Maternal Immunometabolism Adaptation in Pregnancy

April Rees, BSc

Swansea University
Prifysgol Abertawe

Medical School
Ysgol Feddygaeth

Submitted to Swansea University in fulfilment of the requirements for the Degree of Doctor of Philosophy (PhD)

2022

Summary

Pregnant women undergo a series of metabolic and immunologic changes to ensure provision of nutrients to, and prevent rejection of, the fetus. To ensure continuous supply of glucose to the fetus, the mother increases glucose production, glucose intolerance and insulin resistance. To meet her own energy demands, the mother transitions from lipid storage to lipolysis. To prevent rejection of the fetal semi-allograft, the mother's immune system must be regulated, whilst maintaining protection against pathogens.

Hypothesis: *Well-recognised metabolic changes in pregnancy could impact maternal immune function.*

The aims of this project are to landscape the lipidomic profile using novel mass spectrometry techniques, and to determine whether monocytes undergo metabolic adaptation, if this occurs at 28 weeks of gestation, and if maternal obesity sabotages immunological adaptations. In addition, aims included investigation into the mechanisms which may protect the mother and fetus against SARS-CoV-2.

Key findings unveiled significant phenotypic adaptations in the monocyte subsets during pregnancy, which are sabotaged by obesity. As the effect of maternal obesity is poorly understood, other immunological adaptations were investigated which revealed a shift to a Th1 and Th17 response which might contribute to the detrimental effects of obesity on pregnancy. At term, the monocytes illustrate a strong metabolic adaptation where their oxidative phosphorylation capabilities are reduced, confirmed by alterations in their mitochondria, with a downstream effect on their functionality with reduced production of lipid mediators and cytokines.

While risk of infection with SARS-CoV-2 is low to pregnant women and the fetus, there is increased risk of preterm birth and admission into ICU. The fetus is relatively protected against infection, with cases of vertical transmission being rare. This thesis illustrates an elevated presence of soluble SARS-CoV-2 related molecules in breast milk and amniotic fluid which are postulated to act as decoy traps for the virus, which protects the neonate.

In conclusion, this thesis has revealed novel findings into the immunometabolism adaptation to pregnancy.

Declarations

This work has not previously been accepted in substance for any degree and is not being concurrently submitted in candidature for any degree.

Signed .....  te)

Date .....15/03/2022.....

STATEMENT 1

This thesis is the result of my own investigations, except where otherwise stated. Where correction services have been used, the extent and nature of the correction is clearly marked in a footnote(s).

Other sources are acknowledged by footnotes giving explicit references. A bibliography is appended.

Signed .....  didate)

Date .....15/03/2022.....

STATEMENT 2

I hereby give consent for my thesis, if accepted, to be available for photocopying and for inter-library loan, and for the title and summary to be made available to outside organisations.

Signed ..  didate)

Date .....15/03/2022.....

Table of Contents

List of figures

List of tables

Abbreviations

2-DG	2-Deoxy-D-glucose
2-ME	2-Mercaptoethanol
ADP	Adenosine diphosphate
AMP	Adenosine monophosphate
AMPK	AMP-activated protein kinase
APC	Antigen presenting cell
AT	Adipose tissue
ATP	Adenosine triphosphate
BMI	Body mass index
BODIPY	Boron-dipyrromethene
BPTES	Bis-2-(5-phenylacetamido-1,3,4-thiadiazol-2-yl)ethyl sulfide
BSA	Bovine serum albumin
CCR	C-C chemokine receptor
CD	Cluster of differentiation
CL	Cardiolipin
CPT1A	Carnitine Palmitoyl Transferase 1 A
CRP	C-reactive protein
CXCR	C-X-C motif chemokine receptor
DC	Dendritic cell
DRAQ7	Deep Red Anthraquinone 7
ECAR	Extracellular acidification rate
EDTA	Ethylenediaminetetraacetic acid
ELISA	Enzyme linked immunosorbent assay
Eto	Etomoxir
FACS	Fluorescence-activated cell sorting
FAO	Fatty acid oxidation
FAT	Fatty acid transporter
FBS	Fetal bovine serum
FCCP	Carbonyl cyanide-*p*-trifluoromethoxyphenylhydrazone
FcγR	Fc gamma receptor
FFA	Free fatty acids
FSC	Forward scatter
GAPDH	Glyceraldehyde 3-phosphate dehydrogenase
GDM	Gestational diabetes mellitus
GLUT	Glucose transporter
HK	Hexokinase
HLA	Human leukocyte antigen
IFN-	Interferon
Ig	Immunoglobulin
IL-	Interleukin
ILC	Innate lymphoid cell
LAT1	Large amino acid transporter 1
LC-MS/MS	Liquid chromatography with tandem mass spectrometry
LDH	Lactate dehydrogenase
LPC	Lysophosphotidylcholine
LPS	Lipid polysaccharide

MACS	Magnetic activated cell sorting
MAIT	Mucosal-associated invariant T cell
MALDI-ToF	Matrix-assisted laser desorption/ionisation - time of flight
MAPK	Mitogen-activated protein kinase
MDP	Muramyl Dipeptide
MFI	Median fluorescence intensity
MHC	Major histocompatability complex
MNCs	Mononuclear cells
mTOR	Mammalian target of rapamycin
NAD	Nicotinamide adenine dinucleotide
NK cell	Natural killer cell
NOD2	Nucleotide-binding oligomerization domain-containing protein 2
OCR	Oxygen consumption rate
Oligo	Oligomycin
OXPHOS	Oxidative phosphorylation
PAMP	Pathogen-associated molecular patterns
PBMCs	Peripheral blood mononuclear cells
PBS	Phosphate buffer saline
PC	Phosphotidylcholine
PCR	Polymerase chain reaction
PD-1	Programmed cell death protein 1
PMN	Polymorphonuclear cell
POLY I:C	Polyinosinic:polycytidylic acid
PRR	Pattern recogniton receptor
R848	Resiquimod 848
ROS	Reactive oxygen species
RPMI	Roswell Park Memorial Institute medium
RT	Room temperature
SARS-CoV-2	Severe acute respiratory syndrome coronavirus 2
SDS	Sodium dodecyl sulfate
SEM	Standard error of the mean
SSC	Side scatter
TBS	Tris-buffered saline
TBST	TBS with tween
TCA	Tricarboxylic acid
TCR	T cell receptor
TGF	Transforming growth factor
Th	T helper cell
TLR	Toll-like receptor
TNF	Tumour necrosis factor
Treg	Regulatory T cell
UK5099	Acyano—(1-phenylindol-3-yl)-acrylate

CD molecule identification

CD3	T cell marker
CD4	CD4 T cell marker
CD8	CD8 T cell marker
CD11b	Integrin alpha M; activation marker
CD14	Monocyte marker
CD15	Neutrophil marker
CD16	FcγRIII; monocyte subset differentiation marker
CD19	B cell marker
CD36	Fatty acid translocase, scaveger receptor
CD38	Cyclic ADP ribose hydrolase
CD56	NK cell marker
CD62L	L-selectin; adhesion molecule
CD64	FcγRI
CD69	C-type lectin protein; activation marker
CD80	APC co-stimulatory molecule for T cells
CD86	APC co-stimulatory molecule for T cells
CD98	Long chain neutral amino acid transporter
CD163	High affinity scavenger receptor for hemoglobin-haptoglobin complex
CD169	Sialoadhesion; binds sialic acids
CD220	Insulin receptor
CD295	Leptin receptor

Conferences

1. Rees A, Jones N, Cronin J and Thornton C.A. Maternal Immunological Adaptation in Pregnancy. **Medical School Post-Graduate Research Conference**, 17th-18th May 2018. Poster Presentation. Awarded Post-Graduate Research Poster Presentation Prize.
2. Rees A, Jones N, Cronin J and Thornton C.A. Maternal Immunological Adaptation in Pregnancy. **Medical School Post-Graduate Research Conference**, 16th-17th May 2019. Flash Presentation. Awarded Post-Graduate Research Flash Presentation Runner Up.
3. Rees A, Jones N, Cronin J and Thornton C.A. Maternal Immunological Adaptation in Pregnancy. **IUIS 17th International Congress of Immunology, Beijing**, 19th-23rd October 2019. Poster Presentation.
4. Rees A, Stanton R, Turner S, Thornton C.A. Potential protective effects of breast milk and amniotic fluid against novel coronavirus SARS-CoV-2. **British Society of Immunology Annual Congress, Virtual**, 1st – 2nd December 2020. Poster Presentation.
5. Rees A, Richard O, Jones N, Thornton C.A. The immunological profile of maternal obesity at 28 weeks of gestation underpins negative pregnancy outcomes. **American Association of Immunologists Annual Meeting, Virtual**, 10th – 15th May 2021. Poster presentation.
6. Rees A, Jones N, Cronin J., Thornton C.A. Maternal immunometabolism adaptation in monocytes underpins functional changes during pregnancy. **British Society of Immunology Annual Congress,** 28th November – 1st December 2021. Poster Presentation.

Publications

Rees A, Richards O, Jones N, Allen-Kormylo A, Thornton CA (2022) Maternal body mass index is associated with an altered immunological profile at 28 weeks of gestation. Accepted - *Clinical & Experimental Immunology.*

Rees A, Richards O, Chambers M, Jenkins BJ, Cronin JG, Thornton CA (2022) Immunometabolic adaptation and immune plasticity in pregnancy and the bi-directional effects of obesity. Accepted – *Clinical & Experimental Immunology.*

Rees A, Turner S, Thornton CA (2022) Potential protective effects of breast milk and amniotic fluid against novel coronavirus SARS-CoV-2 through decoy receptors. *Paediatric allergy and immunity,* 33: e13672

Jenkins BJ, **Rees A,** Jones N, Thornton CA (2021) Does altered cellular metabolism underpin the normal changes to the maternal immune system during pregnancy? *Immunometabolism,* 3(4): e210031

Holm S, Jenkins BJ, **Rees A**, Cronin JG, Jones N, and Thornton CA (2021) A role for metabolism in determining neonatal immune function. *Pediatric Allergy and Immunology.* 00: 1-13

Jones N, Blagih J, Zani F, **Rees A**, Hill DG, Jenkins BJ, Bull CJ, Moreira D, Bantan AIM, Cronin JG, Avancini D, Jones GW, Finlay DK, Vousden KH, Vincent EE, and Thornton CA (2021) Fructose reprograms glutamine-dependent oxidative metabolism to support LPS-induced inflammation. *Nature Communications*, 12: 1209.

Chambers M, **Rees A,** Cronin JG, Nair M, Jones N, and Thornton CA (2021) Macrophage Plasticity in Reproduction and Environmental Influences on Their Function. *Frontiers in Immunology* 11: 3491.

Scott LM, Bryant AH, **Rees A**, Down B, Jones RH, and Thornton CA (2017) Production and regulation of interleukin-1 family cytokines at the materno-fetal interface. *Cytokine* 99: 194-202.

Acknowledgements

These 4 years of PhD life has definitely been interesting, to say the least. I have enjoyed the experience as a whole and have grown a lot through these short years. That has mostly been down to the best supervisor someone could ask for. The support that Prof Cathy Thornton has provided means the world to me, and I couldn't have asked for someone better to push me to reach my potential. I thank her so much for always believing in me. I am also very grateful to my two other supervisors, Dr James Cronin and especially Dr Nick Jones, who has always been kind to lend an ear to the many rants about machines not working and experiments gone wrong.

I'd also like to thank Dr Roberto Angelini, who has been incredibly patient with me with sharing the world of lipidomics with me and helping me wrap my head around the mass spec. Dr Ruth Jones has been instrumental in recruiting patients onto the studies, but I am particularly grateful for her insight to making snazzy spreadsheets! From my time as a PGR rep, I thank the PGR office – Georgie, Ian and Nici – and the PGR directors, - Dr James Cronin and Dr Martin Clift – for giving me another dimension of PGR life to enjoy, and for giving me to the opportunity to organise an amazing PGR conference (especially the important after-party).

A big thank you goes to all those in the CT group (of whom there are too many to name), for helping keep me sane. I am particularly grateful for those who have accompanied me on walks along the beach to get a much-needed iced coffee or ice cream when there's been a lull in lab work and writer's block has gotten to be too much. Those in the PhD office from other groups I am indebted to, with always making sure I get my caffeine-fix and brightening my life with Cake Thursday – something I deeply miss post-lockdown.

Survival of the PhD could also have not been done without the friendship of Rosie, Faith, Tamsin and Becky. Our weekends away have always provided a much-needed break, and I really value our friendship.

Most importantly, I could not have done this without support from my family. I hope my mum, dad, Hallie, and Nana realise how much their love and support mean to me, and I appreciate them so much. There aren't enough words to describe how lucky I am to have the family that I do. I am especially grateful to the one person who is my rock and has been with my every step of this journey, my best friend and partner, Kieran.

All in all, a massive thank you to everyone who has helped shape me into the person who has submitted this thesis after 4 short years.

*"**To the stars who listen and the dreams that are answered**"*

-Sarah J Maas

I dedicate this thesis to my Nana

and in memorial of

my Bampi and my brother,

always in my heart

Chapter 1 - Introduction

1.1 Overview

To meet the high energy demands of pregnancy, mandatory maternal physiological changes are required to provide a suitable and continuous metabolic supply from the mother to the fetus [1]. Some metabolic adaptations include the switch from accumulating lipids, to lipolysis, and the development of insulin resistance through gestation (Figure 1.1)[2]. In addition to metabolic changes, immunological changes are required to prevent maternal rejection of the fetus, which expresses paternal antigens and is referred to as a semi-allograft. The work presented in this thesis investigates the interaction between the immune response and cellular metabolism – now called immunometabolism – in pregnancy concentrating on peripheral blood monocytes.

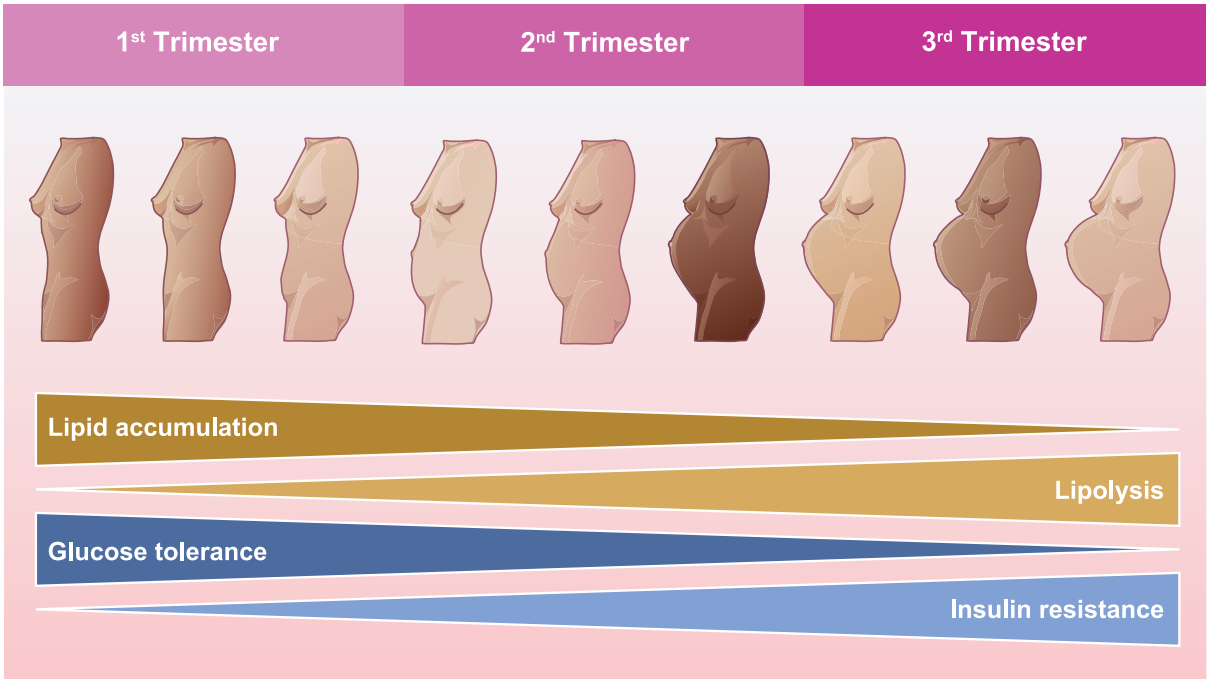

Figure 1.1: As gestation progresses, various metabolic changes occur. The accumulation of lipids decreases with pregnancy while lipolysis increases. The mother becomes less tolerant to glucose and insulin resistance is induced. Image created for Rees et al.

1.2 Pregnancy

1.2.1 Immunological adaptation in pregnancy – an overview

The maternal immune system undergoes dynamic adaptation to pregnancy at both the materno-fetal interface and systemically with the systemic changes the focus of this thesis. Many of these changes are driven by the presence of the fetus that has been likened to a "semi-allogenic graft" that the mother ("host") recognises as half-*self* and half *non-self* [3] accompanied by the hormonal changes that occur. Thus, the mother's immune system must

be well regulated to prevent rejection of the fetus but maintain protection against pathogens. Many immunological changes occur in pregnancy and include suppression of cytotoxic T and natural killer (NK) cells; increased regulatory T cells (Treg); increased B cell activity; decreased immunoglobulin and phagocytic activity; and increased oestrogen and corticosteroids in the reproductive tract [4, 5]. The total number of circulating leukocytes increases during pregnancy. This is mostly due to neutrophils, with no significant changes in the counts of other granulocytes, namely eosinophils and basophils, [6] and a sharp increase in monocytes in the first trimester, which plateaus with advancing gestation [6]. T cells play a vital role in graft rejection, so changes in the number and/or function of different T cell subsets observed in pregnant women is essential to pregnancy success. The greatest reduction of T cells is seen in the 1st trimester, and normal T cell responses are restored 1 month postpartum [7]. Recent years have seen a shift from a T helper type (Th)1/Th2 centric view of immune adaptation in pregnancy [8] to one that also considers the balance of Th17 and regulatory T cells (Treg) [9, 10]. This T cell plasticity likely underpins amelioration, e.g., multiple sclerosis and rheumatoid arthritis, or exacerbation, e.g., systemic lupus erythematosus, of various autoimmune diseases recognised to occur with pregnancy [11-13]. During the 2nd and 3rd trimesters of pregnancy, conventional lymphocytes have a reduced ability to proliferate against soluble antigens or foreign lymphocytes [14], and T cells have a diminished ability to kill foreign cells [15, 16]. To supplement maternal defence against bacterial invasion, elevated levels of maternal serum complement proteins enhance opsonisation of immunoglobulins and chemotaxis from week 11 of gestation [17]. A delay in the activation of the complement pathways prevents attack of the fetus and placental trophoblast [17]. Macrophage levels fluctuate during the menstrual cycle and increase in the uterus and then decidua after fertilisation, where they have been deemed necessary for implantation [18]. The immunological profile of the uterus adapts with pregnancy with the development of the maternal-fetal interface (Figure 1.2)[19] to ensure fetal survival. These changes are driven by signals from the fetus, as well as maternal and placental mediated hormonal and other mediator changes. Uterine natural killer (uNK) cells become the dominant leukocyte in the first trimester decidua [20, 21], with smaller numbers of macrophages and T cells accounting for the rest of the immune cell populations [22]. The main role of these cells is to promote trophoblast invasion and spiral artery vascular modelling, whilst regulating the immune response to the semi-allogenic fetus [22].

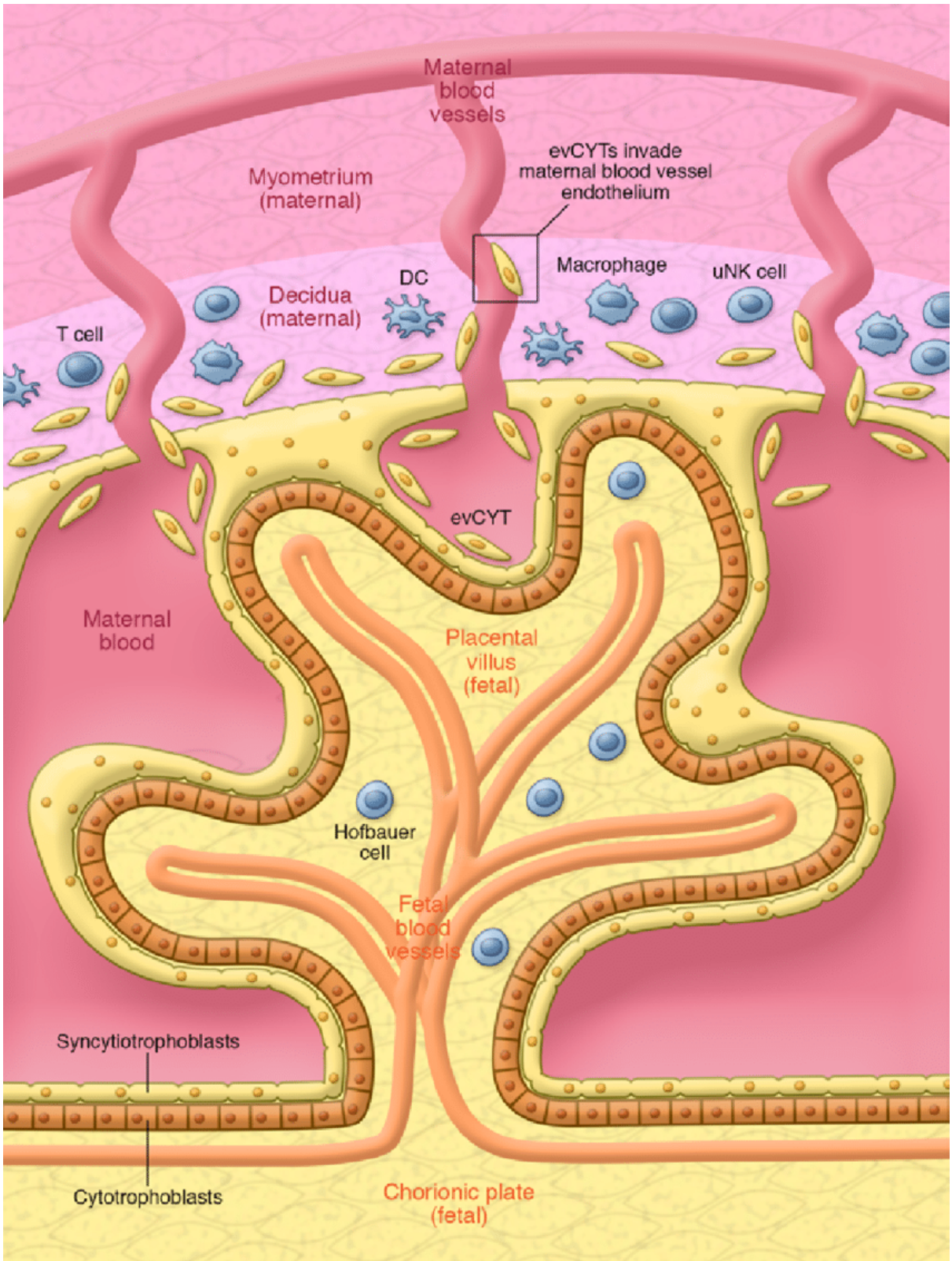

Figure 1.2: The maternal-fetal interface. The maternal-fetal interface is composed of the fetal-derived placenta and the maternal-derived decidua, connected by the invasion of extravillous cytotrophoblasts (evCYTs) into the decidua to initiate nutrient circulation. To facilitate nutrient and waste exchange, the maternal blood is in direct contact with the placental villus. The decidua contains the maternal leukocytes including uterine NK (uNK) cells, macrophages, dendritic cells (DCs) and T cells, whereas the fetal macrophages (Hofbauer cells) surround the fetal blood vessels in the placenta. Image taken from Racicot & Mor 2017 [19].

Both pro- and anti-inflammatory changes occur within the uterus as a healthy pregnancy progresses and these are stage specific. At the maternal-fetal interface, pro-inflammatory M1 macrophages are dominant in the first stage of pregnancy for implantation, contributing to the high levels of tumour necrosis factor-alpha (TNFα), interleukin (IL)-6 and IL-1β observed [23, 24]. With the emergence of the developing placenta, an anti-inflammatory M2 milieu becomes dominant supporting trophoblast invasion and vascular remodelling, and includes secretion of mediators such as IL-10 and TGFβ [25]. The expansion of paternal antigen specific Treg cells and a switch to a Th2 profile with the secretion of IL-4 and IL-10 assists in the prevention of allograft rejection [26, 27]. The induction of labour is associated with a pro-inflammatory state, with pro-inflammatory macrophages infiltrating the decidua to promote uterine contractions [28]. Prior to this, in preparation for delivery, elevated levels of predominantly pro-inflammatory cytokines are observed (e.g., IL-1β, IL-1α, IL-6, IL-8) [29, 30].

During the last two trimesters of pregnancy, maternal systemic immunity has an anti-inflammatory innate phenotype [31]. A number of studies demonstrate that plasma levels of many pro-inflammatory cytokines (e.g. IL-18, TNFα, CCL2, CXCL10, IL-6) are decreased in pregnancy, whereas mediators with immunomodulatory and anti-inflammatory properties (e.g. IL-1 Receptor Agonist (RA), soluble (s) TNF-receptor (R) I, sTNF-RII) are elevated [31, 32]. Consequently, perturbed levels of pro-inflammatory cytokines are associated with adverse obstetric outcomes. For example, systemic elevation of IL-6 is associated with preeclampsia [33]. Obesity is a low grade chronic systemic inflammatory disorder characterised by increased circulating levels of inflammatory markers such as IL-6, TNFα, C-reactive protein (CRP), and the pro-inflammatory satiety hormone leptin [34, 35] recognised to have negative effects on pregnancy [36].

1.2.2 Metabolic adaptations in pregnancy

Pregnancy has been described as a diabetogenic state due to increased maternal glucose production, glucose intolerance, and insulin resistance [37]. This is to ensure a continuous supply of glucose to the fetus for growth and development. To fuel her own energy demands over the term of her pregnancy the mother transitions from an anabolic state in which she stores lipids, to a catabolic state of breaking them down via lipolysis [38]. This is evidenced by a

decrease in maternal adipose tissue deposits, and an increase in levels of postprandial free FAs (FFA) in late pregnancy [39].

To meet these energy demands, appetite and therefore food intake is increased, and activity is reduced. Over the course of pregnancy, approximately 30,000 kcal of energy reserves are established, ~3.5 kg of fat is accumulated, and the mother, fetus and placenta synthesise 900 g of new protein. Hytten estimated that the net energy cost of reproduction to be between 75,000 kcal and 85,000 kcal [40] which is equivalent roughly to running 850 miles. During early pregnancy, glycogen and protein synthesis in muscle is increased, whereas in the liver glycogenolysis is increased and glycolysis is decreased. Insulin levels are increased at the start of pregnancy but insulin resistance starts as early as 12-14 weeks of gestation [41]. During the third trimester there is an increase in maternal ketone production, intestinal dietary fat absorption is increased, and, in the liver, gluconeogenesis is decreased [42]. Maternal protein storage is also increased during the first half of pregnancy, with these utilised more economically than in the non-pregnant setting in the second half of pregnancy [43, 44].

In the first two trimesters, heightened lipogenesis allows for the accumulation of maternal adipose tissue deposits which are catabolised in the last trimester [45]. The synthesis of triglycerides increases by 40% by 18 weeks of gestation, and by 250% by term [45, 46]. High-density lipoprotein (HDL), very-low-density lipoprotein (VLDL) and low-density lipoprotein (LDL) are part of a family termed lipoproteins which are a combination of various types of fats and proteins. They are necessary for the transport of cholesterol and triglycerides through the blood. In the first 24 weeks of gestation, HDL levels increase progressively before decreasing until 32 weeks where they plateau [45]. LDL levels undergo a small decrease during the initial stages of pregnancy before rising steadily [45]. During the second and third trimester, VLDL levels increase threefold. These net increases of lipoprotein levels are due to cholesterol levels being 50% higher in late pregnancy in comparison to pre-pregnancy [45, 46].

Metabolic processes during pregnancy are influenced by hormones such as oestrogen, human placental lactogen (hPL), progesterone and potentially the satiety hormone leptin. These hormones can alter the action of insulin and the utilisation of glucose, leading to the observed diabetic state which pregnancy has been likened to. This can also induce changes in the

metabolism of proteins and lipids, as well as increase amino acid and glucose availability for the fetus, whilst meeting the maternal needs by providing FFAs as an alternative energy substrate to maintain homeostasis.

Alterations in complement and T cells occur predominantly in the 1st trimester [7, 17]. It would be an assumption that immunometabolism changes occur around these times. Typically, research has focussed on metabolic changes related to adipose tissue, muscle, and liver, but the emergent field of immunometabolism highlights potential effects on immune function. This novel field explores the link between cellular metabolism and immune cell fate and function. There appears to be very little research surrounding specific immune cell bioenergetics in pregnancy. It has been shown that PBMCs in normal pregnancy have reduced glycolytic capacity and basal glycolysis but elevated bioenergetic health index [47].

Early evidence of important immunometabolic changes with pregnancy are emerging and an example of this is CD38. Cyclic ADP ribose hydrolase (CD38) is a glycoprotein found on the surface of many leukocytes. It is a multi-functional ectoenzyme which catalyses reactions that produce cyclic ADP-ribose and nicotinic acid adenine dinucleotide phosphate (NAADP) from NAD+ and NADP+ respectively. CD38 has been implicated to have critical roles in pregnancy. Soluble CD38 (sCD38) from seminal fluid has a vital role in the establishment of maternal immune tolerance in mice [48]. sCD38 promotes the development of forkhead box $P3^+$ ($Foxp3^+$) Treg cells and uterine tolerogenic DCs to prevent rejection of the allogeneic fetus, with knockout models showing that pregnancy loss occurs [48]. CD38 is also more highly expressed on NK cells during pregnancy where it is postulated to have role in enhancing their ability to combat infected cells [49].

Expression of metabolic transporters is an important consideration in pregnancy. The fatty acid translocase (FAT) CD36 is expressed by the placenta supporting responsiveness to lipoproteins in maternal plasma [50]. Upregulation of other transporters in the placenta such as long chain neutral amino acid transporter (LAT1; CD98) and sodium-coupled neutral amino acid transporter (SNAT) 2 have been linked with fetal macrosomia secondary to maternal obesity in murine models [51]. Glucose is transported across the cell plasma membrane via glucose transporters (GLUT). GLUTs have differential distributions and functions. GLUT1 is

expressed on all cells but is expressed most highly in erythrocytes [52] and barrier tissue endothelial cells [53]; GLUT3 is expressed predominantly in neurons [54] and the placenta [55] and GLUT4 in AT [56] and striated muscle [57]. Glucose intolerance is observed commonly in pregnancy, and in rat models impaired glucose tolerance is further exacerbated in pregnancies with obesity [58]. GLUT3 is vitally important for fetal growth in pregnancy, with mutation of GLUT3 in mice reported to induce fetal loss during early gestation, or growth restriction in later pregnancy [59].

1.2.3 Monocytes in pregnancy

Innate immunity is non-specific and occurs quickly in response to pathogens and other danger signals which breach the anatomical and physiological barriers. Innate immune cells recognise specific motifs on pathogens called pattern associated molecular patterns (PAMPs) [60]. PAMPs are recognised by pattern recognition receptors (PRRs) on immune and other cells and can either be membrane bound (toll-like receptors (TLRs), e.g. TLR4, TLR7, TLR8, or C-type lectin receptors (CLRs)), cytoplasmic (nucleotide binding oligomerisation domain [NOD]-like receptors (NLRs), e.g. NOD2, RIG-I-like receptors (RLRs)) or soluble in the blood (complement system) [60]. TLRs were found to initiate the activation of an immune response by synthesising and secreting cytokines, and through other inflammatory responses. Specific PAMPs interact with specific TLRs, e.g. lipopolysaccharide (LPS) with TLR4 and polyinosinic:polycytidylic acid (POLY I:C) with TLR3. POLY I:C is structurally similar to double stranded RNA and is commonly used to simulate viral infections. PAMP/TLR interaction is mediated via either a myeloid differentiation primary response gene 88 (MyD88)-dependent pathway, or a toll interleukin receptor [TIR]-domain-containing adaptor-inducing interferon-β (TRIF)-dependent pathway [61]. The MyD88-dependent pathway initiates a proinflammatory cytokine response through nuclear factor-kappa B (NF-κB) and mitogen-activated protein (MAP) kinase (MAPK) pathways [61]. NLRs recognise PAMPs like muramyl dipeptide (MDP), which in turn activates caspases to cleave and activate inflammatory cytokines and initiate NF-κB signalling via receptor-interacting-serine/threonine-protein kinase 2 (RIP2) to produce inflammatory molecules [60].

Monocytes are the largest form of leukocyte, and whilst they are key contributors to innate immunity, they also have an impact on the adaptive immune processes due to also serving as antigen presenting cells (APC). They are produced in the bone marrow from precursors as seen in Figure 1.3. Whilst circulating in the blood stream, monocytes have a half-life of approximately one to three days [62], before typically migrating into tissues to differentiate into macrophages[63]. The total leukocyte population in the human body tends to be composed of 2-10% of monocytes, and they contribute to 10-30% of peripheral blood mononuclear cells (PBMCs). More than half of the body's monocytes can be found in the spleen in masses in the cords of the subcapsular red pulp [64] where they are stored and primed for rapid deployment to regulate inflammation [64]. PBMCs are typically made up of monocytes, lymphocytes, and to a lesser degree dendritic cells, and can be extracted via density centrifugation of whole blood. Monocytes have several roles, including macrophage replenishing, differentiation into the appropriate progeny to assist an immune response, and migrate to inflammation signals. Monocytes function in assisting the immune system by producing cytokines, presenting antigens, and performing phagocytosis. Phagocytosis by monocytes can occur via binding directly to the pathogen or indirectly via opsonisation of the pathogen. Monocytosis refers to an excessive count of monocytes; it can be indicative of several diseases such as atherosclerosis and diabetes [65, 66].

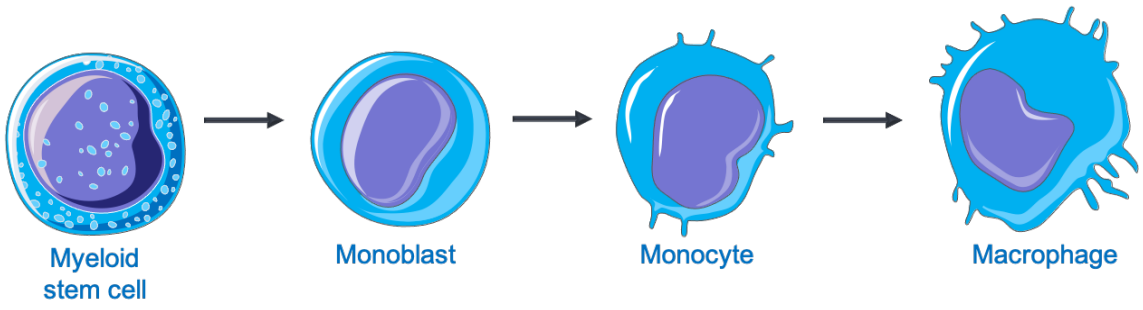

Figure 1.3: Differentiation of monocytes. Monocytes originate from haematopoietic stem cells in the bone marrow via myeloid progenitor cells and monoblasts. Monocytes can further differentiate into macrophages upon leaving the circulation and entry into tissues. Unless otherwise stated, all images in this thesis are self-made, with some manipulation of images from Servier Medical Art https://smart.servier.com/ .

Monocytes are a heterogenic population. They can be characterised into classical (CD14++CD16-), intermediate (CD14++CD16+), and non-classical (CD14+CD16++). Classical monocytes are more prevalent than intermediate or non-classical accounting typically for 90-95%, <1% and 5-10% of total monocyte population respectively [67]. Non-classical monocytes are elevated in inflammatory states such as sepsis and rheumatoid arthritis. Studies have

illustrated an increase in the non-classical subpopulations in obese subjects [68]. Non-classical and classical monocytes can also be identified as $CX_3CR1^{high}/CCR2^{low}$ or $CX_3CR1^{low}/CCR2^{high}$, respectively.

Most studies typically only differentiate between $CD16^-$ and $CD16^+$, due to the low frequency of the intermediate monocytes. Certain immunological markers (i.e., PD-1, chemokine receptors, activation markers etc) have been found to differ in levels of expression between the two subsets. The $CD16^+$ subset has reduced phagocytic capabilities and secretes less ROS [69]. $CD16^-$ monocytes secrete low levels of TNFα and high levels of IL-10, with the converse seen in $CD16^+$ monocytes [70]. In mice, monocyte subsets are described as lymphocyte antigen 6 complex, locus C positive ($Ly6C^+$) and $Ly6C^-$, and these might correlate to classical and non-classical human monocytes respectively due to their functional and phenotypical similarities and their $CX_3CR1/CCR2$ expression [69]. In mice, it is believed that the $Ly6C^+$ and the $Ly6C^-$ monocytes differentiate preferentially into M1 and M2 macrophages, respectively [71]. In humans, non-classical monocytes mostly differentiate into macrophages, whereas classical monocytes differentiate into mostly dendritic cells, and few macrophages; intermediate monocytes have the potential to differentiate into some macrophages and cells with dendrites on occasion [70].

Functionally, studies have shown that the classical and non-classical monocytes have similar capabilities in phagocytosing fungal infections such as that caused by *Candida albicans* [72]. This study also illustrated similar IL-6 and IL-10 production by the two different subsets, but the production of IL-1β and prostaglandin E2 (PGE2), which are mediators for initiating Th17 responses, are elevated in the non-classical monocytes that were shown to induce greater Th17 responses in response to *C. albicans*.

Increased expression of the activation markers CD14, CD64 and CD11b highlight that monocytes are typically activated during pregnancy [73]. Monocytes in pregnancy also produce more oxygen free radicals [73] but their ability to produce cytokines in comparison to those from not pregnant women seems to depend on the cell stimulation used. There are also conflicting reports from different studies; for example, some investigators have observed increased cytokine production in non-stimulated monocytes from pregnant in comparison to

non-pregnant women [74] , whereas others have not [75]. LPS stimulation has been shown in some *in vitro* studies to decrease the number of monocytes secreting cytokines in pregnant women [75], but stimulation with a combination of LPS and IFNγ increases cytokine production [76] [77]. Very little is known about the effects of maternal obesity on monocytes and given the dramatic effects on monocytes in obesity in the non-pregnant state [68, 78, 79], further consideration in pregnancy is certainly warranted. We know that pregnancy-associated monocyte activation is further exacerbated in for example preeclampsia, driving maturation into non-classical monocytes (classical monocytes differentiate into intermediate monocytes which in turn mature into non-classical), [77] and obesity is a risk factor for preeclampsia [80, 81]. The effect of maternal obesity on neonatal monocytes has been explored more. Umbilical cord monocytes from neonates of mothers with obesity have reduced TLR1/2- and TLR4-stimulated TNFα and IL-6 possibly contributing to dysregulation of the offspring's immune function [82, 83].

Dendritic cells

In pregnancy, the circulatory myeloid DC phenotype is altered to favour Th2 responses, by up-regulating expression of CD86 and secreting more IL-10 [84]. Myeloid DCs (mDCs) expressing CD86 and HLA-DR are reduced in the third trimester of pregnancy in comparison to not pregnant women [84]. Monocyte-derived DCs are also phenotypically less mature expressing lower levels of HLA-DR, CD80 (another co-stimulatory molecule for T cells) and CD86, although in response to TNFα and IL-1β stimulation these DCs showed greater upregulation of CD86 than CD80 and secreted more IL-10 [84].

Macrophages

Macrophages, which are differentiated from monocytes in tissue, are critical to the development of the placenta [85]. They are abundant in the decidua where they contribute to the local tissue microenvironment and in the cycling endometrium in non-pregnant women where, due to their fluctuating numbers during the menstrual cycle, they are thought to be regulated by hormonal signalling [86]. Decidual macrophages, which are maternal in origin, have a vital role in implantation. They produce factors to promote angiogenesis, tissue remodelling and the clearing of apoptotic cells to prevent release of pro-inflammatory products in preparation for trophoblast invasion [87, 88]. The balance of decidual M1/M2 macrophages is

critical to successful pregnancy with imbalances linked to complications such as preeclampsia and miscarriage [89-91]. Decidual M1 macrophages are associated with the onset of labour as during the third trimester they infiltrate the decidua and this can occur prematurely in preterm delivery [28].

Maternal obesity has been associated with changes to macrophages in placenta and decidua [85, 92]. Briefly, increased inflammation including heightened gene expression of IL-6, IL-1, TNFα and CCL2 linked to increased number of macrophages have been described to occur in the placenta of pregnant women with versus without obesity [93], although there are some conflicting findings regarding changes to the number of placental macrophages with maternal obesity [94]. In contrast, decidual macrophage levels are reduced in pregnant women with versus without obesity [95]. These changes have been postulated to be linked to placental dysfunction and fetal programming of later child health [93]. It is obviously difficult to study any tissue in pregnancy aside from the placenta. Adipose tissue (AT) however, would be key to investigate, especially in the consideration of macrophages. Murine studies have shown elevated macrophage infiltration in the AT of pregnant mice, and a higher M1/M2 ratio in comparison to non-pregnant mice [96] but these observations have not been extended to consider the effects of obesity. One study using visceral adipose tissue collected from the omentum during caesarean section observed that pregnant women who were overweight or obese had adipocyte hypertrophy and changes to specific populations of macrophages in AT. This included fewer resident $HLA^{-}DR^{low/-}$ macrophages, higher expression of CD206 on resident and recruited macrophages, and elevated CD11c expression on resident $HLA\text{-}DR^{+}$ macrophages [97].

1.2.4 Other innate leukocyte-specific changes in pregnancy

Neutrophils

Neutrophilia is a typical feature of normal pregnancy but an abnormally elevated neutrophil count, especially in the first trimester, is typically indicative of the development of adverse pregnancy outcomes including gestational diabetes mellitus (GDM) [98-101]. Neutrophils are typically more active during pregnancy, evidenced by increased expression of activation markers such as CD11b, increased ROS production [73], degranulation and phagocytosis [102]. During pregnancy, neutrophils are also more inclined to produce neutrophil extracellular traps (NETs) [102]. The increase in neutrophil activity is vital to combat invasive pathogens, to

compensate for a down-regulation of the adaptive response, vital to protect the semi-allograft fetus.

Eosinophils

Eosinopenia is observed in pregnancy, with the nadir reached around delivery. Whilst very little is currently known about the role of eosinophils in pregnancy, degranulation activity is increased until the 2nd trimester as evidenced by elevated levels of eosinophil-derived neurotoxin (EDN) in urine samples of pregnant women [103]. Thus, eosinophil degranulation might play an as yet undetermined role in the progression of pregnancy, possibly through the provision of cytokines [104]. Given how little we know about eosinophils in pregnancy and the emergent understanding of their role in tissue homeostasis, including in the uterus [105], there is a clear need for further study for eosinophils more generally in pregnancy.

Natural killer cells

Like macrophages, NK cells have important roles in ensuring pregnancy success. Two NK cell subsets are well characterised in the circulation: $CD56^{dim}CD16^{+}$, and $CD56^{bright}CD16^{-}$. Phenotypic and functional shifts of blood NK cells such as elevated expression of activation markers (e.g. CD38, CD11b) and select functional markers (e.g. PD-1, CD27) occur with normal pregnancy [49]. However, other than some reported changes in overweight women with gestational diabetes the effects of maternal obesity on blood NK cells have not been studied extensively [106]. Decidual NK cells have a vital role in placental development and uterine artery remodelling. Maternal obesity diminishes the numbers of these uterine resident cells and alters their contribution to extracellular matrix remodelling and growth factor signalling to compromise trophoblast survival and artery remodelling [107]. More recently this has been demonstrated to be linked to altered expression of NK receptors altering the balance of inhibitory and activating receptors [108.] These findings suggest that the altered state of NK cells in maternal obesity impairs function at the maternal-fetal interface and could underpin adverse obstetric outcomes such as altered fetal growth and hypertensive disorders such as preeclampsia [109, 110]. It is worth considering whether obesity-associated defects in NK cell phenotype and function within the uterus can be mapped to peripheral blood for ease of monitoring and tracking of interventions.

1.2.5 The adaptive immune system in pregnancy

Adaptive immunity is specific and is responsible for providing 'immunological memory'[111]. The adaptive response recognises *non-self* peptides presented by APCs, and produces a response which can eliminate specific pathogens, or infected cells. It is highly specific unlike the innate immune response and acts more slowly initially; evolution has driven adaptive immunity in order to combat the variability of pathogens and host evasion [111]. Once exposed to a particular pathogen, the immune system "remembers" it upon subsequent exposures and acts more quickly and specifically. Vaccines are based on the premise of adaptive immunity: live attenuated versions are given to a patient in order to prime an immune response [112]; the novel mRNA vaccines, successful in combating COVID-19, instructs the host cell to produce the viral spike protein which induces the immune system to produce antibodies against it. If the patient then encounters the naturally occurring pathogen, their immune response is primed ready to respond. The adaptive immune response is linked to the innate immune response via antigen presentation by APCs.

T cells

T lymphocytes are produced in the thymus and are identified by their expression of TCR. When they first emerge from the thymus T cells are naïve and upon activation by peptide bearing APCs generate effector and central memory population. This is the basic activation process for both $CD4^+$ or $CD8^+$ T cells. Helper $CD4^+$ T cells recognise peptides presented by MHC class II molecules and their primary role is to assist other lymphocytes. There are subsets of $CD4^+$ T cells including Th1, Th2, Th17, Th9, and Tfh that secrete different cytokines and have slightly different roles, e.g. IL-4 producing Th2 cells assist B cells in their production of IgE for example, and Th17 cell defend against pathogens in the gut. Cytotoxic $CD8^+$ T cells that can directly kill target cells, recognise by peptides presented by MHC class I molecules. A specialised subset of T cells, $CD4^+FoxP3^+$ regulatory T (Treg) cells, limit excess immune responses and are key in maintaining immunological self-tolerance by down-regulating self-reactive immune cells [113]; indeed the depletion of dysfunction of Treg cells leads to autoimmune disease development [114, 115].

The balance between Th1 and Th2 cells is often discussed. Traditionally, in regards to host defence, the Th1 response is typically proinflammatory, with IFNγ being the main Th1-type

cytokine [116]. To counteract an excessive Th1 response, Th2 cells should respond with anti-inflammatory cytokines such as IL-4, -5 and -13 [116]. The reality of the Th1 and Th2 response is much more complicated; for example, while Th2 cells are anti-inflammatory in classical inflammation, in asthma they are very inflammatory [117]. The type 1 and type 2 cytokine classification is also referred to in regards to cell types which are not T cell originated; for example group 2 innate lymphoid cells (ILC2s) are a prime example of a cell which produces type 2 cytokines. The Th1/Th2 balance is compromised in various conditions. Leptin, levels of which are elevated in pregnancy and obesity amongst other conditions, induces a shift towards Th2-type cytokine production [118].

Pregnancy is associated with a shift to Th2 and Treg cells in order to produce pregnancy beneficial cytokines such as transforming growth factor (TGF)-β, IL-4, IL-6, and IL-10, as excesses of Th1 and Th17 cytokines such as IFNγ and TNFα are considered detrimental to pregnancy [119]. Treg cells have a key role in pregnancy success contributing to a tissue environment within the uterus that supports fetal development and survival[120, 121]. Populations of Treg cells expand in both the peripheral blood and the decidua [122]. In murine models, Treg cells create a pro-implantation microenvironment [123] and the absence of Treg cells results in rejection of the semi-allogenic fetus in a syngeneic pregnancy[124]. The immunosuppressive capabilities of Treg cells are especially vital in monitoring infiltrating NK cells (Treg cells are at peak populace at the same time as uterine NK cells) and cytotoxic T cells by the release of immunosuppressive cytokines such as IL-10 and TGF-β [10, 125]. Regulating the maternal immune response to fetal alloantigens is a key Treg response [126]. Immune homeostasis is maintained by complex networks between Th17 and Treg cells and, as mentioned previously, this balance shifts to favour Treg cells, in addition to Th2 cells, in pregnancy [10]. Various strands of evidence support a role for Treg cells in pregnancy success. For example, murine peripheral Treg cells have a key role in suppressing the maternal effector T cell response in response to recognition of paternal antigens [127]. In humans a deficiency of peripheral Treg cells has been correlated with pre-term birth [128] and unexplained recurrent pregnancy loss [129].

Other rare lymphocyte populations are of increasing interest in tissue and immune homeostasis. Treg/ILC2 homeostasis can be disrupted by the soluble isoform of IL-33

receptor ST2 (sST2), which in turn is augmented by the fat-specific depletion of Zbtbt7b. sST2 is elevated with pregnancy, and further heightened in pre-eclamptic pregnancies [130] and adverse changes could manifest as altered Treg and/or ILC2 function linked to adverse obstetric outcome. NKT cells are a type of T cell with properties and markers of NK cells. In pregnancy, maternal obesity is associated with a lower percentage of circulating NKT cells which is correlated negatively to levels of CRP [131] although the functional effects of this remain unknown. Recent studies have started to unravel the role of mucosal-associated invariant T (MAIT) cells in pregnancy. They have been shown to accumulate in the maternal blood in the intervillous space of the placenta at term [132] while no changes in the periphery were found throughout gestation [133, 134]. Despite the lack in change of frequency, during the third trimester the circulatory MAIT cells have been found to be more activated in pregnancy compared to non-pregnant, with increased expression of markers such as CD56 and CD69, and an elevated functional response with increased expression of IFNγ, granzyme B and PD-1 unstimulated or in response to stimulation with IL-2 and IL-18 [135]. It has been proposed that this is due to the enhancement of the innate response due to pregnancy to compensate for the dampened adaptive response, in conjunction with the activation states of monocytes and neutrophils [135].

B cells

Pregnancy is accompanied by a decline in circulating B cell numbers [136] although they play a vital role in tolerance to the fetus; for example, B cells can produce protective antibodies against paternal antigens and regulatory B cells (Breg) are elevated in pregnancy and produce anti-inflammatory IL-10 to inhibit undesirable actions by T cells [137]. It has been suggested that Breg cells in particular have a pivotal role in pregnancy, and might be a logical immunotherapeutic target to restore maternal immune tolerance and remedy recurrent miscarriages [138]. Antibodies are key for passive immunisation of the fetus. As the humoral response in the fetus is unrefined, the placental transfer of maternal IgG antibodies is vital for conferring protection [139]. Systemically, IgG and IgA are found to be significantly elevated at the first stage of pregnancy, and decrease after the 17th week of gestation, whereas IgM was found to decrease immediately following conception [140].

1.2.6 Leptin in pregnancy

Leptin, produced by AT, has been described classically as the "satiety hormone" and was initially described to only have a role in appetite control [141]. However, it has since been discovered to have many other roles, including for example in immune homeostasis [142]. Interaction with the leptin receptor (OB-R; CD295) expressed on innate and adaptive immune cells primarily increases expression of chemokine receptors, cell surface adhesion molecules and cytokines [142]. Whilst leptin classically controls food intake by interacting with OB-R in the brain [143], leptin resistance emerges leading to over-indulgence and further fat storage [144]. Leptin is also responsive to other hormones, such as insulin and cortisol which induce upregulation [145] while catecholamines downregulate leptin [146]. Leptin expression is regulated by a multitude of other factors such as TNFα which increases secretion [147] and by glucose and fatty acids [148]. Functionally, leptin has effects on both innate and adaptive immune features. It can activate innate cells (e.g. monocytes, NK cells, neutrophils), improve their survival by downregulating apoptosis and upregulating cell proliferation and chemotaxis [149], and enhance their functions such as cytotoxicity (NK cells), phagocytosis (macrophages) and cytokine release (PMNs) [150]. Leptin also favours pro-inflammatory $CD16^{+}$ non-classical monocytes [151] and induces the proliferation of most adaptive cell types, except Tregs, and improves their responsiveness to chemotactic signalling, whilst promoting a switch toward pro-inflammatory Th1 [150]. Overall, leptin promotes a pro-inflammatory phenotype.

Leptin is essential for some reproductive functions, with leptin injections improving the likelihood of conception in infertile mice [152] and leptin initiating the onset of puberty in human females [153]. In normal pregnancy, elevated levels of leptin occur due to not only AT accumulation but also placental production [154]; leptin resistance develops during the second trimester [155]. Maternal obesity has been linked with the development of placental leptin resistance [156]. It has been speculated that the mechanisms of leptin resistance in pregnancy differ to those that occur in maternal and general obesity and it seems that leptin resistance mechanisms might differ in lean versus pregnant women with obesity [157]. Fetal growth is supported through central leptin resistance mechanisms in healthy weight pregnant women, but leptin resistance at the placental level in women with obesity adversely affects feto-placental growth and development [157]. Leptin has been described as having various

gestational regulatory roles including placental angiogenesis, nutrient transport and immunomodulation [158].

1.2.7 Novel coronavirus SARS-CoV-2 and pregnancy

Pregnancy poses a unique risk factor to any new infectious disease, such as outbreaks of Zika [159], severe acute respiratory syndrome (SARS) [160] and influenza [161]. These diseases highlight the potential immediate and long-term detrimental health affects for the mother and fetus. Pregnant women are more at risk of severe influenza [161], Zika has been shown to cause birth defects such as microcephaly [159, 162], and SARS to induce premature delivery [160]. Novel coronavirus, SARS-CoV-2, is responsible for the disruptive and deadly COVID-19 pandemic; research into this virus is vital. While it would be logical to assume that pregnant women are therefore at higher risk for severe illness or mortality in comparison to a non-pregnant woman, observations have disputed this[163], with the risk being no different to non-pregnant women [164]. While the majority of pregnant women infected with SARS-CoV-2 have mild or no symptoms [165], some are at risk of severe disease. In this case, the risk of preterm birth, admission to intensive care, and stillbirth are all increased [164].

There are several risk factors associated with disease severity and morbidity of COVID-19 patients [166]. A study from the UK Obstetric Surveillance system has shown that, as with the wider population, Asian and Black pregnant women are more likely to be admitted to hospital with SARS-CoV-2 infection [167]. This study also found that most pregnant women admitted to hospital were in the late second or third trimester [167]. Overweight or obesity also contributed to a large percentage (69%) of pregnant women infected with SARS-CoV-2 and admitted to hospital [167]. A link between levels of IL-6 and risk of mortality has been shown in the general population, a cytokine that is typically observed to be elevated in maternal obesity [168, 169].

1.3 Immunometabolism

Immunometabolism is a burgeoning field with the underlying understanding being that the metabolism (summary: Figure 1.4) of immune cells impacts function [170]. Upon activation, many leukocytes appear to prefer glycolysis over oxidative phosphorylation: despite less adenosine trisphosphate (ATP) being produced per molecule of glucose, glycolysis provides

more rapid ATP production along with key biosynthetic intermediates, supporting a rapid effector response [170]. This is evidenced by the elevated appetite for glucose of activated macrophages and CD4+ T cells[171, 172], and experiments with 2-deoxy-D-glucose (2-DG) (an inhibitor of glycolysis) have shown that it inhibits macrophage activation *in vitro* and suppresses inflammation *in vivo* [173, 174]. However, other ATP and metabolite generating pathways have a role in immune function. Differentiation of macrophages, and production and maintenance of memory CD8+ T cells require fatty acid oxidation (FAO) [170]. These CD8+ T cells proliferate slowly but use FAO to respond rapidly to immune activation [175].

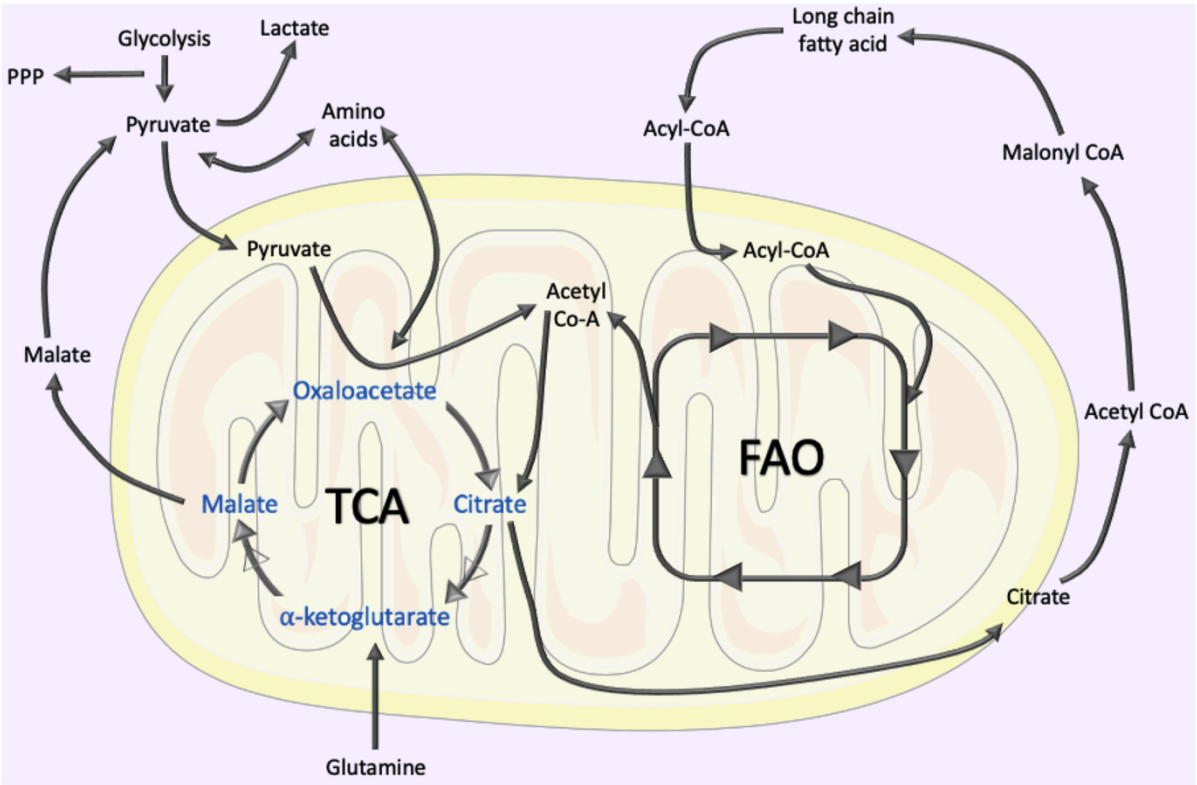

Figure 1.4: Cellular metabolism summary. Pathways for metabolising glucose, fatty acids and amino acids are shown.

1.3.1 Glycolysis and the pentose phosphate pathway

Glucose, a monosaccharide abundant in carbohydrates, is broken down in a process called glycolysis which occurs in the cytosol of cells (Figure 1.5). Glucose is transported into cells via integral membrane proteins called GLUTs which bind to glucose on one side of the membrane and undergo a conformational change to transport glucose to the other side of the membrane. GLUTs can also transport related hexoses such as galactose and fructose. GLUT proteins are encoded by SLC2 (solute carrier family 2) genes and are divided into three classes (I, II, III) based on their sequence similarities, with different isoforms within those classes; GLUT1-GLUT4 comprise class I, GLUTs 5, 7, 9 and 11 for class II, and GLUTs 6, 8, 10, 12 and 13

for class III [176]. The different isoforms have specific roles in hexose metabolism, and differ in substrate specificity, kinetics of transport, tissue expression and how they are regulated in diverse physiological conditions. GLUT1 levels in cell membranes are inversely related to the presence of glucose; in environments of high glucose levels there is decreased expression of GLUT1 to ensure regulation. GLUT3 is a protein expressed primarily in the placenta and in neurons, and GLUT5 is responsible for the transport of fructose in enterocytes [55, 176].

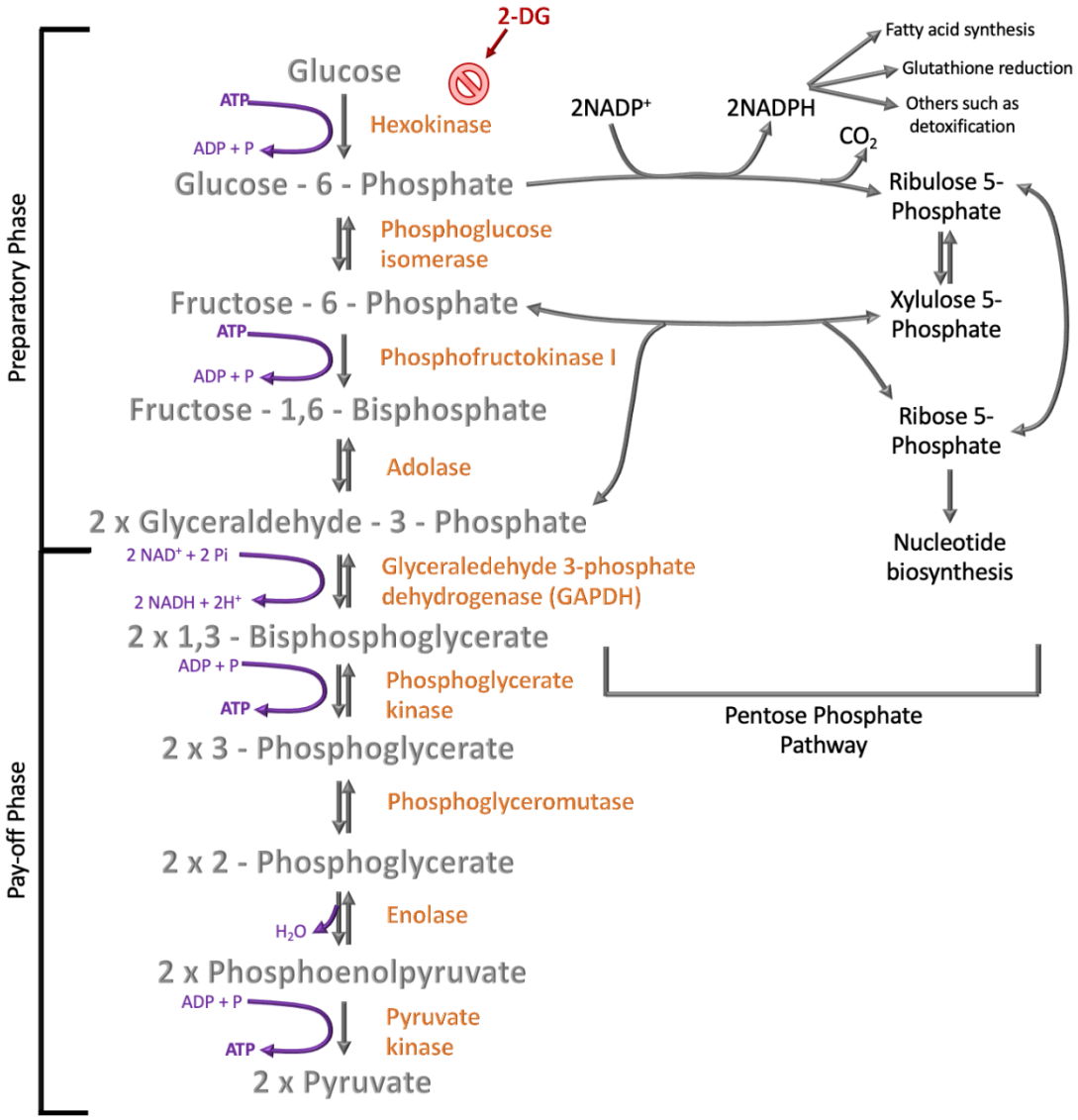

Figure 1.5: Glycolysis pathway. Glucose is first metabolised to glucose-6-phosphate in an irreversible reaction catalysed by hexokinase; an enzyme which can be competitively inhibited by 2-deoxy-D-glucose (2-DG). Glucose-6-phosphate is converted to fructose-6-phosphate by phosphoglucose isomerase. This is converted to fructose-1,6-bisphosphate by phosphofructokinase I, which in turn is converted to 2 molecules of glyceraldehyde-3-phosphate by adolase. This is then converted to pyruvate in the pay-off phase of glycolysis, with the intermediates 1,3-bisphosphoglycerate, 3-phosphoglycerate, 2-phosphoglycerate and phosphoenolpyruvate occurring first; these steps were catalysed by glyceraldehyde 3-phosphate dehydrogenase, phosphoglycerate kinase, phosphoglyceromutase, enolase and pyruvate kinases respectively. The pentose phosphate pathway (PPP) occurs in parallel to glycolysis and uses the intermediates glucose-6-phosphate and fructose-6-phosphate for reactions such as FA synthesis, glutathione reduction, detoxification and nucleotide biosynthesis.

Glycolysis is a metabolic pathway that can proceed in both the presence and absence of oxygen typically producing pyruvate in aerobic conditions and lactate in anaerobic conditions. Pyruvate is metabolised further, and whilst lactate has been described as toxic to cells as it produces lactic acid , this view is changing [177]. For example, in the brain, neuronal activity signals induce lactate production in astrocytes for transfer to the neurons to meet their energetic needs, exhibiting metabolic coupling of cells and the requirement for lactate to be produced other than as a waste product [178]. The intermediates of the glycolytic pathway can be converted from other monosaccharides such as fructose and galactose. These intermediates can also be used in processes other than glycolysis, such as dihydroxyacetone phosphate (DHAP) which is a source of glycerol and forms fat by combining with FAs. Glycolysis occurs in two phases: a preparatory phase and a pay-off phase. In the first phase, which is composed of the first five steps, energy is expended to produce glyceraldehyde-3-phosphaste. The second phase has a net gain of ATP and NADH.

Glycolysis can occur aerobically, in a phenomenon known as the 'Warburg effect' [179]. Whilst being an inefficient way to produce ATP, most cancer cells depend on aerobic glycolysis in comparison to normal cells which primarily utilise mitochondrial oxidative phosphorylation, due to the greater amount of ATP produced in a shorter period. Otto Warburg observed that cancer cells metabolised glucose into lactate, even in the presence of oxygen [180].

Glycolysis is usually enhanced in activated leukocytes such as macrophages, DCs, NK cells, effector T cells and B cells [181-185]. In response to stimulation of antigen and cytokine receptors and PRRs, elevated glycolysis is considered a hallmark metabolic change in most immune cells. LPS induces hypoxia-inducible factor 1α (HIF1α) activation, a transcription factor vital for some glycolytic enzymes to be induced that can also activate TANK-binding kinase 1 (TBK1) or hexokinase 2 and the inhibitor of NF-κB kinase ε (IKKε), to initiate glycolysis in DCs [186, 187]. A key mechanism for the heightened glycolysis of LPS-activated macrophages is increased expression of pyruvate kinase isoenzyme M2 (PKM2) [188]. Pyruvate kinase catalyses the stage in glycolysis which converts phosphoenolpyruvate to pyruvate accompanied by the production of ATP. The PKM2 isoform of this enzyme is regulated to allow the diversion of the glycolytic intermediates to other biosynthetic pathways by slowing the glycolytic flux. PKM2 has been described as having a pro-inflammatory role in inflammatory macrophages

and monocytes. Hexokinase 1 has been illustrated in macrophages to act as a NOD-, LRR-, and pyrin domain-containing 3 (NLRP3) inflammasome regulator, which itself regulates caspase 1 [189]. Caspase 1 generates the mature forms of IL-1β and IL-18, and induces pyroptosis, a highly inflammatory type of programmed cell death. Hexokinase 1 enables the activation of NLRP3 by interacting with the inflammasome in the outer mitochondrial membrane [189].

The pentose phosphate pathway (PPP) occurs in parallel to glycolysis in the cytoplasm. Nicotinamide adenine dinucleotide phosphate ($NADP^+$) is reduced in the PPP to NADPH, and precursors for nucleotides are generated. NADPH can be used in the synthesis of fatty acids (FAs) and cholesterol. Reactive oxygen species (ROS) are generated by the catalysis of NADPH, produced from the PPP, by NADPH oxidase. The PPP also has a protective role in assisting in the prevention of oxidative stress by reducing glutathione via glutathione reductase which reduces hydrogen peroxide (H_2O_2) into water (H_2O). This prevents H_2O_2 from being converted into hydroxyl free radicals. ROS such as H_2O_2 are produced in a respiratory burst that accompanies phagocytosis in monocytes and other phagocytes.

1.3.2 The tricarboxylic acid cycle

The tricarboxylic acid (TCA) cycle is also known as the citric acid cycle (CAC) or the Krebs cycle. It is an aerobic mechanism which produces ATP and carbon dioxide (CO_2) from acetyl-CoA. Pyruvate from glycolysis (of which two molecules are made from every single molecule of glucose) is oxidatively decarboxylated to form acetyl-CoA. Pyruvate enters the mitochondrion from the cytosol via a transport protein called pyruvate translocase. It has been suggested that this protein is a voltage-dependent anion channel (VDAC) which translocates the pyruvate across the mitochondrial membrane with a proton gradient, which is a process that consumes energy. Once in the mitochondrial matrix, pyruvate is converted into acetyl-CoA by an enzyme complex dubbed the pyruvate dehydrogenase complex. The net products from one molecule of pyruvate, as well as NAD^+ and CoA molecules, is one molecule of acetyl-CoA, NADH, CO_2 and a H^+. Acetyl-CoA can also be produced from the metabolism of fats and proteins; this will be discussed in sections *1.3.6 Lipolysis and fatty acid oxidation* and *1.3.7 Amino acid metabolism*.

Glycolysis produces NADH molecules which contain electrons which can be transferred to the electron transport chain for energy generation. As mentioned, glycolysis occurs in the cytosol, whereas further metabolism occurs in the mitochondria. The inner membrane of the mitochondria is not permeable to NADH. The malate-aspartate shuttle (Figure 1.6) is the mechanism by which these electrons can cross the mitochondrial membrane to enter the mitochondrial matrix. Oxaloacetate is converted into malate via malate dehydrogenase with the electron from NADH which was formed during glycolysis. Malate can be transported into the mitochondria via the malate-α-ketoglutarate transporter where it is converted back into oxaloacetate with the release of an electron to form NADH again. Oxaloacetate is transformed into aspartate with the addition of an amino radical, for extraditing to the cytosol as oxaloacetate cannot be transported. The amino radical is supplied by glutamate, which is transferred into the mitochondria at the same time as aspartate translocases to the cytosol. Aspartate is converted back to oxaloacetate via aspartate aminotransferase, for another cycle of electron collection. With the loss of the amino radical, glutamate is converted into α-ketoglutarate, which flows in the opposite direction to malate in the malate-α-ketoglutarate transporter. Malate and oxaloacetate can be produced and supplemented into the TCA cycle.

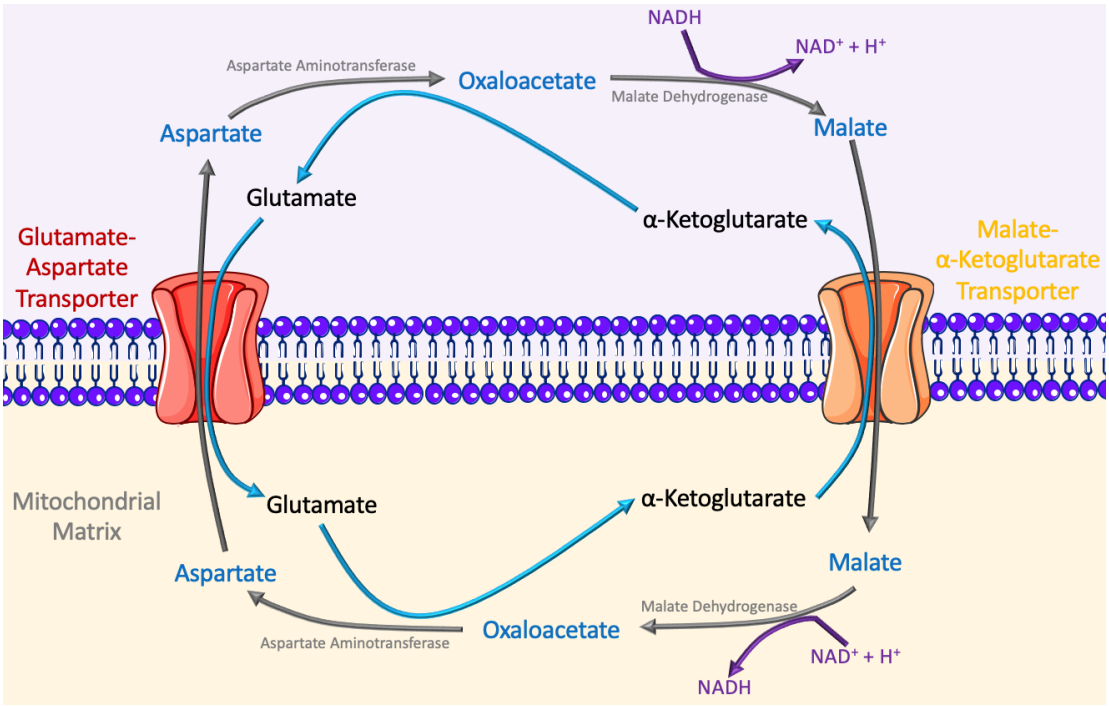

Figure 1.6: Malate-aspartate shuttle. NADH from glycolysis loses its electron to convert oxaloacetate into malate in the cytosol. Malate can then be transported into the mitochondrial matrix via a malate-α-ketoglutarate transporter, and at the same time α-ketoglutarate is transferred into the cytosol. Malate is then oxidised back to oxaloacetate and reduces NAD back into NADH. Oxaloacetate converts into aspartate for transport back out of the mitochondria via a glutamate-aspartate transporter, at which point glutamate is translocated into the mitochondrial matrix.

The TCA cycle essentially connects the metabolism of fats, proteins, and carbohydrates. The reactions of the TCA cycle can be visualised in Figure 1.7. Acetyl-CoA donates its two-carbon acetyl group to oxaloacetate (a four-carbon molecule) to produce citrate (a six-carbon molecule). This kickstarts the TCA cycle, and citrate undergoes a cycle of chemical transformations before forming oxaloacetate again and allowing the TCA cycle to undergo several turns. CO_2 is produced from the loss of two carboxyl groups during the cycle, and electrons are transferred to NAD^+ to form NADH in the oxidative stages of the TCA (D-isocitrate conversion to α-ketoglutarate to succinyl Co-A, and malate to oxaloacetate). $FADH_2$ is also reduced from FAD (flavin adenine dinucleotide), a cofactor of succinate dehydrogenase, in the oxidative step of converting succinate to fumarate. NADH and $FADH_2$ molecules are subsequently utilised in oxidative phosphorylation to produce 2.5 and 1.5 molecules of ATP respectively.

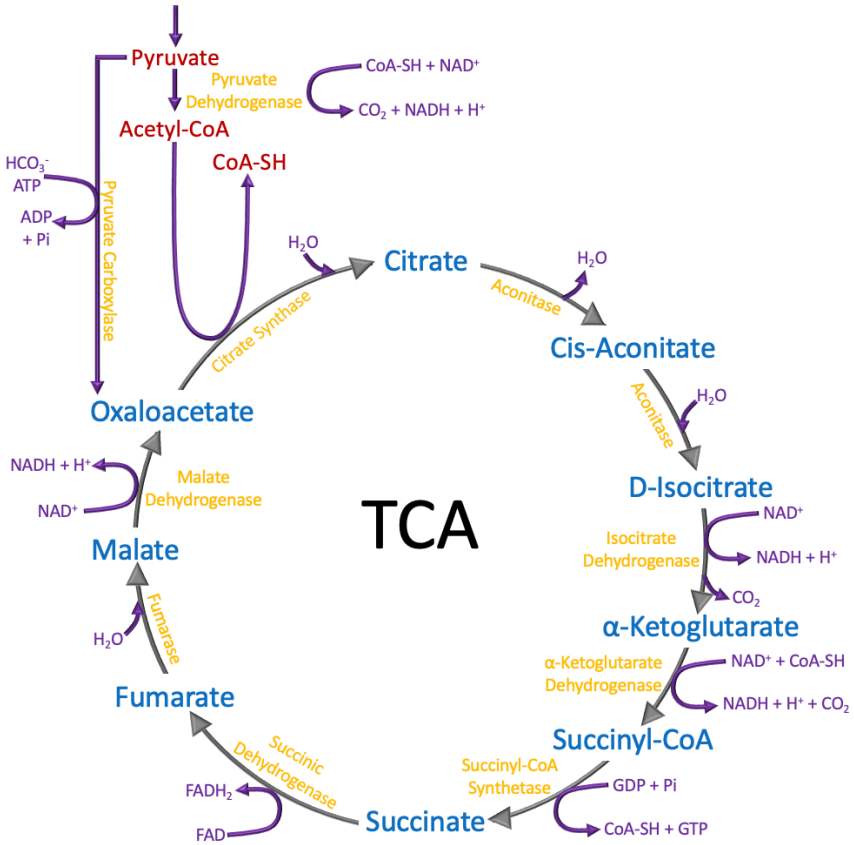

Figure 1.7: TCA Cycle. Pyruvate is first transported into the mitochondrial matrix from the cytosol, where it is converted into acetyl CoA by pyruvate dehydrogenase. Pyruvate can also enter the TCA by conversion into oxaloacetate by pyruvate carboxylase, but this expends energy. Acetyl-CoA enters the TCA cycle by transferring its two-carbon acetyl group to oxaloacetate, a four-carbon acceptor to form citrate, a six-carbon molecule. Citrate is then converted in turn to cis-aconitate, d-isocitrate, α-ketoglutarate, succinyl-CoA, succinate, fumarate, malate, oxaloacetate, which is then converted back into citrate. This process is catalysed by a number of enzymes and produces a net gain of two molecules CO_2 and three molecules NADH.

In macrophages, there are distinct differences in the TCA cycle between the two subsets. M2 macrophages, the TCA cycle is intact and is coupled to OXPHOS [186]. UDP-GlcNAc intermediates are produced which are vital for the glycosylation of M2-associated receptors. In M1 macrophages however, the TCA cycle is broken in two places: after succinate and after citrate [186]. The accumulated citrate is exported from the mitochondria via the citrate transporter to be utilised for the synthesis of FAs. These FAs are then used for membrane biogenesis. The excess citrate can also enter pathways which produce prostaglandins (effector molecules), itaconic acid (bactericidal) and nitric oxide (which can inactivate the electron transport chain (ETC) in macrophages) [190, 191]. The accumulation of succinate can lead to the stabilisation of HIF1α and maintained IL-1β production by inhibiting prolyl hydroxylases [186].

1.3.3 Oxidative phosphorylation

Electrons from glycolysis, pyruvate oxidation and the citric acid cycle, carried by electron carriers NADH and $FADH_2$, are fed into the ETC so that their reducing power is used to fuel ATP synthesis. The ETC is especially important for ATP synthesis during glucose metabolism as it produces 34 ATP molecules per glucose molecule created. It involves four enzyme complexes and is coupled with ATP synthase (also termed Complex V) for oxidative phosphorylation as seen in Figure 1.8.

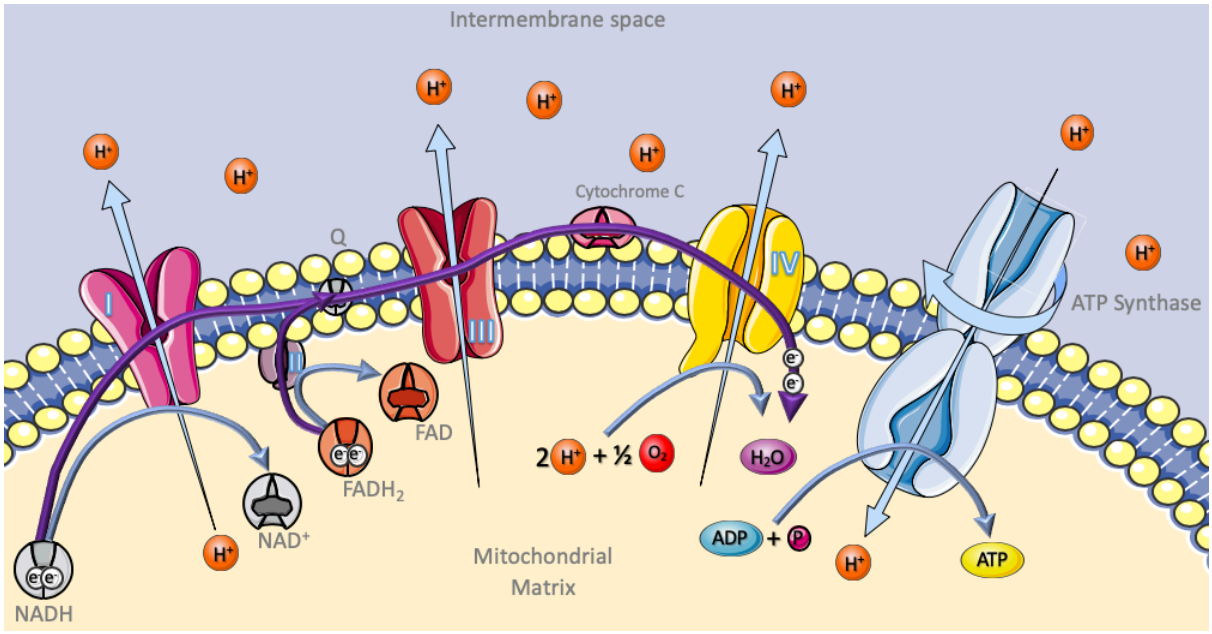

Figure 1.8: Oxidative Phosphorylation. The flow of electrons through the electron transport chain (complexes I-IV) generating a proton gradient due to the accumulation of protons in the intermembrane space. Complex I – NADH Q Reductase; Complex II – Succinate Dehydrogenase; Complex III – Cytochrome C Reductase; Complex IV – Cytochrome C Oxidase. This is used to power ATP synthase with an electrochemical gradient; as it rotates, it catalyses the generation of ATP in a process called chemiosmosis.

NADH and $FADH_2$ are molecules which are energy rich as they contain a pair of electrons which have a high transfer potential. In the ETC, they are used to liberate a vast amount of free energy by reducing molecular oxygen to water. This free energy can then be utilised to generate ATP. The flow of electrons through the protein complexes results in the pumping of protons out of the mitochondrial matrix. This leads to the generation of a pH gradient and a transmembrane electrical potential due to the imbalanced dispersal of protons and generates a proton-motive force. ATP synthase, an enzyme complex at the end of the ETC, allows the protons to flow back into the mitochondrial matrix, which allows for the synthesis of ATP. The complexes I, III and IV (NADH-Q oxidoreductase, Q-cytochrome *c* oxidoreductase, and cytochrome *c* oxidase) convert electron-motive force into proton-motive force.

Complex I is the first protein in the ETC and starts the reaction by binding to an NADH molecule, which donates two electrons via the flavin mononucleotide (FMN), which reduces it to $FMNH_2$. Iron-sulphur clusters allow for the transfer of electrons through the complex, and four protons are pumped into the membrane space. The electrons are then transferred to a ubiquinone (Q) molecule which reduces it to ubiquinol (QH_2), and this also contributes to the proton gradient. The electrons can enter complex II (succinate-Q oxidoreductase). Complex II is an enzyme that is also part of the TCA cycle and consists of iron-sulphur clusters, a bound FAD cofactor, and a heme group. It has been suggested that the heme group may be vital in regulating the production of ROS as it does not participate in the transfer of electrons [192]. Complex II oxidises succinate to fumarate which transfers electrons to FAD to form $FADH_2$. The electrons are then transferred to Q to reduce it to QH_2. Complex II does not contribute to the proton gradient. An enzyme called electron transfer flavoprotein-ubiquinone oxidoreductase (ETF-Q oxidoreductase) is a third entry point for electrons into the ETC. It accepts electrons from flavoproteins to reduce ubiquinone and accepts electrons from several acetyl CoA dehydrogenases during FA β oxidation, and amino acid and choline catabolism. Electrons pass through complex III which has an iron-sulphur cluster, and three cytochromes: one c_1 and two b cytochromes. A cytochrome has a minimum of one heme group and transfers electrons. Within complex III's heme group, when electrons are transferred through the complex, the iron atoms alternate between an oxidised and a reduced ferrous state. QH_2 is oxidised in complex III along with two molecules of cytochrome *c* – which carries only one electron - being reduced. The Q cycle occurs here and can be seen

in Figure 1.9. Complex IV facilitates the final reaction of the ETC and is responsible for the transfer of electrons to oxygen to produce water whilst pumping protons out of the mitochondrial matrix. It has two heme groups and various metal ion cofactors including atoms of magnesium, zinc and copper. Oxygen is dictated as the terminal electron acceptor.

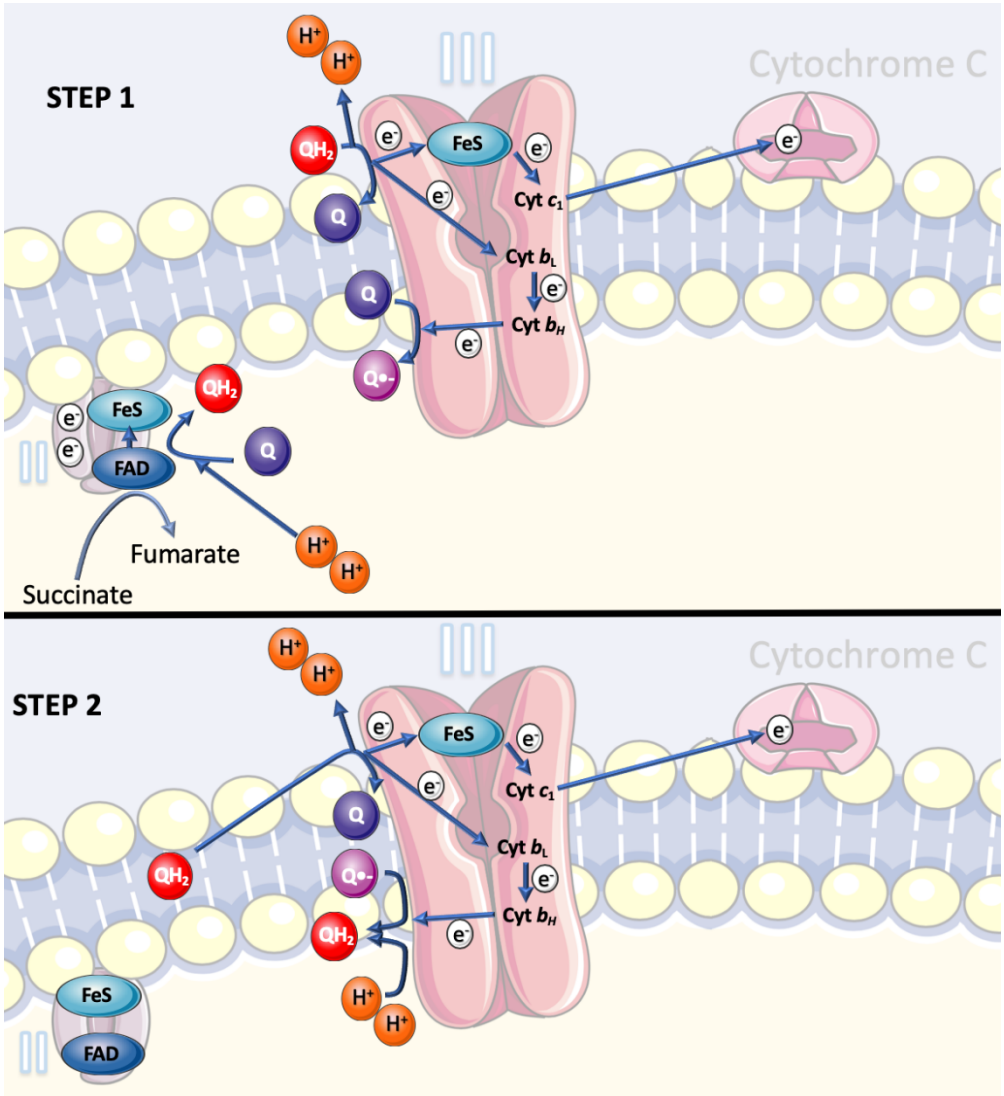

Figure 1.9: Q cycle. Step 1: succinate is oxidised to fumarate, and stimulates the path of two electrons to involve FAD and iron-sulphur centres (FeS). FAD is reduced to $FADH_2$, which reduces Q to QH_2 with the addition of two protons in the matrix. QH_2 binds to the outer-Q binding site on complex III, loses its two protons to the intermembrane space, and is oxidised to Q. It transfers one of the electrons via the Rieske FeS to cytochrome c_1 (Cyt c_1) which is then transferred to cytochrome c. The other electron is transferred via two b-type cytochromes (Cyt b_L, low potential, and Cyt b_H, high potential) to an inner Q-binding site where it is donated to a Q to be converted to a semiquinone, a free radical. Step 2: Most of the reactions in step 2 are the same as step 1. Instead of an electron transferring to a Q molecule at the inner Q-binding site, the electrons is transferred to a semiquinone to produce ubiquinol with the addition of two protons. With each Q cycle, four protons are exported out of the mitochondria.

ATP synthase, otherwise known at complex V, is the terminal enzyme of the oxidative phosphorylation pathway. The proton gradient produced by the complexes of the ETC drives the synthesis of ATP from ADP and P_i. The enzyme complex is characterised in two portions;

the top portion is called F_O and the bottom portion is F_1. F_O is embedded within the membrane and consists of a proton channel and a ring of c subunits, whereas F_1 is the site of ATP synthesis. F_1 itself is composed of a ball-shaped complex with three α subunits and three β subunits, and a "stalk" section which has a γ subunit. The α and β subunits both bind nucleotides, but the ATP synthesis reaction is catalysed only by the β subunit. The F_O proton driven motor rotates when protons cross the membrane in the base of the enzyme. It has been suggested that the rotation may be caused by electrostatic interactions because of amino acid ionisation in the ring of c subunits. This rotation in turn drives the rotation of the γ subunit within the α and β subunits, which themselves remain static. Energy for the active sites is provided by this rotation, allowing the β subunit to undergo the binding change mechanism. The β subunit has three states: an 'open' state where ADP and phosphate enter the active site; a 'loose site' where the protein binds around the molecules loosely; a 'tight' shape where the protein constrains the substrates together to produce ATP. The β subunit cycles back to 'open' state to release the ATP and take in more ADP and phosphate.

Some electrons can leak into a molecule of oxygen to form a reactive oxygen species, superoxide, which is involved in oxidative stress [193]. Heightened oxidative stress has been exhibited in aging and disease [194]. The biggest producer of ROS in the ETC is Complex I, with Complex III also contributing. One of Complex I's inhibitors is rotenone; when present, it inhibits electron transfer to Coenzyme Q [195]. This creates a backlog of electrons, allowing some to leak into oxygen molecules to form ROS. Physiologically, ROS are usually dealt with by superoxide dismutase and catalase enzymes. Superoxide dismutase forms hydrogen peroxide from superoxide, and catalase then breaks this down into oxygen and water. Oxidative stress is caused when there is an imbalance between this biological system to deal with the species and the production of the ROS. ROS can cause damage to mitochondrial proteins, lipids and DNA [193].

1.3.4 Fatty acid metabolism

Fatty acids (FA) are key components of the phospholipids in the phospholipid bilayers of cell membranes, as well as serving as intracellular signalling and local hormones. FAs produce the most ATP on an energy per gram basis when compared to carbohydrates and proteins. This

is when they are fully oxidised to CO_2 and H_2O by the TCA cycle and β-oxidation. β-oxidation of a single palmitate molecule, which is a major FA, has the potential to yield over 100 ATP molecules. FAs are typically stored as triglycerides in adipose tissue. FAs are released from adipose tissue by decreasing glucose levels which heightens glucagon and epinephrine levels in the blood. These hormones activate lipases which induce lipolysis of the FAs and frees them to the circulation. Globular proteins termed plasma albumins transport the free FAs through the bloodstream. Solute carrier proteins such as SLC27 transport long-chain FAs into cells to be metabolised. CD36, also known as FA translocase (FAT), is an integral membrane protein that is known to import FAs and has been implicated in lipid metabolism among other roles [196]. Inside the cell, a fatty acyl-adenylate is formed from the catalysed reaction between the FA and ATP. The fatty acyl-adenylate then reacts with a free coenzyme A to produce fatty acyl-CoA. This enters the mitochondrion via carnitine which shuttles it into the mitochondria via carnitine palmitoyltransferase I (CPT1), which can be inhibited by etomoxir [197]. Medium and long-chain FAs are transferred via CPT-1, whereas short-chain FAs (those with fewer than six carbons in the aliphatic tail) can passively diffuse into the mitochondria. β-oxidation then occurs in the mitochondrial matrix. This involves splicing the acyl-CoA molecules into acetate units which combines with co-enzyme A and can be seen in Figure 1.10. This then condenses with oxaloacetate and enters the TCA cycle.

Lipids can be generated from precursors produced from other metabolic pathways such as citrate from the TCA cycle, glycerol from glycolysis and reducing equivalents of NADPH from the pentose phosphate pathway. FA synthesis is necessary for cellular growth and proliferation. This pathway is closely coupled to mTOR signalling. mTOR signalling promotes this pathway via regulation of key enzymes required for *de novo* synthesis of lipids including FA synthase (FASN), sterol regulatory element binding protein (SREBP) and acetyl CoA carboxylase (ACC). Branched chain amino acids, like valine and leucine, are used as substrates for elongation to yield branched chain FAs. Straight chain FAs can be generated from citrate which is shunted into the cytosol from the mitochondria via citrate carrier. In the cytosol, it is converted into acetyl-CoA and oxaloacetate by ATP citrate lyase. The acetyl-CoA can then be carboxylated to synthesise malonyl-CoA by ACC. Palmitic acid can be produced by elongating the nascent FA chain by FASN in an NADPH-dependent manner. Palmitic acid can be elongated or desaturated to produce alternative chain lengths or unsaturated FAs

respectively. Combinations of phospholipids and triacylglycerides can be generated from the condensation of FAs with glycerol.

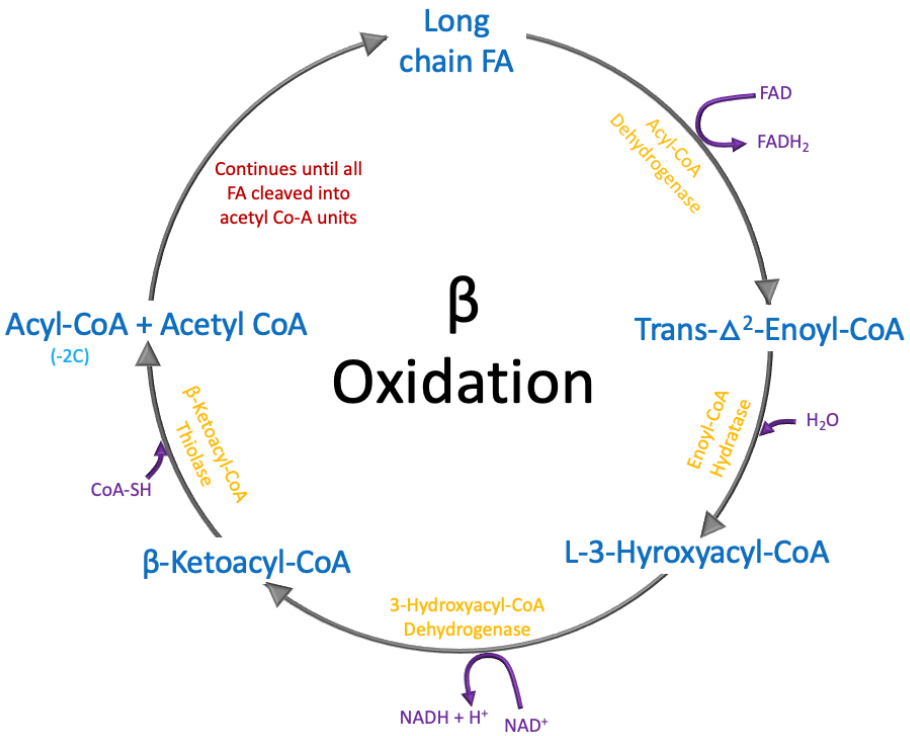

Figure 1.10: β Oxidation. The long chain FA is dehydrogenated by FAD and Acyl-CoA-Dehydrogenase to form a double bond between C-2 and C-3. The bond between the C-2 and C-3 is then hydrated in a stereospecific reaction. The hydroxyl group is then oxidised by NAD+ into a keto group. The β-ketoacyl CoA is cleaved between the C-2 and C-3 in the final step by a thiol group from Coenzyme A. The acyl-CoA molecule is two carbons shorter than when it started. The cycle continues until the chain is cleaved into acetyl Co-A molecules, with the final sequence producing two molecules of acetyl CoA and no acyl CoA.

FAO reliance in immune cells is observed in those not considered pro-inflammatory in nature to increase their cellular life span. These cells include M2 macrophages, memory T cells and T_{reg} cells [175, 184, 198]. Increasing the expression of active CPT1A in macrophage cell-lines, reduces lipid accumulation and increases FAO accompanied by reduction of inflammatory cytokine production. Therefore, the inflammatory potential of inflammatory macrophages can be reduced by the promotion of FAO [198].

Unsurprisingly, FA synthesis promotes the synthesis and function of pro-inflammatory cells, in contrast to the anti-inflammatory function of FAO. An increase in FA synthesis is observed when macrophages are exposed to inflammatory stimuli such as cytokines and LPS [199]. TLR induced activation leads to the accumulation of triacylglycerides in macrophages, along with elevated uptake of free FAs, associated with uptake by fatty acid translocase (CD36) [199]. Upon the differentiation of monocytes into macrophages after treatment with macrophage colony

stimulating factor (M-CSF), sterol regulatory element-binding protein 1 (SREBP1c) was found to be upregulated. This induced elevated expression of FASN and other FA synthesis related target genes, thus increasing FA biosynthesis [200].

1.3.5 Amino acid metabolism

Amino acids enter the body via dietary proteins. Amino acids tend to fall into one of three categories: ketogenic, glucogenic, or both. Those which fall under the glucogenic category produce pyruvate or TCA intermediates such as oxaloacetate or α-ketoglutarate. These are precursors in gluconeogenesis. Apart from lysine and leucine which are only ketogenic, other amino acids are at minimum partly glucogenic. Leucine and lysine cannot contribute to glucose production, as they give rise only to acetoacetyl-CoA or acetyl-CoA. Amino acids which can be characterised as both glucogenic and ketogenic are those which can produce precursors for glucose and FAs; these are isoleucine, phenylalanine, threonine, tryptophan, and tyrosine. In the event of starvation, the carbon skeleton of amino acids can be oxidised to CO_2 and H_2O for energy. Amino acids and their properties can be visualised in Table 1.1 [201].

Amino Acids	3-letter	1-letter	Essential	Glucogenic	Ketogenic	Polar	Aromaticity	Charge	Size
Alanine	Ala	A	✓	✓	-	-	Aliphatic	-	Medium
Arginine	Arg	R	-	✓	-	✓	Basic	+ve	Small
Asparagine	Asn	N	✓	✓	-	✓	Amidic	-	Large
Aspartate	Asp	D	✓	✓	-	✓	Acidic	-ve	Large
Cysteine	Cys	C	✓	✓	-	✓	+Sulphur	-	Small
Glutamate	Glu	E	✓	✓	-	✓	Acidic	-ve	Small
Glutamine	Gln	Q	✓	✓	-	✓	Amidic	-	Small
Glycine	Gly	G	✓	✓	-	-	Aliphatic	-	Medium
Histidine	His	H	-	✓	-	✓	Basic	+ve	Small
Isoleucine	Ile	I	-	✓	✓	-	Aliphatic	-	Small
Leucine	Leu	L	-	-	✓	-	Aliphatic	-	Small
Lysine	Lys	K	-	-	✓	✓	Basic	+ve	Small
Methionine	Met	M	-	✓	-	✓	+Sulphur	-	Small
Phenylalanine	Phe	F	-	✓	✓	NA	Aromatic	-	Small
Proline	Pro	P	✓	✓	-	-	Aliphatic	-	Medium
Serine	Ser	S	✓	✓	-	✓	Hydroxylic	-	Medium
Threonine	Thr	T	-	✓	✓	✓	Hydroxylic	-	Large
Tryptophan	Trp	W	-	✓	✓	NA	Aromatic	-	Small
Tyrosine	Tyr	Y	✓	✓	✓	NA	Aromatic	-	Small
Valine	Val	V	-	✓	-	-	Aliphatic	-	Small

Table 1.1: Properties of amino acids. Essential amino acids are those which the body cannot synthesise, and so must be derived via the diet. Charge is either positive (+ve), negative (-ve) or neutral.

Amino acids are transported into cells via specific transport systems which are part of the SLC family. There are dibasic transporters, neutral transporters, and acidic transporters. CD98, is a large neutral amino acid transporter (LAT1) which is a glycoprotein composed of SLC3A2

and SLC7A5 [202]. Aromatic and branched chain amino acids are preferentially transported by CD98. Glutamine, tryptophan, and arginine are the most extensively studied amino acids.

Glutamine is the most abundant free amino acid. It has various roles including protein synthesis, lipid synthesis, cellular energy, nitrogen, and carbon donation, and is a precursor to glutamate, a neurotransmitter. Macrophages in particular utilise glutamine at high rates to promote either a M1 or M2 phenotype depending on the route of consumption [203]. Glutamine can act as a precursor for the synthesis of arginine, and generates nitric oxide, illustrating its role in antimicrobial and cytotoxic macrophage functions [204]. Nitric oxide is produced by the conversion of arginine mediated by inducible nitric oxide synthase (iNOS). Murine iNOS deficiency induces defective killing of bacteria by macrophages [205]. Macrophages can also utilise arginine for a more tolerant response via the arginase pathway, which leads to the biosynthesis of l-ornithine and urea. Macrophages expressing arginase-1 restrict the inflammatory potential of effector T cells [206]. The primary role of arginase-1 in macrophages is to restrict excessive nitric oxide production, to prevent inflammatory tissue damage [207], whereas it has been shown that an isoform of arginase – arginase-2 – is up-regulated by LPS-activation of macrophages to induce the production of pro-inflammatory cytokines and ox-LDL [208].

The immunological role of tryptophan metabolism has become an area of interest due to its contribution to immune evasion by cancer cells. Levels of indoleamine-2,3-dioxygenase (IDO) have been observed to be elevated in poor prognosis of some forms of cancer [209]. IDO is a rate-limiting enzyme in tryptophan catabolism. Both LPS and IFNγ stimulation induces IDO expression, increasing tryptophan catabolism [210, 211]. By denying bacterial and parasitic pathogens necessary substrates, tryptophan metabolism in host cells can prevent their anabolic growth [212]. Kynurenine, a product of tryptophan catabolism, has also been suggested to have an important role in immune cell function. Studies have suggested it modulates via acryl hydrocarbon receptor (AHR), a ligand-activate transcription factor, activation [213]. During the second and third trimesters of pregnancy, maternal plasma levels of tryptophan are found to decrease as gestation progresses; however, kynurenine levels remain stable throughout pregnancy resulting in an increase in the kynurenine to tryptophan ratio [214, 215]. As tryptophan starvation has been found to induce a Treg phenotype, this observation of tryptophan in

pregnancy could further promote the Treg cells [216]. Altered IDO expression and activity has been illustrated to be vital for a successful pregnancy as it contributes to immune tolerance, with dysfunction resulting in pathological pregnancies such as preeclampsia and miscarriage [217, 218].

1.3.6 Gluconeogenesis

Gluconeogenesis is the process by which glucose is generated from non-carbohydrate carbon substrates. It is an important mechanism in maintaining blood glucose levels to avoid hypoglycaemia during periods like intense exercise and fasting. The catabolism of proteins and lipids produces the substrates for gluconeogenesis, such as glucogenic amino acids and triglycerides. The primary precursors are glycerol, alanine, glutamine, and lactate. Lactate, which is produced in exercising muscles as they perform anaerobic glycolysis, can be converted back into pyruvate via the Cori cycle, which in turn produces glucose. Pyruvate can also be derived from succinyl-CoA, which in turn can be yielded from the product of odd-chain FAO, propionyl-CoA. Gluconeogenesis is localised to the kidneys, intestine, liver, muscles and placenta [219].

1.3.7 Mitochondrial health

The mitochondrion is an important organelle required for generation of energy in cells. Mitochondria have their own DNA which contains various genes such as those for proteins of the respiratory chain. A mitochondrion has a double membrane, comprising of phospholipid bilayers (including the lipid cardiolipin) and proteins; it has an inner and an outer membrane, with an intermembrane space. The inner membrane forms infoldings called cristae, and the matrix exists within the inner membrane. The inner membrane hosts the enzymes required for oxidative phosphorylation, which induces a membrane potential, as well as specific metabolic transport proteins. The outer membrane contains porins, whereas the inner membrane is impermeable. Mitochondria undergo multiple fusion and fission events (mitochondrial dynamics) (Figure 1.11); they are constantly fusing and dividing [220]. This is vital for the maintenance of functions in the mitochondria, and mitochondrial inheritance.

In eukaryotes, the mitochondrion is responsible for various respiratory processes such as oxidative phosphorylation, β-oxidation of fatty acids, the TCA cycle, and the biosynthesis of certain phospholipids, haem, and other metabolites. Mitochondria also participate in ageing, developmental processes, and are key regulators of apoptosis. The morphology of mitochondria adapts in cells when activated; fusion of the mitochondria is increased to produce large mitochondrial networks, in order to contribute towards energy dissipation [221]. Mitochondria are heterogenous in their function and morphology. Quiescent mitochondria are functionally and morphologically distinct as short rods or small spheres. The dispersion of mitochondria appears to be determined by activation; highly energised mitochondria are found to aggregate more in the periphery of cells [221]. These peripheral mitochondria have a higher membrane potential ($\Delta\Psi_{mit}$) than those found in perinuclear regions, suggesting they are functionally different.

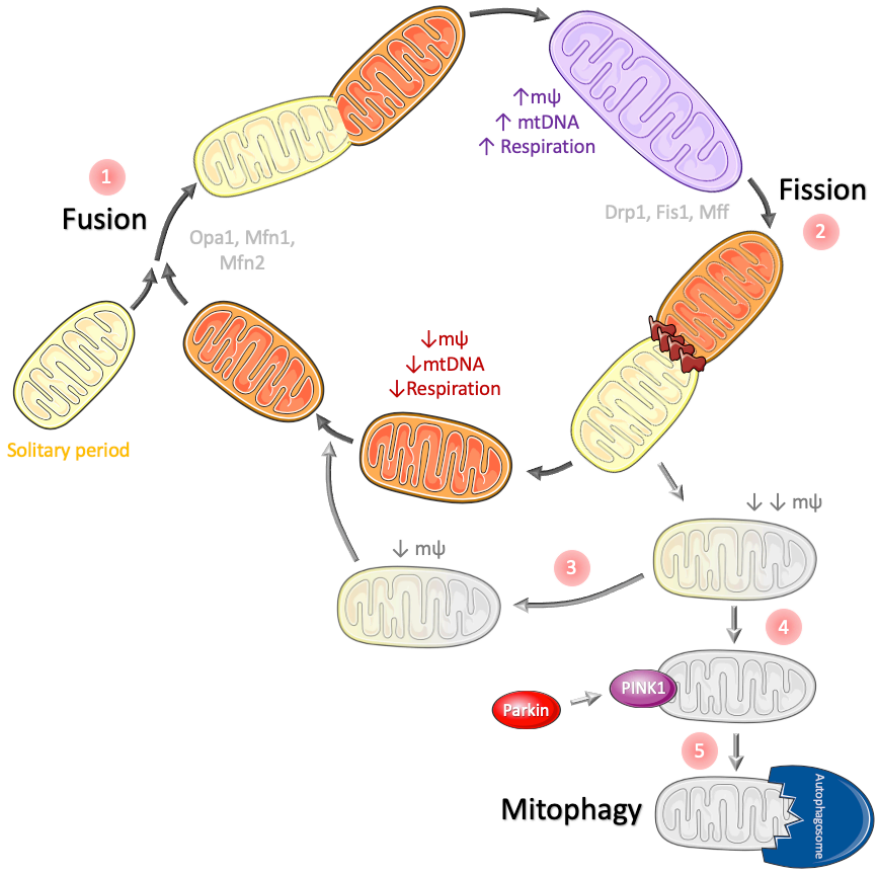

Figure 1.11: Mitochondrial biogenesis; fusion and fission events. (1) Two mitochondria fuse together to form elongated, tubular interconnected networks of mitochondria under the regulation of enzymes optic atrophy (Opa1), mitofusin 1 and 2 (Mfn1 and Mfn2). This tubular mitochondrion has a high membrane potential (mψ), high quantity of mitochondrial DNA (mtDNA) and high respiration. (2) Fission occurs to form small, rounded mitochondria from the tubular mitochondrion via dynamin-relation protein 1 (Drp1), fission protein 1 (Fis1) and mitochondrial fission factor (Mff). The daughter units produced have lower mψ than the tubular mitochondria, as well as lowered respiration and mtDNA, and the two units typically have different mψ with some being depolarised. (3) Polarisation can be restored by fusing with other mitochondria. (4) If the depolarisation is sustained, Opa1 is cleaved, reducing the capacity of Mfn. Parkin and PINK1 is recruited to the mitochondria. (5) PINK1 targets the dysfunctional mitochondrion to undergo mitophagy, where it is destroyed by an autophagosome.

Selective autophagy of the mitochondria is termed mitophagy. It is a regulatory feature of the cell, removing damaged or stressed mitochondria, and it also allows the adjustment of mitochondrial numbers to meet altered metabolic needs of the cell. In mammals, mitophagy is mediated by NIP3-like protein X (NIX) and regulated by phosphatase and tensin homolog (PTEN)-induced kinase 1 (PINK1) and Parkin. As by-products of mitochondrial metabolism, including ROS, can lead to cytotoxicity and DNA damage, mitophagy is a critical process. Defective mitophagy, especially dysfunctional Parkin, has been implicated in various diseases such as Parkinson's and metabolic disorders [222].

There are few studies which have investigated the effect on mitochondria during pregnancy, with the focus primarily on adverse pregnancy events rather than characteristics associated with a healthy pregnancy. Due to the high energy demands of pregnancy, mitochondrial function must be vital for a successful outcome. Women with mitochondrial disease or dysfunction have exhibited aggravation of constitutional and neurological symptoms with pregnancy and are also associated with adverse obstetric outcomes such as GDM, pre-eclampsia, miscarriage, and fetal congenital anomalies [223, 224]. In skeletal muscle, the mitochondria have been observed to be disrupted in pregnancies complicated with obesity and GDM, with impaired mitochondrial respiratory chain enzyme activity [225]. Interestingly, a high prevalence of anticardiolipin autoantibodies, a characteristic of antiphospholipid syndrome, have been observed in women who suffer from recurrent miscarriages [226].

1.4 Rationale

Many adverse pregnancy outcomes such as GDM are difficult and intrusive to diagnose. As the lipidomic environment changes throughout pregnancy, and some markers are indicative of inflammation, novel mass spectrometry techniques could be used as new diagnostic tools, as well as offer further insight into the lipidomic profile of pregnancy. The immunological changes in pregnancy are still poorly described, particularly concerning the maternal systemic changes. Additionally, the field of immunometabolism is still in its early stages and as of yet, not been considered in regard to a healthy pregnancy. Given the vast changes of metabolism in pregnancy that we are aware of, immune cells must adapt metabolically which will have an impact on their function. While investigation into the adaptive response in pregnancy is vital, the innate response is underappreciated, especially considering the changes in inflammation.

As such, monocytes are the primary focus for much of this thesis. This will include examination of their metabolic state (including mitochondrial content and activity) and their consequential functional adaptations. While a study of the monocytes at term will allow for full appreciation of how they are affected by a long-term accumulation of maternal changes, it is also necessary to determine when in pregnancy these changes occur, and if they are deterred by other conditions such as obesity. The introduction of novel SARS-CoV-2 into the population requires urgent consideration of the mechanisms of pregnancy which may offer protection to the mother and fetus.

1.5 Hypothesis

The lipidomic profile in pregnancy changes and contributes as a driving factor for metabolic adaptation of monocytes which underpins functional changes observed in pregnancy, which are compromised by obesity. The maternal environment is rich in factors which offer specific protection for the fetus against SARS-CoV-2.

1.6 Aims and Objectives

1. To investigate the lipid profile of maternal serum and plasma using novel mass spectrometry techniques.
2. To characterise the immunometabolic adaptations of monocytes during pregnancy at term.
3. To investigate if changes observed at term also occur earlier in gestation at 28 weeks.
4. To explore the effect of obesity on leukocyte populations and their bioenergetics during pregnancy.
5. To unravel the potential protective maternal effects during pregnancy and lactation against novel coronavirus SARS-CoV-2.

Chapter 2 – Materials and Methods

2.1 Human blood collection

Blood was donated by healthy female volunteers between the ages of 18 and 40 years for non-pregnant controls at Swansea University Medical School's Clinical Research Facility. A research passport was obtained for personal access to recruitment of participants from antenatal clinic to enable collection of peripheral blood from women at 28 weeks of gestation from the glucose tolerance testing (GTT) clinic and full-term (37+ weeks of gestation) pregnant women at their scheduled pre-caesarean section assessment at Singleton Hospital, Swansea. A maximum of 120 ml of blood could be obtained from non-pregnant women and a maximum of 35 ml from pregnant women. Bloods for cell analysis were collected in 9 ml BD Vacutainer® heparin blood collection tubes (Greiner Bio-one, Frickenhausen, Germany) to prevent coagulation. Bloods were also collected into 4 ml EDTA BD Vacutainer® and 5 ml serum BD Vacutainer® blood collection tubes for plasma and serum analysis respectively. Blood donation was always voluntary, all donors had the right to refuse at any point, and any personal information was confidential. Volunteers were informed how much blood would be taken and what their blood would be used for. Ethical approval for all groups was provided by a Health Research Authority (HRA) Research Ethics Committee (13/WA/0190 – healthy volunteers; 11/WA/0040 – full term pregnant women; 19/LO/0722 – GTT clinic). Informed written consent was obtained from all donors.

2.2 Mononuclear cell isolation

Blood was diluted 1:4 in phosphate buffered saline (PBS; Life Technologies) before 35 ml was layered onto 15 ml LymphoPrep™ (Stem Cell Technologies, UK; density 1.077 g/ml). The blood was then centrifuged at 400 *x g* for 40 mins at room temperature with no brake and no acceleration to allow density separation (layers illustrated in Figure 2.1). The diluted plasma layer was removed and discarded. The mononuclear cell (MNC) layer was extracted and washed with RPMI 1640/Glutmax (Gibco) at 515 *x g* for 10 mins at room temperature. Where MNCs were in more than one tube, they were combined into a single tube before being washed again with RPMI 1640/Glutamax at 515 *x g* for 7 mins at 4°C. MNCs were then resuspended in 1 ml RPMI 1640/Glutamax and an aliquot diluted dependent on starting volume of blood in preparation for cell counting.

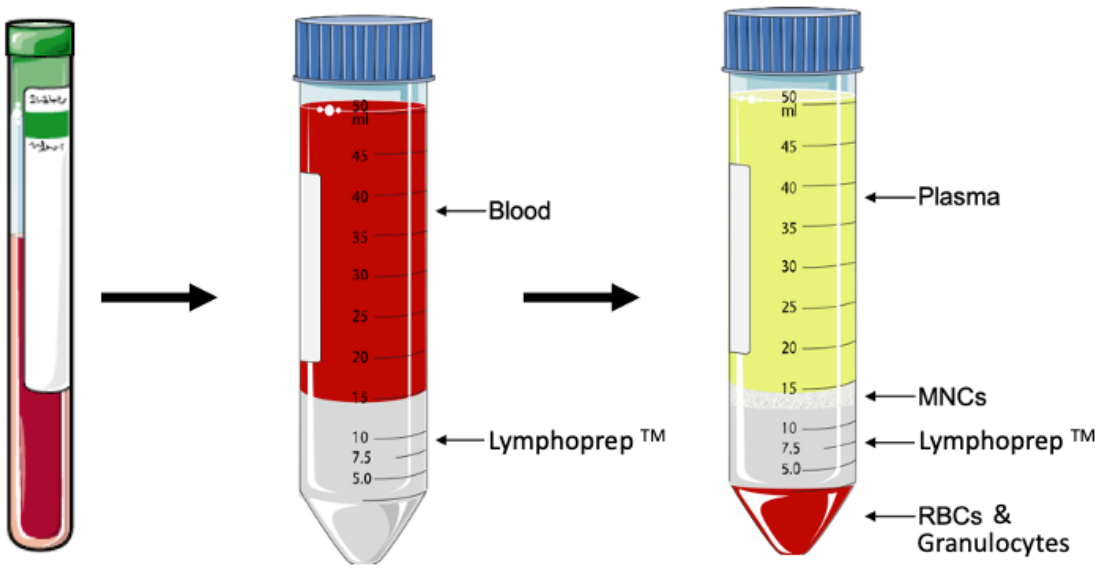

Figure 2.1: Density gradient centrifugation. Blood collected in heparin tubes was diluted 1:4 with PBS, before 35 ml was layered onto 15 ml Lymphoprep ™. After density gradient centrifugation, four layers were produced: diluted plasma, MNCs, Lymphoprep ™, and red blood cells (RBCs) and granulocytes.

2.3 Cell counting

10 µl of a diluted aliquot of cells was mixed 1:1 with the cell viability stain Trypan Blue (0.4%; NanoEntek, Cambridge Bioscience, UK) for cell counting using EVE ™ cell counting slides (NanoEntek, Cambridge Bioscience, UK) in the Countess® automated cell counter (Life Technologies). The total number of cells present in 1 ml was then calculated according to the dilution factor used.

2.4 Monocyte Isolation

Once the MNCs were counted, they were centrifuged at 300 *x g* for 10 mins. For positive selection of cells, microbeads coated with anti-CD14 antibodies were used (Figure 2.2). Cells and microbeads were incubated as described by the manufacturer and washed by centrifugation with magnetically activated cell sorting (MACS) buffer (PBS with 2% HyClone fetal bovine serum; FBS; Cytiva, Austria) at 300 *x g* for 10 mins. The cells were resuspended in 500 µl MACS buffer before being transferred to the autoMACS Pro Separator (Figure 2.3). Here, the MNCs were passed onto a column containing a proprietary material which is placed in a strong magnetic field. Cells which do not have the microbeads bound to them pass through the column, whilst the cells which do have the beads attached stay on the column. Once the magnetic field is no longer applied to the column, cells with microbeads attached to them can be washed out of the column into a new tube. This is known as positive selection.

In contrast, for negative selection the cells of interest are not labelled with microbeads and so pass through the column. For monocyte selection, cells are run through the separator twice for optimal purity.

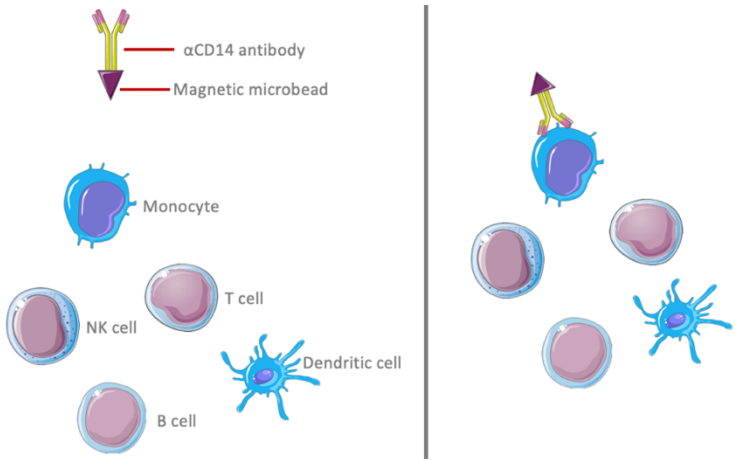

Figure 2.2: Positive selection. The labelled magnetic microbead (anti (α) – CD14) selectively attaches to only the monocytes in the MNC preparation.

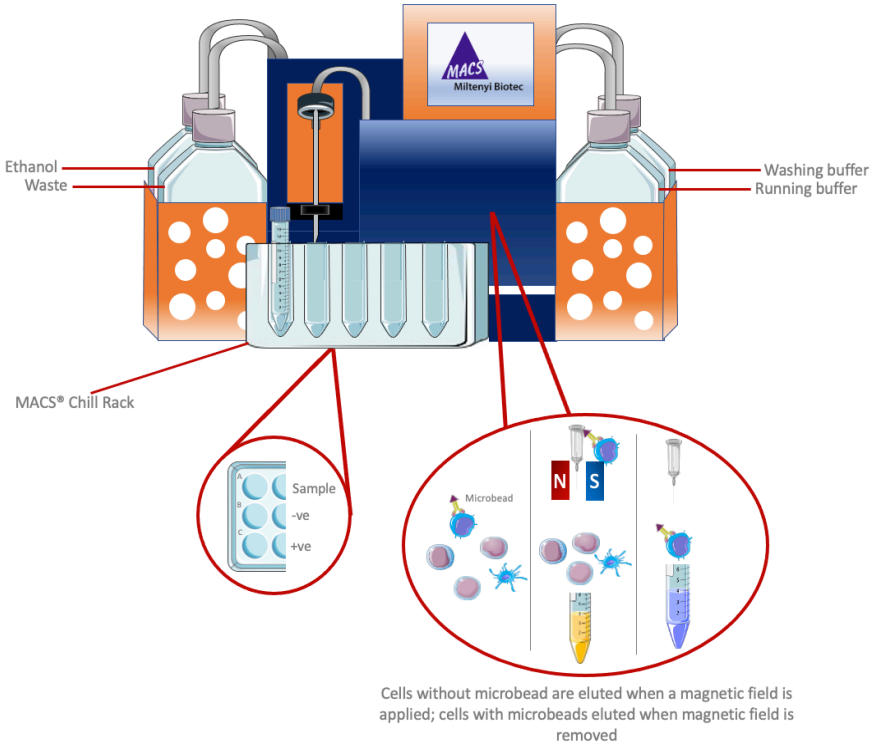

Figure 2.3: Schematic of the autoMACS Pro separator. Cells with and without the antigen-specific magnetic microbeads attached to them are run through the column. When a magnetic field is applied, the cells attached to microbeads stick to the column, allowing the other cells to be collected in a negative fraction tube. Once all the cells have been eluted, the magnetic field is removed, allowing the cells attached to the microbeads to be collected in a positive fraction tube.

Once the monocytes were isolated, they were centrifuged at 300 *x g* for 10 mins, the media discarded, and the cell pellet resuspended in 500 µl of preferred media (dependent on subsequent experiments). An aliquot was diluted and mixed 1:1 with Trypan Blue and

counted as before. The live cell count and viability was noted and adjusted according to the dilution used.

2.5 Flow cytometry

Flow cytometry is commonly used in clinical and research practices, particularly in disorder diagnosis, as it is useful for counting and sorting cells, detecting biomarkers and protein engineering. It does this by exposing cells in a suspension to a laser source; detectors then measure forward scatter, side scatter and fluorescence. Fluorescently labelled antibodies are commonly used to identify cell populations of interest, as they can be chosen for their antigen-specific properties and label cells that then can be separated on plots which measure the fluorescence intensity. A diagram of the flow cytometer used, with an illustration of the scattering of light by the cells is shown in Figure 2.4.

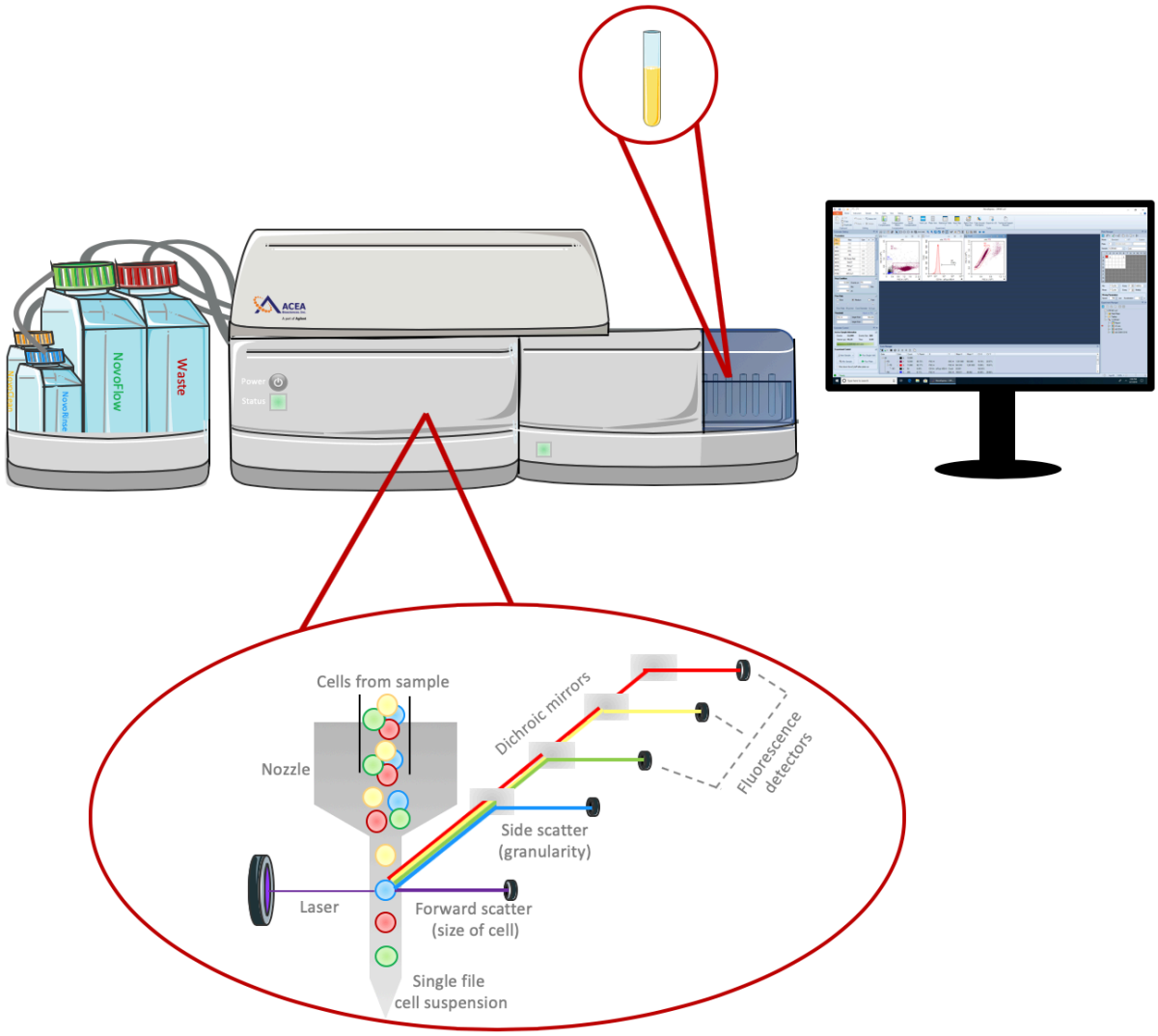

Figure 2.4: The Acea NovoCyte flow cytometer. The schematic shows the cells running through a nozzle into a single file suspension, being subjected to a laser, and the light scattering based on size, granularity and fluorescence then detected via a series of detectors.

MNCs or monocytes isolated as in *2.3 Monocyte isolation* were used for flow cytometry. The volume containing the number of cells required is topped up to 100 µl with fluorescence-activated cell sorting (FACS) buffer (PBS with 0.2% bovine serum albumin – BSA; Sigma, USA –and 0.05% sodium azide – Sigma, China). Cells were stained using fluorescently stained antibodies with the volume used as per the manufacturers' guidelines and incubated for 30 mins on ice in the dark, before being washed with 2 ml FACS buffer. Cells were centrifuged at 4°C 515 x *g* for 7 mins, and fixed with 200 µl Cell Fix ™ (BD Biosciences ™, 1 ml diluted in 9 ml distilled water) prior to acquisition with the flow cytometer (NovoCyte; ACEA) and using analysis FlowJo™ (version 10.1; BD Biosciences).

2.4.1 Purity

The purity of the monocytes was always confirmed using flow cytometry. Optimisation of the isolation method was carried out as initial methods brought an excessive quantity of platelets and inclusion of band neutrophils with "pure" monocytes from pregnant women. As such, the dilution of the blood in the first steps alongside a slower and longer density centrifugation minimised these contaminations (as seen in *2.2 Mononuclear cell isolation*). The gating strategy (Figure 2.5.) for the purity of the monocytes begins with the exclusion of doublet cells. Monocytes are then selected based on their FSC vs SSC profile, so that the population of platelets could be monitored. Due to the effect of platelets particularly on metabolism [227], only cells which contained more than 80% monocytes (based on their FSC vs SSC profile) were used for further analysis (excluding flow cytometry where gating strategies allow for platelet exclusion). Anti-CD14 eFluor® 450 fluorochrome (Biolegend; isotype Mouse IgG1a, κ; clone M5E2) was used to confirm the monocytes, where a purity <98% was used for experiments.

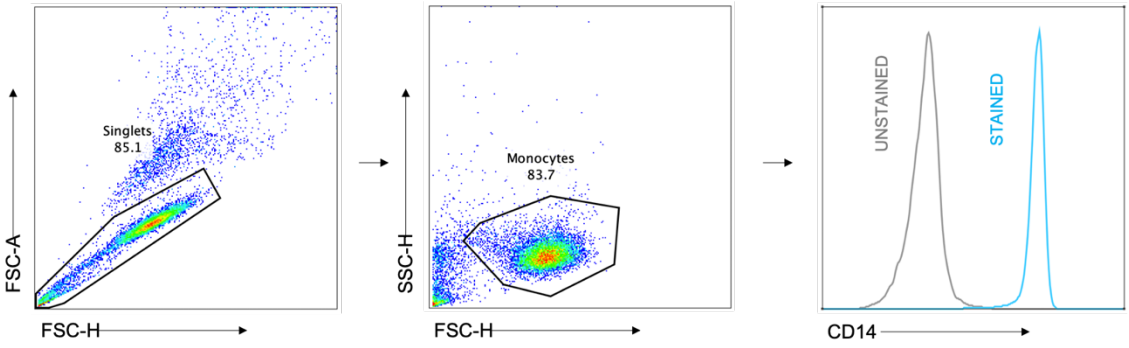

Figure 2.5: Isolated monocyte purity check. Doublets are first excluded using a forward scatter (FSC) height (H) vs area (A) plot. A FSC-H vs side scatter (SSC-H) dot plot is then utilised to exclude debris such as platelets and dead cells. Histograms of the unstained monocytes and the monocytes stained with pacific blue anti-CD14 was used to calculate purity.

2.4.2 Gating strategy for selection of monocytes

Throughout this thesis, monocytes were analysed via flow cytometry from a series of different samples: whole blood (Figure 2.6), MNCs (Figure 2.7) and pure monocytes (Figure 2.8). Singlet cells were first always selected. The use of forward scatter (FSC) vs side scatter (SSC) plots allowed for the rough selection of monocytes according to their size and granularity profile. CD14 expression was then used to confirm that monocytes are selected from whole blood and MNC populations. The CD14 and CD16 expression of the monocytes was then used to determine the individual subsets: CD14++CD16- (classical), CD14++CD16+ (intermediate) and CD14+CD16++ (non-classical). Median fluorescence intensity (MFI) or percentage of positive cells was then used to analyse phenotypic markers.

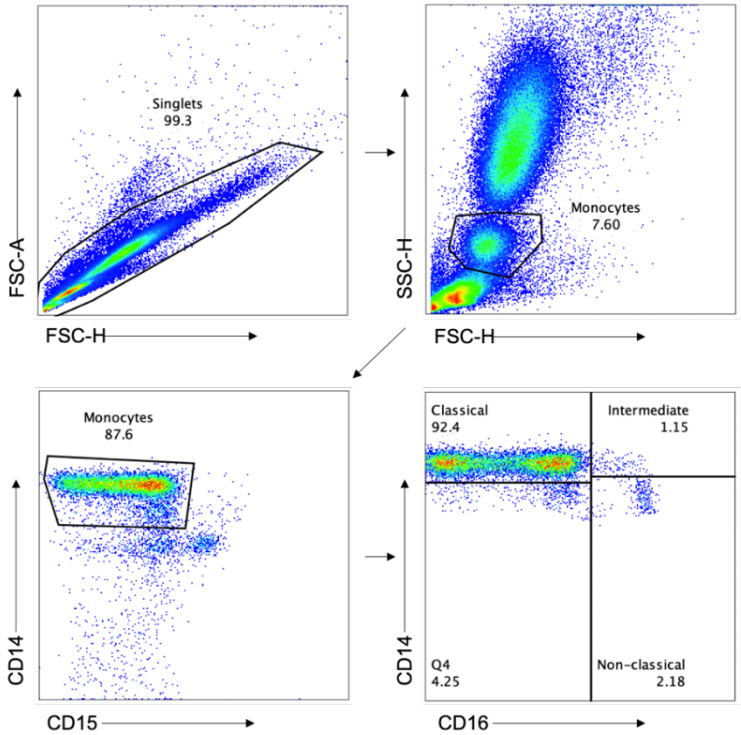

Figure 2.6: Gating strategy for monocytes and their subsets in whole blood. Singlets were first selected using a FSC-H vs FSC-A dot plot. Using a FSC-H vs SSC-H dot plot, monocytes were identified according to their relative size and granularity. Neutrophils (CD15+) and other leukocytes (CD14-CD15-) were removed using a CD15 vs CD14 dot plot. Monocyte subsets were then identified according to their CD14/CD16 profile.

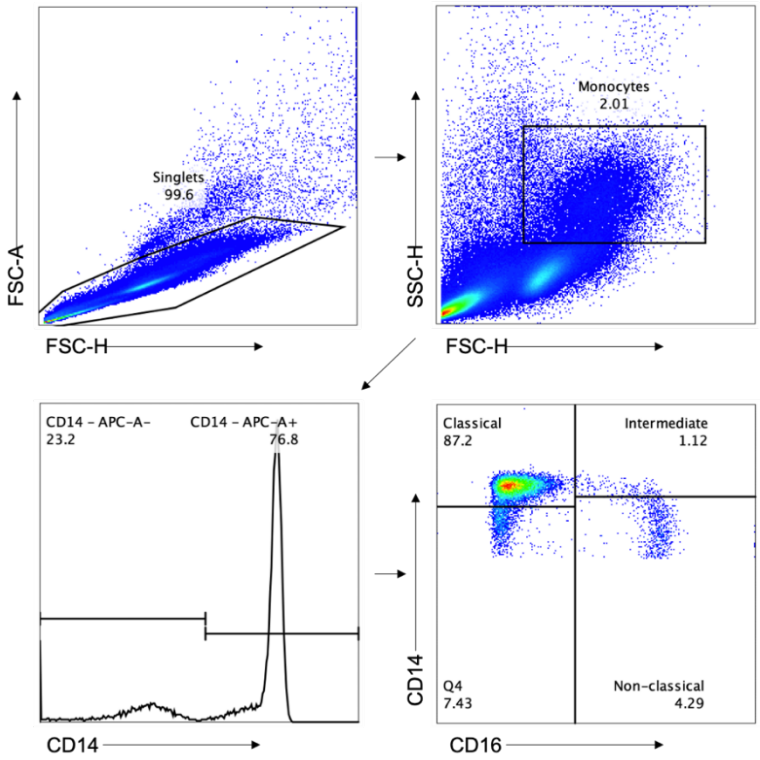

Figure 2.7: Gating strategy for the selection of monocytes and their subsets in MNCs. Singlets were first selected using a FSC-H vs FSC-A dot plot. Using a FSC-H vs SSC-H dot plot, monocytes were identified according to their relative size and granularity. A histogram visualising the CD14 expression enabled gating on the CD14-positive peak. Monocyte subsets were then identified according to their CD14/CD16 profile.

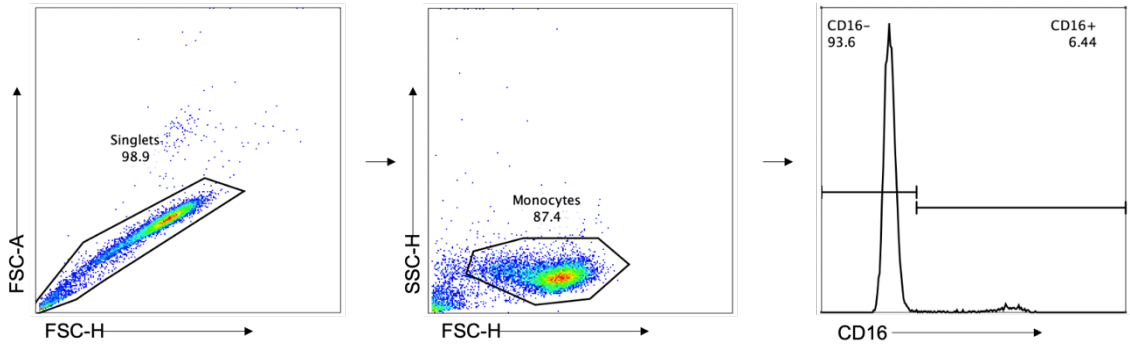

Figure 2.8: Gating strategy for selection of CD16+ and CD16- monocytes from isolated monocytes. Singlets were first selected using a FSC-H vs FSC-A dot plot. Using a FSC-H vs SSC-H dot plot, debris such as platelets and dead cells were gated out. CD16+ and CD16- monocytes were then selected using a histogram for CD16.

2.4.3 Data analysis

NovoExpress® experiment files were converted to .fcs files to be analysed using FlowJo™ version 10.1 (BD Biosciences). Median fluorescence intensity (MFI) or percentage values were collated into GraphPad Prism© V9 (GraphPad) and the appropriate statistical analysis was determined per experiment. Percentage values represent the number of cells which express antibody of interest; MFI was used when all cells express the antibody of interest, but with different levels of expression.

2.4.4 Compensation

When multiple antibodies are used with different fluorophores, samples must be compensated to account for overlap of the emission wavelengths of the fluorophores. Compensation is achieved using single stains of the antibodies which will be used in tandem and using the compensation tool on FlowJo™ to select for the negative and positive peaks of the sample. The tool creates a matrix which compensates for any overlaps, and this matrix can be applied to all samples with that mixture of antibodies.

2.6 Cell culture

Isolated monocytes were stimulated with lipopolysaccharide (LPS), muramyl dipeptide (MDP), or LPS and Resiquimod 848 (R848) to induce immune responses in the cells.

0.25 x10^6 cells in 250 µl culture media (10% autologous plasma, 100 µl 2-mercaptoethanol – 2-ME; Life Technologies, UK –, RPMI 1640/Glutamax) were seeded onto a flat bottomed 96 well plate in duplicate for: unstimulated, LPS-stimulated, MDP-Stimulated or LPS/R848-stimulated. LPS stock (ultra-pure LPS from *E. coli* 0.111:B4 strain – TLR4 ligand; InvivoGen™) was made up with 1 ml endotoxin-free water which was provided with the lyophilised LPS to give a concentration of 5 mg/ml. The final concentration of LPS in cultures needed to be 10 ng/ml, and so was diluted 1/50 with media, which was then diluted 1/100 into the experimental culture well. MDP stock (muramyl dipeptide; L-D isoform, active – NOD2 ligand; InvivoGen™) was 1 mg/ml, and the concentration in culture needed to be 1 µg/ml. A 1/10 dilution was made, and then a 1/100 dilution made into the experimental culture well. R848 stock (Imidazoquinoline compound = a TLR7/8 ligand; InvivoGen™) solution of 1 mg/ml was made by re-suspension with 500 µl endotoxin-free water. Final concentration in culture needed to be 400 ng/ml; stock was diluted 1/25 with media, before the 1/100 dilution into the experimental culture well. The final concentrations were from pre-optimisation experiments previously in the research group [47, 228]. Plates were lightly covered with their lids (allowing for gaseous exchange) and incubated at 37°C in a 5% CO_2-in-air incubator for 24 hrs. After incubation, plates were centrifuged at 4°C, 515 x *g* for 7 mins. The cell free supernatant was aliquoted into microtubes and frozen at -20°C until analysis.

2.7 Bioenergetic analysis

Bioenergetics is the study of the flow of energy through living systems with a focus on metabolic pathways. A goal of the study of bioenergetics is understanding the production and use of energy in the form of molecules such as ATP (adenosine triphosphate). Seahorse Bioscience XF Extracellular Flux Analyser™ profiles the metabolic activity of cells by measuring glycolysis rates, production of ATP, consumption of oxygen, and respiratory capacity. This analyser is ideal for its label-free and real-time capabilities. A schematic of the Seahorse XF^{e}96 machine and how it measures oxygen consumption and extracellular acid rate is shown in Figure 2.9.

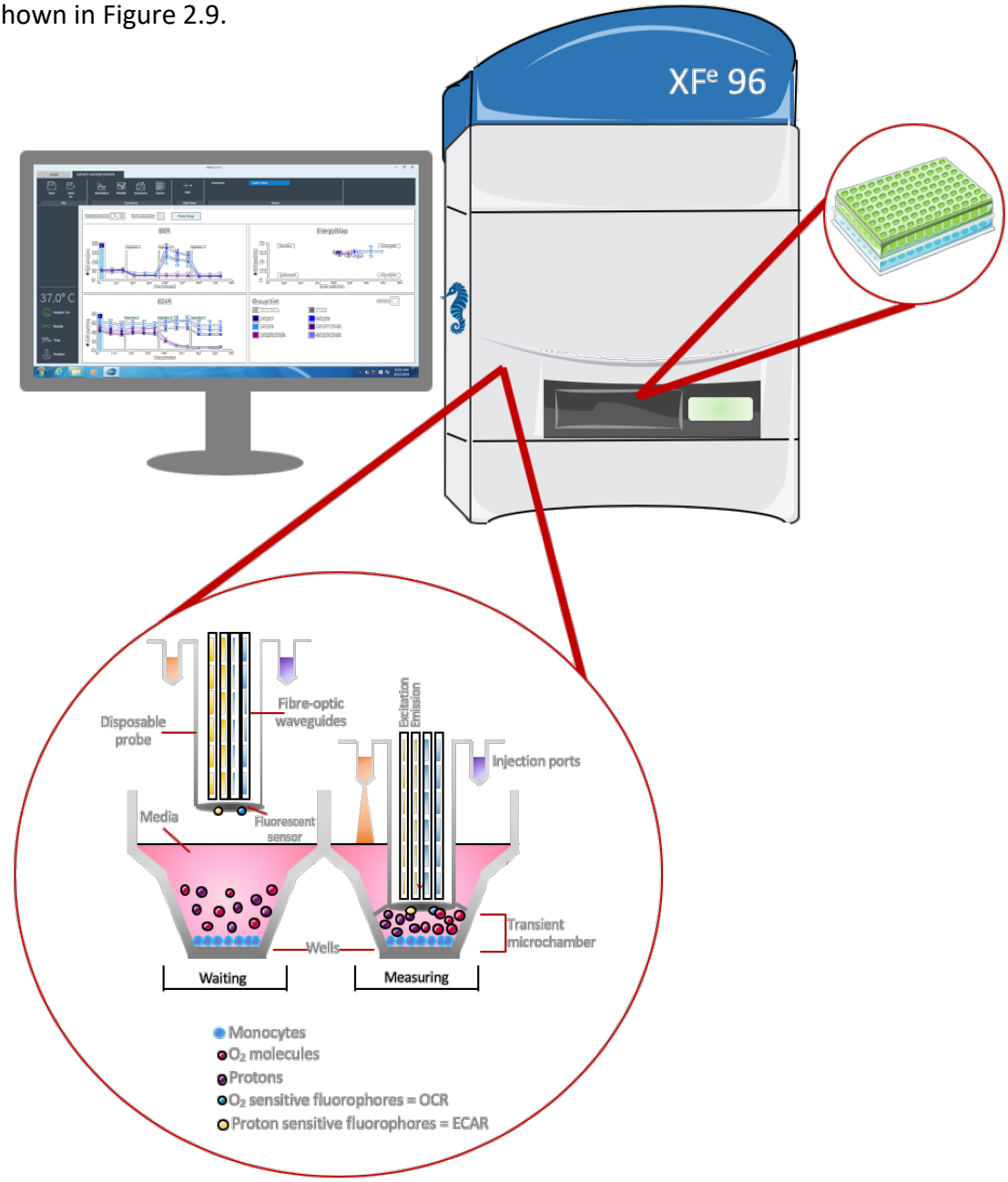

Figure 2.9: The Seahorse XF^{e}96 for bioenergetic analysis. Extracellular acidification rate (ECAR) and oxygen consumption rate (OCR) are measured using proton and oxygen sensitive fluorophores, respectively.

2.7.1 Preparation of cell adhesion and calibration plates

A Cell-Tak© (Corning, USA) coated plate was prepared up to a week in advance; this ensured that the cells would adhere to the plate. A stock of Cell-Tak© (22.4 µg/ml) was prepared with 0.1 M sodium bicarbonate (Sigma). 25 µl of this was added to each well of a barcoded 96-well cell-culture plate (Agilent) the plate and left for 20 mins at room temperature. 200 µl sterile water was added to each plate and then all liquid was carefully removed. The plate was allowed to dry completely before storing at 4°C. The day before the assay, the Seahorse Bioscience™ XF Extracellular Flux Analyser was set to reach 37°C. 200 µl of calibration fluid was added to each well of the calibration cartridge (Agilent) before re-assembling it and placing it in a sealed bag to leave in a 37°C oven overnight.

2.7.2 Mito Stress Assay

The Mito Stress assay analyses mitochondrial function by measuring production of ATP, basal respiration, leaking protons, non-mitochondrial respiration, maximal respiration, and spare respiratory capacity (Figure 2.10). Injections of oligomycin, carbonyl cyanide-p-trifluoromethoxyphenylhydrazone (FCCP), and rotenone/antimycin A are used to target specific components of the electron transport chain (ETC). Oligomycin inhibits ATP synthase. FCCP is an ionophore that acts as an uncoupling agent by collapsing the proton gradient and disrupting the mitochondrial membrane potential. This allows uninhibited flow of electrons through the ETC, and the maximum consumption of oxygen by complex IV. Rotenone and antimycin A inhibit complexes I and III respectively, shutting down oxidative phosphorylation. Glycolysis is measured using ECAR (extracellular acidification rate) to track the production of lactate; however, acidification can be caused by other cellular functions such as by the citric acid cycle via the production of carbon dioxide.

On the day of the assay, the Cell-Tak™ coated plate was first placed in a 37°C oven (no CO_2 flux). To make up the assay media, glucose (Agilent), pyruvate (Agilent) and glutamine (Sigma) were used to supplement XF assay media minimal DMEM (Agilent); volumes and concentrations are provided in **Error! Reference source not found.**. The concentrations for the media and injections were optimised from Jones et al. 2015 [47] for MNCs and Jones et al. 2021 [228] for monocytes. The remaining 40 ml of volume was supplemented with the Seahorse media with minimal DMEM (Agilent). The media was brought to 37°C in a water bath and a

pH of 7.4 for each media was achieved by adding small increments of 1M sodium hydroxide. Media was then sterilised by filtering (Millex ® 33 mm sterile filter unit with Millipore Express® PES membrane with 0.22 µm pore, Ireland) and returned to the water bath.

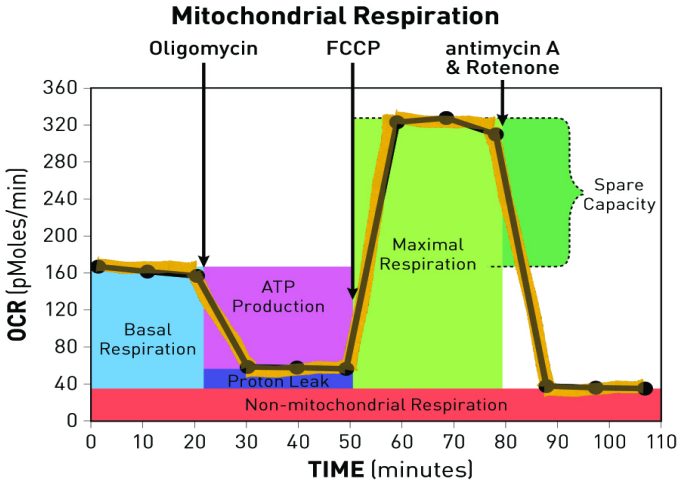

Figure 2.10: MitoStress assay parameters. Non-mitochondrial respiration is measured by the OCR below the final injection (antimycin A and rotenone) that acts as a base for the other measurements. Measurements of basal respiration are taken before the first injection of oligomycin. ATP production is determined by the difference in measurements taken between the first (oligomycin) and second (FCCP) injection. Maximal respiration is measured after the second injection, and spare respiratory capacity is determined by the difference in OCR between basal respiration and the peak of maximal respiration. Image taken from Agilent XF Mito Stress Test User guide, accessed 30/07/2021, https://www.agilent.com/cs/library/usermanuals/public/XF_Cell_Mito_Stress_Test_Kit_User_Guide.pdf

	Stock (M)	Final concentration (mM)	Volume needed in 40ml total (ml)
Glucose	1	5.5	0.22
Pyruvate	1	1	0.4
Glutamine	0.2	2	0.4

Table 2.1: OXPHOS media recipe. The stock concentrations of supplementary glucose, pyruvate and glutamine, and the concentrations required in the final media along with the volumes needed to acquire those concentrations.

Monocytes were isolated as in *2.3 Monocyte isolation*. After the final centrifugation, cells were re-suspended in 500 µl of Seahorse assay media before being counted as described in 2.3 Cell counting. The working concentration was determined to ensure that there were five replicates of 0.2 x10^6 monocytes per 100 µl per well. This was calculated by preparing 1.2 x 10^6 cells (excess required) in a total of 600 µl, before seeding 100 µl into wells. Remaining wells were seeded with 100 µl of media only (blanks). The plate was centrifuged at 200 x *g* with no brake and 1 acceleration for 1 min at room temperature. 50 µl/well assay media was

then added to give a total volume of 150 µl/well. The plate was then transferred to a 37°C oven for 45mins.

Injections (all from Sigma) were prepared as optimised [47] as in Table 2.2. Approximately 15 minutes before the end of the incubation in the 37°C oven, injections were added to the ports in the calibration plate as in Table 2.2. The calibration plate was then loaded onto the machine. Once the calibration had finished and passed the quality control, the plate containing the cells was loaded into the machine. Live OCR and ECAR levels were measured.

	Stock Concentration (mM)	**Volume (µl)**	**Volume media (µl)**	**Volume into port (µl)**	**Final concentration (µM)**
Oligo	2.5	7	2493	25 (A)	1.0
FCCP	2.5	8	2492	25 (B)	1.0
Antimycin A/ rotenone	2.5 (each)	9 + 9	2482	25 (C)	1.0 (each)

Table 2.2: Injection preparation. Stock concentrations of the injections - oligomycin (oligo), FCCP, and antimycin A and rotenone. The volumes of stock and media required to attain final concentrations in the wells is shown.

2.7.3 Mito Fuel Flex test

Various types of fuels can contribute to the TCA and oxidative phosphorylation functions of the cell. Broadly, carbohydrates, fatty acids and amino acids are the key molecules involved. Despite the vast range of molecules under these umbrella terms, it is possible to investigate the fuel dependency and capacity of the cells by investigating specific examples of those molecules.

BPTES (bis-2-(5-phenylacetamido-1,3,4-thiadiazol-2-yl)ethyl sulphide) is classically used to inhibit glutaminase, as it is a selective inhibitor of glutaminase (GLS1). This is a key enzyme which converts glutamine to glutamate from which α-ketoglutarate can be formed to be oxidised by the TCA cycle. By utilising BPTES it is possible to get insight into the bioenergetic dependence on amino acids.

Etomoxir (Eto; 2[6(4-chlorophenoxy)hexyl]oxirane-2-carboxylate) prevents the transport of long chain fatty acyl chains into the mitochondria from the cytosol. It is an irreversible

inhibitor of carnitine palmitoyltransferase-1 (CPT-1). CPT-1 is present on the cytosol side of the inner mitochondrial membrane and forms acyl carnitines, an essential step for the transportation of fatty acyl chains. By inhibiting CPT-1 and obstructing fatty acid oxidation (FAO), Eto prevents the production of ATP. High concentrations of Eto have also been observed to have a secondary effect on the metabolism of Coenzyme-A (Co-A) [229].

UK5099 (2-cyano-3-(1-phenyl-1H-indol-3-yl)-2-propenoic acid) is classically used to prevent the transportation of pyruvate into the mitochondria by inhibiting the mitochondrial pyruvate carrier (MPC). Pyruvate is produced during glycolysis and can be transported into the mitochondria to contribute to the TCA cycle after conversion to acetyl-Co-A. Therefore, this can yield data on the use of carbohydrates by the cells.

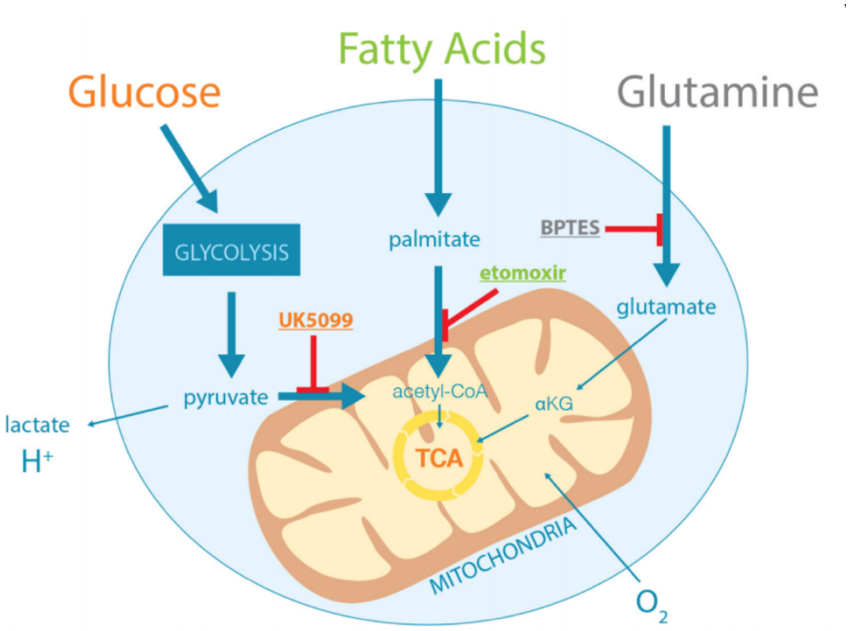

Figure 2.11: The inhibition of specific fuels for the TCA cycle and oxidative phosphorylation. BPTES, etomoxir and UK5099 inhibit the transport of either amino acids, fatty acids or carbohydrates, respectively into the mitochondria for oxidation. Image taken from Agilent XF Mito Fuel Flex Test User guide, accessed 30/07/2021,https://www.agilent.com/cs/library/usermanuals/public/XF_Mito_Fuel_Flex_Test_Kit_User_Guide%20old.pdf

The principle of the assay utilises the MitoStress assay already described, with the addition of these inhibitors. The media preparation is unchanged, and the injections only have slight changes due to the shift of injection ports to allow the first injection to be either media (control), BPTES, Etomoxir or UK5099 (all from Sigma; Table 2.3). A minimum of 2 wells per condition were used at the same seeding concentration used for the MitoStress assay, and

the plate was segregated four-ways for the different conditions. The dependency of the cell on that fuel source was determined by the decrease in fuel oxidation (OCR).

	Stock Concentration (mM)	Volume (µl)	Volume media (µl)	Volume into well (µl)	Final concentration (µM)
CTRL (media)				25 (A)	
BPTES	10	4	1900	25 (A)	3.0
Etomoxir	10	4	1900	25 (A)	3.0
UK5099	10	2	1428	25 (A)	2.0
Oligo	2.5	8	2492	25 (B)	1.0
FCCP	2.5	9	2491	25 (C)	1.0
Anti-mycin A /rotenone	2.5 (each)	10 + 10	2480	25 (D)	1.0 (each)

Table 2.3: The injections and their concentrations for the fuels flex MitoStress test.

2.7.4 Data analysis

The Seahorse Wave™ desktop software provides values for the OCR and ECAR over time. Data from here was converted into a GraphPad Prism© V8 file and collated into groups for analysis as described in results chapters.

2.8 Enzyme linked immunosorbent assay

Enzyme-linked immunosorbent assays (ELISAs) are designed to use antibodies to detect a desired substance via colour change. There are several types of ELISAs, but throughout this thesis sandwich ELISAs were used (Figure 2.12). This is when a plate is first coated using an antigen-specific capture antibody, which will bind to antigen present in test samples. Then a specific biotinylated detection antibody is added which also binds to the antigen, and thus the antigen is bound – sandwiched - between two antibodies. Streptavidin-HRP is added to bind to the biotinylated detection antibody. Substrate solution is then added which the HRP converts into a detectable colour; this colour changes again once a 'stop' solution is added to prevent the reaction from continuing. This is then measured as absorbance with this value used to quantify the antigen. A standard curve on every ELISA plate is best practice so that unknown concentrations can be plotted on a graph with known concentrations.

ELISAs were carried out as per R&D Systems™ guidelines. Capture antibodies were diluted as required in PBS. This was added 50 µl/well on a half-area 96 well plate (Greiner Bio-One) and incubated over-night, or over the weekend, in the fridge. The coating antibody was tipped off

and blocking/assay buffer (1% BSA in PBS) was added at 150 µl/well to bind to nonspecific binding sites. This was incubated for 1hr at room temperature with shaking at 450 rpm (Titramax 1000, Heidolph). Aspiration and washing 3 times with wash buffer (PBS with 0.05% Tween-20) was then done. Samples (diluted as optimised with assay buffer) and standards were added at 50 µl/well. This was incubated at room temperature for 2 hrs and then aspirated and washed 4 times. Biotinylated detection antibody was diluted 1/60 in assay buffer, added 50 µl/well, incubated 2hrs room temperature, and aspirated before the plate was washed 4 times. Streptavidin-HRP was diluted 1/40 in assay buffer, incubated 20 mins at room temperature, and then aspirated before the plate was washed 6 times. 3,3',5,5' tetramethylbenzidine (TMB) substrate solution (BD Biosciences) was made by mixing equal volumes of Substrate A (containing hydrogen peroxide) and Substrate B (containing TMB; light sensitive) and added 50 µl/well. The blue colour was allowed to develop in the dark. The reaction was then stopped with 50 µl/well 1 M sulphuric acid (H_2SO_4) up to 20 minutes later once a gradient appeared in the standard curve wells. This changed the bright blue colour to a yellow. The absorbance was then measured at λ 450 nm using a plate reader (POLARstar Omega, BMG Labtech).

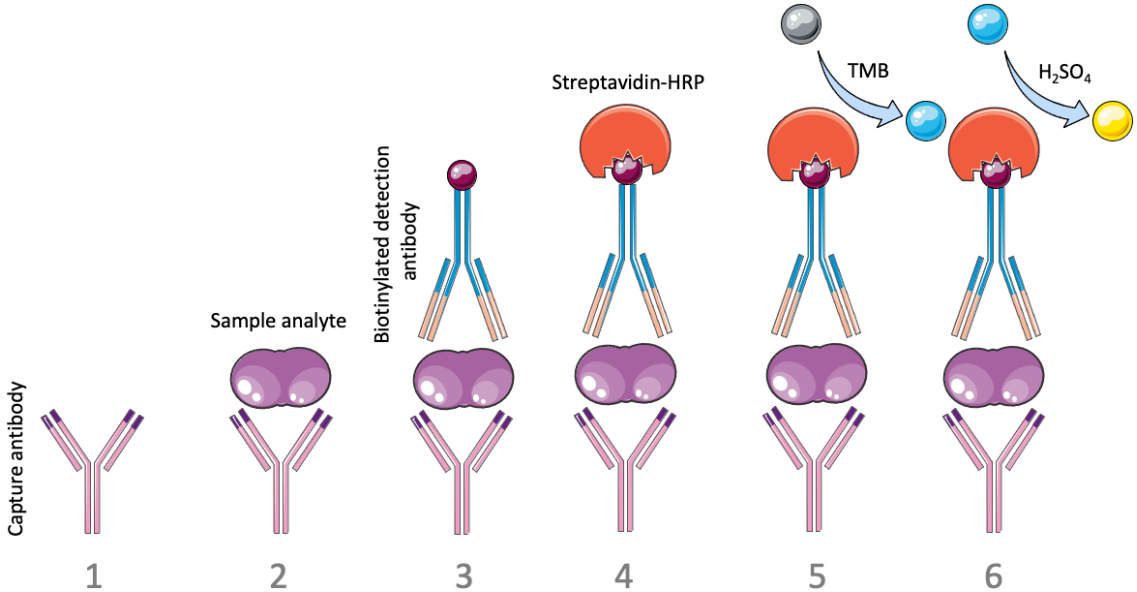

Figure 2.12: A sandwich ELISA. 1. Capture antibody; 2. Sample is added, and antigens bind to capture antibody; 3. Detection antibody added and also binds to antigen; 4. Streptavidin-HRP is added and binds to detection antibody; 5. A TMB substrate solution is added to convert the enzyme into a detectable colour; 6. A 'stop' solution is added to prevent on-going reaction, and changes the colour again. The absorbance of this colour is then measured.

2.7.1 Data analysis

Data from the Mars™ data analysis program (version 3.20 R2, BMG Labtech) which collected the data from the ELISA experiments was exported into Excel™. A polynomial standard curve

was generated using the known concentrations of the standards and their optical readings. The equation and R^2 value were displayed. The R^2 value gave an indication as to how well the experiment was carried out, i.e., how well the trendline fits the data points. An R^2 of 1 infers the data points perfectly fit the line, whereas a lower R^2 is indicative of the data points being more scattered. The equation then allows extrapolation of data using optical readings of the unknown concentrations from the samples. This was then collated onto GraphPad Prism© V8 and plotted onto scatter graphs in groups of non-pregnant vs pregnant to determine variances.

2.9 Immunoblotting

Immunoblotting can be used to quantify the amount of a chosen protein or enzyme in a sample and provide additional information including molecular weights and isoforms. For normalisation purposes, the same amount of total protein is used for the samples. Samples are loaded onto an acrylamide gel for sodium dodecyl sulphate–polyacrylamide gel electrophoresis (SDS-PAGE), whereby the proteins are separated based on their molecular masses; the larger the protein, the longer it takes to separate and thus sits higher on a gel. Once SDS-PAGE is completed, the protein molecules are transferred from the gel to a membrane. This membrane can be incubated with a primary antibody (for chosen protein of study) and then with a secondary antibody which is HRP-labelled. When the samples are ready for imaging, they are incubated with the chemiluminescent substrate and HRP catalyses release of a signal that can be detected by an imaging system. This process is seen simplified in Figure 2.13.

2.8.1 Protein quantification

Protein quantification was first needed to ensure that the same amount of protein was loaded onto the gel. The Qubit® protein assay kit (Life Technologies) was used for this purpose. By diluting the Qubit® protein reagent 1/200 in Qubit® protein buffer, this produced the Qubit® working solution with which the standards and samples were prepared. Three pre-diluted BSA Qubit® standards (0 ng/ml, 200 ng/ml, 400 ng/ml) were diluted further - 1/20 - with the working solution. Samples were diluted 1/100 with working solution. This was prepared in Qubit® assay tubes where the total volume for each tube was 200 µl. Each assay tube was

vortexed briefly and incubated for 15 mins at room temperature. The standards and samples were then read using protein protocol on the Qubit® 4.0 Fluorometer (Life Technologies). Protein amount was provided as µg per µl.

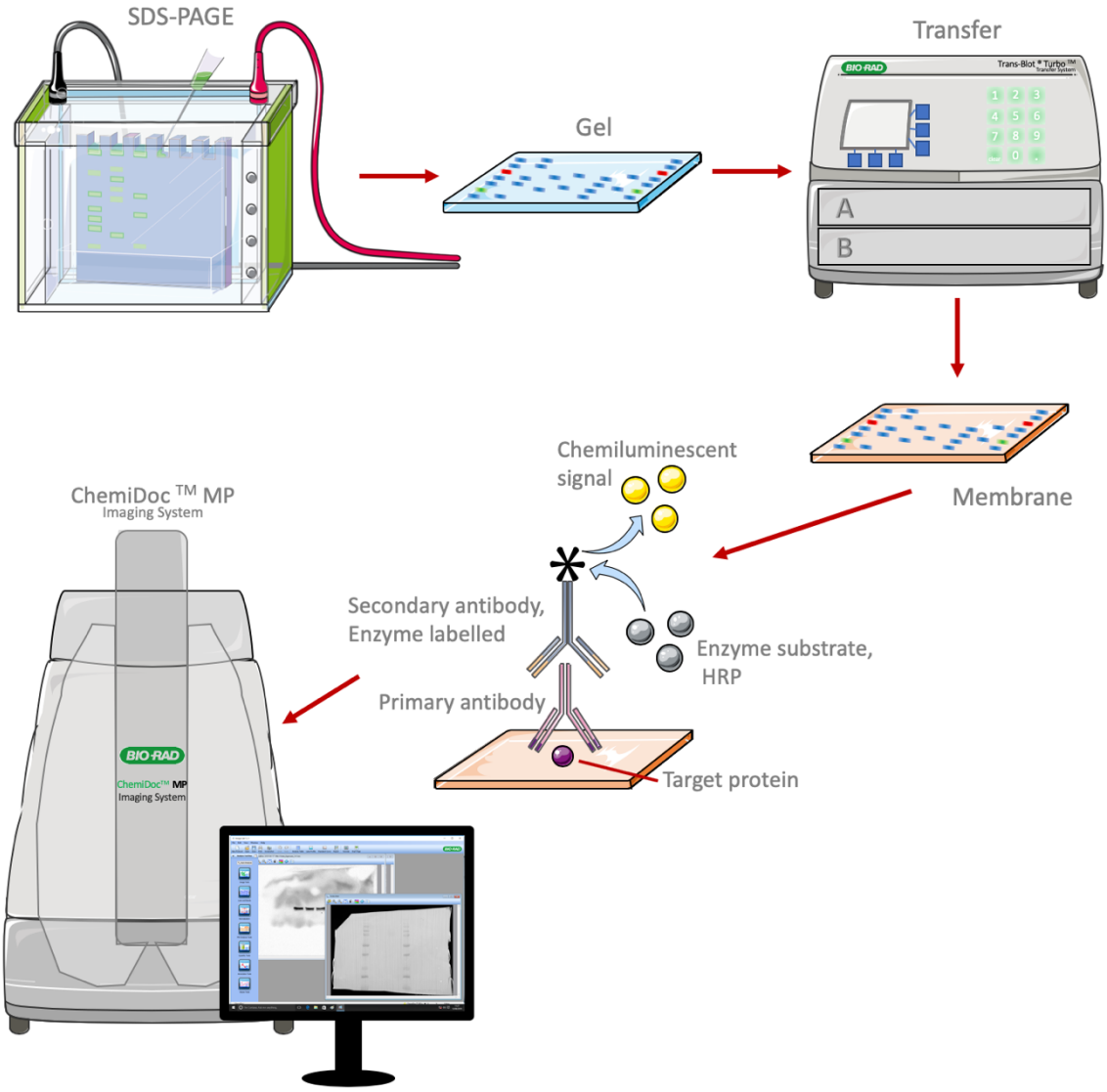

Figure 2.13: Steps of immunoblotting. Proteins in samples are separated by SDS-PAGE. Samples are transferred onto a membrane and primary antibodies are added before secondary enzyme (HRP) conjugated antibodies. Chemiluminescent substrate is then added to produce a chemiluminescent signal which is detected by an imaging system.

2.8.2 Gel preparation

Gels were made up as either: 6%, 8%, 10% or 12% acrylamide. Gel percentage is chosen based on the size of the protein of interest. Table 2.4 is for guidance on which gel to use. Clean spacer and short plates (Bio-Rad) were clamped together. Resolving gel was made up as in Table 2.5 in order of solutions listed (all from Bio-Rad except ammonium persulfate; APS, Sigma). After the final solution tetramethylethylenediamine (TEMED) was added to the mixture, it was gently mixed and added into the plates, filling until approx. 1 cm was left at

the top. Ethanol (70%) was added to the top of the gel to remove any bubbles. The gels were allowed to polymerise. Once polymerised and the ethanol removed, stacking gel (made up as in Table 2.6) filled the remaining space at the top, and combs for the wells (Bio-Rad) were inserted into the stacking gel; this was also then allowed to polymerise.

Size of Protein (kDa)	Gel Percentage (%)
10-70	12
15-100	10
25-200	8

Table 2.4: Guidance for gel percentage to use depending on the size of protein of interest.

Gel %	6%	8%	10%	12%
ddH_2O	8 ml	7 ml	6 ml	5 ml
30% Acrylamide	3 ml	4 ml	5 ml	6 ml
1.5M Tris (pH 8.8)	3.75 ml	3.75 ml	3.75 ml	3.75 ml
10% SDS	150 µl	150 µl	150 µl	150 µl
10% APS	75 µl	75 µl	75 µl	75 µl
TEMED	15 µl	15 µl	15 µl	15 µl

Table 2.5: Resolving gel recipes. The volumes needed to produce two resolving gels for varying percentage gels

.

ddH_2O	3 ml
30% Acrylamide	650 µl
1.5M Tris (pH 8.8)	1.25 ml
10% SDS	50 µl
10% APS	25 µl
TEMED	5 µl

Table 2.6: Stacking gel recipe. The volumes needed to produce two stacking gels

2.8.3 Blotting

The calculated volumes for 20 µg of protein for each sample were added into individually labelled 500 µl tubes. 5X reducing buffer was diluted 1/5 onto the samples. Samples were then heated at 95°C for 5 minutes, and then left to cool. A gel was loaded with an accompanying second or blank gel, into the blotting tank with loading buffer (900ml diH_2O and 100ml tris-buffered saline; TBS, Bio-rad). 5µl of protein plus protein dual colour standard (Bio-Rad) was added to each of wells 1 and 10. Samples were loaded into the other wells, alternating between non-pregnant and pregnant. Voltage was set to 120 V for one hour.

Extra thick blot filter paper (Bio-rad) was placed in transfer buffer (700 ml diH_2O, 200 ml methanol, 100 ml tris-glycine buffer; TG, Bio-Rad) for 20 minutes, and the membrane (Immobilon-P PVDF membrane, 0.45 µm pore size, Sigma) was soaked in 100% methanol for 30 seconds before being placed underneath the filter papers. The gel was removed from the tank and cracked open from its protective case. The gel was placed onto the membrane which was on top of one piece of filter paper. The other filter paper was placed carefully on top of the gel as in Figure 2.14. This sandwich was then placed in the Bio-Rad Trans-Blot® Turbo™ transfer system on standard protocol A for 30 minutes. The membrane was then separated from the gel and paper, and placed in blocking buffer (5 % BSA, TBST; 10X TBS diluted with dH_2O and 0.1% Tween-20) with gentle agitation for 1 hour at room temperature. The membrane was then placed in a tightly heat-sealed bag with the primary antibody (diluted as required with blocking buffer). This was then placed back in the blocking buffer with gentle agitation at 4°C overnight.

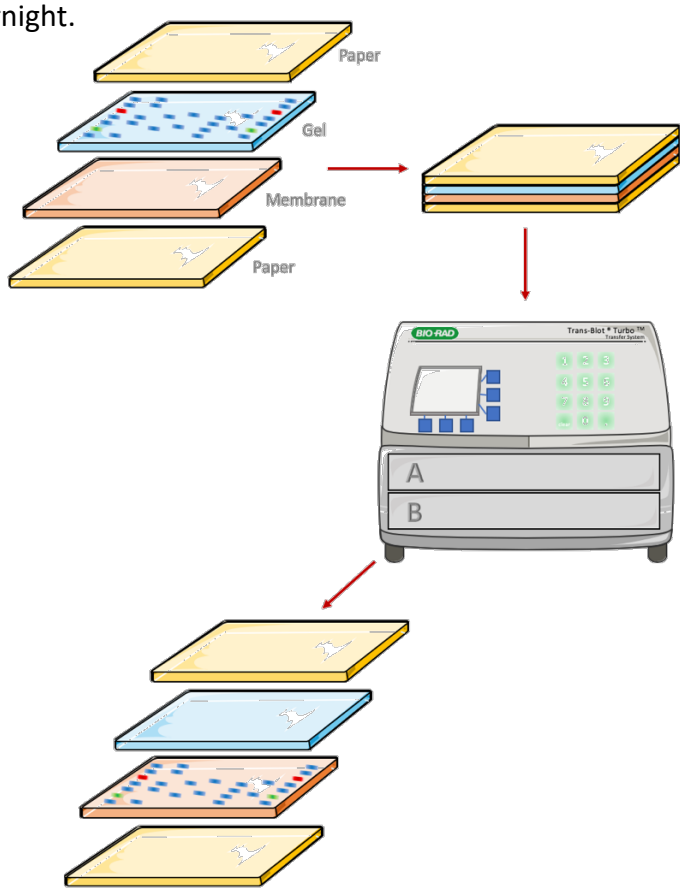

Figure 2.14: Gel transfer. Diagram of the sandwich of the post-run gel ready for transfer, the Bio-rad transfer machine, and the resulting transfer onto the membrane.

The membrane was removed from the bag the next day and washed three times with TBST for 5 minutes each wash with gentle agitation. The membrane was then placed in a new

tightly heat-sealed bag with the secondary antibody (diluted as required with TBST) and agitated gently for 1 hour at room temperature. The membrane was washed 3 times again and run on the Bio-Rad © ChemiDoc ™ MP Imaging System with equal volumes of solutions A (luminol solution) and B (peroxide solution; Amersham™, Cytiva) coating the membrane for visualisation of the protein.

After imaging, the first antibody needed to be stripped from the membrane so that it could be used for re-probing with a new antibody. The new antibody is typically a house-keeping protein which assesses whether the same amount of protein was loaded from different samples. The membrane was washed twice with TBST and then coated with stripping buffer (Thermofisher), which was left on for no longer than 10 minutes at room temperature with gentle agitation. The membrane was washed again 3 times and coated with blocking buffer for 1 hour. The rest of the assay with the primary and secondary assay was as mentioned previously.

2.10 Mass spectrometry

Monocytes were prepared for mass spectrometry analysis. 1 x 10^6 monocytes were aliquoted and washed with 1 ml RPMI 1640/Glutamax, centrifuged at 400 x *g* for 5 mins. The pellet was then washed twice with 1 ml PBS, ensuring all the supernatant was removed at each step, and centrifuged in the same conditions. The PBS was completely removed, and the pellet was frozen at -80°C until use. They were then washed with 100 µl of dH_2O and centrifuged at 400 x *g* for 5 mins, with the supernatant being completely removed. The pellet was carefully re-suspended in 50 µl of dH_2O. Protein concentration was calculated using the protein estimation assay in *2.8.1 Protein quantification.* This sample could then be used for intact analysis, and/or the lipids extracted.

2.10.1 Lipid extraction

In order to investigate the lipidomics of the monocytes, the lipids need to be extracted from the samples. A 14:0 cardiolipin standard (Avanti) was used to normalise results on MALDI. To prevent unreliable normalisation, a lipid extraction of monocytes without the internal standard was performed to ensure there was no natural peak at the same m/z of the

standard. The cardiolipin standard was used at a working concentration of 1.25 nM/μg of protein. From a 7.84 mM stock, the cardiolipin was diluted using chloroform to 12.5 nM. Samples were standardised to contain 10 μg of protein.

All materials were kept on ice for the protocol. 10 μg of sample was added to glass tubes (Corning), and volumes were brought to 400 μl using HPLC grade H_2O (Fisher Scientific); a blank sample of just 400μl of H_2O was processed in parallel. 400 μl of HPLC grade methanol (MetOH; Fisher Scientific) was added to each sample, along with 400 μl of 12.5 nM cardiolipin standard. Samples were vortexed thoroughly and then centrifuged at 1800 *x g* for 30 mins at 4°C. Once centrifuged, the solutions separated into three layers; the top layer is MetOH, middle layer contains proteins, and the bottom layer is where the lipids lie. Avoiding taking up any MetOH, a glass Pasteur pipette was used to take up the lipid layer to a fresh glass tube. 400 μl of chloroform (Fisher Scientific) was added to the original tube (with the MetOH and proteins), vortexed thoroughly and centrifuged again at 1800 *x g* for 30 mins at 4°C. The lipid layer was again collected and added to the original lipid layer, ensuring the majority of lipids is preserved. The chloroform was then evaporated with nitrogen at 50°C in a fume hood for approximately 30 mins. 50 μl of MetOH:$CHCl_3$ (methanol and chloroform in a 1:1 ratio) was added to each sample, including the blank, and vortexed. The mixture was transferred to 1.5 ml glass vials (Kinesis). Another 50 μl of the MetOH:$CHCl_3$ solution was added to the samples and transferred to the same vials to ensure all lipids were transferred. The solution was then evaporated using nitrogen at 50°C (approximately 10 mins), and 20 μl of MetOH:$CHCl_3$ was added to each vial. Vials were vortexed and frozen at -20°C until analysis.

2.10.2 Matrix assisted laser desorption/ionisation (MALDI) time of flight (ToF)

MALDI-ToF can be used to directly investigate lipid profiles of cells. The matrix is a small organic molecule which can absorb the UV light from the laser and assist in the ionisation process. The sample is sandwiched in a crystalline matrix (Figure 2.15) and subjected to a pulsing laser (Figure 2.16). Molecules from the sample vaporise into the vacuum and are either protonated (positive-ion mode) or deprotonated (negative-ion mode) without decomposing. The time of flight is responsible for separating the ions based on their mass to charge ratio. This is determined by the time it takes for the ions to reach the detector; in some

machines, reflectors are used in order to extend the flight distance and focus the masses of the ions to achieve a higher resolution. The ions which take the longest to reach the detector are the largest.

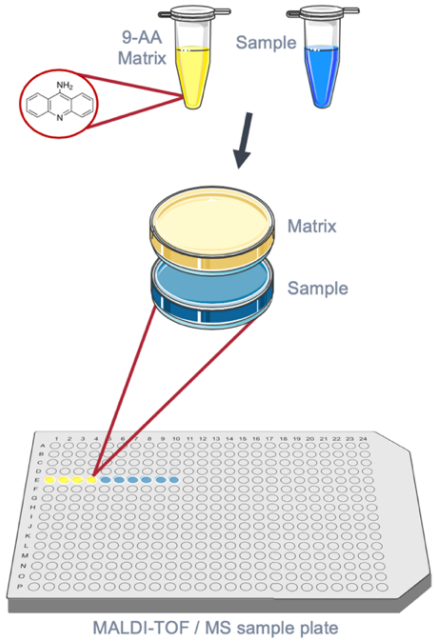

Figure 2.15: MALDI sample preparation. The sample is first aliquoted onto a MALDI-ToF plate, with the 9-AA matrix layered on top of the sample.

For intact analysis, samples were kept on ice when ready to be used. 1 µl of the suspension was aliquoted onto the MALDI target plate (Bruker) and allowed to dry. A 0.4 µl droplet of a 9-aminoacridine (9-AA; Acros Organics) matrix solution, (30 mg/ml in a 60:40 ratio with 2-propanol-acetonitrile; Fisher Scientific) was added onto the dried suspension.

Lipid extracted samples were mixed in a 1:1 ratio with 30 mg/ml of the 9-AA matrix solution. 1 µl of this solution was spotted onto the MALDI target plate. An Ultraflex mass spectrometer (Bruker, Germany) was used to acquire the spectra for both sample types but operating in the positive polarity for intact analysis and negative polarity for lipid extractions.

2.10.3 Data analysis

Data was exported to OpenMS© software (Version 2.5.0, TOPPAS) where peaks were identified as specific lipids using their m/z value with the assistance of LIPID MAPS® (https://www.lipidmaps.org/). The intensity of their peaks were used for analysis.

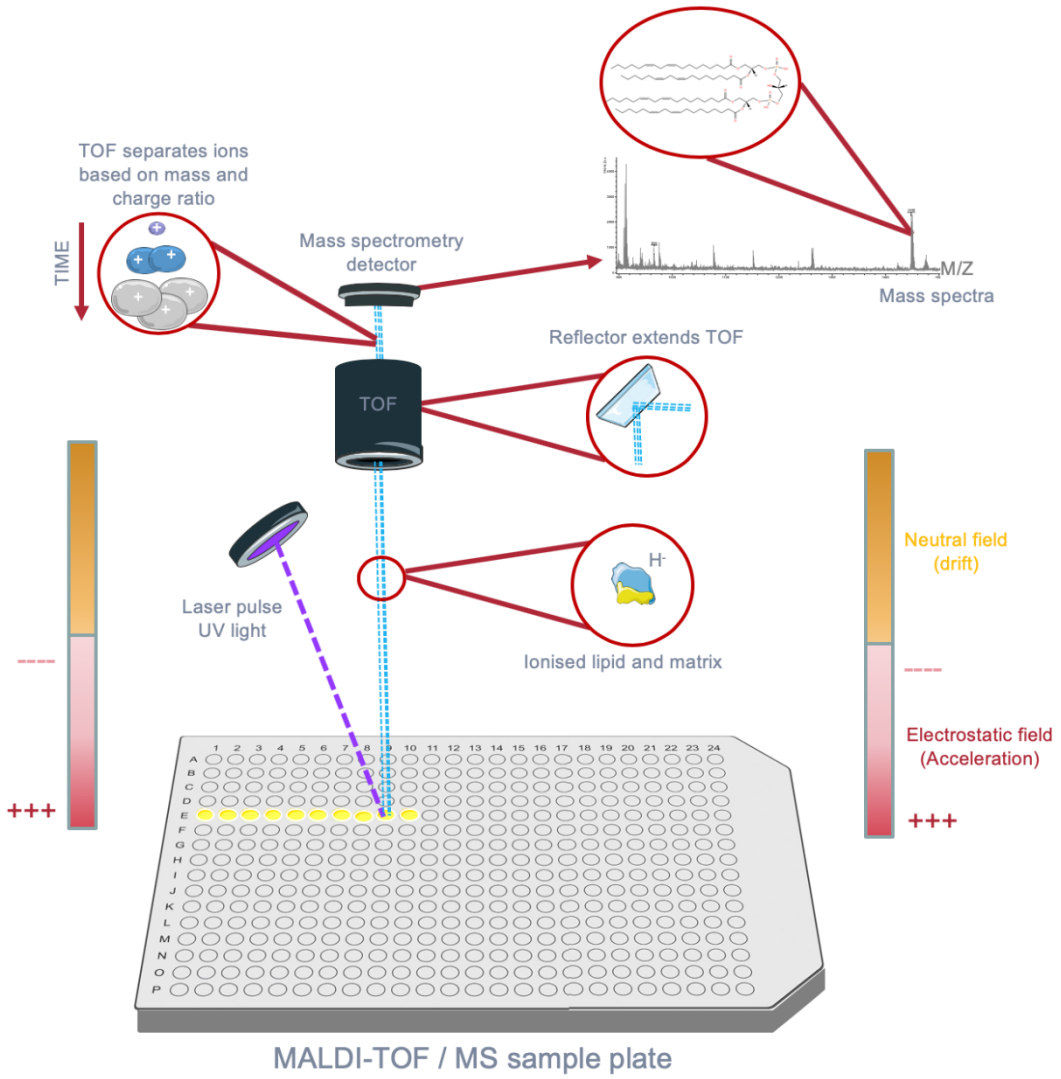

Figure 2.16: How a MALDI-ToF spectra is generated. The sample in the matrix is subjected to pulses of UV light. The electrostatic field charges the plate to assist in the ionisation of the lipids. The deprotonated lipid molecules pass through a ToF, where a reflector extends the time of flight. The ToF separates the ions based on the mass to charge ratio (m/z) and ions are detected to produce a spectrum of lipids.

2.11 NanoString

NanoString© nCounter® SPRINT profiler allows for the analysis of up to 800 gene targets simultaneously from RNA or cell lysates. NanoString has various pre-defined panels such as the nCounter® Metabolic Pathways Panel. This specific panel investigates the expression of 768 human genes including genes which are specific for: biosynthesis and anabolic pathways, cell stress, nutrient capture and catabolic pathways, metabolic signalling, and transcriptional regulation. It utilises molecular barcodes for direct digital detection of individual target molecules. The process by which the nCounter® SPRINT profiler works can be observed in Figure 2.17. The samples first need to be hybridised for the reporter probe and capture probe to pair to the target nucleic acid to produce a target-probe complex. The capture probe has

50 bases and is biotinylated and the 50 base reporter probe is directly adjacent to it and has a 6-spot fluorescent barcode. Each target is assigned a unique colour combination for identification. Excess probes are removed after the hybridisation process and the purified complexes are loaded into the sample cartridge allowing for random binding to the surface. Upon insertion into the SPRINT profiler, an electric current is applied to induce the complexes to be orientated in the same direction for immobilisation. To count the captured barcodes, imaging software and fluorescent microscopy is utilised which generates digital data where one count is equal to one molecule.

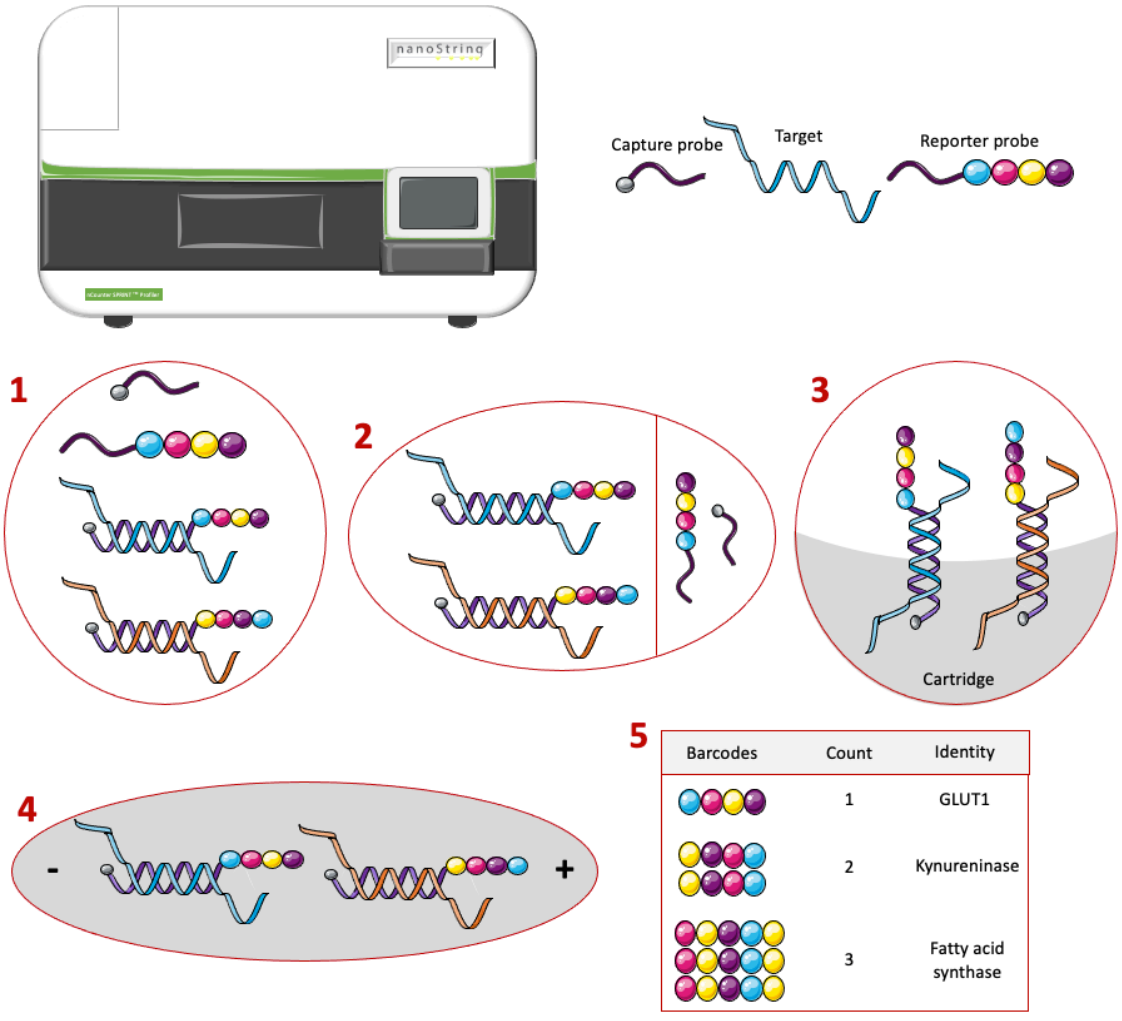

Figure 2.17: Schematic of the NanoString nCounter™ SPRINT profiler. (1) The hybridisation process occurs. A reporter probe with a unique barcode binds to a target sequence as well as a capture probe to produce reporter complexes. **(2)** Reporter complexes are immobilised and excess probes are washed away. **(3)** The immobilised complexes bind to the cartridge. **(4)** An electric current is applied inducing the complexes to orient in the same direction. **(5)** The individual colour barcodes are counted and collated.

2.11.1 Sample preparation

1 x 10^6 of monocytes were washed with 1 ml RPMI 1640/Glutamax and centrifuged at 8,000 *x g* for 4 mins. The cells were re-suspended with diluted RLT buffer (Qiagen, UK) (1/3 with

RNase-free water; Invitrogen) so that the concentration is at 10,000 cells / µl, and frozen at -80°C.

2.11.2 Hybridisation

To attach reporter and capture probes to sample RNA, a hybridisation reaction must occur. A master mix is first prepared by the addition of 70 µl hybridisation buffer (NanoString, USA) to the reporter CodeSet (NanoString, USA). 8 µl of this master mix is aliquoted into PCR tubes with 4.5 µl cell lysate and 0.5 µl RNase-free water to bring total volume to 13 µl per tube. The Capture ProbeSet (NanoString, USA) is then added at 2 µl per tube (final volume 15 µl). Samples are then placed in a ThermoCycler for 20 hrs where the sample temperature was set at 65°C and the lid temperature at 70°C.

2.11.3 Running cartridge

The cartridge is brought to room temperature 15 mins before the hybridisation reaction is completed. Samples are brought to 35 µl final volume with RNase-free water (also accounting for any evaporation in the hybridisation process). 33 µl of samples were added to the sample ports on the cartridge and run immediately on the nCounter® SPRINT (NanoString, USA).

2.11.4 Data analysis

Data analysis was performed using the advanced analysis package (2.0.134 within the nSolver analysis software (Version 4.0, NanoString). XQuartz (version 2.8.1 for macOS) was required to use this wizard.

2.12 Statistics

All statistics were carried out using GraphPad Prism© V9. Data sets were first tested for normality using the Kolmogorov-Smirnov (K-S) one sample test, where a significant value <0.05 indicated signification deviation from normality. Where only two data sets are analysed and were not paired samples (e.g., non-pregnant versus pregnant), an unpaired t-test was used if the data was parametric, and a Mann-Whitney tests if the data was non-parametric. In the rare cases where the samples are paired (e.g., serum and plasma from the same donor), a Wilcoxon matched-pairs signed rank test was used, as these were all non-parametric. In

instances where more than two data sets were analysed (e.g., non-pregnant versus pregnant versus cord), a one-way analysis of variance (ANOVA) with a Tukey post-hoc test was performed. ANOVAs determine the variability between three or more groups. Multiple comparison post-hoc tests are required to detect differences between each group, i.e. compare each column mean with every other mean. An example of this: we are measuring an analyte in plasma from non-pregnant, pregnant, and cord blood; the post-hoc tests allow for comparison between non-pregnant and pregnant, non-pregnant and cord, and pregnant and cord. A 2-way ANOVA with a Šídák's multiple comparisons post-hoc test was used when more than two groups analysed (e.g., non-pregnant versus pregnant classical and non-classical monocytes). Depending on if the data reported as parametric or non-parametric, where analysis was needed to observe the degree in which two variables correlate (e.g., BMI versus monocyte percentage) a Pearson or Spearman correlation test was used respectively. The r values are reported to indicate direction (negative values a downward trend; positive values upward trend) and weight of correlation. In all statistical analysis, a p value < 0.05 was determined to be significant.

Chapter 3 - The changing lipidomic profile of pregnancy can be monitored using novel mass spectrometry techniques

3.1 Introduction

Lipidomics, the large-scale study of lipids, has been an emerging field in recent years due to the realisation that lipids are involved in more than membrane structure and energy production. Lipids are now also recognised as involved in signal transduction, regulation of membrane proteins, vesicular trafficking, cytoskeletal rearrangements, and secretion. Because of these vital roles, disruption of lipid metabolism is involved in various pathologies, such as neurological disorders [230], cancer [231], and cardiovascular diseases [232].

3.1.1 PC/LPC

Phosphotidylcholines (PC) are a class of phospholipids that are a major component of cells and vital in supporting membrane bilayers and can be found systemically in the blood bound to lipoproteins. PC itself is produced from phosphatidylethanolamine (PE) via three sequential methylations by S-adenosyl methionine (SAM) catalysed by phosphatidylethanolamine N-methyltransferase (PEMT). PC can also be converted from choline obtained by dietary consumption or metabolism of lipids which contain choline. Cleavage of PC by phospholipase A_2 (PLA_2) produces lysophosphotidylcholine (LPC; Figure 3.1) with free-fatty acids released as by-products such as the precursors for eicosanoids, polyunsaturated fatty acids (PUFAs). Oxidised low-density lipoproteins (oxLDL) are rich in LPC and when the LPC is released by apoptotic cells this stimulates the recruitment of phagocytes [233]. Due to its immune activating properties, for example specifically inducing chemoattractant molecules such as MCP-1 for monocytes [234], high levels of LPC are synonymous with inflammation and have been observed in inflammatory diseases such as atherosclerosis [235]. The metabolism of PC to LPC, measurable as a PC/LPC ratio, then is vital to the pathogenesis of various diseases.

As pregnancy is naturally accompanied by various inflammatory states throughout gestation, the monitoring of the PC/LPC ratio might predict adverse obstetric outcomes known to be associated with inflammation, such as gestational diabetes mellitus (GDM) and preeclampsia. Studies have implicated elevated PCs in the risk of developing GDM, independently of maternal BMI [236-238], increased LPCs in preterm delivery [239], and reduced PCs in preeclampsia [240]. However, traditional methods for the determination of lipid content, including for the PC/LPC ratio, are convoluted and time-consuming, requiring lipids to first be extracted before analysis with mass spectrometry. Angelini et al have produced a method to use 'intact'

samples, (i.e., no processing of the sample required) with the MALDI-ToF to quickly and accurately determine the PC/LPC ratio [241].

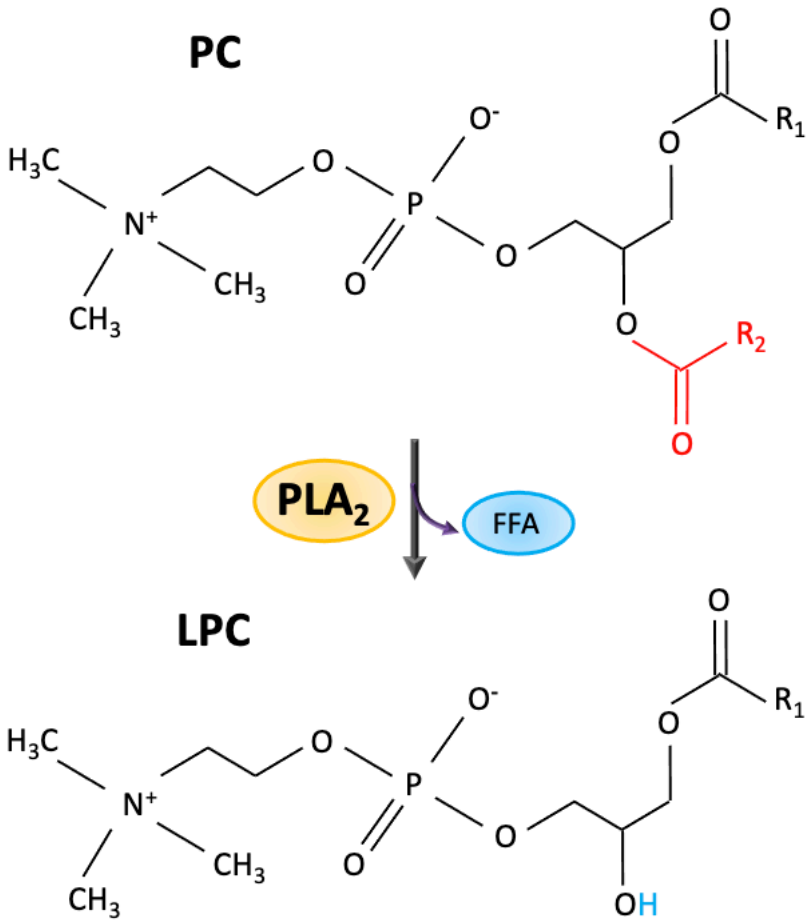

Figure 3.1: The production of LPC from PC in a reaction catalysed by PLA_2.

3.1.2 Lipid Mediators

Inflammation is a protective response instigated by injury or infection, with the intention of removing the initiating stimulus. It also links innate and adaptive immune processes to underpin the establishment of immunological memory providing a quicker and specific response if encountered again. Inflammation also promotes the repair of tissue in the case of injury. Many soluble mediators are produced by tissue resident cells during the inflammatory response, including complement, cytokines, free radicals, eicosanoids such as prostaglandins (PGs), and cytokines. Inflammation needs to be regulated and terminated appropriately. Lipid mediators are immunomodulating molecules which counter regulate the inflammatory process with some sub-types potent pro-inflammatory mediators and others with critical roles in resolution of inflammation. These mediators are derived from PUFAs including docosahexaenoic acid (DHA), eicosapentaenoic acid (EPA) and arachidonic acid (AA).

AA is the main eicosanoid precursor and is found in all cells. Eicosanoids are oxygenated products that are released from a cell and act in a paracrine or autocrine manner on target cells. AAs are metabolised by specific enzymes to form specific eicosanoids. For example, cyclooxygenase (COX) catalyses the production of the prostanoids, namely PGs and thromboxanes (TX); leukotrienes (LTs) and lipoxins (LXs) are produced by lipoxygenases (LOXs); and cytochrome p450 (CYP) enzymes metabolise AAs into epoxyeicosatrienoic acids (EETs) (Figure 3.1).

The biosynthesis of prostanoids is the target of nonsteroidal anti-inflammatory drugs (NSAIDs). Prostanoids have a diversity of functions, for example PGI_2 and PGE_2 enhance oedema through effects on vasodilation and vascular permeability [242]. Whilst typically exhibiting various proinflammatory properties, there are several prostanoids which induce immunosuppressive effects. PGI_2 and PGE_2 can diminish the phagocytosis ability of leukocytes and inhibit downstream proinflammatory mediator production, despite increasing IL-6 and IL-10 production [243-246].

LTs convey information either by paracrine or autocrine signalling and are produced at sites of inflammation. They are generated by granular leukocytes including mast cells as well as macrophages and have a proinflammatory mediator role. Different LTs have distinct roles in compelling various inflammation phases. For example, LTD_4 attracts eosinophils, and LTB_4 is a chemoattractant and activator of monocytes, lymphocytes and neutrophils [247].

5-LOX is one of the various types of LOX enzymes that as well as generating LT, can also produce 5-oxo-6,8.11,14-eicosatetraenoic acid (5-oxo-ETE). 5-oxo-ETE is an autocrine molecule that can be produced by monocytes, neutrophils, eosinophils and basophils. Emerging evidence suggests that 5-oxo-ETE is a potent chemoattractant for eosinophils, but it also induces CD11b expression, calcium mobilisation, L-selectin shedding and actin polymerisation [248, 249]. It can also stimulate survival factors for eosinophils by inducing the secretion of granulocyte-macrophage colony-stimulating factor (GM-CSF) by monocytes [250]. Leukocytes which are primed with GM-CSF and TNFα can also be induced to degranulate and produce superoxides [251].

LXs control the entry of monocytes and granulocytes into sites of inflammation inhibiting the infiltration of granulocytes whilst stimulating noninflammatory monocyte entry for wound healing and inflammatory resolution [252, 253]. Thereby, LXs act as anti-inflammatory mediators. other pro-resolution roles for LCs include promoting macrophage clearance of apoptotic neutrophils and inducing anti-inflammatory cytokines like transforming growth factor β1 (TGF-β1) [254, 255].

EETs also tend to anti-inflammatory mediators. The expression of cell adhesion molecules on granulocytes are supressed by EETs and prevent the cells from adhering to the vascular wall [256]. Platelet aggregation can be inhibited by EETs to prevent or halt thrombosis [257]. Hydroxyeicosatraenoic acid (HETE) can also be produced from catalysis by CYP. EETs can also inhibit leukocytes adhering to the endothelium, but also suppresses LT synthesis [258]. In response to the activation of phospholipases, granulocytes release specific HETEs (20- and 16-HETE) which block platelet aggregation induced by TXs [259].

Specialised pro-resolving mediators (SPM) of inflammation encompass a group of omega-3 PUFA-derived products: resolvins (Rvs; resolution phase interaction products), protectins (PDs) and maresins (MaRs; macrophage mediator in resolving inflammation). Some of the roles of Rvs include blocking the accumulation of dendritic cells and neutrophils at sites of inflammation, inhibiting neutrophil ROS, stimulating the phagocytosis of apoptotic neutrophils by macrophages, regulation of pro-inflammatory cell surface markers on leukocytes, and termination of chemokine signalling [260-263]. The total effect of Rvs are to initiate the resolution of inflammation and induce a decrease of granulocytes at inflammation sites. Like Rvs, there are various members in the PD family. The most well documented is PD1, which is synthesised by PBMCs. It can exert its immunoregulatory effects by inhibiting the migration of neutrophils, inhibiting TLR-mediated activation, suppressing production of proinflammatory lipid mediators and Th2 inflammatory cytokines, and promoting the apoptosis of T cells [264-267]. PD1 has also been shown to have protective effects in oxidative stress. Less is known about MaRs due to their more recent discovery, but it is known that they inhibit granulocyte infiltration and induce macrophage phagocytosis [268].

Lipid mediators are especially important in pregnancy in moderating inflammation. Whilst pregnancy is described as a state of heightened inflammation, persistent and excessive inflammation can result in adverse maternal-fetal outcomes. A pro-inflammatory intrauterine environment poses a higher risk in preterm infants for severe complications [269]. Dietary supplementary of long chain PUFAs (LC-PUFA) in pregnancy has been shown to lower risk of preterm delivery, increased birth weight of the infant, and reduced incidence of maternal allergic conditions such as asthma [270-272].

Pre-eclampsia, which is underpinned excessive inflammation, has been associated with a deficiency in LXA_4, an anti-inflammatory mediator, as well as its receptor and biosynthesis enzyme [273]. Due to this deficiency, pro-inflammatory cytokines induced by LPS are increased, and IL-10, an anti-inflammatory cytokine, levels are reduced; this has been rectified in rat models treated with LXA_4 [273].

3.1.3 Rationale

Pregnancy is associated with many changes in inflammation. The use of novel and more time-efficient techniques to determine changes in PC/LPC ratios or eicosanoids, would allow determination of alterations in gross inflammatory status. Firstly, utility of this approach needs to be confirmed and a range for healthy pregnancy established.

3.1.4 Hypothesis

Novel mass spectrometry techniques will allow for quick determination of inflammatory status using maternal blood samples and predict adverse pregnancy outcomes.

3.2 Materials and Methods

3.2.1 Samples

Cells and plasma from heparin coagulated Vacuettes ©, and serum were obtained from non-pregnant and pregnant women, and umbilical cord as described in *2.1 Human blood collection*.

3.2.2 Monocyte isolation

Monocytes were isolated as in *2.4 Monocyte isolation.*

3.2.3 PC/LPC ratio determination

For intact MALDI, serum samples were diluted in a 1:2 (v:v) ratio with HPLC-grade water (e.g. 10 µl serum with 20 µl water), and intact monocytes were spotted neat. A 10 mg/ml matrix solution of 9-aminoacrinide (9-AA) was produced 1:1, v:v with 2-propanol/acetonitrile (60/40, v/v). 1 µl of the diluted serum or 1 µl of monocytes (equivalent to 20,000 cells) is spotted onto the MALDI target; once dried, 0.5 µl of the 9-AA matrix solution was spotted on top in a "sandwich method". Once the solvents had evaporated, samples were directly analysed by MALDI-TOF MS. This method is described in *2.10 Mass spectrometry*.

The peaks and their identifiers for PC and LPC from sera are shown in Table 3.1. Fewer species of PC and LPC were identifiable in monocytes; those assigned are in Table 3.2. The sum of the intensity of specific PC peaks and the intensity of specific LPC peaks was determined, and the ratio was calculated; $^{\Sigma PC}/_{\Sigma LPC}$.

Assignment (positive ion spectra)	Peak m/z
LPC 16:0 (+H+)	496.3398
LPC 16:0 (+Na+)	518.3241
LPC 18:0 (+H+)	524.2854
LPC 18:0 (+Na+)	546.3554
PC 16:0/18:2 (+H+)	758.5694
PC 16:0/18:1 (+H+)	760.5851
PC 16:0/18:2 (+Na+)	780.5538
PC 16:0/18:1 (+Na+) and PC 16:0/20:4 (+H+)	782.5694
PC 18:0/18:3 (+H+)	784.5851
PC 18:0/18:2 (+H+)	786.6454
PC 16:0/20:4 (+Na+)	804.5749
PC 18:0/18:3 (+Na+)	806.5694
PC 18:0/18:2 (+Na+)	808.5851

Table 3.1: The peak m/z and their assigned molecules as observed in the MALDI-TOF positive ion spectra for human sera.

Assignment (positive ion spectra)	Peak m/z
LPC 16:0 (+H+)	496.3398
LPC 18:0 (+H+)	524.2854
PC 16:0/18:2 (+H+)	758.5694
PC 16:0/18:1 (+H+)	760.5851
PC 16:0/18:1 (+Na+) and PC 16:0/20:4 (+H+)	782.5694
PC 18:0/18:3 (+H+)	784.5851
PC 18:0/18:2 (+H+)	786.6454
PC 18:0/18:2 (+Na+)	808.5851

Table 3.2: The peak m/z and their assigned molecules as observed in the MALDI-TOF positive ion spectra for human monocytes.

3.2.4 Eicosanoids with LC-MS/MS

Plasma samples from non-pregnant women, pregnant women at term (37+ weeks) and cord were sent to Toulouse Institute for Infectious and Inflammatory Disease for analysis on their lipidomic platform, using the method from Le Faouder et al [274]. Eicosanoids which were measurable can be seen in Figure 3.2, and those that were actually detectable in the plasma samples can be seen in Table 3.3. The eicosanoids are classified as by Le Faouder at al [274].

Inactive products	Pro-Inflammatory mediators	Oxidative stress markers
TXB_2	PGE_2	9-HODE
5,6-DiHETE	PGF_{2a}	13-HODE
Pathway markers	5-oxo-ETE	8-iso-PGA_2
5-HETE	**Pro-resolving mediators**	**Bioactive mediators**
15-HETE	RvD5	8-HETE
14-HDoHE	LxA4	12-HETE
17-HDoHE	PDx	
18-HEPE	PGD_2	

Table 3.3: The classification of each eicosanoid which was quantifiable in plasma samples for non-pregnant, pregnant and cord.

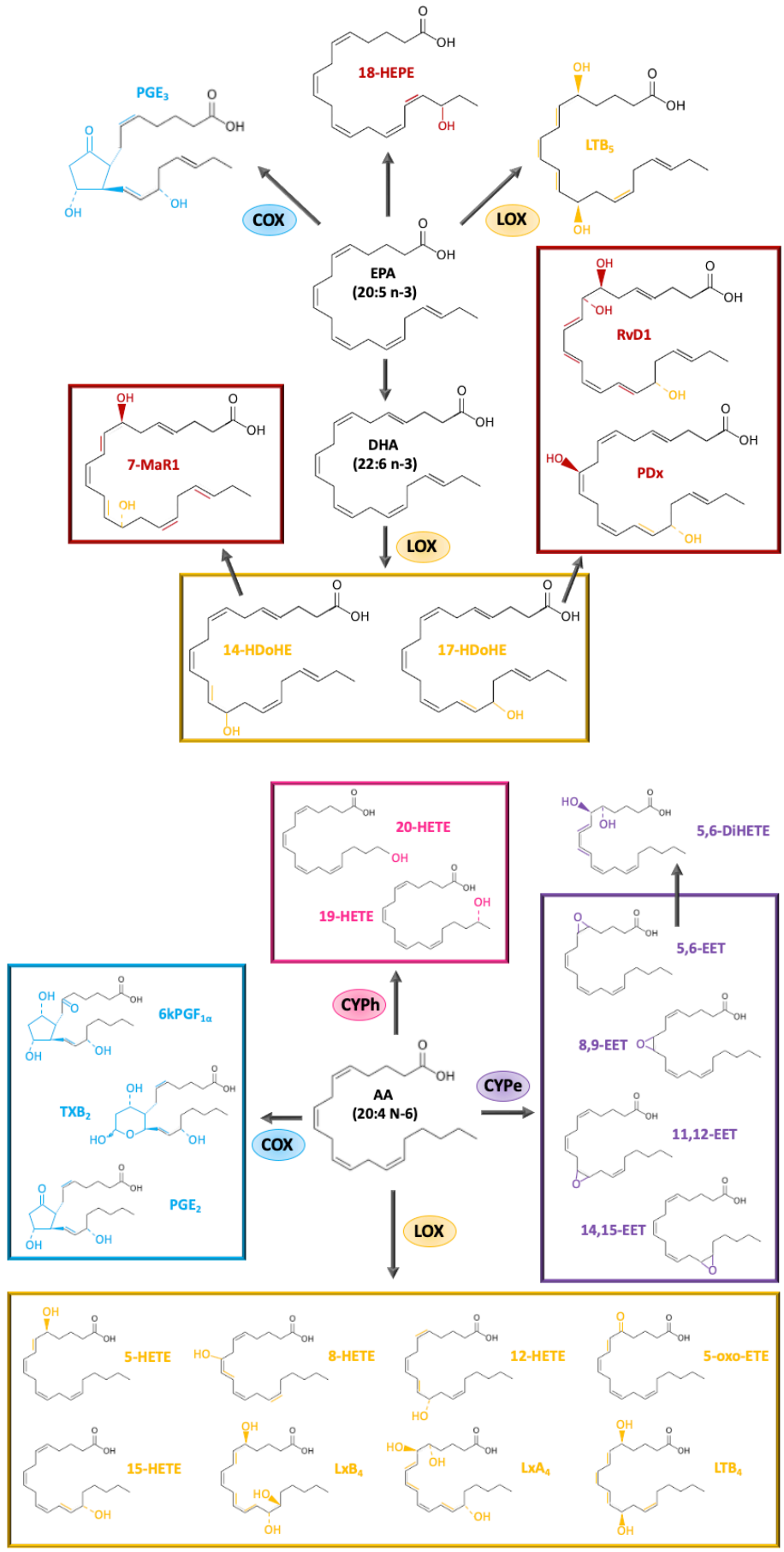

Figure 3.2: The synthesis of eicosanoids from the precursor arachidonic acid (AA), and the enzymes involved.

3.3 Results

3.3.1 Serum is chosen over plasma for the determination of PC/LPC

The development of the method for determining the PC/LPC ratio using MALDI-ToF was developed using horse serum samples [241]. While serum was easier to attain for multiple stages of gestation for this project, the first step was to investigate if there was a difference between heparin-plasma and serum. Samples used for this were matched, i.e., the blood for plasma and serum was taken from the same non-pregnant patient at the same time. There was a substantial increase in the PC/LPC ratio for plasma in comparison to serum, however the plasma also had a larger standard deviation (SD; Figure 3.3).

The use of serum for the determination of the PC/LPC ratio range for further work, was due in part to the low SD across all the samples, and it is also in line with the method development by Angelini et al [241]. While plasma is typically considered by our group and others to be the optimal type of sample to use, due to the absence of coagulation allowing a closer resemblance to the individual's systemic blood, LPC levels are also increased in serum samples [275]. Some studies have induced the release of LPC from blood lipoproteins by treating plasma with peptide hydrolytic enzymes such as pepsin to allow for better quantification of LPC [276]. That LPC is already higher in the serum removes the need for treatment with pepsin as the clotting process naturally releases LPC [275].

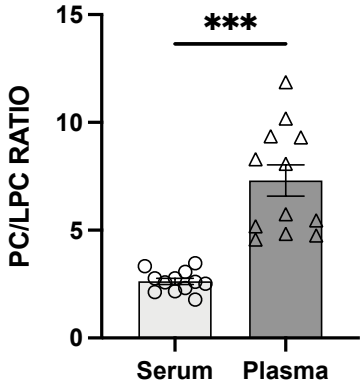

Figure 3.3: The comparison of plasma vs serum for the determination of the PC/LPC ratio. Matched serum and plasma samples from non-pregnant women (n = 12) were analysed using MALDI-ToF for determination of their PC/LPC ratio. Statistical difference was determined using a Wilcoxon test, where a $p < 0.05$ was significant. The samples for serum (SD = 0.4963) were compared with plasma (SD = 2.511, $p = 0.0005$).

3.3.2 The PC/LPC ratio is significantly altered throughout gestation in sera

Archived serum samples from non-pregnant women (aged 18-40), pregnant women (at 16, 28 and 37+ weeks) and umbilical cord were analysed using MALDI-ToF to determine the

PC/LPC ratio. 15 samples were used for each group, except for pregnant at 16 weeks where 11 were used due to lack of available samples.

The PC/LPC ratio increases significantly as gestation progresses (Figure 3.4), with their reference values seen in Table 3.4. This indicates that the maternal circulation in pregnancy is becoming more anti-inflammatory as pregnancy progresses. Cord serum has a similar PC/LPC ratio to that of non-pregnant adults rather than pregnant women. Example whole spectra for each group can be observed in Figure 3.5. Example spectra focussing specifically on the PC region (Figure 3.6) and the LPC region (Figure 3.7) for each group analysed can also be observed separately.

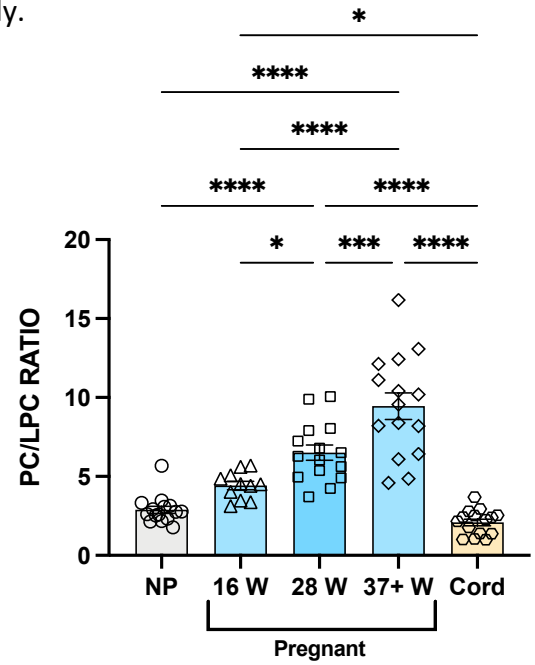

Figure 3.4: The determination of the PC/LPC ratio throughout pregnancy and in cord blood. Serum samples from non-pregnant (NP; n = 15), pregnant (P) at 16 weeks (16W; n = 11), 28 weeks (28W; n = 15) and term (37+W; n = 15), and cord (C; n = 15), were analysed using MALDI-ToF to determine their PC/LPC ratio. Statistics were performed using an ordinary one-way ANOVA and a Tukey post-hoc test, where $p < 0.05$ was significant. All groups were compared with each other: NP vs P-16W ($p = 0.2320$), NP vs P-28W ($p < 0.0001$), NP vs P-37+W ($p < 0.0001$), NP vs C ($p = 0.7643$), P-16W vs P-28W ($p = 0.0460$), P-16W vs P-37+W ($p < 0.0001$), P-16W vs C ($p = 0.0182$), P-28W vs P-37+W ($p = 0.0004$), P-28W vs C ($p < 0.0001$), and P-37+W vs C ($p < 0.0001$).d

		Range	Mean	SD	SEM
Non-Pregnant		1.780 - 5.675	2.884	0.901	0.233
Pregnant	**16W**	3.120 - 5.684	4.425	0.865	0.261
	28W	3.708 - 10.060	6.506	1.875	0.484
	37+W	4.685 - 16.18	9.456	3.253	0.840
Cord		0.995 - 3.688	2.090	0.802	0.207

Table 3.4: PC/LPC reference ranges for serum from non-pregnant and pregnant women, and umbilical cord. The mean, standard deviation (SD) and standard error of the mean (SEM) are also shown for each group.

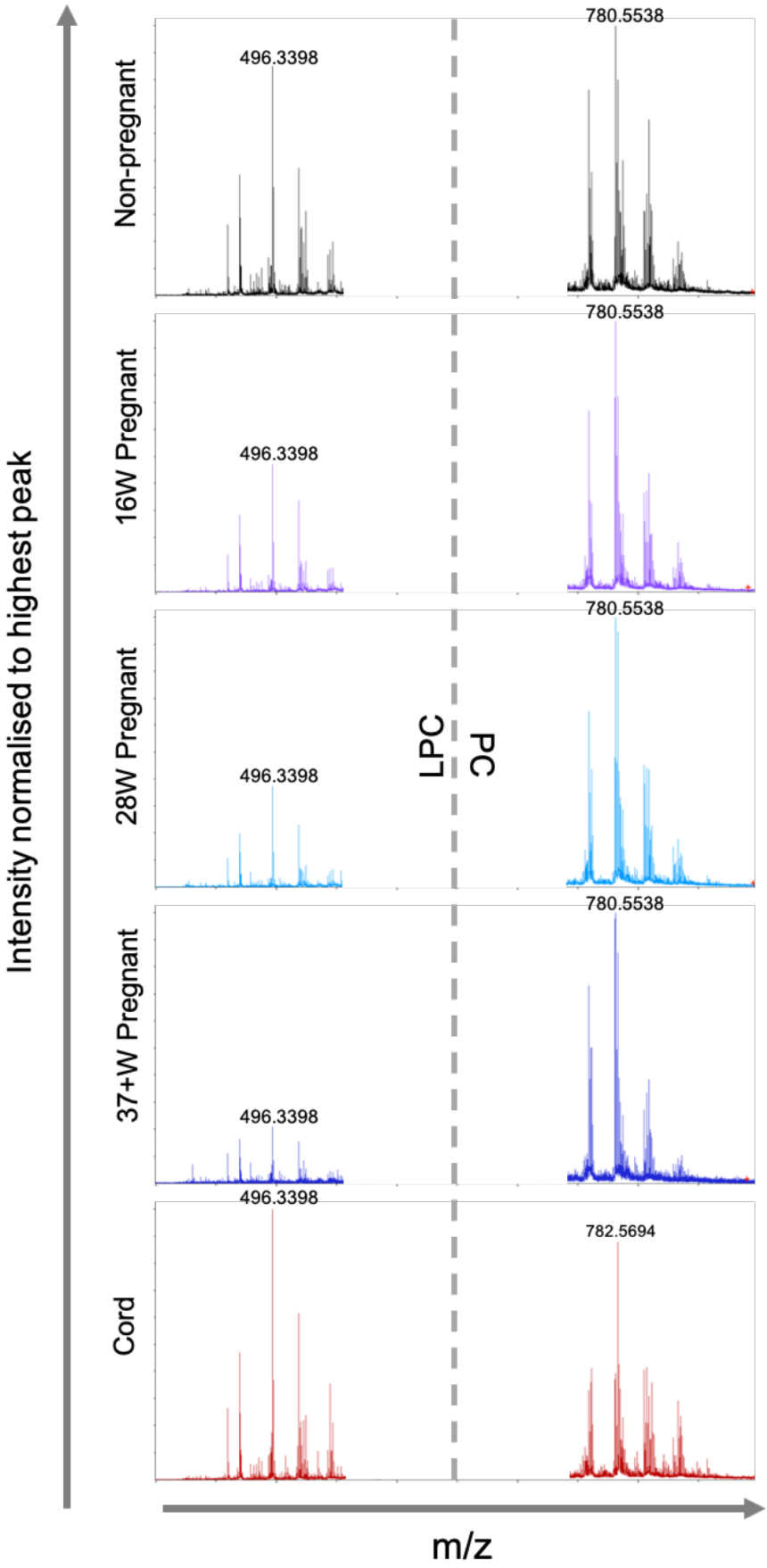

Figure 3.5: Example full spectra for each group analysed. Non-pregnant (black), 16 weeks pregnant (purple), 28 weeks pregnant (light blue), term (37+ weeks) pregnant (dark blue), cord (red). LPC molecules lie in the 490 – 550 m/z range, whereas the PC molecules lie in the 760 – 820 m/z range. Spectra in between these ranges have been excluded due to lack of interest. The most abundant LPC and PC molecules are labelled with their m/z value.

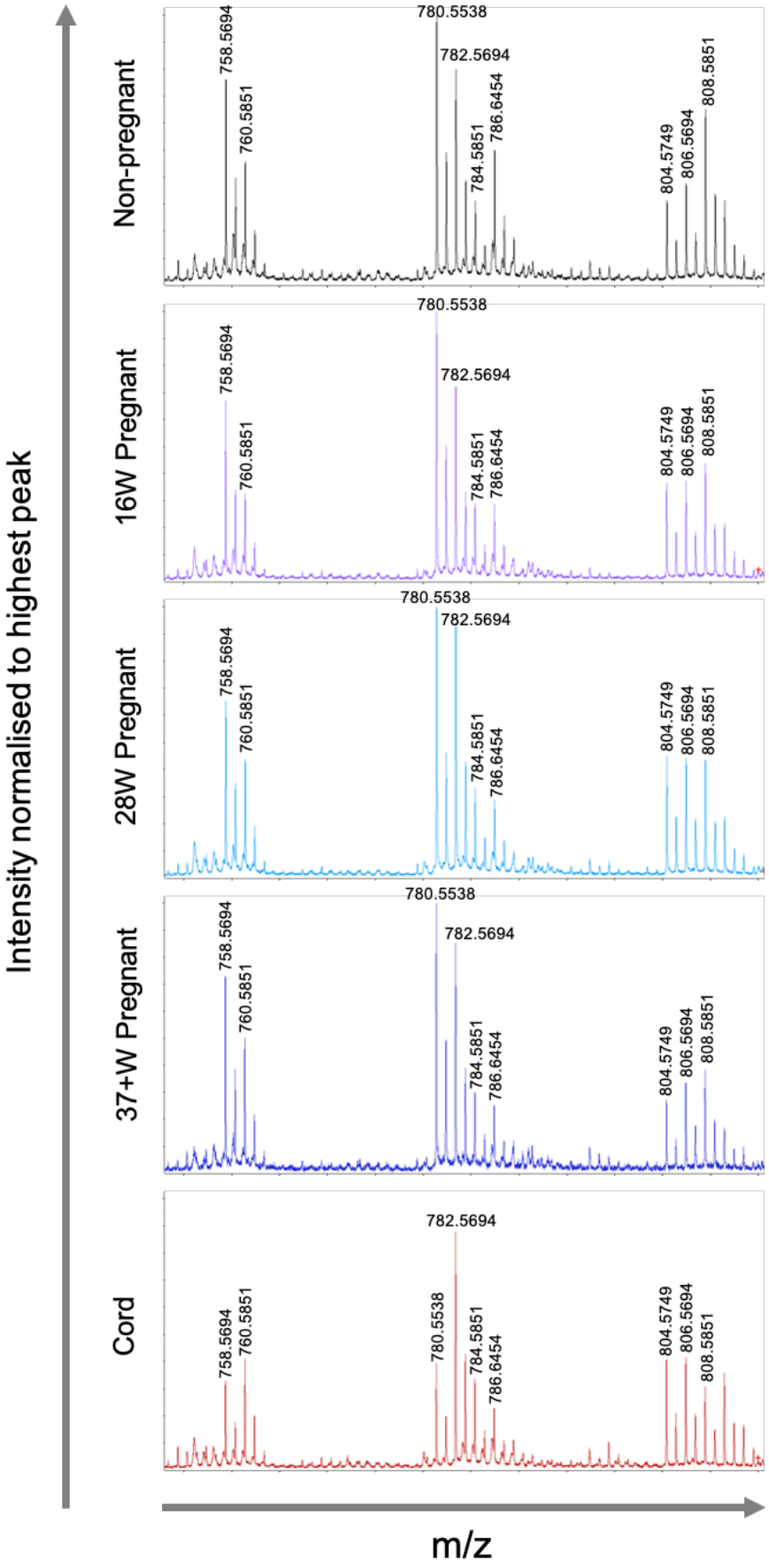

Figure 3.6: Example spectra for each group analysed, with a focus on the PC molecule region. Non-pregnant (black), 16 weeks pregnant (purple), 28 weeks pregnant (light blue), term (37+ weeks) pregnant (dark blue), cord (red). Peaks which were used for analysis are labelled with their m/z value.

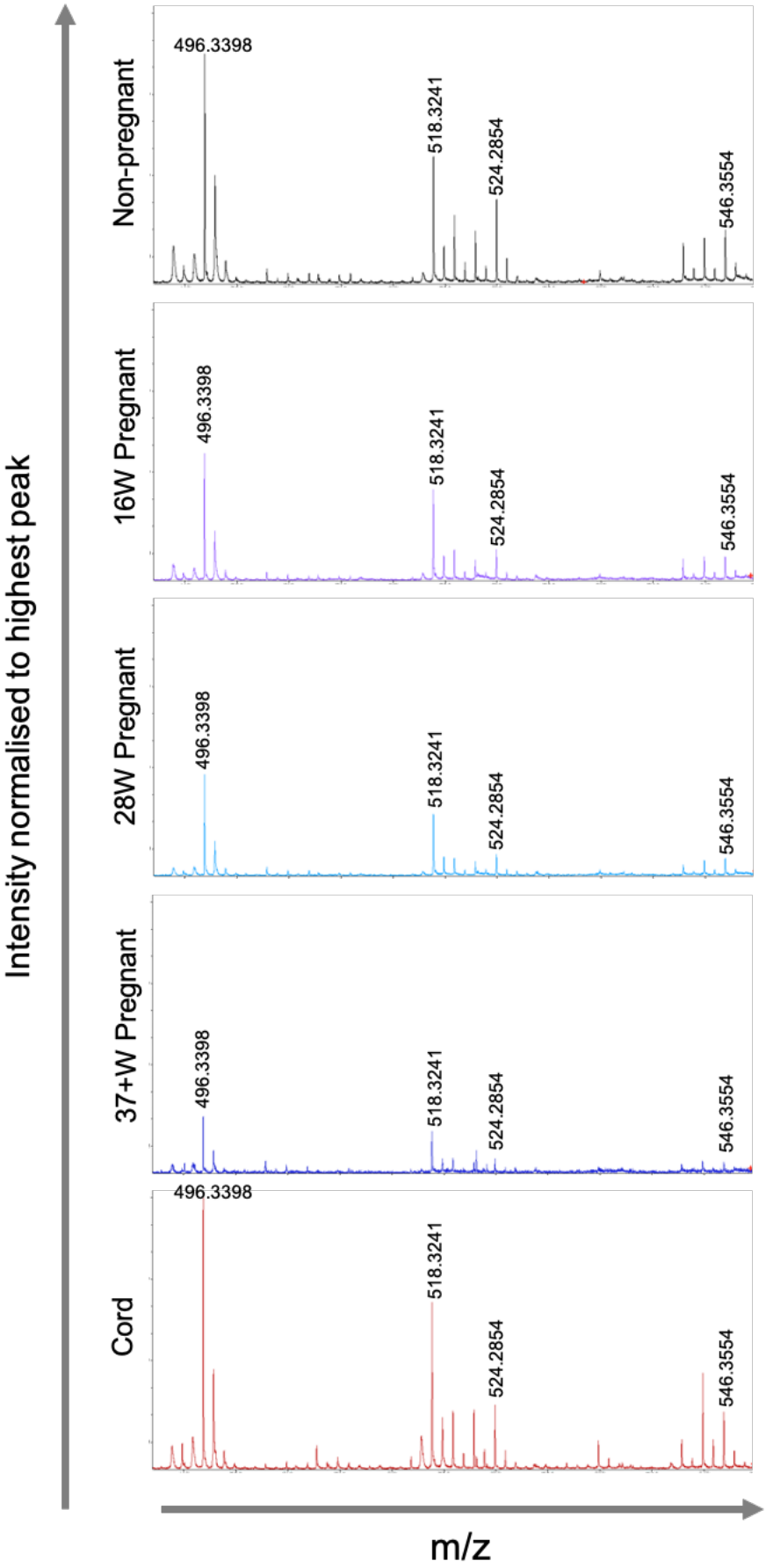

Figure 3.7: Example spectra for each group analysed, with a focus on the LPC molecule region. Non-pregnant (black), 16 weeks pregnant (purple), 28 weeks pregnant (light blue), term (37+ weeks) pregnant (dark blue), cord (red). Peaks which were used for analysis are labelled with their m/z value.

3.3.3 Obesity does not affect the PC/LPC ratio in serum samples

To determine if obesity influenced the PC/LPC ratios observed, the individual ratio quantities were correlated with the BMI from the patient (in regard to the cord samples, this was the mother's BMI). As observed in Figure 3.8, BMI has no significant correlation to the PC/LPC ratio in serum from any of the groups measured. However, the PC/LPC ratio at 16-weeks of gestation, shows a trend to down-regulation with obesity. This suggests an increase in inflammation with obesity, which is unsurprising. That this is only evident at the earlier gestation time-point could be indicative of the elevated risk of miscarriage at this stage [277].

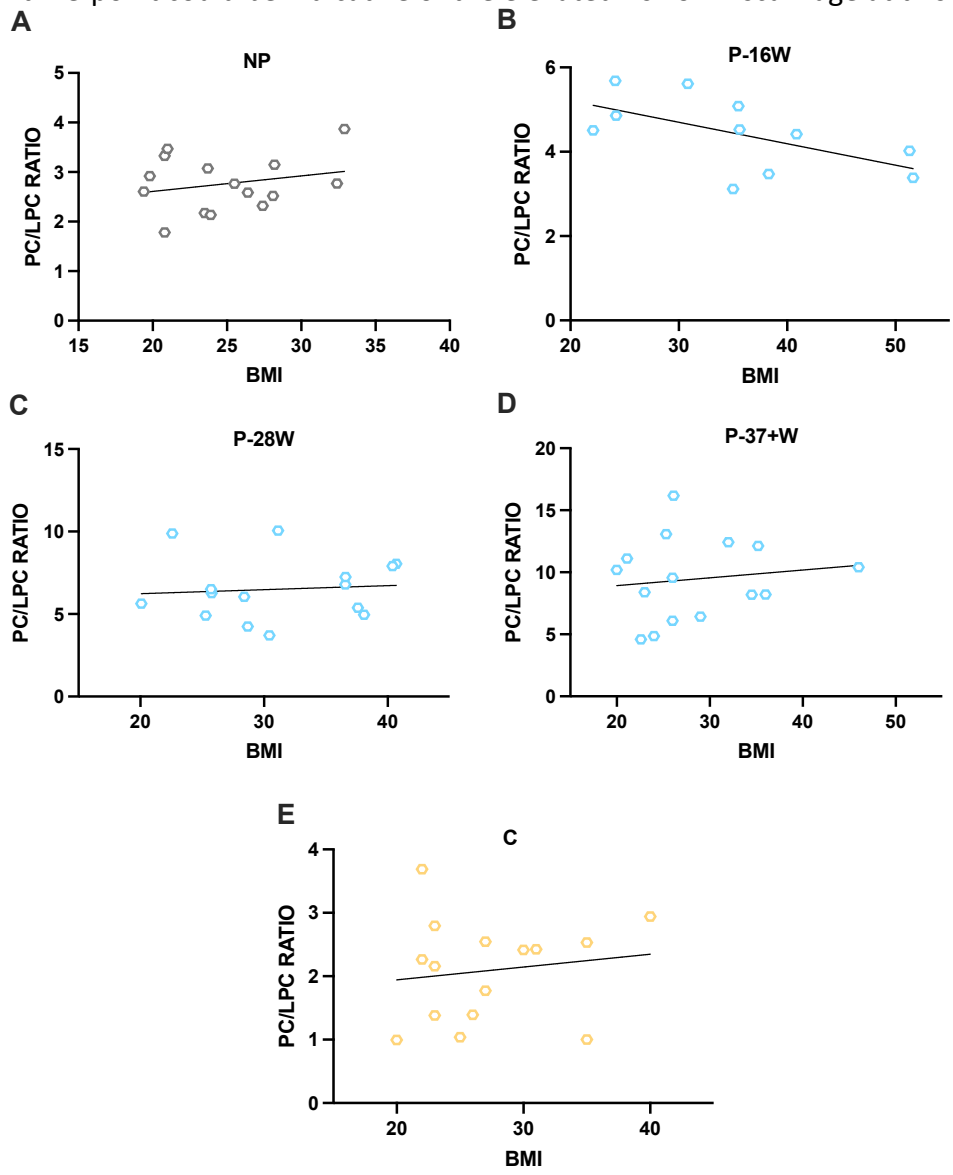

Figure 3.8: The effect of BMI on the PC/LPC ratio in serum from non-pregnant, pregnant at different gestations and cord. The PC/LPC ratio determined for non-pregnant (NP), pregnant (P) at 16 weeks (16W; n = 11), 28 weeks (28W; n = 15) and term (37+W; n = 15), and cord (C; n = 15) was used to determine if BMI influenced individual samples. For the cord samples, the mother's BMI was taken into consideration. All groups passed the Kolmogorov-Smirnov normality test, and so statistics were determined using the Pearson r test, where $p < 0.05$ indicated a significant correlation between BMI and PC/LPC ratio. Groups measured were: **(A)** NP ($r = 0.2426$, $p = 0.3836$), **(B)** P-16W ($r = -0.5890$, $p = 0.0566$), **(C)** P-28W ($r = 0.08717$, $p = 0.7574$), **(D)** P-37+W ($r = 0.1364$, $p = 0.6278$) and **(E)** C ($r = 1464$, $p = 0.6025$).

3.3.4 The PC/LPC ratio is significantly affected by GDM at 16 weeks of gestation, but not at 28 weeks.

To determine if this novel method for determining the PC/LPC ratio can be used as a diagnostic tool, sera from pregnancies complicated with GDM at 16 weeks and 28 weeks of gestation was readily available. These were used in comparison to healthy pregnancies at the two different timepoints. There is a significant decrease in the PC/LPC ratio in the pregnancies complicated with GDM at 16 weeks, but the decrease at 28 weeks is not significant (Figure 3.9). There is also too much overlap in the range to precisely diagnose GDM at 16 weeks of gestation, despite the significant change (Table 3.5).

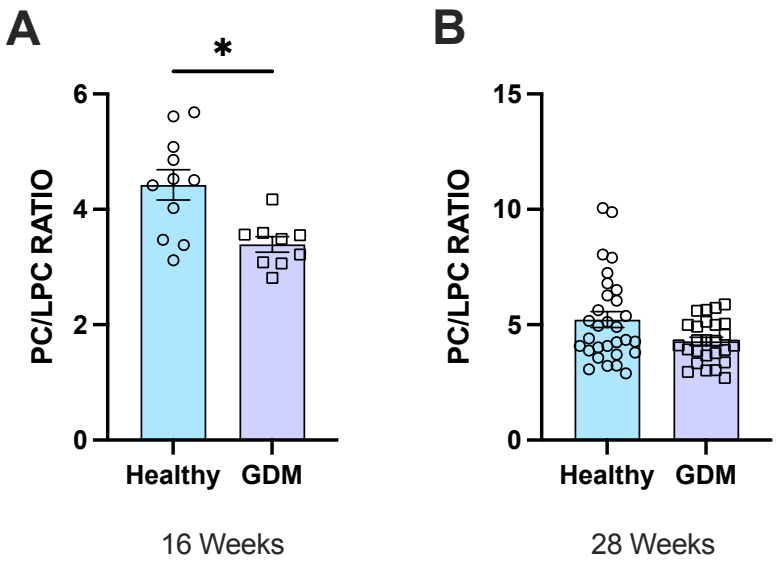

Figure 3.9: The PC/LPC ratio for healthy pregnant women versus pregnant women with GDM at 16 weeks and 28 weeks of gestation. Sera samples from healthy pregnant women (blue; n=11 16W, n=30 28W) and pregnant women with GDM (purple; n=29 16W, n=26 28W) were analysed on the MALDI-ToF as described in the materials and methods. Statistics were determined using a Mann-Whitney t test where $p < 0.05$ was significant. Times of gestation measured were at: **(A)** 16 weeks ($p = 0.0125$) and **(B)** 28 weeks ($p = 0.0990$).

		Range	Mean	SD	SEM
16W	Healthy	3.120 - 5.684	4.425	0.865	0.261
	GDM	2.814 - 4.174	3.394	0.401	0.134
28W	Healthy	2.895 - 10.060	5.224	1.902	0.347
	GDM	2.692 - 5.883	4.277	0.924	0.181

Table 3.5: Descriptive statistics for the PC/LPC ratio for healthy pregnant women versus pregnant women with GDM at 16 weeks and 28 weeks of gestation.

3.3.5 The PC/LPC ratio in monocytes is not affected by pregnancy

To determine if the same MALDI-ToF method which was used for serum could also be used for the measurement of PC/LPC ratio in cells, intact monocytes were used. Monocytes are a key component of inflammation, and so the investigation into this ratio in pregnancy was

logical. Monocytes were isolated from non-pregnant and pregnant women at 37+ weeks and spotted directly onto the MALDI target for analysis. There was no significant difference in the PC/LPC ratio in the monocytes from pregnant women at term in comparison to non-pregnant women (Figure 3.10). Examples of whole spectra (Figure 3.11), and of the specific LPC (Figure 3.12) and PC (Figure 3.13) regions for monocytes can be seen below.

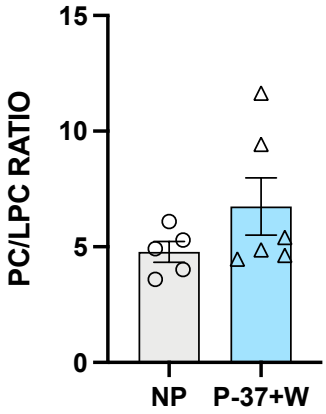

Figure 3.10: The PC/LPC ratio in intact monocytes during pregnancy at term. Isolated monocytes from non-pregnant (n = 5) and term (37+ weeks) pregnant (n = 6) women were analysed intact on the MALDI-ToF. Statistical analysis was with a Mann-Whitney test, where $p < 0.05$ was deemed significant. The PC/LPC ratio was measured for both groups ($p = 0.4286$).

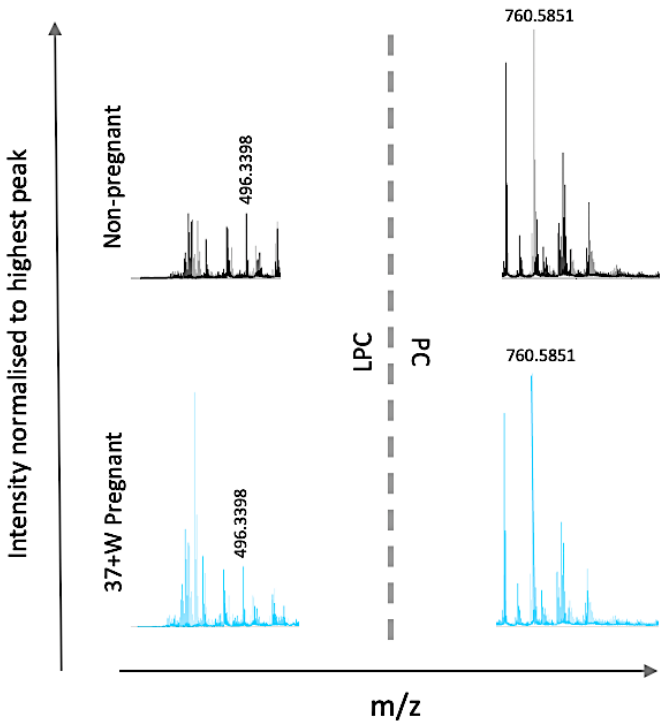

Figure 3.11: Example full spectra for the analysis of monocytes from non-pregnant and pregnant women. Non-pregnant (black) and term (37+ weeks) pregnant (blue) women. LPC molecules lie in the 490 – 550 m/z range, whereas the PC molecules lie in the 760 – 820 m/z range. Spectra in between these ranges have been excluded due to lack of interest. The most abundant LPC and PC molecules are labelled with their m/z value.

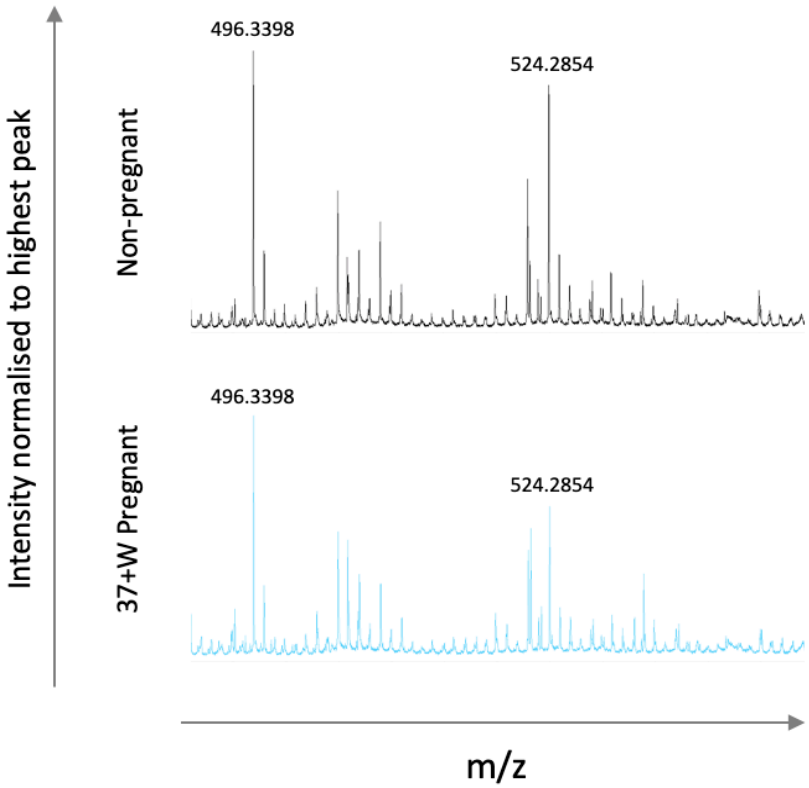

Figure 3.12: Example spectra for each group analysed in monocytes, with a focus on the LPC molecule region. Non-pregnant (black), pregnant at term (blue). Peaks which were used for analysis are labelled with their m/z value.

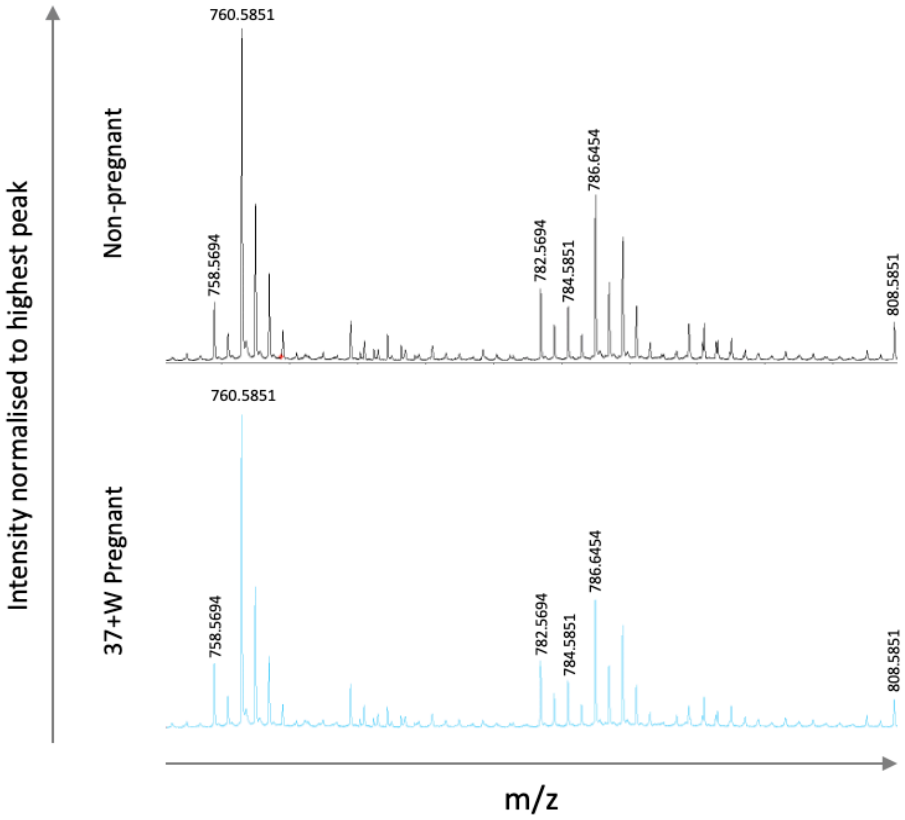

Figure 3.13: **Example spectra for each group analysed in monocytes, with a focus on the PC molecule region**. Non-pregnant (black), pregnant at term (blue). Peaks which were used for analysis are labelled with their m/z value.

3.3.6 Plasmas from the neonate exhibit a marked increase in eicosanoids

Due to the low levels of these molecules, plasma was used for analysis as the clotting factors in serum can conceal some lipid biomarkers [275]. These lipid mediators are sectioned into classifications set out by Le Faouder et al., for ease of discussion [274].

3.3.5.1 Inactive metabolites/products of compounds such as thromboxane A2 and eicosapentaenoic acid are typically removed as waste products.

These include thromboxane B2 (TXB_2) and 5,6-dihydroxyeicosapentaenoic acid (5,6-DiHETE) respectively (Figure 3.14). 5,6-DiHETE has been described recently to have a role in attenuating vascular hyperpermeability [278]. 5,6-DiHETE is elevated in umbilical cord blood plasma in comparison to that of non-pregnant adults (p = 0.0092). It also appears that 5,6-DiHETE is present in much higher levels in pregnant compared to non-pregnant women, but this is significant.

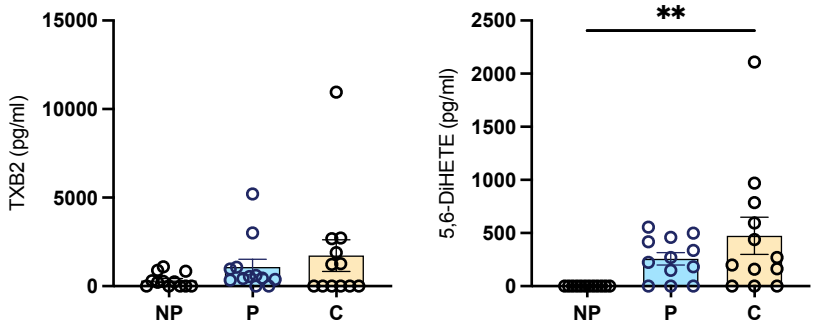

Figure 3.14: Inactive product concentrations in plasma samples from non-pregnant and pregnant women at term, and from cord samples. Plasma from heparin-coagulated tubes from non-pregnant women (grey; NP), pregnant women at 37+ weeks (blue; P) and cord (orange; C) was analysed using LC-MS/MS for the presence of eicosanoids. Statistics were performed using an ordinary one-way ANOVA and a Tukey post-hoc test, where $p < 0.05$ was significant. Inactive products that were measured were: TXB_2 (NP vs P p = 0.6242; NP vs C p = 0.2127; P vs C p = 0.7126) and 5,6-DiHETE (NP vs P p = 0.2145; NP vs C p = 0.0092; P vs C p = 0.3297).

3.3.5.2 There are eicosanoids which are pathway markers, which signify biosynthesis of specific marker activation.

5-hydroxyeicosatetraenoic acid (5-HETE) is a metabolite of arachidonic acid that induces cell activation by binding to the oxoeicosanoid receptor 1 (OXER1) and triggers cell signalling pathways to produce a functional response. This functional response includes activation of pathways such as P13K/Akt and the MAPK/ERK. 5-HETE can also inhibit neutrophils NETs formation [279]. As the neonate is less capable of forming NETs than adults [280], the significant increase in 5-HETE (Figure 3.15) could contribute to this. 15-HETE can activate cells via the leukotriene B4 receptor 2 (BLT2) or peroxisome proliferator-activated receptor gamma

(PPARγ). Like 5-HETE, 15-HETE mimics autocrine and paracrine signalling agents to regulate inflammation. The increase in 15-HETE observed in the cord plasma compared to both the non-pregnant (p = 0.0044) and pregnant (p = 0.0290) adults is significant (Figure 3.15). 14- and 17-hydroxydocosahexaenoic acid (14-HDoHE, 17-HDoHE) are both human xenobiotic metabolites and are also significantly elevated in the neonate compared to the non-pregnant adult (p = 0.0054, p = 0.0087 respectively; Figure 3.15). 18-hydroxyleicosapentaenoic acid (18-HEPE) has been found to inhibit macrophage-mediate proinflammatory activation [281]. This is elevated in the neonate compared to the non-pregnant adult (p = 0.0372; Figure 3.15).

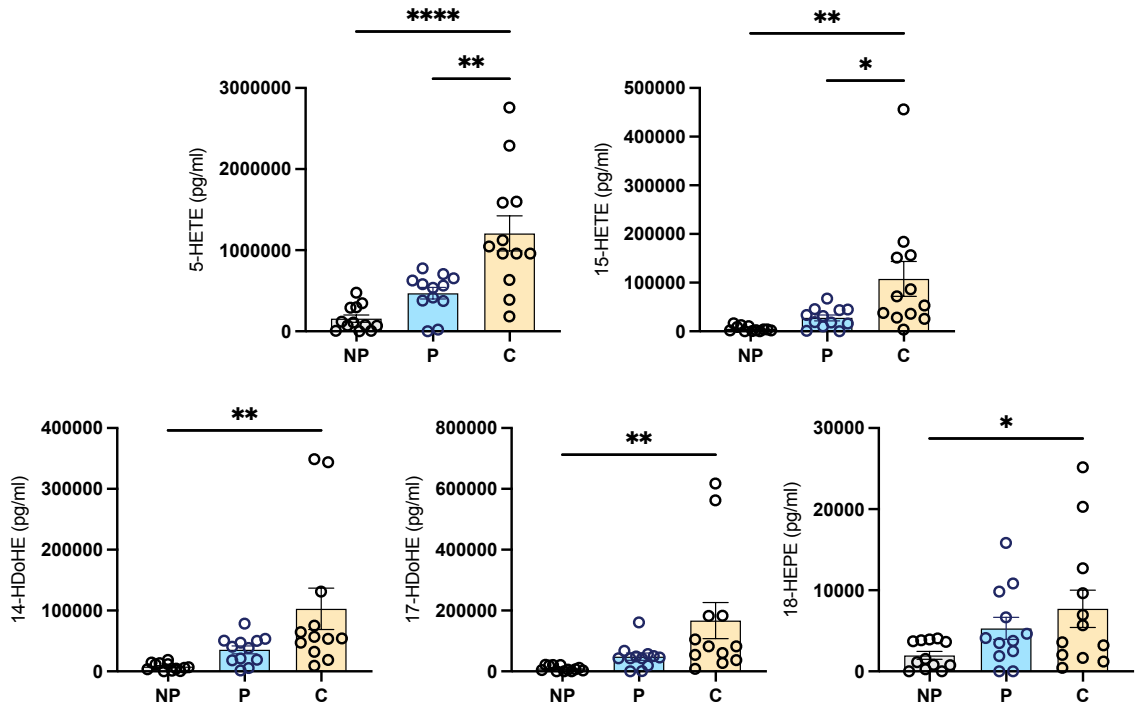

Figure 3.15: Pathway marker concentrations in plasma samples from non-pregnant and pregnant women at term, and from cord samples. Plasma from heparin-coagulated tubes from non-pregnant women (grey; NP), pregnant women at 37+ weeks (blue; P) and cord (orange; C) was analysed using LC-MS/MS for the presence of eicosanoids. Statistics were performed using an ordinary one-way ANOVA and a Tukey post-hoc test, where $p < 0.05$ was significant. Pathway markers that were measured were: 5-HETE (NP vs P p = 0.2369; NP vs C p < 0.0001; P vs C p = 0.0013, 15-HETE (NP vs P p = 0.7367; NP vs C p = 0.0044; P vs C p = 0.0290), 14-HDoHE (NP vs P p = 0.5970; NP vs C p = 0.0054; P vs C p = 0.0580), 17-HDoHE (NP vs P p = 0.7138; NP vs C p = 0.0087; P vs C p = 0.0566), and 18-HEPE (NP vs P p = 0.3062; NP vs C p = 0.0372; P vs C p = 0.5273).

3.3.5.3 Other eicosanoids can be termed bioactive mediators, those which do not demonstrate clear-cut pro-resolving or pro-inflammatory properties.

8-HETE is a natural agonist of PPAR alpha (PPARα), whereas 12-HETE is involved in many inflammatory responses. 12-HETE is involved in chemotaxis and aggregation of neutrophils, localisation of monocytes to vascular endothelial cells, and local accumulation of neutrophils and MNCs at sites of injection. It has been implicated in various diseases such as rheumatoid arthritis [282], and cholestasis [283]. As such, 12-HETE could act as a biomarker for intrahepatic

cholestasis (liver disorder exhibits with intense itching) in pregnancy. Both 8-HETE and 12-HETE appear to be increased in pregnant versus non-pregnant women, although this is not significant, with umbilical cord levels significantly higher than both (8-HETE NP p= 0.0003, P p = 0.0291; 12-HETE NP p = 0.0003, P p = 0.0333; Figure 3.16).

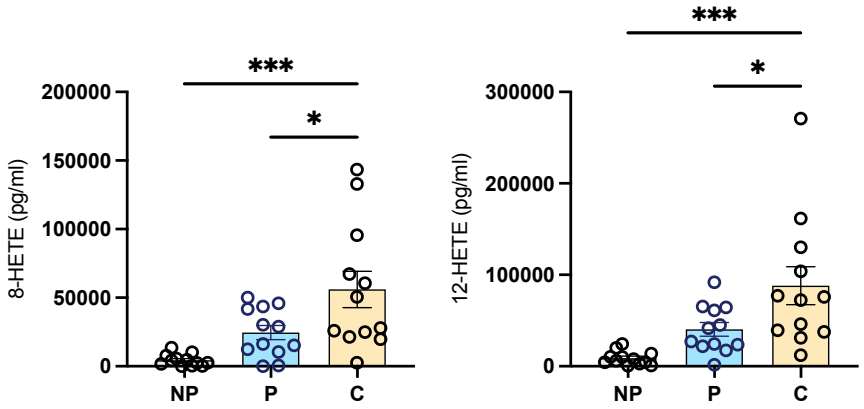

Figure 3.16: Bioactive mediator concentrations in plasma samples from non-pregnant and pregnant women at term, and from cord samples. Plasma from heparin-coagulated tubes from non-pregnant women (grey; NP), pregnant women at 37+ weeks (blue; P) and cord (orange; C) was analysed using LC-MS/MS for the presence of eicosanoids. Statistics were performed using an ordinary one-way ANOVA and a Tukey post-hoc test, where $p < 0.05$ was significant. Bioactive mediators that were measured were: 8-HETE (NP vs P p = 0.2104; NP vs C p = 0.0003; P vs C p = 0.0291), and 12-HETE (NP vs P p = 0.2054; NP vs C p = 0.0003; P vs C p = 0.0333).

3.3.5.4 Some lipid mediators are well recognised for their potent pro-inflammatory effects.

Prostaglandin E_2 (PGE2) has oxytocic properties and can be used as medication to induce labour [284], terminate a pregnancy [285] and is also used on neonates with congenital heart defects [286]. It is also involved in the regulation of lymphocyte function and promotes Th2, Th17 and Treg responses [287]. There is a significant increase of PGE2 in the plasma from both the pregnant women (p = 0.0024) and the cord (p = 0.0175) in comparison to the non-pregnant (Figure 3.17). PGF2a has also been used to induce labour [288], and is active in the menstrual cycle to cause luteolysis [289]. The significant elevation of PGF2a in the cord compared to adults (p = 0.0011) and pregnant women (p = 0.0016) is novel (Figure 3.17). 5-oxo-eicosatetraenoic acid (5-oxo-ETE) is a potent cell signalling metabolite of the 5-HETE family and is particularly effective in stimulating eosinophils. It has various interactions with leukocytes and enhances chemotaxis, production of other eicosanoids, degranulation, and oxidative metabolism [290]. As well as eosinophils, 5-oxo-ETE exerts these enhancements on monocytes and other PMNs [291]. Pregnancy has significantly higher levels of 5-oxo-ETE than non-pregnant adults (p = 0.0003) and cord (p = 0.0060), indicative of an environment rich in monocytes and neutrophils [6, 292].

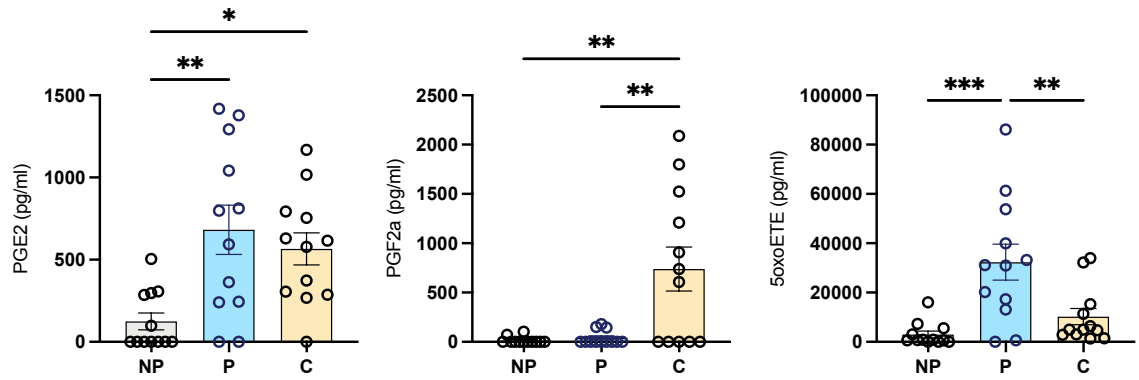

Figure 3.17: Proinflammatory mediator concentrations in plasma samples from non-pregnant and pregnant women at term, and from cord samples. Plasma from heparin-coagulated tubes from non-pregnant women (grey; NP), pregnant women at 37+ weeks (blue; P) and cord (orange; C) was analysed using LC-MS/MS for the presence of eicosanoids. Statistics were performed using an ordinary one-way ANOVA and a Tukey post-hoc test, where $p < 0.05$ was significant. Proinflammatory mediators that were measured were: PGE2 (NP vs P $p = 0.0024$; NP vs C $p = 0.0175$; P vs C $p = 0.7275$), PGF2a (NP vs P $p = 0.9896$; NP vs C $p = 0.0011$; P vs C $p = 0.0016$), and 5-oxo-ETE (NP vs P $p = 0.0003$; NP vs C $p = 0.5262$; P vs C $p = 0.0060$).

3.3.5.5 Anti-inflammatory, pro-resolution biological effects are characteristic of another subset of lipid mediators.

Resolvin D5 (RvD3) is involved in the resolution of inflammation [293]. There seems to be a higher concentration of RvD5 in pregnancy than in the non-pregnant plasma, but this is not significant; however the plasma from the cord is significantly more rich in RvD5 than in the non-pregnant adults ($p = 0.0152$; Figure 3.18). Lipoxin A4 (LxA4) is an example of an autacoid which inhibit inflammatory processes such as superoxide production, NF-κB activation, chemotaxis and proinflammatory cytokine production by PMNs and monocytes [294, 295]. LxA4 is present in cord plasma in significantly higher concentrations than both the non-pregnant ($p = 0.0002$) and pregnant ($p = 0.0051$) adults (Figure 3.18). Some of the pro-resolving actions that protectin DX (PDx) has involves the inhibition of COX-1 and COX-2 to prevent further production of pro-inflammatory prostaglandins, as well as blocking ROS production by neutrophils [296]. PDx is also significantly elevated in the plasma of the cord compared to both non-pregnant ($p = 0.0035$) and pregnant ($p = 0.0286$) adults (Figure 3.18). There are some prostaglandins that have anti-inflammatory effects such as PGD2. PGD2 is produced by mast cells to entice Th2 cells [297]. This mediator is rich in the plasma from pregnant women, significantly higher than both non-pregnant women ($p = 0.0204$) and cord ($p = 0.0059$) plasma (Figure 3.18).

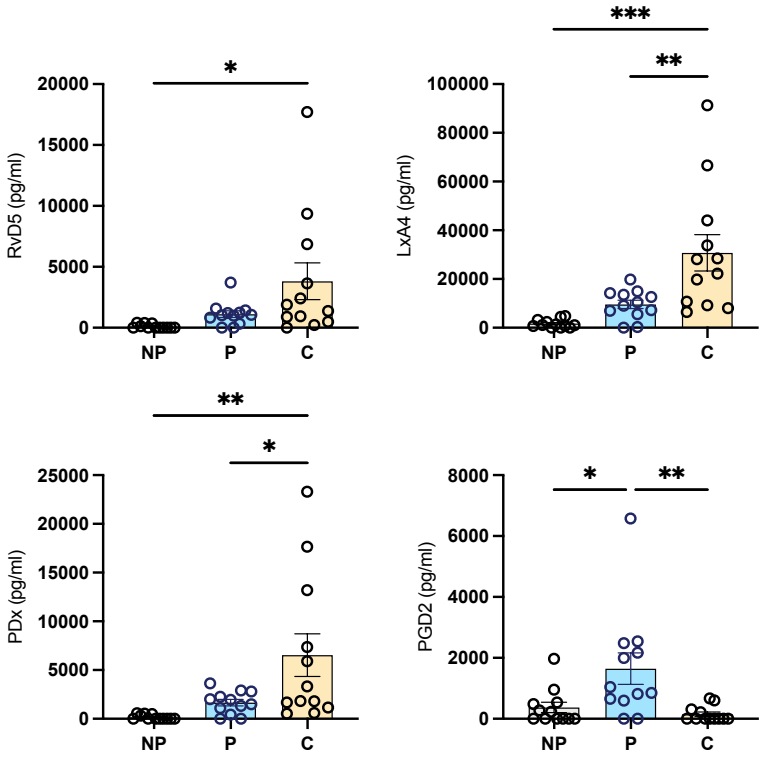

Figure 3.18: Pro-resolving mediator concentrations in plasma samples from non-pregnant and pregnant women at term, and from cord samples. Plasma from heparin-coagulated tubes from non-pregnant women (grey; NP), pregnant women at 37+ weeks (blue; P) and cord (orange; C) was analysed using LC-MS/MS for the presence of eicosanoids. Statistics were performed using an ordinary one-way ANOVA and a Tukey post-hoc test, where $p < 0.05$ was significant. Pro-resolving mediators that were measured were: RvD5 (NP vs P $p = 0.7024$; NP vs C $p = 0.0152$; P vs C $p = 0.0944$), LxA4 (NP vs P $p = 0.4264$; NP vs C $p = 0.0002$; P vs C $p = 0.0051$), PDx (NP vs P $p = 0.6865$; NP vs C $p = 0.0035$; P vs C $p = 0.02866$), and PGD2 (NP vs P $p = 0.0204$; NP vs C $p = 0.8751$; P vs C $p = 0.0059$).

3.3.5.6 Lipid mediators can also be markers of oxidative stress.

This includes 9-hydroxyoctadecadienoic acid (9-HODE), 13-HODE and 8-iso-PGA2. Both 9-HODE and 13-HODE have been recognised to be elevated in LDL of patients with rheumatoid arthritis [298]. All three markers share the trend of being increased in the plasma of the pregnant women (9-HODE $p = 0.0022$; 13-HODE $p = 0.0239$; 8-iso-PGA2 $p = 0.0026$) and cord (9-HODE $p = 0.0423$; 13-HODE $p = 0.0050$; 8-iso-PGA2 $p = 0.005$) compared to the non-pregnant adults (Figure 3.19).

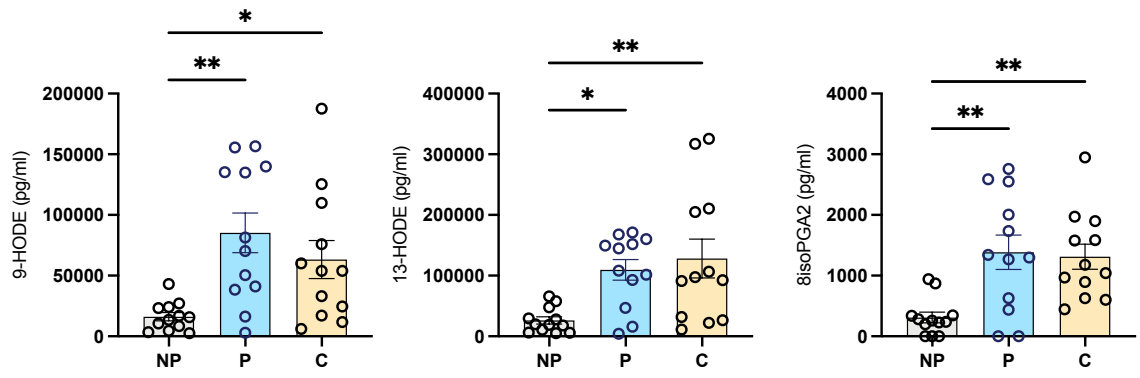

Figure 3.19: Oxidative stress marker concentrations in plasma samples from non-pregnant and pregnant women at term, and from cord samples. Plasma from heparin-coagulated tubes from non-pregnant women (grey; NP), pregnant women at 37+ weeks (blue; P) and cord (orange; C) was analysed using LC-MS/MS for the presence of eicosanoids. Statistics were performed using an ordinary one-way ANOVA and a Tukey post-hoc test, where $p < 0.05$ was significant. Oxidative stress markers that were measured were: 9-HODE (NP vs P $p = 0.0022$; NP vs C $p = 0.0423$; P vs C $p = 0.4754$), 13-HODE (NP vs P $p = 0.0239$; NP vs C $p = 0.0050$; P vs C $p = 0.8113$), and 8-iso-PGA2 (NP vs P $p = 0.0026$; NP vs C $p = 0.0050$; P vs C $p = 0.9668$).

3.3.7 The overarching effect of the lipid mediators lends a more pro-inflammatory effect in pregnancy

As a general trend emerged with the eicosanoids being slightly increased in pregnancy, followed by a higher increase with each molecule measured in cord regardless of function, the ratio between the pro-inflammatory and pro-resolving mediators for each group was considered. Each concentration value was converted to a log value for normalisation. The sum of the values for the pro-inflammatory molecules (PGE2, PGF2a, 5-oxo-ETE) was divided by the sum of the pro-resolving mediators (RvD5, LxA4, PDx, PGD2) for each sample. The ratio shows that the pregnant women plasma is a more pro-inflammatory environment than the non-pregnant ($p = 0.0408$) and cord ($p = 0.0203$) plasma (Figure 3.20).

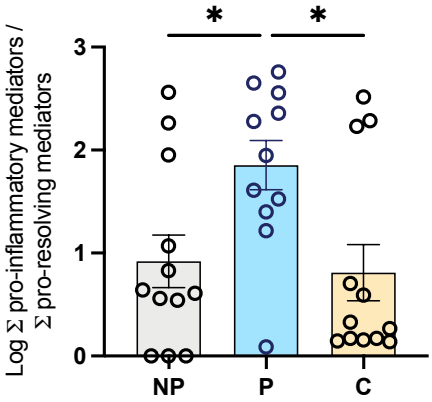

Figure 3.20: The ratio between the pro-inflammatory and pro-resolving mediators for non-pregnant, pregnant, and cord plasma. The ratio was calculated by dividing the sum of the log values for each pro-resolving mediator, by the sum of the log values for each pro-inflammatory mediator. Statistics were performed using a one-way ANOVA and a Tukey post-hoc test, where $p < 0.05$ was deemed significant. The groups were compared: NP vs P $p = 0.0408$, NP vs C $p = 0.9497$, P vs C $p = 0.0203$.

3.4 Discussion

This chapter illustrates the novel use of mass spectrometry techniques to identify the PC/LPC ratio and eicosanoids in human sera and plasma respectively. With the use of MALDI-ToF, PC/LPC can be quickly and cost-effectively determined.

As discussed in *1.2.1 Immunological adaptation in pregnancy – an overview*, the bookends of pregnancy are marked with a pro-inflammatory load for implantation and labour. As pregnancy progresses however, an anti-inflammatory phenotype dominates the maternal systemic immune system [31]. This is evidenced here by the build-up of PC levels and the minimal conversion to LPC as gestation progresses. All pregnant participants were scheduled for elective caesarean section and display no evidence of labour, it is logical that this does not decrease. Future work should consider planned and emergency caesarean sections versus natural or induced labour to investigate if a change in PC/LPC occurs. Regarding calculating reference ranges for each of the groups measured, there is overlap for each group, and the later gestations have higher standard-deviations. This suggests greater variability in PC metabolism at this stage that could be linked to proximity to natural initiation of labour. Studies have shown the increase in the production of PC is by both PEMT and CDP-choline pathways during pregnancy, but it is the PC produced by the PEMT pathway that is selectively transferred to the fetus in the third trimester [299]. Dietary supplements of choline are recommended for pregnant women, due to the heightened requirement [299]. This studies, like others which investigate lipids, use lipid extraction methods, which is timely and expensive and quantified using liquid chromatography – tandem mass spectrometry (LC-MS/MS).

Obesity is an inflammatory state, and studies have shown a decrease in LPC in obese subjects [300]. Non-pregnant volunteers used in this study are typically not obese, and so the data here only includes two women with BMIs above 30. With all cohorts measured here, there was no significant correlation found between BMI and PC/LPC ratio. However, for women at 16 weeks of pregnancy, the negative correlation (suggesting increased inflammation with increased LPC) is almost significant ($p = 0.0566$). This suggests that obesity has more of an effect in maternal inflammation earlier in gestation perhaps linked to increased risk of miscarriage [277] and fetal programming effects. As pregnancy progresses and maternal

metabolism changes this might over-ride any overt effect on obesity-related measures but only a prospective analysis could address this.

Further work investigating the PC/LPC ratio considered adverse obstetric outcomes such as GDM. As mentioned previously, some studies have already shown a correlation between elevated PCs and GDM [236-238], however it has yet to been discovered if intact serum analysis with MALDI-ToF can quickly and cost-effectively diagnose GDM. While a significant difference was observed at 16 weeks of gestation for pregnancies complicated with GDM, this was not the case at 28 weeks when the majority of GDM diagnoses are made. Like BMI at 16 weeks, GDM induces a lower PC/LPC ratio, suggesting a higher inflammatory burden at this stage of gestation. The range of values currently overlaps too much to be able to confidently diagnose GDM; however long-term data of these women is not yet available (collection of this data has been prevented by COVID-19), and it is possible that the women with the lower range of PC/LPC in the healthy group may have developed GDM later in pregnancy. Women are only typically tested at 16 weeks of gestation when they are at even higher risk of developing GDM, i.e., GDM in a previous pregnancy or glucosuria.

Given the pregnancy-related differences demonstrated using a MALDI-ToF analysis of intact serum, it was also considered if intact cell analysis of the PC/LPC ratio using MALDI-ToF might also prove useful. It also provided a novel approach to analysing this content in intact cells. Intact monocytes were spotted and the PC and LPC molecules were identified. Monocytes have fewer species of PC and LPC molecules compared to serum, but enough to determine a PC/LPC ratio. Using monocytes isolated from the blood of non-pregnant and pregnant women, there was no significant difference in their PC/LPC ratio. Historically, lipid extraction has been required to investigate these molecules in cells but using this method originally devised using serum [241] and validated here for use with human serum, extensions of this analysis approach to intact cells was determined to be possible. In the future, the metabolism of PC in leukocytes would be key to investigate. For example, in multiple sclerosis (MS), the production of PUFAs by monocytes, a by-product of PC metabolism, predicts relapses [301]. Investigating the PC/LPC ratio in leukocytes in various disease states will provide knowledge on their inflammatory status and how this might change in pregnant women with autoimmune and other diseases.

Various lipid mediators were measured, including those which are identified as inactive products, pathway markers, bioactive mediators, proinflammatory and pro-resolving mediators, and oxidative stress markers. In almost all the eicosanoids measured, the overall trend was an increase in the plasma from pregnant versus non-pregnant women, and a much larger and mostly significant increase in the plasma from cord. Whether this is due to a supply from the placenta, or the neonate is yet to be determined. Future work should investigate the presence of these molecules in placental tissue. That the molecules measured are high in cord plasma regardless of their properties, such as being pro- or anti-inflammatory, suggests a tight balance between the mediators. Higher levels in the cord might reflect the low PC/LPC ratio observed earlier; despite trafficking PEMT-PC to the fetus, cord PC/LPC is low suggesting a higher conversion rate of PC to LPC, thereby producing the higher levels of eicosanoids as by-products. This may explain the difference observed between the pregnant and cord samples, however the PC/LPC ratio for cord in comparison to the non-pregnant samples are relatively equal. An issue with the MALDI-ToF intact method to determine the PC/LPC ratio, is the inability to quantify the amount of PC and LPC present. The cord samples may contain more total PC and LPC, but this will have to be determined by extracting the lipids and spiking the sample with an internal standard to quantify. That the eicosanoids all appear increased in pregnant compared to non-pregnant plasma, probably reflects the build-up of lipids from earlier gestation before switching to a catabolic state which is evidenced by increased levels of free fatty acids in later pregnancy [39]. As this trend mostly illustrates marked increase of most of the lipid mediators measured, the ratio between the pro-inflammatory and pro-resolving mediators was calculated for each sample. It appears the plasma from pregnant women favours a more pro-inflammatory environment compared to both adult and cord which resemble each other more closely. This contradicts the trend observed from the PC/LPC results. As already discussed, the pregnant women in this study were undergoing c-sections the following day, and so labour wasn't induced. As specific pro-inflammatory factors such as PGE2, which is used to induce labour [284], is increased, this suggests that the overarching PC/LPC ratio masks early signs of labour. Future work should include profiling the pro-inflammatory/pro-resolving lipid mediator profile over pregnancy, to determine if it follows the same tend as the PC/LPC ratio, but perhaps at a quicker pace, and the establishment of the PC/LPC ratio in women during labour versus *c*-section.

The main exception to the trend of increased lipid mediators in pregnant women is 5-oxo-ETE, where the plasma from pregnant women had significantly higher levels than both the non-pregnant and cord. This mediator provides the maternal immune system with a more attractive environment for monocytes and neutrophils, both of which are elevated in pregnancy. PGD2 is also an exception to this trend, which is hardly detectable in the plasma from cord. High levels of PGD2 have been implicated in the inhibition of conventional dendritic cell (cDC) maturation, which are impaired in neonates during paramyxoviral infection [302]. Thus, low levels are required for immune function in the neonate which is more reliant on innate immunity.

3.5 Conclusion

The maternal systemic environment has an increasing anti-inflammatory status as gestation progresses, evidenced by an increase in PC/LPC ratio, though this is contradicted by an increase in the pro-resolving/pro-inflammatory lipid mediator ratio at term. Further work needs to explore the impact of labour on these measurements. This chapter highlights a novel technique to quantify lipids of interest quickly and effectively, and the ability to use intact monocytes should provide insight into how their PC metabolism is altered with different disease states.

Chapter 4 - Immunometabolic adaptations of monocytes in pregnancy at 37+ weeks gestation

4.1 Introduction

4.1.1 Monocytes

Monocytes are phagocytes; they ingest foreign objects and expose them to lysosomal enzymes for digestion. Phagocytosis can be either non-opsonic or opsonic (Figure 4.1). Non-opsonic phagocytosis does not require the target molecule to be primed with immunoglobulins and the phagocyte directly recognises the PAMPs. Non-opsonic PAMP receptors include C-type lectin receptors [303], mannose receptors [304], CD14 [305] and scavenger receptors (e.g., CD36) [306]. CD36 and CD14 can recognise oxidised phosphatidyl serine (oxPS) and lysophosphatidylcholine (LPC) which are exposed on the membrane of apoptotic cells for clearance by phagocytes [307-309].

During opsonic phagocytosis, pathogens are opsonised with immunoglobulins, the Fc fragment of which can bind to Fc gamma receptors (FcγR) on phagocytic cells [310]. FcγRs in this immunoglobulin superfamily include: FcγRI (CD64), FcγRIIA (CD32a), FcγRIIB (CD32b), FcγRIIIA (CD16a), and FcγRIIIB (CD16b). Upon crosslinking with the IgG-coated molecule, the FcγRs cluster and trigger a signalling cascade within their cytoplasmic domain initiated by the tyrosine phosphorylation of immunoreceptor tyrosine-based activation motifs (ITAM) by SRC kinases [310]. SYK-family kinases are then recruited followed by activation of downstream targets such as phosphoinositide 3-kinase (P13K) which in turn activates phospholipase Cγ (PLCγ) [311]. This triggers the calcium signalling pathways by increasing intracellular calcium. The phagosomes are formed upon actin cytoskeleton and membrane remodelling (including changes to the lipid composition) initiated by ITAM tyrosine phosphorylation. The signalling cascade results in lysosomal degradation of the pathogen to the accompaniment of a respiratory burst where ROS, such as hydrogen peroxide (H_2O_2) and superoxide anion (O^2), are produced. Whilst ROS are natural by-products and have roles in homeostasis, oxidative stress can occur by ROS accumulation in response to environmental and other stressors. This can cause significant damage to cells and their organelles, usually resulting in autophagy of said damaged structures as a form of autoregulation.

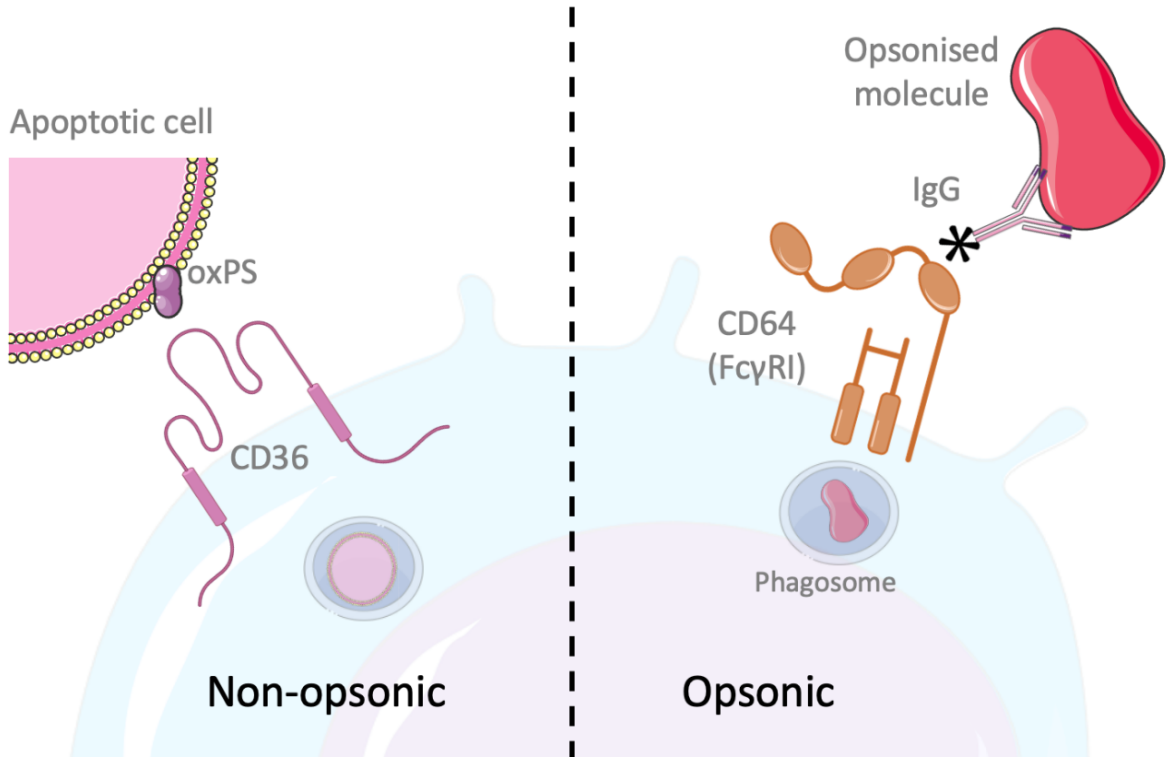

Figure 4.1: Two different mechanisms of phagocytosis. Phagocytes can recognise apoptotic cells and PAMPs which have oxPS or LPC molecules exposed on the membrane, by receptors such as CD36 (a scavenger receptor) for clearance. Pathogens can also be coated with opsonins where they can be recognised by immunoglobulin receptors such as CD64 for clearance.

The three monocyte subsets (classical, intermediate, and non-classical) are phenotypically and functionally different, as touched upon in *1.2.3.1 Classical and non-classical monocytes*. Table 4.1, adapted from Sampath et al. [312], illustrates some of the phenotypic cell surface marker expression of the different subsets. In response to cell surface TLRs such as LPS, non-classical monocytes do not produce cytokines or ROS and as such, are weak phagocytes in comparison to the classical monocytes [313]. However, upon stimulation with immune complexes containing nucleic acids or viruses they secrete IL-1β, CCL3 and TNFα via the TLR7-TLR8 mediated myeloid differentiation primary response (MyD88)/mitogen-activated protein kinase kinase (MEK) pathway [314]. Classical monocytes in contrast, do respond to the TLR4 agonist LPS, and preferentially produce IL-6, IL-8, IL-10, CCL2, CCL5, G-CSF and TNFα [70].

	Classical	Intermediate	Non-Classical
CCR2	+++	+/-	-
CCR5	++	+++	+/-
CD11b	+++	+++	+/-
CD36	+++	++	+/-
CD62L	+	++	-
CD64	+++	+++	+/-
CD80	+	+++	+/-
CD86	+	+++	++
CD163	++	+++	+/-
CX_3CR1	+/-	++	+++
HLA-DR	+/-	+++	++

Table 4.1: A selection of cell surface markers expressed by monocyte subsets.

4.1.1 Monocytes in pregnancy

Monocytes are typically more activated during pregnancy when compared to not-pregnant women evidence by increased expression of the activation markers CD14, CD64 and CD11b [73]. Monocytes in pregnancy also produce more oxygen free radicals, and cytokine production is decreased on stimulation with LPS in comparison to not-pregnant, but increased on stimulation with a combination of LPS and IFNγ [77]. These alterations in normal pregnancy are further exacerbated in preeclampsia, with further elevation of activation markers [77]. A study has investigated the production of type 1 and type 2 cytokines from monocytes, to determine if they contribute to the overarching Th2 environment of pregnancy. This study used intracellular flow cytometry analysis and endotoxin stimulation to reveal that the monocytes in pregnancy are primed to express IL-12, a type 1 cytokine [76], further implicating monocytes as being in a state of heightened activation in pregnancy.

Zika virus (ZIKV) has been known to cause adverse obstetric outcomes if contracted during pregnancy and causes birth defects such as microcephaly [159, 162]. Several studies have shown that in the general population, to establish viremia, ZIKV targets peripheral monocytes, specifically $CD16^+$ monocytes [315-317]. Monocytes are an ideal target for ZIKV to infiltrate tissue such as the placenta [318]. There are different lineages of ZIKV, and a study has unveiled that during Asian-lineage infection in pregnancy, the non-classical monocytes are suppressed in an exacerbated M2-skewed manner (increased expression of CD163, VEGF, IL-10) [319]. Similarly, to the general population, ZIKV targets peripheral monocytes in pregnancy and

induces a more dramatic expansion of non-classical monocytes than in the non-pregnant population in the first and second trimester [319]. Transcriptome analysis of the monocytes upon ZIKV infection revealed a higher occurrence of genes in the first and second trimester which are implicated in adverse obstetric outcomes, such as ADAMTS9 (arrest of cervical dilation) and fibronectin 1 (preeclampsia) [319-321].

4.1.2 Monocyte immunometabolism

Glycolysis is often ramped up by cells for quick production of ATP, despite the low yield per molecule of glucose in comparison to OXPHOS. Glycolysis is more rapidly initiated via upregulation of enzymes involved in the pathway, whilst increasing OXPHOS is a much slower process requiring mitochondrial biogenesis. Glycolysis at higher rates also enables production of biosynthetic intermediates to support cell growth and proliferation. Therefore, cells which have a more immediate need for rapid ATP production will typically switch to glycolysis.

Monocyte metabolism has been described mostly in tandem with macrophages and dendritic cells, with very little investigation into only monocytes. Some studies have investigated TLR4 and TLR2 microbial stimuli (LPS and Pam_3CysSK_4 [P3C] respectively) to show that an increase in glycolysis only occurred in monocytes stimulated with LPS but not in those stimulated with P3C or alternative bacterial lysates [322]. In order to retain their phagocytic and cytokine activity in response to P3C, increased OXPHOS by monocytes was necessary. It was speculated that the metabolic programmes which govern immune cell function are therefore unique to individual stimuli [322]. This supports the emerging data that a "one size fits all" switch to glycolysis is not always the case. When complex I of the ETC was inhibited the P3C-stimulated monocytes had reduced phagocytosis and cytokine production, in comparison to stimulation with LPS which showed no change in these functions, further highlighting that the LPS-stimulated monocytes do not rely on OXPHOS[322]. OXPHOS capabilities in monocytes appear linked with their ability to phagocytose, probably due to the high energy requirements necessary for phagocytosis and the high ATP yield of OXPHOS. Mitochondrial morphology may contribute to the differences in OXPHOS between the two types of stimuli, as larger mitochondria were observed in the monocytes stimulated with LPS in comparison with P3C after 24-hr stimulation [322].

Sites of inflammation are usually hypoglycaemic so understanding cellular metabolic processes in low glucose settings is critical. To compensate for increased energy demands upon LPS stimulation in glucose deprived conditions, monocytes increase their OXPHOS. This has also been evidenced on exposure to fructose as an alternative carbon source to glucose; LPS-stimulated monocytes now rely heavily on OXPHOS with reduced glycolytic flexibility on exposure to fructose in place of glucose, with the increase in mTORC1 activity driving an increase in the production of pro-inflammatory cytokines [228].

Over a short period of time, glycolysis produces more ATP than OXPHOS due to its fast conversion rate. However, one molecule of a long-chain FA has an even greater ATP yield [323]. Under low glucose conditions the monocyte switch to OXPHOS is seemingly fuelled mostly by FAO, with FA derived from lipid droplets (LD), illustrating a switch from FA synthesis to consumption [324]. LDs are a source of FA for oxidation, and store mostly cholesterol esters and triglycerides within a phospholipid layer. LDs interact with the mitochondria to efficiently supply FAs for β-oxidation [325]. These LD-mitochondria interactions are orchestrated by AMP-activated protein kinase (AMPK), the main cellular energy sensor [325]. AMPK has been found to be activated in the monocytes under glucose deprivation conditions [324]. AMPK was actually found to be the vital regulator for the switch to OXPHOS, as inhibition of AMPK blocks this metabolic switch [324]. Functionally, these changes in metabolism under hypoglycaemic conditions had no effect on monocyte viability, phagocytosis capabilities, cytokine production or chemotactic migration [324]. ROS generation is limited in glucose deprivation with a decrease in LPS-induced NADPH oxidase-dependent respiratory burst, due to the direct effect of the activation of AMPK [324]. Levels of succinate are unchanged in monocytes under hypoglycaemic conditions, and the utilisation of glutamine makes a minor contribution to the oxygen consumption.

Clearly, cellular metabolism has a central role in determining monocyte function yet very little is understood about the metabolic adaptations the monocytes undergo during a healthy pregnancy. Given the many metabolic adaptations of pregnancy as discussed in *1.2.2 Metabolic adaptations in pregnancy*, fuel availability and thereby alterations in the bioenergetic flux within immune cells including monocytes is feasible.

4.1.3 Rationale

Immunometabolism of heterogeneous MNCs – mostly lymphocytes and monocytes - is altered at 37+ weeks of gestation in comparison to non-pregnant, where a reduction in glycolysis was observed [47]. It is important to determine whether discrete MNC populations themselves show immunometabolic adaptation. Due to the inflammatory profile of pregnancy [29-31], the innate immune system needs to be considered. Monocytes are a key inflammatory cell population within MNCs that can be prepared readily and ethically from the blood of pregnant women and are known to undergo metabolic adaptation in response to different environmental cues.

4.1.4 Hypothesis

Metabolic adaptation by monocytes underpins pregnancy-related changes in their function.

4.2 Materials and Methods

4.2.1 Samples

Blood samples were donated as in *2.1 Human blood collection*. All women recruited for this study were healthy or overweight, with obese and morbidly obese individuals excluded. Obesity was defined as BMI of ≥ 30, where BMI is calculated as:

$$BMI\ \left({}^{kg}/_{m^2}\right) = \frac{Mass\ (kg)}{Height\ (m)^2}$$

4.2.2 Monocyte isolation

MNCs were first separated from the blood and monocytes isolated subsequently from the MNCs via the isolation protocol as in *2.2 Monocyte isolation.*

4.2.3 NanoString

The NanoString © nCounter ® Metabolic Pathways Panel was utilised with monocytes as described in *2.11 NanoString* and differential expression p-value adjustment was done with Benjamini-Hochberg.

4.2.4 Flow cytometry

Basic phenotyping was performed as in *2.3 Flow cytometry*. Antibodies used are shown in Table 4.2.

Antibody	Fluorochrome	Isotype	Clone	Company
CD11b	PE	Mouse IgG1, κ	CBRM 1/5	Biolegend
CD14	eFluor ® 450	Mouse IgG2a, κ	M5E2	Biolegend
CD16	VioBlue	Mouse IgM, κ	VEP13	Miltenyi Biotec
CD16	Alexa Fluor 488	Mouse IgG1, κ	3G8	Biolegend
CD163	PE	Mouse IgG1, κ	GHI/61.1	Miltenyi Biotec
CD169	PE	Mouse IgG1, κ	7-239	Miltenyi Biotec
CD192 (CCR2)	PE	Human IgG1	REA624	Miltenyi Biotec
CD195 (CCR5)	PE	Human IgG1	REA245	Miltenyi Biotec
CD220	PE	Human IgG1	REA260	Miltenyi Biotec
CD279 (PD-1)	PE	Mouse IgG2b, κ	PD1.3.1.3	Miltenyi Biotec
CD295 (LEPR)	PE	Human IgG1	REA361	Miltenyi Biotec
CD36	PE	Mouse IgG2a, κ	5-271	Biolegend
CD38	PE	Mouse IgG1, κ	HB-7	Biolegend
CD62L	PE	Mouse IgG1, κ	DREG-56	Biolegend
CD64	PE	Mouse IgG1, κ	10.1.1	Miltenyi Biotec
CD69	APC	Mouse IgG1, κ	FN50	Biolegend
CD80	PE	Mouse IgG1, κ	2D10	Miltenyi Biotec
CD86	PE	Mouse IgG1, κ	FM95	Miltenyi Biotec
CD98	FITC	Mouse BALB/c IgG1, κ	UM7F8	BD Horizon
CX3CR1	PE	Rat IgG2b, κ	2A9-1	Miltenyi Biotec
GLUT1	PE	Mouse IgG2b, κ	FAB1418P	R&D Systems
HLA-DR	Brilliant Violet 421	Mouse IgG2a, κ	L243	Biolegend

Table 4.2: Antibodies used for phenotypic analysis. List includes their fluorochrome, isotype, clone and manufacturer.

4.2.4.1 Mitochondrial dyes

MitoTracker Green FM ™ (ThermoFisher) is a stain for mitochondria which fluoresces equivalently to FITC (Ex/Em 490/516 nm); it localises to the mitochondria in live cells irrespective of mitochondrial membrane potential. 50 μg of MitoTracker Green FM ™ (MW 671.8797) was reconstituted with 74.4 μl of DMSO in the dark to give a stock of 1 mM concentration. This was diluted 1/50 with FACS buffer then diluted a further 1/10 (concentration 2 μM). This 2 μM dilution was added 1/100 to 0.5 x 10^6 cells in 500 μl for a final concentration of 20 nM. Cells were incubated in the dark for 30 mins at 37°C before being washed with 2 ml FACS buffer and centrifuged at 512 *x g* for 7 mins at 4°C. A CD16 antibody (VioBlue)was added once the supernatant was discarded, and the protocol as in *2.3 Flow cytometry* finished the experiment.

MitoSOX ™ Red (ThermoFisher) is a mitochondrial superoxide indicator. It targets the mitochondria in live cells and is oxidised by superoxides only to produce a red fluorescence (Ex/Em 510/580 nm). 50 μg of MitoSOX ™ Red (MW 759.71) is reconstituted with 13 μl DMSO in the dark to produce a stock concentration of 5 mM. This was diluted 1/10 with FACS buffer (concentration now 500 μM), before being diluted 1/100 into 0.5 x 10^6 cells in 500 μl for a final concentration of 5 μM. Cells were incubated in the dark for 15 mins at 37°C before being washed with 2 ml FACS buffer and centrifuged at 512 *x g* for 7 mins at 4°C. α-CD16 antibody (VioBlue) was added once the supernatant was discarded, and the protocol as in *2.3 Flow cytometry* finished the experiment.

4.2.4.2 DCFDA Assay

Dichlorofluorescin diacetate (DCFDA) is a dye which diffuses into a cell to be oxidised by hydroxyl, peroxyl and other ROS into a fluorescent molecule (2',7'-dichlorofluorescein; Ex/Em 485 nm/535 nm). Thus, it is a tool to measure ROS activity of a cell. Monocytes were seeded at 2 x 10^5 cells per 200 μl total culture media. To investigate the effect of activation on ROS production, cells were left unstimulated or stimulated with oligomycin (1 μM), FCCP (1 μM) or a combination of both. Stock of oligomycin (2.5 mM) and FCCP (2.5 mM) was first diluted 1/312.5 in culture media to produce a new stock of 8 μM. This was diluted 1/8 into experiment wells. Oligomycin was added first, before incubation for 20 mins at 37°C, 5% CO_2.

FCCP was then added at the same time as 2 µl DCFDA (5 µM; Abcam) and incubated for 30 mins at 37°C with 5% CO_2. Cells were centrifuged at 515 *x g* for 7 mins at 4°C. Supernatant was aspirated and cells resuspended with 100 µl FACS buffer. A anti-CD16 antibody (APC, Clone 3G8, FCγRIII, Biolegend) was added and the protocol as in *2.3 Flow cytometry* finished the experiment.

4.2.4.3 BODIPY

Boron-dipyrromethene (BODIPY) fluorophore dyes are a series of products which have specific spectral characteristics which can assist in the analysis of various molecules such as fatty acids. BODIPY 493 (Ex/Em 500/509 nm) and BODIPY 500 (Ex/Em 508/514nm) allow for investigation into fatty acid storage and uptake respectively. These experiments were always performed in the dark.

Stock of BODIPY 493 (10 mg, ThermoFisher ©) was re-suspended in 10ml DMSO to give a concentration of 1 mg/ml. This was aliquoted and frozen at -20°C until needed. Buffer used was 2 mM EDTA with 0.5% BSA in PBS. BODIPY 493 was further diluted 1/10 with buffer to give a concentration of 100 µg/ml. 2 µl of the dye was added to 2 x 10^5 of cells in 200 µl of buffer, final concentration 1 µg/ml. Cells were incubated for 1 hr at 4°C in the dark. 2 ml FACS buffer was added, and cells were centrifuged 512 *x g* for 7 mins at 4°C. α-CD16 antibody was added once the supernatant was discarded, and the protocol as in *2.3 Flow cytometry* finished the experiment.

Stock of BODIPY 500 (1 mg, ThermoFisher ©) was re-suspended in DMSO to give a concentration of 1 mM; this was aliquoted and stored at -20°C. This was diluted 1/10 (concentration 100 µM) with FACS buffer and then 2 µl added to 2 x 10^5 of cells in 200 µl of FACS buffer (final concentration 1 µg/ml). This was then incubated for 20 mins at 37°C before being washed with 2 ml FACS buffer and centrifuged 512 *x g* for 7 mins at 4°C. α-CD16 antibody was added once the supernatant was discarded, and the protocol as in *2.3 Flow cytometry* finished the experiment.

4.2.4.4 Kynurenine assay

Kynurenine is produced from the amino acid tryptophan (Figure 4.2). It is involved in immune regulation and is produced when an immune response is activated. It has been implicated in various diseases such as depression where its production is compromised [326]. Investigation into the uptake of kynurenine by monocytes in pregnant and non-pregnant women was done based on an assay described by Sinclair et al [327] and is based on the autofluorescence of kynurenine (Ex/Em 380/480 nm – equivalent to Pacific Blue). Controls to block the uptake of kynurenine were set up in order to conclude the shift in fluorescence observed is due to actual kynurenine uptake. These controls are 4°C incubation, system L blocker 2-aminobicyclo-(2,2,1)-heptane-2-carboxylic acid (BCH), and lysine which blocks system y + L.

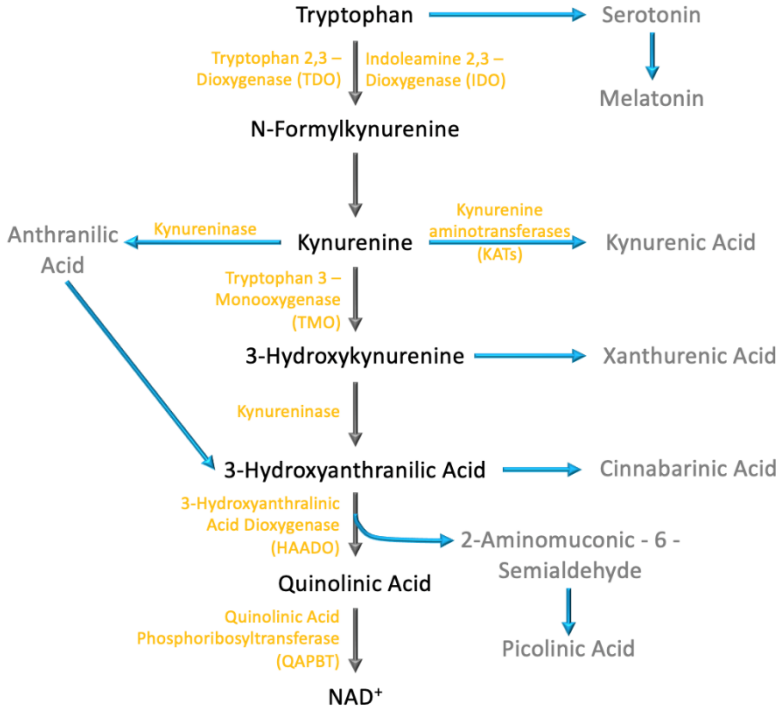

Figure 4.2: Tryptophan metabolism. Tryptophan can produce by-products such as serotonin which in turn produces melatonin. Kynurenine is generated from tryptophan via N-formylkynurenine in a reaction catalysed by tryptophan 2,3-dioxygenase (TDO) and indoleamine 2,3-dioxygenase (IDO). Kynurenine can then be further metabolised to produce a number of other products. Kynurenic acid is produced with a reaction catalysed by kynurenine aminotransferases (KATs). Kynurenine is catalysed with kynureninase to produce anthranilic acid. To produce the final product NAD+, kynurenine undergoes four reaction steps catalysed by tryptophan 3-monooxygenase (TMO), kynureninase, 3-hydroxyanthralinic acid dioxygenase (HAADO), and quinolinic acid phosphoribosyltransferase (QAPBT) via 3-hydroxykynurenine, 3-hydroxyantharlinic acid and quinolinic acid respectively. Xanthurenic acid, cinnabarinic acid, 2-aminomuconic-6-semialdehyde and picolinic acid are various by-products produced by the various steps.

0.5 x10^6 cells in 100 µl RPMI 1640/Glutamax were stained in quintuplet with FITC anti-CD16 antibody (BioLegend), with one unstained test, and incubated for 30 mins at 4°C. The cells were then washed with 2 ml FACS buffer and centrifuged at 512 *x g* for 7 mins at 4°C. The

supernatant was discarded, and the cells re-suspended in 200 µl warmed Hanks' Balanced Salt Solution (HBSS; Life Technologies). All solutions were kept at 37°C. Kynurenine (Tocris) was added so that the final concentration was 200 µM; it was first diluted 1:12.5 from 10 mM stock. A control with an inhibitor of system L amino acid transporters, BCH, and a control with lysine was used to ensure specificity. BCH (Sigma) was diluted from stock (50 mM) to 40mM (1:1.25) for a final concentration of 10 mM for the uptake. Lysine (Sigma) did not need to be diluted, the stock was 20 mM, to provide a final concentration of 5 mM. A control of uptake at 4°C also confirmed surface binding did not occur, and that it was transported kynurenine being measured. Additions to the individual 6 tubes as in Table 4.3.

Unstained	200 µl HBSS
No-kynurenine + CD16	200 µl HBSS
Kynurenine + CD16	100 µl HBSS + 100 µl Kynurenine
BCH + CD16	100 µl BCH + 100 µl Kynurenine
4°C + CD16	100 µl HBSS + 100 µl Kynurenine
Lysine + CD16	100 µl Lysine + 100 µl Kynurenine

Table 4.3: Conditions for the kynurenine assay and their respective components

Kynurenine was added last and simultaneously to all the conditions. Samples were left for 4 mins and then 125 µl of 4% paraformaldehyde (PFA; Sigma) was added to stop uptake. Samples were incubated for 30 mins in the dark at RT, and washed twice with 0.5% BSA in PBS, and finally re-suspended in 200 µl 0.5% BSA in PBS for acquisition on the flow cytometer. An example histogram of kynurenine and the controls can be visualised in Figure 4.3.

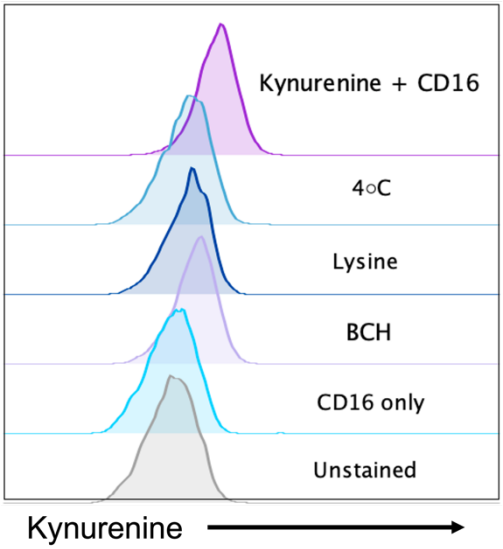

Figure 4.3: An example of histogram for the kynurenine assay with the controls. The pacific blue (kynurenine) fluorescence for the unstained, CD16 only, BCH + kynurenine, lysine + kynurenine, kynurenine at 4°C, kynurenine + CD16 under optimal conditions with no inhibitor.

4.2.4.5 Phagocytosis assay

pHrodo ™ red *E. coli* BioParticles ™ conjugate for phagocytosis (ThermoFisher; Max Ex/Em 560/585 nm, equivalent to PE) are pH-sensitive and only fluoresce inside phagosomes as the pH becomes more acidic. The BioParticles were re-constituted with uptake buffer (ThermoFisher) to produce a 1 mg/ml stock. 2 x 10^5 monocytes were seeded at 200 µl per well in culture media. BioParticles were added at either 10 µg/ml or 25 µg/ml and the cells were incubated at 37°C in 5% CO_2 for 1 hr. Cells were placed on ice to prevent further phagocytosis and stained with anti-CD16 (APC, Clone 3G8, FCγRIII, Biolegend) for 30 mins. Samples were centrifuged at 515 *x g* for 7 mins at 4°C, supernatant discarded, cells re-suspended in 200 µl FACS buffer and then acquired on the flow cytometer.

4.2.5 Bioenergetics

Glycolytic and oxidative phosphorylation capabilities were determined as in *2.6 Bioenergetic analysis.* The mitochondrial use of fuels was determined as in *2.6.4 Mito Fuel Flex test*.

4.2.6 Cardiolipin quantification

During the lipid extraction process, the monocytes were spiked with a 14:0 cardiolipin standard (Avanti) and analysed via MALDI-ToF as described in *2.10 Mass spectrometry*.

4.2.7 Cell culture

Monocytes were left unstimulated or stimulated with LPS, MDP, or LPS and R848 as in *2.6 Cell culture* with autologous plasma culture media for 24 hrs. Autologous plasma was used instead of FBS to provide a semblance of the native non-pregnant or pregnant environment.

4.2.8 ELISAs

ELISAs were carried out as *in 2.7 Enzyme linked immunosorbent assay (ELISA)*, using the R&D Systems kits for IL-1β, TNFα, IL-6, IL-8, IL-10, and IL-12p70. Due to the use of autologous plasma, cytokine measurements observed in media only were checked, but no detectable cytokines were present.

4.2.9 Eicosanoids with LC-MS/MS

1 x 10^6 monocytes were left unstimulated or stimulated with LPS (10 ng/ml) in 1 ml autologous culture media for 22 hr at 37°C with 5% CO_2. Samples were centrifuged at 515 *x g* for 7 mins at 4°C end the cell-free supernatant extracted. Supernatants were frozen at -80°C until shipping to the Lipidomic Core Facility, Université de Toulouse for analysis with LC-MS/MS [274]. Eicosanoids which were detectable from the monocyte supernatants can be seen in Table 4.4. Measurements from the autologous media was subtracted from the supernatants.

Inactive products	**Pro-Inflammatory mediators**	**Pro-resolving mediators**
TXB_2	PGE_2	PGA_1
Pathway markers	PGF_{2a}	**Bioactive mediators**
5-HETE	LTB4	8-HETE
15-HETE	**Oxidative stress markers**	12-HETE
14-HDoHE	9-HODE	
17-HDoHE	13-HODE	
18-HEPE	8-iso-PGA_2	

Table 4.4: The classification of each eicosanoid which was quantifiable in the supernatants from monocyte cultures.

4.3 Results

4.3.1 Non-classical monocyte levels are elevated in pregnancy

As discussed in *1.2.3Monocytes in pregnancy*, monocytes are heterogenous and with pregnancy being a state of heightened inflammation, the levels of classical vs non-classical monocytes needed to be considered. Figure 4.4 illustrates the histograms of monocytes for non-pregnant and pregnant donors, and the percentage of $CD16^-$ and $CD16^+$ monocytes in the two groups. The percentage of CD16+ in non-pregnant women ranges between 3 and 10%. In pregnant women, this percentage significantly increases to a range between 11 and 30% which is in keeping with findings from other groups [328, 329].

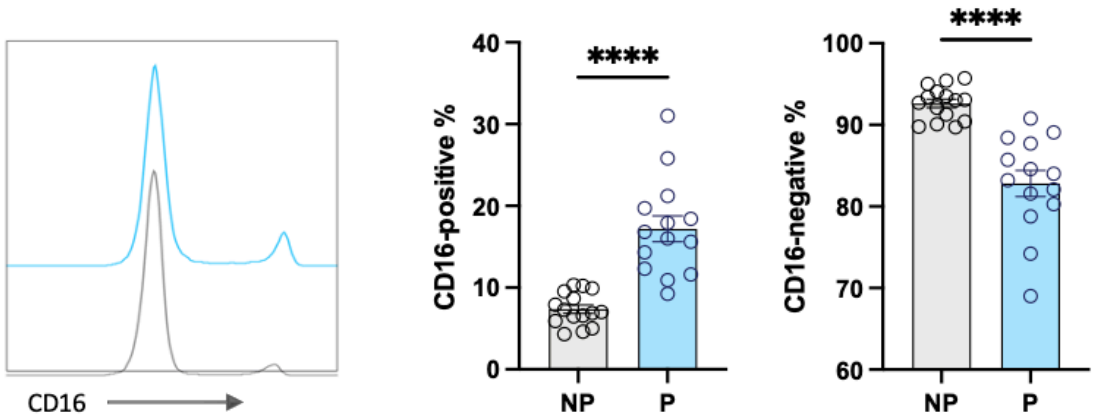

Figure 4.4: The ratio of CD16+/CD16- monocytes in non-pregnant and pregnant women. Monocytes from non-pregnant (grey; n=15) and pregnant women (blue; n=14) were stained with CD16 antibody as described in the Materials and Methods. Example histograms are shown for the staining of CD16 on the monocytes. The percentage of CD16-positive ($p < 0.0001$) and CD16-negative ($p < 0.0001$) monocytes was calculated. Statistics were determined using a Mann-Whitney test where a p value < 0.05 was deemed significant.

4.3.2 Monocytes are phenotypically altered to adapt to the pregnant environment

To determine the activity of the monocytes in pregnancy, expression of common activation markers was investigated. CD62L, also known as L-selectin, is a cell adhesion molecule. This marker is unchanged for both monocyte subsets (Figure 4.5 A). CD69 is an early activation marker and is the human transmembrane C-Type lectin protein. This marker is unchanged in both subsets of monocytes in pregnancy (Figure 4.5 B). Integrin-α-M (ITGAM), also known as CD11b, regulates the adhesion and migration of leukocytes. CD11b is significantly increased in the $CD16^+$ population of monocytes in pregnancy (Figure 4.5 C). Human leukocyte antigen – DR isotype (HLA-DR) - is an MHC class II molecule whose primary role is to present foreign peptides to elicit a CD4 T cell response along with other factors such as costimulatory and

coinhibitory molecules which determine the tenor of response. HLA-DR is significantly upregulated in both CD16+ and CD16- monocytes in pregnancy (Figure 4.5 D).

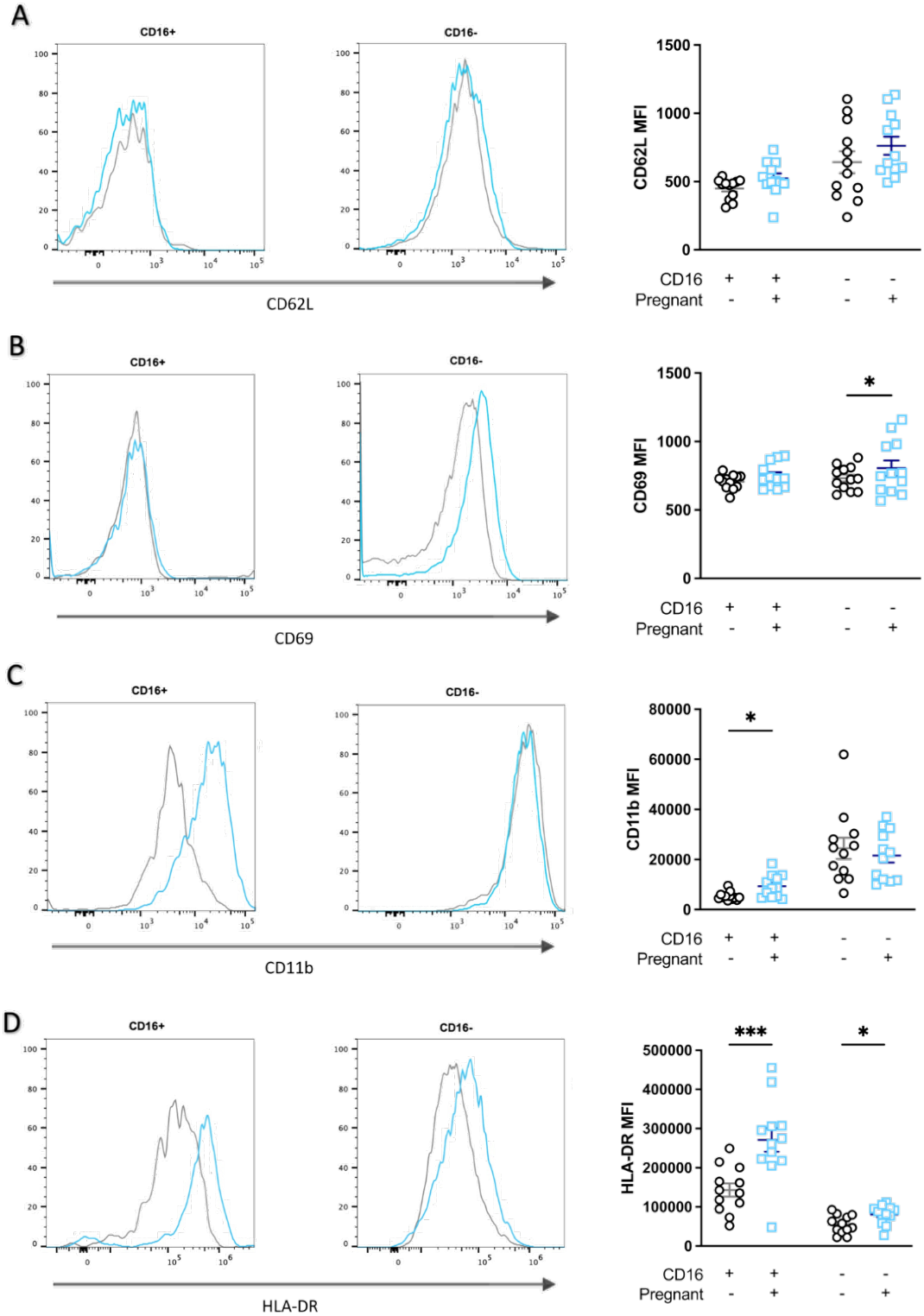

Figure 4.5: Activation marker expression on CD16+ and CD16- monocytes from non-pregnant and pregnant women. Non-pregnant (NP) is illustrated in grey (n=12), and pregnant (P) in blue (n=12). An example histogram for each group is shown on the left and summary data on the right as scatter plots. Statistical analysis was by 2-way ANOVA and a Šídák's post-hoc test, where $p < 0.05$ was deemed significant. Activation markers which were measured were: **(A)** CD62L ($p = 0.1334$ CD16+, $p = 0.6407$ CD16-), **(B)** CD69 ($p = 0.1922$ CD16+, $p = 0.0268$ CD16-), **(C)** CD11b ($p = 0.0328$ CD16+, $p = 0.7540$ CD16-) and **(D)** HLA-DR ($p = 0.0006$ CD16+, $p = 0.0212$ CD16-).

Chemokine receptors interact with a particular type of cytokine, called a chemokine, the name of which is derived from their aptitude to induce directed chemotaxis in responsive cells. Chemokines interact with their specific receptors to trigger a flux in intracellular calcium ions, to induce cell responses including chemotaxis. There are four main subfamilies of chemokines and chemokine receptors: CXC, CC, CX_3C and XC. C-C chemokine receptor type 2 (CCR2) exclusively mediates monocyte chemotaxis via interaction with monocyte chemoattractant protein-1 (MCP-1; CCL2). CD16- monocytes are said to be CCR2 negative/low with CD16+ monocytes CCR2 positive, assisting in distinguishing between the two subsets. In pregnancy, the CD16+ monocytes appear to increase their CCR2 expression, although this change is not significant, and expression on the CD16- population remains unchanged (Figure 4.6 A). C-C chemokine receptor type 5 (CCR5) is present on all leukocytes and interacts with various ligands such as CCL3 (MIP 1α), CCL4 (MIP 1β), CCL5 (RANTES) and CCL_3L_1. The normal immune function of CCR5 is still unclear, although it is known that it is used by HIV-1 to enter immune cells [330], and during the cancer transformation process it is selectively induced [331]. CCR5 is significantly elevated on CD16+ monocytes during pregnancy, with no change in the CD16- subset (Figure 4.6 B). CX_3C chemokine receptor 1 (CX_3CR1) is a fractalkine receptor which binds specifically to the fractalkine CX_3CL1. CX_3CR1 is present on leukocytes and is involved in their migration and adhesion. It is also another chemokine receptor which can be used to assist in distinguishing between CD16+ and CD16- monocytes, as it is positively and negatively expressed respectively. CX_3CR1 promotes monocyte cell survival, and is required for their homeostasis [332]. In pregnancy, expression of CX_3CR1 by CD16+ monocytes is reduced with no change on the CD16- subset (Figure 4.6 C).

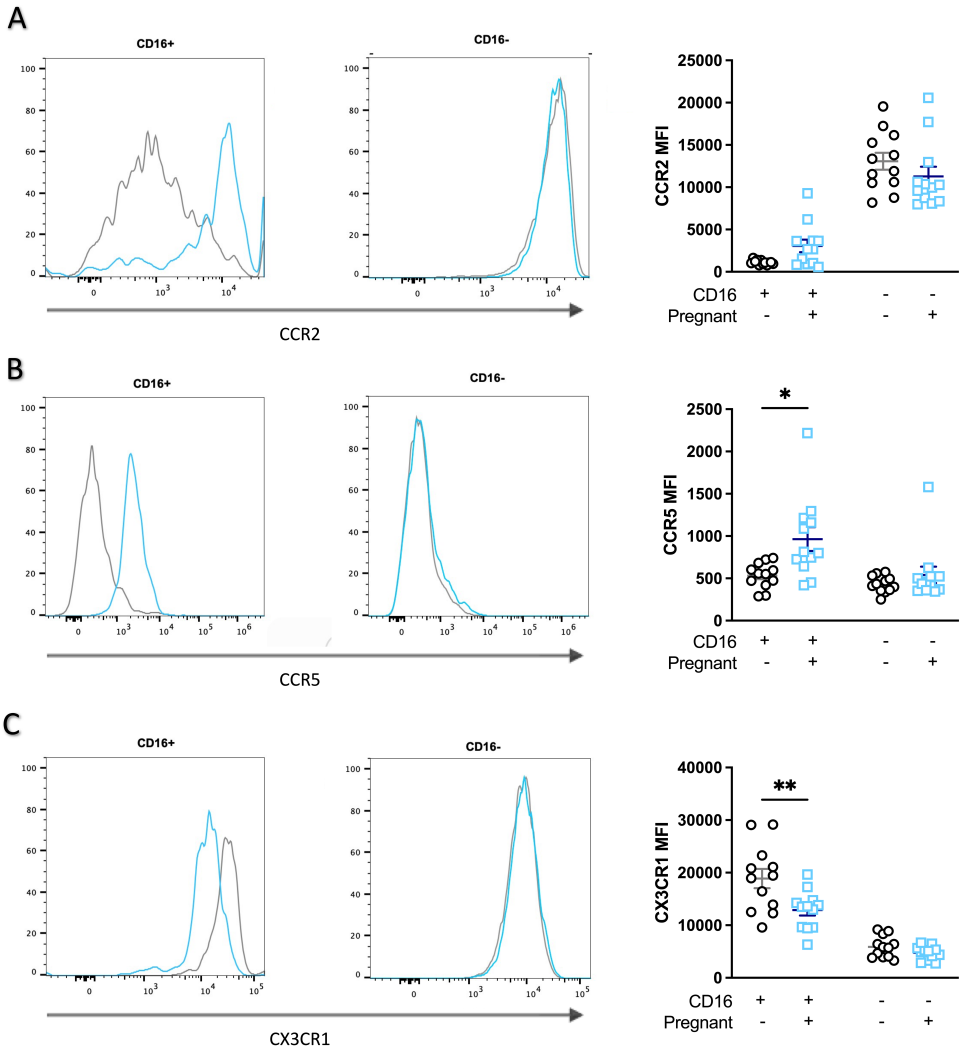

Figure 4.6: Chemokine receptor expression on CD16+ and CD16- monocytes in pregnancy. Non-pregnant (NP) is illustrated in grey (n=12), and pregnant (P) in blue (n=12). An example histogram for each group is shown on the left and summary data on the right as scatter plots. Statistics were determined using 2-way ANOVA and a Šídák's post-hoc test, where $p < 0.05$ was deemed significant. Chemokine receptor expressions which were measured were: **(A)** CCR2 ($p = 0.0532$ CD16+, $p = 0.1824$ CD16-), **(B)** CCR5 ($p = 0.0290$ CD16+, $p = 0.4462$ CD16-) and **(C)** CX3CR1 ($p = 0.0023$ CD16+, $p = 0.6675$ CD16-).

Pregnancy is accompanied by various hormonal adaptations, including those of a metabolic nature. As discussed in *1.2.2 Metabolic adaptations in pregnancy*, insulin resistance is a common feature which develops over the course of pregnancy, and excessive resistance to insulin leads to adverse pregnancy outcomes like gestation diabetes mellitus [333, 334]. Monocytes are sensitive to insulin, and illustrate enhanced inflammatory properties, such as increasing the production of IL-6 and TNFα on exposure to insulin [335, 336]. The insulin receptor (CD220) is present on monocytes as well as other cells and allows insulin molecules to bind and induce glycogen synthesis and regulates gene expression such as MAPK [337, 338]. Flow cytometry analysis illustrates that there is no change in the expression of CD220 in either subset of monocytes in pregnancy (Figure 4.7 A). Leptin is another metabolic hormone which

is increased in pregnancy [339]. Its primary function is to assist in the regulation of energy balance by inhibiting hunger, which leads to the diminishing of fat storage. Leptin also has various roles in immune cells, for example it is required for T_h17 differentiation, it can suppress Treg differentiation, inhibit NK cell activation, and inhibition of the leptin receptor (CD295) prevents phagocytic and microbicidal functions of macrophages and dendritic cell maturation [340]. In regards to monocytes, leptin can stimulate migration, cytokine secretion and CD16 expression [151]. CD295 is significantly elevated on both subsets of monocytes in pregnancy (Figure 4.7 B).

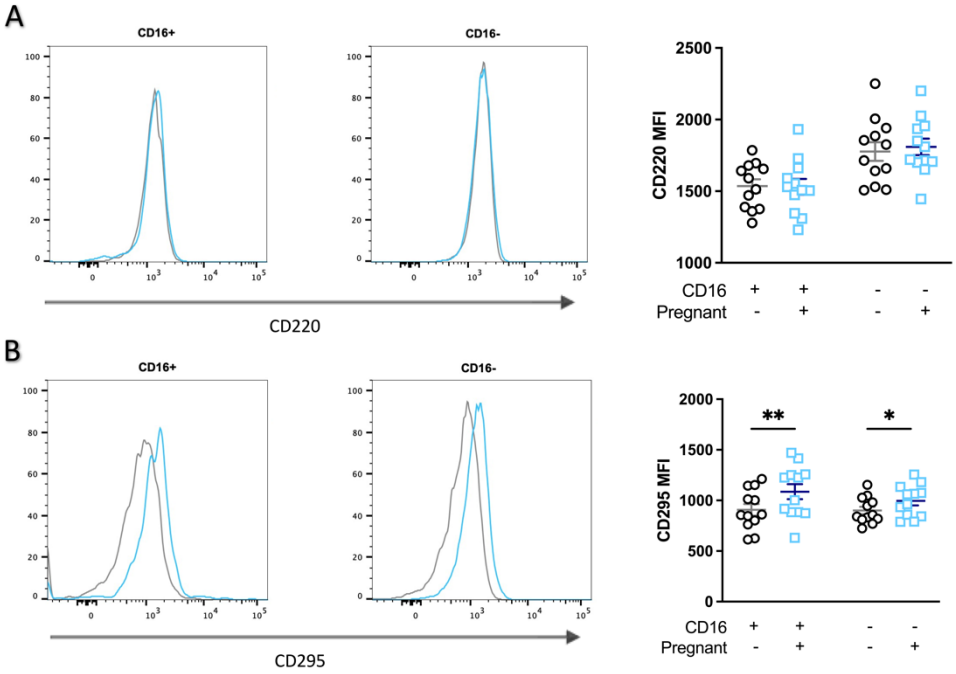

Figure 4.7: Metabolic hormone receptor expression on CD16+ and CD16- monocytes in pregnancy. Non-pregnant (NP) is illustrated in grey (n=12), and pregnant (P) in blue (n=12). An example histogram for each group is shown on the left and summary data on the right as scatter plots. Statistics were determined using 2-way ANOVA and a Šídák's post-hoc test, where $p < 0.05$ was deemed significant. The metabolic hormone receptor expressions which were measured were: **(A)** CD220 ($p = 0.9953$ CD16+, $p = 0.8496$ CD16-) and **(B)** CD295 ($p = 0.0026$ CD16+, $p = 0.0313$ CD16-).

Monocytes can serve as antigen presenting cells (APCs) and CD80 (B7-1) and CD86 (B7-2) work in tandem to stimulate a T cell response via interaction without counter co-stimulatory/inhibitory molecules on the T cell. CD80/CD86 bind to co-stimulatory CD28 on T cells but can also bind to co-inhibitory CTLA-4 on Treg cells, with CD86 possessing a greater affinity for CTLA-4 rather than CD28. CD80 has also been suggested to interact with a discrete ligand on NK cells which triggers NK cell-mediated cytotoxicity of the CD80 expressing cell [341]. CD80 expression is up-regulated in both subsets of monocytes in pregnancy (Figure 4.8 A) whilst CD86 expression is unchanged (Figure 4.8 B).

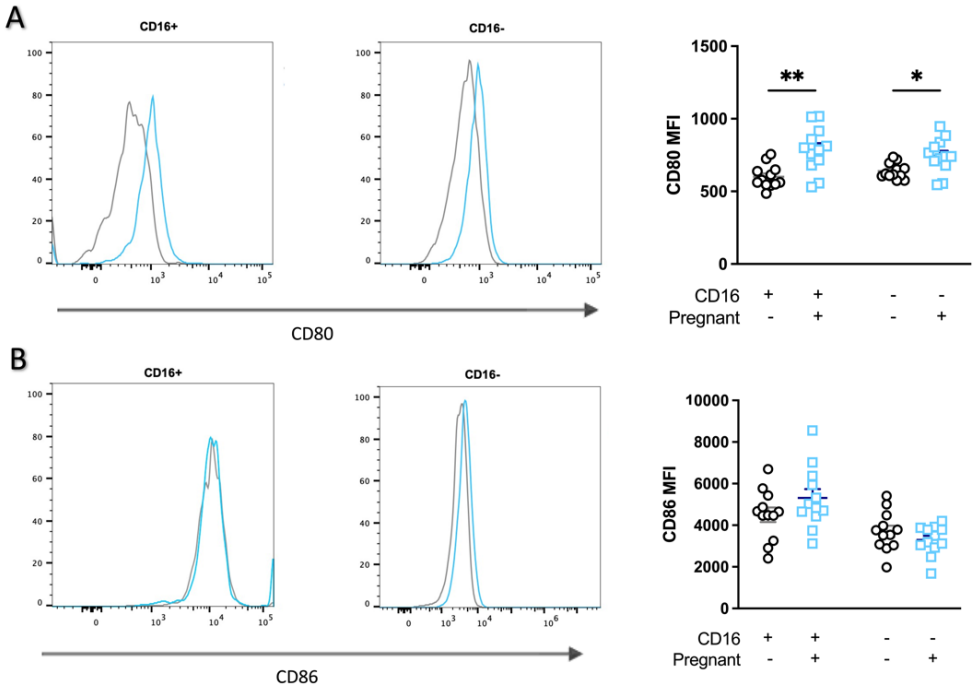

Figure 4.8: T cell co-stimulatory counter-receptors on CD16+ and CD16- monocytes in pregnancy. Non-pregnant (NP) is illustrated in grey (n=12), and pregnant (P) in blue (n=12). An example histogram for each group is shown on the left and summary data on the right as scatter plots. Statistics were determined using 2-way ANOVAs and a Šídák's post-hoc test, where $p < 0.05$ was deemed significant. The expression of T cell co-stimulatory markers which were measured were: **(A)** CD80 ($p = 0.0033$ CD16+, $p = 0.0219$ CD16-) and **(B)** CD86 ($p = 0.3074$ CD16+, $p = 0.5380$ CD16-).

Analysis of other surface molecules can provide insight into potential functional changes in monocytes. Cyclic ADP ribose hydrolase (CD38) is a glycoprotein whose function is implicated in signal transduction, cell adhesion and calcium signalling. It is a multifunctional ectoenzyme (nucleotide metabolising enzyme) responsible for the synthesis of cyclic ADP-ribose and nicotinic acid-adenine dinucleotide phosphate (NAADP), products which are essential for intracellular calcium regulation. CD38 in malignant myeloma cells is required for oxidative phosphorylation and mitochondrial content, as knock down murine models have illustrated a decrease in both [342]. Conversely, studies in aging have found that the increasing levels of CD38 are inversely proportional to the mitochondrial function of cells [343]. In pregnancy, CD38 expression is increased in both subsets of monocytes (Figure 4.9 A).

Monocytes can bind immunoglobulins as one of their ways to perform phagocytosis (opsonisation – see Figure 4.1) They can bind monomeric IgG via FcγRI (CD64) to trigger cellular activation. CD64 expression in pregnancy is increased in both CD16+ and CD16- subsets of monocytes (Figure 4.9 B).

A scavenger receptor for haemoglobin and the haemoglobin-haptoglobin complex (CD163) is a monocyte lineage marker. It also acts as a sensor for Gram-negative and Gram-positive bacteria. Once bound to the haemoglobin-haptoglobin complex, the complex is internalised and the globin and heme are metabolised leading to iron metabolism and antioxidant pathway changes and polarisation. In pregnancy, no changes are observed in expression of CD163 in either subset of monocytes (Figure 4.9 C). Sialic acids are found in glycoproteins and gangliosides, and are found on cell surfaces of certain bacteria, and vertebrates and some invertebrates. Sialoadhesion (CD169 or siglec-1) is a macrophage I-type lectin cell adhesion molecule which binds sialic acids. A salt bridge is produced between the sialic acid carboxylate group and a highly conserved arginine residue. CD169 mediates juxtracrine signalling with predominantly neutrophils, but also monocytes, NK cells, cytotoxic T cells and B cells. In both subsets of monocytes, CD169 expression is elevated in pregnancy (Figure 4.9 D).

Overall, the phenotype of the monocytes in pregnancy is distinct from that of non-pregnant women. They have more pro-inflammatory and activated markers, suggesting they are either primed for infection, or their constant state of vigilance may leave them excessively activated and contribute to damage expressed by a PAMP or DAMP. Investigation into whether they are produced with this phenotype in the bone marrow, or upon exposure to the environment, is warranted, but not possible with human subjects. This will be discussed in greater detail in *Chapter 8 – General discussion*. The activated phenotype of the monocytes proves a need for their metabolic and functional state need to be determined.

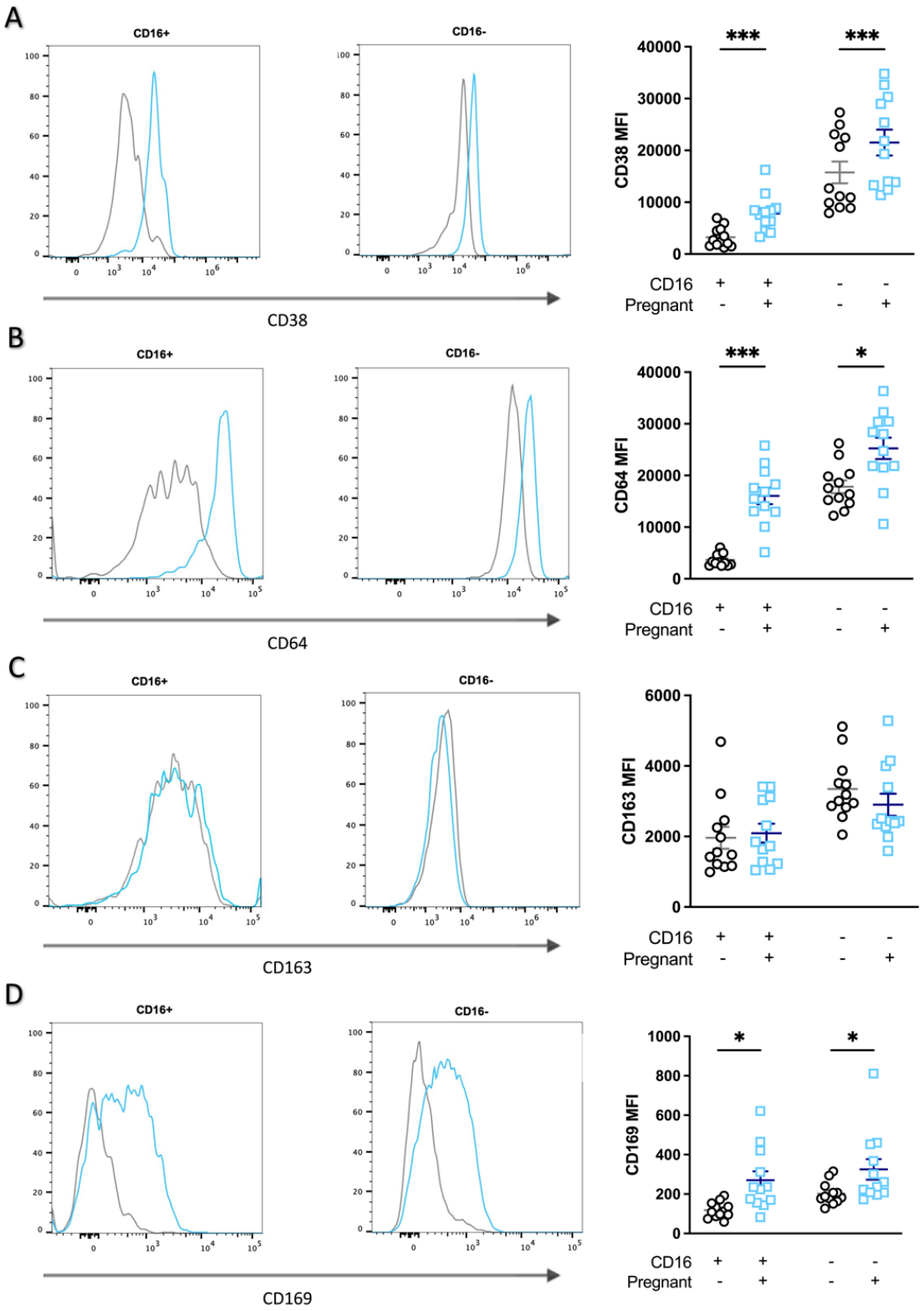

Figure 4.9: Characteristic markers expressed on CD16+ and CD16- monocytes in pregnancy. Non-pregnant (NP) is illustrated in grey (n=12), and pregnant (P) in blue (n=12). An example histogram for each group is shown on the left and summary data on the right as scatter plots. Statistics were determined using 2-way ANOVA and a Šídák's post-hoc test, where $p < 0.05$ was deemed significant. Phenotypic markers which were measured were: **(A)** CD38 ($p = 0.0005$ CD16+, $p = 0.0010$ CD16-), **(B)** CD64 ($p = 0.0004$ CD16+, $p = 0.0160$ CD16-), **(C)** CD163 ($p = 0.8754$ CD16+, $p = 0.4474$ CD16-) and **(D)** CD169 ($p = 0.0259$ CD16+, $p = 0.0490$ CD16-).

4.3.3 Monocytes in pregnancy have genetically altered metabolic pathways

The use of NanoString © technology allows for the investigation into over 700 genes simultaneously in a sample. Monocytes from non-pregnant women aged under 40 years (n=6) were used as a control against age-matched pregnant women at term (n=6) to determine any differences in their metabolic pathways. Figure 4.10 illustrates the overall log2 fold change of the genes measurable in these samples with their relevant p values. The top 40 most significantly altered genes are labelled. There are various different genes which are significant and can be visualised in Figure 4.10.

With the vast number of genes analysed, there appears to be few of significant individual value. However, when considering numerous genes are involved in different processes, it is vital to investigate if there is more of an overarching significant difference by looking at specific pathways. NanoString © data analysis compiles arbitrary pathway scores by condensing the gene expression profiles of each sample. This can be illustrated by a heat map as in Figure 4.11 which shows how the samples cluster based on how similar their pathway scores are.

The pathway scores can also be plotted, and statistics derived (Figure 4.12). Pathways which are indicated to be elevated in the monocytes at 37+ weeks gestation are: AMPK ($p = 0.0004$), cell cycle ($p = 0.0001$), mitochondrial respiration ($p = 0.0288$), TLR signalling ($p < 0.0001$), and transcriptional regulation ($p < 0.0001$). In contrast, the following pathways are downregulated: amino acid transporters ($p = 0.0001$), antigen presentation ($p = 0.0004$), autophagy ($p = 0.0008$), cytokine and chemokine signalling ($p < 0.0001$), hypoxia ($p = 0.0072$), MAPK ($p < 0.0001$), NF-κB ($p = 0.0004$), PI3K ($p < 0.0001$), reactive oxygen response ($p = 0.0002$), TCR & Costimulatory signalling ($p = 0.0002$), and mTOR ($p = 0.0004$).

It is vital to determine if these pathways are actually affected so this was determined with follow on experiments.

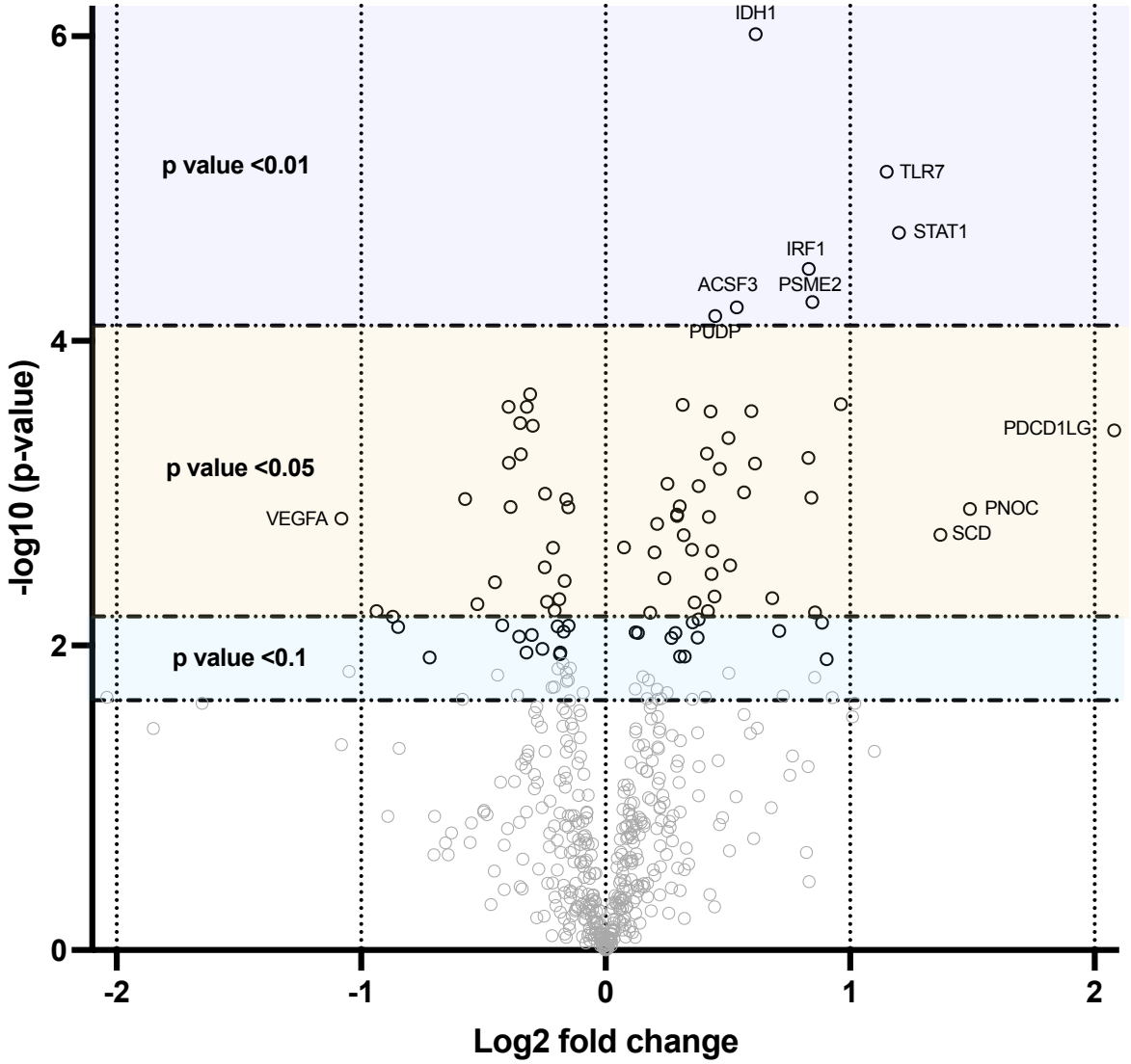

Figure 4.10: Volcano plot of the differential expression of genes in monocytes from non-pregnant vs pregnant women. Using the non-pregnant sample as a baseline, the differential expression of genes in the monocytes of pregnant women are illustrated, where the negative log2 (fold change) suggests a decrease in expression in comparison to the non-pregnant, and the positive log2 (fold change) an increase in expression. The p values calculated using a Benjamini-Hochberg test; $p < 0.05$ is deemed significant. The top 20 genes which were significant are: IDH1 (p = 0.0005), TLR7 (p = 0.0020), STAT1 (p = 0.0034), IRF1 (p = 0.0044), PSME2 (p = 0.0051), ACSF3 (p = 0.0051), PUDP (p = 0.0051), ZNF136 (p = 0.0108), RIMKLB (p = 0.0108), STAT3 (p = 0.0108), SQSTM1 (p = 0.0108), RB1CC1 (p = 0.0108), JAK2 (p = 0.0108), ALOX5 (p = 0.0108), FDX1 (p = 0.0117), PPM1A (p = 0.0117), PDCD1LG2 (p = 0.0118), RBBP5 (p = 0.0125), TLR2 (p = 0.0144), and PEMT (p = 0.0144).

Figure 4.11: Heatmap of pathway scores. The pathway scores are composed by condensing the gene expression profile of each sample. Monocytes from non-pregnant and pregnant women were used for analysis. Blue indicates a decrease in pathway score, whereas yellow indicates an increase.

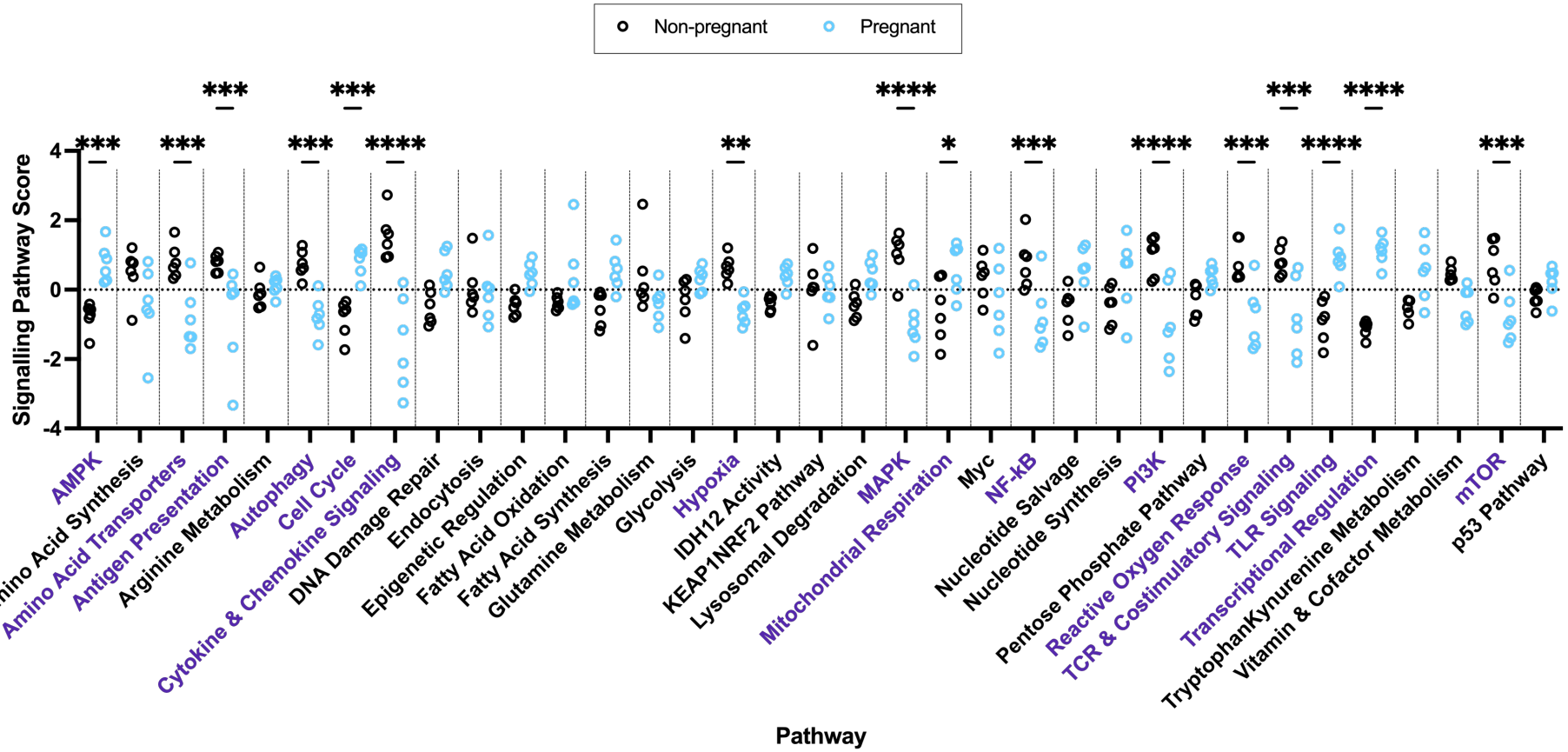

Figure 4.12: The pathway score take into account the various genes involved, with the increasing score corresponding to mostly increasing expression. Monocyte cell lysates were analysed using the NanoString nCounter® Human Metabolism panel and a comparison between the non-pregnant and pregnant samples made. Statistics were determined using a 2-way ANOVA and a Šídák's post-hoc test, where $p < 0.05$ is significant. The pathways for which a score was calculated were: AMPK ($p = 0.0004$), amino acid synthesis ($p = 0.1970$), amino acid transporters ($p = 0.0001$), antigen presentation ($p = 0.0004$), arginine metabolism ($p > 0.9999$), autophagy ($p = 0.0008$), cell cycle ($p = 0.0001$), cytokine and chemokine signalling ($p < 0.0001$), DNA damage repair ($p = 0.0822$), endocytosis ($p > 0.9999$), epigenetic recognition ($p = 0.2612$), fatty acid oxidation ($p = 0.6285$), fatty acid synthesis ($p = 0.0672$), glutamine metabolism ($p = 0.6316$), glycolysis ($p = 0.9371$), hypoxia ($p = 0.0072$), IDH12 activity (0.5766), KEAP1RNF2 pathway ($p > 0.9999$), lysosomal degradation ($p = 0.3570$), MAPK ($p < 0.0001$), mitochondrial respiration ($p = 0.0288$), Myc ($p = 0.8168$), NF-κB ($p = 0.0004$), nucleotide salvage ($p = 0.1882$), nucleotide synthesis ($p = 0.3031$), PI3K ($p < 0.0001$), pentose phosphate pathway ($p = 0.6466$), reactive oxygen response ($p = 0.0002$), TCR and costimulatory signalling ($p = 0.0002$), TLR signalling ($p < 0.0001$), transcriptional regulation ($p < 0.0001$), tryptophan/kynurenine metabolism ($p = 0.0907$), vitamin and cofactor metabolism ($p = 0.2956$), mTOR ($p = 0.0004$) and p53 ($p = 0.9998$).

4.3.4 Monocytes have reduced oxidative phosphorylation capabilities in pregnancy

The NanoString © data suggested that the genes involved in mitochondrial respiration were up regulated. However, the genes involved in the mTOR pathway, a key regulator of mitochondrial oxygen consumption, were downregulated. Treatment with rapamycin, the inhibitor of mTOR, studies have been found to lower oxygen consumption and mitochondrial membrane potential [344]. Bioenergetics of isolated total CD14+ monocytes were therefore used to analyse the oxidative phosphorylation and glycolytic abilities of the cells. Figure 4.13A shows the bioenergetic profile and individual values for the oxygen consumption rate (OCR) of the cells, with the addition of oligomycin, FCCP and then antimycin A and rotenone, to allow the measurement of oxidative phosphorylation. Figure 4.13B also shows the extracellular acidification rate of the cells; this gives an indication of glycolysis. Pregnancy is associated with a significant down-regulation of oxidative phosphorylation especially in its maximal respiration (Figure 3.13C) and spare respiratory capacity value (maximal – basal respiration) and percentage (maximal / basal respiration x 100) profiles (Figure 3.13I&J), whilst showing no change in glycolysis. Despite this, it appears that ATP production is unaffected (Figure 3.13F).

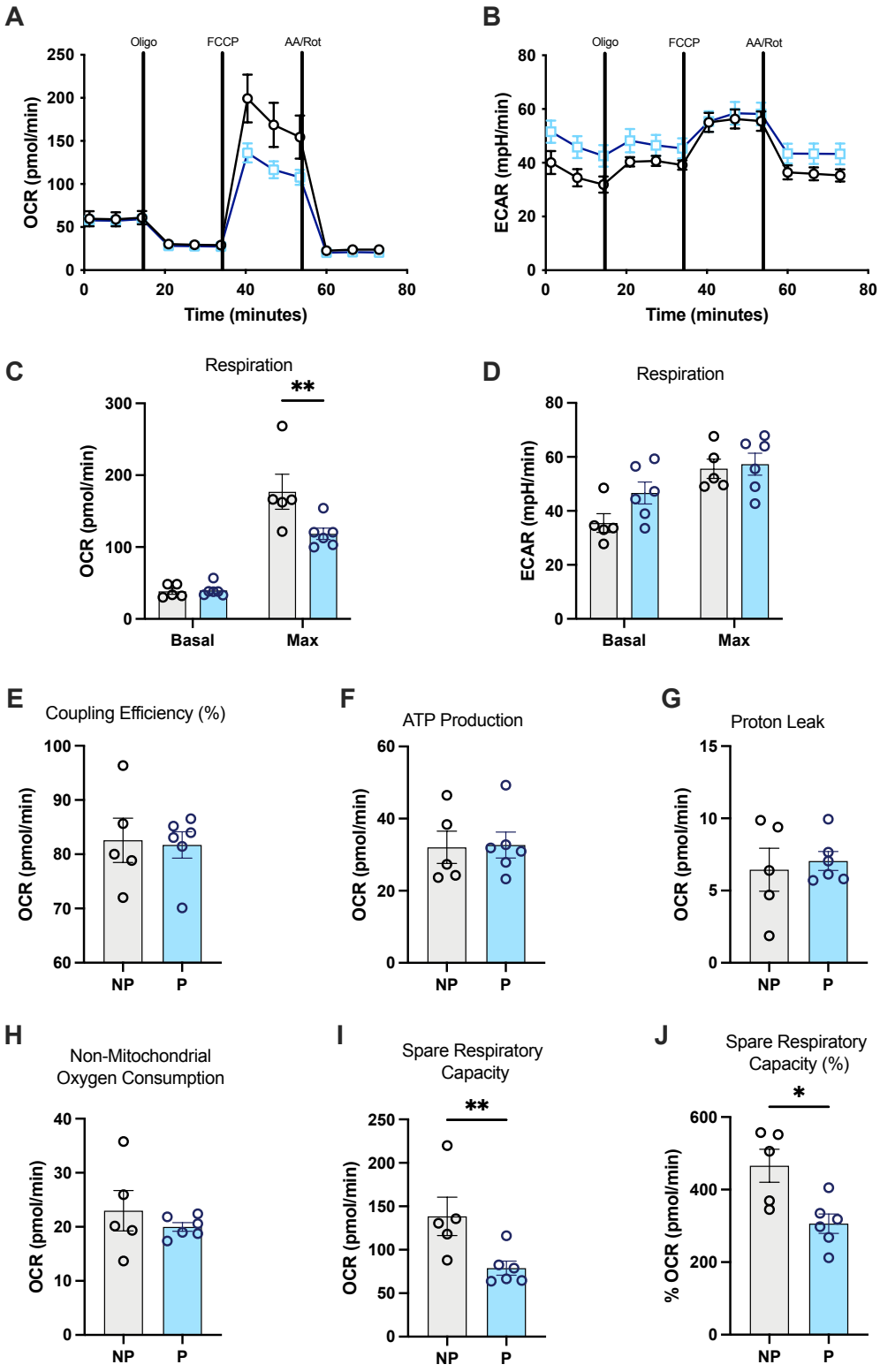

Figure 4.13: The bioenergetic capabilities of total CD14+ monocytes from non-pregnant and pregnant (37+ weeks) women. Total CD14+ monocytes isolated using magnetic microbeads from periperhal blood of non-pregannt (grey; n=5) and pregnant (blue; n=6) women were analysed for their oxidative phosphorylation and glycolysis using the MitoStress assay with the Seahorse© Extracellular Flux analyser. Traces for **(A)** OCR and **(B)** ECAR illustrate the responses of the monocytes to each injection. Statistics were performed using a Mann-Whitney test where $p < 0.05$ was deemed significant. Parameters which were measurable were: **(C)** basal ($p = 0.5368$) and maximal OCR ($p = 0.0087$), **(D)** basal ($p = 0.1255$) and maximal ECAR ($p = 0.9307$), **(E)** coupling efficiency ($p = 0.9307$), **(F)** ATP production ($p = 0.7922$), **(G)** proton leak ($p = 0.7922$), **(H)** non-mitochondrial oxygen consumption ($p = 0.6623$ **(I)** spare respiratory capacity ($p = 0.0087$) and **(J)** the percentage spare respiratory capacity ($p = 0.0173$).

Due to the reduction in OXPHOS in pregnancy, the next step looked at the mitochondria in the monocytes. The use of MitoTracker Green ™ (Figure 4.14A) on the flow cytometer allows for the differentiation of the monocyte subsets and illustrates the depletion of mitochondria in both CD16+ and CD16- monocytes from pregnant women. This is further evidenced by using MALDI-ToF on whole monocytes to investigate the relative quantity of cardiolipin (Figure 4.14B), which shows a reduction in the monocytes from pregnancy. Cardiolipin is an integral lipid of the mitochondria and is synthesised on the matrix side of the inner mitochondrial membrane. The reduction in the quantity of mitochondria likely explains the reduced OXPHOS seen in the total monocytes in Figure 3.13.

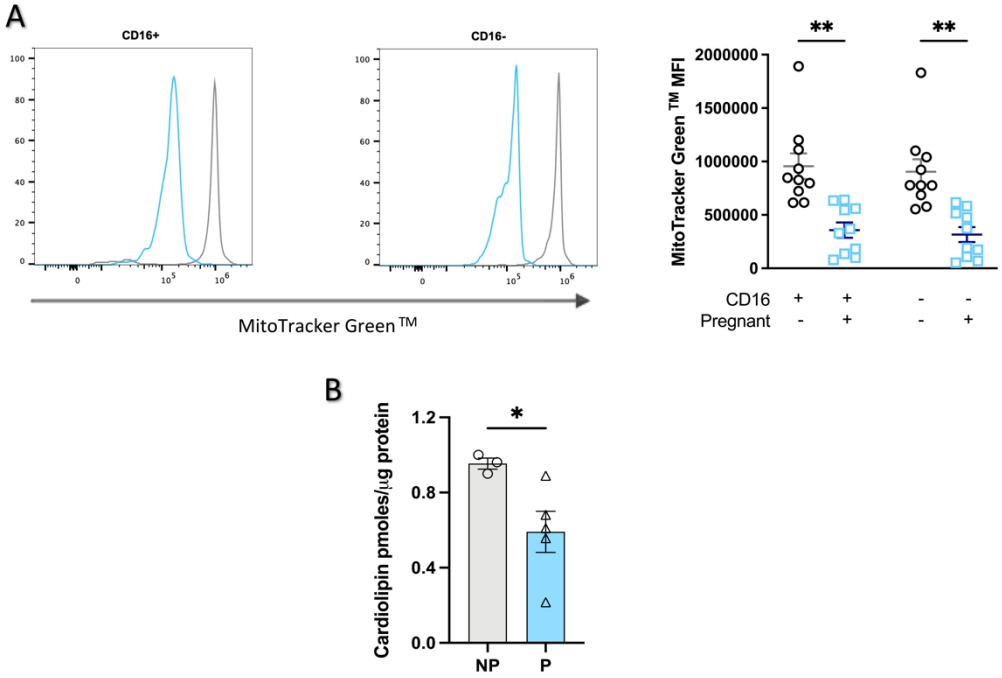

Figure 4.14: Mitochondrial content in monocytes from non-pregnant and pregnant (37+ weeks) women. Monocytes were analysed using flow cytometry or MALDI-ToF to investigate the mitochondrial content in non-pregnant (grey; n=10 MitoTracker, n=3 cardiolipin) and pregnant (blue; n=10 MitoTracker, n=5 cardiolipin) women. Statistics performed was either a two-way ANOVA and a Šídák's post-hoc test, or Mann-Whitney test where $p < 0.05$ was deemed significant. Mitochondrial content was determined using **(A)** MitoTracker Green ™ for CD16+ ($p = 0.0024$) and CD16- ($p = 0.0021$) monocytes and **(B)** relative cardiolipin concentration in total monocytes ($p = 0.0357$).

The pathway scores from the NanoString © suggested that the genes involved in the reactive oxygen response in the monocytes are downregulated. During OXPHOS, mitochondrial ROS (mtROS) are produced, specifically superoxide (caused by the partial reduction of oxygen from leaking electrons from complex I and III) and subsequently hydrogen peroxide. To further delve into the reduced OXPHOS in monocytes from pregnant women, mitochondrial superoxide levels were measured using MitoSOX Red ™ (Figure 4.15A). While not quite

significant, there appears to be a slight decrease in the amount of mitochondrial superoxide in both CD16+ and CD16- monocytes of pregnant women. It is also vital to see if total cellular ROS is affected by pregnancy in the monocytes. This was done with the DCFDA assay (Figure 4.15B), with oligomycin and FCCP to mimic the conditions used in the bioenergetics assay. This yielded no significant changes in cellular ROS production for the monocytes in pregnancy.

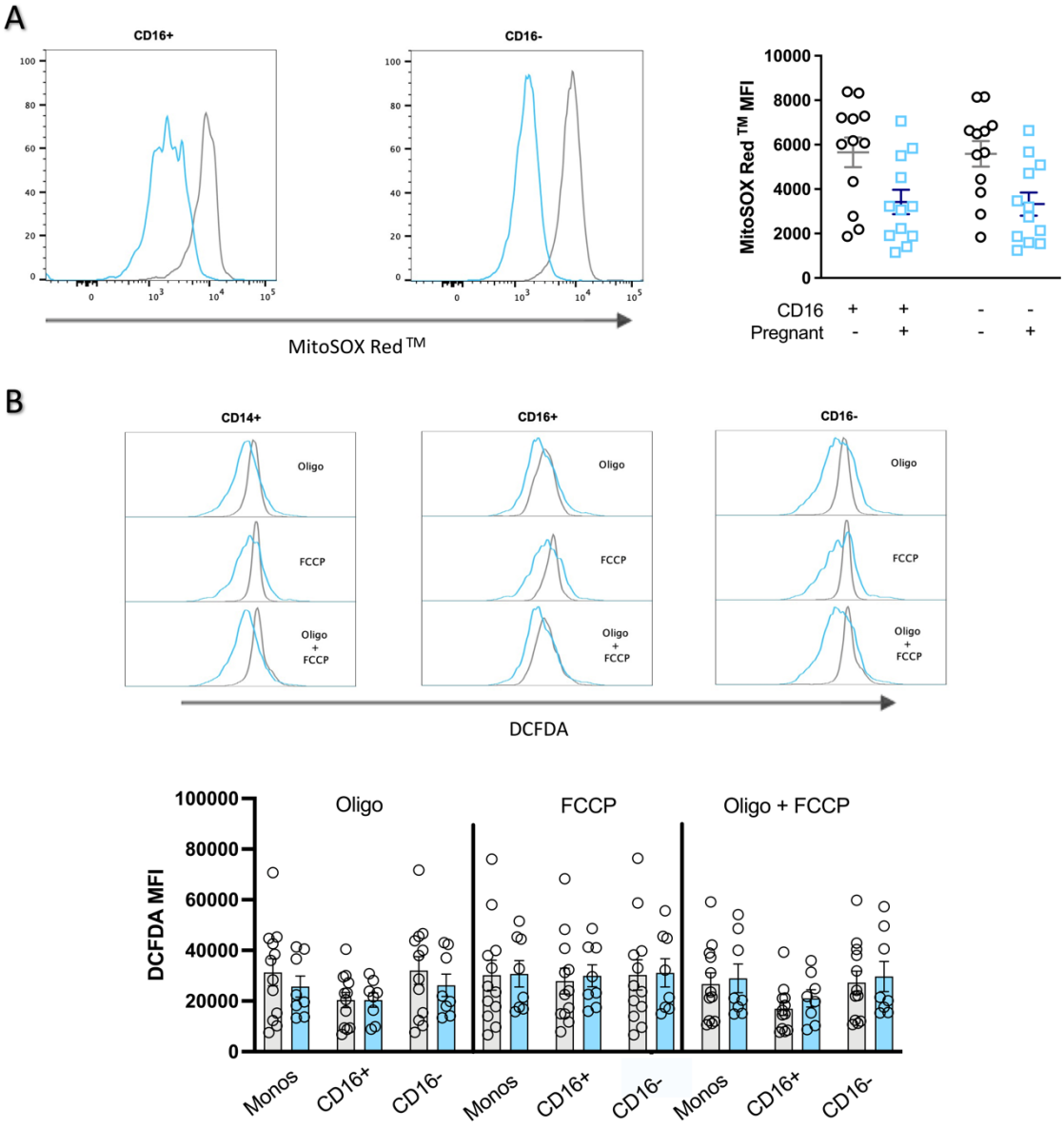

Figure 4.15: Mitochondrial and cellular ROS production by monocytes from non-pregnant and pregnant (37+ weeks) women. Monocytes from non-pregnant (grey; n=12) and pregnant (blue; n =12 MitoSOX, n=8 DCFDA) women were analysed using flow cytometry as described in the materials and methods to determine mitochondrial and cellular ROS activity. Statistics were performed using a 2-way ANOVA and a Šídák's post-hoc test, where $p < 0.05$ was deemed significant. Mitochondrial superoxide activity was determined with **(A)** MitoSOX Red ($p = 0.0629$ CD16+, $p = 0.0572$ CD16-), whereas cellular ROS activity was measured with **(B)** the DCFDA assay with oligomycin ($p = 0.9810$ CD14+, $p > 0.9999$ CD16+, $p = 0.9814$ CD16-), FCCP ($p > 0.9999$ CD14, $p > 0.9999$ CD16+, $p > 0.9999$ CD16-), or a combination of oligomycin/FCCP ($p > 0.9999$ CD14, $p = 0.7040$ CD16+, $p > 0.9999$ CD16-).

4.3.5 CD16+ and CD16- monocytes have altered metabolic transporter expression in pregnancy

Changes in OXPHOS during pregnancy could be due to a change in fuel resource. NanoString © analysis suggested a downregulation in the genes involved in amino acid transporters for example. Therefore, the expression of key metabolic transporters were considered by flow cytometry. CD36, a multi-functional receptor that has a role in importing fatty acids (FA) into cells [345], was increased significantly in both monocyte subsets with pregnancy (Figure 4.16A). Conversely, CD98 which is a heterodimer long chain amino acid transporter (LAT1) [346], was decreased significantly in both subsets in pregnancy (Figure 4.16B). Glucose transporter 1 (GLUT1), responsible for facilitating glucose across the membranes of cells, was found to be unchanged in pregnancy (Figure 4.16C). Despite trying different CD16 antibodies to differentiate the monocytes for intracellular GLUT1 expression, this was not possible.

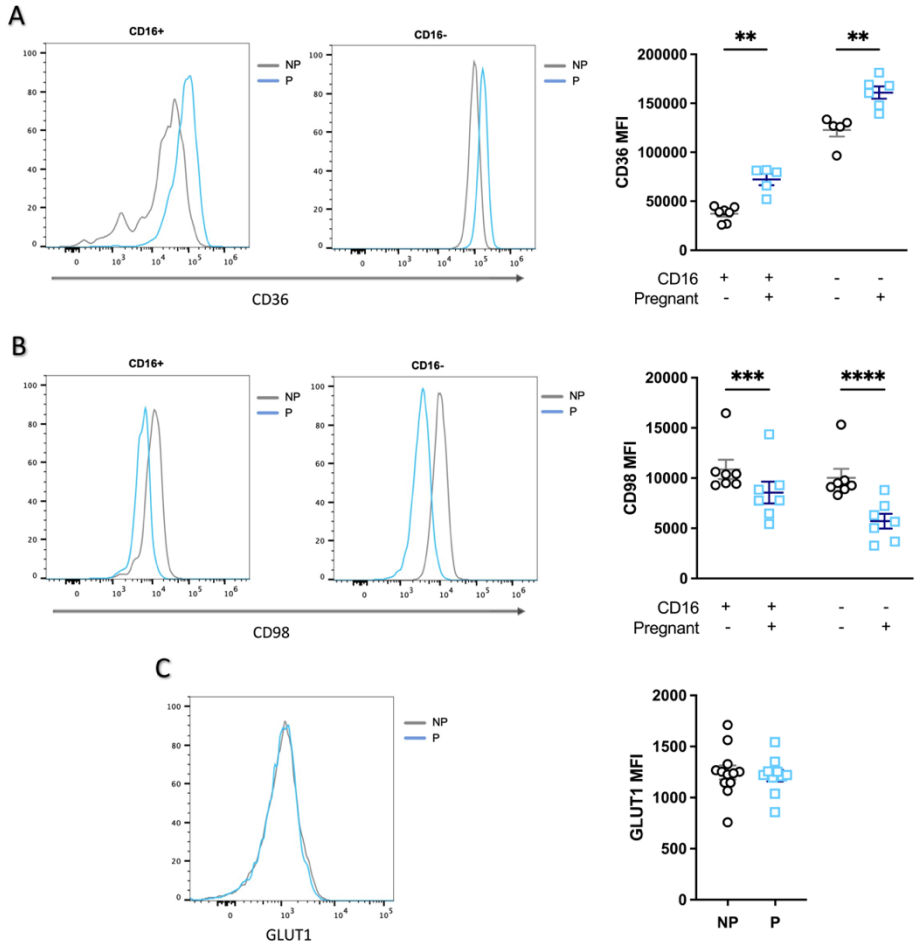

Figure 4.16: Expression of metabolic transporters in CD16+ and CD16- monocytes from non-pregnant and pregnant (37+ weeks) women. Subsets of monocytes from non-pregnant (grey; n=7 CD36, CD98, n=12 GLUT1) and pregnant (blue; n=7 CD36, CD98, n=10 GLUT1) women were analysed for key metabolic transporter expression with flow cytometry as described in the materials and methods. Statistics were performed with a 2-way ANOVA and a Šídák's post-hoc test, or Mann-Whitney test and $p < 0.05$ deemed significant. Receptors measured were: **(A)** CD36 ($p = 0.0025$ CD16+, $p = 0.0043$ CD16-), **(B)** CD98 ($p = 0.0043$ CD16+, $p = 0.0043$ CD16-) and **(C)** GLUT1 ($p = 0.7400$).

4.3.6 Fatty acid uptake and storage is unchanged in the monocytes during pregnancy

Fatty acids are utilised by monocytes as one of their various energy sources. Due to the changes observed above of increased expression of the fatty acid translocase marker CD36 and the reduction in oxidative phosphorylation, investigating fatty acid uptake and storage was deemed necessary. CD36 function, however, is not limited to only fatty acid transport; it has other roles such as phagocytosis, calcium flux and production of prostaglandin E_2 [347, 348]. The BODIPY ® fluorophore dyes are intrinsically lipophilic and intensely fluorescent that mimic *in vivo* natural lipids and provide effective tracers of lipid trafficking. BODIPY 493 is used to specifically stain for cellular neutral lipid droplets and non-polar lipids[349] so provides insight into the lipid content of the cell. BODIPY 500 mimics fatty acids and can become incorporated into the cells, allowing for the measurement of fatty acid uptake. BODIPY 493 was not significantly different in either monocyte subsets in pregnancy (Figure 4.17 A&B) suggesting no difference in lipid content. BODIPY 500 was also unchanged in both subsets of monocytes in pregnancy (Figure 4.17 A&B). The results shown in Figure 3.17 A&B were from analysis of freshly isolated cells, so the effects of cell activation were then considered. Monocytes were cultured for 24hr unstimulated and stimulated with either LPS or MDP. Due to the ability of monocytes to acquire and/or up-regulate CD16 expression over long periods of time, subset analysis was not performed. Both BODIPY 493 and 500 were unchanged for all of the conditions in pregnancy (Figure 4.17C). LipidTOX ™ can also be used to determine steatosis (intracellular accumulation of neutral lipids). The use of this dye on monocytes illustrated no significant difference in their pool of lipids (Figure 4.18). Overall, this means that despite higher expression of CD36 on monocytes from pregnant women there is no evidence of increased fatty acid uptake or accumulation.

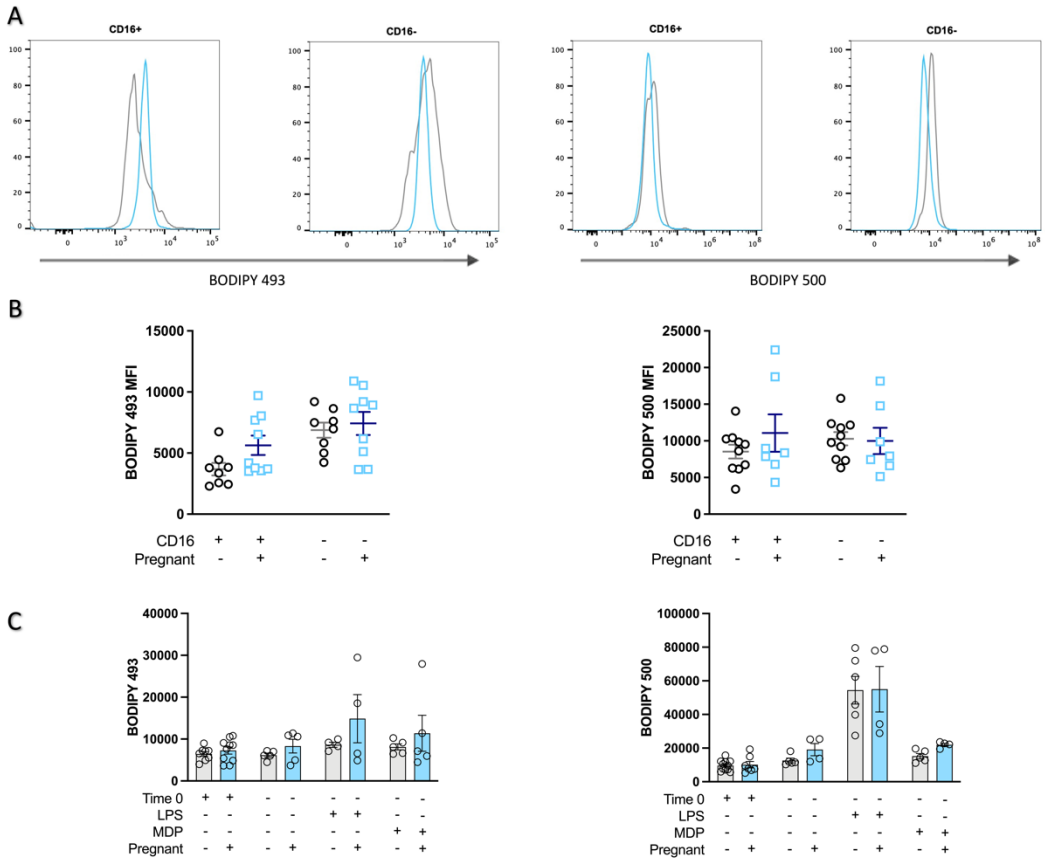

Figure 4.17: Fatty acid uptake and storage in monocytes from non-pregnant and pregnant (37+ weeks) women. Isolated monocytes from frnon-pregnant (grey; n=8 BODIPY 493, n=5 24hr, n=10 BODIPY500, n=6 24hr) and pregnant (blue; n=9 BODIPY 493, n=5 24hr, n=7 BODIPY 500, n=4 24hr) women were anlaysed with BODIPY 493 for FA storage and BODIPY 500 for FA uptake. Statistics were determined using 2-way ANOVAs and a Šídák's post-hoc test, where $p < 0.05$ was deemed significant. **(A)** Example histograms of BODIPY 493 and BODIPY 500. **(B)** Basal expression of the monocyte subsets were measured for: BODIPY 493 ($p = 0.1861$ CD16+, $p = 0.8415$ CD16-) and BODIPY 500 ($p = 0.1861$ CD16+, $p = 0.8415$ CD16-). **(C)** Expression of BODIPY 493 and BODIPY 500 was measured in total monocytes for time 0 ($p = 0.9374$ BODIPY 493; $p = 0.9921$ BODIPY 500) and post-24 hrs for unstimulated ($p = 0.9374$ BODIPY 493; $p = 0.1993$ BODIPY 500), LPS ($p > 0.9999$ BODIPY 493; $p > 0.9999$ BODIPY 500) and MDP ($p > 0.9999$ BODIPY 493; $p = 0.1211$ BODIPY 500).

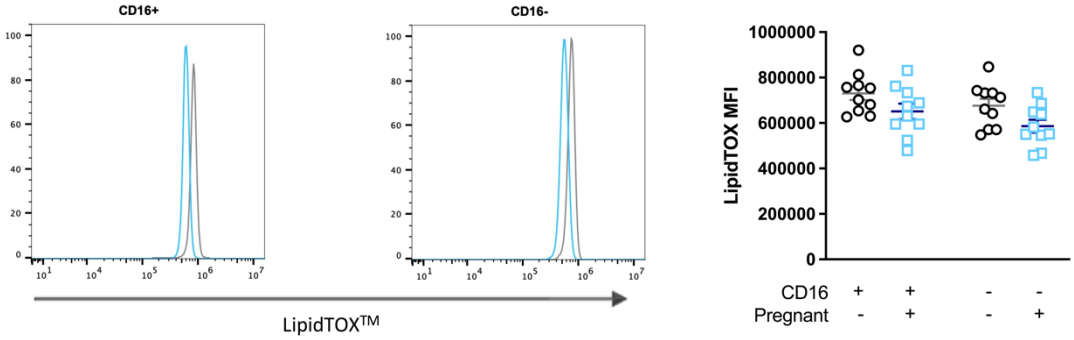

Figure 4.18: The accumulation of neutral lipids in monocytes from non-pregnant and pregnant (37+ weeks) women. Monocytes from non-pregnant (grey; n=10) and pregnant (blue; n=10) women were stained with LipidTOX ™ and analysed using flow cytometry as described in the Materials and Methods. Statistics were performed using a 2-way ANOVA and a Šídák's post-hoc test, where $p < 0.05$ was deemed significant. CD16+ ($p = 0.2865$) and CD16- ($p = 0.1910$) subsets were analysed.

4.3.7 Kynurenine uptake is increased in CD16+ monocytes only in pregnancy

Amino acids are another energy source utilised by monocytes, albeit more difficult to investigate. Amino acid transporter genes are downregulated in total monocytes (Figure 4.16A), and CD98 (LAT1) expression is decreased in both monocyte subsets with pregnancy (Figure 4.16B). While no significant difference was found using NanoString © with regards to tryptophan/kynurenine metabolism, it did appear to be increased. A simple assay can be undertaken to investigate the uptake of kynurenine, a product of tryptophan metabolism, due to its autofluorescence (Ex/Em 380/480 nm) which can be monitored using flow cytometry[327, 350]. Tryptophan is an aromatic amino acid and can be transported via CD98. Kynurenine and its further metabolised products have various roles including regulating the immune response [351]. Some of the metabolites of kynurenine can suppress T cell responses. In response to inflammatory signalling such as via LPS stimulation, IDO, the enzyme which catalyses the transformation of tryptophan into kynurenine, is strongly induced in APCs [352]. Tryptophan is an essential amino acid required in pregnancy: fetal growth and development and elevated synthesis of proteins for the mother; NAD^+ synthesis; kynurenine for subduing rejection of the fetus [353]. In late pregnancy, tryptophan availability is maintained in order to increase the flux through its metabolic pathway to increase immunosuppressive kynurenine [353]. In monocytes, an increase in the uptake of kynurenine in the CD16+ monocytes in pregnancy was observed, with no change in this capability in the CD16- monocytes (Figure 4.19).

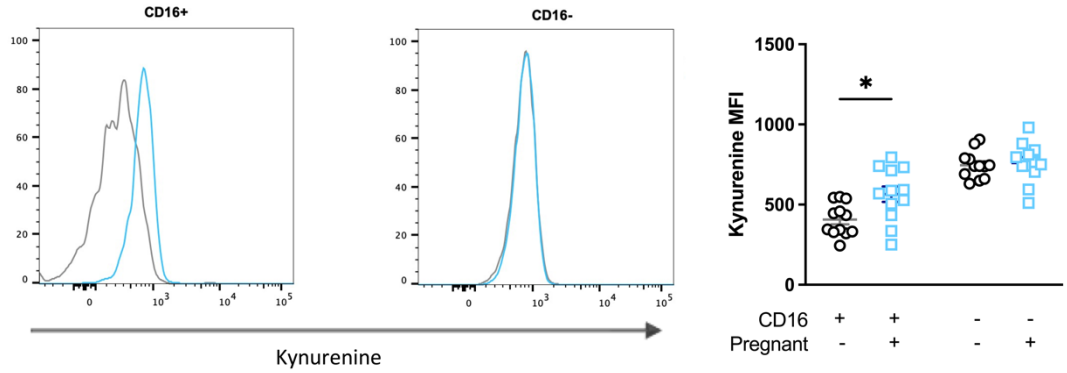

Figure 4.19: Uptake of kynurenine in monocytes from non-pregnant and pregnant (37+ weeks) women. Isolated monocytes from non-pregnant (grey; n=12) and pregnant (blue; n=12) women and used for uptake of kynuerinine awith appopriate controls as described in the material and methods. Statistics were determined using 2-way ANOVAs and a Šídák's post-hoc test, where $p < 0.05$ was deemed significant. Uptake of kynurenine was determined by MFI ($p = 0.0488$ CD16+, $p = 0.9500$ CD16-).

4.3.8 Monocytes from pregnant women are less reliant on glutamine than monocytes from non-pregnant women

As the metabolic transporter receptors (Figure 4.16) showed differences in expression on the monocytes during pregnancy, which led to the realisation that the lipid content is unchanged (Figure 4.17,Figure 4.18) but the kynurenine uptake was elevated (Figure 4.19), the next logical step was to determine if the monocytes have a preferential fuel for respiration. Tweaking the MitoStress assay on the Seahorse extracellular flux analyser allows insight into this, with the addition of a first injection with an inhibitor relevant to utilisation of a particular fuel. The injection for the control sample was only media. To investigate the use of carbohydrates, fatty acids and amino acids in OXPHOS, inhibitors for glutaminase (GLS1; inhibitor BPTES), carnitine palmitoyltransferase I (CPT1; inhibitor etomoxir) and mitochondrial pyruvate carrier (MPC; inhibitor UK5099) were used respectively. This has its limitations in that it only targets subsets of these fuel groups, but it can increase our understanding of the mechanisms of respirational control of the monocytes in pregnancy.

The traces for the OCR for monocytes from non-pregnant (Figure 4.20A) and pregnant (Figure 4.20B) women hint at different fuel dependencies. The monocytes from pregnant women appear to be more flexible in their use of fuels; on inhibition with UK5099, monocytes from non-pregnant women struggle more with their non-mitochondrial oxygen consumption (Figure 4.20E), and ATP production (Figure 4.20G), leading to potentially damaged mitochondria as evidenced by increased proton leak (Figure 4.20F). There was no significant difference between their basal and maximal respiration however, as well as no difference in their coupling efficiency and spare respiratory capacity. There were no significant changes for the other inhibitors (BPTES, Etomoxir) either.

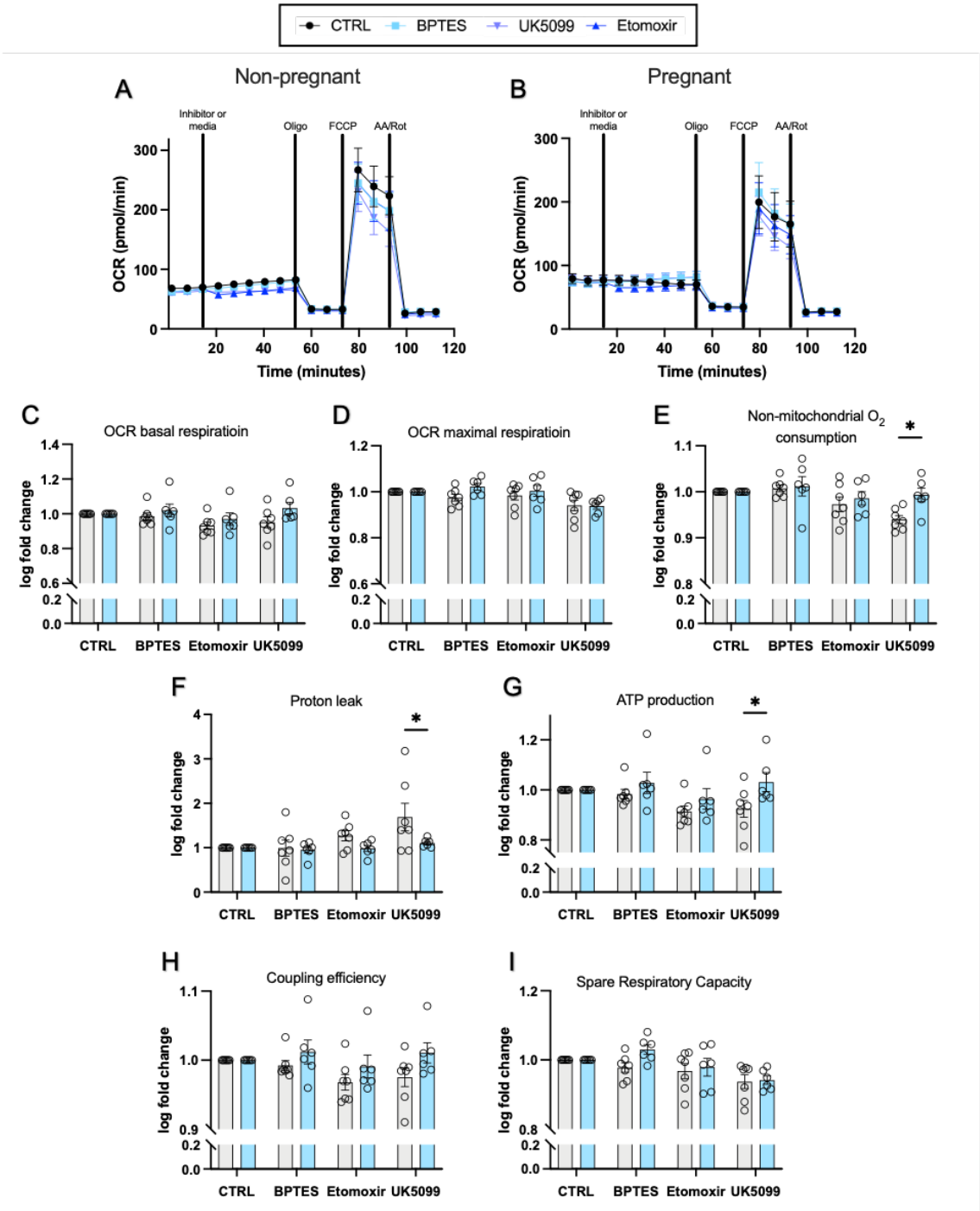

Figure 4.20: The dependency on different fuels of monocytes from non-pregnant and pregnant (37+ weeks) women. The effect of inhibitors on monocyte oxidative phosphorylation was analysed in non-pregnant (grey; n=7) women versus pregnant (blue; n=6) women using a modified MitoStress assay. The use of these inhibitors (BPTES (B) for amino acids, Etomoxir (E) for fatty acids and UK5099 (U) for pyruvate) provides insight into the reliance of the cells on these fuel sources. Statistics were performed using a 2-way ANOVA and a Šídák's post-hoc test, where a p value < 0.05 was deemed significant. Traces for the OCR of the monocytes from non-pregnant **(A)** and pregnant **(B)** women illustrate the effect of the inhibitors. To determine the effect of the inhibitors, values were normalised against their individual control values, by calculating a log value. Parameters which were measurable were: **(C)** OCR basal respiration (B p = 0.8298; E p = 0.7615; U p = 0.1120), **(D)** OCR maximal respiration (B p = 0.1714; E p = 0.8680; U p > 0.9999), **(E)** non-mitochondrial oxygen consumption (B p = 0.9983; E p = 0.9068; U p = 0.0138), **(F)** proton leak (B p = 0.9996; E p = 0.5507; U p = 0.0319), **(G)** ATP production (B p = 0.7236; E p = 0.6300; U p = 0.0418), **(H)** coupling efficiency (B p = 0.6795; E p = 0.5358; U p = 0.1485), and **(I)** spare respiratory capacity (B p = 0.1042; E p = 0.9809; U p = 0.9994).

4.3.9 Monocytes from pregnant women produce lowered levels of pro-inflammatory cytokines when left unstimulated or MDP-stimulated

With evidence of some alteration to fuel utilisation and reduced oxidative phosphorylation with pregnancy the next step was to consider the functional consequences of this. The NanoString © data suggests a downregulation of the genes involved in cytokine and chemokine signalling in the monocytes, and so it is necessary to determine if this is functional.

When unstimulated, monocytes from pregnant women produce significantly less IL-1β (Figure 4.21A), IL-6 (Figure 4.21B) and TNFα (Figure 4.21D) in comparison to non-pregnant women. Whilst not significant, the secretion of IL-8 (Figure 4.21C) from monocytes in pregnancy also appears reduced.

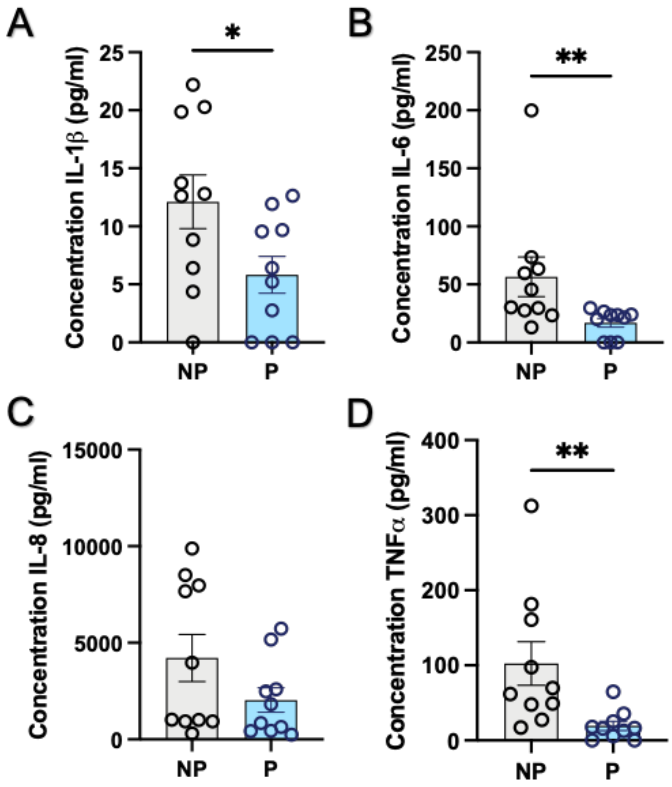

Figure 4.21: Cytokine production from unstimulated monocytes from non-pregnant and pregnant (37+ weeks) women. Supernatants from monocytes unstimulated for 24 hrs were analysed for cytokines produced in non-pregnant (grey; n=10) versus pregnant (blue; n=10) women as described in the Materials and Methods. Statistical analysis was performed using a Mann-Whitney t test where $p < 0.05$ was deemed significant. Cytokines measured were: **(A)** IL-1β ($p = 0.0492$), **(B)** IL-6 ($p = 0.0052$), **(C)** IL-8 ($p = 0.1655$) and **(D)** TNFα ($p = 0.0010$).

In contrast to the decrease in the genes involved in cytokine and chemokine signalling, those involved in TLR signalling are suggested to be elevated in the monocytes in pregnancy, especially TLR7 ($p = 0.0137$) and, to a much lesser extent, TLR4 ($p = 0.1330$). As pregnant

women are notorious for increased severity when contracting infectious diseases like influenza [161] and middle eastern respiratory syndrome (MERS) [354], it is vital to determine the ability of monocytes from pregnant and non-pregnant women to combat pathogens. This can be imitated by specific immunosimulators.

When stimulated with LPS (extracellularly binds TLR4), the secretion of IL-1β (Figure 4.22A), IL-8 (Figure 4.22C), and IL-10 (Figure 4.22D) from monocytes of pregnant women does not differ significantly different to that from monocytes from non-pregnant women. Whilst not significant, the production of IL-6 (Figure 4.22B) and TNFα (Figure 4.22E) from monocytes in pregnancy appear reduced in comparison to monocytes from non-pregnant women.

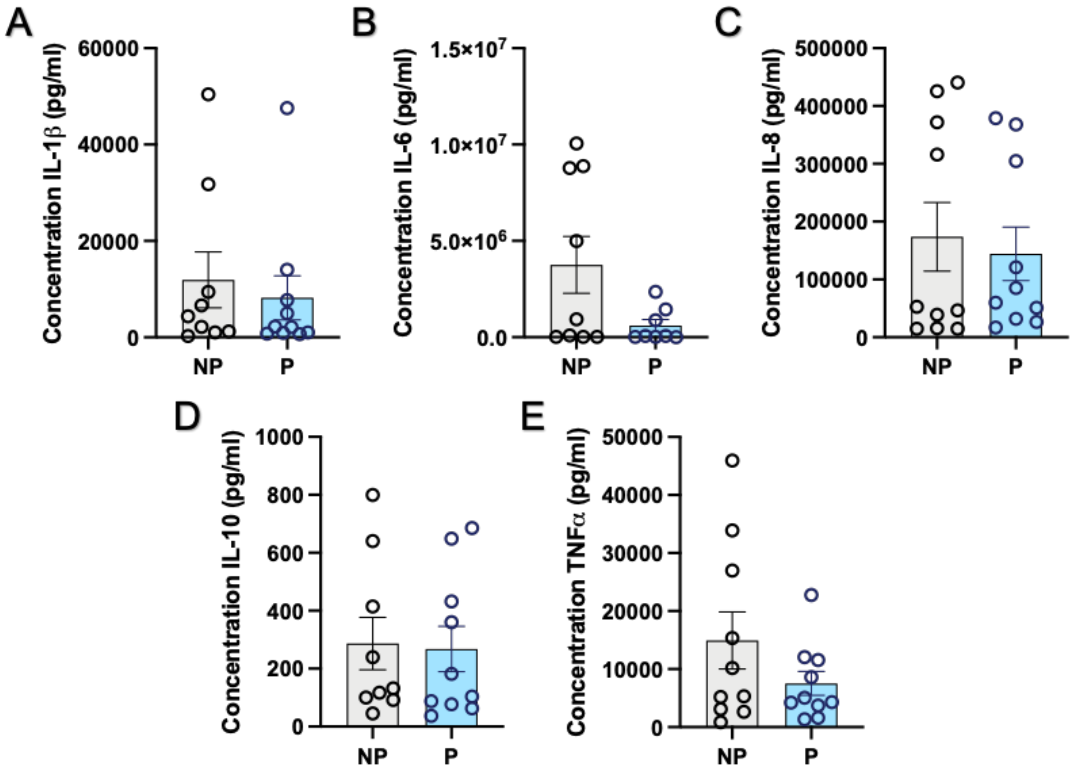

Figure 4.22: Cytokine production from LPS stimulated monocytes from non-pregnant and pregnant (37+ weeks) women. Supernatants from monocytes stimulated with LPS for 24 hrs were used for cytokine analysis in non-pregnant (grey; n=10) versus pregnant (blue; n=10) women as described in the Materials and Methods. Statistical analysis was performed using a Mann-Whitney t test where $p < 0.05$ was deemed significant. Cytokines measured were: **(A)** IL-1β ($p = 0.1220$), **(B)** IL-6 ($p = 0.2370$), **(C)** IL-8 ($p = 0.9654$), **(D)** IL-10 ($p = 0.6516$) and **(E)** TNFα ($p = 0.2370$).

Monocytes stimulated with MDP (intracellularly binds NOD2) produce significantly less IL-6 (Figure 4.23B) and TNFα (Figure 4.23D) with pregnancy. The secretion of IL-1β also appears reduced in pregnancy, but this is not significant (Figure 4.23A) whilst the secretion of IL-8 (Figure 4.23C) is unchanged.

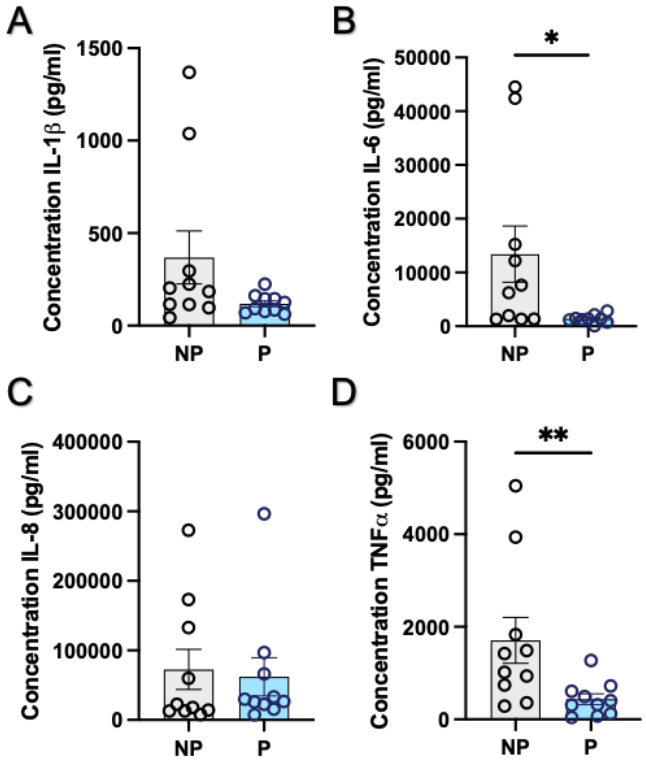

Figure 4.23: Cytokine production from MDP stimulated monocytes from non-pregnant and pregnant (37+ weeks) women. Monocytes were stimulated for 24 hr with MDP, from which the supernatant was used for cytokine analysis in non-pregnant (grey; n=10) versus pregnant (blue; n=10) women as described in the Materials and Methods. Statistical analysis was performed using a Mann-Whitney t test where $p < 0.05$ was deemed significant. Cytokines measured were: **(A)** IL-1β ($p = 0.0892$), **(B)** IL-6 ($p = 0.0172$), **(C)** IL-8 ($p = 0.6305$) and **(D)** TNFα ($p = 0.0068$).

In order to produce IL-12p70, a cytokine involved in mediating T cell and NK cell responses, monocytes need to be stimulated via both TLR4 and TLR8 [355]. IL-12 has previously been shown to be increased intracellularly in monocytes in pregnancy [76]. Thus, when stimulated with LPS (TLR4) and R848 (TLR7/8) monocytes can produce IL-12p70. However, there was no significant difference in the production of any cytokines measured in pregnancy in comparison to non-pregnant; IL-1β (Figure 4.24A), IL-6 (Figure 4.24B), IL-8 (Figure 4.24C), IL-10 (Figure 4.24D), IL-12p70 (Figure 4.24E) and TNFα (Figure 4.24F). Whilst there are no significant changes, the production of IL-1β and TNFα does appear reduced.

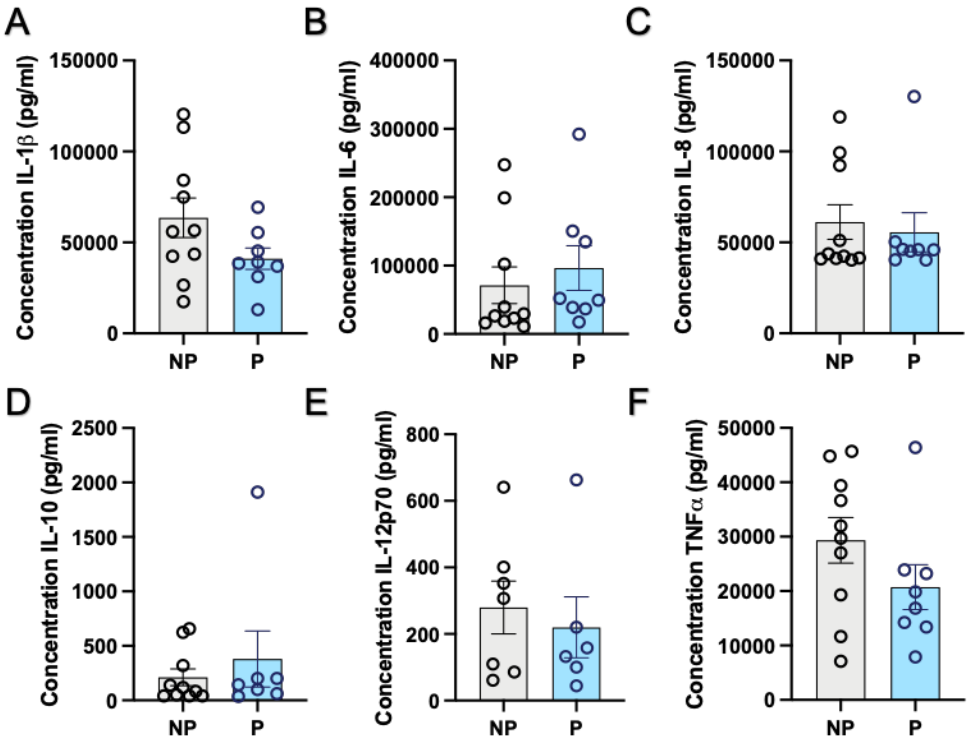

Figure 4.24: Cytokine production from LPS/R848 stimulated monocytes from non-pregnant and pregnant (37+ weeks) women. The supernatants from monocytes stimulated with a combination of LPS and R848 were used for the measurement of cytokines produced in non-pregnant (grey; n=10) versus pregnant (blue; n=10) women as in the Materials and Methods. Statistical analysis was performed using a Mann-Whitney t test where $p < 0.05$ was deemed significant. Cytokines measured were: **(A)** IL-1β ($p = 0.1220$), **(B)** IL-6 ($p = 0.2370$), **(C)** IL-8 ($p = 0.9654$), **(D)** IL-10 ($p = 0.6516$), **(E)** IL-12p70 ($p = 0.7308$) and **(F)** TNFα ($p = 0.2370$).

4.3.10 Phagocytic capabilities of monocytes are heightened in pregnancy

CD36 is a scavenger receptor, and while its most recognisable role is as a FAT, it is also involved in non-opsonic phagocytosis. As CD36 expression is increased in monocytes (Figure 4.16A), and yet this does not translate to elevated lipid uptake and storage, (Figure 4.17) its other roles must be considered. CD64, involved in opsonic phagocytosis, was also upregulated on the monocytes during pregnancy (Figure 4.9). The combination of increased CD36 and CD64 warranted investigation of the phagocytic function of the monocytes. To determine this, pHrodo *E. coli* BioParticles ™ and flow cytometry were used. These are not opsonised and the experiment was devoid of a source of IgG so the approach chosen investigates more the role of CD36 rather than CD64. As CD16 is mobilised and shed during opsonic phagocytosis, only total monocytes could be analysed and not the subsets [356]. Two different concentrations of the *E. coli* BioParticles ™ were used (10 µg, 25 µg [357]), with a significantly higher rate of

phagocytosis by the monocytes of pregnant women in response to the higher concentration (Figure 4.25).

Unfortunately, due to COVID-19, this finding could not be pursued further within the timeframe. Plans involved repeating the experiment with human plasma to introduce IgG for opsonic phagocytosis and using an inhibitor for CD36 (sulfo-N-succinimidyl oleate [SSO]) to determine its role in phagocytosis of monocytes in pregnancy.

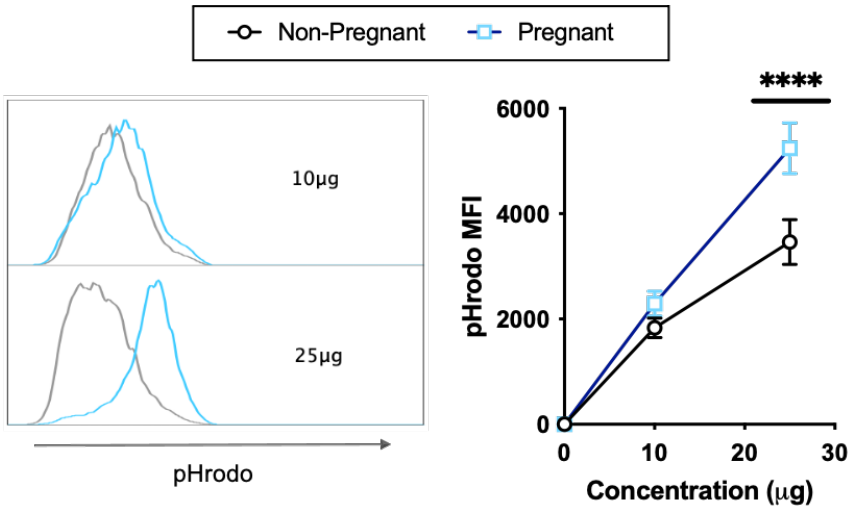

Figure 4.25: The measurement of the phagocytic capabilities of the monocytes from non-pregnant and pregnant (37+ weeks) women. Monocytes are cultured with different concentrations of pHrodo Red E. coli BioParticles to illustrate phagocytosis in non-pregnant (grey; n=12) women versus pregnant (blue; n=12) women as described in the Materials and Methods and analysed using the flow cytometer. Statistics were performed using a 2-way ANOVA and a Šídák's post-hoc test, where $p < 0.05$ were determined to be significant. Concentrations of pHrodo which was used were: 10 µg ($p = 0.1621$) and 25 µg ($p < 0.0001$).

4.3.11 Monocytes from pregnant women are less efficient at producing lipid mediators

Supernatants from monocytes stimulated with and without LPS were sent to Toulouse Lipidomic Centre for lipidomic analysis. Traditionally, to determine the functional capabilities of monocytes, cytokines and their phagocytic capabilities are discussed. As discussed in more detail in the earlier *Chapter 3- The changing lipidomic profile of pregnancy can be monitored using novel mass spectrometry techniques,* lipid mediators are key immunomodulatory molecules which regulate the severity of inflammation and can be produced by monocytes. As monocytes in pregnancy have reduced OXPHOS capabilities (Figure 4.13), yet little functional difference in cytokine output (Figure 4.21-24), it is rational to determine if other monocyte outputs are effected. In the first instance, n=1 was sent to test whether an approach adapted from analysis of plasma/serum [274] could be used on either cells or cell

culture supernatants. A further n=6 was sent after confirmation, producing data with n=7 total.

TXB_2 is an inactive waste product. Upon stimulation with LPS, the monocytes from pregnancy appear perturbed in their ability to produce TBX_2, but this is not significant (Figure 4.26).

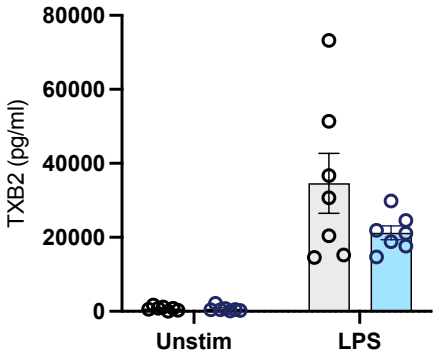

Figure 4.26: Inactive product concentrations in the supernatants of monocytes from non-pregnant and pregnant (37+ weeks) women stimulated with or without LPS. Monocytes from a non-pregnant (grey) and a pregnant (blue) woman were cultured with or without LPS so that the supernatant could be analysed for the presence of eicosanoids using LC-MS/MS. Statistics were performed with a 2-way ANOVA and a Šídák's post-hoc test, where <0.05 was significant. Inactive products that were detectable: TXB_2 (unstim p = 0.0998, LPS p = 0.0643).

The ability of monocytes to produce eicosanoids classified as pathway markers depends on the molecule in question. The monocytes from a pregnant woman appear to produce more 14-HDoHE when left unstimulated or stimulated with LPS, in comparison to the monocytes from the non-pregnant woman, but this is not significant. There are no significant changes to the production of 5-HETE, 17-HDoHE an 18-HEPE. Conversely, the production of 15-HETE is significantly hindered upon LPS stimulation in the monocytes from a pregnant woman (p = 0.0408; Figure 4.27).

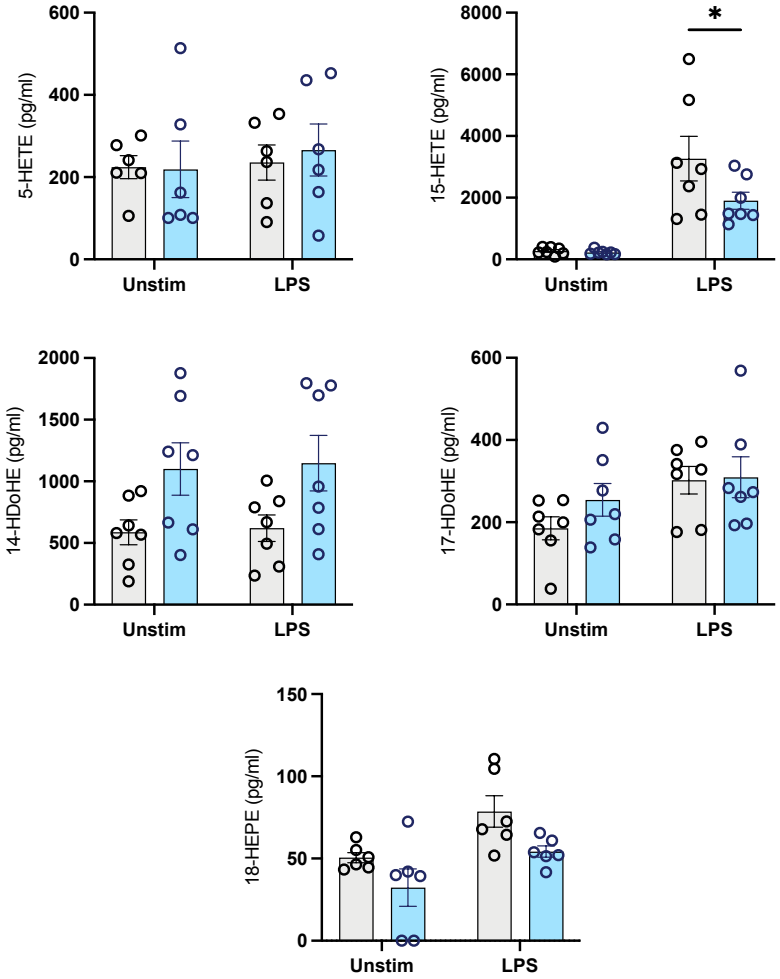

Figure 4.27: Pathway marker concentrations in the supernatants of monocytes from non-pregnant and pregnant (37+ weeks) women stimulated with or without LPS. Monocytes from a non-pregnant (grey) and a pregnant (blue) woman were cultured with or without LPS so that the supernatant could be analysed for the presence of eicosanoids using LC-MS/MS. Statistics were performed with a 2-way ANOVA and a Šídák's post-hoc test, where <0.05 was significant. Bioactive mediators that were detectable: 5-HETE (unstim p = 0.9968, LPS p = 0.9049) 15-HETE (unstim p = 0.9959, LPS p = 0.0408), 14-HDoHE (unstim p = 0.0878, LPS p = 0.0775), 17-HDoHE (unstim p = 0.3872, LPS p = 0.9897) and 18-HEPE (unstim p = 0.2149, LPS p = 0.0764).

There is no significant differences in the ability of the monocytes in pregnancy to produce the bioactive mediators, 8-HETE and 12-HETE (Figure 4.28).

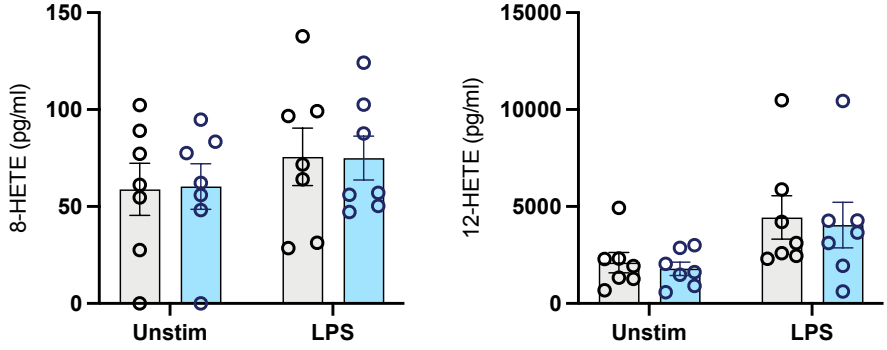

Figure 4.28: Bioactive mediator concentrations in the supernatants of monocytes from non-pregnant and pregnant (37+ weeks) women stimulated with or without LPS. Monocytes from a non-pregnant (grey) and a pregnant (blue) woman were cultured with or without LPS so that the supernatant could be analysed for the presence of eicosanoids using LC-MS/MS. Statistics were performed with a 2-way ANOVA and a Šídák's post-hoc test, where <0.05 was significant. Bioactive mediators that were detectable: 8-HETE (unstim p = 0.9961, LPS p = 0.9993), and 12-HETE (unstim p = 0.9590, LPS p = 0.9393).

The production of proinflammatory mediators is relatively lower for all molecules measured in the monocyte supernatants from the pregnant women, however most of these are not significant. The production of PGE2 is significantly lower from the LPS-stimulated monocytes n pregnancy (p = 0.0079; Figure 4.29).

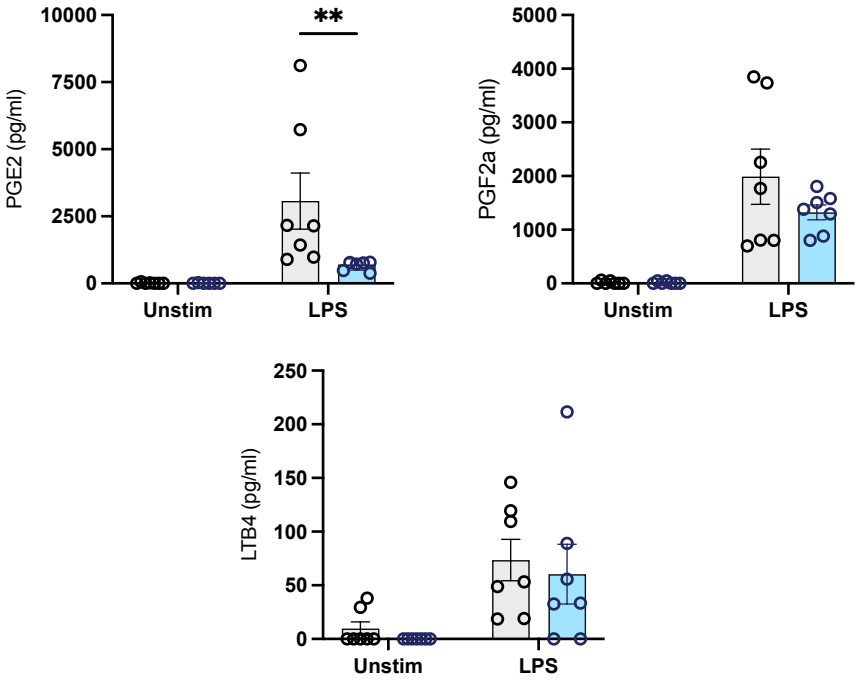

Figure 4.29: Proinflammatory mediator concentrations in the supernatants of monocytes from non-pregnant and pregnant (37+ weeks) women stimulated with or without LPS. Monocytes from a non-pregnant (grey) and pregnant (blue) woman were cultured with or without LPS so that the supernatant could be analysed for the presence of eicosanoids using LC-MS/MS. Statistics were performed with a 2-way ANOVA and a Šídák's post-hoc test, where <0.05 was significant. Proinflammatory mediators that were detectable was: PGE2 (unstim >0.9999, LPS p = 0.0079), PGF2a (unstim >0.9999, LPS p = 0.1715), and LTB4 (unstim = 0.9076, LPS p = 0.8353).

The eicosanoids classified as pro-resolving mediators also appear to be present only in low concentrations in the supernatants. The secretion of PGA1 from monocytes is no different in pregnant women compared to non-pregnant (Figure 4.30).

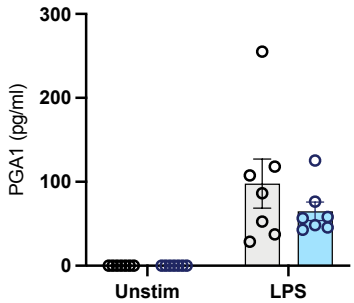

Figure 4.30: Pro-resolving mediator concentrations in the supernatants of monocytes from non-pregnant and pregnant (37+ weeks) women stimulated with or without LPS. Monocytes from a non-pregnant (grey) and a pregnant (blue) woman were cultured with or without LPS so that the supernatant could be analysed using LC-MS/MS for the presence of eicosanoids using LC-MS/MS. Statistics were performed with a 2-way ANOVA and a Šídák's post-hoc test, where <0.05 was significant. Pro-resolving mediators that were detectable was: PGA1 (unstim p > 0.9990, LPS p = 0.2709).

Some eicosanoids also act as oxidative stress markers. The production of all three molecules (9-HODE, 13-HODE and 8-iso-PGA2) is not significantly different from the monocytes in pregnancy, although 8-iso-PGA2 does appear reduced (Figure 4.31).

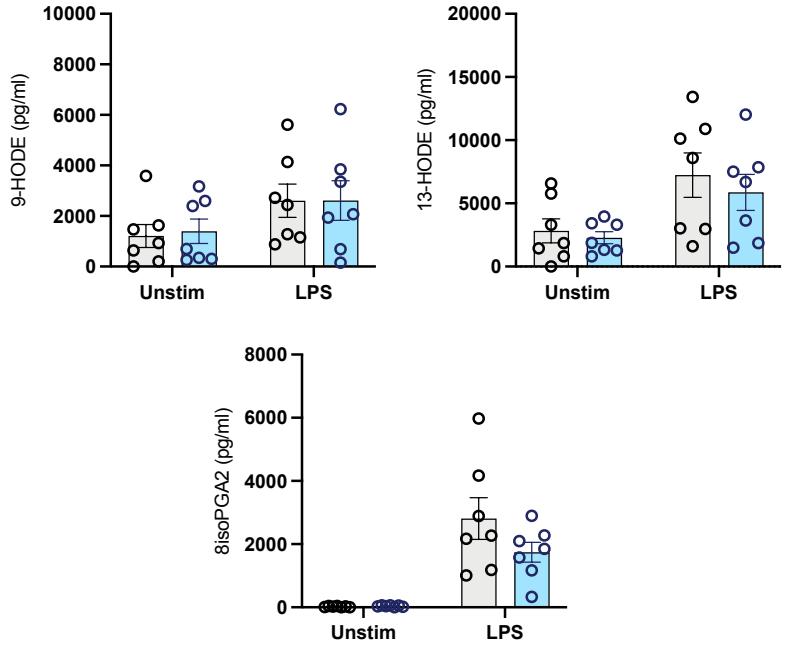

Figure 4.31: Oxidative stress mediator concentrations in the supernatants of monocytes from non-pregnant and pregnant (37+ weeks) women stimulated with or without LPS. Monocytes from a non-pregnant (grey) and pregnant (blue) woman were cultured with or without LPS so that the supernatant could be analysed using LC-MS/MS for the presence of eicosanoids using LC-MS/MS. Statistics were performed with a 2-way ANOVA and a Šídák's post-hoc test, where <0.05 was significant.Oxidative stress mediators that were detectable was: 9-HODE (unstim p = 0.9711, LPS p > 0.9999), 13-HODE (unstim p = 0.9428, LPS p = 0.6930), and 8-iso-PGA2 (unstim p = 0.9996, LPS p = 0.0984).

Overall, while not always significant, there appears to be a decrease in the ability of monocytes to produce eicosanoids. A radar plot which summarises these changes can be seen in Figure 4.32.

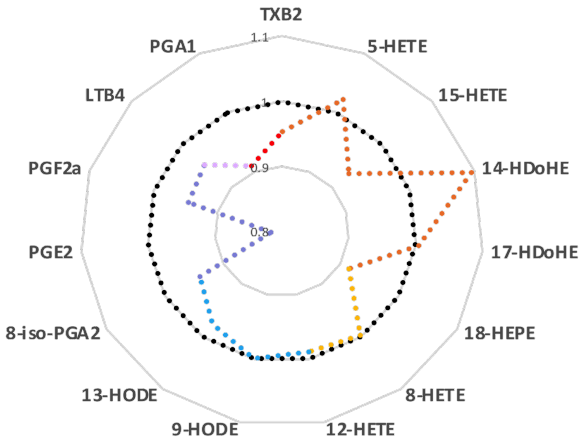

Lipid Mediator	p values
Inactive products	
TXB_2	0.0643
Pathway markers	
5-HETE	0.9049
15-HETE	0.0408
14-HDoHE	0.0775
17-HDoHE	0.9897
18-HEPE	0.0764
Bioactive mediators	
8-HETE	0.9993
12-HETE	0.9393
Oxidative stress markers	
9-HODE	>0.9999
13-HODE	0.693
8-iso-PGA_2	0.0984
Pro-Inflammatory	
PGE_2	0.0079
PGF_{2a}	0.1715
LTB4	0.8353
Pro-resolving	
PGA_1	0.2709

Figure 4.32: A radar plot summary of the eicosanoids produced from the LPS-stimulated monocytes of non-pregnant and pregnant (37+ weeks) women. The log values of the mean for pregnancy (coloured) for each lipid mediator is calculated relative to the mean from the non-pregnant (black).

4.3.12 Summary of results

A heatmap is provided in Figure 4.33 to summarise the findings of this chapter. It does not include the summary of the lipid mediator data as that has been surmised on the previous page.

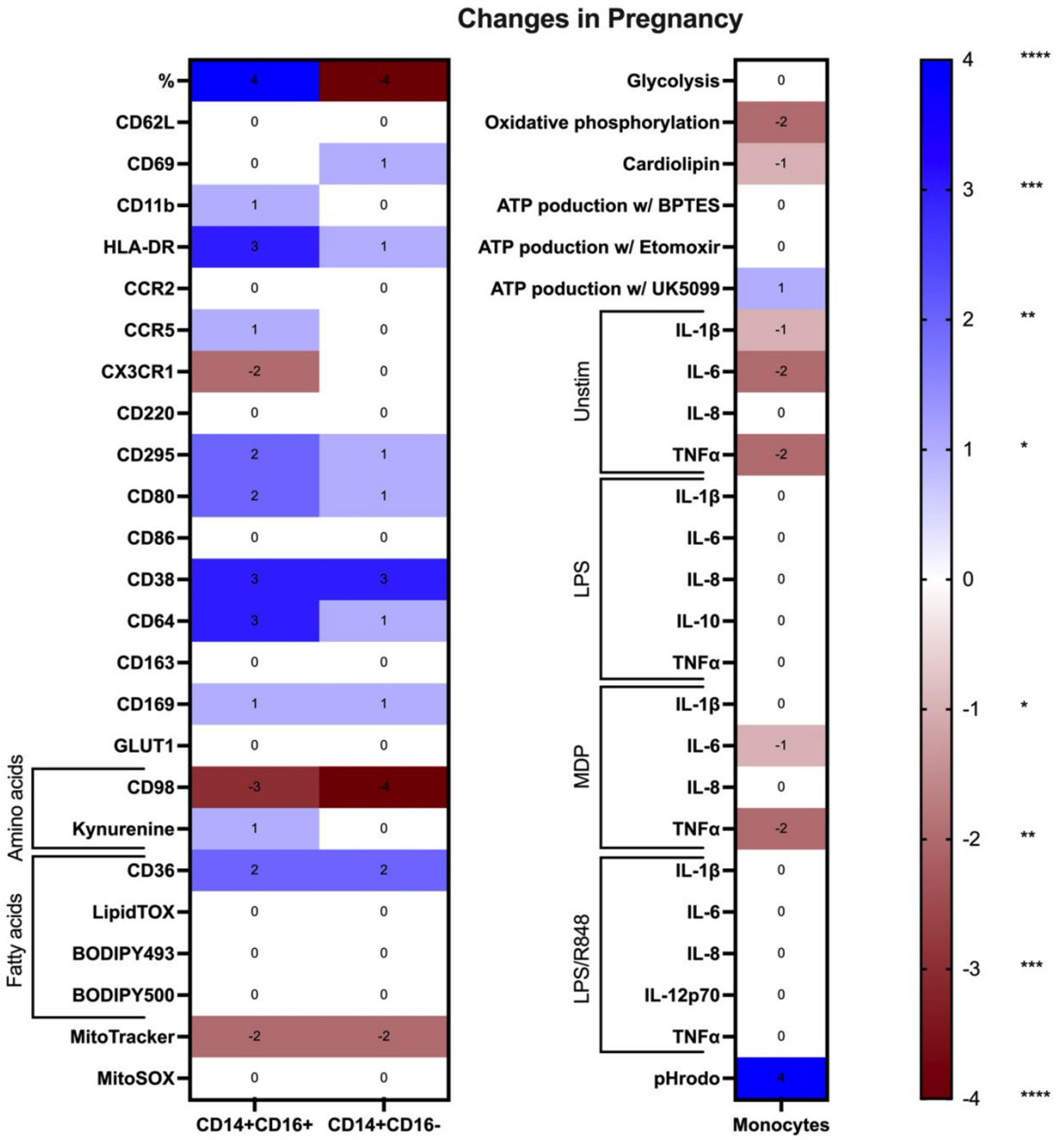

Figure 4.33: A heatmap summary of the findings of Chapter 4: Immunometabolic adaptations of monocytes in pregnancy at 37+ weeks gestation. Blue indicates a significant increase of the monocytes from pregnant women in comparison to the red which illustrates a decrease of the expression or activity of the monocytes. Some findings have been condensed to the most important, such as overall OXPHOS rather than showing each measurement.

4.4 Discussion

Monocytes from pregnant women at term are clearly altered phenotypically and metabolically to adapt to their environment. This is evidenced at the gene, protein, and functional level. The most striking discovery is the stark difference in the oxidative phosphorylation of the monocytes may lead to diminished function.

Initial phenotypic analysis of the monocytes revealed an abundance of non-classical monocytes with pregnancy and an activated phenotype showing adaptation to pregnancy, in line with what other studies have illustrated [328]. Studies have shown increased expression of the activation markers CD14, CD64 and CD11b highlight that monocytes are typically activated during pregnancy [73]. These studies in pregnancy have been carried out on total monocytes; therefore, the phenotypic analysis shown here is novel as it takes into consideration the monocyte subsets. Phenotypic analysis also revealed monocytes to be more activated (HLA-DR, CD11b, CD69) and have functional alterations such as increased CD38, CD64 and CD169. The leptin receptor (CD295) is elevated on the monocytes from pregnancy, most likely due to the leptin-rich environment pregnancy presents [154]. Leptin has been shown to promote CD16+ monocytes [151]. Investigation into the effect of leptin on monocytes from non-pregnant women, in conjunction with hormones which are typically found in high levels in pregnancy (prolactin and human placental lactogen [hPL]) was started to attempt to mimic the monocytic changes observed in pregnancy. However, results were not particularly exciting, and this line of investigation was dropped in favour of other avenues. CD80, of the T cell co-stimulatory counter receptors was found to be elevated significantly on both subsets of monocytes in pregnancy, suggesting a heightened inclination to induce T cell activation at this stage of pregnancy.

Transcriptomics analysis with NanoString © then kickstarted the investigation into the metabolic adaptability of monocytes during pregnancy at term. This stage of gestation was chosen to drive discovery at a time where there are more likely drastic differences to the non-pregnant environment, which should provide an inclination in what lines of investigation to home in on for earlier stages. This revealed significant differential expression of several genes and an impact on specific cellular and metabolic pathways. The pathway scores from the NanoString © implicated an increase in the genes involved in mitochondrial respiration in the

monocytes from pregnancy. In contrast however, the genes involved in the mTOR pathway are significantly decreased, coupled to an increase in those involved in the AMPK pathway. mTOR, which AMPK inhibits, has been shown to correlate with mitochondrial activity, with inhibition of mTOR resulting in reduced oxygen consumption, ATP synthetic capacity and mitochondrial membrane potential [344]. Bioenergetics analysis revealed that monocytes from pregnant women do indeed have diminished capability for maximal oxidative phosphorylation. The reduced mitochondrial content of the monocytes from pregnant women shown using both flow cytometry with MitoTracker Green ™ and cardiolipin (CL) content by mass spectrometry would provide an explanation for reduced oxidative phosphorylation. CLs are necessary for normal electron transport and OXPHOS [358]. Complexes IV and III require cardiolipin molecules to maintain full enzymatic function [358]. This reduction in CL could also explain why the genes involved in mitochondrial respiration, namely the ones involved in OXPHOS complexes, are elevated. The complexes could be present in higher concentrations but are unable to reach their functional capacity. Using an antibody cocktail of the OXPHOS complexes (Abcam) it is possible to semi-quantify this using immunoblotting. However, optimisation of blotting with monocytes from pregnancy is proving difficult due to altered β-actin expression, possibly due to having altered membrane composition. Due to a lack of samples and national reagent shortage due to COVID-19, this analysis is progressing more slowly than anticipated. Lower mitochondrial content and reduced oxidative phosphorylation promoted analysis of other features of mitochondrial function. A by-product of OXPHOS is ROS and the NanoString © pathway score for the reactive oxygen response indicated a down-regulation in monocytes from pregnant women. Flow cytometry analysis for this also suggested reduced mitochondrial ROS with pregnancy but this was not significant. Further experiments should include investigating the production of mitochondrial ROS when stimulated. Total cellular ROS yielded no significant differences upon stimulation.

As pregnancy is accompanied by various metabolic differences as described in *Chapter 1*, and data supported cellular metabolic adaptation by monocytes of pregnant women, further investigation into the role of fatty acids, amino acids and carbohydrates was undertaken. Examination of metabolic transporters using flow cytometry revealed higher expression of CD36 (FAT), lower expression of CD98 (LAT) and unchanged expression of GLUT1 in the monocytes from pregnant women. These data can be compared to gene expression data and

functional assays to elaborate any biological role. Despite an increase in CD36 expression, fatty acid uptake and storage and lipid accumulation were no different in the monocytes from pregnant compared to non-pregnant women prompting subsequent analysis of the role of CD36 in phagocytosis discussed below. This was in line with the lack of significant difference in the pathway score for fatty acid synthesis and fatty acid oxidation from the NanoString ©. The lack of change with GLUT1 is unsurprising given no differences were observed in ECAR from the bioenergetics analysis. However, flow cytometry analysis of GLUT1 is flawed as the antibody used shows little to no expression with a myriad of cell types, even with intracellular flow cytometry techniques. Glucose uptake analysis on the flow cytometer using a fluorescent analogue for 2-DG, 2-(N-(7-Nitrobenz-2-oxa-1,3-diazol-4-yl)Amino)-2-deoxyglycose (2-NBDG), is also notorious for its unreliability as it has been illustrated that there is a large disparity between 2-NBDG labelling and glucose transport capacity [359]. The reduction of CD98 is in line with the downregulation of the genes involved in amino acid transport observed with the NanoString ©; both SLC3A2 and SLC7A5, which form CD98, were found to be decreased with the NanoString © data ($p = 0.0824$ and $p = 0.1620$), though these were not significant. Amino acid uptake is much more challenging to discern experimentally, and future experiments could include using heavy labelled amino acids to trace through the TCA, but we can take advantage of the natural autofluorescence of kynurenine to study uptake in monocyte subsets [327]. Kynurenine is involved in immune regulation and produced from the amino acid tryptophan. An increase in the uptake of kynurenine was observed in the CD16+ monocytes of pregnant women only; the tryptophan and kynurenine pathway also appear to have an inclination of up-regulated genes. Kynurenine 3-monooxygenase (KMO) is a gene which is significantly upregulated ($p = 0.0144$ in the monocytes from pregnancy and is responsible for converting kynurenine to 3-hydroxykynurenine, illustrating kynurenine catabolism potential. It has been shown that the transport of kynurenine is restricted to activated cells [327]. The elevated activation status of the monocytes in pregnancy (evidenced by increased expression of activation markers) may allow for increased transport capacity of the monocytes despite the reduced expression of CD98. Kynurenine has been shown in mice models to augment CCL2-mediated chemotaxis and proinflammatory capabilities of monocytes [360]. Given that CCR2 is also increased on this population, albeit not significantly, then analysis of chemotaxis by this subset would be a worthy follow-on experiment.

Having explored the expression and activity of some fuel transporters, the next step was to try and determine if there were differences in the ability of monocytes from pregnant women to use three types of fuels (pyruvate, fatty acids, and amino acids) for OXPHOS. For this, an adaptation of the MitoStress assay on the Seahorse extracellular flux analyser was used. This involved injection of an inhibitor specific to those fuels: BPTES for amino acids, Eto for fatty acids, and UK5099 for pyruvate. This assay has its limitations in that only specific molecules for each type of fuel utilisation pathway are targeted. This revealed that inhibition of transferring pyruvate into the mitochondria with UK5099 had a more dramatic effect on monocytes from non-pregnant women; monocytes from pregnant women were not as susceptible suggesting greater fuel use plasticity of monocytes in pregnancy and a reduced reliance on carbohydrates.

It is vital to determine if these metabolic adaptations result in the function of the monocytes being affected. Firstly, a typical analysis of cytokine production was undertaken. This revealed a reduction in IL-1β, IL-6 and TNFα from unstimulated monocytes during pregnancy, and reduced IL-6 and TNFα production from MDP-stimulated monocytes of pregnant women, with no differences observed in the cytokines produced upon LPS- or LPS/R848-stimulation. No significant changes in the production of cytokines from LPS-stimulated monocytes in pregnancy is unsurprising linked with the no difference in glycolysis observed; as discussed earlier in *4.1.2 Monocyte immunometabolism*, LPS-stimulated cells are reliant on glycolysis [322]. Other stimuli do not always show this reliance, hence one of the reasons why others were investigated. Consequently, it has been shown with murine macrophages that MDP targets the mitochondria by inducing mitochondrial proton leak and rendering OXPHOS inefficient [361, 362]. El-Khoury et al. has shown it does this by upregulating uncoupling protein 2 and production of ROS [361]. This provides an explanation for why the cytokine production by the MDP-stimulated monocytes from a pregnant woman is significantly reduced; MDP renders the already down-regulated OXPHOS of the cells even more inefficient. To further prove the reduction in OXPHOS (caused by a lack of mitochondria) results in this functional change, future experiments include the confirmation of the effect of MDP on OXPHOS, by performing the MitoStress assay on 24hr MDP-stimulated monocytes from non-pregnant women; this experiment will be performed as described by Lachmandas et al [322]. The effect on cytokine production of the monocytes from pregnancy with P3C, which has been shown to rely on

OXPHOS [322], will also be considered to consolidate this effect. This study is the first to show cytokine production from monocytes in pregnancy when stimulated with MDP and LPS/R848. Despite the elevated expression of TLR7 shown with Nanostring © there was no difference to the cytokine response in the presence of R848. A combination of LPS and R848 was used to incite the IL-12p70 response and to mimic a hyperinflammatory response. Stimulation with R848 alone, or a TLR7-specific agonist (e.g., imiquimod) could unveil a difference in the cytokine response which the LPS may be masking. There are also conflicting reports from other studies in regards to cytokine production by monocytes in pregnancy; for example, some investigators have observed increased cytokine production in non-stimulated monocytes from pregnant in comparison to non-pregnant women [74] , whereas others have not [75]. LPS stimulation has been shown in some *in vitro* studies to decrease the number of monocytes secreting cytokines in pregnant women [75], but stimulation with a combination of LPS and IFNγ increases cytokine production [76, 77].

There have been conflicting reports on phagocytosis capabilities of monocytes in pregnancy; some have suggested enhanced phagocytosis [363] while another has disputed this and claimed the monocytes have a lower phagocytic index [364]. As no differences were observed in lipid accumulation of the monocytes in pregnancy, it was curious that CD36 was more highly expressed on both subsets of monocytes from pregnant women. CD36 is a scavenger receptor and has other roles beside fatty acid translocation including non-opsonic phagocytosis. Elevation of both CD36 and CD64, a receptor for opsonic phagocytosis, suggested that phagocytosis might be elevated in the monocytes from pregnant women. This turned out to be the case when the higher concentration of pHrodo *E. coli* BioParticles ™ was used although the experimental set up only allowed non-opsonic phagocytosis to be examined and COVID-19 prevented further planned experiments to examine this in more detail. These experiments would include neutralising or inhibiting CD36 and repeating experiments in the presence of serum to provide IgG for opsonisation. However, some of the other data generated sheds light on this finding. Phagocytosis is dependent on glycolysis [170], so a lack of any difference in the glycolytic capabilities of monocytes from pregnant and non-pregnant women means this is unlikely to contribute to any difference in their ability to phagocytose. In contrast, while not significant, the pathway score for fatty acid synthesis (FAS) appears elevated in the monocytes from pregnant women, with *ACSF3* upregulation significant. ACSF3 is a gene which

encodes the enzyme Acyl-CoA synthetase family member 3 which can bind malonate with high specificity and activates fatty acids. Induction of FAS is a key requirement for phagocytic function [319]. While unstimulated and stimulated total cellular ROS, and unstimulated mtROS has been found to be unchanged in the monocytes in pregnancy, investigating the mtROS upon stimulation is the next step. Increased phagocytosis and decreased mtROS production might make pregnant women more susceptible to intracellular pathogens including viruses and some bacteria. This is very speculative at this stage but could explain findings like increased Zika virus in monocytes of pregnant women [319] for example.

Future work includes investigating the mitochondrial dynamics of monocytes from pregnant versus non-pregnant women. This work has been delayed due to COVID-19 affecting the ability to train on new techniques. This will include visualisation of the mitochondria to reveal the relative size and shape of the mitochondria [365]. This could also provide answers as to why the monocytes from pregnant women have an increased phagocytosis ability, as the state of fission or fusion mitochondria influences this function [366, 367] with fusion linked to increased phagocytosis [368]. This allows for speculation that the mitochondria in the monocytes from pregnancy may skew towards the fusion dynamic.

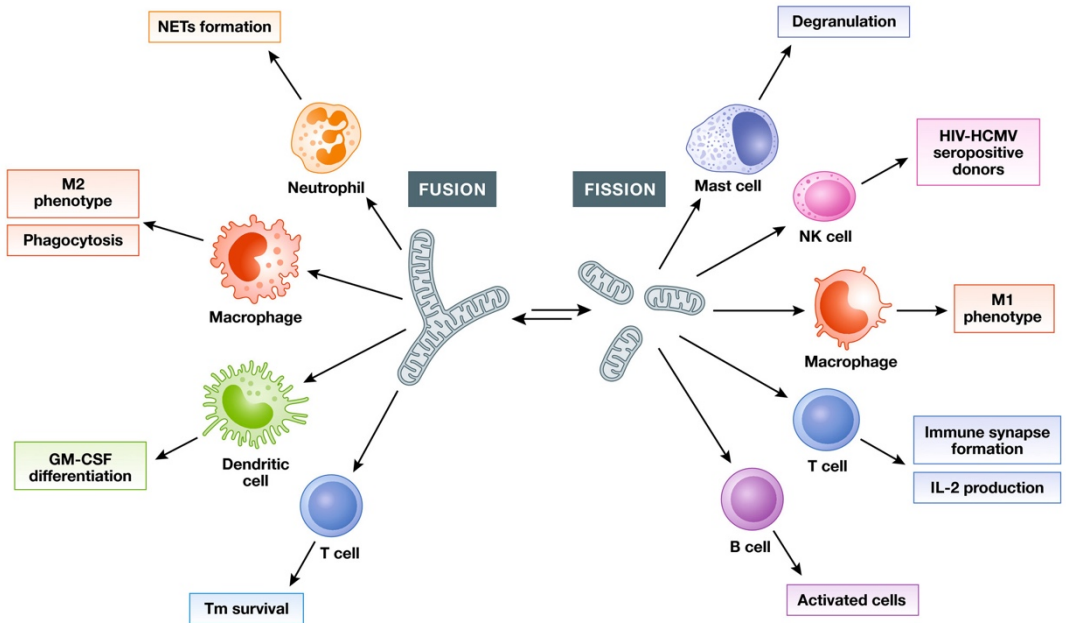

Figure 4.34: The effect of mitochondrial dynamics on immune cell function. Mitochondrial fusion promotes NETs formation (neutrophils), M2 phenotype and phagocytosis (macrophages), GM-CSF differentiation (DCs) and Tim survival (T cells), while mitochondrial fission endorses degranulation (mast cells), M1 phenotype (macrophages), immune synapse formation and IL-2 production (T cells) and activation (B cells). Image taken from Cervantes-Silva et al. [365]

Cytokine production and phagocytosis are fairly typical measures of monocyte functionality that are largely dependent on glycolysis which was unaffected by pregnancy. Therefore, alternative measures of monocyte function that might be linked to OXPHOS were sought and so the production of lipid mediators was considered. As evidenced in *Chapter 3,* the systemic environment in pregnancy is rich in lipid mediators, and so it is logical to consider if the monocytes contribute to this. It appears that the monocytes from pregnancy have an overall diminished ability to produce eicosanoids. The plasma from pregnant women is rich in all lipid mediators in comparison to that from non-pregnant women due to the build-up of lipid stores earlier in gestation leading to the release of free fatty acids in late gestation through enhanced lipolysis [39]. This would suggest a reduced need for monocytes to produce lipid mediators themselves as the maternal systemic environment is already rich in these molecules and this does appear to be the case. Whether the monocytes were hyperactive earlier in gestation to assist in the production of these lipid mediators and this has led to a depletion of their mitochondrial stores, reduced OXPHOS capabilities and reduced secretion of eicosanoids as gestation ends would be interesting to explore. Ethical approval has been obtained for peripheral blood from pregnant women of earlier than 37+ weeks gestation and some of this analysis is shown in later chapters. The finding that PGE2 production is significantly impaired in the LPS-stimulated monocytes from pregnant women, is particularly interesting from a metabolism standpoint. In macrophages, stimulation with LPS has been shown to increase the expression of the mitochondrial citrate carrier (CIC; exports citrate from the mitochondria to the cytoplasm) [190], and to activate ATP-citrate lyase (ACLY; transforms cytoplasmic citrate into acetyl-CoA and oxaloacetate) via NF-κB and STAT signalling pathways [369]. Studies have shown that both ACLY and CIC are essential to produce PGE2, with the inhibition of either results in reduced production of the prostaglandin [190, 369, 370]. Data from the NanoString © analysis show a reduction in the pathway score for the genes related to NF-κB signalling ($p = 0.0004$), which could offer part of the explanation for the decrease in PGE2 production from monocytes in pregnancy. Future work should explore the use of citrate in the monocytes from pregnant women compared to non-pregnant. As described in *Chapter 3 – The changing lipidomic profile of pregnancy can be monitored using novel mass spectrometry techniques*, PUFAs (the precursors of lipid mediators) are a by-product of the cleavage of PC into LPC. PC itself is produced from PE in a reaction catalysed by PEMT. From the NanoString © data, PEMT is significantly downregulated ($p = 0.0144$) in

the monocytes from pregnant women. This suggests that there may be a build-up of PE, and less PC to be converted into LPC, thereby not producing as many PUFAs as a by-product. Chapter 3 also showed no change in the PC/LPC ratio in the monocytes. The PE/PC ratio should then be considered. Additionally, future work also includes investigating the expression of COX and LOX in the monocytes to determine if a lack of these enzymes contributes to the reduced production of the lipid mediators.

4.5 Conclusions

Pregnancy programmes late gestation monocytes to influence their environment by downregulating their metabolic abilities. This is evidenced at their gene, protein, and functional level. The most striking discovery is the reduced mitochondrial content of the monocytes which translates to a reduction in their OXPHOS capabilities and results in diminished function, evidenced by the cytokines produced when stimulated with MDP (Figure 4.35). Additional to further work noted in the discussion, future work includes spiking the monocytes with heavy labelled glucose, glutamine, and choline to trace their paths through the TCA cycle. Citrate is a key metabolite involved in the TCA that is exported from mitochondria is involved in the production of lipids so analysis of citrate might provide understanding of the underpinning mechanisms of the changes seen.

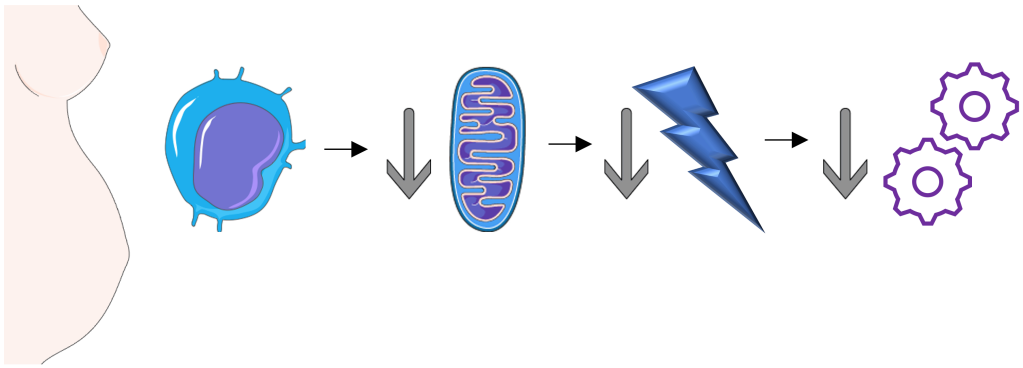

Figure 4.35: Monocytes from pregnant women have fewer mitochondria, are less capable of OXPHOS and are functionally impaired.

Chapter 5 - Key functional immune changes occur at 28 weeks of gestation, particularly in monocytes

5.1 Introduction

Pregnancy is commonly split into three trimesters and counted from day 1 of the previous menstrual cycle: first trimester is 0-13 weeks of gestation; second is 14-26 weeks and the third trimester is 27 to 40 weeks, with 40 weeks being full-term. There are various maternal physiological changes that accompany each trimester to allow for growth of the fetus. Human chorionic gonadotropin (hCG) is a hormone that is commonly used for diagnosing pregnancy due to its role in rescuing the corpus luteum to assist in trophoblast implantation [371]. hCG reaches its peak production in the first trimester (between the eight and tenth week), after which it plateaus at lower level for the rest of gestation [371]. Sex hormones - estrogens, progesterone, and prolactin - all increase throughout gestation and reach their peak at term, as well as the adipokine leptin [372, 373]. Human placental lactogen (hPL) is a hormone produced exclusively by the placenta to assist in providing fuel for the growing fetus and is partly responsible for maternal insulin resistance and glucose intolerance as gestation progresses [39]. Human placental growth hormone (hPGH) also increases during gestation and it is thought to also contribute to the insulin resistance observed in pregnancy [39]. Accompanying these endocrine changes, metabolic adaptations occur as gestation proceeds. Early pregnancy is a metabolically anabolic state associated with increasing maternal fat storage and insulin sensitivity, whereas late gestation is a catabolic state where lipolysis and insulin resistance occurs [374].

The immunological adaptations which occur during pregnancy have been discussed in previous chapters. Due to the significant role T cells play in graft rejection, the greatest reduction of T cell numbers is observed in the 1st trimester, with a reduction of their ability to eliminate foreign cells occurring during the 2nd and 3rd trimester [7]. T_{reg} cells were shown to actually increase during early pregnancy and peak in the 2nd trimester, before declining in the 3rd trimester [120]. This alteration of T_{reg} numbers is consistent with the immunological stimulus of the semi-allogenic fetus and assists in immunosuppression to assist materno-fetal tolerance; during the 2nd trimester, the maternal decidua is at maximal trophoblast invasion. Monocytosis occurs overall in pregnancy, with a sharp increase observed in the first trimester before it plateaus as pregnancy progresses [6]. To prevent an attack of the fetus and placental trophoblast, the activity of the complement pathway is suppressed at the maternal-fetal

interface until week 11 of gestation, where it assists in maternal defence against bacterial invasion with an increase in complement proteins [17].

Changes in the symptoms of autoimmune diseases also accompany pregnancy. For example, women with multiple sclerosis (MS) have decreased frequency of relapses during pregnancy (Figure 5.1); this is a potent example of the immunological adaptations that occur throughout pregnancy. The frequency of relapse is lowest during the third trimester [375]. *Chapter 3- The changing lipidomic profile of pregnancy can be monitored using novel mass spectrometry techniques,* clearly illustrated a change in the PC/LPC ratio, which increased over gestation, as a result of diminishing LPC. LPCs have been implicated in the demyelination observed in MS [376], as they have been shown to stimulate phagocytosis of the myelin sheath by macrophages [377], and so this reduction in LPC during pregnancy asserts its protectiveness against demyelination. Monocytes are a key marker of MS attacks in the general population. The secretion of prostaglandins (which are also a by-product from the production of LPC from PC by phospholipase A2) from peripheral monocytes predict relapses, and clinical activity is accompanied by increased activation markers and release of IL-1 and TNFα [301]. Increases in the non-classical subset of monocytes, the more pro-inflammatory subset, has also been found in MS patients [378]. As these changes to the monocyte phenotype (increased activation and non-classical monocytes) are typically observed in pregnancy, the monocytes from patients with MS are already pre-disposed to the required phenotype but are instead directed to a beneficial role rather than contribution to the inflammation and demyelination of the central nervous system (CNS).

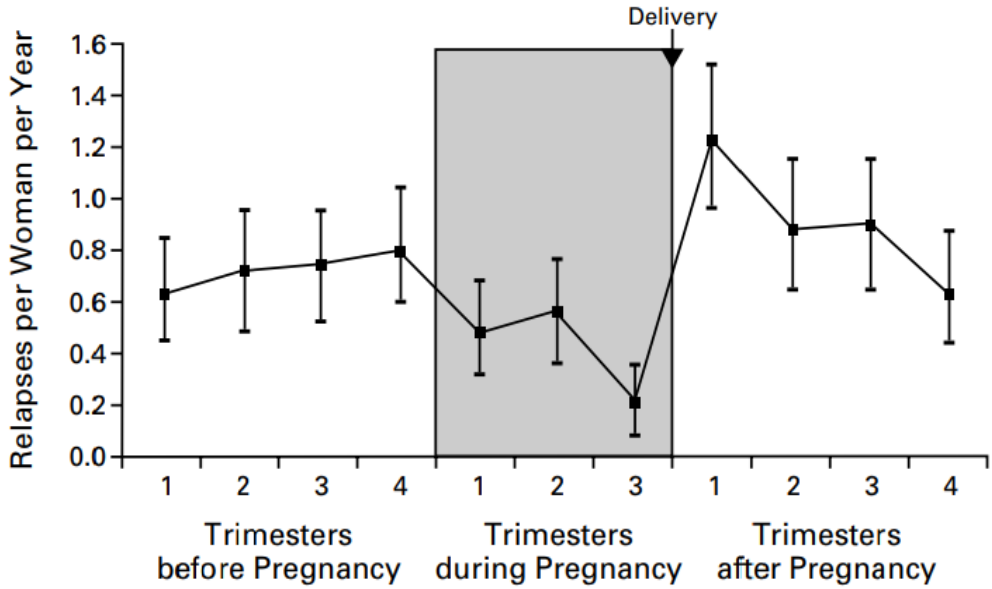

Figure 5.1: MS relapse rate of women before, during and after pregnancy. Women experience a steady rate of relapses before pregnancy. This is seen to drop significantly during pregnancy, with the lowest relapse rate occurring in the third and final trimester. Immediately post-pregnancy, the relapse rate skyrockets before slowly reducing to the same rate as pre-pregnancy. Graph has been taken from Confavreux et al [375].

5.1.1 Rationale

The metabolic and endocrine changes that occur with each gestational stage must have an impact immunologically. Previous chapters have discussed how monocytes are altered at term, but it is vital to understand at which point in pregnancy these changes occur.

5.1.2 Hypothesis

Systemic immunological adaptations during pregnancy induce an altered monocyte phenotype at 28 weeks of gestation.

5.2 Materials and Methods

5.2.1 Samples

Heparin anti-coagulated peripheral blood (Vacuette ™; Greiner Bio-one, Frickenhausen, Germany) was collected from healthy, non-pregnant women (aged 18-40 years) and fasted pregnant women (between 26- and 28-weeks' gestation, mean 27.5 weeks) and processed within 30 minutes of collection. These pregnant women were being tested for gestational diabetes mellitus (GDM) and obtained a negative result from the oral glucose tolerance test (OGTT). These women were also non-obese (BMI <30). All samples were collected with informed written consent and ethical approval obtained from a Health Research Authority (HRA) Research Ethic Committee (REC approval 19/LO/0722). All donors were either healthy or overweight BMI; samples from women with obesity were excluded.

***Disclaimer**:* The experiments where the samples were used to determine leukocyte populations (section 5.3.1) were performed by a fellow PhD student Oliver Richards for a different analysis. He has kindly allowed me to extract the raw data for the normal weight and overweight pregnant women from his large cohort of healthy pregnant women for this analysis.

5.2.2 MNC isolation

MNCs were prepared via density centrifugation as in *2.2 Mononuclear cell Isolation*. Due to the limited availability of the blood (one 9 ml tube for pregnant women), monocytes were not isolated.

5.2.3 Flow cytometry

An 8-colour immunophenotyping kit (Miltenyi) was used on whole blood to investigate the frequency of key leukocyte populations. 10 µl of the antibody cocktail and 10 µl of the 7-AAD (a viability stain) were added to 100 µl of whole blood. Samples were incubated at room temperature in the dark for 10 mins. The 10X lysis buffer was diluted 1:10, and 2 ml of the lysis buffer was added to the blood, which was vortexed for 5 secs before incubating in the dark at room temperature for 10 mins. The blood was centrifuged at 515 *x g* for 7 mins at 4°C, supernatant aspirated, washed with 2 ml FACS buffer and centrifuged again. The cells were

resuspended in 100 µl FACS buffer and run on the flow cytometer. Specific leukocyte populations were identified as in Figure 5.2.

Monocytes were analysed in the MNC population via flow cytometry as in *2.4 Flow Cytometry*. Antibodies used for the analysis of monocytes are shown in Table 5.1. Mitochondrial content of monocytes was monitored using 2 nM MitoTracker Green (Life Technologies).

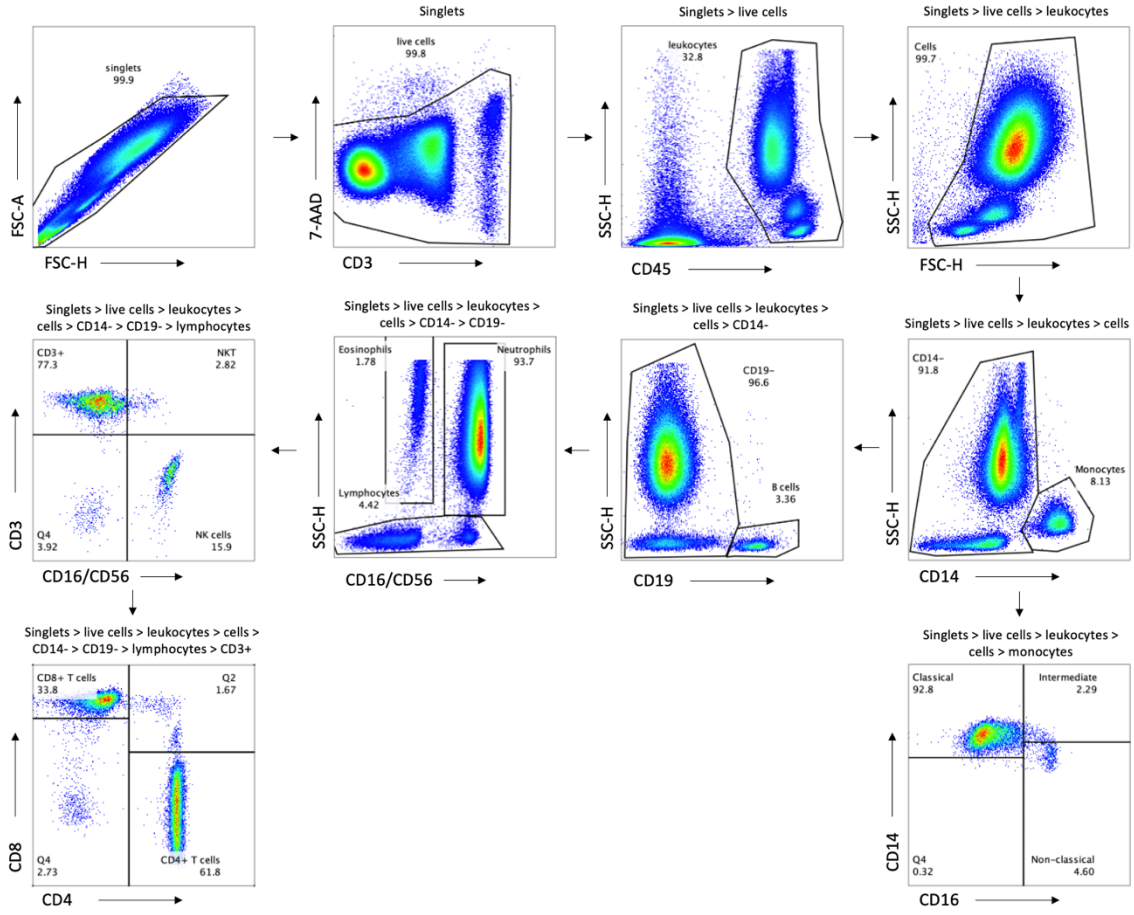

Figure 5.2: Identification of specific leukocyte populations from whole blood. Singlets are first selected via a forward scatter (FSC) height (H) vs area (A). Dead cells (7-AAD positive) are excluded. Only leukocytes (CD45+) are then selected, before debris is removed from the gating strategy on a FSC-H vs side-scatter (SSC)-H plot. Monocytes are identified by being CD14+ and further separated into their subsets based on CD14 and CD16 expression. From the CD14-negative cells, B cells (CD19+) are identified. It is possible to identify eosinophils (CD16/CD56-negative), neutrophils (CD16/CD56-positive) and lymphocytes (low SSC profile). In the lymphocyte profile, T cells (CD3+), NKT cells (CD3+CD16/CD56+) and NK cells (CD3-CD16/CD56+) are identified. T cells can be segregated by their CD4 and CD8 expression.

Antibody	Fluorochrome	Manufacturer	Clone	Isotype
anti-CD14	Alexa Fluor ® 647	BioLegend	53D3	IgG1
anti-CD16	VioBlue ®	Miltenyi	VEP13	IgMκ
anti-CD11b	PE	BioLegend	CBRM1/5	IgG1
anti-CD36	PE	BioLegend	5-271	IgG2a
anti-CD38	PE	BioLegend	HB-7	IgG1
anti-CD220	PE	Miltenyi	REA260	IgG1
anti-CD98	PE	Miltenyi	REA387	IgG1
anti-CD80	PE	Miltenyi	REA661	IgG1
anti-CD86	PE	Miltenyi	REA968	IgG1
anti-CD64	PE	Miltenyi	REA978	IgG1
anti-CD163	PE	Miltenyi	REA812	IgG1
anti-CD192 (CCR2)	PE	Miltenyi	REA264	IgG1
anti-CX_3CR1	PE	Miltenyi	REA385	IgG1

Table 5.1: Details of the antibodies used to phenotype monocytes within MNC preparation.

5.2.4 Cytokine analysis

MNCs cultures were prepared as in *2.5 Cell culture* with LPS (10 ng/ml), MDP (1 µg/ml), LPS (10 ng/ml) and R848 (400 ng/ml), or POLY I:C (25 µg/ml). Polysinosinic:polycytidylic acid (POLY I:C) is typically used to simulate viral infections due to it being a synthetic analogue of double-stranded RNA. POLY I:C interacts with TLR3 to initiate signalling. Cytokine analysis was done via multiplexing.

5.2.5 Multiplex cytokine analysis

A multiplex flow cytometry approach to cytokine analysis was performed uisng LEGENDplex™ (BioLegend) kits. This is a bead-based panel which employs fluorescently encoded beads for quantification on a flow cytometer and operates on the same principle as a sandwich ELISA. Mixed capture beads are directly added to samples, and the analytes will bind to the capture beads. These beads are of two sizes: smaller Beads A and larger Beads B. These can be distinguished by their side scatter (SSC) and forward scatter (FSC). Beads A can consist of up to 6 bead populations with specific cytokine antibodies attached, and Beads B of up to 7 bead populations that are distinguished by their unique internal fluorescence intensities (Figure 5.3). This internal dye is detected by the APC channel (λ Em 660 nm) on the ACEA Novocyte flow cytometer used for this analysis. After washing, biotinylated detection antibodies are added which bind to the specific analyte on the capture beads. Streptavidin-phycoerythrin (SA-PE) will then bind to the biotin when it is added, and this is responsible for producing a

fluorescent signal in the PE channel (λ Em 572 nm). The intensity of this signal is proportional to the quantity of analytes that have bound to the APC-equivalent-labelled bead.

MNCs stimulated with LPS, MDP, LPS/R848 and POLY I:C were analysed using the LEGENDplex ™ Human Inflammation panel 1 (13-plex; BioLegend). LPS stimulated samples were diluted 1:3 with assay buffer and the other samples were run neat. The analysis was performed as per the manufacturer's guidelines. The standard cocktail was reconstituted with 250 µl assay buffer to give the top standard (standard concentrations for each cytokine in the panel can be seen in Table 5.2), which was then serially diluted 1:4 with assay buffer. 25 µl of assay buffer was added to all sample wells. 25 µl of standard or sample was then added. A vial of the mixed capture beads was vortexed for 30 sec, and 25 µl of this was added to the plate. The plate was sealed, protected from light and placed on a plate shaker at 800 rpm for 2 hr at room temperature. After the incubation, the plate was centrifuged at 250 *x g* for 5 mins. The supernatant was aspirated, and the plate was washed twice with 200 µl wash buffer. 25 µl of detection antibodies were added to each well, and the plate was incubated on the shaker in the dark for 1 hr. SA-PE was added at 25 µl per well, before returning to incubation for 30 mins. The plate was washed again by centrifugation, removing the supernatant, adding wash buffer, and removing the supernatant again. The beads were then resuspended in 150 µl of wash buffer and the plate was run on the flow cytometer with high-speed mixing in between each sample to prevent the settling of the beads. Data was loaded onto the Qognit LEGENDplex ™ software which extrapolated the concentrations of each cytokine in each sample against the standard curve produced. It took into consideration the dilution and produced a report that was used for further analysis on GraphPad Prism ©.

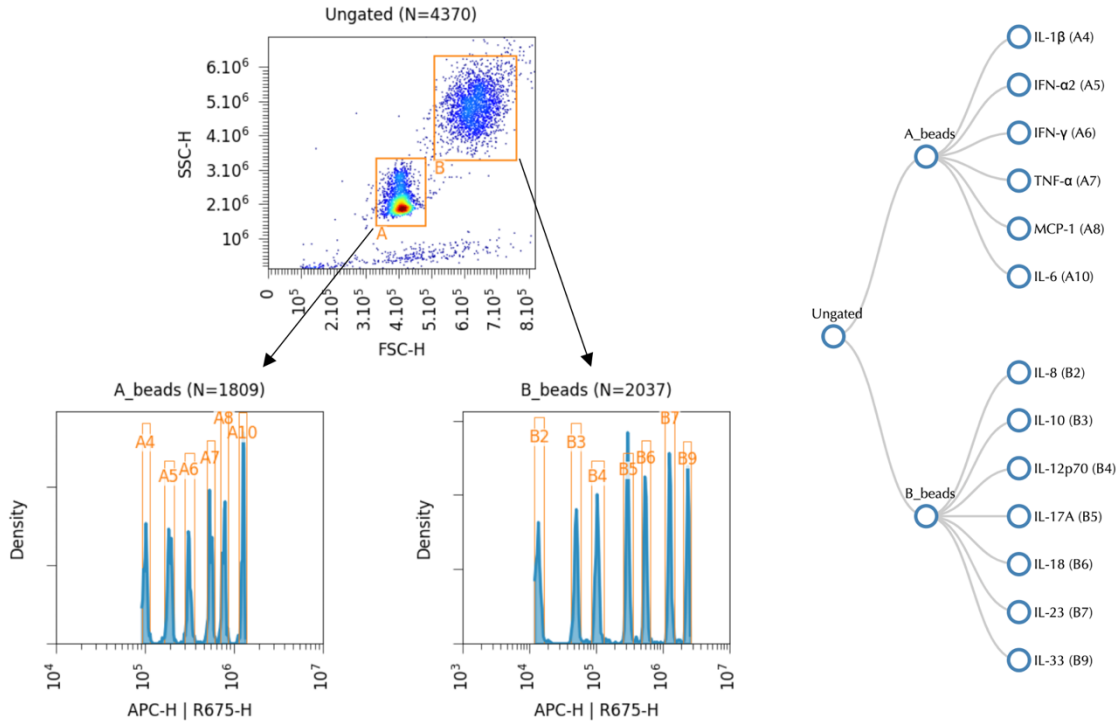

Figure 5.3: Gating strategy from the LEGENDplex ™ qognit software. The beads are first separated by size and labelled A or B. The individual cytokines are then distinguished by their unique APC fluorescence intensity. The frequency of those cytokines are then analysed using MFI of their PE fluorescence and extrapolated from a standard curve.

Inflammation	
IL-1β	11 ng/ml
IFN-α2	13 ng/ml
IFN-γ	9 ng/ml
TNFα	11.5 ng/ml
MCP-1	10 ng/ml
IL-6	10 ng/ml
IL-8	11 ng/ml
IL-10	11 ng/ml
IL-12p70	14 ng/ml
IL-17A	3.3 ng/ml
IL-18	17 ng/ml
IL-23	15 ng/ml
IL-33	100 ng/ml

Table 5.2: The top standards which were subsequently serially diluted four-fold for the different LEGENDplex ™ assays.

5.2.6 Bioenergetic analysis

OXPHOS and glycolytic capabilities of the MNCs were determined as in *2.6 Bioenergetic analysis* with an additional final injection (port D) of the ionophore monensin (20 µM) to increase the rate of ATP production [379]. Monensin does this by driving the increase in ATP demand by Na^+/K^+ -ATPase.

5.3 Results

5.3.1 Proportions of leukocytes are significantly altered in pregnancy at 28 weeks of gestation

While leukocyte changes in pregnancy are well documented, here it was a good starting point to confirm or negate previous studies. It is evident that most leukocyte subsets are affected by pregnancy (Figure 5.4). Neutrophilia is the most prominent ($p = 0.0001$), whereas in contrast the lymphocytes (T cells $p < 0.0001$; B cells $p < 0.0001$) and NK cells ($p = 0.0063$) are decreased in pregnancy at 28 weeks. Despite the difference in total T cell contribution to the leukocyte population, there are no significant differences between the T cell subsets CD4+ and CD8+ as a percentage of total T cells. While total monocytes are not statistically altered as a percentage of total CD45+ cells, the monocytes from pregnant women appear to be enriched with the classical subset ($p = 0.0398$).

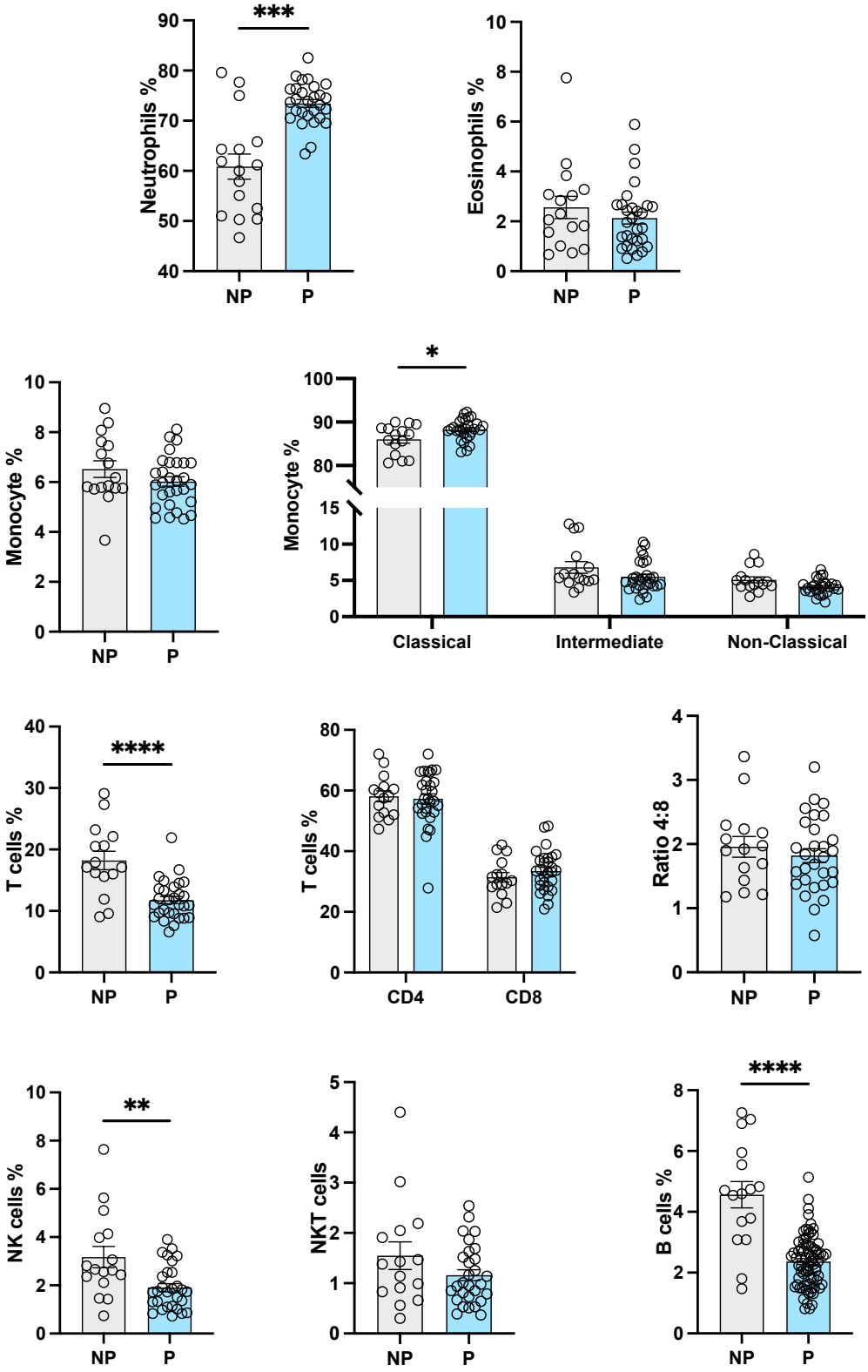

Figure 5.4: Populations of leukocytes in peripheral blood of non-pregnant women versus 28 week pregnant women. Specific leukocyte populations were identified in blood from non-pregnant women and pregnant women at 28 weeks of gestation using an 8-colour phenotyping panel via flow cytometry as described in the Materials and Methods. Statistics were measured using a Mann-Whitney t test where a p value < 0.05 was determined to be significant. Leukocytes which were identified were: neutrophils ($p = 0.0001$), eosinophils ($p = 0.4451$), monocytes ($p = 0.2507$) and its subsets classical ($p = 0.0398$), intermediate ($p = 0.4067$) and non-classical ($p = 0.0895$), T cells ($p < 0.0001$) and its subsets CD4 ($p = 0.9561$), CD8 ($p = 0.5333$) and the CD4:CD8 ratio ($p = 0.5402$), NK cells ($p = 0.0063$), NKT cells ($p = 0.2935$) and B cells ($p < 0.0001$).

5.3.2 MNCs are less capable of producing inflammatory cytokines upon interaction with a combined stimuli in pregnant women at 28 weeks' gestation

To determine if the MNCs from pregnant women were affected in their ability to produce cytokines in comparison to non-pregnant women, supernatants from cells left unstimulated or stimulated with either LPS (TLR4), MDP (NOD2), LPS/R848 (TLR7/8) or POLY I:C (TLR3) were analysed with a multiplex approach. Cytokines in this human inflammation panel included: IL-1β, IFNα2, IFNγ, TNFα, MCP-1, IL-6, IL-8, IL-10, IL-12p70, IL-17A, IL-18, IL-23 and IL-33. IL-17A was not detectable in any sample, whereas most or all other cytokines were in response to at least one of the stimuli used. The data are shown in Figures 5.5 – 5.9.

Pregnancy at 28 weeks of gestation appears to have little effect on the inflammatory cytokine output of MNCs in the unstimulated (Figure 5.5), LPS-stimulated (Figure 5.6), MDP-stimulated (Figure 5.7) or POLY I:C stimulated (Figure 5.9). The exception was the decreased production of IL-1β from the MNCs in pregnancy ($p = 0.0467$).

Upon interaction with a combination of LPS and R848 however, the output of various cytokines was significantly diminished in pregnancy: IL-1β ($p = 0.0041$), IFNα2 ($p = 0.0066$), IFNγ ($p = 0.0282$), MCP-1 ($p = 0.0388$), IL-6 ($p = 0.0308$), IL-8 ($p = 0.0270$), IL-10 ($p = 0.0214$) and IL-33 ($p = 0.0075$).

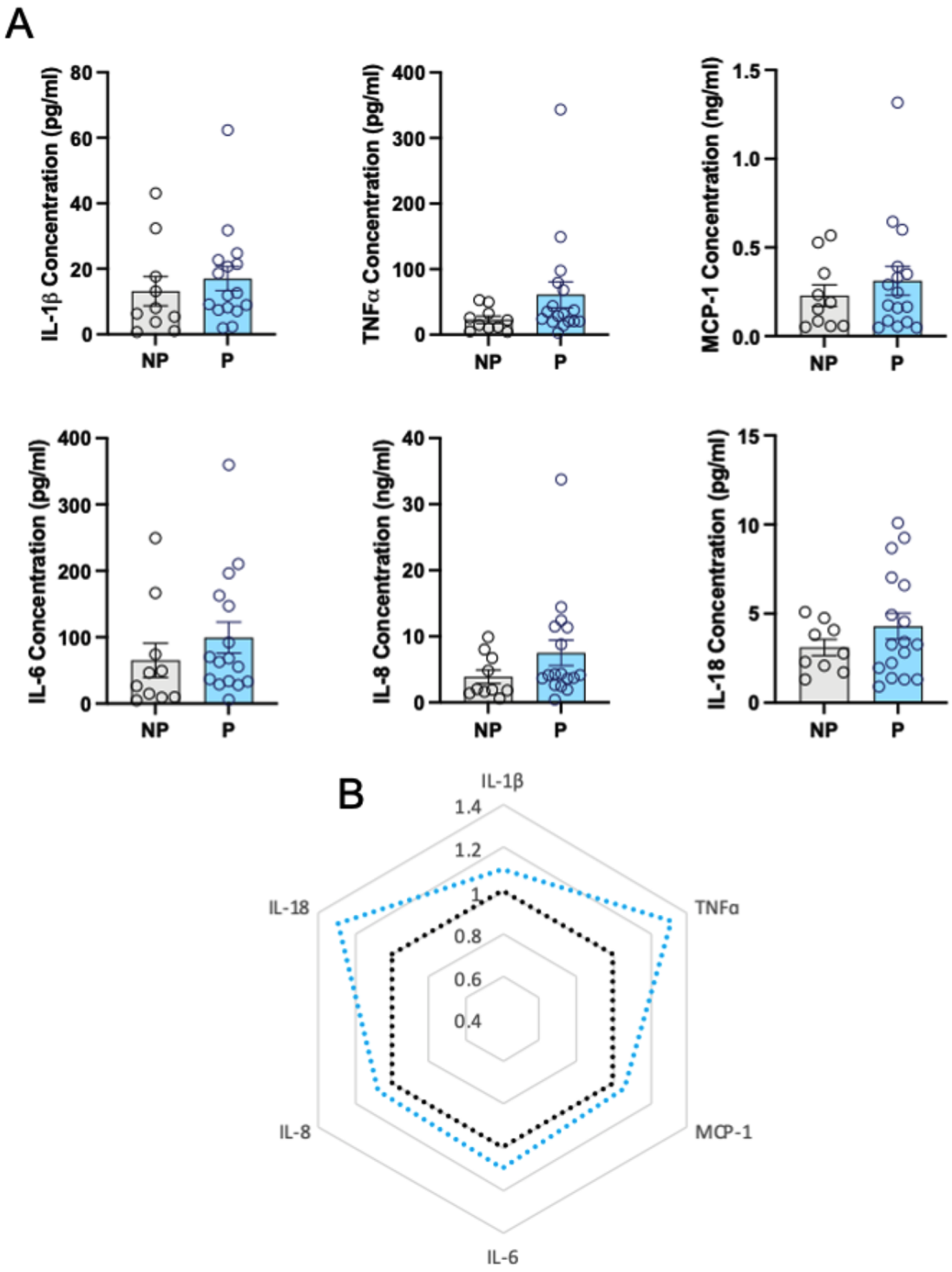

Figure 5.5: Cytokine production from unstimulated MNCs of non-pregnant women versus pregnant women at 28 weeks of gestation. Supernatants from MNCs from non-pregnant and pregnant women at 28 weeks of gestation left unstimulated for 24hr were analysed using a multiplex approach as described in the materials and methods. Statistical analysis was with a Mann-Whitney t test where $p < 0.05$ was significant. Some cytokines were not detectable in the supernatants. (A) Cytokines measured were: IL-1β ($p = 0.2625$), TNFα ($p = 0.1035$), MCP-1 ($p = 0.6599$), IL-6 ($p = 0.1824$), IL-8 ($p = 0.1035$) and IL-18 ($p = 0.5877$). (B) Radar plot whereby the means of each cytokine in pregnancy were used to calculate a log value against the means from the non-pregnant group.

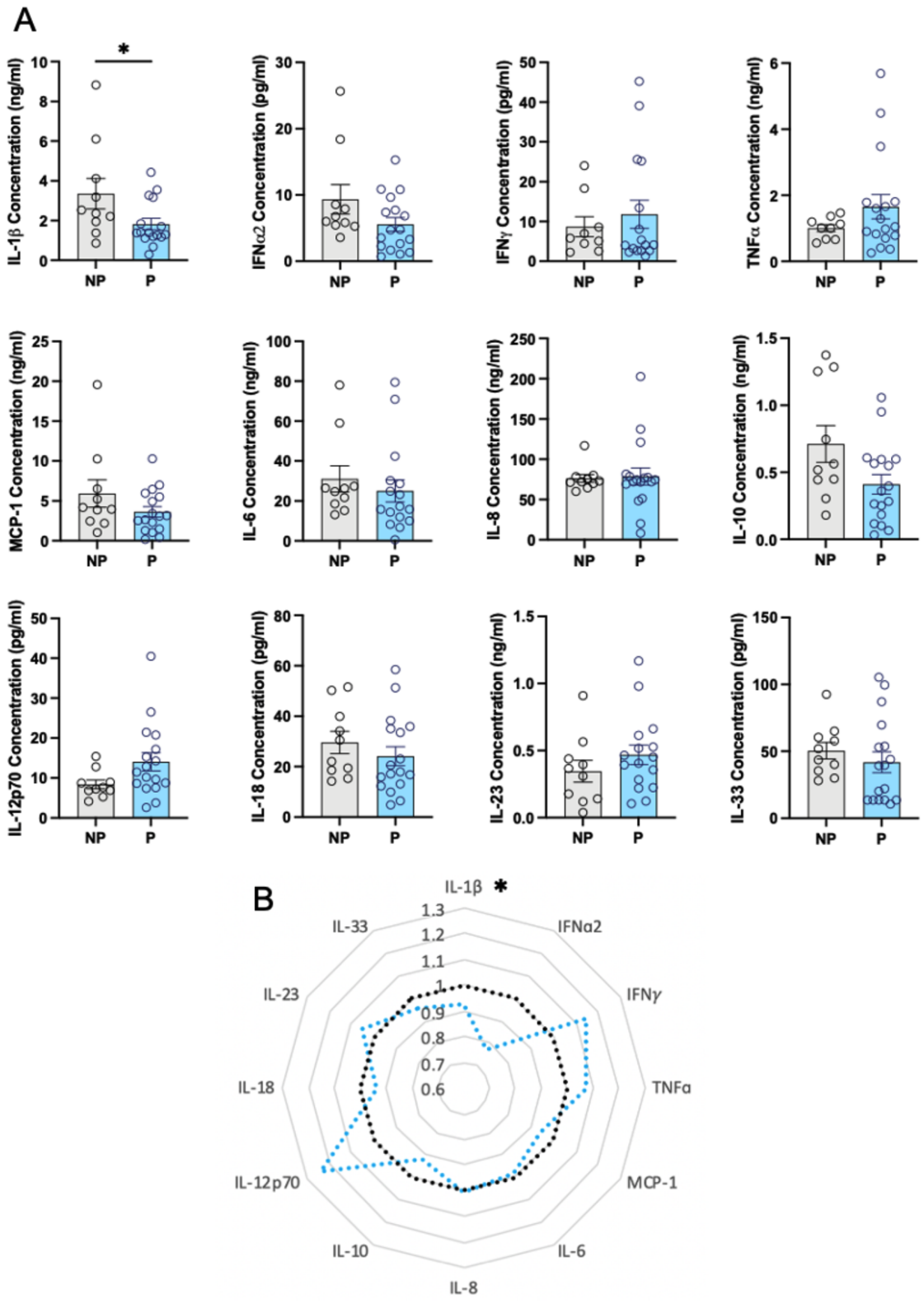

Figure 5.6: Cytokine production from LPS-stimulated MNCs of non-pregnant women versus pregnant women at 28 weeks of gestation. Supernatants from MNCs from non-pregnant and pregnant women at 28 weeks of gestation stimulated with LPS for 24hr were analysed using a multiplex approach as described in the materials and methods. Statistics were determined using a Mann-Whitney t test where $p < 0.05$ was significant. Only IL-17A was not detectable in the supernatants. (A) Cytokines measured were: IL-1β ($p = 0.0467$), IFNα2 ($p = 0.1035$), IFNγ ($p = 0.8459$), TNFα ($p = 0.4910$), MCP-1 ($p = 0.2860$), IL-6 ($p = 0.2857$), IL-8 ($p = 0.8630$), IL-10 ($p = 0.0929$), IL-12p70 ($p = 0.0520$), IL-18 ($p = 0.2860$), IL-23 ($p = 0.2406$) and IL-33 ($p = 0.2413$). (B) Radar plot whereby the means of each cytokine in pregnancy were used to calculate a log value against the means from the non-pregnant group.

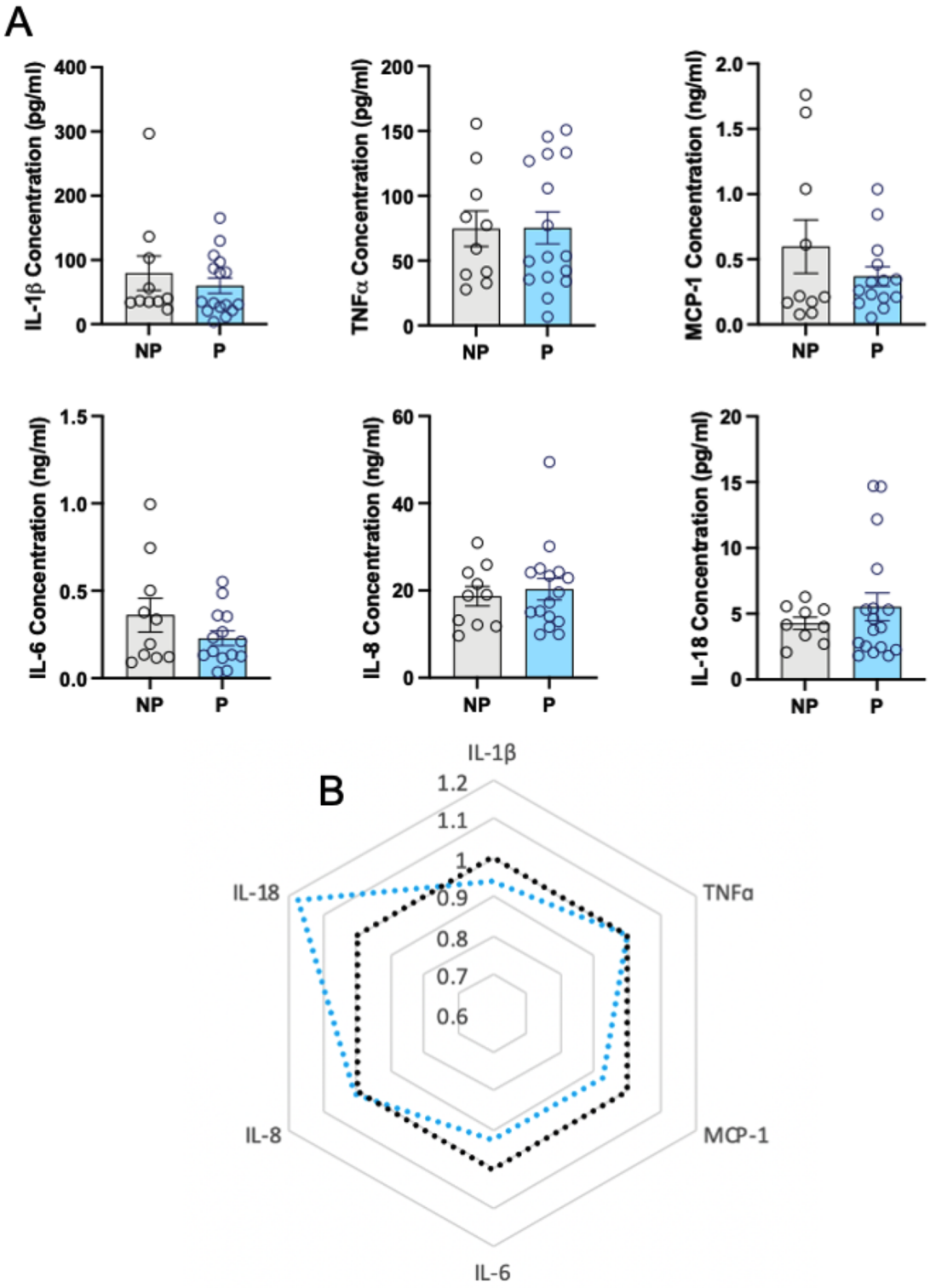

Figure 5.7: Cytokine production from MDP-stimulated MNCs of non-pregnant women versus pregnant women at 28 weeks of gestation. Supernatants from MNCs from non-pregnant and pregnant women at 28 weeks of gestation stimulated with MDP for 24hr were analysed using a multiplex approach as described in the materials and methods. Statistics were determined using a Mann-Whitney t test where $p < 0.05$ was significant. Some cytokines were not detectable in the supernatants. (A) Cytokines measured were: IL-1β ($p = 0.3102$), TNFα ($p = 0.9794$), MCP-1 ($p = 0.9314$), IL-6 ($p = 0.4716$), IL-8 ($p = 0.8159$) and IL-18 ($p = 0.7811$). (B) Radar plot whereby the means of each cytokine in pregnancy were used to calculate a log value against the means from the non-pregnant group.

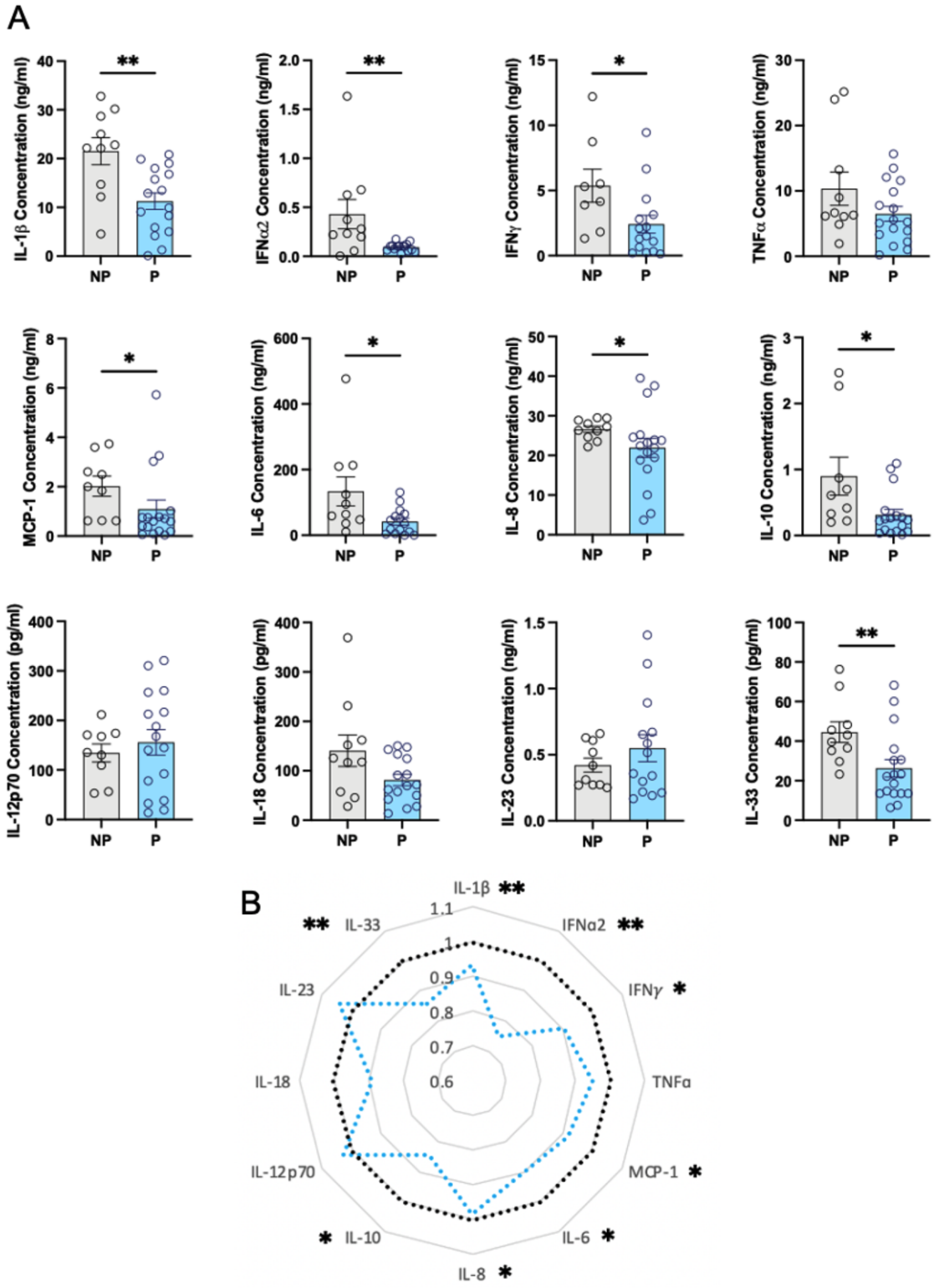

Figure 5.8: Cytokine production from LPS/R848-stimulated MNCs of non-pregnant women versus pregnant women at 28 weeks of gestation. Supernatants from MNCs from non-pregnant and pregnant women at 28 weeks of gestation stimulated with a combination of LPS and R848 for 24hr were analysed using a multiplex approach as described in the materials and methods. Statistics were determined using a Mann-Whitney t test where $p < 0.05$ was significant. Only IL-17A was not detectable in the supernatants. (A) Cytokines measured were: IL-1β ($p = 0.0041$), IFNα2 ($p = 0.0066$), IFNγ ($p = 0.0282$), TNFα ($p = 0.2044$), MCP-1 ($p = 0.0388$), IL-6 ($p = 0.0308$), IL-8 ($p = 0.0270$), IL-10 ($p = 0.0214$), IL-12p70 ($p = 0.6368$), IL-18 ($p = 0.1214$), IL-23 ($p = 0.7521$) and IL-33 ($p = 0.0075$). (B) Radar plot whereby the means of each cytokine in pregnancy were used to calculate a log value against the means from the non-pregnant group.

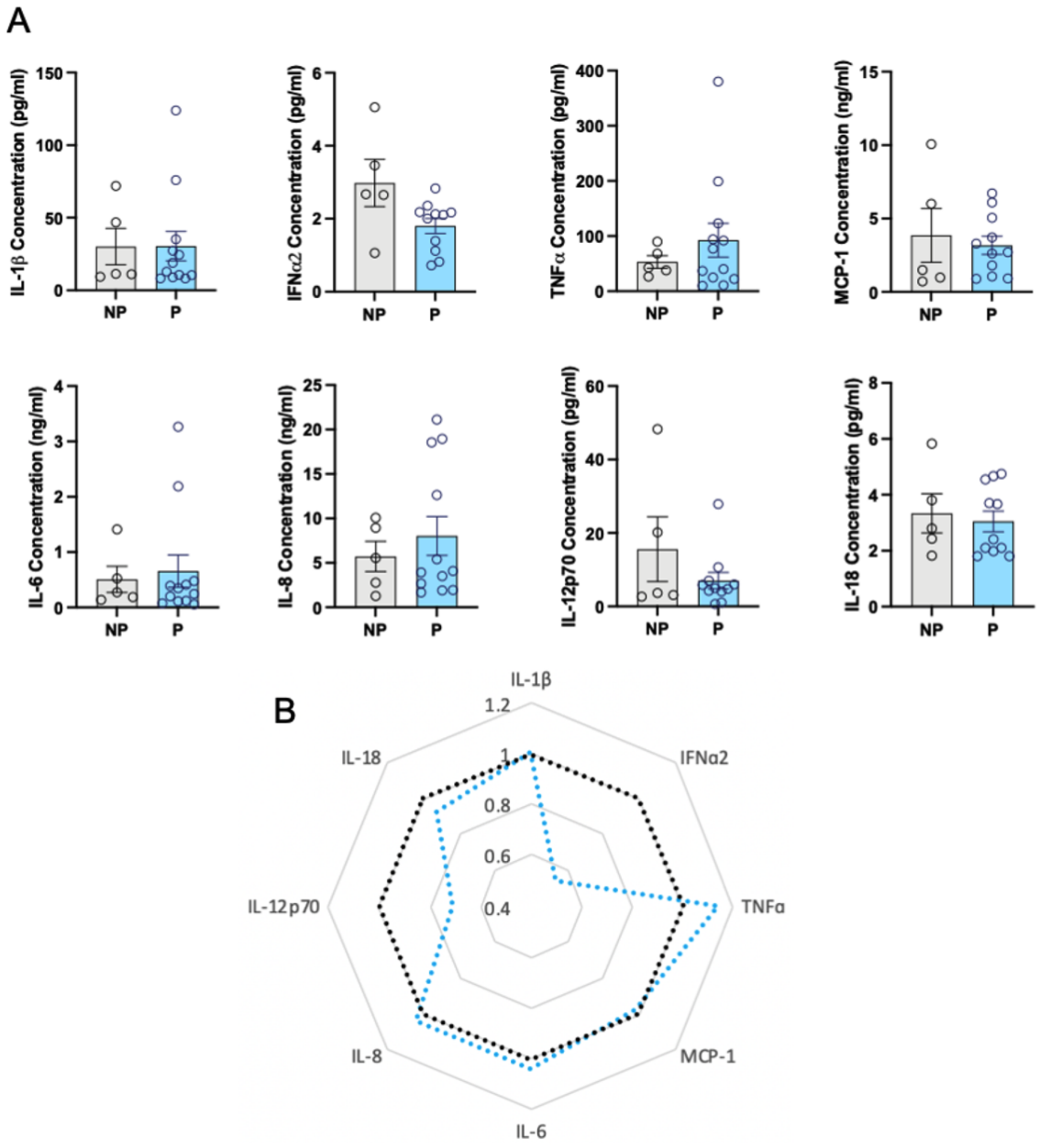

Figure 5.9: Cytokine production from POLY I:C-stimulated MNCs of non-pregnant women versus pregnant women at 28 weeks of gestation. Supernatants from MNCs from non-pregnant and pregnant women at 28 weeks of gestation stimulated with POLY I:C for 24hr were analysed using a multiplex approach as described in the materials and methods. Statistics were determined using a Mann-Whitney t test where $p < 0.05$ was significant. Some cytokines were not detectable in the supernatants. (A) Cytokines measured were: IL-1β ($p = 0.7796$), IFNα2 ($p = 0.0687$), TNFα ($p = 0.8788$), MCP-1 ($p = 0.8269$), IL-6 ($p = 0.7214$), IL-8 ($p = 0.8788$), IL-12p70 ($p > 0.9999$) and IL-18 ($p = 0.5618$). (B) Radar plot whereby the means of each cytokine in pregnancy were used to calculate a log value against the means from the non-pregnant group.

5.3.3 The phenotype of monocytes is significantly altered in pregnancy at 28 weeks of gestation

As illustrated in *Chapter 4- Immunometabolic adaptations of monocytes in pregnancy at 37+ weeks gestation*, the phenotype of monocytes is significantly altered at term pregnancy. To investigate if these changes occur at earlier gestation (~28 weeks), flow cytometry of MNCs was conducted.

Firstly, the expression of chemokine receptors (CCR2 and CX_3CR1) was examined (Figure 5.10). While there appears to be a decrease in expression of both receptors by monocyte subsets in pregnancy in comparison to non-pregnant women, the only significant decrease was observed in the non-classical monocytes for CCR2 ($p = 0.0280$).

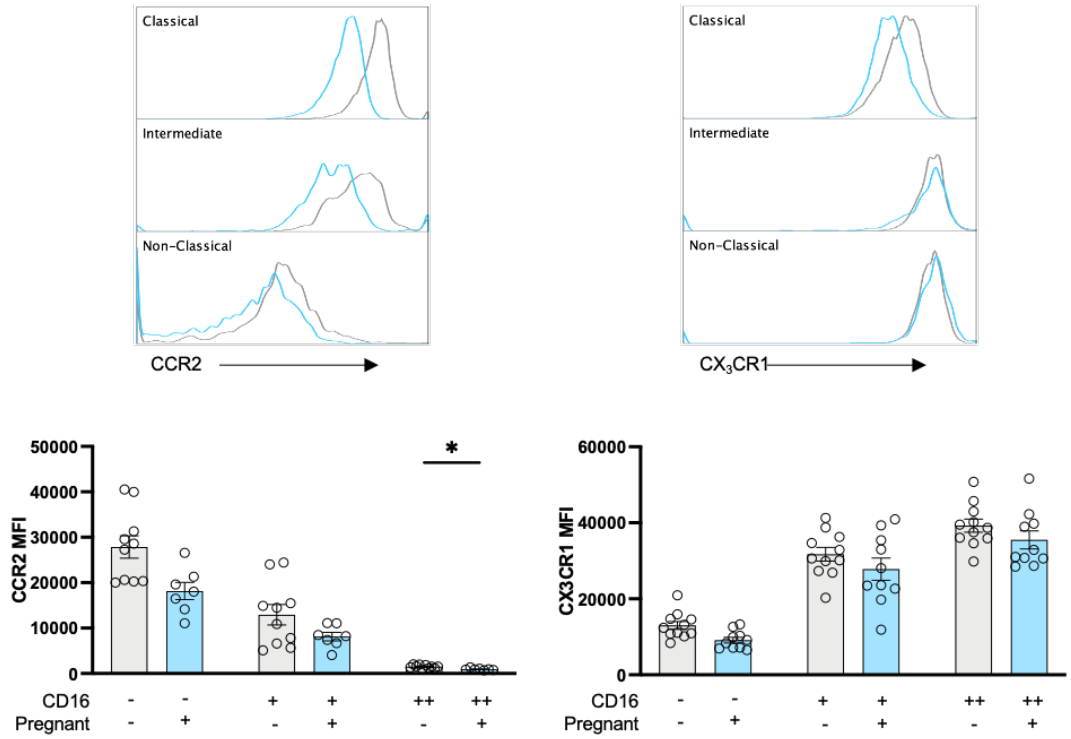

Figure 5.10: The chemokine receptor profile of monocyte subsets at 28 weeks of gestation and in non-pregnant women. The expression of chemokine receptors on monocyte subsets (classical = C; intermediate = I; non-classical = NC) was determined by flow cytometry of the MNCs as described in the materials and methods. Statistics were measured by a Šidák's multiple comparisons test and a p value < 0.05 was deemed significant. Chemokine receptors which were measured were: CCR2 (C $p = 0.0890$; I $p = 0.4849$; NC $p = 0.0280$) and CX_3CR1 (C $p = 0.0877$; I $p = 0.6924$; NC $p = 0.6408$).

Looking at some typical phenotype markers of monocytes (Figure 5.11) demonstrated changes in the monocytic profile in pregnancy at 28 weeks of gestation. No significant differences were detected for CD163, CD86 or CD220. Increased expression of the activation marker CD11b was observed for classical ($p = 0.0134$) and intermediate ($p = 0.0087$)

monocytes, and for CD64 on the intermediate (p = 0.0021) subset. In contrast, a decrease in the expression of CD80 on non-classical monocytes (p = 0.0078) in pregnancy in comparison to non-pregnant was seen.

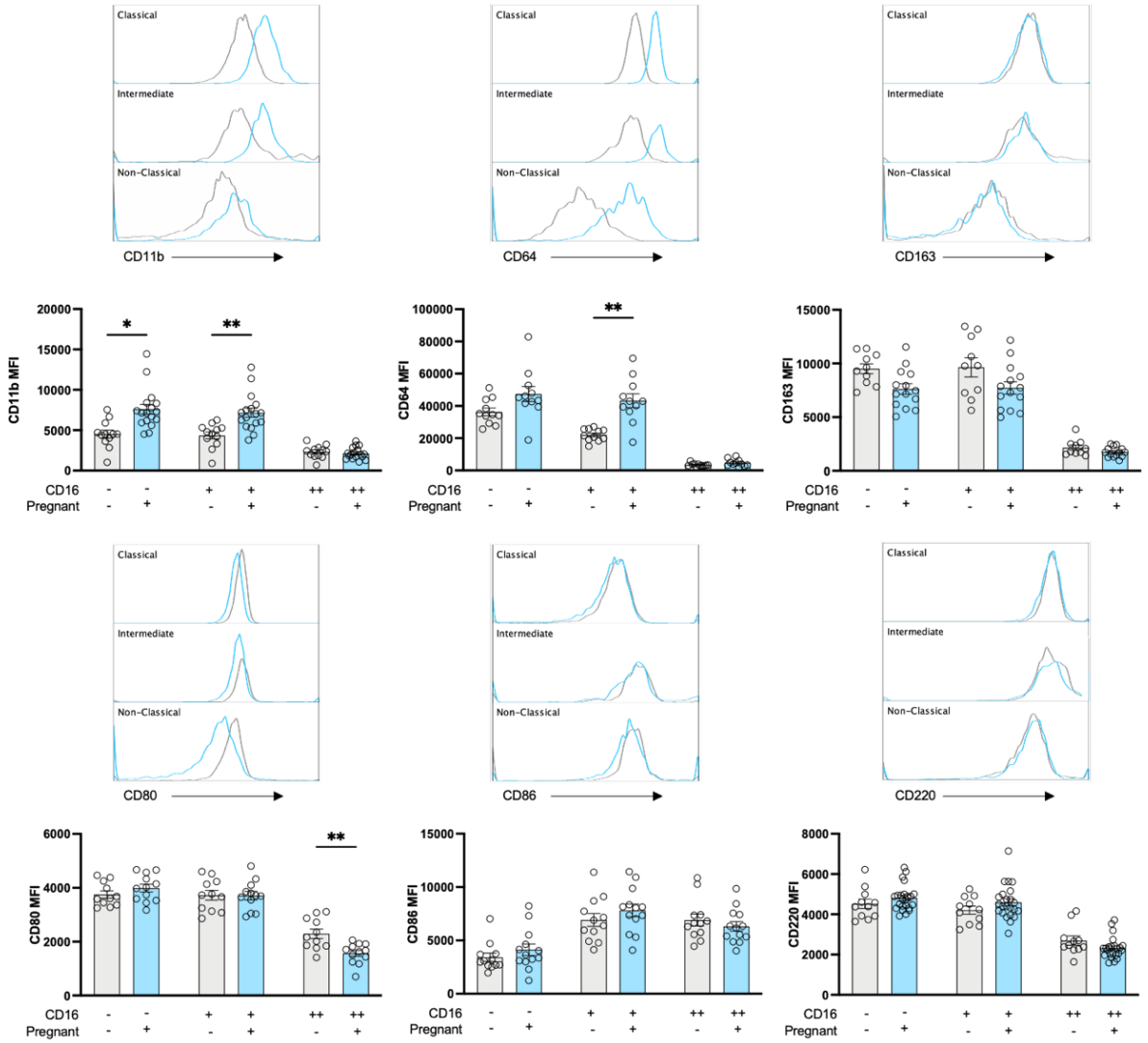

Figure 5.11: Typical phenotypic markers of monocytes in pregnancy at 28 weeks of gestation and in non-pregnant women. The expression of typical phenotypic markers on monocyte subsets (classical = C; intermediate = I; non-classical = NC) was determined by flow cytometry of the MNCs as described in the materials and methods. Statistics were measured by a Šidák's multiple comparisons test and a p value < 0.05 was deemed significant. Molecules which were measured were: CD11b (C p = 0.0134; I p = 0.0087; NC p = 0.8735), CD64 (C p = 0.0994; I p = 0.0021; NC p = 0.1899), CD163 (C p = 0.0671; I p = 0.2826; NC p = 0.3977), CD80 (C p = 0.6065; I p = 0.9998; NC p = 0.0078), CD86 (C p = 0.6856; I p = 0.6674; NC p = 0.7977) and CD220 (C p = 0.7231; I p = 0.6565; NC p = 0.5125).

As demonstrated in the previous Chapter 4, clear metabolic adaptations occur in monocytes in pregnancy at term. Therefore, investigation of these same markers was made for pregnancy at 28 weeks of gestation (Figure 5.12). CD36 (FAT) and CD98 (LAT) are both significantly elevated on the classical (p = 0.0133; p = 0.0078 respectively) and intermediate (p = 0.0131; p = 0.0045) monocytes, as well as CD38 (cyclic ADP ribose hydrolase) on the classical monocytes (p = 0.0326) of pregnant women. Interestingly, the mitochondrial

quantity is also increased in the classical (p = 0.0252) and intermediate (p = 0.0054) monocytes in pregnancy at 28 weeks of gestation in comparison to non-pregnant.

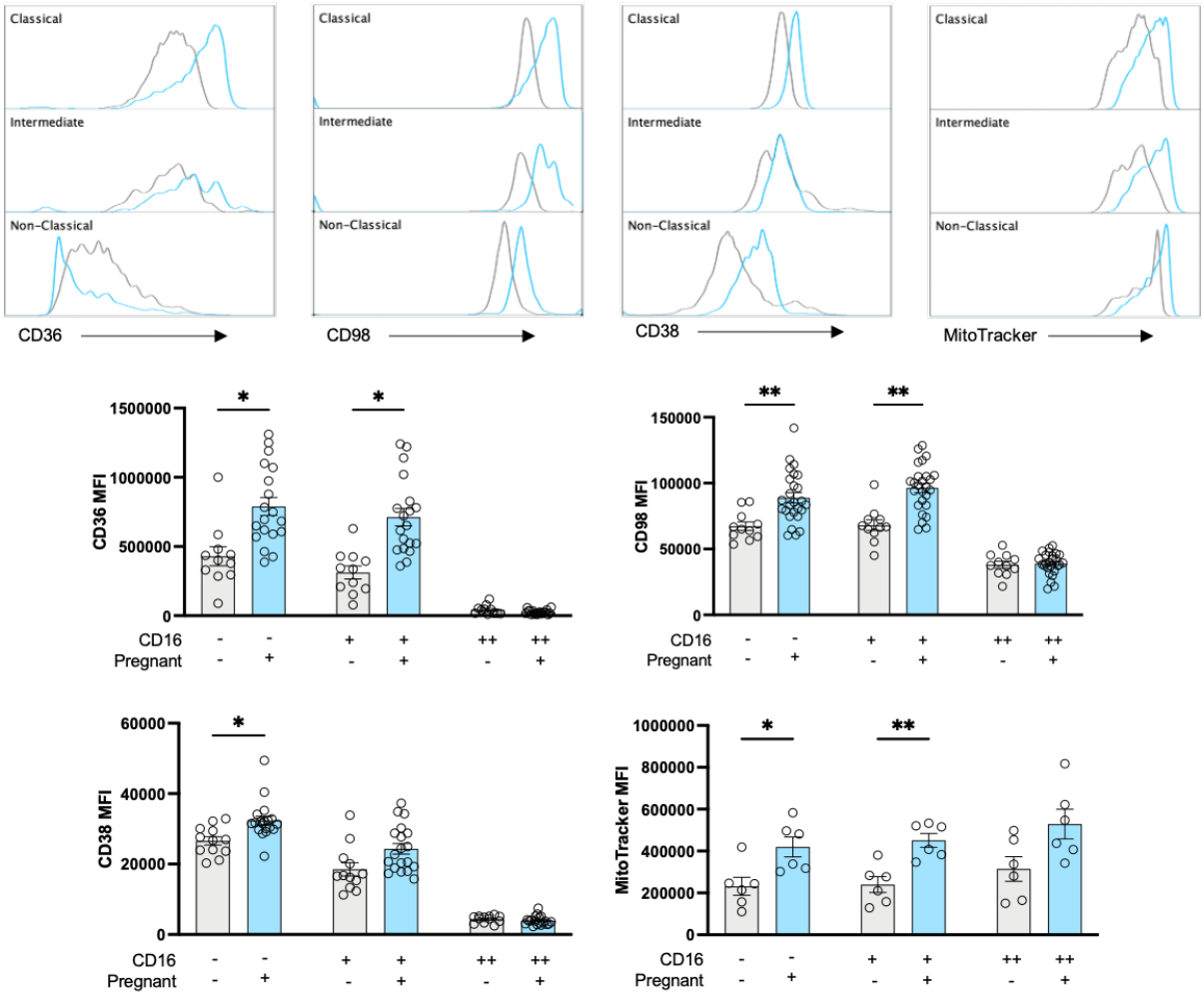

Figure 5.12: Metabolic markers on monocyte subsets in pregnancy at 28 weeks of gestation and in non-pregnant women. The expression of typical metabolic markers on monocyte subsets (classical = C; intermediate = I; non-classical = NC) was determined by flow cytometry of the MNCs as described in the materials and methods. Statistics were measured by a Šidák's multiple comparisons test and a p value < 0.05 was deemed significant. Molecules which were measured were: CD36 (C p = 0.0133; I p = 0.0131; NC p = 0.3572), CD98 (C p = 0.0078; I p = 0.0045; NC p = 0.9893), CD38 (C p = 0.0326; I p = 0.1126; NC p = 0.7931) and MitoTracker (C p = 0.0252; I p = 0.0054; NC p = 0.1957).

5.3.4 MNCs in pregnant women at 28 weeks of gestation are not metabolically altered

As monocytes contribute to the heterogeneity of MNCs, and there were obvious metabolic changes in pregnancy at 28 weeks (i.e., higher mitochondria), the OXPHOS and glycolytic capacity of the MNCs was then determined (Figure 5.13). However, there were no difference in either OCR or ECAR, nor in any of the parameters that it is possible to calculate.

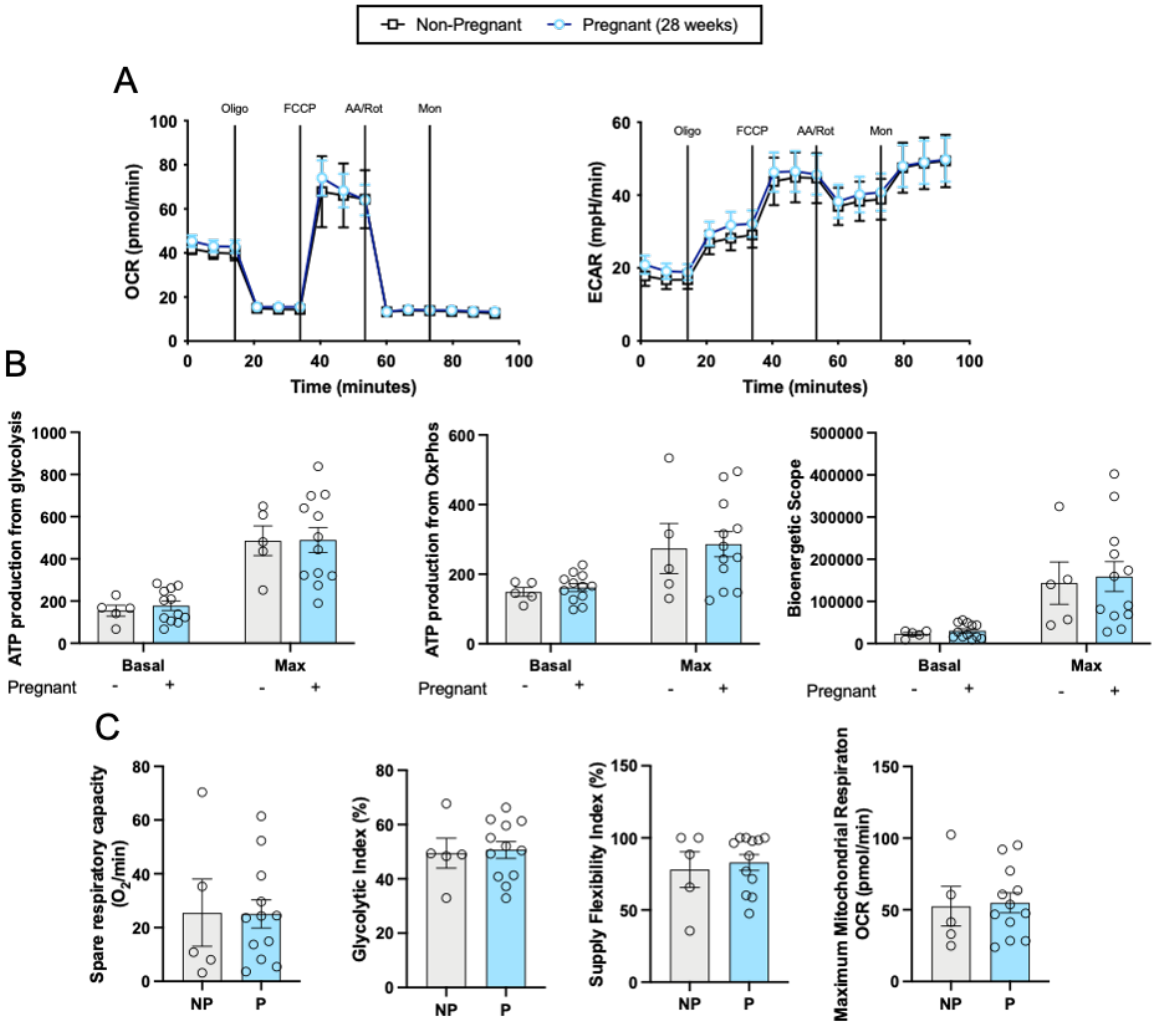

Figure 5.13: The bioenergetic capabilities of MNCs of pregnant women at 28 weeks of gestation in comparison to non-pregnant women. MNCs were used for bioenergetic analysis on the Seahorse Extracellular flux analyser as described in the materials and methods. Both oxidative phosphorylation (OXPHOS; OCR) and glycolytic (ECAR) parameters were measured. Statistics were performed using a Mann-Whitney t test where a p value < 0.05 was significant. (A) The OCR and ECAR traces for pregnant and non-pregnant MNCs with their responses to the injections. (B) ATP production for glycolysis (basal p = 0.7214; max p. =. 0.9593) and OXPHOS (basal p = 0.6461; max p =0.7214), and the bioenergetic scope (basal p = 0.6461; max p = 0.7214) were measured. (C) Other parameters which were measured were: spare respiratory capacity (p = 0.7214), glycolytic index (p = 0.7214), supply flexibility index (p > 0.9999) and maximum mitochondrial respiration (p = 0.7214).

5.3.5 Summary of results

A heatmap is provided in Figure 5.14 to summarise the findings of this chapter.

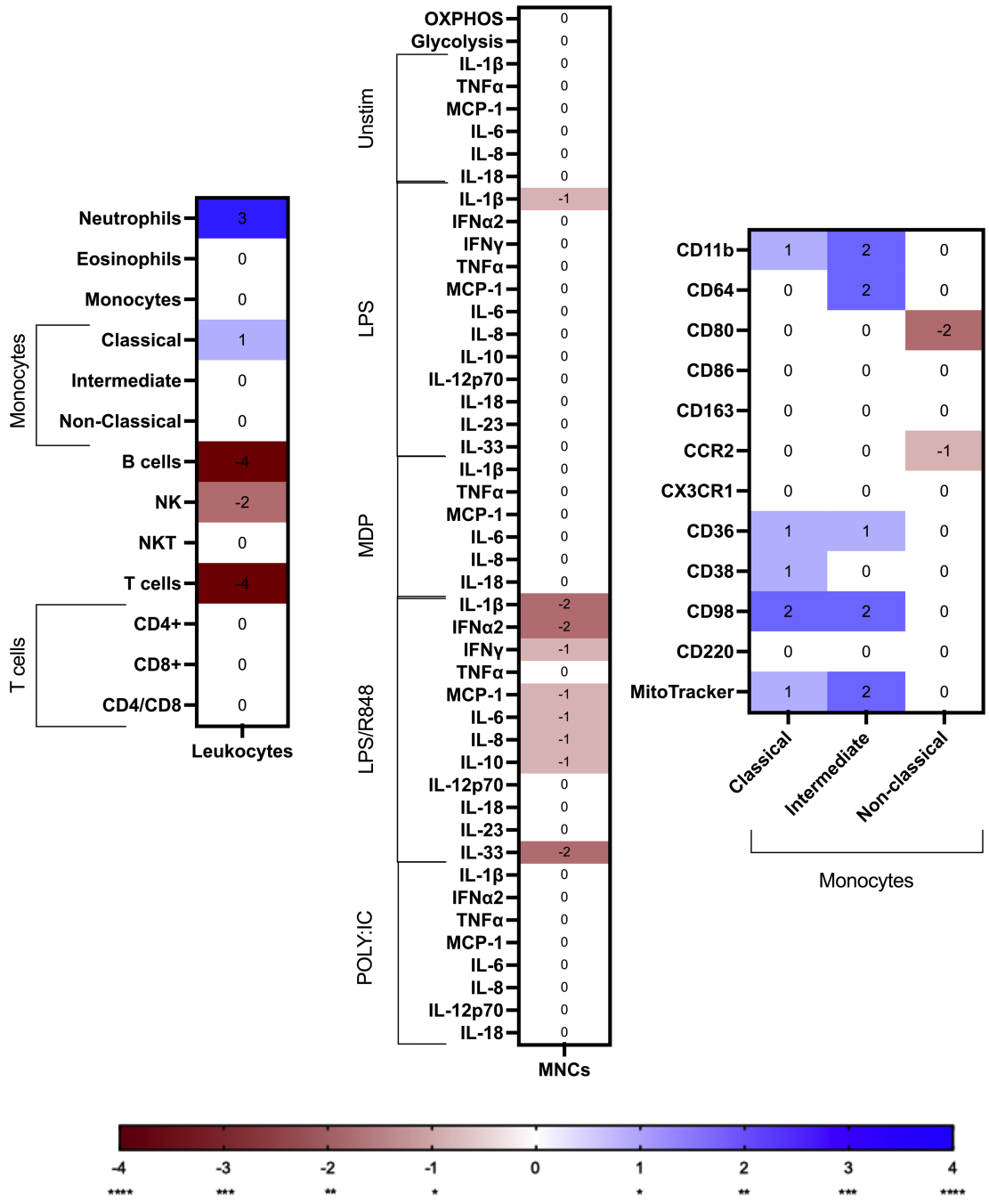

Figure 5.14: A heatmap summary of the findings of Chapter 5. Blue indicates a significant increase in the measurements from pregnant women in comparison to non-pregnant, whereas red specifies a derease. Some findings have been condensed to the most important, such as overall OXPHOS rather than showing each measurement.

5.4 Discussion

This chapter clearly illustrates immunological adaptations which occur at 28 weeks of pregnancy. Along with different proportions of leukocytes, the cytokine producing ability of MNCs and the phenotype of monocytes from pregnant women are affected when compared to those from non-pregnant women. The most notable differences are the effect of stimuli on cytokine production in MNCs, and a suggested metabolic and chemotaxis phenotype of the monocytes at 28 weeks of gestation. It must be acknowledged that a down-side to this investigation is that the pregnant women were fasted, whereas it was not possible to have the non-pregnant women fast; there have been some studies showing an effect of fasting on immune cells [380].

It is difficult to pinpoint the literature that describes the actual leukocyte population changes that occur throughout the stages of gestation. Early reports only classify total white blood cells, granulocytes, monocytes and lymphocytes, and even recent reports generated using automated haematology analysers do not differentiate between the subsets. Here, this chapter clearly illustrates a collection of the changes in different leukocyte proportions at 28 weeks of gestation. Confirming previous reports, neutrophils are elevated at 28 weeks of gestation [381]. Neutrophilia has been shown to be a key component of the leucocytosis observed in pregnancy [6]. The reduction in T cells and B cells also confirms what has been found previously [7, 136]. Studies have shown a slight reduction in NK cell populations as the pregnancy progresses [382-384], and here the reduction in NK cell percentage is more substantial. This could be due to the cluster of women in the cohort; women of similar BMI at the same stage of gestation, and blood taken at the same time to account for circadian rhythm. It has been suggested that elevated peripheral NK cells is associated with recurrent miscarriage (RM) [385-387], though this has been a source of debate. A systemic review by Seshadri et al which showed the number of peripheral NK cells were elevated in infertile women and women with RM in comparison to fertile controls, and also an increase in the percentage of these cells in women with RM in comparison to controls, though no significant changes in uNK cells [388]. Seshadri et al did however conclude that the variability between the studies demonstrates the inadequacy of using NK cell marker as a tool for diagnostics[388]. Another study has shown that primary RM (pRM; no previous live births) presented with higher absolute number of peripheral NK cells in comparison to secondary RM (sRM; ≥1 previous live

births) [389]. This could account for some of the heterogeneity found in other studies. The elevation of peripheral NK cells may only be a marker of RM and not a causative factor, and more work needs to be done to explore their role. With regards to the monocytes, in contrast to what is observed here with an increase in the classical subset of monocytes, elevated non-classical monocytes and a depletion of the classical subset is usually observed [328, 329]. However, another study by Al-Ofi et al also showed an increase in the classical monocytes [390]. In their review, Faas & Vos [77] discussed the discrepancies between these three studies and theorised the conflicting reports were attributed to the analysis on whole blood [328, 329] vs MNCs [390]. However, as this study, which utilises whole blood, shows what is observed by Al-Ofi et al in MNCs, this theory can be rejected. The women from these three studies and this present study are all at approximately the same gestational age, and complications such as GDM were excluded. The three studies collected venous blood in the same way, into a tube with EDTA anticoagulant, whereas this study used a tube containing heparin anticoagulant.

Despite a reduction in the production of IL-1β by LPS-stimulated MNCs from pregnant women, stimulation with LPS, MDP or POLY I:C had no significant changes in their ability to produce the cytokines measured in pregnancy; there were also no differences in the unstimulated controls. However, stimulation with a combination of LPS and R848, revealed numerous differences between the response of MNCs from pregnant versus non-pregnant women. Significant decreases in the levels of IL-1β, IFNα2, IFNγ, MCP-1, IL-6, IL-8, IL-10, and IL-33 were observed in the MNCs from pregnant women in comparison to those from non-pregnant women. This suggests that pregnant women might have a reduced capability to combat pathogens, especially viral pathogens that trigger TLR7/8. This reduced ability to produce these cytokines upon interaction with LPS/R848 might provide insight into the SARS-CoV-2 interaction with pregnancy. A cytokine storm is synonymous with disease severity in infections with SARS-CoV-2 [391]; the inability of MNCs from pregnant women to mount a significant cytokine response in response to LPS/R848 suggests protection against hyperinflammation and disease severity with SARS-CoV-2. The response of whole blood leukocytes to SARS-CoV-2 has been studied extensively during the COVID-19 pandemic with some studies revealing a correlation between the ability to produce IFNs and disease severity (reduced ability leads to severe disease), and conversely showing that increased production of other inflammatory cytokines (e.g. IL-6, IL-10, TNFα) also lead to increased severity [392].

While the decrease in IFNα2 and IFNγ observed in pregnancy suggests a lessened ability to combat SARS-CoV-2, the reduction in the other inflammatory cytokines (IL-6, IL-10) indicates a reduced inclination to disease severity. It has been shown that pregnant women are not more susceptible than non-pregnant women to the development of severe COVID-19; however, instances of severe COVID-19 in pregnant women brings increased risk of preterm birth and intensive care admission [164]. An inflammatory state like obesity may increase the production of these inflammatory cytokines, leading to increased risk of disease severity during pregnancy, as maternal obesity has been found to be linked with severe COVID-19 [167].

While the reduced production of inflammatory cytokines from MNCs of pregnant women might be beneficial in preventing a cytokine storm, in contrast this illustrates the increased susceptibility to typical viruses and other pathogens [161] as inflammatory cytokines are required for the clearance of pathogens. The reduction of MCP-1 in particular suggests a diminished ability to recruit monocytes to a site of infection, thereby resulting in reduced leukocyte activity. Very few studies have investigated the production of cytokines by MNCs in pregnancy. One study did culture MNCs with serum to illustrate a significant reduction in TNFα, IFNγ and MCP-1 over gestation, but no significant changes in IL-12p70, IL-6, IL-8, IL-1β or IL-10 [393]. The adaptive response, especially the Th paradigms, is more commonly researched, than the innate response which is investigated here. NK cells and T cells have been observed to have reduced IL-6, IFNγ, and TNFα upon stimulation with IL-12/IL-15 and toxic shock syndrome toxin-1 (TSST) respectively during the second and third trimester [384]. This suggests an overarching down-regulated of Th1-type proinflammatory cytokines (i.e., IFNγ) with the innate and adaptive response. Pregnancy is characterised by increased inflammation at implantation and parturition [394] but is predominantly anti-inflammatory for the development of the fetus, where a successful pregnancy is driven by a Th2 response [395]. The reduction of the Th2 type anti-inflammatory cytokines (i.e., IL-10) observed here with an innate stimulus may be compensation for an increase in these types of cytokines if a TCR-dependent stimuli was used.

As significant differences in the monocytes from pregnant women at term were observed as discussed in Chapter 4, the investigation into whether these changes occur at an earlier stage of gestation was necessary. In this chapter, monocyte phenotype was determined using

MNCs, where it was possible to distinguish between all three monocyte subsets using their CD14 and CD16 expression. At 28 weeks, the CCR2 expression of the monocytes appear to be downregulated in comparison to non-pregnant, but this difference was only significant for the non-classical monocytes. This suggests that at this stage of gestation they might be less efficient at chemotaxis – at least to CCL2 (also referred to as MCP-1). This could be due to the requirements for monocytes and their bioactivity at different stages of pregnancy. At implantation and parturition, where the inflammation balance tips in favour of pro-inflammatory, it might be expected that the monocytes would have high expression of CCR2 to infiltrate the decidua and polarise to macrophages [292], a key cell at these stages of pregnancy supporting the invasion of the trophoblast and expulsion of the fetus. During the early stages of the third trimester at 28 weeks, we might assume there would be less of a requirement for the monocytes to promote inflammation within gestation-associated tissues. Labour is associated with elevated leukocyte infiltration (notedly elevated decidual macrophages), with the expression of certain chemokines (CCL2, CCL4, CCL5, CXCL8, CXCL10) being markedly upregulated [396]. The low expression of CCR2 at 28 weeks of gestation therefore is to prevent the likelihood of a preterm labour.

The significant increase in CD11b suggests an increase in the activation state of the classical and intermediate monocytes at 28 weeks of gestation. Together, with the elevation of CD64 expression, which could be indicative of their phagocytosis abilities, this illustrates a likely primed innate response to combat potential pathogens. The elevated expression of these markers has been shown previously in other studies which investigated pregnant women at similar stages of gestation (28-32 weeks) [73, 397]. The decrease in the expression of CD80 (a co-stimulatory molecule for T cells) indicates a reduced capability to induce an adaptive response to protect the fetus, and also confirms what other studies have observed [398].

Metabolically, the monocytes are very interesting at 28 weeks of gestation. Their fatty acid (CD36) and amino acid transporters (CD98), mitochondrial content and CD38 are all elevated in the classical and intermediate monocytes. This implies that the monocytes are more metabolically activate and capable at this stage of gestation than the non-pregnant. These findings are novel regarding monocytes in pregnancy. CD36 also has other roles such as in non-opsonic phagocytosis; combined with the elevated expression of CD64, a molecule

involved in opsonic phagocytosis, further study of the phagocytic abilities of monocytes at 28 weeks of gestation is warranted.

Due to the significant changes in the metabolic markers and mitochondrial content of the monocytes, it was logical to assess the oxidative phosphorylation and glycolytic capabilities of the MNCs. In addition, Jones et al showed a reduction in the glycolytic capabilities of MNCs from pregnant women at term, and so inquiry into gestational age was warranted [47]. Investigating these parameters for isolated monocytes was not possible in this instance due to the low volume of blood available from the pregnant women. Despite the likely possibility that monocytes have higher oxidative phosphorylation capabilities at 28 weeks of gestation than in the absence of pregnancy, if this is the case it is hidden in the heterogenous population of MNCs. There were no significant changes observed with either the OCR or ECAR measurements.

Ethics for investigating isolated monocytes in greater detail at different stages of pregnancy was approved shortly before the COVID-19 pandemic. As a result of this pandemic however, samples were not able to be collected.

5.5 Conclusion

Monocytes from pregnant women at 28 weeks of gestation appear primed to respond to pathogens, with potentially upregulated metabolism and phagocytosis potential. However, in the heterogenous pool of MNCs, cytokine production is stunted on exposure to LPS/R848, and the MNCs do not appear to be metabolically compromised. Future studies should investigate homogenous cell populations to characterise functionality and metabolic capabilities of the cells and how this contributes to the heterogenous population.

Chapter 6 – Maternal body mass index is associated with an altered immunological profile at 28 weeks of gestation

6.1 Introduction

Maternal obesity during pregnancy is associated with adverse pregnancy outcomes such as miscarriage [399], preeclampsia [400] and gestational diabetes mellitus [401], and poses an increased risk of fetal mortality and childhood obesity as a result of macrosomia and metabolic syndromes [402]. With the prevalence of obesity in women of reproductive age recently reported as between 20% and 28% in England [403], reflecting the increasing prevalence of obesity worldwide, maternal obesity and the health consequences for mother and child are an endemic problem. In the not pregnant general population, we have good mechanistic insight into the links between excessive fat accumulation, systemic low-grade inflammation, and obesity-associated health risks such as type 2 diabetes mellitus (T2DM), reproductive dysfunction and cardiovascular disease [404-406]. Elevated circulating inflammatory markers such as IL-6, TNF and C-reactive protein (CRP) characterise the systemic inflammation that typically occurs with increasing adiposity [34]. The current COVID-19 pandemic highlights the detrimental impact of obesity on inflammation, immune function, and risk from infectious disease with, for example, obesity and high CRP levels indicate for severity of COVID-19 symptoms [407].

How obesity in pregnancy might mechanistically underpin the well documented adverse pregnancy and child health outcomes is relatively unknown. The effects of maternal obesity on inflammation and immune function in the term placenta [93] and first trimester uterus [107] have received some attention revealing impact on immune cell number and function that could contribute to adverse pregnancy outcomes. This includes depleted decidual macrophages [95] and increased numbers of placental macrophages in obesity [93], although there are some conflicting findings regarding the number of placental macrophages with maternal obesity (Figure 6.1) [94]. Maternal obesity also diminishes the numbers of uterine resident NK cells and alters their contribution to extracellular matrix remodelling and growth factor signalling to compromise trophoblast survival and spiral artery remodelling [107].

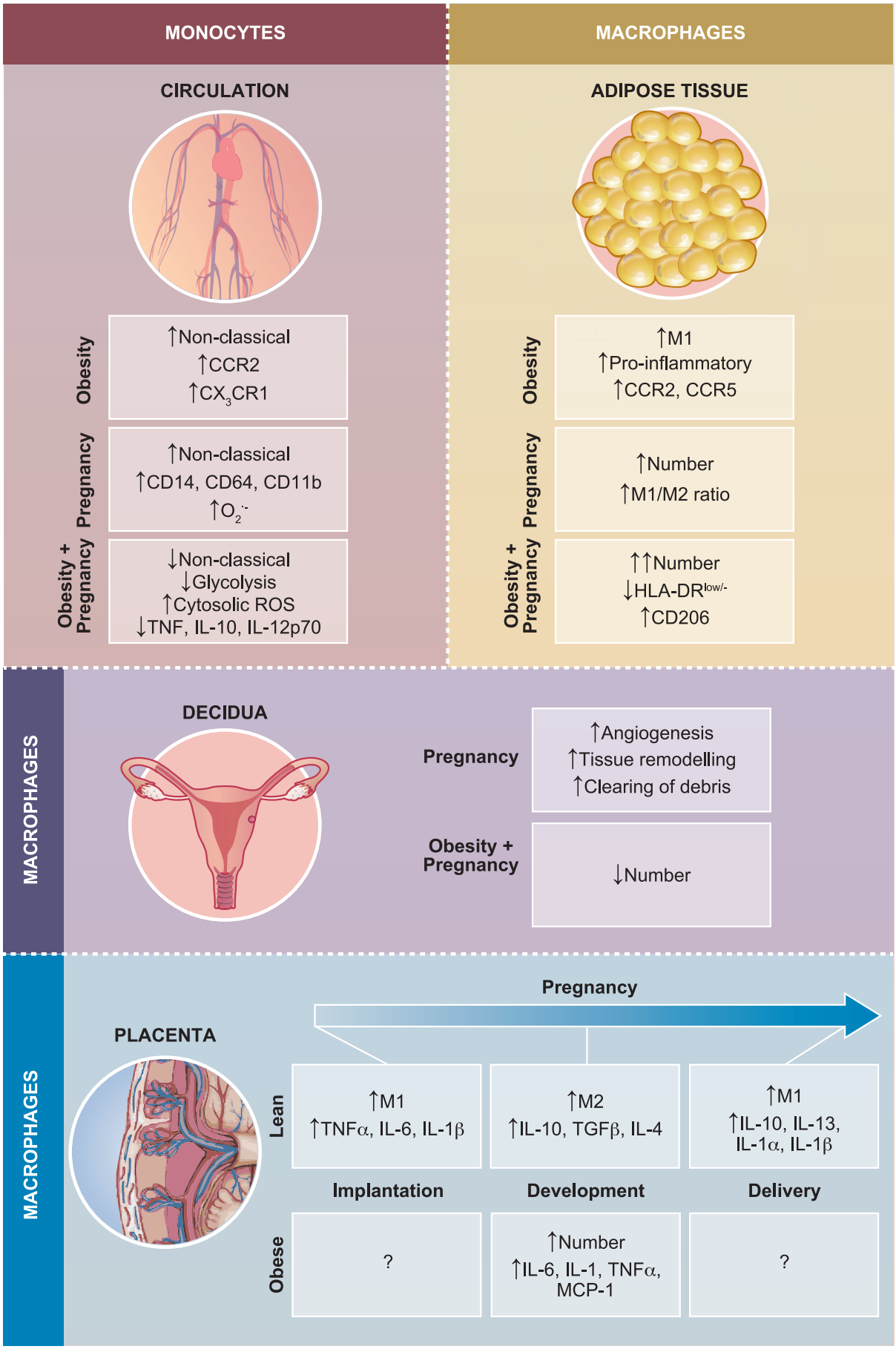
MONOCYTES
MACROPHAGES
CIRCULATION
ADIPOSE TISSUE
Obesity
↑Non-classical
↑CCR2
↑CX3CR1
Pregnancy
↑Non-classical
↑CD14, CD64, CD11b
↑O2·-
Obesity + Pregnancy
↓Non-classical
↓Glycolysis
↑Cytosolic ROS
↓TNF, IL-10, IL-12p70
Obesity
↑M1
↑Pro-inflammatory
↑CCR2, CCR5
Pregnancy
↑Number
↑M1/M2 ratio
Obesity + Pregnancy
↑↑Number
↓HLA-DRlow/-
↑CD206
MACROPHAGES
DECIDUA
Pregnancy
↑Angiogenesis
↑Tissue remodelling
↑Clearing of debris
Obesity + Pregnancy
↓Number
MACROPHAGES
PLACENTA
Pregnancy
Lean
↑M1
↑TNFα, IL-6, IL-1β
↑M2
↑IL-10, TGFβ, IL-4
↑M1
↑IL-10, IL-13, IL-1α, IL-1β
Implantation
Development
Delivery
Obese
?
↑Number
↑IL-6, IL-1, TNFα, MCP-1
?

Figure 6.1: A summary of the effects obesity has on monocytes, and on macrophages in adipose tissue, decidua and in the placenta. Monocytes: In comparison to lean, obesity is associated with an increase in non-classical ($CD14^{dim}CD16^{+}$) monocytes [408], which are thought to be more pro-inflammatory, as well as an increase in the expression of CCR2 and CX_3CR1 [67, 409]. Pregnancy is also accompanied by an increase in non-classical monocytes. Monocytes in pregnancy also have increased expression of CD14, CD11b and CD64, as well as increased superoxide production [410]. **Adipose tissue**: Obesity is associated with an increase in M1 macrophages, inducing a more pro-inflammatory environment [83]. These macrophages also have elevated expression of chemokine receptors CCR2 and CCR5. During a healthy pregnancy, the number of total macrophages increases in adipose tissue and there is an increase in the M1/M2 ratio. The effect obesity has on pregnancy shows that the number of macrophages is further exacerbated, and also increases the induction of apoptosis. Surface markers on these macrophage changes: lower $HLA\text{-}DR^{low/-}$ and elevated CD206 [91]. **Decidua**: during a healthy gestation, decidual macrophages promote angiogenesis, tissue remodelling and the clearance of apoptotic cells [84, 411]. Very little is currently understood about decidual macrophages in an obese environment, but their overall numbers are reduced [89]. **Placenta**: throughout a healthy pregnancy placental macrophage undergo many changes. At implantation, M1 macrophages are dominant and contribute to the high levels of TNFα, IL-6 and IL-1β observed [16, 17]. As pregnancy develops, a switch occurs so that M2 are the dominant macrophage phenotype, along with the increased production of IL-10, TGF-β and IL-4 [412]. At delivery, the macrophages switch back to an M1 phenotype which coincides with elevated production of IL-10, IL-13, IL-1α and IL-1β [23-25]. Little is known about the effect obesity has on macrophages in the placenta but it has been shown that there are more placental macrophages in obesity, and an increase in pro-inflammatory cytokines IL-6, IL-1, TNFα and MCP-1 [93]. Image created for Rees et al. [2]

In contrast, the systemic effects of obesity in pregnant women are largely unknown. Like the general population, maternal IL-6, CRP and leptin levels are elevated in pregnant women with obesity compared to their lean counterparts [93, 413]. This suggests a common outcome of systemic inflammation in pregnant and not pregnant adults with obesity. It also highlights that obesity-related changes can occur over and above the systemic inflammatory alterations that are a normal feature of pregnancy, including reduced pro-inflammatory cytokines (e.g. IL-6, CCL2, CXCL10, IL-18, TNF) and increased immunomodulatory and anti-inflammatory mediators (e.g. soluble TNF-receptor I, sTNF-RII, IL-1 Receptor Agonist (RA))[32].

Pregnancy per se is also associated with cellular changes linked to inflammation and innate immune function such as increases in peripheral blood neutrophils and monocytes for example [6]; maternal obesity exacerbates the neutrophil count even further [101]. The effects of obesity on the general population and in pregnancy on granulocytes is summarised in Figure 6.2. Functional effects have also been described and include evidence of monocyte activation such as increased expression of CD14, CD64 and CD11b and heightened production of oxygen free radicals [73]. In the general population, monocytes seem particularly susceptible to the effects of obesity including increases in the non-classical subset of monocytes [68], elevated expression of CCR2 by classical and intermediate monocytes and higher expression of CX_3CR1 by all three subsets likely leading to increased intrinsic migratory capacity in response to chemokines such as CX_3CL1 and CCL2 secreted by adipose tissue [79]. Beyond reported increased production of LPS-stimulated IL-1β and RANTES and ssRNA-stimulated TNF and IL-

10 in monocytes of the general population with obesity [79] little is known about the effects of maternal obesity on myeloid effectors of innate immunity and inflammation. One recent study has shown that at term, monocytes of pregnant women with obesity appear to be disrupted in their ability to adapt to pregnancy, perhaps explaining their increased susceptibility to infections [414]. With both atypical levels of circulating pro-inflammatory cytokines such as IL-6 [33] and exacerbated activation and maturation of monocytes to the non-classical subset [77] linked to preeclampsia for which obesity is a risk factor [80], there is real need to address this shortcoming. A summary on the changes in monocytes can be visualised in Figure 6.1.

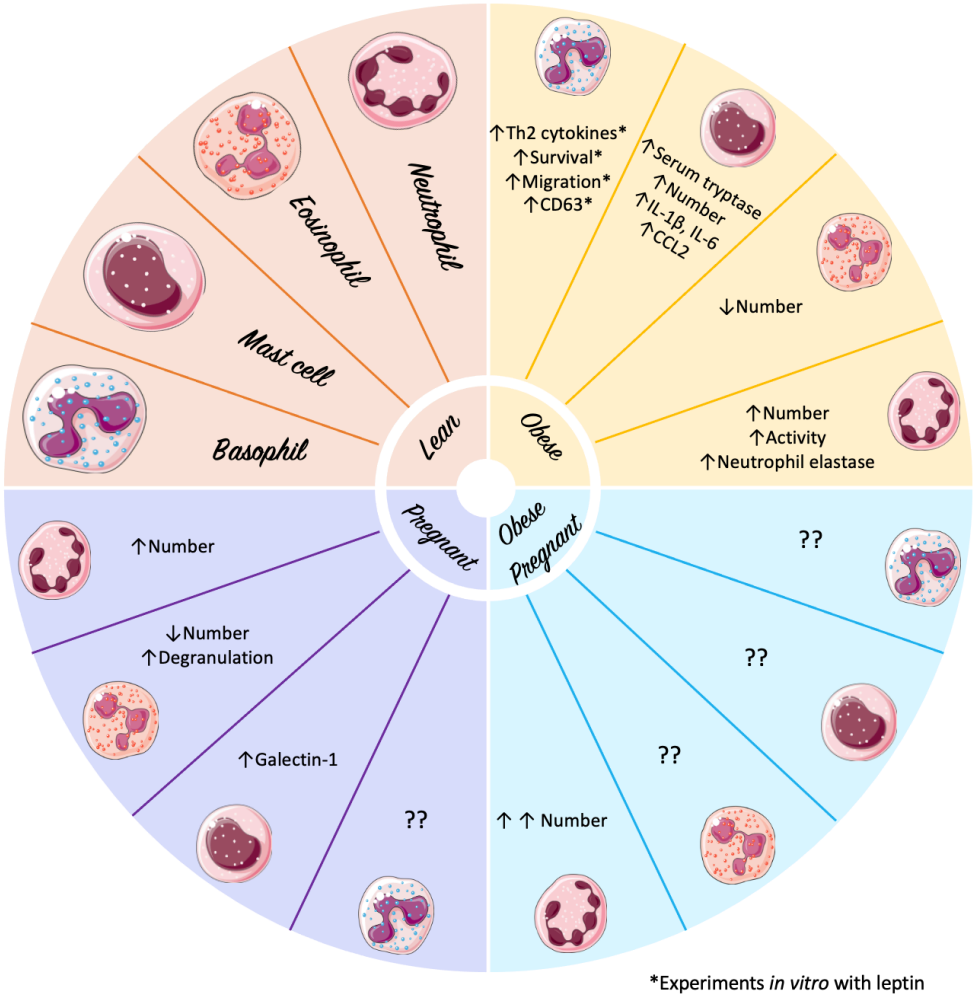

Figure 6.2: The effect of obesity and pregnancy on granulocytes, in comparison to lean non-pregnant. Neutrophils: obesity induces an elevation in the number of neutrophils and increases their activity [41] and production of neutrophil elastase [42]. The population of neutrophils is also increased in pregnancy, and further exacerbated in obese pregnancies [409]. Eosinophils: the population is significantly depleted in obesity [410] and in pregnancy, and their degranulation capacities are elevated in pregnancy [103]. The effect of obesity on pregnancy for eosinophils is not defined. Basophils: obesity-simulation with leptin observes an increase in Th2 cytokines; the survival and migration of the basophils increase, and CD63 expression is elevated [411]. It is unknown how basophils are affected by pregnancy and obese pregnancy. Mast cells: the production and release of tryptase is increased in obesity [412]; mast cell number, production of IL-1β and IL-6, and expression of CCL2 are all increased in obesity [413]. The production of galectin-1 is increased in pregnancy [105,107], and the effect of obesity on pregnancy for mast cells is not yet understood.

Obesity in the general population is also recognised to negatively affect the function of multiple lymphocyte populations. This ranges from suppression of T and natural killer (NK) cell function – including reductions in cytotoxicity, IFNγ production and expression of perforin and granzymes [420] - and altered B cell activity that manifests as reduced class-switching and immunoglobulin activity [421]. A reduced CD8+ T cell count in peripheral blood with obesity in both the general population [422] and pregnant women [131] has been described and possibly links to their accumulation in adipose tissue that, from mouse models, precedes that of macrophages [422]. The cytokine producing capacity of T cells also changes with obesity in the general population and obesity-associated inflammation is in part driven by a shift to Th1 and Th17 which is thought to be mediated by leptin [423]. Th1 and Th17 cytokines such as TNF and IFNγ are detrimental to pregnancy [119]. Conversely, a Th2 and regulatory T cell (Treg) dominated environment is considered essential to pregnancy success [119]. Maladaptation of adaptive immune processes could very much underpin obesity-associated adverse obstetric outcomes with upregulation of Th1 described in GDM [424].

6.1.1 Rationale

As shown in previous chapters, there are vast immunological adaptations which happen in pregnancy, especially in monocytes. It is known that obesity is a risk factor for several negative obstetric outcomes, and so understanding the immunological factors underlying this is vital. Very little is currently known regarding a healthy pregnancy, let alone a pregnancy affected by obesity. The main goal of the work here was to describe the changes in the immune environment of GDM-negative, pregnant women of differing pre-pregnancy BMI at 28 weeks of gestation and reveal a phenotype of systemic inflammation, monocyte activation and altered Th1/Th2/Th17 balance.

6.1.2 Hypothesis

The immunological changes in pregnancy are sabotaged by maternal obesity.

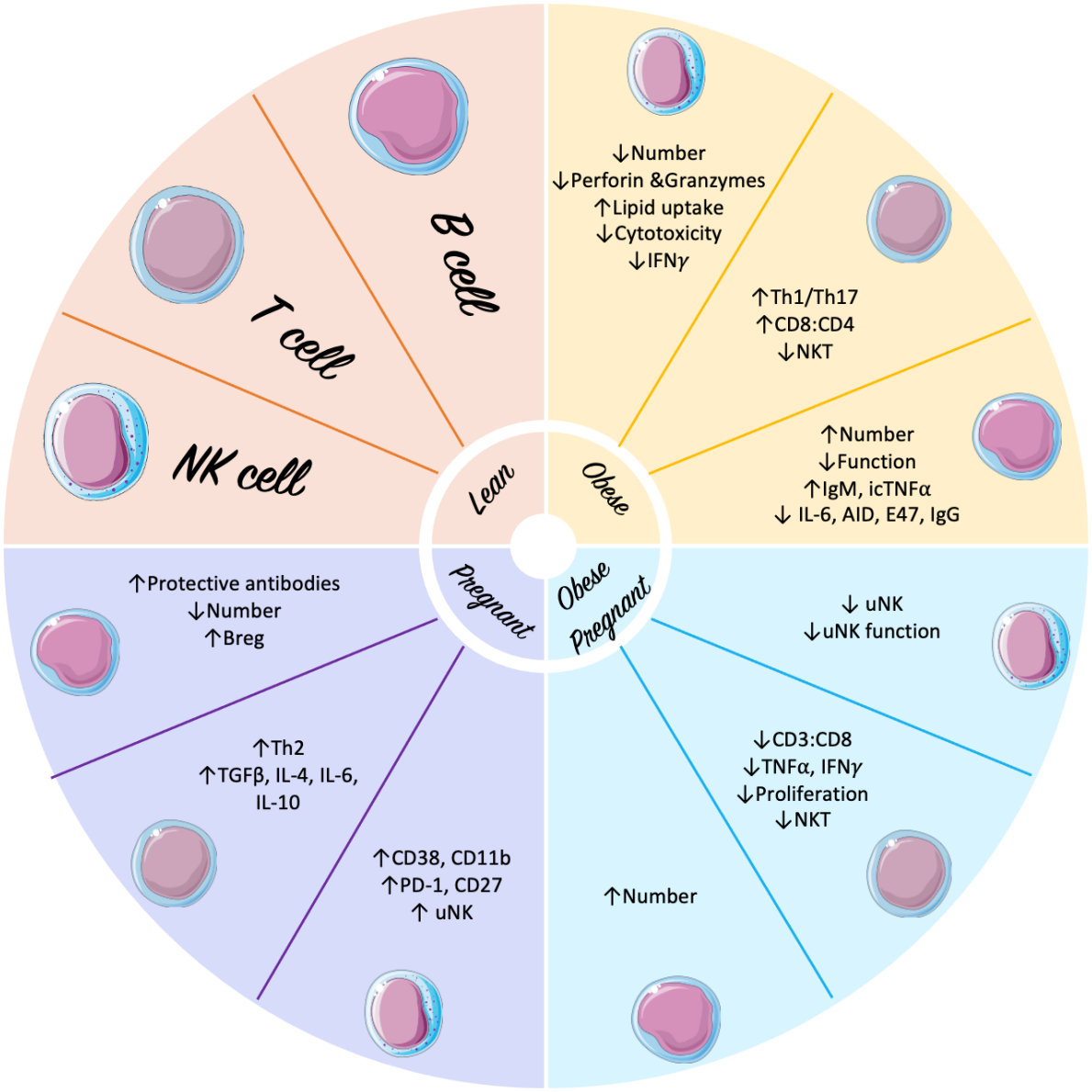

Figure 6.3: Lymphocytes are altered in pregnancy and in obesity, and further modified in obese pregnancy. NK cells: obesity is associated with a decrease in the number of NK cells and their activity [97]. Their cytotoxicity abilities are diminished, and they produce less perforin, granzymes and IFNγ, perhaps due to their increased lipid uptake [97]. In pregnancy, NK cells are abundant in the uterus (uNK) and have increased expression of activation markers CD38 and CD11b, and immune checkpoint molecules PD-1 and CD27 [98]. In obese pregnancies, the vital uNK cells are depleted and their function weakened [419]. T cells: the Th1/Th17 response is increased in obesity [419,109], as well as the CD8:CD4 ratio [110,112], whereas NKT cell numbers are reduced [420,421]. In contrast, pregnancy is associated with a shift to a Th2 environment, with the elevation of the production of TGF-β, IL-4, IL-6 and IL-10 [111]. Obesity effects T cells in pregnancy by decreasing the CD3:CD8 ratio [417,] the number of NKT cells [422] and reducing the proliferation of the cells and the production of TNFα and IFNγ [422]. B cells: the number of B cells increases in obesity [423] as well as the production of IgM [423] and intracellular TNFα, but their function is negatively altered [424] as well as their production of IL-6, AID, E47 and IgG [423,424.] Conversely, the number of B cells decrease in pregnancy [425], but the subset of Breg cells is increased, as well as the production of protective antibodies [425]. The effect of obesity on pregnancy for B cells is still poorly understood, but it has been observed that their numbers increase [427].

6.2 Materials and Methods

6.2.1 Samples

Peripheral blood was collected from healthy, fasted pregnant women into one 9 ml heparinised Vacuette ™, one 4 ml EDTA Vacuette ™ and one 5 ml serum Vacuette ™ (Greiner Bio-one, Frickenhausen, Germany), and processed within 30 minutes of collection. These women were being tested for gestational diabetes mellitus (GDM) and obtained a negative result from the oral glucose tolerance test (OGTT). All samples were collected with informed written consent and ethical approval obtained from a health Research Authority (HRA) Research Ethic Committee (REC approval 19/LO/0722). The demographics of the women analysed are shown in Table 6.1. Ethnicity is significantly different between the groups; this likely reflects the screening process whereby ethnicity is recognised as a risk factor for GDM as set out by the National Institute for Health and Care Excellence (NICE) guidelines. Women with a BMI over 30 gave birth to neonates of lower weights on average, compared to women with a BMI under 30 ($p = 0.0492$), in line with studies observing higher incidences of intrauterine growth restriction with maternal obesity [433, 434]. It needs to be acknowledged that within the complications measured, one pregnancy resulted in a still birth at term (BMI > 30), and two pregnancies resulted in preterm but healthy neonate (one BMI < 30 and one BMI > 30). All pregnancies were healthy at time of blood sampling.

		BMI ≤ 29.9		BMI ≥ 30.0		p-value
		Mean	± SEM	Mean	± SEM	
Age (years)		30.06	0.7304	29.74	0.6182	0.7157
Ethnicity (%)	Caucasian	76.00	n/a	95.00	n/a	0.0001
	Middle Eastern	15.00	n/a	2.00	n/a	
	South Asian	10.00	n/a	1.00	n/a	
	African	0.00	n/a	1.00	n/a	
Gestation at sample collection (weeks)		27.48	0.2328	27.25	0.1436	0.3732
Gravidity		2.50	0.2289	2.65	0.1753	0.5281
Parity		0.98	0.1466	1.01	0.1104	0.8893
Fasting glucose (mmol)		4.44	0.0456	4.52	0.0464	0.2288
2 hr glucose (mmol)		5.57	0.1359	5.40	0.1119	0.3850
BMI (kg/m^2)		24.44	0.4203	35.63	0.5291	<0.0001
Pregnancy outcomes						
Live birth (%)		100.00	n/a	98.50	n/a	0.4002
Fetal sex (% male)		54.35	n/a	48.48	n/a	0.5415
Fetal weight (kg)		3.52	0.0081	3.31	0.0081	0.0492
Gestation at delivery (weeks)		39.42	0.2775	38.91	0.2312	0.1031
Mode of delivery (% vaginal)		65.96	n/a	64.18	n/a	0.8447
Complications (%)		17.39	n/a	30.30	n/a	0.1205

Table 6.1: Summary data for study participants. All women were GDM-negative on oral glucose tolerance test at time of blood sampling. Numerical data (e.g., age) were analysed using a Mann-Whitney test, and grouped data (e.g. fetal sex) were analysed using a Chi-Squared test, where a p value < 0.05 is considered significant. Complications are grouped and include preeclampsia, hypertension, obstetric cholestasis, and infection.

EDTA and serum Vacuettes were centrifuged at 1800 *x g* for 10 mins. The plasma or serum was then extracted and stored at -80°C.

***Disclaimer**:* Experiments where the samples were stimulated with CytoStim ™ were performed by a fellow PhD student Oliver Richards for a different analysis. He has kindly allowed the use of the supernatants for this analysis. The flow cytometry experiments and initial data analysis for the 8-colour panel and Th subsets were also performed by Oliver. He donated the raw data from his large cohort of healthy pregnant women for me to extract the obese vs not-obese data.

6.2.2 MNC isolation

MNCs were prepared via density centrifugation as in *2.2 Mononuclear cell Isolation*. Due to the limited availability of the blood, monocytes were not isolated.

6.2.3 Bioenergetics

OXPHOS and glycolytic capabilities of the MNCs were determined as in *2.6 Bioenergetic analysis* and, with the addition of a monensin injection as described in *5.2.6 Bioenergetic analysis*.

6.2.4 Cytokines

MNCs cultures were prepared as in *2.5 Cell culture* with LPS (10 ng/ml), MDP (1 µg/ml), LPS (10 ng/ml) and R848 (400 ng/ml), POLY I:C (25 µg/ml) or CytoStim ™ (diluted 1:200) (Miltenyi). Polysinosinic:polycytidylic acid (POLY I:C) is typically used to simulate viral infections due to it being a synthetic analogue of double-stranded RNA. POLY I:C interacts with TLR3 to initiate signalling. CytoStim ™ is a specialised TCR activator used to produce a T cell response. Cytokine analysis was done via multiplexing (*7.2.6 Multiplex cytokine analysis*) or high sensitivity quantikine ELISAs (*7.2.7 High sensitivity ELISAs*).

6.2.5 Flow cytometry

An 8-colour immunophenotyping kit (Miltenyi) was used on whole blood to investigate the frequency of key leukocyte populations as in *5.2.3 Flow cytometry*.

Monocytes and Th subsets were analysed in the MNC population via flow cytometry as in *2.4 Flow Cytometry.* Antibodies used for the monocytes are shown in Table 6.2. Mitochondrial content of monocytes was monitored using 2 nM MitoTracker Green (Life Technologies).

Antibody	Fluorochrome	Manufacturer	Clone	Isotype
anti-CD14	Alexa Fluor ® 647	BioLegend	53D3	IgG1
anti-CD16	VioBlue ®	Miltenyi	VEP13	IgMκ
anti-CD11b	PE	BioLegend	CBRM1/5	IgG1
anti-CD36	PE	BioLegend	5-271	IgG2a
anti-CD38	PE	BioLegend	HB-7	IgG1
anti-CD220	PE	Miltenyi	REA260	IgG1
anti-CD98	PE	Miltenyi	REA387	IgG1
anti-CD80	PE	Miltenyi	REA661	IgG1
anti-CD86	PE	Miltenyi	REA968	IgG1
anti-CD64	PE	Miltenyi	REA978	IgG1
anti-CD163	PE	Miltenyi	REA812	IgG1
anti-CD192 (CCR2)	PE	Miltenyi	REA264	IgG1
anti-CX_3CR1	PE	Miltenyi	REA385	IgG1

Table 6.2: Details of the antibodies used to phenotype monocytes in MNCs.

The relative abundance of different Th subsets was determined based on their chemokine expression profile, as set out by Miltenyi Biotec [435]. Th cells are functionally heterogeneous, and the subsets have distinct features which define them (Table 6.3). The $CD4^+$ subsets can be identified based on their chemokine receptor expression, the cytokines they produce, and their transcription factors [436, 437]. The expression of chemokine receptors on these T cells determine the signals they receive and their trafficking patterns [438-440], as the different effector functions of the subsets implies that they will be differentially recruited to sites of inflammation. For the most comprehensive segregation of Th subsets, the best method has been suggested to utilise a Golgi system inhibitor, to prevent cytokine release, and intracellular staining for cytokines for identification as in Table 6.3, e.g., IL-22 for Th22 identification [441]. However, due to the limited availability of samples, this was not possible. Studies have confirmed the validity of using chemokine receptor profile for Th subset identification; using a gating strategy based on their chemokine profile, the T cell subsets were sorted, and their cytokine secretion profile was analysed, along with their transcription factor mRNA expression [442]. As such, this method of identification was deemed appropriate for this study. The antibodies used can be seen in Table 6.4 and the gating strategy used in Figure 6.4.

Th subset	Chemokine receptors	Cytokines induced by	Cytokines secreted	Transcription factors
Th1	CXCR3+	IL-12	IFN-γ	T-bet
Th2	CCR4+	IL-4, IL-25	IL-4, IL-5, IL-13	STAT6, GATA3
Th9	CCR6+	TGFβ, IL-4	IL-9	IRF-4
Th17	CCR4+CCR6+	TGFβ, IL-6	IL-17A, IL-17F	RORγt
Th22	CCR4+CCR6+CCR10+	IL-6, TNFα	IL-22	BNC2, FOXO4

Table 6.3: Th subset characteristics. The Th subsets' heterogeneity is reflected in distinct features. These include: chemokine receptors, cytokines which induce their production, and cytokines they secrete, and transcription factors.

Antibody	Fluorochrome	Manufacturer	Clone	Isotype
anti-CD3	VioBlue ®	Miltenyi	REA613	IgG1
anti-CD4	VioGreen ™	Miltenyi	REA623	IgG1
anti-CD194 (CCR4)	APC	Miltenyi	REA279	IgG1
anti-CD196 (CCR6)	PE-Vio ® 615	Miltenyi	REA190	IgG1
anti-CD184 (CXCR3)	VioBright ™ FITC	Miltenyi	REA232	IgG1
anti-CCR10	PE	Miltenyi	REA326	IgG1

Table 6.4: The antibodies and their information used to distinguish the Th subsets.

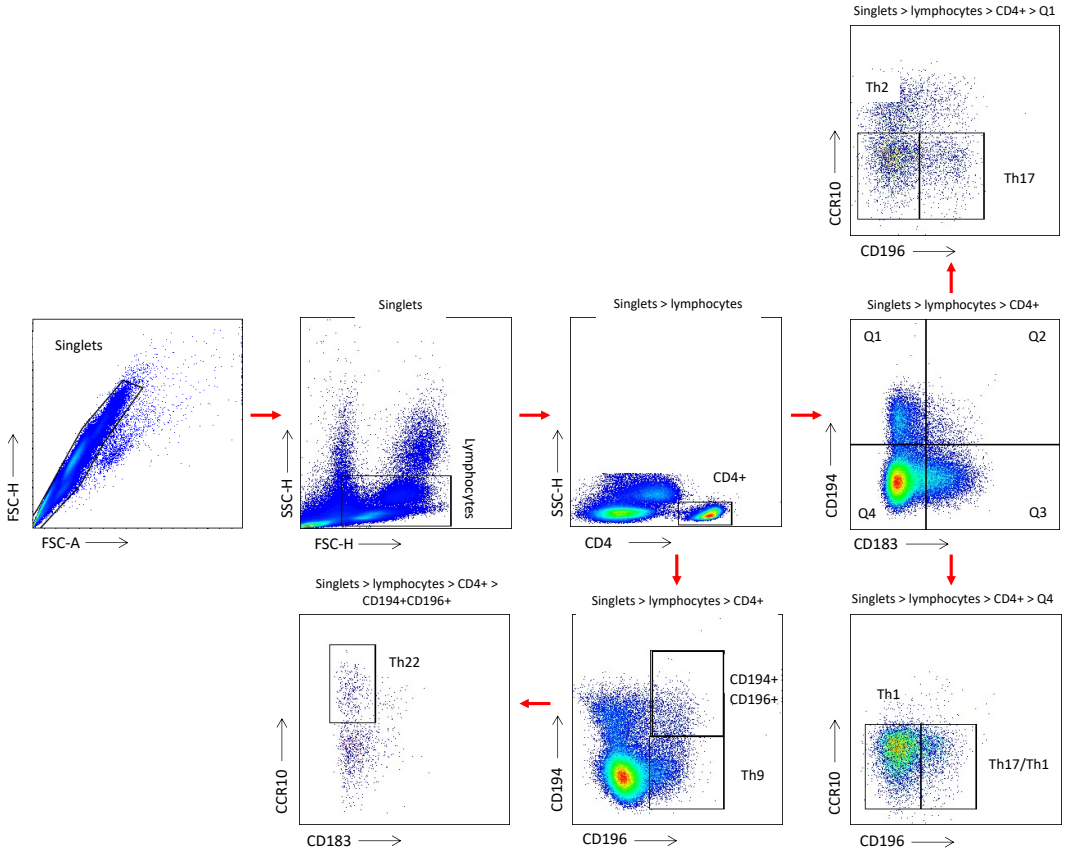

Figure 6.4: Gating strategy for identifying the Th subsets using flow cytometry and chemokine receptor profile. Singlets are first selected using a FSC-H vs FSC-A plot. The relative location of the lymphocytes are determined based on their size and granularity (SSC-H vs FSC-H). CD4+ T cells are then selected before distinguishing between the subsets based on their chemokine profile. CCR4-CXCR3-CCR10-CCR6- Th1; CCR4+CXCR3-CCR10-CCR6- Th2; CCR4-CCR6+ Th9; CCR4+CXCR3-CCR10-CCR6+ Th17; CCR4-CXCR3-CCR10-CCR6+ Th17/1; CCR4+CCR6+CCR10+ Th22.

6.2.6 Multiplex cytokine analysis

A multiplex flow cytometry approach to cytokine analysis was performed with LEGENDplex ™ (BioLegend) kits as described in *5.2.5 Multiplex cytokine analysis.*

EDTA-plasma was analysed using the LEGENDplex ™ Human Diabesity panel (4-plex; BioLegend). The analysis was performed as per the manufacturer's guidelines with the plasma samples diluted 1:8 with assay buffer and the analysis was performed as per the manufacturer's guidelines. The standard cocktail was reconstituted with 250 µl assay buffer which gave the top standard (standard concentrations for each cytokine in the panel can be observed in Table 6.5), which was serially diluted 1:4 with assay buffer. 25 µl of Matrix B was added to the wells which would contain the standards, to account for the plasma in the sample wells, and 25 µl of assay buffer was added to all sample wells. 25 µl of standard or sample was loaded on top. 100X Human Diabesity Cortisol Tracer was diluted 1:100 with assay buffer, and 25 µl of this was added to each well. A vial of the mixed capture beads was vortexed for 30 sec, and 25 µl of this was added to the plate. The rest of the protocol was performed as in *5.2.5 Multiplex cytokine analysis*.

Diabesity		Inflammation		T-helper	
PAI-1	400 ng/ml	IL-1β	11 ng/ml	IL-5	11 ng/ml
Insulin	100 ng/ml	IFN-α2	13 ng/ml	IL-13	12 ng/ml
Leptin	50 ng/ml	IFN-γ	9 ng/ml	IL-2	10 ng/ml
Cortisol	5 µg/ml	TNFα	11.5 ng/ml	IL-6	18 ng/ml
		MCP-1	10 ng/ml	IL-9	13 ng/ml
		IL-6	10 ng/ml	IL-10	11 ng/ml
		IL-8	11 ng/ml	IFN-γ	14 ng/ml
		IL-10	11 ng/ml	TNFα	16 ng/ml
		IL-12p70	14 ng/ml	IL-17A	5 ng/ml
		IL-17A	3.3 ng/ml	IL-17F	14 ng/ml
		IL-18	17 ng/ml	IL-4	13 ng/ml
		IL-23	15 ng/ml	IL-22	11 ng/ml
		IL-33	100 ng/ml		

Table 6.5: The top standards which were subsequently serially diluted four-fold for the different LEGENDplex ™ assays.

MNCs stimulated with LPS, MDP, LPS/R848 and POLY I:C were analysed using the LEGENDplex ™ Human Inflammation panel 1 (13-plex; BioLegend), and those stimulated with CytoStim ™ were analysed using the LEGENDplex ™ Human T-helper cytokine panel 2 (12-plex; BioLegend). Unstimulated supernatants were analysed on both panels. LPS stimulated

samples were diluted 1:3, and the other samples were run neat. These panels were run the same as the Diabesity panel with a few exceptions. Assay buffer was used instead of Matrix B for the standard wells, and no cortisol tracer was required.

6.2.7 High sensitivity ELISAs

High sensitivity Quantikine™ ELISAs for IL-6, IL-8, MCP-1 and TNFα (R&D systems) were performed according to the manufacturer's instructions. Each kit had slightly different protocols. EDTA-plasma samples were run neat for all except for MCP-1 where they were diluted 2-fold. While incubation times varied with some of the steps, they followed the same procedure. Equal volumes of assay diluent and standard or sample was added to each well on a provided pre-coated plate and incubated at room temperature on a shaker. The wells were aspirated and washed before specific conjugates were added to each well. Incubation and wash steps were repeated before the addition of streptavidin polymer-HRP (IL-6, TNFα), or substrate solution was added (MCP-1, IL-8). IL-8 required an amplifier solution at this stage with an incubation period. Substrate solution was added to IL-6 and TNFα. Stop solution was added to all ELISAs after a dedicated period, and the plates were read with a microplate reader.

6.2.8 Duoset ELISA

ELISAs for CD26, CD147 and NRP-1 were performed as in *2.7 Enzyme linked immunosorbent assay (ELISA).*

6.2.9 Data analysis

The data sets were first tested for normality using the Kolmogorov-Smirnov (K-S) one sample test, where a significant p value <0.05 indicated significant deviation from normality. Depending on if the data reported as parametric or non-parametric, a Pearson or Spearman correlation test was used respectively. The r values are reported to indicate direction (negative values a downward trend; positive values upward trend) and weight of correlation, and a p value <0.05 determined the r value to be significant.

6.3 Results

6.3.1 Leptin, IL-6 and MCP-1 levels are directly correlated to increasing BMI at 28 weeks of pregnancy

To evaluate systemic inflammation at 28 weeks of pregnancy in this population of fasted, GDM-negative women of varying pre-pregnancy BMI (n=80) key inflammatory mediators present in plasma were measured. Plasma rather than serum was chosen for analysis as this reflects the liquid phase of blood as it circulates in the body rather than after clotting has occurred. Leptin ($p < 0.0001$) and IL-6 ($p < 0.0001$) had a significant positive correlation with BMI (Figure 6.5), as described previously [93], and here is the first illustration of MCP-1 ($p = 0.0064$) increasing with BMI in pregnant women (Figure 6.5) in keeping with the same relationship in not pregnant adults [443, 444]. PAI-1, insulin, cortisol, TNFα and IL-8 did not vary with BMI (Figure 6.5).

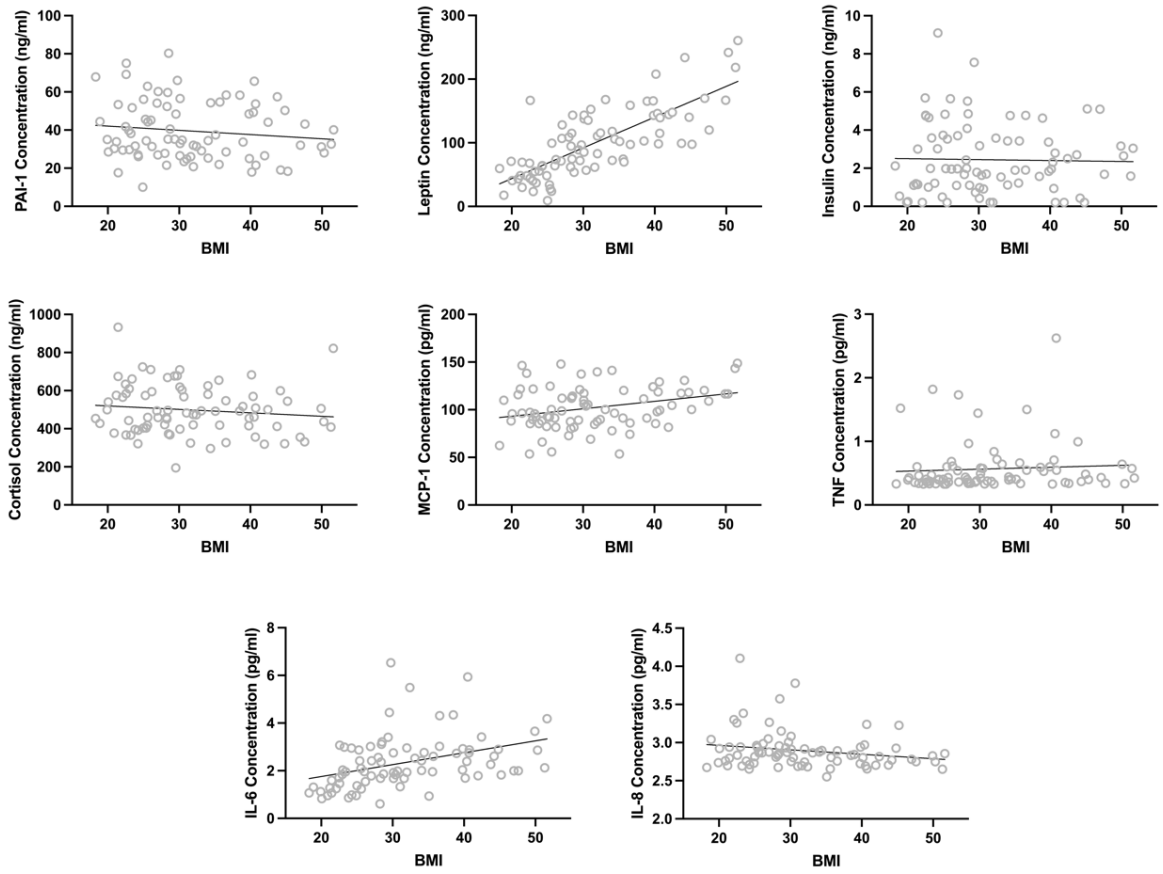

Figure 6.5: Plasma levels of inflammatory mediators in GDM-negative women of varying pre-pregnant BMI at 28 weeks of gestation. Plasma was available from fasted pregnant women of approximately 28 weeks of gestation (n=80) and was used for analysis as described in the Materials and Methods and correlated to BMI. Statistics were determined using either a Pearson r or Spearman r test dependent on their K-S test result, where $p < 0.05$ was determined significant. Analytes measured were: PAI-1 ($r = -0.1242$; $p = 0.2722$), leptin ($r = 0.7635$; $p < 0.0001$), insulin ($r = 0.0017$; $p = 0.9882$), cortisol ($r = -0.1196$; $p = 0.2937$), MCP-1 ($r = 0.3024$; $p = 0.0064$), TNF ($r = 0.1931$; $p = 0.0861$), IL-6 ($r = 0.4895$; $p < 0.0001$) and IL-8 ($r = -0.1923$; $p = 0.0875$).

In addition to these classically analysed molecules, soluble forms of CD26, CD147 and NRP-1 was also measured against BMI in pregnancy. These molecules have been highly implicated in SARS-CoV-2 cell entry and infectivity [445]. Results show that CD26 and CD147 concentrations were unaffected by BMI (Figure 6.6), but NRP-1 levels positively correlated significantly to BMI (Figure 6.6)

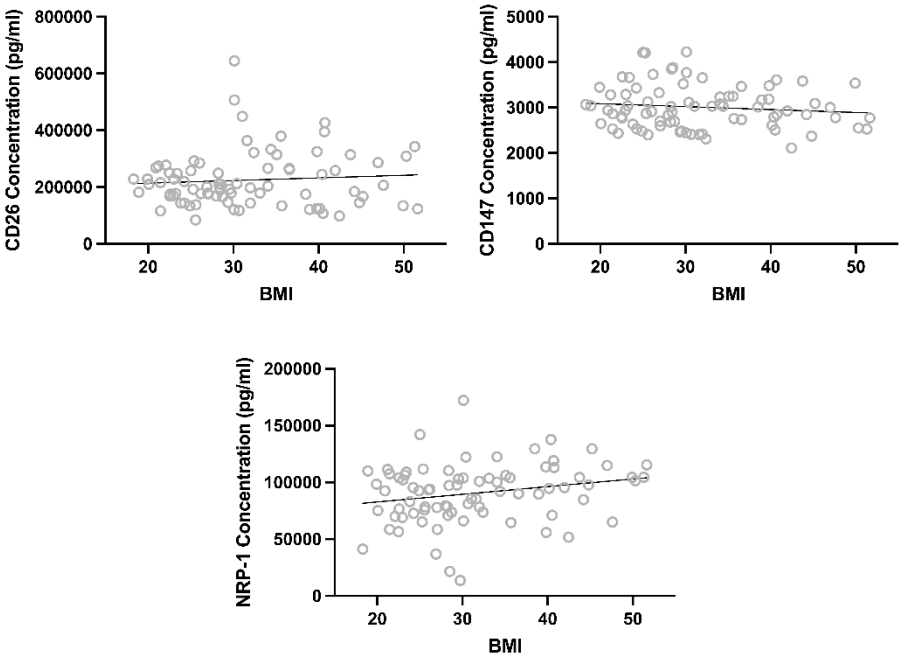

Figure 6.6: Levels of molecules associated with facilitating SARS-CoV-2 entry and infectivity and their relationship to maternal BMI. Plasma was available from fasted pregnant women of approximately 28 weeks of gestation (n=80) and was used for analysis as described in the Materials and Methods and correlated to BMI. Statistics were determined using either a Pearson r or Spearman r test dependent on their K-S test result, where $p < 0.05$ was determined significant. Soluble forms receptors which were measured were: CD26 ($r = 0.05273$; $p = 0.6422$), CD147 ($r = -0.1173$; $p = 0.3003$) and NRP-1 ($r = 0.2247$; $p = 0.0451$).

6.3.2 Circulating leukocyte numbers are altered with increasing maternal BMI

Whilst obesity in general is associated with increased levels of neutrophils [446], B cells [447] and non-classical monocytes [68] but decreased levels of eosinophils [448], NK cells [420], and NKT cells [449], little is known about the effects on circulating leukocyte numbers in obese pregnant women. Using flow cytometry, several changes in key blood immune cell populations was observed. Increasing BMI was associated with a decrease in the intermediate subset ($p = 0.0372$) of monocytes (Figure 6.7). BMI did not have any effect on the total T cell number, however, increasing BMI was correlated with an increasing CD4:CD8 ratio ($p = 0.0140$) directly attributable to a significant increase in CD4+ ($p = 0.0137$) T cells accompanied by a significant decrease in CD8+ ($p = 0.0299$) T cells (Figure 6.7). This decline in CD8+ T cells is in keeping with studies in both pregnant women [131] and the general population [422] with obesity. From

animal studies it has been suggested that this decline in CD8+ T cells in the peripheral blood is attributable to infiltration of CD8+ T cells into adipose tissue that precedes macrophage accumulation [422]. Whilst other studies also have shown a reduction in the proportion of $CD3^+/CD8^+$ T cells in pregnancies with obesity [131], the question as to whether they have accumulated in the adipose tissue remains unanswered. NKT cells ($p = 0.0123$) also showed a decrease with increasing BMI (Figure 6.7) which is also in keeping with observations in the general population [449] and in pregnancy [131]. While neutrophils tended to increase with BMI and eosinophils tended to decrease with BMI this was not significant; other populations did not show any differences with maternal BMI.

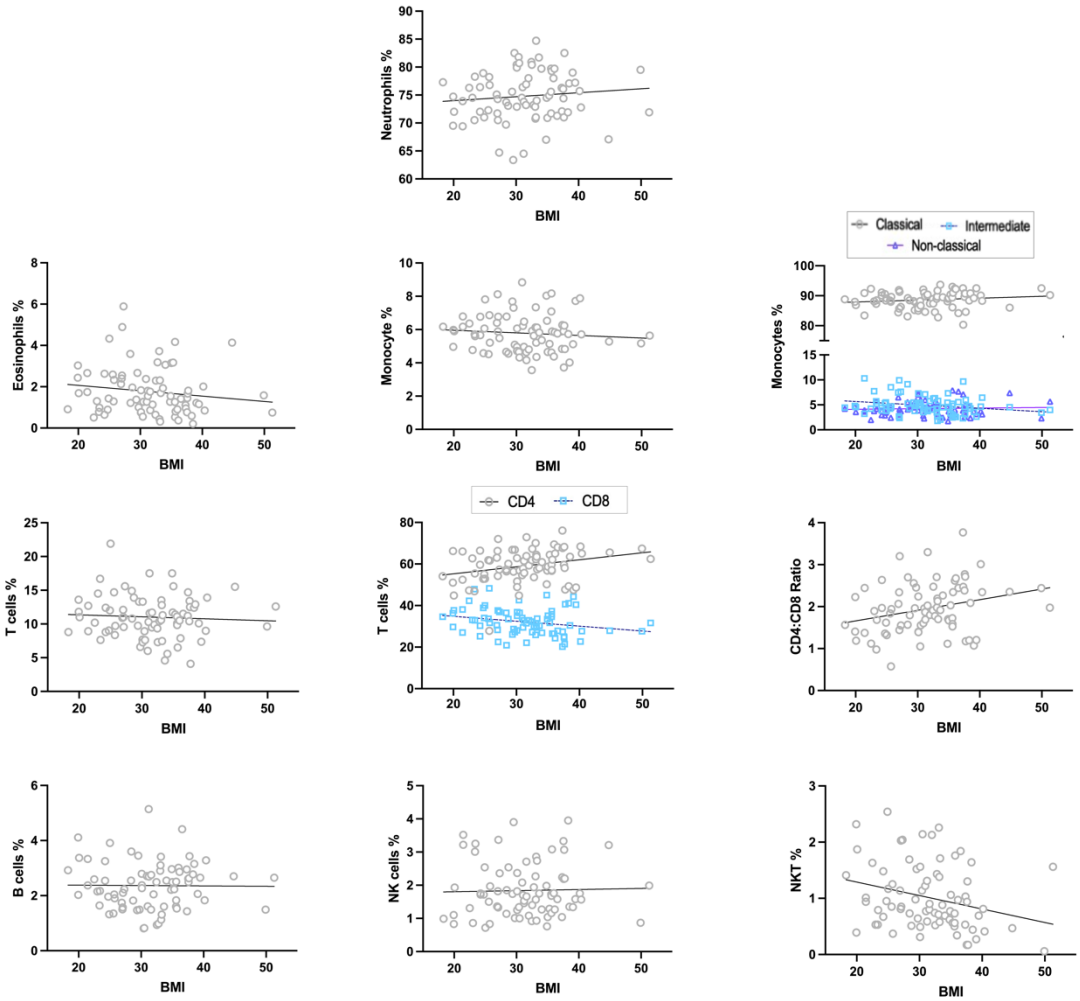

Figure 6.7: The impact of BMI on leukocyte populations in pregnancy. Whole blood (n=77) from fasted pregnant women of approximately 28 weeks of gestation was used for leukocyte phenotyping as described in the materials and methods. They were correlated to BMI. Statistics were determined using either a Pearson r or Spearman r test dependent on their K-S test result, where $p < 0.05$ was determined significant. Leukocyte populations which were determined where: neutrophils ($r = 0.1053$; $p = 0.3654$), eosinophils ($r = -0.2034$; $p = 0.0760$), total monocytes ($r = -0.898$; $p = 0.4375$), classical monocytes ($r = 0.2138$; $p = 0.0637$), intermediate monocytes ($r = -0.2394$; $p = 0.0372$), non-classical monocytes ($r = -0.0354$; $p = 0.7614$), total T cells ($r = -0.0606$; $p = 0.6004$), CD4 T cells ($r = 0.2798$; $p = 0.0137$), CD8 T cells ($r = -0.2476$; $p = 0.0299$), CD4:CD8 ratio ($r = 0.2789$; $p = 0.0140$), B cells ($r = -0.0105$; $p = 0.9276$), NK cells ($r = 0.0628$; $p = 0.5877$) and NKT cells ($r = -0.2842$; $p = 0.0123$).

6.3.3 The inflammatory cytokine profile of MNCs in maternal obesity is mostly unchanged

Having confirmed systemic inflammation occurs with increasing BMI in pregnant women (Figure 6.5) and that there are differences in the relative abundance of some peripheral blood leukocytes with changing BMI in pregnancy (Figure 6.6), the next consideration was whether the inflammatory response of blood mononuclear cells (MNCs) might differ with BMI. MNCs were isolated and left unstimulated or challenged with MDP (NOD2), LPS (TLR4), LPS and R848 (TLR7/8) or POLY I:C (TLR3) as a prototypic inflammatory stimulus with thirteen cytokines (IL-1β, IFNα2, IFNγ, TNFα, MCP-1, IL-6, IL-8, IL-10, IL-12p70, IL-17A, IL-18, IL-23 and IL-33) measured using a multiplex approach. IL-17A was not detectable in any sample but all other cytokines were, and data are shown in Figures 7.5 – 7.9.

Obesity appears to have little effect on inflammatory cytokine output of MNCs whether unstimulated (Figure 6.8), MDP-stimulated (Figure 6.10), LPS-stimulated (Figure 6.9), LPS/R848-stimulated (Figure 6.11) or POLY I:C-stimulated (Figure 6.12). The majority of alterations in cytokine levels in pregnant women with obesity were not statistically significant. The only exceptions were on stimulation with LPS/R848 (Figure 6.11), where a positive correlation is observed with IL-1β (p = 0.0489) and IL-10 (p = 0.0408), and with POLY I:C (Figure 6.12) where IL-18 (p = 0.0027) increases significantly with BMI.

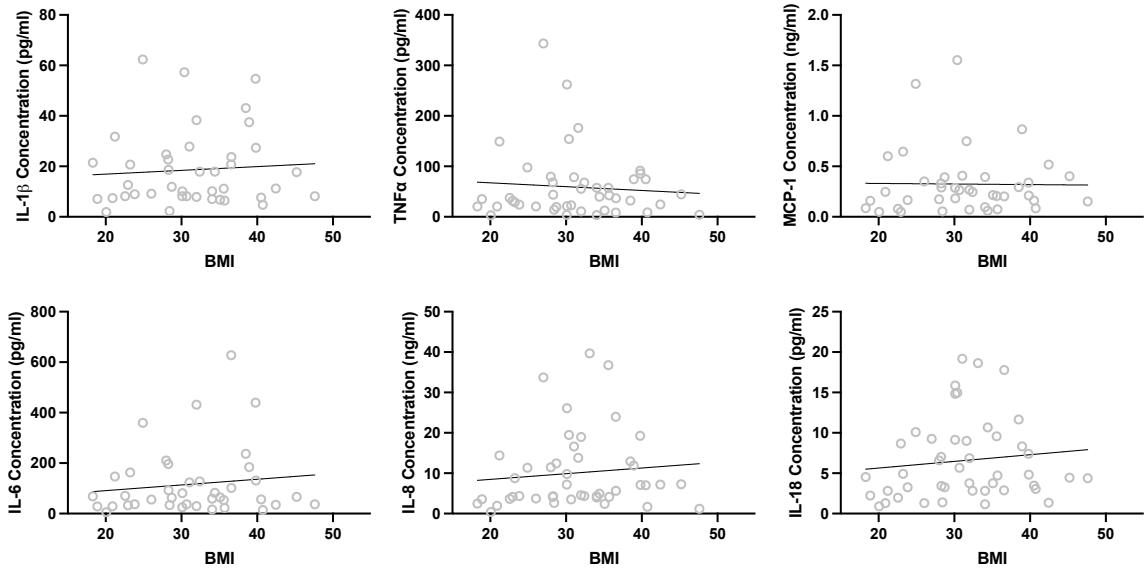

Figure 6.8: Unstimulated cytokine production by peripheral blood mononuclear cells from GDM-negative women of varying pre-pregnant BMI at 28 weeks of gestation. MNCs (n=45) were left unstimulated for 24 hr and then levels of cytokines (ng/ml or pg/ml) measured using a multiplex bead array for flow cytometry. Statistics were determined using either a Pearson r or Spearman r test dependent on their K-S test result, where $p < 0.05$ was determined significant. Cytokines which were detectable were: IL-1β ($r = 0.0630$; $p = 0.6956$), TNFα ($r = 0.0315$; $p = 0.8391$), MCP-1 ($r = 0.0872$; $p = 0.5877$), IL-6 ($r = 0.1009$; $p = 0.5358$), IL-8 ($r = 0.1917$; $p = 0.2071$) and IL-18 ($r = 0.1751$; $p = 0.2500$).

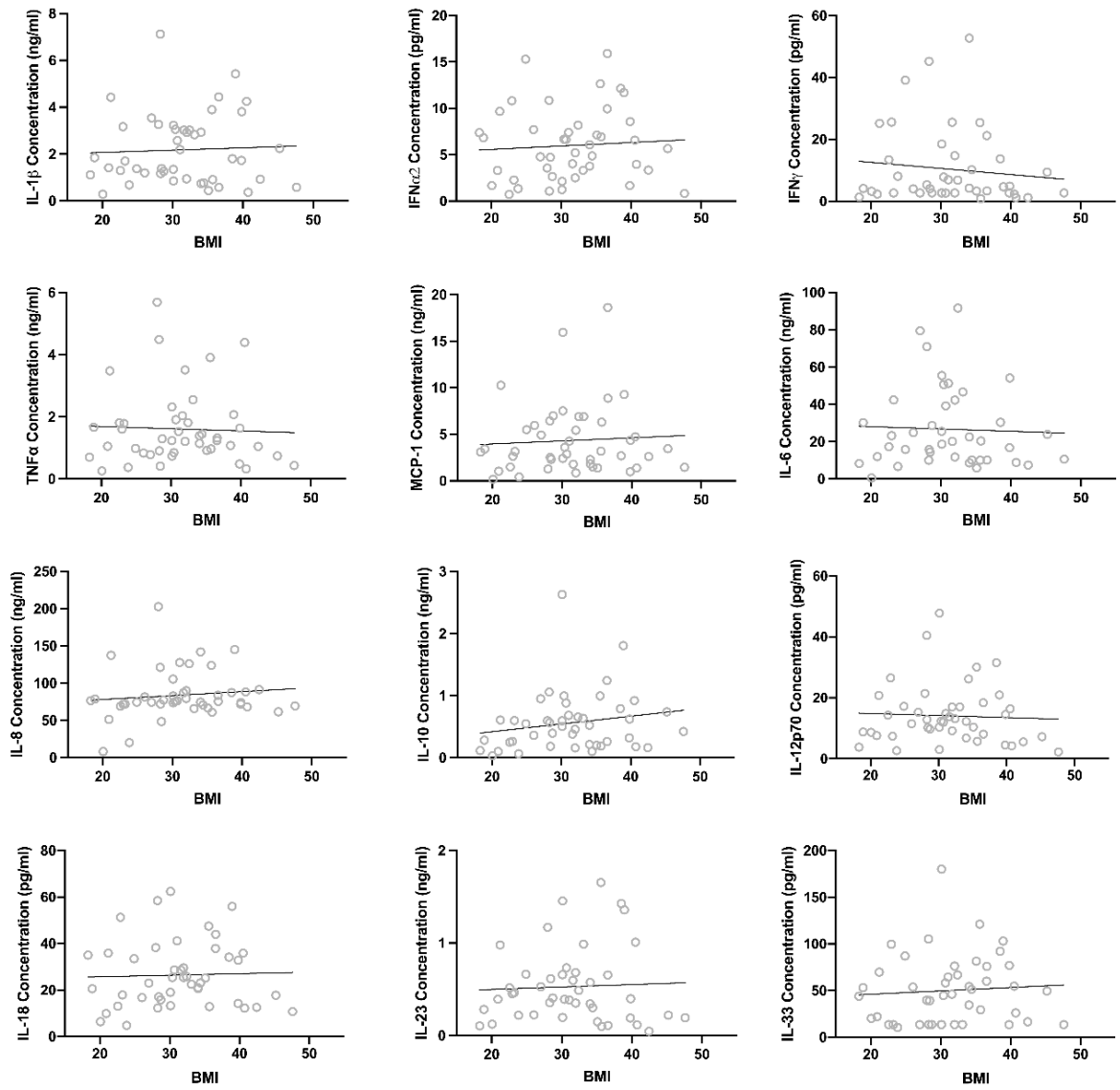

Figure 6.9: LPS-stimulated cytokine production by peripheral blood mononuclear cells from GDM-negative women of varying pre-pregnant BMI at 28 weeks of gestation. MNCs (n=45) were stimulated with LPS and then levels of cytokines (ng/ml or pg/ml) measured using a multiplex bead array for flow cytometry. Statistics were determined using either a Pearson r or Spearman r test dependent on their K-S test result, where $p < 0.05$ was determined significant. Cytokines measured were: IL-1β ($r = -0.0040$; $p = 0.9791$), IFNα2 ($r = 0.0687$; $p = 0.6579$), IFNγ ($r = -0.1182$; $p = 0.4503$), TNF ($r = -0.0144$; $p = 0.9254$), MCP-1 ($r = 0.0651$; $p = 0.6710$), IL-6 ($r = -0.0602$; $p = 0.7085$), IL-8 ($r = 0.0083$; $p = 0.5642$), IL-10 ($r = 0.2085$; $p = 0.1694$), IL-12p70 ($r = -0.0596$; $p = 0.6972$), IL-18 ($r = 0.0331$; $p = 0.8290$), IL-23 ($r = -0.0791$; $p = 0.6099$) and IL-33 ($r = 0.1555$; $p = 0.3078$).

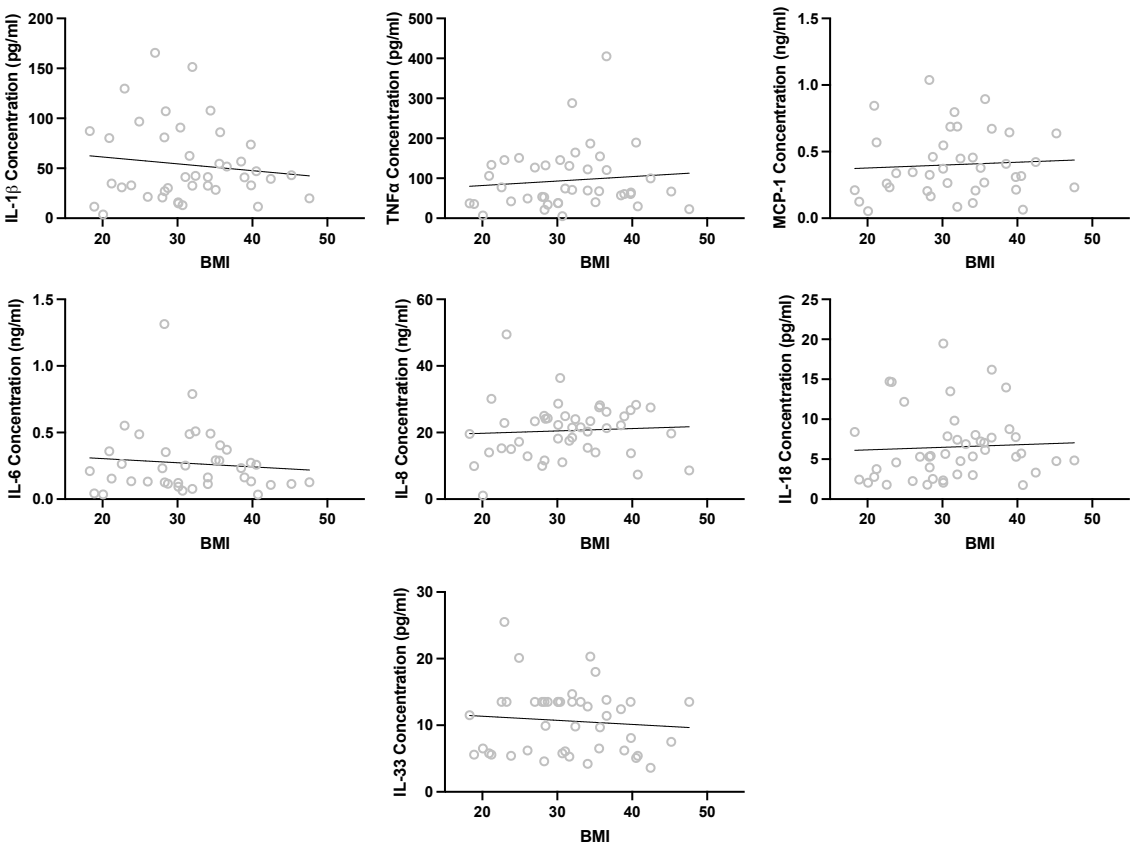

Figure 6.10: MDP-stimulated cytokine production by peripheral blood mononuclear cells from GDM-negative women of varying pre-pregnant BMI at 28 weeks of gestation. MNCs (n=45) were stimulated with MDP and then levels of cytokines (ng/ml or pg/ml) measured using a multiplex bead array for flow cytometry. Statistics were determined using either a Pearson r or Spearman r test dependent on their K-S test result, where $p < 0.05$ was determined significant. Cytokines which were detectable were: IL-1β ($r = 0.01472$; $p = 0.9272$), TNFα ($r = 0.1327$; $p = 0.4020$), MCP-1 ($r = 0.0652$; $p = 0.6973$), IL-6 ($r = -0.0404$; $p = 0.8071$), IL-8 ($r = 0.0606$; $p = 0.6924$), IL-18 ($r = 0.1947$; $p = 0.1999$) and IL-33 ($r = -0.0727$; $p = 0.6391$).

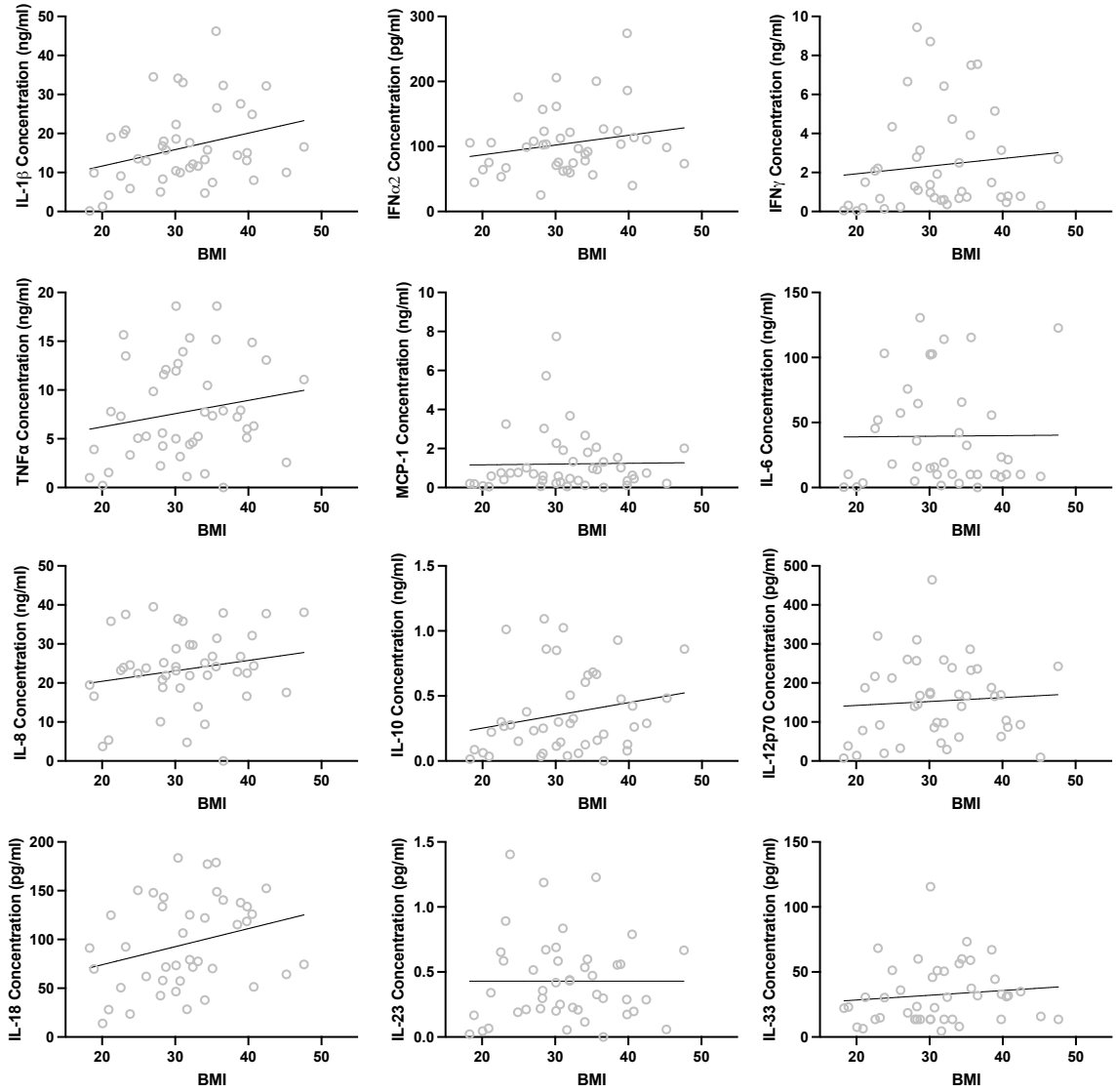

Figure 6.11: LPS/R848-stimulated cytokine production by peripheral blood mononuclear cells from GDM-negative women of varying pre-pregnant BMI at 28 weeks of gestation. MNCs (n=45) were stimulated with LPS/R848 and then levels of cytokines (ng/ml or pg/ml) measured using a multiplex bead array for flow cytometry. Statistics were determined using either a Pearson r or Spearman r test dependent on their K-S test result, where $p < 0.05$ was determined significant. Cytokines measurable were: IL-1β ($r = 0.3022$; $p = 0.0489$), IFNα2 ($r = 0.1894$; $p = 0.2356$), IFNγ ($r = 0.2104$; $p = 0.1757$), TNF ($r = 0.2661$; $p = 0.0809$), MCP-1 ($r = 0.1818$; $p = 0.2377$), IL-6 ($r = -0.0042$; $p = 0.9793$), IL-8 ($r = 0.2570$; $p = 0.0922$), IL-10 ($r = 0.3133$; $p = 0.0408$), IL-12p70 ($r = 0.0719$; $p = 0.6428$), IL-18 ($r = 0.2855$; $p = 0.0668$), IL-23 ($r = 0.0240$; $p = 0.8775$) and IL-33 ($r = 0.2227$; $p = 0.1463$).

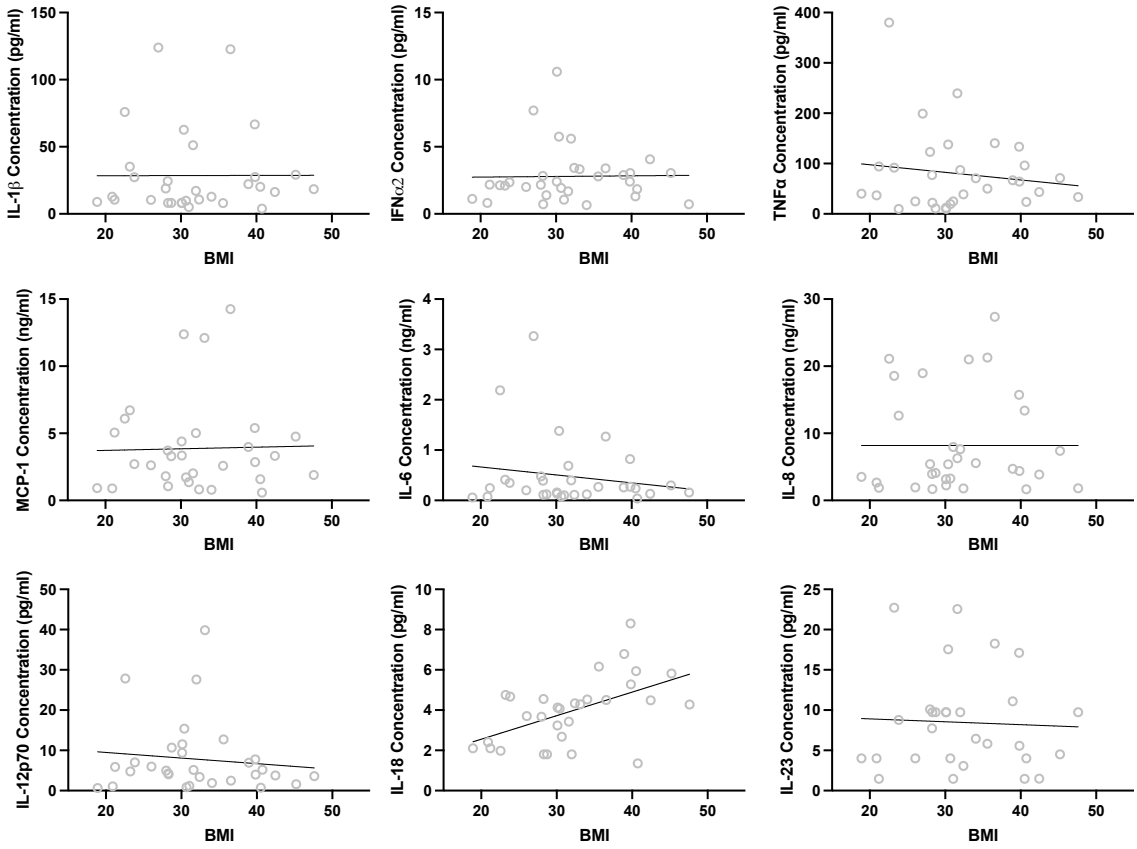

Figure 6.12: POLY I:C-stimulated cytokine production by peripheral blood mononuclear cells from GDM-negative women of varying pre-pregnant BMI at 28 weeks of gestation. MNCs (n=32) were stimulated with POLY I:C and then levels of cytokines (ng/ml or pg/ml) measured using a multiplex bead array for flow cytometry. Statistics were determined using either a Pearson r or Spearman r test dependent on their K-S test result, where $p < 0.05$ was determined significant. Cytokines measurable were: IL-1β ($r = 0.0388$; $p = 0.8350$), IFNα2 ($r = 0.1668$; $p = 0.3615$), TNF ($r = 0.0266$; $p = 0.8870$), MCP-1 ($r = -0.0186$; $p = 0.9211$), IL-6 ($r = -0.0436$; $p = 0.8161$), IL-8 ($r = 0.0708$; $p = 0.7004$), IL-12p70 ($r = -0.1274$; $p = 0.4946$), IL-18 ($r = 0.5278$; $p = 0.0027$), IL-23 ($r = -0.0387$; $p = 0.8420$).

6.3.4 Monocytes have an adapted phenotype in response to obesity at 28 weeks of gestation

Given the decline in intermediate monocytes with BMI and the well-recognised role of mononuclear phagocytes in obesity-associated inflammation [68, 79], flow cytometry was used to further phenotype the classical ($CD14^{++}CD16^{-}$), intermediate ($CD14^{++}CD16^{+}$) and non-classical ($CD14^{+}CD16^{++}$) subsets of monocytes. The markers chosen for study were those commonly used for phenotyping monocytes linked to various effector functions (CD11b, CD64, CD80, CD86 and CD163; Figure 6.14A-E), chemokine receptors (CCR2 and CX3CR1; Figure 6.14F-G) and metabolism associated transporters and receptors (CD36, CD38, CD98 and CD220; Figure 6.14H-L) including mitochondria. Examples of the histograms of these markers for each subset can be visualised in Figure 6.13.

CD163 (haemoglobin scavenger receptor) expression was increased in intermediate ($p = 0.0241$) and non-classical ($p = 0.0163$) monocytes with increasing maternal BMI (Figure 6.14E). Several studies have shown a correlation between soluble CD163 and BMI which might act as an indicator for risk of insulin resistance [450]. Except for decreased expression of the co-stimulatory molecule CD86 (Figure 6.14D) on intermediate monocytes ($p = 0.0263$) the other markers in this group (CD11b activation marker, Figure 6.14A; CD64 Fcγ receptor 1, Figure 6.14B; CD80 costimulatory molecules, Figure 6.14C) were unchanged.

Both CCR2 and CX3CR1 are commonly studied in obesity [79] and are also differentially expressed on monocyte subsets, i.e., classical monocytes are $CCR2^{high}CX3CR1^{low}$, intermediates $CCR2^{high}CX3CR1^{high}$, and non-classical $CCR2^{low}CX3CR1^{high}$. While CX3CR1 did not differ on any of the monocyte subsets with maternal obesity (Figure 6.14G), CCR2 expression on all subsets of monocytes (C $p = 0.0083$, I $p = 0.0121$, NC $p = 0.0317$) was elevated with increasing BMI (Figure 6.14F). Combined with MCP-1 levels that also increased with BMI (Figure 6.5) this suggests that the CCL2/CCR2 axis that contributes to obesity related inflammation in the general population is likely also activated in pregnant women with obesity and warrants further investigation.

With growing interest in the role of immunometabolism in determining cell fate and function, the expression of key metabolic transporters CD36 (fatty acid translocator), CD98 (long-chain neutral amino acid transporter) and CD220 (insulin receptor) was considered; the mitochondrial content (MitoTracker Green™) was also quantified. No differences were found in the CD36 (Figure 6.14H), CD98 (Figure 6.14J) or insulin receptor (Figure 6.14K) with increasing BMI. However, all three subsets of monocytes had decreased mitochondrial content as BMI increased (C p = 0.0103, I p = 0.0467, NC p = 0.0438; Figure 6.14L). While deficient and dysfunctional mitochondria have been linked with obesity [451], this is the first to show this occurs in pregnancies with obesity and in leukocytes specifically. CD38 (cyclic ADP ribose hydrolase that metabolises NAD+) has been suggested to play a vital role in pregnancy and here it is shown on classical (p = 0.0478) and intermediate (p = 0.0269) monocytes at 28 weeks of gestation that CD38 expression was significantly decreased with increasing BMI (Figure 6.14I).

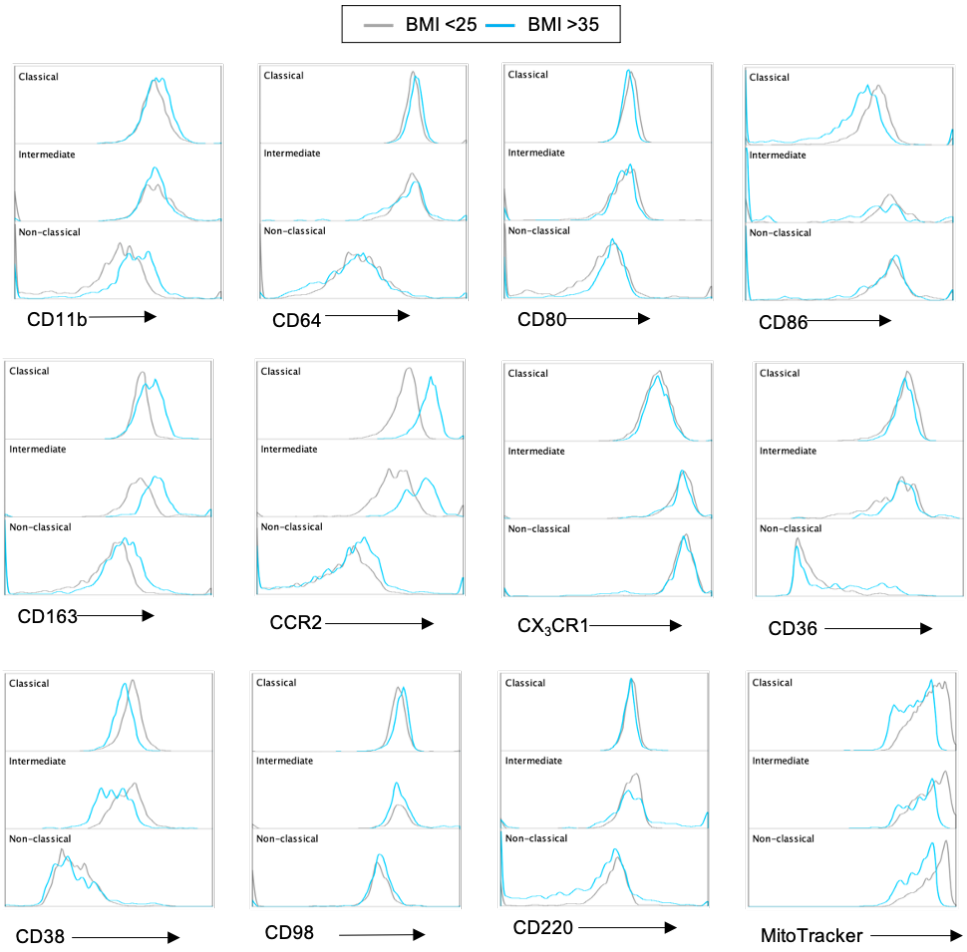

Figure 6.13: Histograms for the expression of the receptors measured. Each receptor has overlaid histograms for classical (top), intermediate (middle) and non-classical (bottom) monocytes for BMI less than 25 (grey) and over 35 (blue). Molecules measured were: CD11b, CD64, CD80, CD86, CD163, CCR2, CX_3CR1, CD36, CD38, CD98, CD220 and MitoTracker ™ Green.

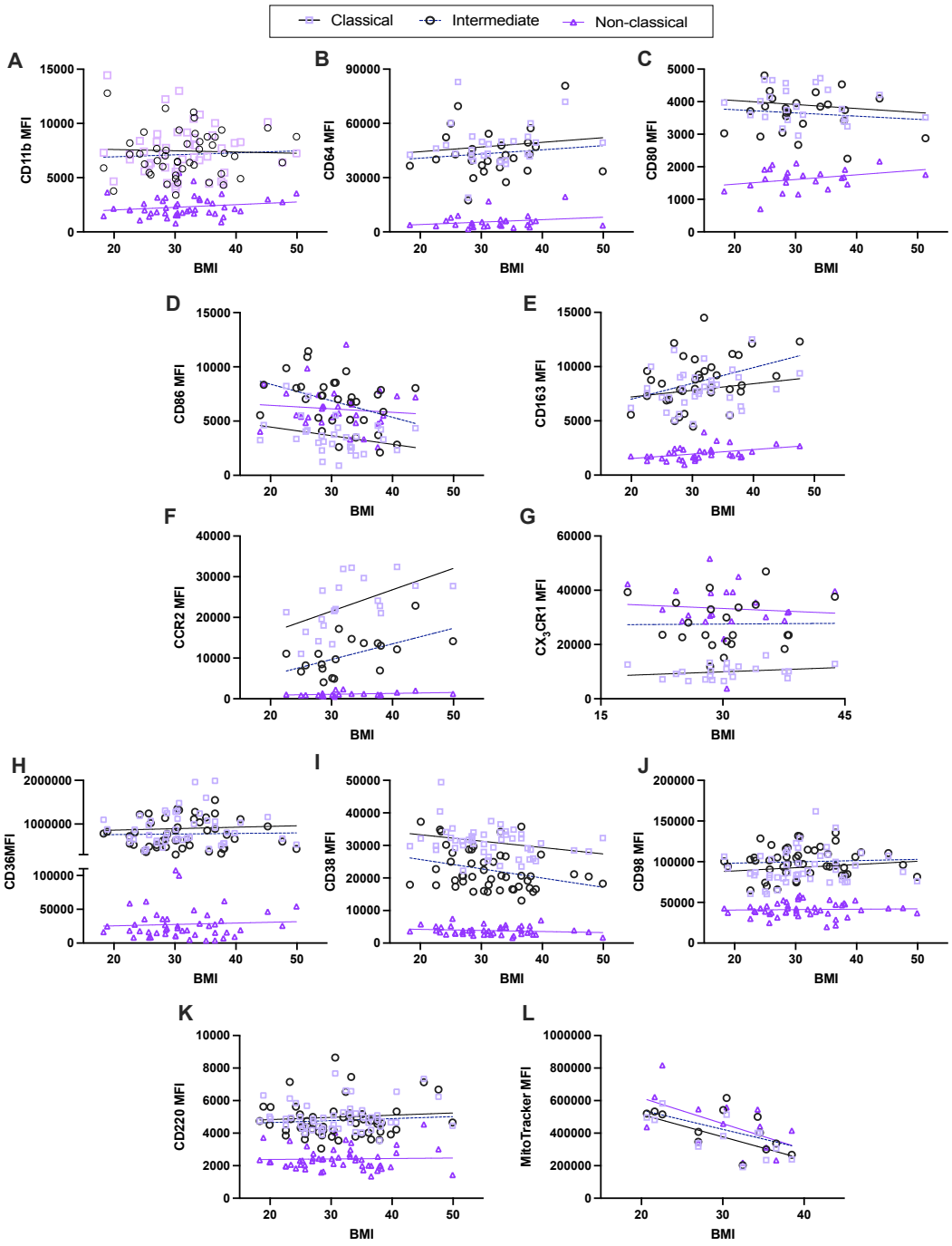

Figure 6.14: Phenotype of classical, intermediate, and non-classical peripheral blood monocytes of GDM-negative women of varying pre-pregnant BMI at 28 weeks of gestation. CD14 and CD16 expression were used to define classical (C; CD14++/CD16-), intermediate (I; CD14++, CD16+) and non-classical (NC; CD14+, CD16++) monocytes for further analysis of key surface antigens; MFI values are reported for correlation with BMI for each subset. Statistics were determined using either a Pearson r or Spearman r test dependent on their K-S test result, where $p < 0.05$ was determined significant. Molecules measured were: **(A)** CD11b (n=46; C r = -0.0339, p = 0.8228; I r = 0.0592, p = 0.6960; NC r = 0.1953, p = 0.1934), **(B)** CD64 (n=28; C r = 0.1248, p = 0.5269; I r = 0.1201, p = 0.5427; NC r = 0.1880, p = 0.5499), **(C)** CD80 (n=24; C r = -0.1713, p = 0.4235; I r = -0.1178, p = 0.5834; NC r = 0.3106, p = 0.1396), **(D)** CD86 (n=30; C r = -0.2969, p = 0.1110; I r = -0.3924, p = 0.0263; NC r = -0.1029, p = 0.5753), **(E)** CD163 (n=35; C r = 0.2085, p = 0.2293; I r = 0.3806, p = 0.0241; NC r = 0.4034, p = 0.0163). **(F)** CCR2 (n=19; C r = 0.5596, p = 0.0083; I r = 0.5627, p = 0.0121; NC r = 0.4696, p = 0.0317), **(G)** CX_3CR1 (n=22; C r = 0.2466, p = 0.2685; I r = -0.0515, p = 0.8199; NC r = -0.0587, p = 0.7951), **(H)** CD36 (n=47; C r = 0.0761, p = 0.6073; I r = 0.0274, p = 0.8533; NC r = 0.0372, p = 0.8040), **(I)** CD38 (n=47; C r = -0.2872, p = 0.0478; I r = -0.3195, p = 0.0269; NC r = -0.1711, p = 0.2501), **(J)** CD98 (n=47; C r = 0.1307, p = 0.3791; I r = 0.0612, p = 0.6828; NC r = 0.0382, p = 0.7966), **(K)** CD220 (n=53; C r = 0.0316, p = 0.8222; I r = -0.0105, p = 0.9407; NC r = -0.0233, p = 0.8682) and **(L)** MitoTracker™ Green (n=13; C r = -0.6818, p = 0.0103; I r = 0.5597, p = 0.0467; NC r = -0.5659, p = 0.0438).

6.3.5 Cellular metabolism is not altered by maternal BMI

Given decreased mitochondrial content was common to all monocyte subsets (Figure 6.14L) and adipocytes in obesity have shown downregulated OXPHOS proteins, lowered mitochondrial oxidative capabilities and reduced mitochondrial biogenesis [452] it is then logical to consider whether OXPHOS might be altered with increasing BMI. Summary data for oxidative phosphorylation as oxygen consumption rate (OCR) and glycolysis as extracellular acidification rate (ECAR) are shown as grouped BMIs (BMI $\leq$ 29.9 versus BMI $\geq$ 30; Figure 6.15A). OXPHOS and glycolysis parameters were calculated (ATP production, bioenergetic scope, bioenergetic capacity, glycolytic index, supply flexibility index, spare respiratory capacity) and compared by BMI (Figure 6.15B). There were no significant differences in any OXPHOS or glycolysis parameters with BMI at 28 weeks of gestation. MNCs in pregnancy at term have previously been found to have decreased basal glycolysis and glycolytic capacity in conjunction with increased bioenergetic health index [47]. Very little otherwise is known about specific immune cell bioenergetics in obesity or pregnancy.

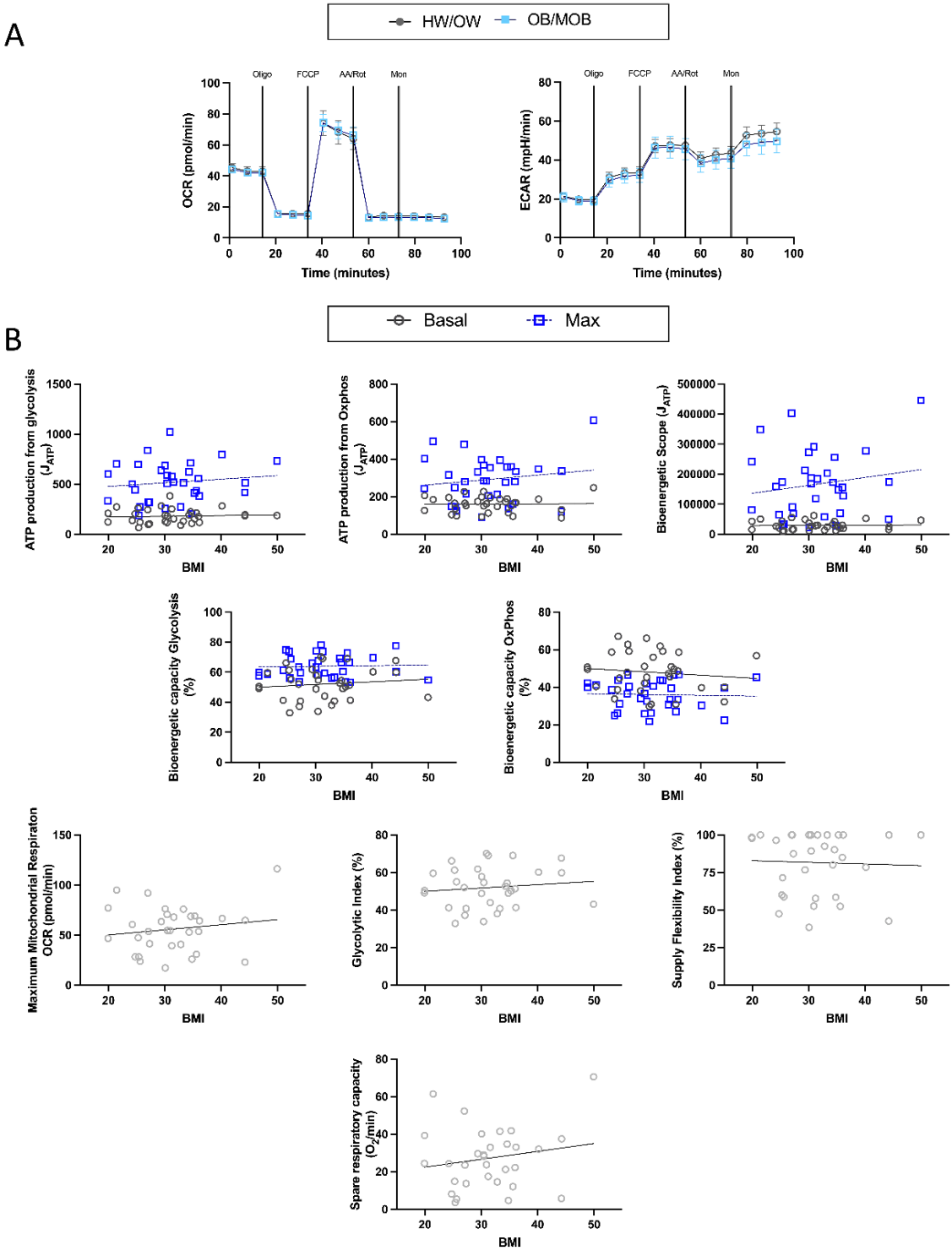

Figure 6.15: The bioenergetic capacity of mononuclear cells from GDM-negative women of varying pre-pregnant BMI at 28 weeks of gestation. OCR and ECAR of MNCs from pregnant women at approximately 28 weeks (n=32) were measured using the Seahorse extracellular flux analyser as described in the Materials and Methods and correlated to maternal obesity. (A) The trace of OCR and ECAR against time for grouped not-obese vs obese. (B) Specific glycolytic or oxidative phosphorylation parameters were extracted and correlated against BMI. Statistics were determined using either a Pearson r or Spearman r test dependent on their K-S test result, where $p < 0.05$ was determined significant. These parameters included: ATP production from glycolysis (basal r = 0.0650, p = 0.7239; max r = 0.1268, p = 0.4894) and OXPHOS (basal r = 0.0226, p = 0.9025; max r = 0.1549, p = 0.3972), bioenergetic scope (basal r = 0.0386, p = 0.8339; max r = 0.1668, p = 0.3617), bioenergetic capacity for glycolysis (basal r = 0.1155, p = 0.5289; max r = 0.0405, p = 0.8259) and OXPHOS (basal r = -0.1155, p = 0.5289; max r = -0.0405, p = 0.8259), maximum mitochondrial respiration (r = 0.1549; p = 0.3972), supply flexibility index (r = 0.0168; p = 0.9271), glycolytic index (r = 0.1156; p = 0.5288) and spare respiratory capacity (r = 0.1814; p = 0.3286).

6.3.6 Pregnant women with obesity show altered Th1/Th2/Th17

Given the dramatic effect of maternal obesity on T cell numbers (Figure 6.7) and the role of immune plasticity related to Th1/Th2/Th17 in pregnancy success [453] it is worth considering the effect of BMI on CD4+ T cell subsets. The relative abundance of different Th subsets was determined based on their chemokine expression profile – CXCR3, CX3CR1, CCR4, CCR6 and CCR10 - to identify Th1 (CXCR3-CCR4-CCR10-CCR6-), Th2 (CXCR3-CCR4+CCR10-CCR6-), Th9 (CCR4-CCR6+), Th17 (CXCR3-CCR4+CCR10-CCR6+), Th17/1 (CXCR3-CCR4-CCR10-CCR6+) and Th22 (CCR4+CCR6+CCR10+CXCR3-) subsets [454]. The percentage of Th2 cells as well as closely related Th9 cells decreased with increasing maternal BMI (Figure 6.16) but other subsets were unaffected.

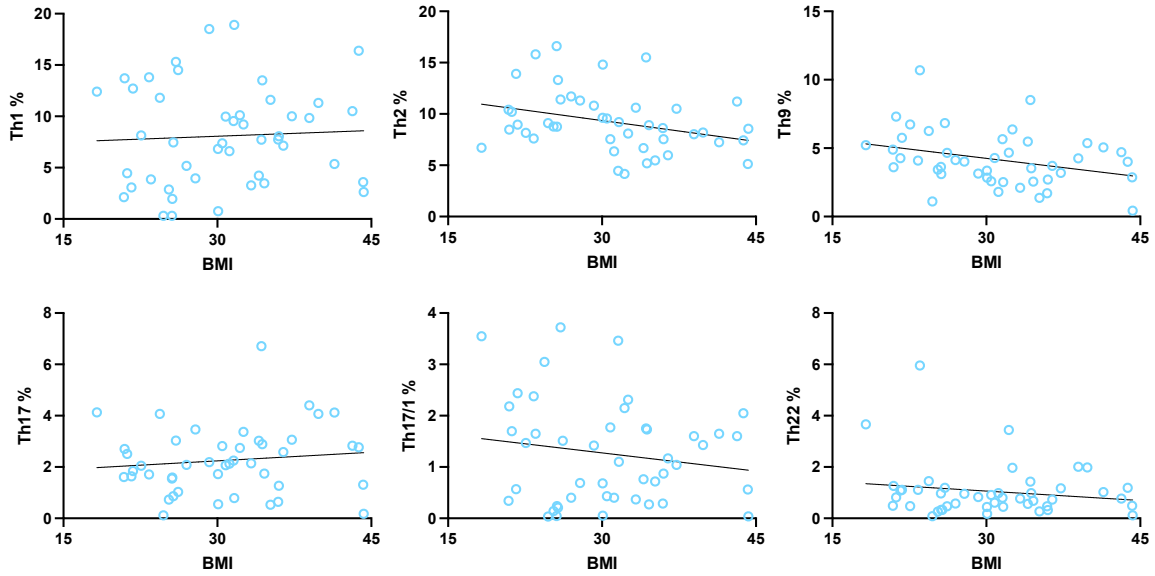

Figure 6.16: The Th profile of GDM-negative women of varying pre-pregnant BMI at 28 weeks of gestation. Th subsets were identified using flow cytometry and their chemokine receptor profile – CCR4-CXCR3-CCR10-CCR6- Th1; CCR4+CXCR3-CCR10-CCR6- Th2; CCR4-CCR6+ Th9; CCR4+CXCR3-CCR10-CCR6+ Th17; CCR4-CXCR3-CCR10-CCR6+ Th17/1; CCR4+CCR6+CCR10+ Th22. Statistics were determined using either a Pearson r or Spearman r test dependent on their K-S test result, where $p < 0.05$ was determined significant. The populations identified were (n=46): Th1 ($r = 0.0538$; $p = 0.7225$), Th2 ($r = -0.3202$; $p = 0.0341$), Th9 ($r = -0.3205$; $p = 0.0319$), Th17 ($r = 0.1202$; $p = 0.4315$), Th17/1 ($r = -0.1662$; $p = 0.2696$) and Th22 ($r = -0.0705$; $p = 0.6415$).

When the examination of the cytokine profile induced in response to the TCR activator CytoStim™ and measured using a multiplex approach, it was found that IL-4 production was also decreased with increasing BMI (Figure 6.17). This decrease in IL-4 was accompanied by increases in IL-6, IL-17A, IL-17F and IL-22 (Figure 6.17). Overall, this suggests a decrease in Th2 accompanied by an increase in Th17 that could underpin adverse obstetric outcomes in pregnant women with obesity.

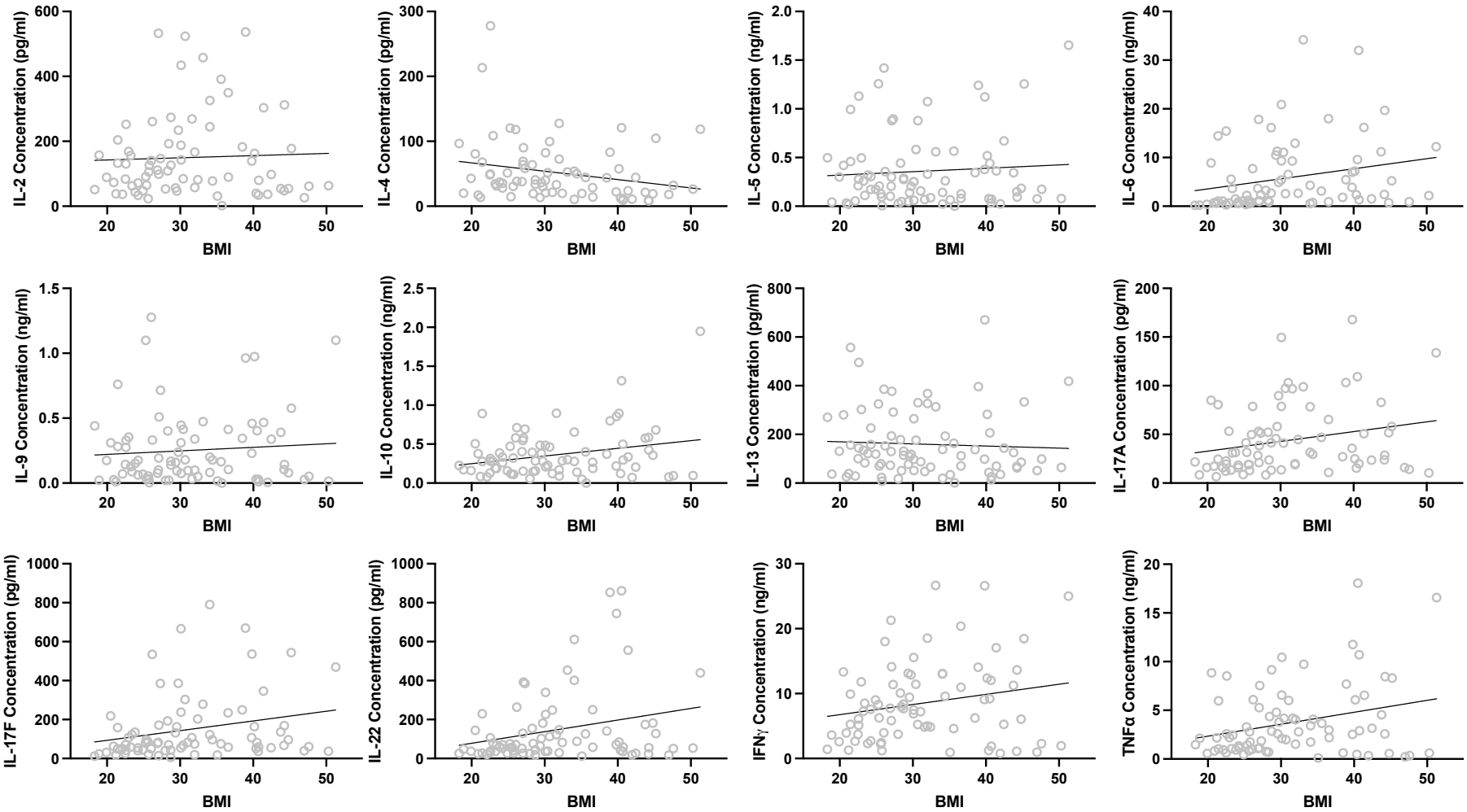

Figure 6.17: CytoStim™-stimulated Th cytokine production by peripheral blood mononuclear cells from GDM-negative women of varying pre-pregnant BMI at 28 weeks of gestation. MNCs (n=74) were stimulated with CytoStim™ and then levels of Th cytokines (ng/ml or pg/ml) measured using a multiplex bead array for flow cytometry. Statistics were determined using either a Pearson r or Spearman r test dependent on their K-S test result, where $p < 0.05$ was determined significant. Cytokines measured were: IL-2 ($r = 0.0295$; $p = 0.8046$), IL-4 ($r = -0.2806$; $p = 0.0162$), IL-5 ($r = -0.0158$; $p = 0.8898$), IL-6 ($r = 0.4166$; $p = 0.0002$), IL-9 ($r = 0.0240$; $p = 0.8339$), IL-10 ($r = 0.1193$; $p = 0.2983$), IL-13 ($r = -0.1013$; $p = 0.3745$), IL-17A ($r = 0.2753$; $p = 0.0168$), IL-17F ($r = 0.2973$; $p = 0.0091$), IL-22 ($r = 0.2257$; $p = 0.0484$), IFNγ ($r = 0.1762$; $p = 0.1228$) and TNF ($r = 0.1979$; $p = 0.0824$).

6.3.7 Summary of results

A heatmap is provided in Figure 6.18 to summarise the findings of this chapter.

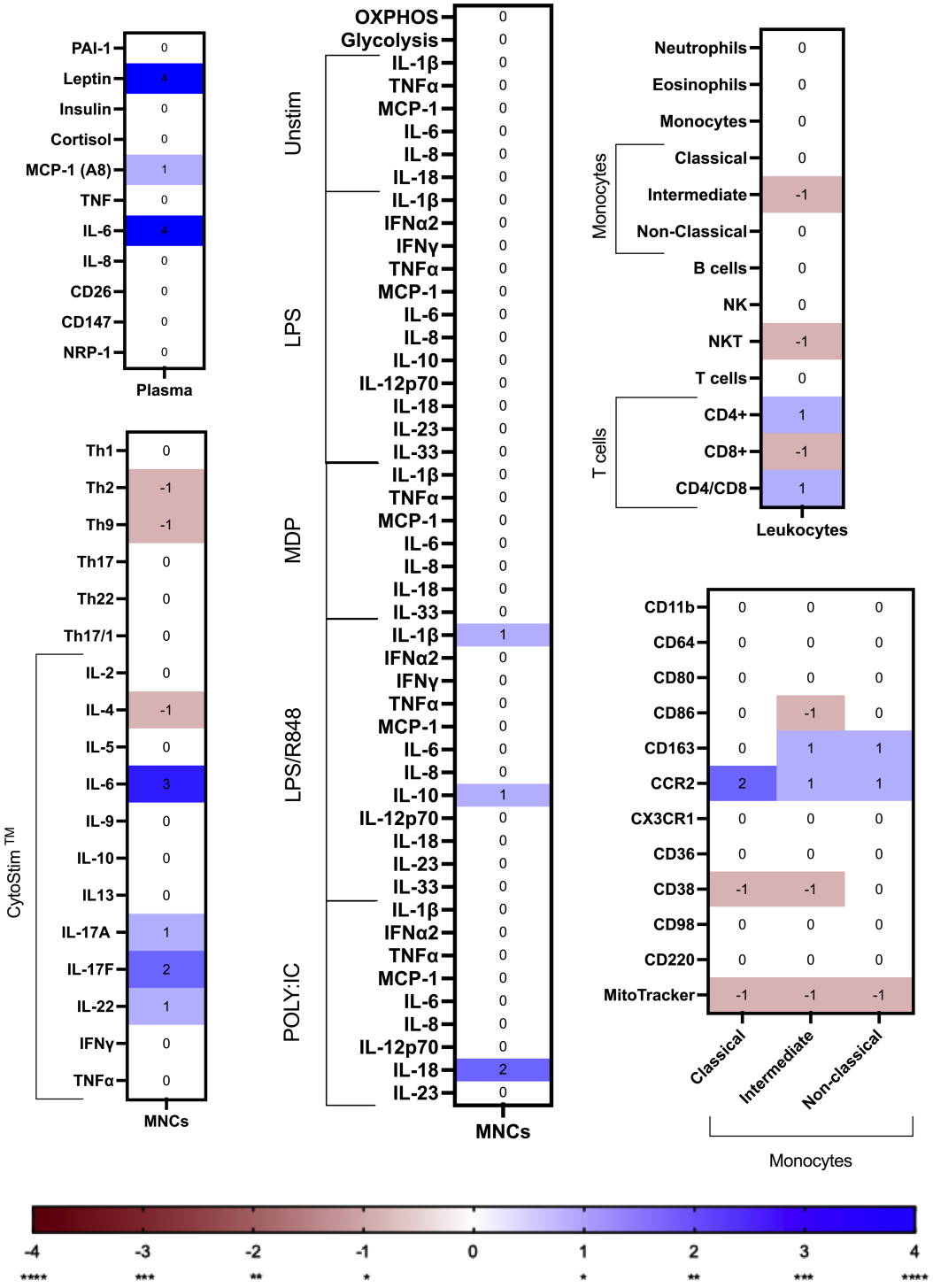

Figure 6.18: A heatmap summary of the findings of Chapter 6. Blue indicates a significant positive correlation between BMI and the measurement, whereas red indicates a significant negative correlation with BMI. Some findings have been condensed to the most important, such as overall OXPHOS rather than showing each measurement.

6.4 Discussion

Using a cohort of women of varying BMI but of very similar gestation and confirmed as negative for GDM by glucose tolerance testing, in contrast to many other studies of obesity in pregnancy, we have been able to establish the effects of obesity on systemic maternal immunity early in the third trimester. This chapter confirms that maternal obesity is associated with systemic inflammation and monocyte activation and extend this to suggest activation of the CCL2/CCR2 axis, as in the general population, with obesity. It is also showing a profound effect of increasing BMI on loss of mitochondrial content; while this did not seem to affect oxidative phosphorylation capacity this measure was made on total mononuclear cells rather than isolated monocytes as would have been ideal. Finally, using both phenotypic and functional analysis this chapter shows for the first time that maternal obesity causes downregulation of Th2 cells and responses favouring heightened Th17 in particular.

Increased leptin and IL-6 in pregnant women with obesity has been described previously [93] and this phenotype of systemic inflammation is extended to include CCL2/MCP-1. Importantly, this study confirms increasing leptin with increasing maternal BMI in a cohort that does not include women with either current or a history of hyperglycaemia and/or GDM/T2DM. Together with Wang et al [453], it supports that this relationship likely occurs throughout pregnancy. Similarly, the systemic elevation of IL-6 but not TNF with increasing maternal BMI is confirmed [93]. While CCL2/MCP-1, a pro-inflammatory chemokine, is reported to be decreased in healthy pregnancy [455], herein obesity in pregnant women was associated with increased CCL2/MCP-1 as has been observed in the general population [413]. Given maternal CCL2/MCP-1 levels have been suggested to be a marker of labour [455], levels with maternal obesity could contribute to increased risk of early labour or miscarriage [456]. Combined with our observation of elevated CCR2 on all monocyte subsets with increasing maternal BMI, as in the general population [79], it is likely that the CCL2/CCR2 axis is also active in pregnant women and manifests as increased intrinsic migratory capacity of monocytes but this remains to be formally investigated. The suspected increased intrinsic migratory capacity of monocytes in pregnancies with obesity would suggest altered macrophage phenotype in adipose and placental tissue. Macrophages have been reported to accumulate in the placenta of pregnant women with obesity [93] but whether this is CCL2/CCR2 mediated recruitment of maternal monocytes remains to be determined.

Obesity in the general population has been shown to be an indicator for severity of COVID-19 symptoms, with high levels of CRP indicating strong critical illness risk [407]. While CRP levels were not measured here, it has been reported that CRP levels are exacerbated in pregnant women with obesity [93]. Despite the initial concern for increased susceptibility for pregnancy with SARS-CoV-2 (based on previous influenza [161], SARS [160] and zika [159] outbreaks), studies have shown that pregnant women are not at severe risk [457]. This is discussed further in *Chapter 7 - The potential protective effects of pregnancy against novel coronavirus SARS-CoV-2*. However, several studies across the globe have described a relationship in pregnancy between severe disease and obesity [458-461]. Obesity and its contribution to immunopathology with SARS-CoV-2 in pregnant women has recently been reviewed by McCartney et al[462]. While soluble forms of the key viral entry receptor for SARS-CoV-2, ACE2 were not measured due to not-detectable levels of the soluble form in plasma, other key molecules CD26 [463], CD147 [464] and NRP-1 [465] were measured. Only NRP-1 showed a correlation between plasma concentration and BMI. Soluble forms of ACE2 (sACE2) have been speculated to act as 'traps' for SARS-CoV-2 to prevent it binding cellular ACE2 [466]. One study investigating the relationship between sNRP1 levels and SARS-CoV-2 disease susceptibility in women suffering with PCOS indicated that depleted plasma sNRP1 correlates to increased vulnerability [467]. This suggests that the elevated sNRP1 observed in maternal obesity is not involved in conferring protection from SARS-CoV-2 during pregnancy.

Independently of facilitating SARS-CoV-2 entry into the cell, NRP-1 plays a vital role at the maternal-fetal interface due to its interaction with vascular endothelial growth factor (VEGF) and its role in angiogenesis [468]. A study has shown a relationship between significantly down-regulated placental NRP-1 and pregnancies with fetal growth restriction [469]. BMI and pregnancy complications such as preeclampsia and preterm labour have been described as being in an antiangiogenic state [470-473]. Due to the relationship between obesity and these pregnancy complications, it would be worth investigating if elevated plasma sNRP-1 as BMI increases, is due to a shedding of membrane NRP-1 from the placenta. The shedding or export of sNRP1 from the placenta is evidenced in healthy pregnant women *in 7.3.4 The placenta, amnion and choriodecidua express both membrane-bound and soluble receptors linked to SARS-CoV-2 infectivity*.

The many obesity-associated changes in monocytes prompted a closer scrutiny of this population. In contrast to the increase in the non-classical subpopulation seen in the general population [68], diminished intermediate monocytes with increasing maternal BMI was observed. Despite being the rarest subpopulation of monocytes, the intermediate subset has been implicated in various diseases. An increase in this subset has been associated with cardiac complications [474, 475], obesity [476, 477], pregnancy [328, 329] and preeclampsia [328]. That the intermediate monocytes are decreasing with BMI, suggests that the elevation already seen in obesity in the general population might be accelerated too early in pregnancy, thereby reducing their expansion in later pregnancy. The functional aspects of the intermediate monocytes in disease are thus far unexplored. Other highlights of the effect of increasing maternal BMI include changes in CD163, CD86 and CD38 which are all novel findings for maternal obesity. An increased expression of CD163 is typical of monocytes and macrophages in response to inflammation [478] and was seen on intermediate and non-classical monocytes with increasing maternal BMI. Increased monocyte expression of CD163 has been associated with improved immune control [479]. Soluble CD163 was not measured here, but this is elevated in sepsis [480] and other inflammatory conditions and would be worth considering in further studies. CD86 was decreased with increasing maternal BMI on intermediate monocytes – in contrast to the general population, where CD86 expression has been found to be elevated on non-classical monocytes in obesity [481]. This suggests a disinclination to stimulate lymphocyte activation. CD38 expression on monocytes and macrophages is induced in inflammatory conditions [482] and a decrease in the expression of CD38 correlates with suppression of adipogenesis and lipogenesis in adipose tissue in mouse models [483]. The data shows a decrease in CD38 expression on classical and intermediate monocytes, and together with CD163 and CD86 observations, suggests that the monocytes might be attempting to counter the exacerbated inflammatory state of maternal obesity. CD38 also has a role in metabolism, with the ability to produce cyclic ADP-ribose and nicotinic acid adenine dinucleotide phosphate (NAADP) from NAD+ and NADP+ respectively. Inhibitors of CD38, such as the flavonoid apigenin from foods such as parsley, have shown beneficial effects in tackling obesity in animal models [484]. In these models elevated cellular levels of NAD^+ are beneficial, and CD38 knockout increases the NAD^+ levels and protects against obesity [484].

Metabolically, while the data on fatty acid and amino acid transporters revealed no differences related to maternal BMI, all three subsets of monocytes had reduced mitochondrial content suggesting that monocyte metabolism – especially OXPHOS - is compromised in maternal obesity. Therefore, the bioenergetic capabilities of MNCs was also considered. It would have been ideal to undertake this analysis on isolated monocytes to better match the flow cytometry finding but this was not possible – this was a study of MNCs and only flow cytometry allowed delineation of effects of maternal obesity on discrete cell types within this heterogenous mix. There appears to be very little research surrounding specific immune cell bioenergetics in obesity or pregnancy although the spare respiratory capacity of monocytes has been shown to be negatively correlated with percentage body fat [485]. A study investigating the effect of the bioenergetic function of peripheral monocytes in women with HIV illustrated that monocytes of infected women with obesity had impaired bioenergetic health (reduced basal and maximal oxygen consumption rate as well as decreased bioenergetic health index) in comparison to lean infected women [486]. A recent study by Sureshchandra et al. has shown that at term, monocytes from pregnant women with obesity have reduced ECAR at baseline and following LPS and glucose injections, in comparison to lean pregnant women that might support their maladaptive phenotype [414]. There are no other studies of the effects of obesity on the bioenergetic profile of MNCs in pregnancy or in obesity in general. While the results in this chapter show no effect of maternal BMI, using a similar approach it is observed that MNCs of pregnant women with GDM have reduced oxidative phosphorylation compared to their GDM-negative counterparts (see *Chapter 8* - General Discussion). Given the absence of any difference in cellular bioenergetics with maternal obesity it is perhaps not surprising that no differences in LPS-stimulated cytokine production was seen, despite differences in such responses in the general population with obesity such as increased production of IL-1β and RANTES upon LPS stimulation of classical monocytes [79] and heightened LPS-stimulated TNF, IL-2, and IFNγ and decreased IL-10 production from LPS-stimulated MNCs [487]. However, cytokine production by monocytes is underpinned by glycolysis [170] which does not depend on mitochondria and was also unchanged with maternal BMI. It would be worthwhile investigating the effects of maternal BMI on monocyte effector functions supported by the mitochondria including ROS production and fatty acid oxidation. All of this does suggest however that it is vital to further investigate phenotypic and functional adaptation of monocytes to both obesity and GDM. This is

especially so as pregnancy-associated monocyte activation is exacerbated in for example preeclampsia [77], and obesity is a risk factor for preeclampsia [80].

Monocytes are not the only cell type affected by maternal obesity. The immunophenotyping performed on MNCs revealed that T cells are particularly susceptible to the effects of maternal BMI. As already reported [131], this study also found a negative correlation between maternal obesity and the abundance of iNKT cells. Due to their ability to influence both innate and adaptive responses, iNKT cells been implicated in various diseases [488]. In the general population, iNKT cells are depleted in adipose tissue of people with obesity [41] and the addition of iNKT cells resolves increased body fat, leptin and insulin sensitivity [449]. While no change in the number of iNKT cells have been observed in pregnancy, they are more activated [489]; further activation of iNKT cells has been shown to induce pregnancy loss in murine models [490]. For conventional T cells, there was no change in total T cells but there was a significant increase in CD4+ T cells accompanied by a decrease in CD8+ T cells which significantly impacted the CD4:CD8 T cell ratio. This decline in peripheral CD8+ T cell counts with obesity in both the general population [422] and in pregnant women [131] appears to be a common finding. While animal studies suggest that this might be explained by the accumulation of CD8+ T cells in adipose tissue [422], little is known about the effects of pregnancy - either with or without obesity - on adipose tissue immune profiles. While there are recent studies exploring the impact of obesity on adipocyte hypertrophy and adipose tissue macrophage populations in visceral adipose tissue from pregnant women with and without obesity [97] there are few studies of the effects of maternal obesity on adipose tissue with most focusing on GDM [491]. Our and other findings in changes to the abundance of some circulating immune cell populations certainly warrant further effort to understand what is happening within adipose tissues in pregnancy and the interrelationship of blood, adipose tissue and placenta. It also is unfortunate that regulatory T cells was not included in this analysis but clearly investigation of these and other important minor cell subsets such as ILCs and MAIT cells is needed.

The effect of maternal BMI on the relative abundance of CD4 and CD8 T cells, combined with the recognised importance of the Th1/Th2/Th17/Treg axis in pregnancy success [10] prompted the consideration of the impact of obesity on this phenotype. Using a flow cytometry based approach based on patterns of chemokine expression by CD4+ T cells [454] it was found that

maternal obesity was associated with a decline in Th2 and Th9 cells. This decline in Th2 cells was accompanied by decreased production of IL-4 upon stimulation of MNCs revealing a negative effect of maternal obesity on Th2 responsiveness in particular. This appears to be accompanied by increased Th1 and Th17 cytokine production suggesting disruption of the Th1/Th2/Th17 axis in pregnant women with obesity. These findings are consistent with the obesity-associated shift to Th1 and Th17 in the general population (Figure 6.19) [423, 492]. In the setting of pregnancy such a shift could lead to recurrent pregnancy loss [129] and pre-term birth [128] for which obesity is a recognised risk factor. Obesity also has been shown to be an indicator for severity of COVID-19 symptoms [407] including in pregnancy [461] and the altered Th1/Th2/Th17 profile shown here could account for this obesity-associated increased risk of severe disease in pregnant women. Overstimulation of Th1-type immunity in particular appears to be a main contributor to miscarriage through the production of IFN-γ and TNFα, with Th1 inhibitors or IL-10 administration combatting the effect in mice [493]. Conversely, studies have indicated that Th2-type immunity may not actually be required for pregnancy, evidenced by mice models with Th2 cytokine knockout [494]. Additionally, the Th1/Th2 paradigm is more prominent at the maternal-fetal interface rather than systemically [495]. There are conflicting studies of Th1 and Th2-type cytokine production in the blood. Some report decreased IFNγ and IL-2 with an increase in IL-4 production (peaking at month 7 of gestation) [496, 497], while others demonstrate a reduction in IL-4 and an increase in IFNγ secretion [498-500]. IL-17 has been observed be increased in maternal peripheral blood but not in spontaneous abortion[501]. However, increased concentrations of IL-17 in maternal sera are seen in pregnancies complicated by fetal growth restriction and preeclampsia [502]. This is corroborated in this study, where there was a significant decrease in fetal birth weight observed when maternal BMI is > 30.

A comparison of lean pregnant women with non-pregnant women at the same time as the comparison with obesity, using the same methodology, would assist in our understanding of the value of a systemic Th1/Th2 (and Th17) paradigm. Most of the women who took part in this study completed successful uncomplicated pregnancies, and so the findings here could further evidence that Th2 type immunity is unessential, at least at this stage of pregnancy. This does not however disregard any potential long-term effect on the mother and the fetus

that these changes may have; further work is required. Additional investigations should consider the Th profile at different stages of pregnancy, with and without obesity, and with and without complications, and ideally in the same women prospectively. If this shift only occurs later in gestation, it could suggest that the pregnancy is too well established to be impacted by any systemic shifts in the Th1/Th2 (and Th17) dichotomy. It is possible this shift only relates to adverse outcomes if it occurs early in gestation when the establishment of the maternal-fetal interface is more sensitive to dysregulation. Due to the difficulty of acquiring samples from pregnant women, animal models are being considered to delve more into the mechanistic aspect of the changes observed, particularly looking at the effect on adipose tissue and other organs.

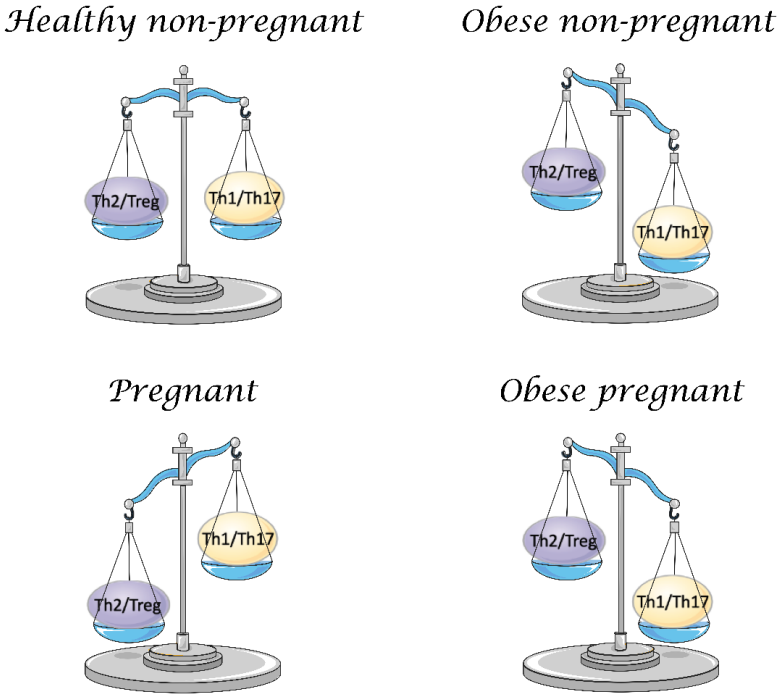

Figure 6.19: Summary of the balancing act of the Th subsets in healthy and obese non-pregnant, and healthy and obese pregnancies. A tight balance is maintained in the general healthy population; this skews to favour the Th1/Th17 in obesity, and towards Th2/Treg in a healthy pregnancy. A pregnancy complicated by obesity mimics the change in balance as observed in the general population with obesity.

Conclusion

BMI is strongly correlated to several differences in pregnant woman at 28 weeks of gestation. These associations may offer explanations for increased risk of adverse obstetric outcomes, and some may offer targets for therapy. Further investigation into isolated cell populations as well as adipose tissue and placenta is required to further our understanding of the influence of obesity on pregnancy outcome. In addition, murine models may extrapolate the significance of the findings described here if it is found that the pregnancies were or were not successful.

Chapter 7 - The potential protective effects of pregnancy against novel coronavirus SARS-CoV-2

7.1 Introduction

Novel coronavirus, SARS-CoV-2, is responsible for the disruptive and deadly COVID-19 pandemic; research into this virus is vital. Pregnancy poses a unique risk factor to any new infectious disease, such as the previous outbreaks of Zika [159], SARS [160] and influenza [161]. These diseases highlight the potential immediate and long-term detrimental health affects for the mother and fetus. Pregnant women are more at risk of severe influenza [161], Zika has been shown to cause birth defects such as microcephaly [159, 162], and SARS to induce premature delivery [160]. However, the characteristics of COVID-19 in pregnant and non-pregnant women are very similar and while severe COVID-19 in pregnancy brings increased risk of preterm birth and intensive care admission [164] most pregnant women, be they symptomatic or asymptomatic for SARS-CoV-2 infection, do not experience severe complications in pregnancy [165]. Similarly, cases of SARS-CoV-2 vertical transmission are rare and there is low risk of serious disease for the neonate [503]. Understanding the mechanisms of resilience against severe COVID-19 in pregnant women and the newborn are critical to ensure ongoing vigilance in care and to provide insight into disease pathogenesis and therapeutic opportunities. The Royal College of Obstetricians & Gynaecologists currently advise in their guidelines for pregnant women to follow the same precautions as a healthy individual as there is no evidence to suggest they are more at risk of contracting COVID-19 [163].

Disease severity and morbidity of COVID-19 patients have been associated with increasing age [166]. Along with age, other factors which induce higher expression of CD147- and ACE2-related genes have included being male, obesity, smoking and hypertension [504]. A study from the UK Obstetric Surveillance System (UKOSS) has shown that, as with the wider population, Asian and Black pregnant women are more likely to be admitted to hospital with SARS-CoV-2 infection [167]. This study also found that most pregnant women admitted to hospital were in the late second or third trimester [164, 167]. Overweight or obesity also contributed to a large percentage (69%) of pregnant women infected with SARS-CoV-2 and admitted to hospital [167]; other studies have observed the same trend with obesity [458, 461, 462]. BMI and ethnicity are also a risk factor for gestation diabetes mellitus [505]; therefore, it is vital to understand how exactly the immune system differs in these pregnancies. Further discussion on the effect of maternal obesity on SARS-CoV-2 can be found in *Chapter 6.*

As discussed in Chapter 1, the maternal pregnant environment becomes skewed towards a Th2 response [8, 506]. The progression of severity by SARS-CoV-2 infection could be initiated by a cytokine storm, which is primarily the excessive activation of Th1 cytokines. Typically, a Th1 environment is more effective at containing viruses, illustrated by pregnant women being more susceptible to influenza. However, the Th2 dominant environment of pregnancy may result in lesser severity as the predominant response to SARS-CoV-2. While it would be logical to assume that pregnant women are therefore at higher risk for severe illness or mortality in comparison to a non-pregnant woman, observations have disputed this, with the risk and severity being no different to non-pregnant. The mortality rates of pregnant women are also surprisingly relatively low in comparison to MERS and SARS pandemics. However, if pregnant women were to contract severe SARS-CoV-2, there is an increased risk of pre-term birth, with risk of hypertension also increasing with severe infection [164, 507].

Vertical transmission of SARS-CoV-2 or any virus to the fetus is a particular worry. One of the roles of the placenta is to act as a barrier against viral and bacterial infections. Zika virus has been shown to infiltrate the placenta to affect the fetus. Studies have suggested that Zika disrupts the placental barrier by directly infecting placental cells, primarily targeting placental macrophages and trophoblasts, including syncytiotrophoblast (STB) cells [318, 508, 509]. The STBs mediate the exchange of waste and nutrients between the fetal and maternal blood, and Zika uses this to infect the fetus. Studies thus far have concluded that the fetus is substantially protected from vertical transmission of SARS-CoV-2 [510], with occurrences being uncommon; less than 3.2% of neonates have been found to be SARS-CoV-2 positive [511]. Angiotensin-converting enzyme 2 (ACE2) is a key molecule which works in tandem with other molecules to allow SARS-CoV-2 entry into cells [512]. ACE2 has been found highly expressed in healthy pregnancies, particularly due to the placenta [513, 514], suggesting that pregnant women may be at an increased risk to SARS-CoV-2 complications. Studies have shown that upon SARS-CoV-2 binding to ACE2, ACE2 is down-regulated and thus blood pressure increases along with other inflammatory effects that occur in preeclampsia [515]. Early reports show that preeclampsia may be more prevalent in pregnancies affected by COVID-19 [516]. However, despite the localisation of ACE2 and the SARS-CoV-2 spike protein being primarily within the outer syncytiotrophoblast layer, no differences between ACE2 expression and cases of vertical

transmission have been found, suggesting that the occurrences of this may be due to a different viral entry pathway [515].

In the case of maternal infection, maternal IgG antibodies against SARS-CoV-2 will cross the placenta to provide the fetus passive immunity [517], providing short-term protection for the last months of pregnancy and for some months after the baby is born; studies have confirmed this phenomenon occurs with SARS-CoV-2 [518, 519]. Antibodies (predominantly IgA but also IgG) will also be provided in the breast milk if the baby is breast fed [520, 521], and this has been confirmed in the case of SARS-CoV-2 natural infection and vaccination [522, 523].

SARS-CoV-2, like most other coronaviruses, has an outer membrane spike (S) protein which is the prime protein for interaction with host cell targets [463, 524]. ACE2 is an enzyme present on cell membranes that has a normal role in lowering blood pressure via the Renin-Angiotensin System (RAS) in which ACE2 catalyses the reaction which produces the vasodilator peptide angiotensin (1-7) from the hydrolysis of vasoconstrictor peptide angiotensin II. However, it also acts as an entry point for coronaviruses into cells (Figure 7.1) [512]. ACE2 is found predominantly on epithelial cells and is ubiquitous in lung, heart, intestine, nasal and kidney epithelium, but is rarely expressed by leukocytes [504]. Epithelial cell surface expression of ACE2 is reduced after interaction with the S-protein of SARS-CoV-2, as it is internalised into endosomes with the viral particles [525]. ACE2 can also exist as a circulating soluble form (sACE2) [526]. Whilst typically present in low quantities in healthy human plasma, sACE2 is elevated in heart failure patients, and thought to have a protective effect. It has been hypothesised that sACE2 can act as a trap for SARS-CoV-2 to prevent it binding membrane ACE2 (Figure 7.1) [466].

Early evidence has shown that CD147 [464] and CD26 [463] are also key viral entry receptors for SARS-CoV-2. CD147, also known as basigin (BSG), is an extracellular matrix metalloproteinase inducer (EMMPRIN). It has various immunological roles, such as intercellular recognition, stimulation of lymphocyte responsiveness [527], and of monocarboxylate transporters [528], such as those which transport lactate and pyruvate across cellular membranes. CD147 was discovered to be a receptor responsible for *Plasmodium falciparum* invasion of cells to cause malaria [529]. The role of CD147 in viral invasion regarding SARS-CoV-2 is still poorly understood

and there are conflicting findings; some have suggested no role in viral entry [530], however, an anti-CD147 antibody drug called Meplazumab has been shown to inhibit SARS-CoV-2 viral entry into host cells [464, 531]. CD26, also known as dipeptidyl peptidase-4 (DPP4), is predominantly associated with apoptosis, regulation of the immune system, and signal transduction. Like ACE2 and CD147, CD26 also has a soluble form present in various body fluids such as blood plasma. CD26 can cleave a broad range of substrates such as neuropeptides, chemokines and vasoactive peptides; it also degrades incretins such as GLP-1, illustrating its role in glucose metabolism [532]. Once degraded, GLP-1 inhibits the release of insulin and stimulates the release of glucagon, thus elevating blood glucose levels [533]; CD26 has been a target for some anti-diabetic drugs [534]. Both CD147 and CD26 are expressed in epithelium and by leukocytes [504].

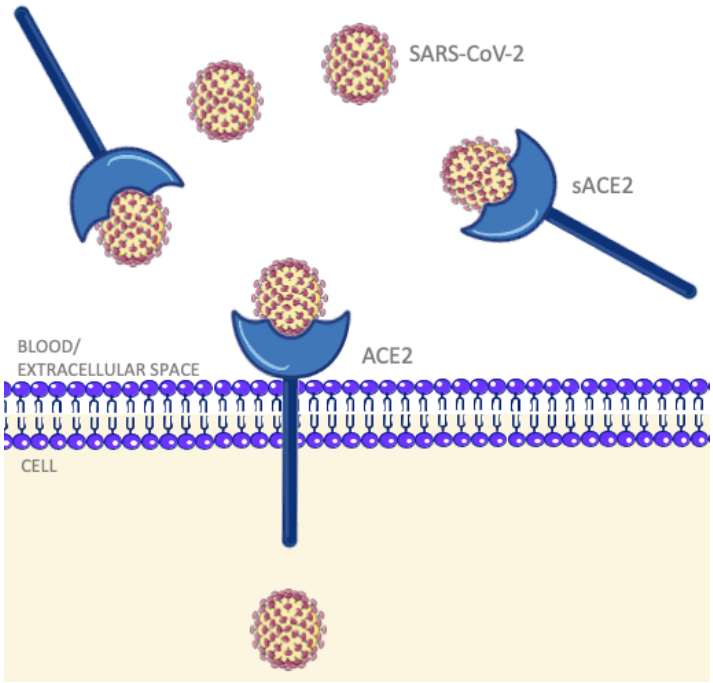

Figure 7.1: The binding of SARS-CoV-2 to ACE2. SARS-CoV-2 can bind to both the membrane-bound and soluble forms of ACE2. Upon binding the membrane-bound ACE2, SARS-CoV-2 can gain entry into the cell to infect it. Soluble ACE2 (sACE2) binds SARS-CoV-2 to prevent it from infecting the cell and acts as a trap for virus particles.

Along with these three molecules, there have been several others described as necessary or desirable for SARS-CoV-2 cell entry (Figure 7.2). Neuropilin-1 (NRP-1) is recognised to be a coreceptor to vascular endothelial growth factor (VEGF) [535] and semaphorin (SEMA3A) [536] supporting its various roles such as angiogenesis and cell survival [468]. In pregnancy, it has been shown that due to its interaction with VEGF, NRP-1 plays a vital role at the maternal-fetal interface. This has been evidenced by significantly down-regulated placental NRP-1 in pregnancies with fetal growth restriction [469]. NRP-1 has also been implicated in

tumorigenesis, promoting the growth and survival of tumours [537], and has been a target for various anti-tumour drugs [538]. NRP-1 has been shown to facilitate SARS-CoV-2 entry into the cell, and also potentiates infectivity [465]. Mayi et al discussed the theorised role of NRP-1 in SARS-CoV-2 [539], and speculated its role in promoting vascular and coagulation dysfunction [540, 541], as well as highlighting the unique role of NRP-1 in facilitating SARS-CoV-2 uptake in the olfactory epithelium and bulb resulting in anosmia symptom presentation [465] (ACE2 is not found on neurons [542]). Soluble NRP-1 (sNRP-1) levels have been linked to SARS-CoV-2 susceptibility in women suffering with polycystic ovary syndrome (PCOS) where increased vulnerability is linked with depleted plasma sNRP-1 levels [467].

A member of the heat shock protein family, glucose regulated protein 78 (GRP-78; binding immunoglobulin protein; BiP) is involved in the folding and assembly of proteins on the endoplasmic reticulum (ER) and is regulated by its allosteric ATPase cycle [543]. GRP-78 has also been discussed to have immunomodulatory functions such as inducing anti-inflammatory cytokine secretion by MNCs [544] and down-regulating vital molecules (e.g. CD86) involved in T cell activation [545], as well as metabolic regulation as it is required in adipose tissue for glucose homeostasis and adipogenesis [546]. GRP-78 is known to interact with a region on the SARS-CoV-2 receptor-binding domain (RBD) that is structurally similar to the cyclic form of Pep42 (a cyclic 13-mer oligopeptide which preferentially binds GRP-78 [547]) allowing the facilitation of viral entry into the cell [548]. GRP-78 is essential for the fertilisation process, involved in the development and proliferation of embryonic cells, and is regulated by maternal oestrogen [549-552]. Under hypoxic conditions and severe preeclampsia pregnancies, placental GRP78 is found to be upregulated, and this has been suggested to occur in an effort to resolve ER stress [553, 554].

A disintegrin and metalloprotease 17 (ADAM17; tumour necrosis factor-α-converting enzyme; TACE) is found on the cell surface and in the intracellular membranes of the Golgi network, with its primary role is understood to be the processing of TNFα [555]. The biological function of transmembrane protease serine 2 (TMPRSS2) is unknown although it is thought to be involved in various physiological processes due to its membership of the serine protease family. Both TMPRSS2 and ADAM17 have been implicated in SARS-CoV-2 through their ability to cleave ACE2 [556]. The spike protein of SARS-CoV induces ADAM-17 interaction with ACE2,

coupled with TNFα production [557], after it has been internalised and proteolytically cleaves the ACE2 ectodomain, and this has been proven to be necessary for infection of cells by SARS-CoV-2 [556, 558]. While it is still unclear how ADAM17 facilitates viral entry, it Zipeto et al speculates that its protease activity may be vital for viral fusion with the cytoplasmic membrane [559], and its increased activity leads to the cleavage of pro-inflammatory molecules such as TNFα [560]. In competition for ACE2 cleavage for viral uptake, TMPRSS2 is also capable of cleaving the ACE2 cytoplasmic tail which can potentiate viral uptake and processing via a cathepsin L (CTSL)-independent pathway [556]. However, augmented SARS-CoV spike (S) protein (SARS-S)-driven entry is only achieved by TMPRSS2 in comparison to ADAM17-cleavage, allowing for activation of the S protein to allow membrane fusion [556]. It has been shown that SARS-CoV-2 entry is primely mediated by ACE2 for entry and TMPRSS2 for S protein priming [561]. CTSL is involved in intracellular protein catabolism, and has various roles including apoptosis and angiogenesis [562]. Once the viral particles are internalised into an endosome after ACE2/TMPRSS2 mediated uptake, CTSL primes the S protein for activation [556].

Due to ADAM17 being a major sheddase for TNFα, some investigation into its role in pregnancy has been necessary. Murine models have suggested ADAM17 activity to be vital for embryonic development, with deficiencies resulting in impaired vessel formation and haemorrhage potentially due to the failure to cleave substrates involved in vascular development [563]. Placental ADAM17 expression has been found to be elevated in preeclampsia, modulated by the hypoxic conditions, contributing to the exacerbated TNFα production observed [564]. Placental expression of both ACE2 and TMPRSS2 has been found to be dependent on gestational age, with the expression highest during the first trimester [565]. The lower expression in the later trimesters could contribute to the infrequent cases of vertical transmission observed; less viral entry receptors for SARS-CoV-2 to bind to cross the placental barrier [566]. Placental CTSL expression is also significantly higher in the first trimester than the latter trimesters as well as having increased enzymatic activity during the invasive phase of placentation [567].

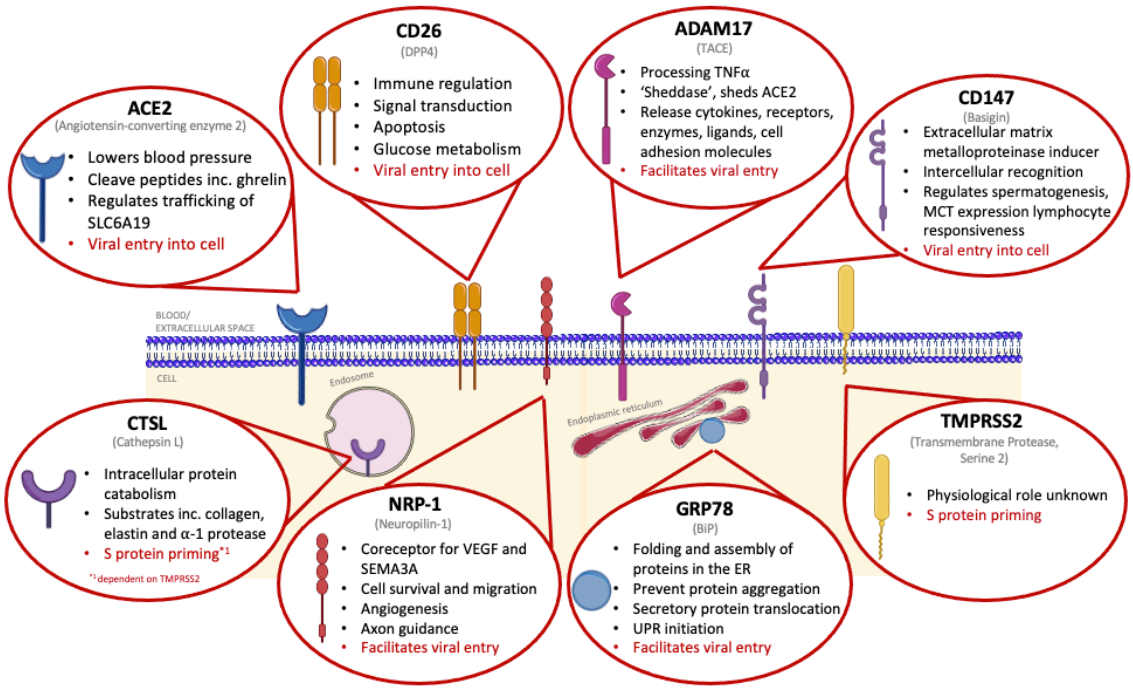

Figure 7.2: Molecules involved in SARS-CoV-2 infectivity and their normal physiological function.

7.1.1 Rationale

Pregnant women are considered a high-risk group for severe effects of SARS-CoV-2. As this virus is resulting in an international pandemic, it is vital to elaborate on why both the mother and fetus appear to be relatively resilient to severe forms of COVID-19, as this may help us identify ways to combat the disease.

7.1.2 Hypothesis

High levels of soluble receptors (e.g., ACE2) in bodily fluids - such as plasma, breast milk and amniotic fluid - act as decoy receptors to stop the virus binding to cells, thus protecting mother and fetus from infection.

7.2 Materials and Methods

7.2.1 Samples

Some samples used for the analysis described in this chapter (serum, plasma, breast milk, amniotic fluid, placental lysates) were archived from previous studies. Cell analysis was performed with peripheral blood donated by male and female volunteers aged 18-40, and pregnant women as described in *2.1 Human blood collection.* At the time of consent for maternal blood, the pregnant women also gave consent for the use of her placenta and blood from the umbilical cord after delivery by elective caesarean section. Samples of amniotic fluid (AF) collected at >37 weeks of gestation (North of Scotland Research Ethics Committee: 06/S0801/77), and breast milk (BM) at 2 (2W) and 6 weeks (6W) postpartum (Wales Research Ethics Committee: 2004/024) archived prior to the COVID-19 pandemic were available.

7.2.2 Flow cytometry

100 µl of peripheral blood or 50 µl of umbilical cord blood was stained with the appropriate volume of antibodies (Table 7.1). Cells were incubated in the dark on ice for 30 mins. 2 ml of FACS lysing solution (10X BD FACS ™ lysing solution diluted to 1X with dH_2O) was added to lyse the red blood cells. Samples were vortexed before incubation for 15 mins in the dark at room temperature and then centrifugation at 515 x g for 7 mins at 4°C. Supernatant was removed and samples were washed with FACS buffer twice as in *2.4 Flow Cytometry*. Monocytes (*2.4.2 Gating strategy for selection of monocytes*), neutrophils (Figure 7.3A), B cells (Figure 7.3B) and T cells (Figure 7.3C) were identified via doublet-exclusion, size and lineage marker expression.

	Fluorochrome	Clone	Isotype	Manufacturer
ACE2	PE	535919	Mouse, IgG2a	R&D Systems
ADAM17	PE	111633	Mouse, IgG1, κ	R&D Systems
CD14	Pacific Blue™	63D3	Mouse, IgG1, κ	BioLegend
CD14	Alexa Fluor® 647	63D3	Mouse, IgG1, κ	BioLegend
CD147	Alexa Fluor® 488	HIM6	Mouse, IgG1, κ	BioLegend
CD15	PE	HI98	Mouse, IgM, κ	BioLegend
CD15	FITC	HI98	Mouse, IgM, κ	BioLegend
CD16	APC	3G8	FcγRIII	BioLegend
CD16	VioBlue	VEP13	Mouse, IgM, κ	Miltenyi
CD19	Percp/Cy5.5	HIB19	Mouse, IgG1, κ	BioLegend
CD26	KIRAVIA Blue 520™	BA5b	Mouse, IgG2a, κ	BioLegend
CD3	PE	HIT3a	Mouse, IgG2a, κ	BioLegend
CD3	APC	OKT3	Mouse, IgG2a, κ	BioLegend
CD4	Alexa Fluor® 647	OKT4	Mouse, IgG2b, κ	BioLegend
CD4	FITC	OKT4	Mouse, IgG2b, κ	BioLegend
CD8a	Pacific Blue™	RPA-T8	Mouse, IgG1, κ	BioLegend
NRP-1	APC/Fire™ 750	12C2	Mouse, IgG2a, κ	BioLegend

Table 7.1: Details of antibodies used to determine the expression of SARS-CoV-2 receptors on leukocytes.

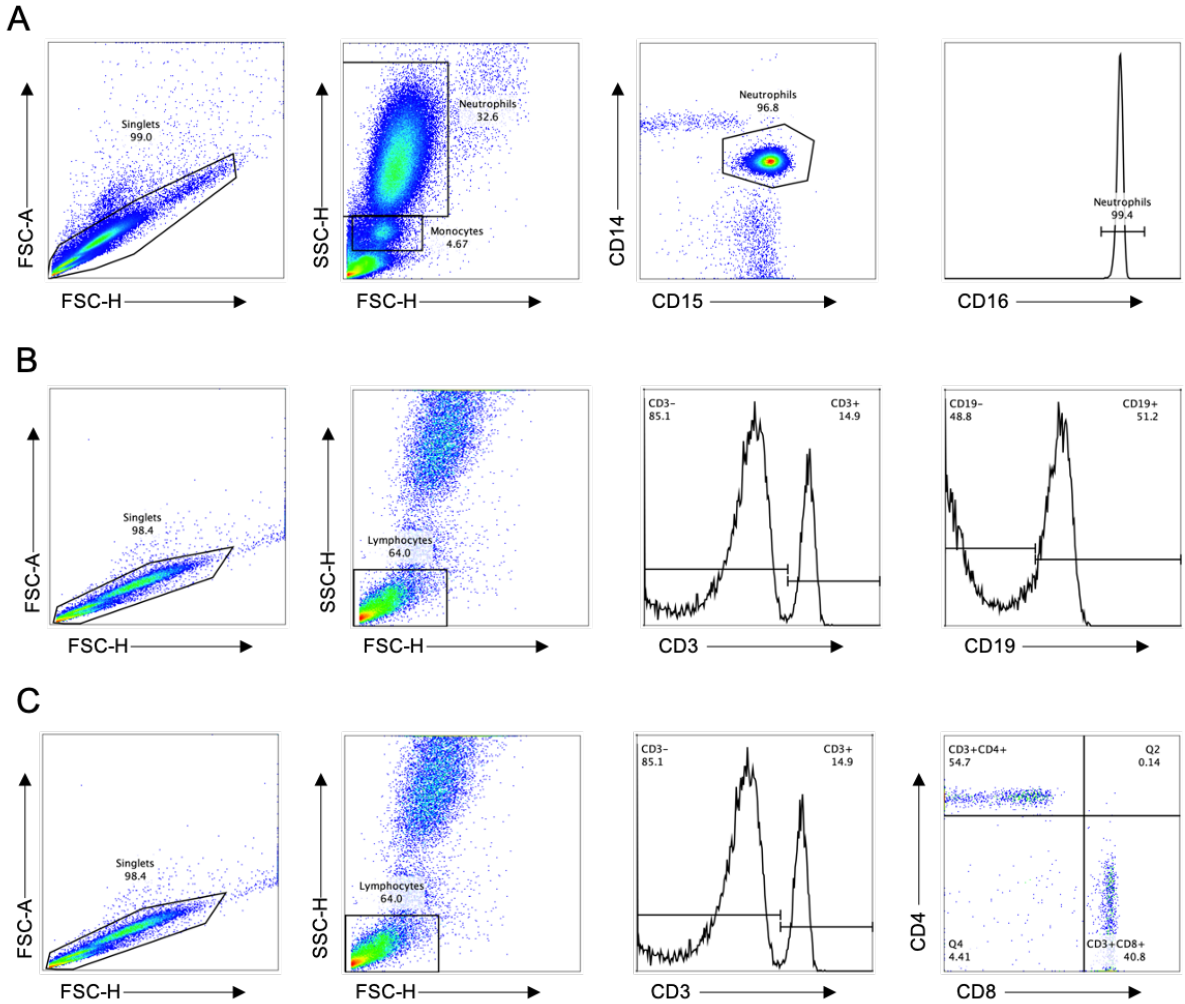

Figure 7.3: Gating strategy for neutrophils, B cells and T cells. **(A)** Neutrophils were identified by first excluding the doublets by a FSC-H vs FSC-A plot. They are then selected by FSC-H vs SSC-H and then confirmed as CD15-positive, CD14-negative (dot plot) and CD16-positive (histogram). **(B)** B cells were identified by first selecting singlets (FSC-H vs FSC-A) followed by using FSC-H vs SSC-H. A CD3-negative population was then selected, and B cells identified as CD19-positive. **(C)** T cells were identified first by the selection of singlets (FSC-H vs FSC-A) and then by using smaller FSC-H vs SSC-H). T cells are identified by being CD3-positive, and subsets by either being CD4-positive of CD8-positive.

7.2.3 MNC preparation

MNCs were prepared from peripheral blood as described in *2.2 Mononuclear cell isolation.*

7.2.4 Cell culture

MNCs were stimulated for 24 hr with LPS, MDP, LPS and R848, POLY I:C or CytoStim ™ as detailed in *2.5 Cell culture*.

7.2.5 Placental lysates

1cm pieces of placenta were cut and placed into PBS, where they were diced into smaller pieces. These were washed six times with PBS to remove blood. 0.2 g of diced placental tissue

was added to tubes with 500 µl PBS/protease inhibitor (cOmplete Mini, EDTA-free, Roche, Germany) solution. Tissue was left on ice for 5 mins before ultrasonication until the tissue was homogenised. A further 500 µl PBS and 10 µl triton X-100 (Sigma) were added. Placental lysates were stored at -80°C until use.

7.2.6 Placental, amnion and chorion decidual explants

Explants of placenta, amnion and choriodecidua were generously produced by fellow PhD colleague Megan Chambers. The choriodecidua and amnion membranes were separated from the placenta and detached from each other. PBS was used to wash the blood from the membranes. Discs of the membranes were cut with an 8-mm biopsy punch (need supplier info). Four discs of choriodecidua per ml of culture media (10% Hyclone FBS, 100 µM 2-ME, RPMI 1640/Glutamax) and six discs of amnion per ml of culture media was cultured.

After removal of the decidua basalis shrouding the maternal slide of the placenta, 1 cm^3 portions of placental villous tissue were extracted and washed repeatedly with PBS. Tissue was further minced to 1 m m^3 piece and 0.2 g of placental tissue was cultured per ml of culture media.

All explants were exposed to the following stimuli: LPS (10 ng/ml), MDP (1 µg/ml), R848 (400 ng/ml) and POLY I:C (25 µg/ml). Cultures were incubated at 37°C in 5% CO_2 for 24 hr. Explant cultures were centrifuged at 515 *x g* for 7 mins at 4°C and tissue-free supernatants were extracted and stored at -20°C until later analysis.

7.2.7 ELISA

ELISAs were performed as in *2.7 Enzyme linked immunosorbent assay (ELISA)*, with the exception being the reagent diluent used to dilute samples and the standards. 50% FBS in PBS was used as the reagent diluent. Soluble receptors which were measured were: ACE2, CD26, CD147 and NRP-1 (Bio-Techne).

7.2.8 Blotting

Western blotting was performed as in *2.8 Immunoblotting*. Plasma samples were diluted 1/10 with PBS. Breast milk and amniotic fluid were run neat. 6 µl of diluted sample (5 µl sample + 1 µl reducing buffer). was loaded into the gel. Antibodies used are shown in Table 7.2.

	Clonality	Isotype	Host species	Predicted MW, kDa	Manufacturer
ACE2	Monoclonal	IgG1	Mouse	120-135	Cell Signalling
ADAM17	Polyclonal	IgG	Rabbit	93	Abcam
CD26	Polyclonal	IgG	Rabbit	90,120	Cell Signalling
CD147	Polyclonal	IgG	Goat	38-50	R&D Technologies
GRP78	Polyclonal	IgG	Rabbit	75	Abcam
NRP-1	Monoclonal	IgG	Rabbit	103	Abcam
TMPRSS2	Polyclonal	IgG	Rabbit	54	Abcam

Table 7.2: Antibodies used for western blotting.

7.2.9 Immunohistochemistry (IHC)

Immunohistochemistry was outsourced to Kate Murphy with the Swansea Bay University Health Board Histology department using archived placental blocks from the research group.

7.3 Results

7.3.1 Leukocyte expression of membrane-bound receptors involved in SARS-CoV-2 infectivity is altered in pregnancy and in umbilical cord blood

Due to the knowledge accumulated in previous chapters, the investigation into the presence and subsequent expression of SARS receptors on leukocytes from men, women, pregnant women, and neonates was a key starting point. Various SARS-CoV-2 receptors which were possible to measure via flow cytometry were: ACE2, ADAM17, CD26, CD147 and NRP-1. There was no significant difference in the expression of any of these receptors on neutrophils (Figure 7.4; Table 7.3), although there appears to be a decrease in the expression of CD26 on cord neutrophils in comparison to the other groups. There were no significant differences observed between any of the groups in any monocyte subset for ACE2, ADAM17, CD17 and NRP1 (Figure 7.5; Table 7.7 - 9.7). A significant difference was found in the classical monocytes between non-pregnant women and neonates for CD26 ($p = 0.0273$) where it was decreased in the neonate (Figure 7.5C; Table 7.4).

B cells lacked detectable ACE2 expression (data not shown), and there were no significant differences in the expression of ADAM17, CD26 and NRP-1 between the groups (Figure 7.6; Table 7.8). However, CD147 expression was decreased significantly on B cells from non-pregnant women compared to men ($p = 0.0169$), and increased significantly on neonatal B cells when compared to men ($p = 0.0005$), non-pregnant ($p < 0.0001$) and pregnant women ($p < 0.0001$; Figure 7.6C; Table 7.8).

Between the different groups analysed, the T cells had more varying expressions of the receptors than the other leukocytes, illustrating that they are more influenced by gender, pregnancy, and age (Figure 7.7). Though not significant, there appeared to be a decrease in the expression of ACE2 on neonatal T cells in comparison to the other groups (Figure 7.7A). Despite the only significant difference for the expression of ADAM17 being between the adult males and neonates in the CD8 T cells ($p = 0.0165$), there also appeared to be a decrease in ADAM17 expression in neonatal total T cells and CD4 T cells compared to adult males and non-pregnant females (Figure 7.7B). The expression of CD26 (Figure 7.7C) was significantly elevated on the total T cells ($p = 0.0233$) and CD4 T cells ($p = 0.0007$) of pregnant women compared to men, and the CD26 expression was vastly higher on the neonatal total T cells,

CD4 and CD8 T cells in comparison to men (p = 0.0002; p = 0.0004; p = 0.0031), non-pregnant (p = 0.0043; p = 0.0057; p = 0.0006) and pregnant women (p = 0.0061; p = 0.0022; p = 0.0194). Elevated expression of CD147 on CD4 T cells (p = 0.0198)was observed in pregnant in comparison to non-pregnant women, as well as in the neonates in comparison to non-pregnant and pregnant women for total T cells (p = 0.0120; p = 0.0008), CD4 T cells (p = 0.0078; p = 0.0026) and CD8 T cells (p = 0.0001; p = 0.0023), and compared to men on CD4 T cells (p = 0.0077; Figure 7.7D). NRP-1 expression was augmented on the T cells from cord in comparison to men (p = 0.0276) and on the cord CD4 T cells compared to men (p = 0.0174) and non-pregnant women (p = 0.0428; Figure 7.7E).

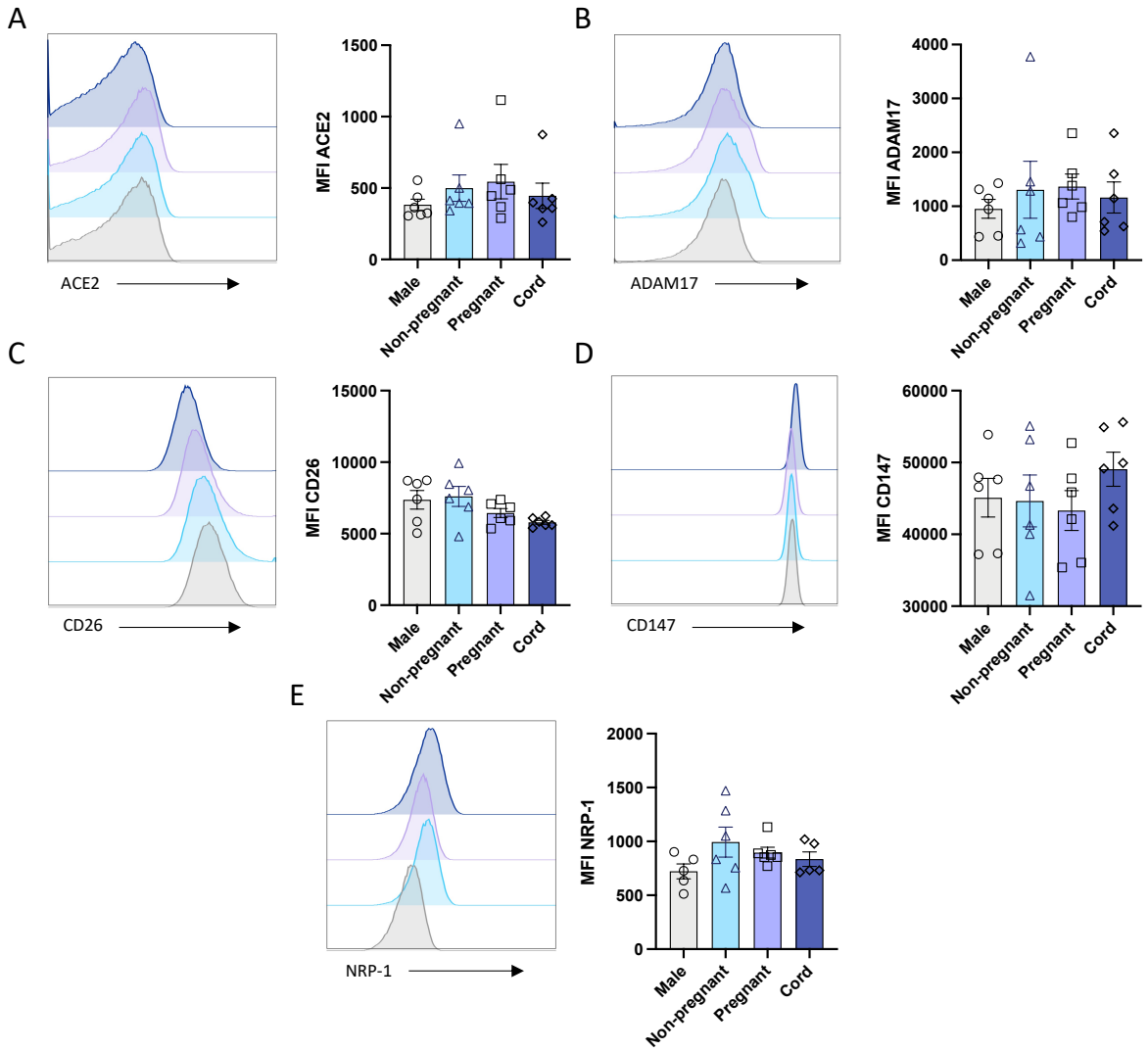

Figure 7.4: **Expression of SARS-CoV-2 receptors on neutrophils from males, females, pregnant *females,* and neonates.** Neutrophils were identified from whole blood from males (M; n=6), non-pregnant females (F; n=6), pregnant (P; n=6) females and cord (C; n=6) and SARS receptor expression was analysed via flow cytometry as described in the Materials and Methods. Statistics were determined using a one-way ANOVA and a Tukey post-hoc test, where $p < 0.05$ was deemed significant. The expression of SARS receptors which were analysed were: **(A)** ACE2 **(B)** ADAM17 **(C)** CD26 **(D)** CD147 **(E)** NRP-1.

ACE2	Male	Non-pregnant	Pregnant	Cord
Male		0.7977	0.5921	0.9596
Non-pregnant			0.9842	0.9743
Pregnant				0.8645
Cord				

ADAM17	Male	Non-pregnant	Pregnant	Cord
Male		0.8767	0.8182	0.9702
Non-pregnant			0.9992	0.9899
Pregnant				0.9725
Cord				

CD26	Male	Non-pregnant	Pregnant	Cord
Male		0.9883	0.5763	0.1574
Non-pregnant			0.3927	0.0870
Pregnant				0.8025
Cord				

CD147	Male	Non-pregnant	Pregnant	Cord
Male		0.9995	0.9718	0.7689
Non-pregnant			0.9879	0.7062
Pregnant				0.5124
Cord				

NRP-1	Male	Non-pregnant	Pregnant	Cord
Male		0.1994	0.5615	0.8425
Non-pregnant			0.8589	0.6270
Pregnant				0.9665
Cord				

Table 7.3: p values for SARS-CoV-2 receptors on neutrophils.

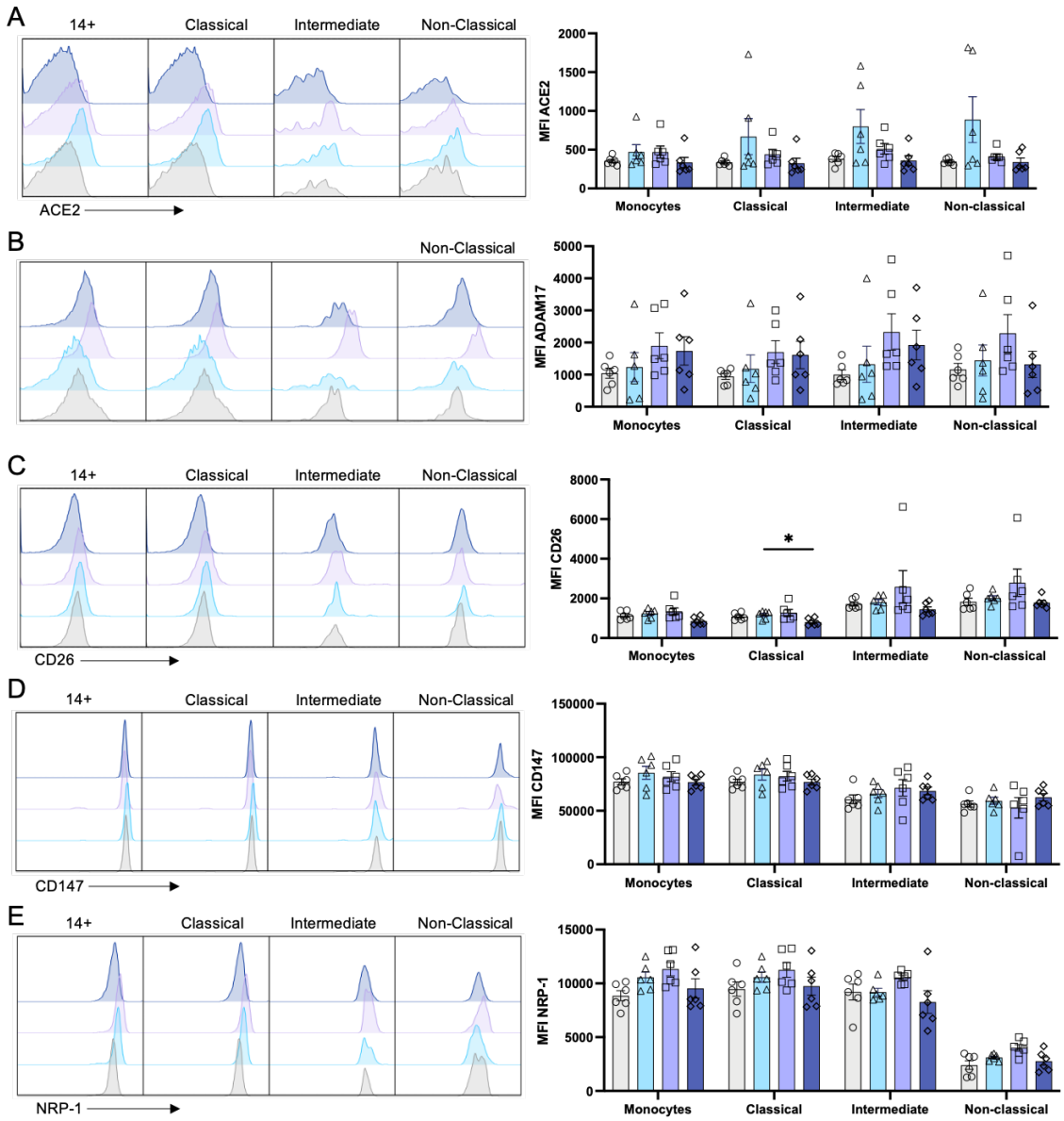

Figure 7.5: Expression of SARS-CoV-2 receptors on monocytes from males, females, pregnant *females,* and neonates. Monocytes and their subsets were identified from whole blood from males (M; n=6), non-pregnant females (F; n=6), pregnant (P; n=6) females and cord (C; n=6) and SARS receptor expression was analysed via flow cytometry as described in the Materials and Methods. Statistics were determined using a two-way ANOVA and a Tukey post-hoc test, where $p < 0.05$ was deemed significant. The expression of SARS receptors which were analysed were: **(A)** ACE2 **(B)** ADAM17 **(C)** CD26 **(D)** CD147 **(E)** NRP-1.

ACE2	Male	Non-pregnant	Pregnant	Cord
Male		0.6930	0.5413	0.9909
Non-pregnant			>0.9999	0.7125
Pregnant				0.6541
Cord				

ADAM17	Male	Non-pregnant	Pregnant	Cord
Male		0.9772	0.4182	0.4921
Non-pregnant			0.8235	0.9126
Pregnant				0.9911
Cord				

CD26	Male	Non-pregnant	Pregnant	Cord
Male		0.4760	0.7607	0.2934
Non-pregnant			0.9258	0.1279
Pregnant				0.1705
Cord				

CD147	Male	Non-pregnant	Pregnant	Cord
Male		0.6498	0.5889	0.9997
Non-pregnant			0.9589	0.5312
Pregnant				0.8324
Cord				

NRP-1	Male	Non-pregnant	Pregnant	Cord
Male		0.1489	0.1728	0.8914
Non-pregnant			0.8085	0.8466
Pregnant				0.2355
Cord				

Table 7.7: p values for SARS-CoV-2 receptors on total monocytes.

ACE2	Male	Non-pregnant	Pregnant	Cord
Male		0.4925	0.4801	0.9979
Non-pregnant			0.7758	0.6051
Pregnant				0.6862
Cord				

ADAM17	Male	Non-pregnant	Pregnant	Cord
Male		0.9441	0.3391	0.4647
Non-pregnant			0.8586	0.6437
Pregnant				0.9988
Cord				

CD26	Male	Non-pregnant	Pregnant	Cord
Male		0.8444	0.7299	0.0951
Non-pregnant			0.9148	0.0273
Pregnant				0.0753
Cord				

CD147	Male	Non-pregnant	Pregnant	Cord
Male		0.6468	0.5865	>0.9999
Non-pregnant			0.9917	0.7393
Pregnant				0.6296
Cord				

NRP-1	Male	Non-pregnant	Pregnant	Cord
Male		0.4527	0.2628	0.9962
Non-pregnant			0.8051	0.8301
Pregnant				0.6739
Cord				

Table 7.4: p values for SARS-CoV-2 receptors on classical monocytes.

ACE2	Male	Non-pregnant	Pregnant	Cord
Male		0.2727	0.3632	0.9904
Non-pregnant			0.6381	0.2332
Pregnant				0.5150
Cord				

ADAM17	Male	Non-pregnant	Pregnant	Cord
Male		0.9336	0.2942	0.1774
Non-pregnant			0.7371	0.6500
Pregnant				0.9522
Cord				

CD26	Male	Non-pregnant	Pregnant	Cord
Male		0.9518	0.7448	0.4150
Non-pregnant			0.8028	0.1607
Pregnant				0.5006
Cord				

CD147	Male	Non-pregnant	Pregnant	Cord
Male		0.6084	0.4372	0.4737
Non-pregnant			0.8565	0.9813
Pregnant				0.9882
Cord				

NRP-1	Male	Non-pregnant	Pregnant	Cord
Male		>0.9999	0.4029	0.9471
Non-pregnant			0.1348	0.8545
Pregnant				0.2803
Cord				

Table 7.5: p values for SARS-CoV-2 receptors on intermediate monocytes.

ACE2	Male	Non-pregnant	Pregnant	Cord
Male		0.3236	0.3857	0.9998
Non-pregnant			0.4663	0.3307
Pregnant				0.7125
Cord				

ADAM17	Male	Non-pregnant	Pregnant	Cord
Male		0.8980	0.4845	0.9613
Non-pregnant			0.8010	0.9894
Pregnant				0.5761
Cord				

CD26	Male	Non-pregnant	Pregnant	Cord
Male		0.9009	0.5345	0.9967
Non-pregnant			0.7176	0.6028
Pregnant				0.3922
Cord				

CD147	Male	Non-pregnant	Pregnant	Cord
Male		0.8510	0.9802	0.3628
Non-pregnant			0.8530	0.9283
Pregnant				0.8240
Cord				

NRP-1	Male	Non-pregnant	Pregnant	Cord
Male		0.3125	0.1996	0.9395
Non-pregnant			0.2470	0.8683
Pregnant				0.0893
Cord				

Table 7.6: p values for SARS-CoV-2 receptors on non-classical monocytes.

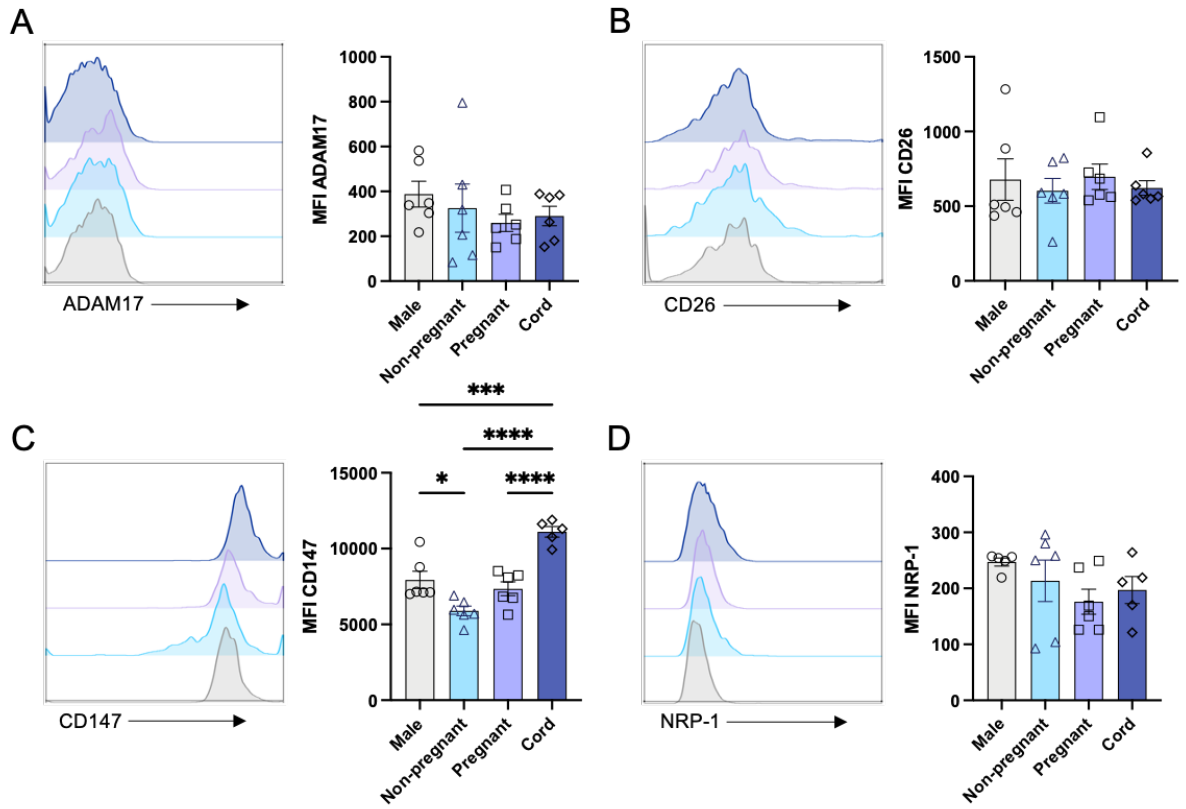

Figure 7.6: Expression of SARS-CoV-2 receptors on B cells in males, females, pregnant females, and neonates. B cells were identified from whole blood from males (M; n=6), non-pregnant females (F; n=6), pregnant (P; n=6) females and cord (C; n=6) and SARS receptor expression was analysed via flow cytometry as described in the Materials and Methods. Statistics were determined using a one-way ANOVA and a Tukey post-hoc test,, where $p < 0.05$ was deemed significant. The expression of SARS receptors which were analysed were: **(A)** ADAM17 (***B***) CD26 (***C***) CD147 (***D***) NRP-1.

ADAM17	Male	Non-pregnant	Pregnant	Cord
Male		0.9126	0.5472	0.7404
Non-pregnant			0.9001	0.983
Pregnant				0.9878
Cord				

CD26	Male	Non-pregnant	Pregnant	Cord
Male		0.9425	0.9989	0.9744
Non-pregnant			0.8942	0.999
Pregnant				0.9418
Cord				

CD147	Male	Non-pregnant	Pregnant	Cord
Male		0.0169	0.7751	0.0005
Non-pregnant			0.1161	<0.0001
Pregnant				<0.0001
Cord				

NRP-1	Male	Non-pregnant	Pregnant	Cord
Male		0.8065	0.2646	0.5859
Non-pregnant			0.7245	0.9705
Pregnant				0.9433
Cord				

Table 7.8: p values for the expression of SARS-CoV-2 receptors on B cells.

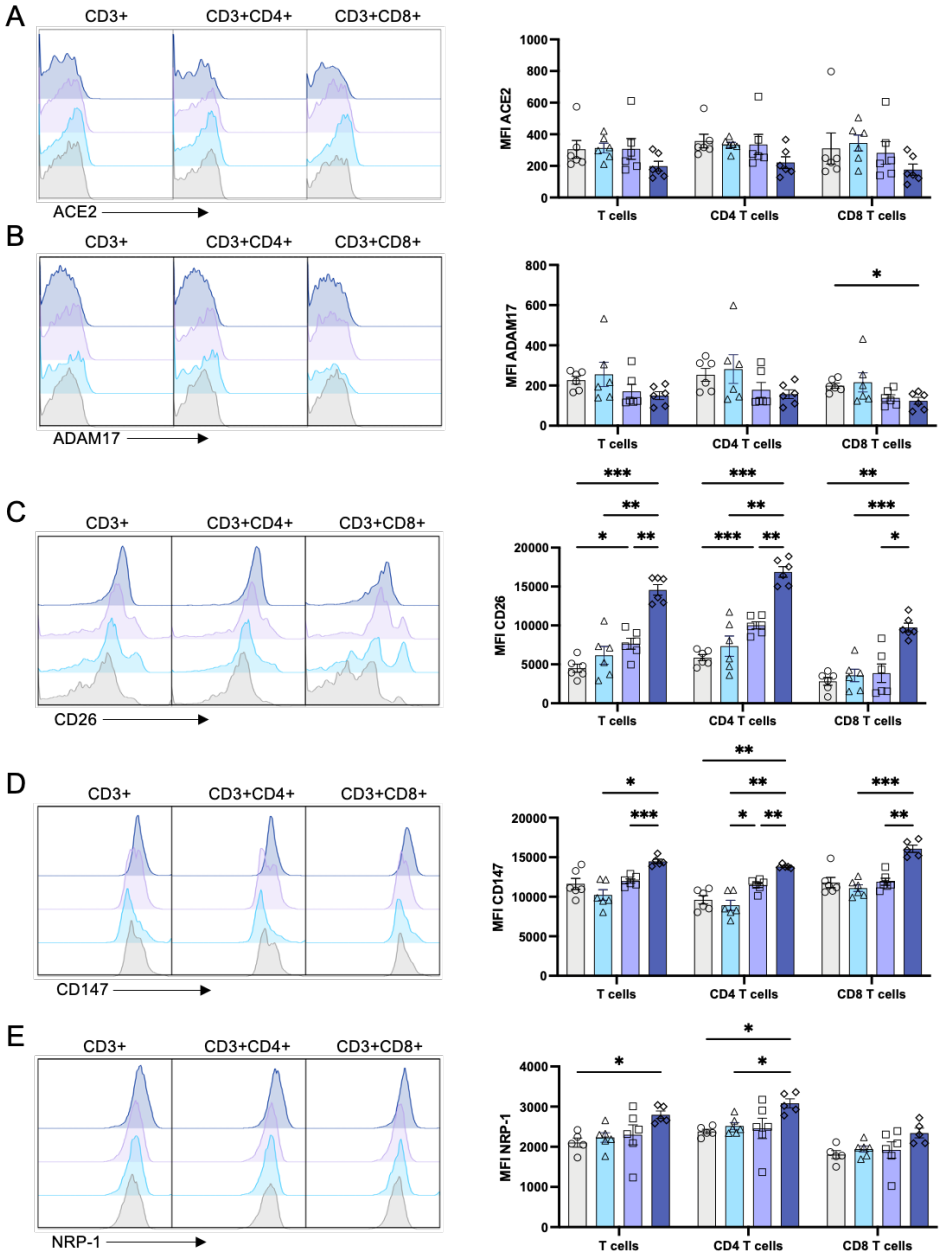

Figure 7.7: Expression of SARS-CoV-2 receptors on T cells in males, female, pregnant females, and neonates. T cells and their subsets were identified from whole blood from males (M; n=6), non-pregnant females (F; n=6), pregnant (P; n=6) females and cord (C; n=6) and SARS receptor expression was analysed via flow cytometry as described in the Materials and Methods. Statistics were determined using a two-way ANOVA and a Tukey post-hoc test,, where $p < 0.05$ was deemed significant. The expression of SARS receptors which were analysed were: **(A)** ACE2 **(B)** ADAM17 **(C)** CD26 **(D)** CD147 **(E)** NRP-1.

ACE2	Male	Non-pregnant	Pregnant	Cord
Male		0.9982	0.9998	0.5617
Non-pregnant			0.9996	0.1055
Pregnant				0.6288
Cord				

ADAM17	Male	Non-pregnant	Pregnant	Cord
Male		0.9473	0.3153	0.0650
Non-pregnant			0.5389	0.2762
Pregnant				0.9603
Cord				

CD26	Male	Non-pregnant	Pregnant	Cord
Male		0.6905	0.0233	0.0002
Non-pregnant			0.8092	0.0043
Pregnant				0.0061
Cord				

CD147	Male	Non-pregnant	Pregnant	Cord
Male		0.6518	0.9782	0.0894
Non-pregnant			0.1270	0.0120
Pregnant				0.0008
Cord				

NRP-1	Male	Non-pregnant	Pregnant	Cord
Male		0.8044	0.8232	0.0276
Non-pregnant			0.9951	0.0760
Pregnant				0.3075
Cord				

Table 7.9: p values for the expression of SARS-CoV-2 receptors on total T cells.

ACE2	Male	Non-pregnant	Pregnant	Cord
Male		0.9346	0.9148	0.2815
Non-pregnant			>0.9999	0.0568
Pregnant				0.5651
Cord				

ADAM17	Male	Non-pregnant	Pregnant	Cord
Male		0.9486	0.1237	0.0721
Non-pregnant			0.337	0.2978
Pregnant				0.9583
Cord				

CD26	Male	Non-pregnant	Pregnant	Cord
Male		0.7622	0.0007	0.0004
Non-pregnant			0.4035	0.0057
Pregnant				0.0022
Cord				

CD147	Male	Non-pregnant	Pregnant	Cord
Male		0.9061	0.1827	0.0077
Non-pregnant			0.0198	0.0078
Pregnant				0.0026
Cord				

NRP-1	Male	Non-pregnant	Pregnant	Cord
Male		0.6149	0.9896	0.0174
Non-pregnant			0.9961	0.0428
Pregnant				0.1861
Cord				

Table 7.10: p values for the expression of SARS-CoV-2 receptors on CD4 T cells.

ACE2	Male	Non-pregnant	Pregnant	Cord
Male		0.9819	0.9322	0.6544
Non-pregnant			0.7490	0.0817
Pregnant				0.6679
Cord				

ADAM17	Male	Non-pregnant	Pregnant	Cord
Male		0.9813	0.1240	0.0165
Non-pregnant			0.4325	0.3415
Pregnant				0.9482
Cord				

CD26	Male	Non-pregnant	Pregnant	Cord
Male		0.9241	0.8259	0.0031
Non-pregnant			0.9980	0.0006
Pregnant				0.0194
Cord				

CD147	Male	Non-pregnant	Pregnant	Cord
Male		0.8939	0.9996	0.0614
Non-pregnant			0.2672	0.0001
Pregnant				0.0023
Cord				

NRP-1	Male	Non-pregnant	Pregnant	Cord
Male		0.7847	0.8836	0.1145
Non-pregnant			0.9997	0.1226
Pregnant				0.3737
Cord				

Table 7.11: p values for the expression of SARS-CoV-2 receptors on CD8 T cells.

7.3.2 MNC sCD26 production in response to stimulation differs in pregnancy and in umbilical cord blood

Due to the significant differences in expression of SARS-CoV-2 receptors on the leukocytes between the groups analysed, it was vital to investigate if these cells shed or release soluble versions of the receptors. To do this, MNCs were left unstimulated for 24 hr or stimulated with either LPS, MDP, LPS and R848, POLY I:C or CytoStim ™. The only detectable soluble receptors of the ones studied were CD26 and CD147.

Mostly there was no significant effect of stimulation on the release of either CD26 or CD147 when compared to the unstimulated group (Figure 7.8; Table 7.12 - 9.13). Pregnant MNCs however were affected by LPS/R848 ($p = 0.0029$), POLY I:C ($p < 0.0001$) and CytoStim ™ ($p < 0.0001$) which all reduced the output of CD26 into the supernatant (Figure 7.8A; Table 7.12), and LPS/R848 which depleted CD147 ($p = 0.0289$; (Figure 7.8B; Table 7.13).

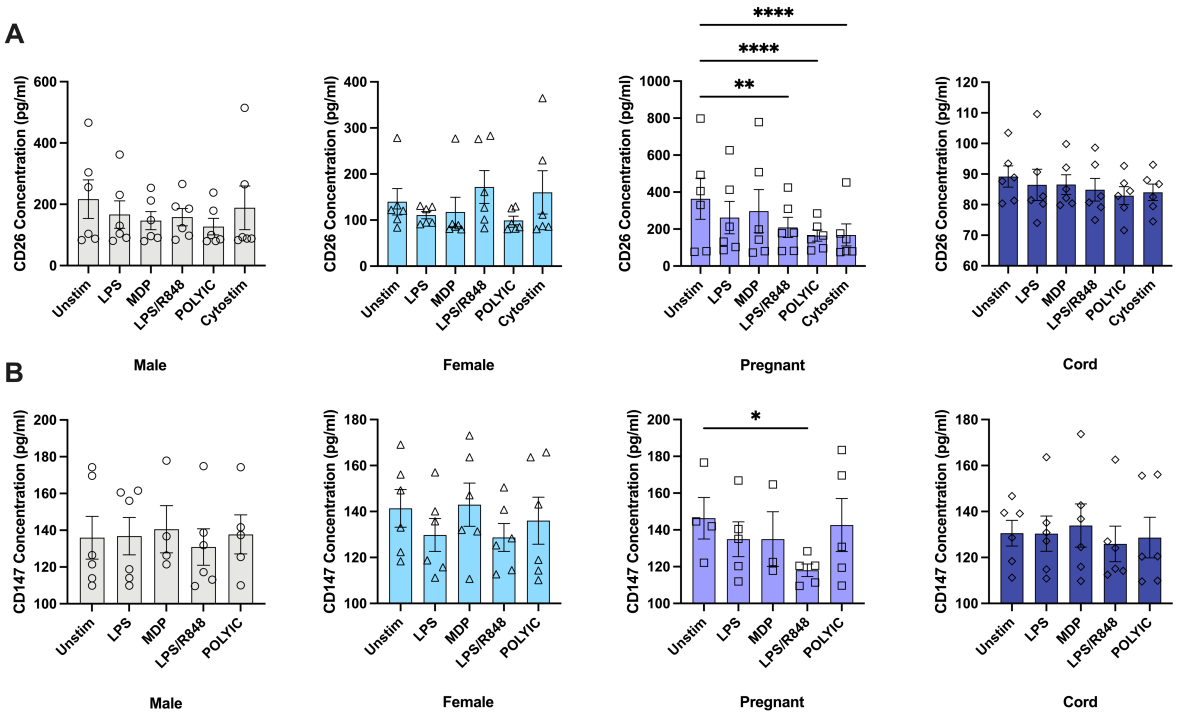

Figure 7.8: The effect of stimulation on the production of soluble receptors from MNCs in males, females, pregnant and cord. MNCs were stimulated with either LPS (L; n=6), MDP (M; n=6), LPS/R848 (LR; n=6), POLY I:C (P; n=6) or CytoStim ™ (C; n=6) and analysed with ELISAs as described in the Materials and Methods. Statistics were determined with a two-way ANOVA and a Tukey's post-hoc test, where the unstimulated (U) were identified as the control group, and a p value < 0.05 was deemed significant. Soluble receptors which were measured were: **(A)** CD26 and **(B)** CD147.

CD26

Male		Female		Pregnant		Cord	
LPS	0.8034	LPS	0.9776	LPS	0.1203	LPS	>0.9999
MDP	0.4987	MDP	0.9932	MDP	0.5425	MDP	>0.9999
LPS/R848	0.6823	LPS/R848	0.9660	LPS/R848	0.0029	LPS/R848	>0.9999
POLY I:C	0.2281	POLY I:C	0.9100	POLY I:C	<0.0001	POLY I:C	>0.9999
CytoStim	0.9805	CytoStim	0.9958	CytoStim	<0.0001	CytoStim	>0.9999

Table 7.12: p values for CD26 measurements in MNC unstimulated versus stimulated supernatants.

CD147

Male		Female		Pregnant		Cord	
LPS	>0.9999	LPS	0.4643	LPS	0.8854	LPS	>0.9999
MDP	0.9316	MDP	0.9993	MDP	0.9747	MDP	0.9891
LPS/R848	0.9512	LPS/R848	0.3720	LPS/R848	0.0289	LPS/R848	0.9621
POLY I:C	0.9968	POLY I:C	0.9386	POLY I:C	>0.9999	POLY I:C	0.9987

Table 7.13: p values for CD147 measurements in MNC unstimulated versus stimulated supernatants.

When unstimulated, the concentration of sCD26 (Figure 7.9A; Table 7.14) was lower in men compared to pregnant women (p = 0.0023) but elevated in comparison to neonatal MNCs (p = 0.0105). The pregnant women also had significantly higher concentrations of sCD26 when compared to non-pregnant women (p = < 0.0001) and neonates (p < 0.0001). sCD147 concentration in MNC supernatants was not significantly altered between any of the groups (Figure 7.9B; Table 7.14).

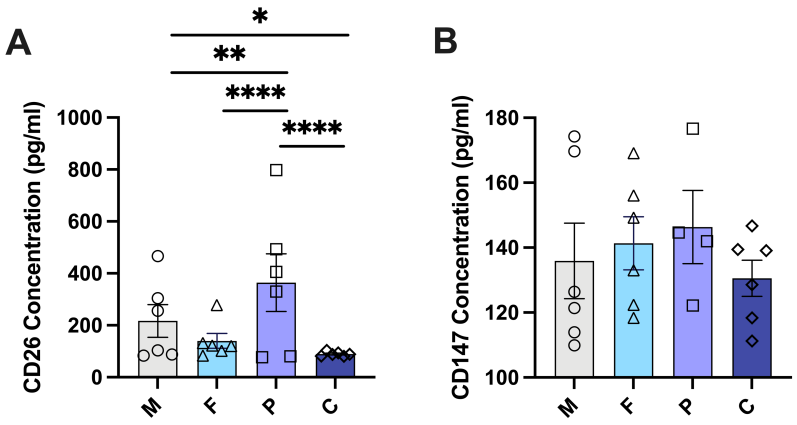

Figure 7.9: The secretion of soluble CD26 and CD147 from MNCs after 24hrs without stimulation. MNCs from males (M; n=6), non-pregnant females (F; n=6), pregnant females (F; n=6) and cord (C; n=6) were cultured unstimulated for 24 hr and supernatants were analysed for the presence of soluble receptors as described in the Materials and Methods. Statistics were performed using a two-way ANOVA and a Tukey's post-hoc test, where a p value < 0.05 was considered significant. Soluble receptors which were detected were: **(A)** CD26 and **(B)** CD147

CD26	Male	Non-pregnant	Pregnant	Cord
Male		0.2230	0.0023	0.0105
Non-pregnant			<0.0001	0.5835
Pregnant				<0.0001
Cord				

CD147	Male	Non-pregnant	Pregnant	Cord
Male		0.9220	0.9816	0.9252
Non-pregnant			0.9973	0.5976
Pregnant				0.7827
Cord				

Table 7.14: p values for CD26 and CD147 measurements in MNC unstimulated supernatants.

7.3.3 Plasma from cord blood and pregnant women's blood have variable CD147 and NRP-1 concentrations in comparison to not pregnant adults

Due to the secretion of soluble receptors from MNCs, the next step was investigating concentrations of the soluble receptors in the plasma of males, females, pregnant and cord. sACE2 was not detectable with all samples (Aviva systems biology). While not significant, sCD26 levels in the plasma of pregnant women is lower in comparison to non-pregnant women and men (Figure 7.10A; Table 7.15). Cord plasma is significantly richer in sCD147 in comparison to all other groups analysed ($p < 0.0001$; Figure 7.10B; Table 7.15). Pregnant plasma has significantly lower levels of sNRP-1 in comparison to male plasma ($p = 0.0030$) and cord plasma ($p < 0.0001$) (Figure 7.10C; Table 7.15).

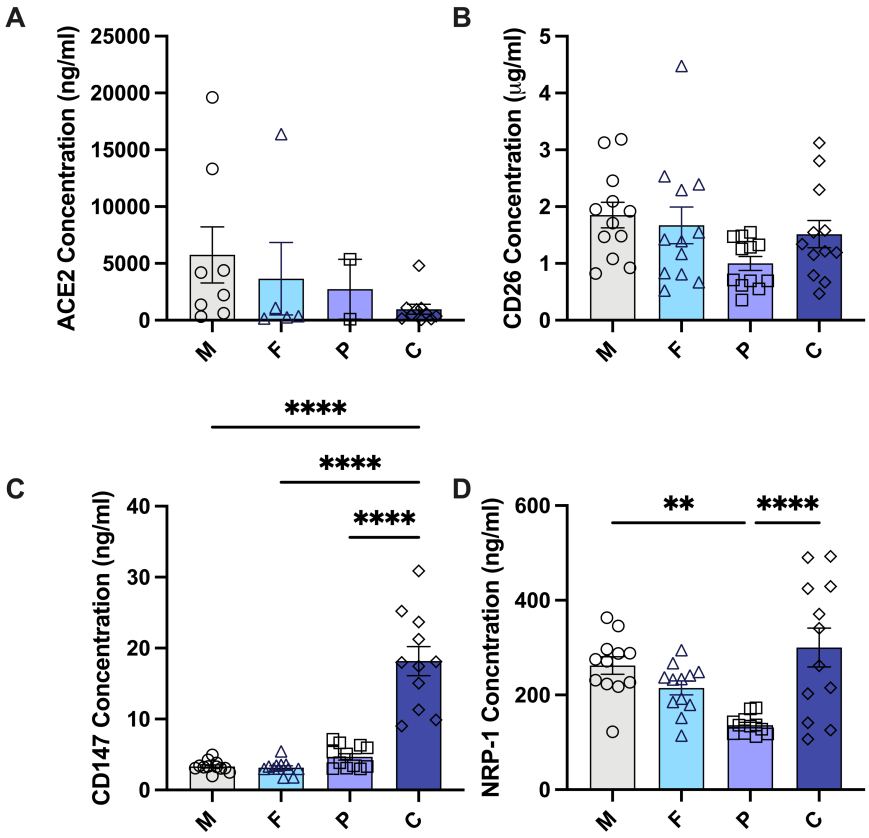

Figure 7.10: Plasma concentrations of soluble SARS receptors in males, females, pregnant females, and neonates. Plasma from men (M; n=12), non-pregnant women (F; n=12), pregnant women (P; n=12), and cords (C; n=12) were used for analysis to determine the concentration of SARS receptors as described in the Materials and Methods. Statistics were determined using a one-way ANOVA and a Tukey's post-hoc test,, where a $p < 0.05$ was deemed significant. The detectable concentrations of SARS receptors which were measured were: **(A)** ACE2 (n=8 M, n=5 F, n=2 P, n=10 C) **(B)** CD26, **(C)** CD147 and **(D)** NRP-1.

ACE2	Male	Non-pregnant	Pregnant	Cord
Male		0.8943	0.8838	0.2471
Non-pregnant			0.9966	0.7859
Pregnant				0.9718
Cord				

CD26	Male	Non-pregnant	Pregnant	Cord
Male		0.9506	0.0696	0.7506
Non-pregnant			0.2059	0.9660
Pregnant				0.4302
Cord				

CD147	Male	Non-pregnant	Pregnant	Cord
Male		0.9993	0.7699	<0.0001
Non-pregnant			0.6978	<0.0001
Pregnant				<0.0001
Cord				

NRP-1	Male	Non-pregnant	Pregnant	Cord
Male		0.5018	0.0030	0.6805
Non-pregnant			0.1092	0.0698
Pregnant				<0.0001
Cord				

Table 7.15: p values for ACE2, CD26, CD147 and NRP-1 measurements in plasma.

Isoforms, with their different glycosylation statuses, of these soluble receptors were detected using immunoblotting (Figure 7.11). It appears that ADAM17 and CD147 have different isoforms present in the plasmas, with the pregnant women having more of the smaller isoform of ADAM17 than the other groups.

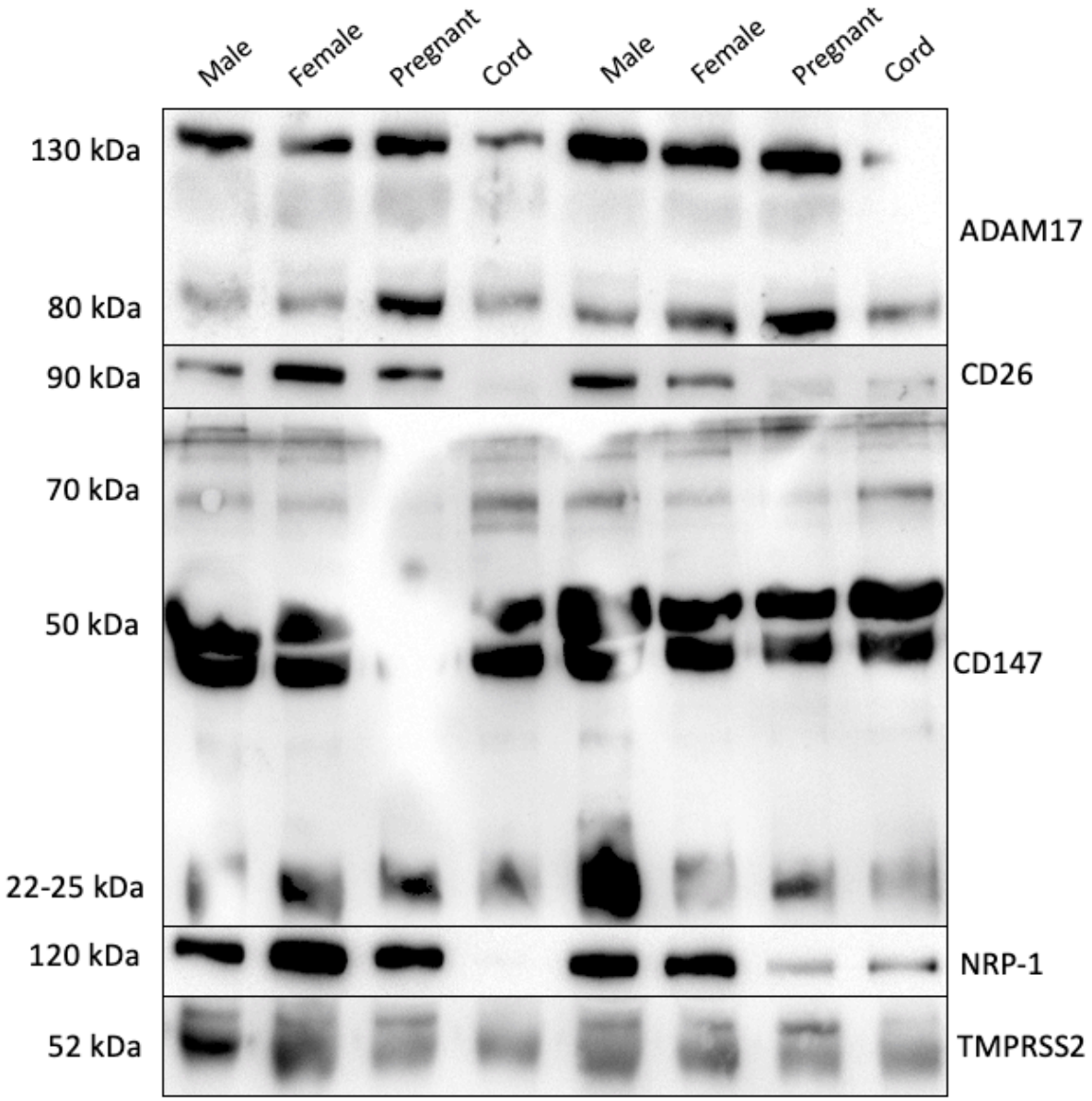

Figure 7.11: Analysis of the expression of different isoforms of soluble SARS-CoV-2 receptors in the plasma of males, females, pregnant females, and neonates, illustrated by western blotting. Plasma from males, females, pregnant females, and cord were diluted 1/10 and analysed for the presence of SARS receptors using western blotting as described in the Materials and Methods. Isoforms of ADAM17 can be observed at 80 kDa and 130 kDa, CD26 at 90 kDa, CD147 at 22-25 kDa, 50 kDa and 70 kDa, NRP-1 at 120 kDa and TMPRSS2 at 52 kDa.

7.3.4 The placenta, amnion and choriodecidua express both membrane-bound and soluble receptors linked to SARS-CoV-2 infectivity

The protection of the fetus is one of the key roles of the maternal-fetal interface. Due to the low rates of vertical transmission with SARS-CoV-2 [510, 511], it is imperative to understand this protective mechanism at the maternal-fetal interface. In addition, from the work described above, any differences in the expression of membrane-bound and soluble forms of the receptors have been predominantly related to the neonate. Therefore, it was deemed essential to determine if the placenta, amnion, and chorion decidua are a source of soluble receptors. Those which were detectable were: ACE2 (except for amnion), CD26, CD147 and NRP-1.

Firstly, to determine if the placenta contains these receptors, placental lysates were used to determine the concentrations expected. The placental tissue is rich in all molecules measured (Figure 7.12).

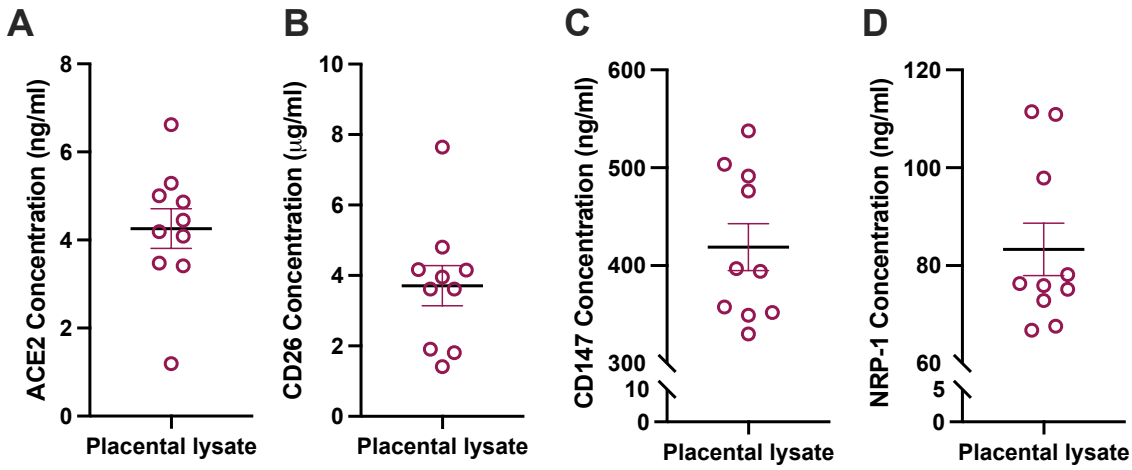

Figure 7.12: The concentration of the soluble receptors in placental lysates. The concentration of soluble SARS-CoV-2 host entry receptors was measured in placental lysates (n=10) using ELISAs (ng/ml or μg/ml). Molecules measured were: **(A)** ACE2, **(B)** CD26, **(C)** CD147 and **(D)** NRP-1.

Explants of placenta, amnion and chorion decidua were stimulated with either LPS, MDP, R848 or POLY I:C. The effect of stimuli on the export of soluble receptors was largely negligible, with an exception being the significant down-regulation of sNRP-1 on POLY I:C-stimulation of the placenta (Figure 7.13).

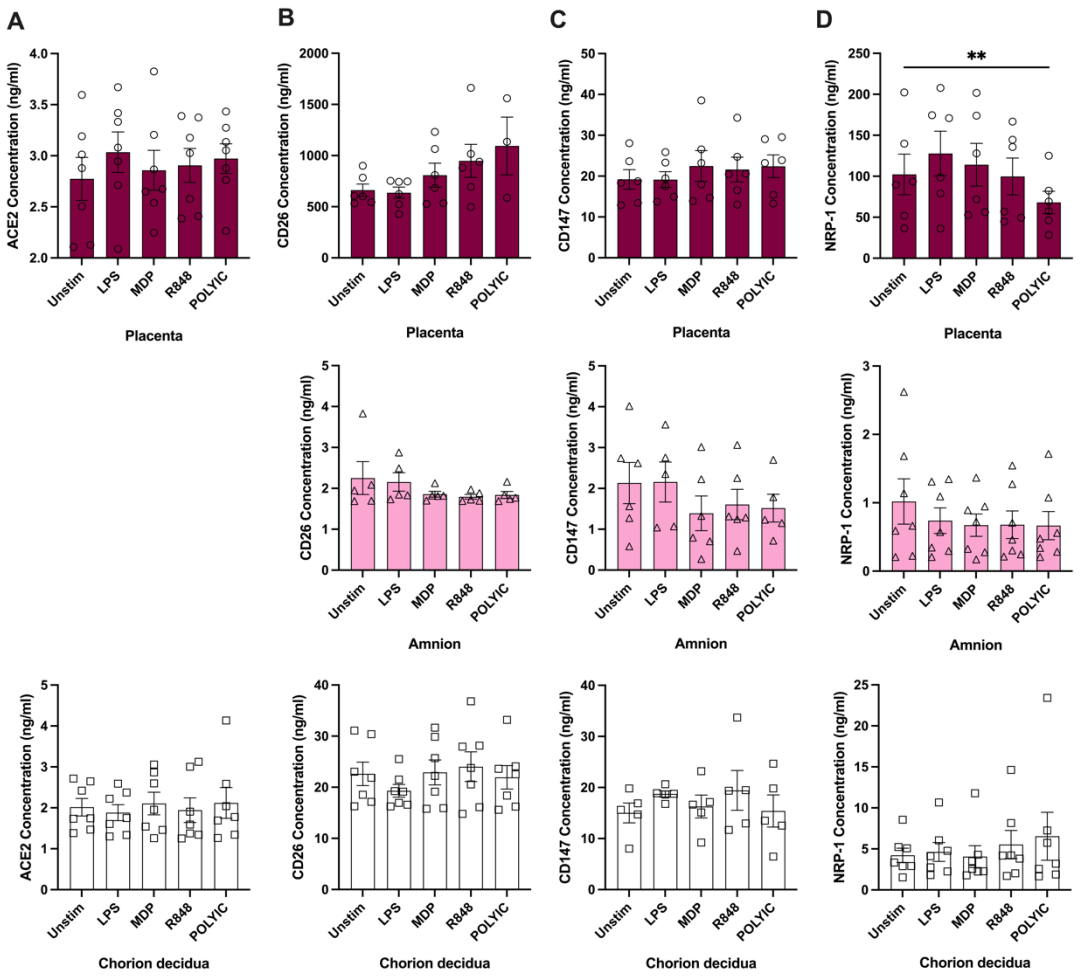

Figure 7.13: The effect of stimuli on the production of soluble SARS receptors by the placenta, amnion, and chorion decidua. Explants of placenta (n=6), amnion (n=6) and chorion decidua (n=6) were stimulated with LPS (L), MDP (M), R848 (R), OR POLY I:C (P) and analysed with ELISAs as described in the Materials and Methods. Statistics were determined with a two-way ANOVA and a Tukey's post-hoc test, where the unstimulated (U) were identified as the control group, and a p value < 0.05 was deemed significant. Soluble receptors which were measured were: **(A)** ACE2, **(B)** CD26, **(C)** CD147 and **(D)** NRP-1.

Placenta

ACE2		CD26		CD147		NRP-1	
LPS	0.7318	LPS	0.9879	LPS	>0.9999	LPS	0.0923
MDP	0.9943	MDP	0.3244	MDP	0.8747	MDP	0.9194
R848	0.9701	R848	0.5554	R848	0.8275	R848	>0.9999
POLY I:C	0.8804	POLY I:C	0.3730	POLY I:C	0.7951	POLY I:C	0.0068

Table 7.16: p values for SARS-CoV-2 soluble receptor measurements in unstimulated versus stimulated placental supernatants.

Amnion

CD26		CD147		NRP-1	
LPS	0.9983	LPS	>0.9999	LPS	>0.9999
MDP	0.8602	MDP	0.1134	MDP	>0.9999
R848	0.8103	R848	0.8652	R848	>0.9999
POLY I:C	0.8456	POLY I:C	0.2690	POLY I:C	>0.9999

Table 7.17: p values for SARS-CoV-2 soluble receptor measurements in unstimulated versus stimulated amnion supernatants.

Chorion decidua

ACE2		CD26		CD147		NRP-1	
LPS	0.9704	LPS	0.2788	LPS	0.4723	LPS	>0.9999
MDP	0.9926	MDP	0.9971	MDP	0.9814	MDP	>0.9999
R848	0.9969	R848	0.7760	R848	0.8768	R848	>0.9999
POLY I:C	0.9875	POLY I:C	0.9905	POLY I:C	>0.9999	POLY I:C	>0.9999

Table 7.18: p values for SARS-CoV-2 soluble receptor measurements in unstimulated versus stimulated chorion decidual supernatants.

The unstimulated samples could be used to reveal the maternal-fetal interface is a rich source of soluble receptors (Figure 7.14). The placenta is the most potent source, exhibiting a higher concentration of CD26, CD147 and NRP-1 in comparison to the amnion ($p = 0.0004$; $p = 0.0029$; $p < 0.0001$) which is devoid of sACE2, and a greater source of ACE2, CD26 and NRP-1 when compared to the choriodecidua ($p = 0.0075$; $p = 0.0002$; $p < 0.0001$). The amnion is the poorest source of all soluble receptors measured in comparison to the placenta and the choriodecidua (CD26 $p = 0.0012$; CD147 $p = 0.0090$).

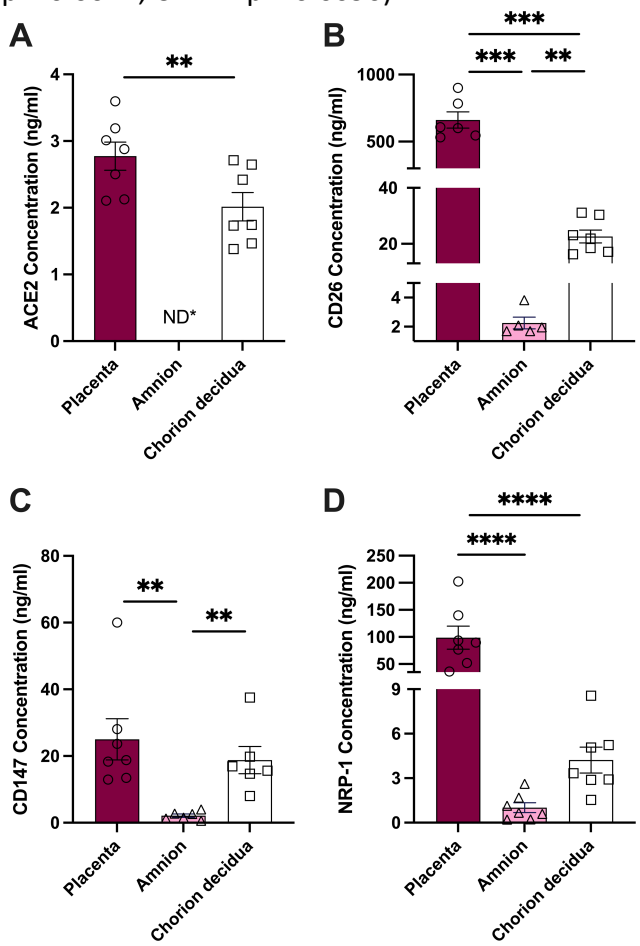

Figure 7.14: The production of soluble SARS receptors by the placenta, amnion, and chorion decidua. Explants were produced from placenta (P; n=6), amnion (A; n=6) and chorion decidua (C; n=6), and the unstimulated supernatants were analysed for soluble SARS receptor concentrations as described in the Materials and Methods. Statistics were determined using a one-way ANOVA and a Tukey's post-hoc test, where a $p < 0.05$ was deemed significant. Soluble receptors which were measured were: **(A)** ACE2 where levels were not detectable (*ND) in supernatants, but were for placenta and chorion decidua ($p = 0.0075$), LPS ($p < 0.0001$), **(B)** CD26 (P vs A $p = 0.0004$; P vs C $p = 0.0002$; A vs C $p = 0.0012$), **(C)** CD147 (P vs A $p = 0.0029$; P vs C $p = 0.4780$; A vs C $p = 0.0090$), **(D)** NRP-1 (P vs A $p < 0.0001$; P vs C $p < 0.0001$; A vs C $p = 0.9797$).

7.3.5 Amniotic fluid and breast milk are rich in soluble receptors

Expanding on the investigation into the protection of the fetus and the neonate, after determining that the maternal-fetal interface is rich in the production of soluble receptors, exploration of the presence of these in amniotic fluid and breast milk was performed. Amniotic fluid from 37+ weeks of gestation, and breast milk from 2 weeks and 6 weeks postpartum were compared to investigate the levels of soluble receptors ingested by the fetus/neonate and, in the case of amniotic fluid, also aspirated.

Figure 7.15 illustrates the high levels of sACE2, sCD26, sCD147 and sNRP-1 in amniotic fluid and breast milk. The breast milk has higher concentrations of sACE2 (Figure 7.15A; Table 7.19) and sNRP-1 (Figure 7.15D) at both 2-weeks ($p = 0.0004$; $p < 0.0001$) and 6-weeks ($p < 0.0001$; $p = 0.0005$) postpartum in comparison to amniotic fluid. The concentration of sNRP-1 was significantly lower in 2-weeks compared to 6-weeks postpartum breast milk ($p < 0.0001$). sCD26 levels (Figure 7.15B) were significantly elevated in amniotic fluid in comparison to breast milk at 2-weeks ($p < 0.0001$) and 6-weeks post-partum ($p < 0.0001$). There were no significant differences in the concentration of sCD147 between amniotic fluid and breast milk (Figure 7.15C).

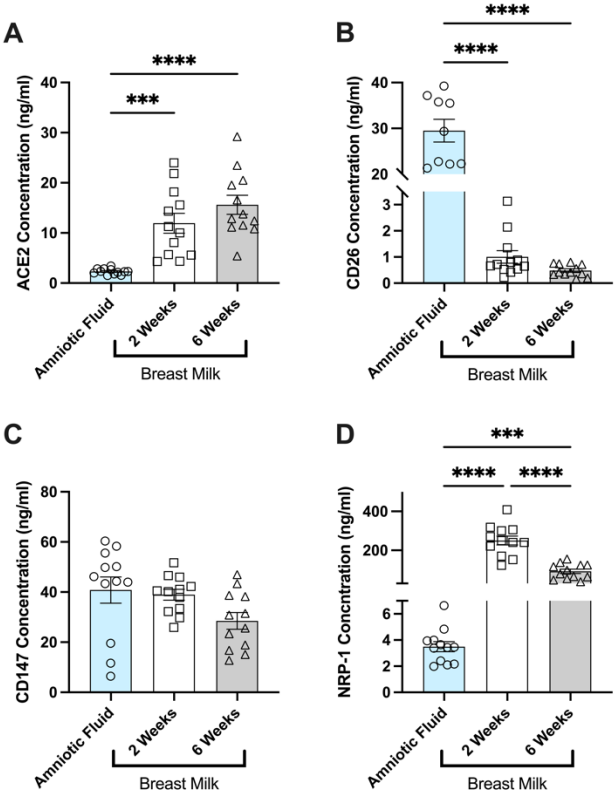

Figure 7.15: Concentrations of soluble receptors in amniotic fluid (AF) and breast milk (BM) at 2-weeks and 6-weeks postpartum. Soluble receptors were measured in AF (n=12) and BM (n=12) using ELISAs as described in the Materials and Methods. Statistics were performed using a one-way ANOVA and a Tukey's post-hoc test, whereby a p value < 0.05 determined significance. Some of the soluble receptors which were measured were not detectable in these samples (i.e. ADAM17). Soluble receptors which were detectable included: **(A)** ACE2, **(B)** CD26, **(C)** CD147 and **(D)** NRP-1.

ACE2	AF	BM2WK	BM6WK	CD26	AF	BM2WK	BM6WK
AF		0.0004	<0.0001	AF		<0.0001	<0.0001
BM2WK			0.2425	BM2WK			0.9434
BM6WK				BM6WK			
CD147	**AF**	**BM2WK**	**BM6WK**	**NRP-1**	**AF**	**BM2WK**	**BM6WK**
AF		0.9368	0.0709	AF		<0.0001	0.0005
BM2WK			0.1414	BM2WK			<0.0001
BM6WK				BM6WK			

Table 7.19: p values for the measurement of SARS-CoV-2 receptors in amniotic fluid (AF) and breast milk (BM) at 2-weeks (2WK) and 6-weeks (6WK) postpartum.

The expression of different isoforms of soluble receptors was detectable via western blotting: ACE2, ADAM17, CD26, CD147, GRP78, NRP-1 and TMPRSS2. The intensity of the bands (typically reflecting levels of receptors) does not confirm that observed by the ELISAs, except for NRP-1 and CD147. However, different isoforms of ACE2, ADAM17, CD26, CD147, GRP78 and TMPRSS2 are observed where typically breast milk exhibits greater variety of isoforms especially for CD147 and preferential expression of any higher molecular weight (MW) isoforms than amniotic fluid, excluding CD26 where the breast milk has a lower MW isoform.

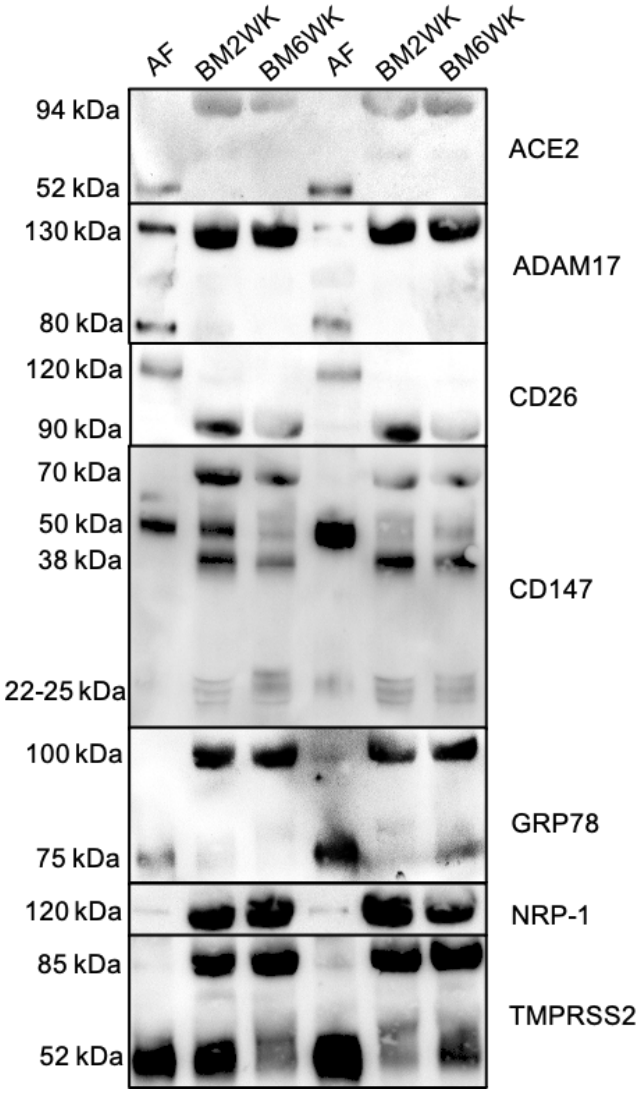

Figure 7.16: Western blot images of receptors associated with SARS-CoV-2 infectivity in amniotic fluid and breast milk at 2- and 6-weeks postpartum. Amniotic fluid and breast milk samples were analysed for soluble receptor expression using western blotting as described in the Materials and Methods. Receptors visualised are: ACE2 (70 kDa, 100 kDa), ADAM17 (80 kDa, 130 kDa), CD26 (90 kDa, 120 kDa), CD147 (22-70 kDa), GRP78 (75 kDa, 100kDa), NRP-1 (120 kDa) and TMPRSS2 (52 kDa, 85 kDa).

7.4 Discussion

While the differences between male and female, non-pregnant and pregnant were not particularly exciting, the data surrounding the abundance of these soluble receptors at the maternal-fetal interface, and in the neonatal environment reveals potential protective mechanisms against SARS-CoV-2.

In previous epidemics SARS-CoV and MERS-CoV illustrated immune cell infectivity [568, 569]. Whether SARS-CoV-2 can also infect leukocytes remains poorly understood, though studies so far have suggested that monocytes, CD4 and CD8 T cells, and B cells are susceptible [570]. Infection of these cells in the previous epidemics induced lymphopenia due to the direct virus destruction of lymphocytes [569], and aberrant cytokine production in monocytes and macrophages [571-574], which could be a driver of the cytokine storm common in severe SARS-CoV-2 patients [391]. Lymphocytopenia has also been reported to be a marker for severe SARS-CoV-2 infection [575, 576]. Aside from the expansion of disease severity, the infection of leukocytes has been theorised to act as "Trojan horses" by transporting the virus from entry sites in the respiratory tract to secondary infection sites [570, 577]. Due to the weak expression of primary SARS-CoV-2 entry receptor ACE2 on leukocytes, it has been speculated that viral entry might depend on other receptors. Pontelli et al. have illustrated that the infection of SARS-CoV-2 in PBMCs is not dependent on TMPRSS2 and that they can also be infected independently of ACE2 [570]. Since CD26 and CD147 have both been described to act as receptors for viral entry into the cell, these along with ADAM17 and NRP-1 which can facilitate viral entry, are key molecules to investigate.

The investigation into the expression of receptors involved in SARS-CoV-2 infectivity on leukocytes from adult male, female, pregnant women, and the neonate led to the observation that for the innate immune subsets, namely monocytes and neutrophils, there was little difference in expression. The leukocytes involved in the adaptive immune response, however, illustrate significant differences specifically regarding the expression of CD26 and CD147. While ADAM17 and NRP-1 expression on CD8 T cells and CD4 T cells were significantly different between adults and neonates, these differences were not as stark as for CD26 and CD147 on T cells and for CD147 on B cells.

The function of CD26 on T cells has been widely studied and discussed. It is more predominantly expressed on CD4 than CD8 T cells as confirmed here and can induce T-cell activation and cytotoxic activity [578]. Its enzymatic function involves the cleavage of polypeptides to amino terminal (L-proline or L-alanine) dipeptides [578]. It can be speculated that a higher expression of CD26 correlates to more severe infection of the T cells with SARS-CoV-2. Results here have illustrated no differences in CD26 expression between genders in adults, but significantly elevated CD26 expression in pregnant women compared to males in CD3 and CD3/CD4 T cells, and a significant increase of expression on all subsets of T cells between the cord and other groups measured. Other studies have also shown the higher expression of CD26 T cells in comparison to adult T cells [579]. As one of its roles inactivates GLP1, the reduced cytokine response by cord T cells could be partially due to the CD26 expression [579].

CD147 plays a vital role in extracellular matrix, fetal and lymphocyte development [580]. Increased expression of CD147 on lymphocytes has been associated with their activation [581, 582]. In reports discussing the infectivity of lymphocytes by SARS-CoV-2, CD147 is more commonly discussed due to the low expression of ACE2 on leukocytes [583]. The data shown here illustrates that CD147 on B cells demonstrates a sex-specific level of expression, with males expressing significantly more than non-pregnant females. CD147-related genes have been shown to be more highly expressed on male peripheral leukocytes than female [445]. B cells and all T cell subsets from cord blood also had significantly higher expression of CD147 than other groups measured. Its expression was also elevated on CD4 T cells from pregnant women when compared to non-pregnant women. While studies have not investigated CD147 expression in the neonate, studies have observed a higher expression of CD147-related genes on MNCs in infants (5-36 months) compared to adolescents and adults [445].

The elevated expression of CD26 on the neonatal T cells, together with the augmented expression of NRP-1, suggest that the lymphocytes of the neonate are more susceptible to viremia. Despite this, neonatal SARS-CoV-2 infection and vertical transmission are exceedingly rare [503]; however this is more likely due to the protection which the placenta offers. Additionally, the implications shown here which suggests that adult leukocytes are at lower risk of viremia, is augmented by studies showing that plasma viremia is uncommon,

occurring only in 13% of outpatients and 27% of hospitalised patients formally diagnosed with COVID-19 [584]. Furthermore, the localisation of SARS-CoV-2 is predominantly in the lungs, together with the lack of viremia suggests a reduced capability to infect other organs [585]. The chances of the virus then to even reach the maternal-fetal interface are low before even the likelihood of vertical transmission. Studies to formally assess the infectivity of neonatal versus adult T cells will clarify if altered expression of CD26 and NRP-1 make neonatal T cells more or less susceptible to infection. An alternative contributing factor to protection of the neonate from infection are high levels of soluble versions of SAR-CoV-2 receptors (i.e., ACE2, CD26, CD147 has already been discussed) that are linked with protection from viral infection by competitively inhibiting the virus from binding to membrane-bound receptors [586-589].

Soluble versions of the receptors/enzymes can be secreted or shed by cells such as leukocytes and epithelial cells. To investigate the release of these receptors by leukocytes from the different study groups, MNCs were left unstimulated for 24 hr or exposed to stimuli: LPS, MDP, LPS/R848, POLY I:C or CytoStim ^{TM}. In general, stimuli had no effect on the release of CD26 or CD147. Interestingly however, the MNCs from pregnant women had significantly less CD26 when exposed to LPS/R848, POLY I:C and CytoStim ^{TM}, and less CD147 upon LPS/R848 stimulation. POLY I:C simulates the response to viral infections. This data suggests that the MNCs from pregnant women might become more sensitive to infection as their ability to secrete soluble versions of these molecules becomes inhibited. The MNCs from pregnant women did however secrete significantly more CD26 than the other groups measured. This could be since leukocytes during pregnancy are typically more activated or permeable. The neonatal MNCs also had significantly lower soluble CD26 in comparison to adult males, despite having heightened membrane-bound forms possibly suggesting reduced shedding and retention of the membrane bound form. This has been found to be the case with other molecules such as reduced L-selectin shedding by neutrophils in the neonate [590, 591]. Nargis et al [592] have identified kallikrein-related peptidase 5 (KLK5) to be the enzyme responsible for the cleavage of CD26 from T cells. To determine if the neonatal T cells do retain their membrane bound form of CD26, investigation into the activity of KLK5 would be rational.

To investigate if these findings translate systemically, the next logical step was to measure the plasma levels of sACE2, sADAM17, sCD26, sCD147 and sNRP-1. sACE2 and sADAM17 were

not detectable with the ELISA kits utilised. Despite no difference in MNC secretion, plasma from the cord is significantly richer in CD147 in comparison to adults and pregnant women. This suggests that another source would be responsible for these circulating levels, such as the placenta. These higher levels of sCD147 in the plasma could offset the theorised increased susceptibility to viremia of the neonate noted above.

Significant lower sNRP-1 was found in pregnant women in comparison to men and neonates. A study involving the investigation of women with PCOS and the correlation between plasma NRP-1 and SARS-CoV-2 susceptibility, indicated a negative correlation [467]. While this is the only study which explored such a correlation, it suggests from the findings in this present study that pregnant women are more susceptible to COVID-19. The mechanisms of these soluble molecules and their potential protective role is very complex, and is unlikely due to a single molecule, but rather a combined effect. This would require formal testing of these biological fluids, or isolation of these soluble molecules, with inhibition assays to confirm.

To further determine the source of protection of the fetus and how the maternal-fetal interface might prevent vertical transmission, placental lysates (untreated at time 0) and explants of the placenta, amnion and chorion decidua were left unstimulated for 24 hr or stimulated with either LPS, MDP, R848 or POLY I:C. The high concentrations observed of CD147 and NRP-1 in the placental lysates could translate to the high levels observed in the cord. The placenta is a particularly concentrated source of CD26, where the average concentration was 3.71 µg/ml. As seen with the MNCs, the secretion of these molecules is largely unaffected by stimuli. The exception here, was the reduced concentrations of NRP-1 in the supernatant from placenta upon interaction with POLY I:C; this could represent the reaction one would observe with SAR-CoV-2. The unstimulated data clearly shows that the placenta, choriodecidua and amnion are, in descending order a rich source of soluble ACE2, CD26, CD147 and NRP-1. Blotting of the placental lysates has proved difficult, and optimisation is currently underway. IHC data has also been held up due to staff shortages with the histology department due to COVID-19.

Samples of amniotic fluid (AF) collected at full term (>37 weeks of gestation) and breast milk (BM) at 2 weeks (2W) and 6 weeks (6W) postpartum that were archived preceding the COVID-19 pandemic were available for analysis. Immunoassays revealed that both AF and BW were rich with sACE2, sCD26, sCD147 and sNRP-1, with BM having significantly higher levels of sACE2 and sNRP-1 than AF, but lower sCD26. Immunoblotting analysis provided further information revealing different isoforms in AF compared to BM. The lower molecular weight (MW) form of CD26 is typically associated with the shed version of the membrane-bound form compared to the higher MW of the naturally occurring soluble form [593] suggesting that BM sCD26 originates by shedding and probably from mammary epithelial cells which are rich in CD26 [594]. These two isoforms have shared and distinct properties, which may affect its ability to bind SARS-CoV-2. The shorter isoform of ACE2 (predominantly found on airway epithelial cells) has been shown to lack SARS-CoV-2 spike high-affinity binding sites [595]. This would suggest that the sACE2 in AF would be less efficient than in BM in acting as a viral decoy. Other molecules involved in SARS-CoV-2 cell entry were distinguishable by immunoblotting: ADAM17, GRP78, and TMPRSS2. These molecules also had isoforms which followed a similar pattern whereby the smaller isoform was more prevalent in the amniotic fluid and the larger isoform in the breast milk. Little is known about the ADAM17 isoforms, but the smaller isoform of GRP78, GRP78va is characterised as a cytosolic protein which is involved in the regulation of PKR-like endoplasmic reticulum kinase (PERK) in response to ER stress [596]. The TMPRSS2 isoforms have been more well characterised in terms of virus (SARS, MERS) activation where the isoforms have been classed as TMPRSS2 isoform 1 and TMPRSS2 isoform 2 [597]. Using the immunoblotting characterisation of these isoforms in the study by Zmora et al [597] it appears as though breast milk contains isoform 1 and amniotic fluid isoform 2. It has been shown that it is isoform 1 which activates the S-spike protein for viral entry into a cell [597].

These results suggest that both AF and BM are rich in soluble SARS-CoV-2 associated molecules that could play a role in protecting the fetus and neonate from infection with SARS-CoV-2 by acting as decoy receptors (Figure 7.17). Future work should focus on evaluating if AF and BM inhibit viral entry into host cells and comparing the relative efficacy of different isoforms in this. If this proves successful, this will reveal a novel protective mechanism for the baby against SARS-CoV-2 and provide further evidence for a protective role for breastfeeding.

Two models were attempted. One involved isolating monocytes and neutrophils and making use of a SARS-CoV-2 Spike protein His-Tag to visualise infection on the flow cytometer in the presence of amniotic fluid, breast milk, placental lysates, and the different plasmas. However, the Spike protein used primarily bound to ACE2, which is present only in small amounts on these leukocytes in comparison to the other receptors. Another model involved the use of airway epithelial cells (VeroE6), where the bodily fluids utilised in this chapter were sent to Dr Rich Stanton in Cardiff University. This assay exposes the epithelial cells to SARS-CoV-2 (229E) and measures the level of infection. By adding the bodily fluids, it should have been possible to determine if the soluble receptors inhibit the virus from entering the cells. However, the bodily fluids either killed the monolayer at higher concentrations or left the cells unhealthy in lower concentrations. This assay has limitations, especially regarding the breast milk and amniotic fluid investigations. Epithelial cells are typically exposed to a flow of these fluids rather than being in stasis. A model where the fluids could flow past the epithelial cells may be beneficial. Isolating the different isoforms of the receptors would also reveal their different properties and could determine their different capabilities of binding to the virus and postulating as a decoy receptor in soluble form.

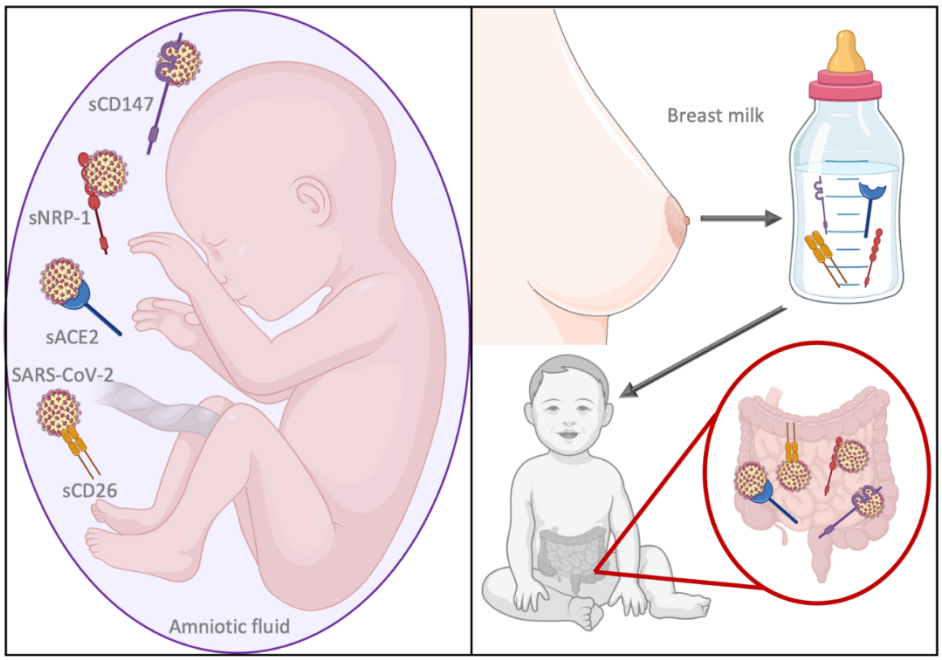

Figure 7.17: The potential protective mechanisms of amniotic fluid and breast milk against novel coronavirus SARS-CoV-2. Amniotic fluid and breast milk are both rich in soluble receptors such as ACE2, CD26, CD147 and NRP-1 which the fetus and neonate ingest. They may act as decoy receptors for the virus, conferring resistance to the baby. This image was created with BioRender ©

7.5 Conclusion

There appears to be no significant differences based on sex and little change with pregnancy with regards to soluble SARS-CoV-2 receptors. However, the maternal-fetal interface has potential mechanisms to protect the fetus from contracting SARS-CoV-2 by being rich with soluble versions of receptors which are involved in host cell entry of the virus, thereby limiting infection of host cells. The placenta, amniotic fluid and fetal circulation during intrauterine life and then breast milk postnatally are rich in these receptors that might act as decoys for the virus to confer resistance to SARS-CoV-2 and COVID-19 in the baby. Further work will determine the ability of these soluble receptors and their isoforms to act as SARS-CoV-2 traps.

Chapter 8 - General Discussion

8.1 Overview

This thesis has clearly presented novel findings in how the immune system adapts in pregnancy to ensure a successful outcome, and how risk factors such as obesity can sabotage this carefully controlled system. Key findings have included: novel methods for the analysis of lipids in plasma, serum and cells; pregnancy programmes late gestation monocytes by downregulating their metabolic capabilities whilst enhancing phagocytosis; monocytes are also effected at earlier gestation, and may have different metabolic capabilities at this stage; obesity disrupts the carefully controlled immunity of pregnancy at 28 weeks and becomes Th1/Th17 skewed; and the neonate may be protected by soluble SARS-CoV-2 receptors which could act as decoy traps for the virus.

8.2 Monocyte changes occur earlier in gestation than at term, with some showing the same trend and others showing the reverse

While one of the aims of this project was to determine at which stage of gestation monocytic adaptations occurred, this was not entirely possible due to COVID-19. The best that was possible used MNCs rather than isolated monocytes at 26-28 weeks of gestation. Due to this, it is difficult to draw conclusions from the comparison between the monocytes at this stage and at term, especially regarding the difficulty in distinguishing the intermediate subset in the isolated monocytes at term. However, it does provide an indication of where to focus the next stage of the study.

CD36 is elevated at both stages of pregnancy investigated; with an increase also observed with CD64 in the intermediate monocytes at 28 weeks, and CD16+ and CD16- monocytes at term. This could suggest increased phagocytic abilities earlier in pregnancy as observed at 28 weeks as well as at term as shown. CD38 is another marker which is elevated at both stages of pregnancy and has been suggested to facilitate phagocytosis [598]. An increase in CD36 could also implicate elevated lipid storage and utilisation at 28 weeks, even though this does not occur at term. To investigate this, the use of the BODIPY and pHrodo dyes would be beneficial. The expression of CD98 at 28 weeks (increased) is the reverse of what is observed at term (decreased). This suggests that the monocytes are likely to be more dependent on amino acids earlier in gestation and this can be assessed using methods outlined in Chapter 4.

Most interesting is the apparent flip in mitochondrial content: at 28 weeks of gestation, the monocytes of pregnant women have more mitochondria than those of non-pregnant women, but at 37+ weeks this pool is significantly depleted to be less than that of the monocytes from non-pregnant women. This suggests that at the earlier gestational stage, the monocytes might be more capable of mitochondrial respiration which would translate to improved functional abilities. The maternal immune system might be more dependent on monocytes at 28 weeks, whereas at term they may have become exhausted. Future work should isolate monocytes at 28 weeks to illustrate their OXPHOS capabilities, and cytokine and lipid mediator output. It would be ideal to track changes in monocytes in the same women from prior to conception to the postpartum to understand when these changes occur, and the implications of this. A comparison of monocytes at term with caesarean section deliveries (shown here) versus labouring deliveries might also show a different phenotype.

8.3 A comparison between pregnancies which are healthy versus complicated with obesity, and how this compares to the non-pregnant immunological profile

While *Chapter 6 – Maternal body mass index is associated with an altered immunological profile at 28 weeks of gestation,* clearly illustrated the effect obesity has on the maternal immune system in comparison to a healthy pregnancy, it was not discussed in terms of how the healthy pregnancy itself differs from the non-pregnant environment.

Key cytokines are reduced in their secretion from healthy pregnant LPS/R848-stimulated MNCs at 28 weeks in comparison to the non-pregnant MNCs: IL-1β ($p = 0.0041$), IL-8 ($p = 0.0270$), and IL-10 ($p = 0.0214$). In contrast, these cytokines were observed to be elevated in the LPS/R848-stimulated MNCs from pregnancies with obesity: IL-1β ($p = 0.0489$), IL-8 ($p = 0.0922$), IL-10 ($p = 0.0408$). While the IL-8 increase is not quite significant, together with the IL-1β and IL-10 it does showcase how the MNCs from pregnancies with obesity struggle to adapt to the maternal environment by mimicking the non-pregnant environment more closely than it does that of healthy pregnancy. A study that follows monocyte phenotype and function from pre-conception to the postpartum should include normal weight and obese women to really understand the effects of obesity on monocyte behaviour in pregnancy.

The depletion of mitochondria in the monocytes of obese pregnant women further consolidates the suggestion that obese pregnant women struggle to establish the appropriate monocyte phenotype. As discussed, during a healthy pregnancy at 28 weeks of gestation monocytes have an elevated pool of mitochondria in comparison to the monocytes of non-pregnant women. That the monocytes from pregnancies complicated with obesity imitate the ones from a non-pregnant woman or perhaps a late pregnant woman who shows fewer mitochondria as shown in Chapter 4, further implies that the monocytes in particular struggle to meet the metabolic and functional requirements that pregnancy dictates if the pregnant woman is obese. While no difference was observed in the bioenergetics of MNCs, isolating monocytes from women with problematic pregnancies may reveal a bioenergetic profile that resembles the non-pregnant monocytes more closely than that expected from a healthy pregnancy.

8.4 SARS-CoV-2 and pregnancy

Outlined in 1.2.7 Novel coronavirus SARS-CoV-2 and pregnancy, and *Chapter 7- The potential protective effects of pregnancy against novel coronavirus SARS-CoV-2*, it has been discussed how the risk of severe infection in pregnancy is no different to a non-pregnant woman, but in cases where severe infection has occurred results in adverse obstetric outcomes such as miscarriage and preeclampsia [516]. Chapter 7 discussed in length the potential protective effects soluble SARS-CoV-2 receptors have by acting as decoy receptors. It was found that these were particularly rich in elements relating to the neonate (cord plasma, amniotic fluid, placenta, and breast milk), which consolidates the low risk associated with the neonate [503, 510]. As discussed earlier, isolating the different isoforms of the soluble receptors from amniotic fluid and breast milk could reveal different viral binding affinities and action as a decoy receptor. However, few differences were found in the mother's systemic environment compared to the non-pregnant women. *Chapter 6* also illustrated relatively no correlation with BMI and the concentration of soluble CD26 and CD147, and minimal change of soluble NRP1 in the plasma of pregnant women. This was surprising as obesity has been well documented as a risk factor for developing severe illness in pregnancy with SARS-CoV-2 [167]. However, the finding that the mother's immune system becomes biased to a Th1/Th17 environment when complicated with obesity during pregnancy, may predispose the mother to a cytokine storm upon SARS-CoV-2 infection, resulting in severe disease. Future work

should consider infecting specific immune cells from pregnant women and non-pregnant women with SARS-CoV-2 to further unravel different mechanisms which may be in place. This should also consider different BMIs and stage of gestation. As discovered in this thesis, some leukocytes may behave differently at term than at earlier stages of gestation.

8.5 Gestational diabetes mellitus

Dysregulation of maternal homeostasis during pregnancy can lead to various adverse outcomes for both mother and fetus. There are several risk factors which can lead to adverse outcomes, such as obesity, smoking, age, and family history.

GDM is characterised by varying severity of glucose intolerance, with onset or recognition during pregnancy and usually resolves postpartum [599]. GDM itself can lead to adverse outcomes including, but not limited to, birth trauma, neonatal hypoglycaemia, and preeclampsia. Obesity, ethnicity, age, and family history of diabetes are strong risk factors for GDM. In the not pregnant setting, obesity induces insulin resistance and type 2 DM (T2DM) through the release of cytokines such as TNFα and IL-6 [600, 601]. Insulin resistance emerges naturally as normal pregnancy progresses and an acceleration of this process driven by lifestyle and genetic factors is potentially what happens in GDM [333, 334].

Offspring from mothers with GDM have an increased risk of developing metabolic and cardiovascular disorders [602, 603]. The enhanced diabetic state in GDM pregnancies alters placental development and function and these alterations include elevated oxidative stress and fetal thrombosis [604, 605]; a recent review aptly describes the pathophysiology of GDM [606]. With regards to immune cell populations, an increase in NK cells in the placentas of GDM mothers has been reported [607]. However, reports of effects on placental macrophage numbers and function are conflicting. Several studies have reported a more pro-inflammatory phenotype [608-610], whilst others show that the M2 phenotype is maintained [611].

With the focus here being the maternal immune system, a study investigating pregnant women with obesity and GDM found upregulation of the Th1 phenotype, altering the Th1/Th2 ratio in comparison to a healthy pregnancy [424]. As the shift to Th2 encourages dynamic antibody production to combat infections and offer fetal passive immunity, the authors of

this study theorised that the provision of passive immunity to the fetus might be compromised in the obese GDM phenotype [424]. A recent review has described the current understanding of the effect of GDM on maternal peripheral leukocytes [612]. This review identified conflicting findings but found that overall GDM is consistent with a pro-inflammatory profile, although most studies are of leukocyte abundance rather than of their function. The reported pro-inflammatory profile is mostly evidenced by increases in NK cells [607] and activated T cells [613].

MNCs in T2DM have illustrated reduced mitochondrial mass, and hyperpolarised mitochondria [614]. The same studies that investigated this also found that the mitochondria occupied less cellular area, were more spherical, less complex and smaller in T2DM [614]. It was also observed that mitochondrial superoxide production is elevated in T2DM [614]. Hyperglycaemia has also been shown to induce excessive superoxide production by the ETC, causing oxidative stress in aortic endothelial cells, and inducing a decrease in GAPDH activity [615]. Changes in the morphology of mitochondria have been associated with ROS overproduction induced by elevated levels of glucose [616].

Monocytes have become indicators of inflammatory changes and innate immune function in T1DM and T2DM. Increased activation of monocytes has been observed in some studies in patients with T2DM compared to healthy controls, whilst other studies have contradicted this. Reports on monocytes in diabetes in general appear contradictory; upon activation with LPS and other immune stimuli, increased production of TNFα, IL-1β, IL-6 and IL-8 has been shown, as well as increased expression of CCR2 and TLR4 in T2DM [617]. In T1DM, studies investigating prediabetic biobreeding (BB) rats (rats that spontaneously develop T1DM) have illustrated the primary role of monocytes by demonstrating that they are the first cells to accumulate in the pancreatic islets [618]. Invasion of T and B cells into the islets is dependent upon prior monocyte infiltration [618]. In Goto-Kakizazki (G-K) rats (T2DM genetic model), monocytes were observed to have lower phagocytic activity in comparison to control rats, whereas there was no differences in granulocytes and lymphocytes [619].

For this thesis, samples were made available from women being tested for GDM by having an oral glucose tolerance test (OGTT). Due to the onset of the COVID-19 pandemic, the collection

of these samples was halted and has yet to restart. As such, data collected has few repeats. However, the results so far look promising (Figure 8.1-8) and should be expanded on when samples become available. Healthy pregnancies here also include pregnancies with obesity but are otherwise healthy. This is because the pregnancies complicated by GDM are also sometimes affected by obesity. MNCs from women who tested positive for GDM at 28 weeks had a disrupted OXPHOS response compared to uncomplicated pregnancies (Figure 8.1). This contrasts with what appears to be happening at 16 weeks, where the MNCs from pregnant women with GDM have increased OXPHOS (n=2, Figure 8.2). This suggests that the MNCs are overly activated earlier in gestation when complicated with GDM, quickening their pace to achieve the respiratory requirements for later in pregnancy. However, this peaks too soon and causes complications. Despite the significant changes in metabolism, functionally it appears as though the MNCs are unchanged by GDM in terms of cytokine production (Figure 8.3-7). As monocytes are a prime cell discussed in this thesis, their phenotype was also considered (Figure 8.8). Replicates here are sorely needed. It appears there are fewer mitochondria in all subsets of monocytes from women with GDM (Figure 8.8A), which contributes to the reduced OXPHOS observed in the heterogenous population of MNCs. CCR2 (Figure 8.8B) expression may also be reduced, with diminished capabilities for chemotaxis. Future work should include isolating monocytes to further investigate their metabolism and chemotaxis capabilities. Investigating this at different gestational stages (i.e., 16 weeks and term) would also highlight when key changes occur.

8.6 Other future work

It has been established here that monocytes are susceptible to adaptations to the pregnant environment and can be incapacitated by risk factors such as obesity, and adverse gestational events such as GDM. Monocytes play a role in the exacerbation of autoimmune diseases such as MS, which diminishes in pregnancy. Investigating how the monocytes are curbed in MS during pregnancy would provide novel insight into management of the disease. The novel use of MALDI-ToF described in this thesis may also be a tool to predict or diagnose MS, if reference ranges can be determined, as LPC has been implicated in demyelination in MS [376].

Due to ethical concerns with human volunteers, it is difficult to obtain more obscure samples, especially with pregnant women. As such, murine models can offer some insight into

questions that have arisen. One such avenue that warrants further work is investigating bone marrow-derived monocytes from dams. *Chapter 4 - Immunometabolic adaptations of monocytes in pregnancy at 37+ weeks gestation* explored the idea that the monocytes at term may be too fatigued to combat PAMPS and DAMPs. It would be interesting to determine if this phenotype is present at production in the bone marrow or develops upon exposure to the peripheral environment. It has been shown that TNF promotes premature release of monocytes from the bone marrow [620], and TNF levels steadily increase as gestation progress [621]. The stress of pregnancy, particularly at term, could impact the ability for hematopoietic stem cells to renew and develop into functional monocytes.

To further the investigation into the effect of obesity on pregnancy, plans are in place to expand on the findings described in this thesis. This includes a more direct focus on the monocytes, particularly on the trafficking capabilities and how their metabolism is modulated. To fully understand the impact of maternal obesity on the immune system, this study will recruit volunteers' pre-conception and will undergo a longitudinal study, covering various trimesters, until birth. In order to encapsulate changes, only groups of women of BMI <25 and >35 will be invited to the study; obstetricians have advised that concerns over BMI are not raised until BMI 35, hence the range selected. To determine if the monocytes are trafficking to the AT to have an effect, murine models would allow for the study of macrophages from visceral and subcutaneous AT at different stages of gestation; collaborations are currently being set up for this. Firstly, it will need to be established if the effect on peripheral monocytes in humans is also observed in mice. If ethical approval allows, obtaining AT from the site of c-section in human pregnancies could also offer insight into the effect of maternal obesity. A fellow PhD student is observing dramatic differences in metabolism and function term placental macrophages from women with obesity (BMI >35) compared to lean (BMI <25). As such, work from that project is tying in with the proposed future work here, by looking at the earlier gestation placental macrophages, which would make use of material from the Human Developmental Biology Resource (HDBR) if the project is accepted.

Monocytes are incriminated in the development of major depression, along with total leucocytosis [622]. It has been found that non-classical monocytes are increased in major

depression, at the expense of classical monocytes [623, 624] which are in an increased state of activation [624]. Treatment of monocytes with ketamine (though classically used as an anaesthetic it has recently been used as an antidepressant [625]) proliferates them into M2c-like macrophages accompanied by the stimulation of CD163 expression and genes associated with mTOR [624]. Pregnancy has been described to increase the vulnerability for anxiety and depression [626]. The monocyte adaptations observed in this thesis in pregnancy also appear to correlate with the monocyte phenotype observed in major depression: increased non-classical monocytes, increased activation state and reduced expression of genes associated with mTOR. This itself shows why there might be increased risk of perinatal and postnatal depression. However, a study into the monocytes during perinatal and postnatal diagnosed depression would provide insight into the disease and may uncover potential treatment or prevention strategies while not undermining the carefully regulated maternal environment.

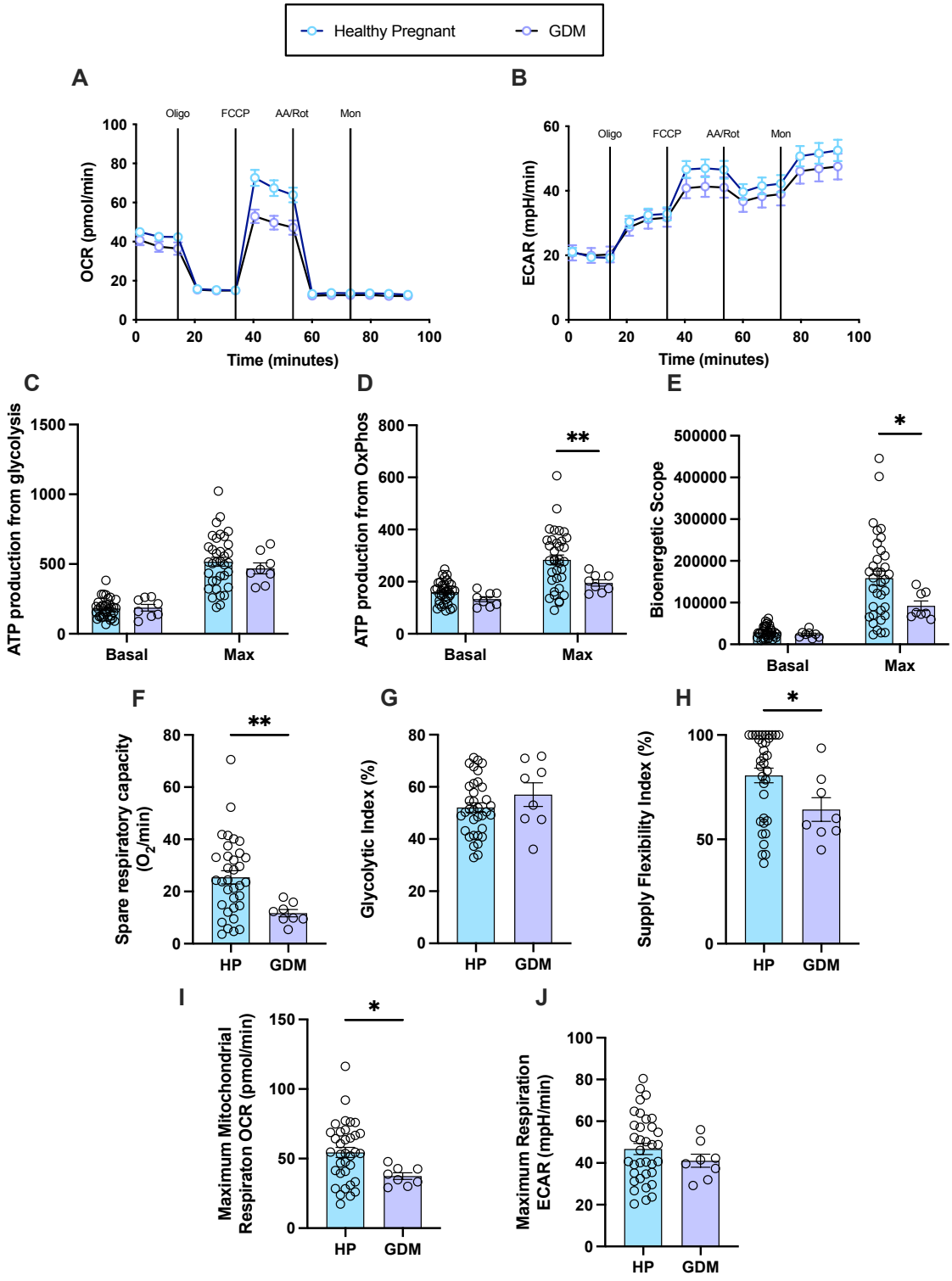

Figure 8.1: Bioenergetic capabilities of MNCs from pregnant women with GDM at 28 weeks of gestation. Bioenergetic analysis was performed on MNCs from pregnant women with (n=8) and without (n=35) GDM at 28 weeks of gestation using the Seahorse Extracellular flux analyser. Statistics performed was either a 2-way ANOVA and a Tukey's post-hoc test, or Mann-Whitney test where p value < 0.05 was significant. Traces for the OCR **(A)** and ECAR **(B)** are shown. Measurements made were: ATP production from **(C)** glycolysis (basal p = 0.9901; max p = 0.6037) and from **(D)** OXPHOS (basal p = 0.6159; max p = 0.0097), **(E)** bioenergetic scope (basal p = 0.9764; max p = 0.0264), **(F)** spare respiratory capacity (p = 0.0081), **(G)** glycolytic index (p = 0.3323), **(H)** supply flexibility index (p = 0.0404), **(I)** maximum mitochondrial respiration (p = 0.0309) and **(J)** maximum ECAR (p = 0.4519).

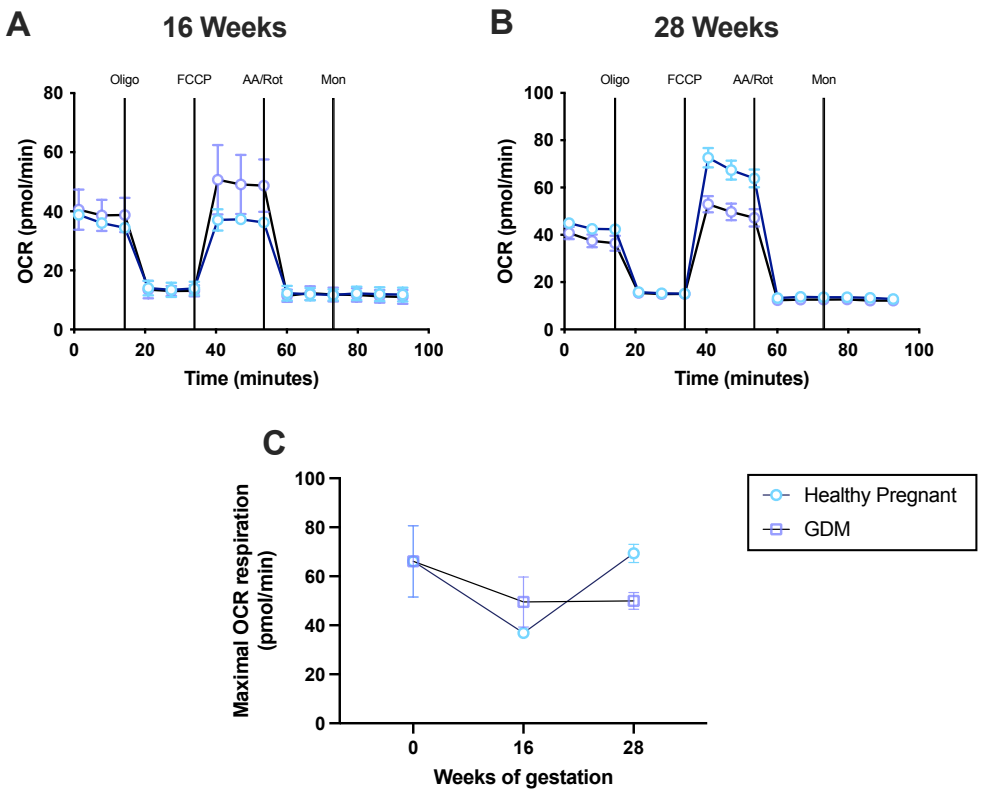

Figure 8.2: OXPHOS capabilities of MNCs from GDM women at 16 weeks and 28 weeks of gestation. MNCs from women with and without GDM at 16 weeks (n=2 for GDM +/-) and 28 weeks of gestation were analysed on the Seahorse extracellular flux analyser for their OXPHOS capabilities. The OCR traces are observed for 16 weeks **(A)** and 28 weeks **(B)** gestation. Their maximal respiration across gestation is observed in **(C)**.

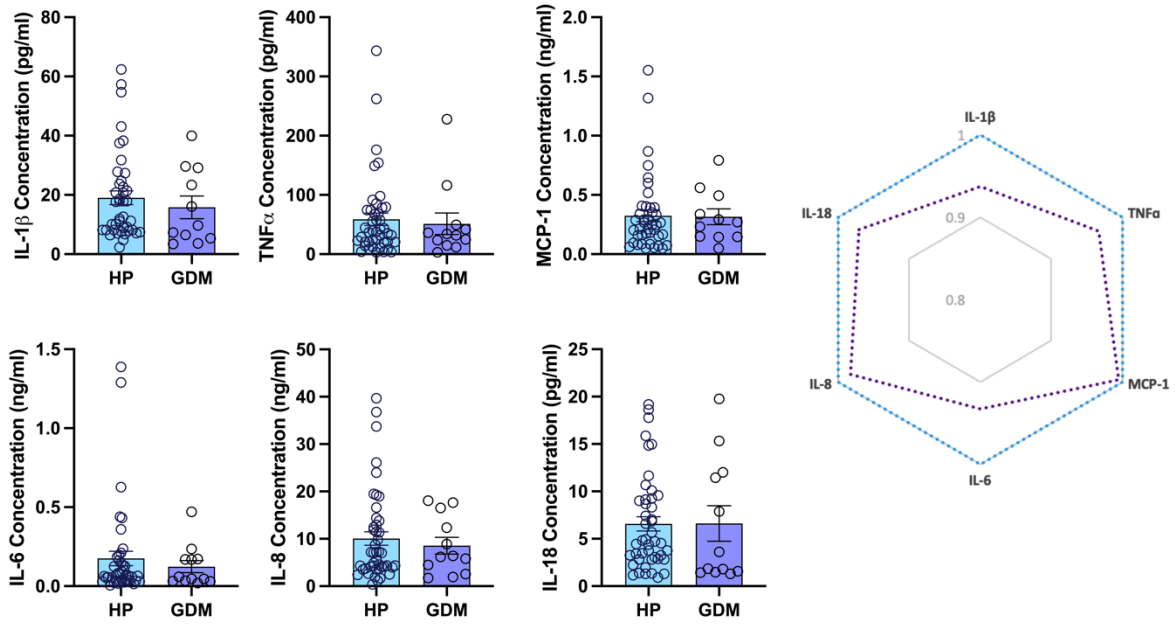

Figure 8.3: Unstimulated MNCs from women with healthy pregnancies and with GDM. MNCs were left unstimulated for 24hr, and the supernatants were used for cytokine analysis using LEGENDplex™ Inflammation kits. Mann-Whitney tests were used to test for significance ($p < 0.05$). Analytes measured were: IL-1β ($p = 0.3614$), TNFα ($p = 0.6573$), MCP-1 ($p = 0.8080$), IL-6 ($p = 0.8776$), IL-8 ($p = 0.9769$) and IL-18 ($p = 0.6186$).

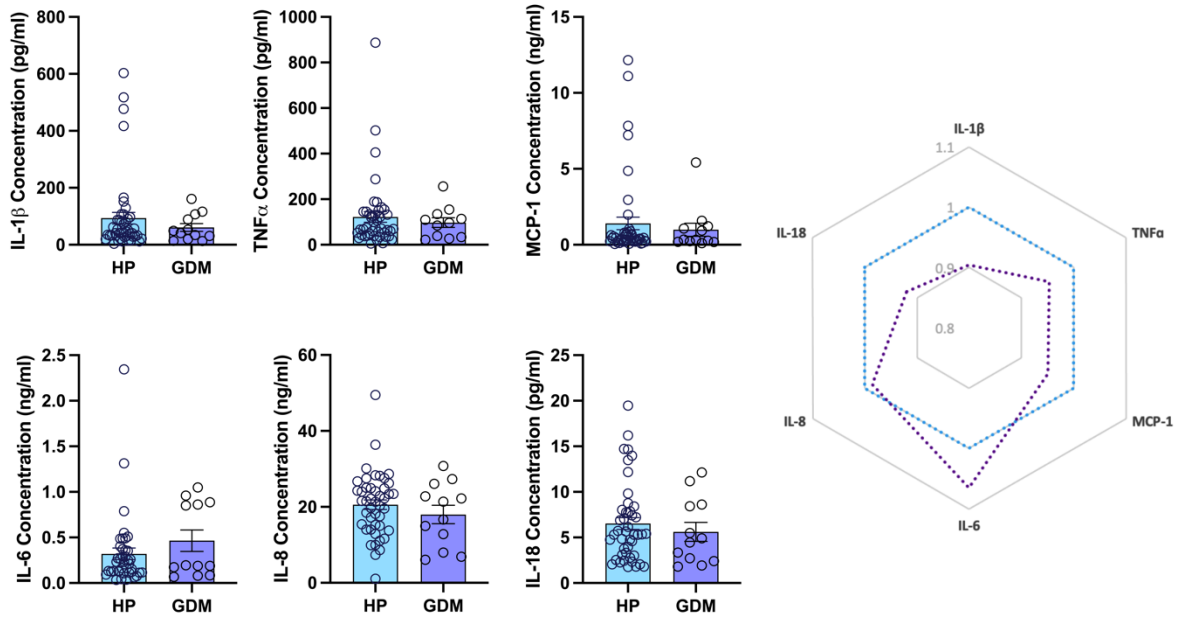

Figure 8.4: MDP-stimulated MNCs from women with healthy pregnancies and with GDM. MNCs were stimulated with MDP for 24hr, and the supernatants were used for cytokine analysis using LEGENDplex™ Inflammation kits. Mann-Whitney tests were used to test for significance ($p < 0.05$). Analytes measured were: IL-1β ($p = 0.8670$), TNFα ($p = 0.8928$), MCP-1 ($p = 0.9923$), IL-6 ($p = 0.3959$), IL-8 ($p = 0.3779$) and IL-18 ($p = 0.5652$).

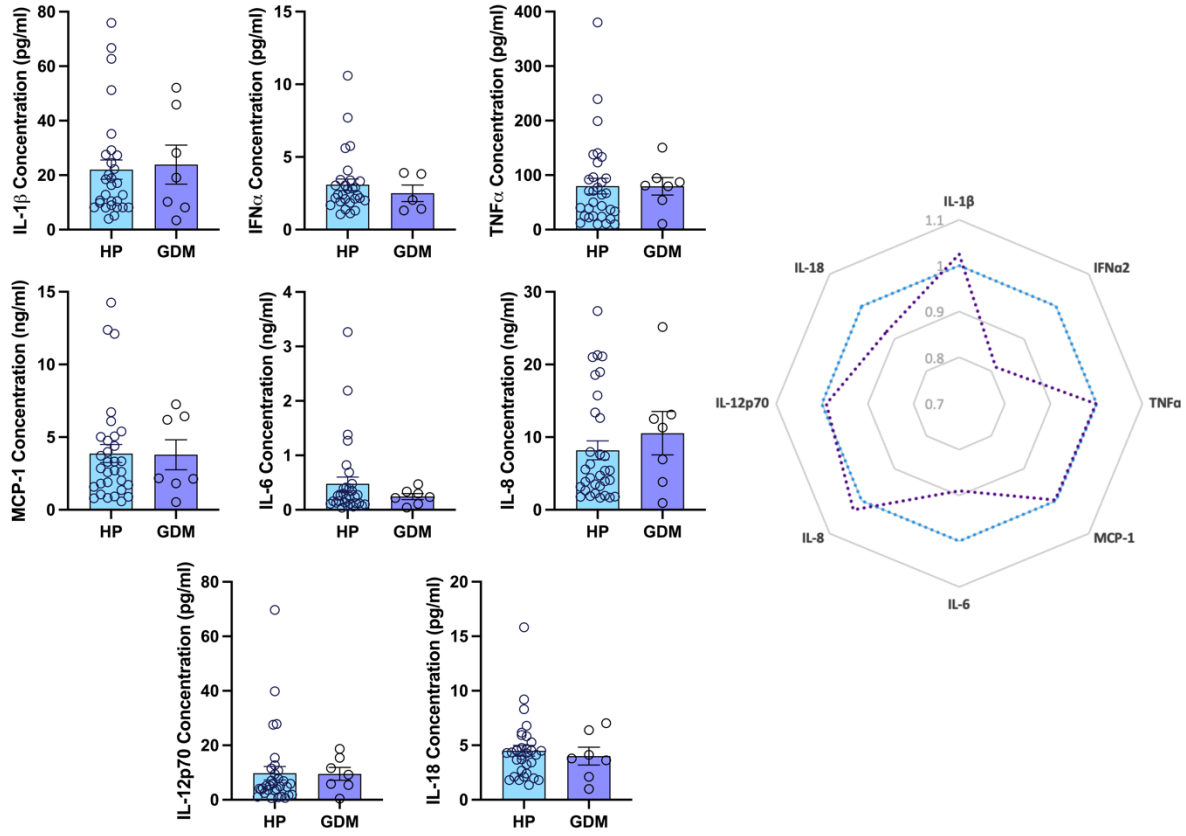

Figure 8.5: POLY:IC-stimulated MNCs from women with healthy pregnancies and with GDM. MNCs were stimulated with POLY:IC for 24hr, and the supernatants were used for cytokine analysis using LEGENDplex™ Inflammation kits. Mann-Whitney tests were used to test for significance ($p < 0.05$). Analytes measured were: IL-1β ($p = 0.8757$), IFNα ($p = 0.6739$), TNFα ($p = 0.4599$), MCP-1 ($p = 0.7966$), IL-6 ($p = 0.6852$), IL-8 ($p = 0.4839$) and IL-18 ($p = 0.7110$).

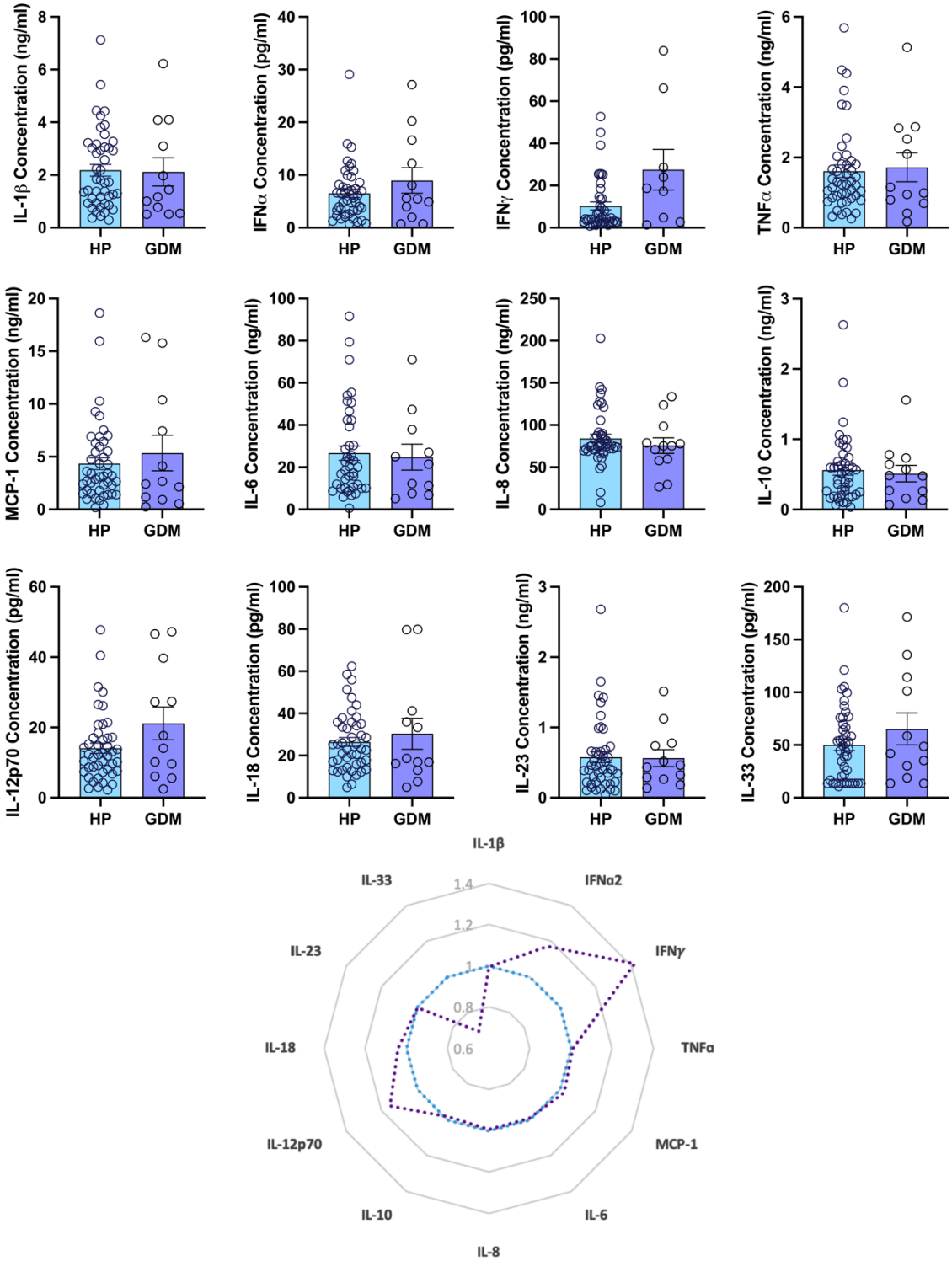

Figure 8.6: LPS-stimulated MNCs from women with healthy pregnancies and with GDM. MNCs were stimulated with LPS for 24hr, and the supernatants were used for cytokine analysis using LEGENDplex™ Inflammation kits. Mann-Whitney tests were used to test for significance ($p < 0.05$). Analytes measured were: IL-1β ($p = 0.6636$), IFNα ($p = 0.6196$), IFNγ ($p = 0.0658$), TNFα ($p = 0.9461$), MCP-1 ($p = 0.7794$), IL-6 ($p = 0.7711$), IL-8 ($p = 0.4921$), IL-10 ($p = 0.7942$), IL-12p70 ($p = 0.2992$), IL-18 ($p = 0.8544$), IL-23 ($p = 0.8092$), and IL-33 ($p = 0.4895$).

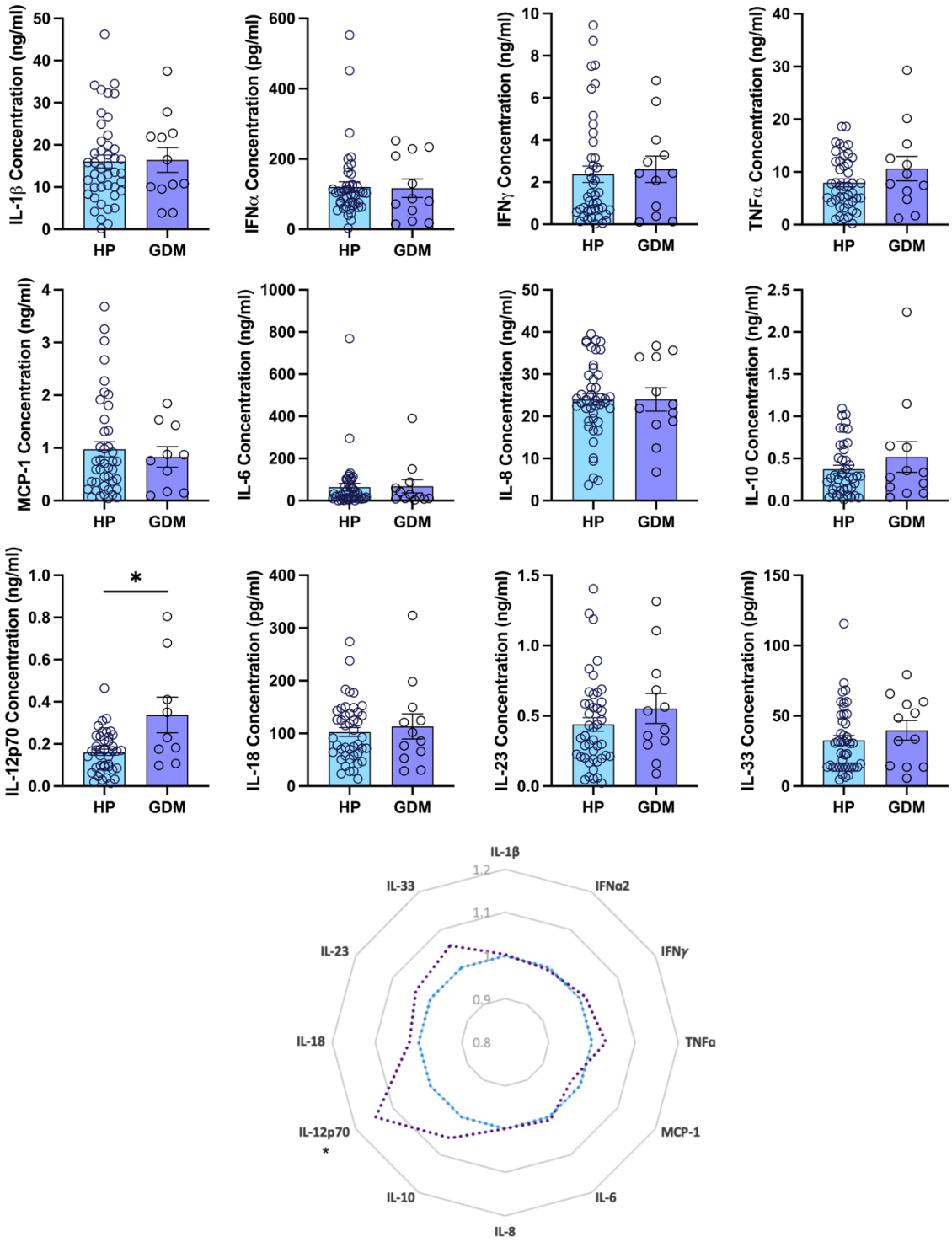

Figure 8.7: LPS/R848-stimulated MNCs from women with healthy pregnancies and with GDM. MNCs were stimulated with LPS and R848 for 24hr, and the supernatants were used for cytokine analysis using LEGENDplex™ Inflammation kits. Mann-Whitney tests were used to test for significance ($p < 0.05$). Analytes measured were: IL-1β ($p = 0.8981$), IFNα ($p = 0.8361$), IFNγ ($p = 0.5798$), TNFα ($p = 0.3578$), MCP-1 ($p = 0.9727$), IL-6 ($p = 0.9558$), IL-8 ($p = 0.7751$), IL-10 ($p = 0.6948$), IL-12p70 ($p = 0.0235$), IL-18 ($p = 0.9294$), IL-23 ($p = 0.3274$), and IL-33 ($p = 0.3080$).

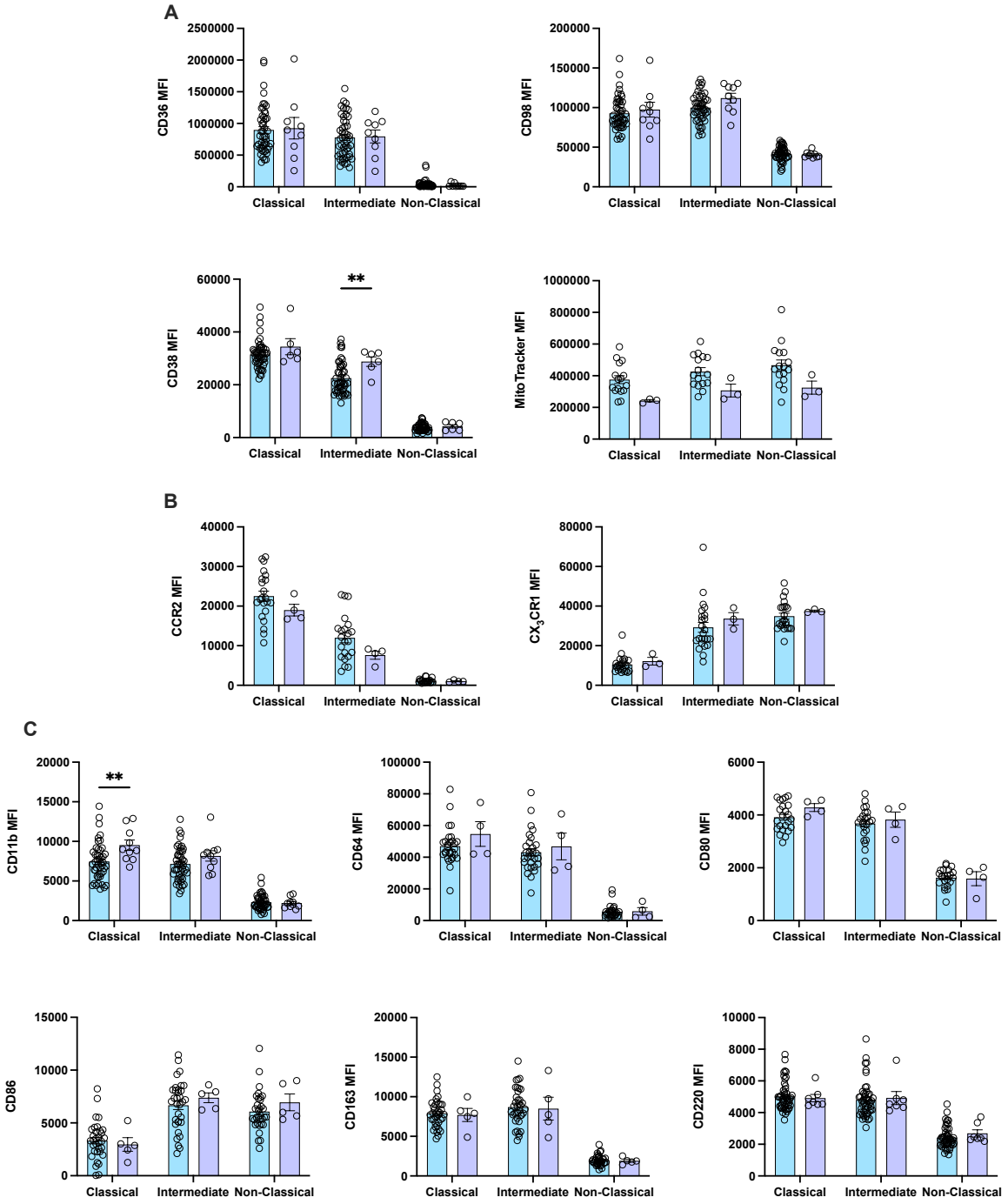

Figure 8.8: Phenotype of monocytes and their subsets from pregnant women with GDM at 28 weeks of gestation. MNCs were stained with antibodies specific for monocytes and their subsets (Classical = C, intermediate = I, non-classical = NC) to determine the phenotypic profile of the monocytes from GDM-positive pregnant women (purple) compared to GDM-negative pregnant women (blue) at 28 weeks of gestation. Statistics were performed with a 2-way ANOVA and a Tukey's post-hoc test,, where $p < 0.05$ was significant. **(A)** Metabolic markers measured were: CD36 (C p = 0.9910, I p = 0.9979, NC p = 0.9986), CD98 (C p = 0.8285, I p = 0.1430, NC p = 0.9972), CD38 (C p = 0.3887, I p = 0.0080, NC p = 0.9975) and MitoTracker Green ™ (C p = 0.1575, I p = 0.2419, NC p = 0.1264). **(B)** Chemokine receptors measured were: CCR2 (C p = 0.4070, I p = 0.2293, NC p > 0.9999) and CX_3CR1 (C p = 0.9832, I p = 0.7746, NC p = 0.9432). **(C)** Other phenotypic markers measured were: CD11b (C p = 0.0061, I p = 0.3136, NC p = 0.9984), CD64 (C p = 0.4449, I p = 0.8865, NC p > 0.9999), CD80 (C p = 0.4469, I p = 0.9301, NC p = 0.9989), CD86 (C p = 0.9729, I p = 0.8326, NC p = 0.7305), CD163 (C p = 0.9936, I p = 0.9938, NC p = 0.9998), and CD220 (C p = 0.9886, I p = 0.9858, NC p = 0.8439).

Chapter 9 – Bibliography

References

1. Mouzon Sylvie H-d, Lassance L. Endocrine and metabolic adaptations to pregnancy; impact of obesity. Hormone Molecular Biology and Clinical Investigation2015. p. 65.
2. Rees A, Richards O, Chambers M, Jenkins BJ, Cronin JG, Thornton CA. Immunometabolic adaptation and immune plasticity in pregnancy and the bi-directional effects of obesity.: *Clinical & Experimental Immunology*; 2022.
3. Head J, Billingham R. Immunobiological aspects of the maternal-fetoplacental relationship. *Clinical aspects of immunology* 1982; **1**: 243œ282.
4. Thornton CA. Immunology of pregnancy. *Proceedings of the Nutrition Society* 2010; **69**: 357-365.
5. PrabhuDas M, Bonney E, Caron K*, et al.* Immune mechanisms at the maternal-fetal interface: perspectives and challenges. *Nature immunology* 2015; **16**: 328-334.
6. Chandra S, Tripathi AK, Mishra S, Amzarul M, Vaish AK. Physiological changes in hematological parameters during pregnancy. *Indian J Hematol Blood Transfus* 2012; **28**: 144-146.
7. Nakamura N, Miyazaki K, Kitano Y, Fujisaki S, Okamura H. Suppression of cytotoxic T-lymphocyte activity during human pregnancy. *J Reprod Immunol* 1993; **23**: 119-130.
8. Wegmann TG, Lin H, Guilbert L, Mosmann TR. Bidirectional cytokine interactions in the maternal-fetal relationship: is successful pregnancy a TH2 phenomenon? *Immunology Today* 1993; **14**: 353-356.
9. Lin H, Mosmann TR, Guilbert L, Tuntipopipat S, Wegmann TG. Synthesis of T helper 2-type cytokines at the maternal-fetal interface. *The Journal of Immunology* 1993; **151**: 4562.
10. Figueiredo AS, Schumacher A. The T helper type 17/regulatory T cell paradigm in pregnancy. *Immunology* 2016; **148**: 13-21.
11. Neuteboom RF, Verbraak E, Wierenga-Wolf AF*, et al.* Pregnancy-induced fluctuations in functional T-cell subsets in multiple sclerosis patients. *Multiple Sclerosis Journal* 2010; **16**: 1073-1078.
12. Iannello A, Rolla S, Maglione A*, et al.* Pregnancy Epigenetic Signature in T Helper 17 and T Regulatory Cells in Multiple Sclerosis. *Front Immunol* (10.3389/fimmu.2018.03075).2019; **9**: 3075.
13. Pannu N, Singh R, Sharma S, Chopra S, Bhatnagar A. Altered Tregs and oxidative stress in pregnancy associated lupus. *Advances in Rheumatology* 2019; **59**: 38.
14. Gehrz RC, Christianson WR, Linner KM, Conroy MM, McCue SA, Balfour HH. A longitudinal analysis of lymphocyte proliferative responses to mitogens and antigens during human pregnancy. *American Journal of Obstetrics and Gynecology* 1981; **140**: 665-670.
15. Djian V, Menu E, Thibault G, Ropert S, Chaouat G. Immunoactive Products of Placenta. V. Immunoregulatory Properties of a Low Molecular Weight Compound Obtained From Human Placental Cultures. *American Journal of Reproductive Immunology* (https://doi.org/10.1111/j.1600-0897.1996.tb00134.x).1996; **36**: 11-24.
16. Aarli Å, Kristoffersen EK, Jensen TS, Ulvestad E, Matre R. Suppressive Effect on Lymphoproliferation In Vitro by Soluble Annexin II Released from Isolated Placental Membranes. *American Journal of Reproductive Immunology* (https://doi.org/10.1111/j.1600-0897.1997.tb00306.x).1997; **38**: 313-319.

17. Blackburn S, Loper D. The hematologic and hemostatic systems. *Maternal, Fetal, and Neonatal Physiology A Clinical Perspective* 1992: 159-200.
18. N. BJ, J. WP, E. LG. Immune cells in the placental bed. *Int J Dev Biol* 2010; **54**: 281-294.
19. Racicot K, Mor G. Risks associated with viral infections during pregnancy. *J Clin Invest* 2017; **127**: 1591-1599.
20. Sojka DK, Yang L, Yokoyama WM. Uterine Natural Killer Cells. *Front Immunol* (10.3389/fimmu.2019.00960).2019; **10**: 960.
21. Faas MM, de Vos P. Uterine NK cells and macrophages in pregnancy. *Placenta* 2017; **56**: 44-52.
22. Erlebacher A. Immunology of the Maternal-Fetal Interface. *Annual Review of Immunology* 2013; **31**: 387-411.
23. Rieger L, Honig A, Sütterlin M*, et al.* Antigen-Presenting Cells in Human Endometrium During the Menstrual Cycle Compared to Early Pregnancy. *The Journal of the Society for Gynecologic Investigation: JSGI* 2004; **11**: 488-493.
24. Ramhorst R, Grasso E, Paparini D*, et al.* Decoding the chemokine network that links leukocytes with decidual cells and the trophoblast during early implantation. *Cell Adh Migr* 2016; **10**: 197-207.
25. Svensson J, Jenmalm MC, Matussek A, Geffers R, Berg G, Ernerudh J. Macrophages at the Fetal–Maternal Interface Express Markers of Alternative Activation and Are Induced by M-CSF and IL-10. *The Journal of Immunology* 2011; **187**: 3671.
26. Svensson-Arvelund J, Mehta RB, Lindau R*, et al.* The Human Fetal Placenta Promotes Tolerance against the Semiallogeneic Fetus by Inducing Regulatory T Cells and Homeostatic M2 Macrophages. *The Journal of Immunology* 2015; **194**: 1534.
27. Tsuda S, Nakashima A, Shima T, Saito S. New Paradigm in the Role of Regulatory T Cells During Pregnancy. *Front Immunol* (10.3389/fimmu.2019.00573).2019; **10**: 573.
28. Hamilton S, Oomomian Y, Stephen G*, et al.* Macrophages Infiltrate the Human and Rat Decidua During Term and Preterm Labor: Evidence That Decidual Inflammation Precedes Labor1. *Biology of Reproduction* 2012; **86**.
29. Dubicke A, Fransson E, Centini G*, et al.* Pro-inflammatory and anti-inflammatory cytokines in human preterm and term cervical ripening. *Journal of Reproductive Immunology* 2010; **84**: 176-185.
30. Osman I, Young A, Ledingham MA*, et al.* Leukocyte density and pro-inflammatory cytokine expression in human fetal membranes, decidua, cervix and myometrium before and during labour at term. *Molecular Human Reproduction* 2003; **9**: 41-45.
31. Graham C, Chooniedass R, Stefura WP*, et al.* In vivo immune signatures of healthy human pregnancy: Inherently inflammatory or anti-inflammatory? *PLOS ONE* 2017; **12**: e0177813.
32. Bränn E, Edvinsson Å, Rostedt Punga A, Sundström-Poromaa I, Skalkidou A. Inflammatory and anti-inflammatory markers in plasma: from late pregnancy to early postpartum. *Scientific Reports* 2019; **9**: 1863.
33. Freeman Dilys J, McManus F, Brown Elizabeth A*, et al.* Short- and Long-Term Changes in Plasma Inflammatory Markers Associated With Preeclampsia. *Hypertension* 2004; **44**: 708-714.
34. Park HS, Park JY, Yu R. Relationship of obesity and visceral adiposity with serum concentrations of CRP, TNF-α and IL-6. *Diabetes Research and Clinical Practice* 2005; **69**: 29-35.

35. Bulló M, García-Lorda P, Megias I, Salas-Salvadó J. Systemic Inflammation, Adipose Tissue Tumor Necrosis Factor, and Leptin Expression. *Obesity Research* 2003; **11**: 525-531.
36. Thornton CA, Jones RH, Doekhie A, Bryant AH, Beynon AL, Davies JS. Inflammation, Obesity, and Neuromodulation in Pregnancy and Fetal Development. *Advances in Neuroimmune Biology* 2011; **1**: 193-203.
37. Hodson K, Dalla Man C, Smith FE*, et al.* Mechanism of Insulin Resistance in Normal Pregnancy. *Horm Metab Res* 2013; **45**: 567-571.
38. Diderholm B, Stridsberg M, Ewald U, Lindeberg-Nordén S, Gustafsson J. Increased lipolysis in non-obese pregnant women studied in the third trimester. *BJOG: An International Journal of Obstetrics & Gynaecology* 2005; **112**: 713-718.
39. Barbour LA, McCurdy CE, Hernandez TL, Kirwan JP, Catalano PM, Friedman JE. Cellular Mechanisms for Insulin Resistance in Normal Pregnancy and Gestational Diabetes. *Diabetes Care* (10.2337/dc07-s202).2007; **30**: S112.
40. Hytten F. Nutritional requirements in pregnancy: What happens if they are not met? *Midwifery* 1990; **6**: 140-145.
41. Catalano PM, Tyzbir ED, Wolfe RR*, et al.* Carbohydrate metabolism during pregnancy in control subjects and women with gestational diabetes. *American Journal of Physiology - Endocrinology And Metabolism* 1993; **264**: E60.
42. Herrera E. Lipid metabolism in pregnancy and its consequences in the fetus and newborn. *Endocrine* 2002; **19**: 43-55.
43. Butte NF, Hopkinson JM, Mehta N, Moon JK, Smith EOB. Adjustments in energy expenditure and substrate utilization during late pregnancy and lactation. *The American Journal of Clinical Nutrition* 1999; **69**: 299-307.
44. Felig P, Kim YJ, Lynch V, Hendler R. Amino acid metabolism during starvation in human pregnancy. *The Journal of clinical investigation* 1972; **51**: 1195-1202.
45. Alvarez JJ, Montelongo A, Iglesias A, Lasunción MA, Herrera E. Longitudinal study on lipoprotein profile, high density lipoprotein subclass, and postheparin lipases during gestation in women. *Journal of Lipid Research* 1996; **37**: 299-308.
46. Sattar N, Greer IA, Louden J*, et al.* Lipoprotein Subfraction Changes in Normal Pregnancy: Threshold Effect of Plasma Triglyceride on Appearance of Small, Dense Low Density Lipoprotein1. *The Journal of Clinical Endocrinology & Metabolism* 1997; **82**: 2483-2491.
47. Jones N, Piasecka J, Bryant AH*, et al.* Bioenergetic analysis of human peripheral blood mononuclear cells. *Clinical and Experimental Immunology* 2015; **182**: 69-80.
48. Kim B-J, Choi Y-M, Rah S-Y*, et al.* Seminal CD38 is a pivotal regulator for fetomaternal tolerance. *Proceedings of the National Academy of Sciences of the United States of America* 2015; **112**: 1559-1564.
49. Le Gars M, Seiler C, Kay AW*, et al.* Pregnancy-Induced Alterations in NK Cell Phenotype and Function. *Front Immunol* (10.3389/fimmu.2019.02469).2019; **10**: 2469.
50. Díaz P, Harris J, Rosario FJ, Powell TL, Jansson T. Increased placental fatty acid transporter 6 and binding protein 3 expression and fetal liver lipid accumulation in a mouse model of obesity in pregnancy. *Am J Physiol Regul Integr Comp Physiol* 2015; **309**: R1569-R1577.
51. Rosario FJ, Kanai Y, Powell TL, Jansson T. Increased placental nutrient transport in a novel mouse model of maternal obesity with fetal overgrowth. *Obesity (Silver Spring)* 2015; **23**: 1663-1670.

52. Zhang J-Z, Ismail-Beigi F. Activation of Glut1 Glucose Transporter in Human Erythrocytes. *Archives of Biochemistry and Biophysics* 1998; **356**: 86-92.
53. Morgello S, Uson RR, Schwartz EJ, Haber RS. The human blood-brain barrier glucose transporter (GLUT1) is a glucose transporter of gray matter astrocytes. *Glia* 1995; **14**: 43-54.
54. Maher F, Davies-Hill TM, Lysko PG, Henneberry RC, Simpson IA. Expression of two glucose transporters, GLUT1 and GLUT3, in cultured cerebellar neurons: Evidence for neuron-specific expression of GLUT3. *Molecular and Cellular Neuroscience* 1991; **2**: 351-360.
55. Brown K, Heller DS, Zamudio S, Illsley NP. Glucose transporter 3 (GLUT3) protein expression in human placenta across gestation. *Placenta* 2011; **32**: 1041-1049.
56. Flores-Opazo M, Boland E, Garnham A, Murphy RM, McGee SL, Hargreaves M. Exercise and GLUT4 in human subcutaneous adipose tissue. *Physiol Rep* 2018; **6**: e13918-e13918.
57. Richter EA, Hargreaves M. Exercise, GLUT4, and Skeletal Muscle Glucose Uptake. *Physiological Reviews* 2013; **93**: 993-1017.
58. Song L, Sun B, Boersma GJ*, et al.* Prenatal high-fat diet alters placental morphology, nutrient transporter expression, and mtorc1 signaling in rat. *Obesity* 2017; **25**: 909-919.
59. Ganguly A, McKnight RA, Raychaudhuri S*, et al.* Glucose transporter isoform-3 mutations cause early pregnancy loss and fetal growth restriction. *American Journal of Physiology-Endocrinology and Metabolism* 2007; **292**: E1241-E1255.
60. Mahla RS, Reddy MC, Prasad DVR, Kumar H. Sweeten PAMPs: Role of Sugar Complexed PAMPs in Innate Immunity and Vaccine Biology. *Front Immunol* 2013; **4**: 248-248.
61. Lim K-H, Staudt LM. Toll-like receptor signaling. *Cold Spring Harb Perspect Biol* 2013; **5**: a011247-a011247.
62. Yang J, Zhang L, Yu C, Yang X-F, Wang H. Monocyte and macrophage differentiation: circulation inflammatory monocyte as biomarker for inflammatory diseases. *Biomarker Research* 2014; **2**: 1-1.
63. Nichols BA, Bainton DF, Farquhar MG. Differentiation of monocytes. Origin, nature, and fate of their azurophil granules. *The Journal of cell biology* 1971; **50**: 498-515.
64. Swirski FK, Nahrendorf M, Etzrodt M*, et al.* Identification of splenic reservoir monocytes and their deployment to inflammatory sites. *Science (New York, NY)* 2009; **325**: 612-616.
65. Swirski FK, Libby P, Aikawa E*, et al.* Ly-6Chi monocytes dominate hypercholesterolemia-associated monocytosis and give rise to macrophages in atheromata. *J Clin Invest* 2007; **117**: 195-205.
66. Min D, Brooks B, Wong J*, et al.* Alterations in Monocyte CD16 in Association with Diabetes Complications. *Mediators of Inflammation* 2012; **2012**: 649083.
67. Ziegler-Heitbrock L. The CD14+ CD16+ blood monocytes: their role in infection and inflammation. *Journal of Leukocyte Biology* 2007; **81**: 584-592.
68. Rogacev KS, Ulrich C, Blömer L*, et al.* Monocyte heterogeneity in obesity and subclinical atherosclerosis. *European Heart Journal* 2009; **31**: 369-376.
69. Geissmann F, Jung S, Littman DR. Blood Monocytes Consist of Two Principal Subsets with Distinct Migratory Properties. *Immunity* 2003; **19**: 71-82.

70. Boyette LB, Macedo C, Hadi K*, et al.* Phenotype, function, and differentiation potential of human monocyte subsets. *PLOS ONE* 2017; **12**: e0176460.
71. Auffray C, Fogg D, Garfa M*, et al.* Monitoring of Blood Vessels and Tissues by a Population of Monocytes with Patrolling Behavior. *Science* 2007; **317**: 666.
72. Smeekens SP, van de Veerdonk FL, Joosten LAB*, et al.* The classical CD14++CD16− monocytes, but not the patrolling CD14+CD16+ monocytes, promote Th17 responses to Candida albicans. *European Journal of Immunology* 2011; **41**: 2915-2924.
73. Sacks GP, Studena K, Sargent IL, Redman CWG. Normal pregnancy and preeclampsia both produce inflammatory changes in peripheral blood leukocytes akin to those of sepsis. *American Journal of Obstetrics and Gynecology* 1998; **179**: 80-86.
74. Luppi P, Haluszczak C, Betters D, Richard CAH, Trucco M, DeLoia JA. Monocytes are progressively activated in the circulation of pregnant women. *Journal of Leukocyte Biology* 2002; **72**: 874-884.
75. Veenstra van Nieuwenhoven AL, Bouman A, Moes H*, et al.* Endotoxin-induced cytokine production of monocytes of third-trimester pregnant women compared with women in the follicular phase of the menstrual cycle. *American Journal of Obstetrics & Gynecology* 2003; **188**: 1073-1077.
76. Sacks GP, Redman CWG, Sargent IL. Monocytes are primed to produce the Th1 type cytokine IL-12 in normal human pregnancy: an intracellular flow cytometric analysis of peripheral blood mononuclear cells. *Clinical & Experimental Immunology* 2003; **131**: 490-497.
77. Faas MM, Spaans F, De Vos P. Monocytes and macrophages in pregnancy and pre-eclampsia. *Front Immunol* 2014; **5**: 298-298.
78. Krinninger P, Ensenauer R, Ehlers K*, et al.* Peripheral Monocytes of Obese Women Display Increased Chemokine Receptor Expression and Migration Capacity. *The Journal of Clinical Endocrinology & Metabolism* 2014; **99**: 2500-2509.
79. Devêvre EF, Renovato-Martins M, Clément K, Sautès-Fridman C, Cremer I, Poitou C. Profiling of the Three Circulating Monocyte Subpopulations in Human Obesity. *The Journal of Immunology* 2015; **194**: 3917.
80. Hauger MS, Gibbons LUZ, Vik T, BelizÁN JM. Prepregnancy weight status and the risk of adverse pregnancy outcome. *Acta Obstetricia et Gynecologica Scandinavica* 2008; **87**: 953-959.
81. Magdaleno R, Pereira BG, Chaim EA, Turato ER. Pregnancy after bariatric surgery: a current view of maternal, obstetrical and perinatal challenges. *Archives of Gynecology and Obstetrics* 2012; **285**: 559-566.
82. Wilson RM, Marshall NE, Jeske DR, Purnell JQ, Thornburg K, Messaoudi I. Maternal obesity alters immune cell frequencies and responses in umbilical cord blood samples. *Pediatric Allergy and Immunology* 2015; **26**: 344-351.
83. Sureshchandra S, Wilson RM, Rais M*, et al.* Maternal Pregravid Obesity Remodels the DNA Methylation Landscape of Cord Blood Monocytes Disrupting Their Inflammatory Program. *The Journal of Immunology* 2017; **199**: 2729.
84. Bachy V, Williams DJ, Ibrahim MAA. Altered dendritic cell function in normal pregnancy. *Journal of Reproductive Immunology* 2008; **78**: 11-21.
85. Chambers M, Rees A, Cronin JG, Nair M, Jones N, Thornton CA. Macrophage Plasticity in Reproduction and Environmental Influences on Their Function. *Front Immunol* (10.3389/fimmu.2020.607328).2021; **11**: 3491.

86. Hunt JS, Miller L, Platt JS. Hormonal regulation of uterine macrophages. *Dev Immunol* 1998; **6**: 105-110.
87. Gustafsson C, Mjösberg J, Matussek A*, et al.* Gene expression profiling of human decidual macrophages: evidence for immunosuppressive phenotype. *PloS one* 2008; **3**: e2078-e2078.
88. Abrahams VM, Kim YM, Straszewski SL, Romero R, Mor G. Macrophages and Apoptotic Cell Clearance During Pregnancy. *American Journal of Reproductive Immunology* 2004; **51**: 275-282.
89. Xu J, Gu Y, Sun J, Zhu H, Lewis DF, Wang Y. Reduced CD200 expression is associated with altered Th1/Th2 cytokine production in placental trophoblasts from preeclampsia. *Am J Reprod Immunol* 2018; **79**: 10.1111/aji.12763.
90. Li Z-H, Wang L-L, Liu H*, et al.* Galectin-9 Alleviates LPS-Induced Preeclampsia-Like Impairment in Rats via Switching Decidual Macrophage Polarization to M2 Subtype. *Front Immunol* 2019; **9**: 3142-3142.
91. Tsao F-Y, Wu M-Y, Chang Y-L, Wu C-T, Ho H-N. M1 macrophages decrease in the deciduae from normal pregnancies but not from spontaneous abortions or unexplained recurrent spontaneous abortions. *Journal of the Formosan Medical Association* 2018; **117**: 204-211.
92. Kelly Amy C, Powell Theresa L, Jansson T. Placental function in maternal obesity. *Clinical Science* 2020; **134**: 961-984.
93. Challier JC, Basu S, Bintein T*, et al.* Obesity in pregnancy stimulates macrophage accumulation and inflammation in the placenta. *Placenta* 2008; **29**: 274-281.
94. Roberts KA, Riley SC, Reynolds RM*, et al.* Placental structure and inflammation in pregnancies associated with obesity. *Placenta* 2011; **32**: 247-254.
95. Laskewitz A, van Benthem KL, Kieffer TEC*, et al.* The influence of maternal obesity on macrophage subsets in the human decidua. *Cellular Immunology* 2019; **336**: 75-82.
96. Zhang L, Sugiyama T, Murabayashi N*, et al.* The inflammatory changes of adipose tissue in late pregnant mice. *Journal of molecular endocrinology* 2011; **47**: 157-165.
97. Bravo-Flores E, Mancilla-Herrera I, Espino Y Sosa S*, et al.* Macrophage Populations in Visceral Adipose Tissue from Pregnant Women: Potential Role of Obesity in Maternal Inflammation. *International journal of molecular sciences* 2018; **19**: 1074.
98. Hahn S, Giaglis S, Hoesli I, Hasler P. Neutrophil NETs in reproduction: from infertility to preeclampsia and the possibility of fetal loss. *Front Immunol* 2012; **3**: 362-362.
99. Gupta AK, Hasler P, Holzgreve W, Gebhardt S, Hahn S. Induction of Neutrophil Extracellular DNA Lattices by Placental Microparticles and IL-8 and Their Presence in Preeclampsia. *Human Immunology* 2005; **66**: 1146-1154.
100. Stoikou M, Grimolizzi F, Giaglis S*, et al.* Gestational Diabetes Mellitus Is Associated with Altered Neutrophil Activity. *Front Immunol* 2017; **8**: 702-702.
101. Sun T, Meng F, Zhao H*, et al.* Elevated First-Trimester Neutrophil Count Is Closely Associated with the Development of Maternal Gestational Diabetes Mellitus and Adverse Pregnancy Outcomes. *Diabetes* 2020: db190976.
102. Giaglis S, Stoikou M, Sur Chowdhury C*, et al.* Multimodal Regulation of NET Formation in Pregnancy: Progesterone Antagonizes the Pro-NETotic Effect of Estrogen and G-CSF. *Front Immunol* 2016; **7**: 565-565.
103. Matsumoto K, Ogasawara T, Kato A*, et al.* Eosinophil degranulation during pregnancy and after delivery by cesarean section. *Int Arch Allergy Immunol* 2003; **131 Suppl 1**: 34-39.

104. Davoine F, Lacy P. Eosinophil cytokines, chemokines, and growth factors: emerging roles in immunity. *Front Immunol* 2014; **5**: 570-570.
105. Marichal T, Mesnil C, Bureau F. Homeostatic Eosinophils: Characteristics and Functions. *Frontiers in Medicine* (10.3389/fmed.2017.00101).2017; **4**: 101.
106. Lobo TF, Borges CdM, Mattar R*, et al.* Impaired Treg and NK cells profile in overweight women with gestational diabetes mellitus. *American Journal of Reproductive Immunology* 2018; **79**: e12810.
107. Perdu S, Castellana B, Kim Y, Chan K, DeLuca L, Beristain AG. Maternal obesity drives functional alterations in uterine NK cells. *JCI Insight* 2016; **1**: e85560-e85560.
108. Castellana B, Perdu S, Kim Y*, et al.* Maternal obesity alters uterine NK activity through a functional KIR2DL1/S1 imbalance. *Immunology & Cell Biology* 2018; **96**: 805-819.
109. Fu B, Zhou Y, Ni X*, et al.* Natural Killer Cells Promote Fetal Development through the Secretion of Growth-Promoting Factors. *Immunity* 2017; **47**: 1100-1113.e1106.
110. Fukui A, Yokota M, Funamizu A*, et al.* Changes of NK Cells in Preeclampsia. *American Journal of Reproductive Immunology* (https://doi.org/10.1111/j.1600-0897.2012.01120.x).2012; **67**: 278-286.
111. Bonilla FA, Oettgen HC. Adaptive immunity. *Journal of Allergy and Clinical Immunology* 2010; **125**: S33-S40.
112. Francis MJ. Recent Advances in Vaccine Technologies. *Vet Clin North Am Small Anim Pract* 2018; **48**: 231-241.
113. Sakaguchi S. Naturally Arising CD4+ Regulatory T Cells for Immunologic Self-Tolerance and Negative Control of Immune Responses. *Annual Review of Immunology* 2004; **22**: 531-562.
114. Ellis JS, Wan X, Braley-Mullen H. Transient depletion of CD4+ CD25+ regulatory T cells results in multiple autoimmune diseases in wild-type and B-cell-deficient NOD mice. *Immunology* 2013; **139**: 179-186.
115. Mohseni YR, Tung SL, Dudreuilh C, Lechler RI, Fruhwirth GO, Lombardi G. The Future of Regulatory T Cell Therapy: Promises and Challenges of Implementing CAR Technology. *Front Immunol* (10.3389/fimmu.2020.01608).2020; **11**: 1608.
116. Berger A. Th1 and Th2 responses: what are they? *BMJ* 2000; **321**: 424-424.
117. Lloyd CM, Snelgrove RJ. Type 2 immunity: Expanding our view. *Science Immunology* 2018; **3**: eaat1604.
118. Suzukawa M, Nagase H, Ogahara I*, et al.* Leptin Enhances Survival and Induces Migration, Degranulation, and Cytokine Synthesis of Human Basophils. *The Journal of Immunology* 2011; **186**: 5254.
119. Hadfield KA, McCracken SA, Ashton AW, Nguyen TG, Morris JM. Regulated suppression of NF-κB throughout pregnancy maintains a favourable cytokine environment necessary for pregnancy success. *Journal of Reproductive Immunology* 2011; **89**: 1-9.
120. Somerset DA, Zheng Y, Kilby MD, Sansom DM, Drayson MT. Normal human pregnancy is associated with an elevation in the immune suppressive CD25+ CD4+ regulatory T-cell subset. *Immunology* 2004; **112**: 38-43.
121. Mjösberg J, Berg G, Ernerudh J, Ekerfelt C. CD4+ CD25+ regulatory T cells in human pregnancy: development of a Treg-MLC-ELISPOT suppression assay and indications of paternal specific Tregs. *Immunology* 2007; **120**: 456-466.

122. Heikkinen J, Möttönen M, Alanen A, Lassila O. Phenotypic characterization of regulatory T cells in the human decidua. *Clinical and experimental immunology* 2004; **136**: 373-378.
123. Wang W-J, Liu F-J, Xin L*, et al.* Adoptive transfer of pregnancy-induced CD4+CD25+ regulatory T cells reverses the increase in abortion rate caused by interleukin 17 in the CBA/J×BALB/c mouse model. *Human Reproduction* 2014; **29**: 946-952.
124. Aluvihare VR, Kallikourdis M, Betz AG. Regulatory T cells mediate maternal tolerance to the fetus. *Nature Immunology* 2004; **5**: 266-271.
125. Nevers T, Kalkunte S, Sharma S. Uterine Regulatory T cells, IL-10 and hypertension. *Am J Reprod Immunol* 2011; **66 Suppl 1**: 88-92.
126. Robertson SA, Green ES, Care AS*, et al.* Therapeutic Potential of Regulatory T Cells in Preeclampsia—Opportunities and Challenges. *Front Immunol* (10.3389/fimmu.2019.00478).2019; **10**: 478.
127. Samstein RM, Josefowicz SZ, Arvey A, Treuting PM, Rudensky AY. Extrathymic generation of regulatory T cells in placental mammals mitigates maternal-fetal conflict. *Cell* 2012; **150**: 29-38.
128. Koucký M, Malíčková K, Cindrová-Davies T*, et al.* Low levels of circulating T-regulatory lymphocytes and short cervical length are associated with preterm labor. *Journal of Reproductive Immunology* 2014; **106**: 110-117.
129. Wang W-J, Hao C-F, Yi L*, et al.* Increased prevalence of T helper 17 (Th17) cells in peripheral blood and decidua in unexplained recurrent spontaneous abortion patients. *Journal of Reproductive Immunology* 2010; **84**: 164-170.
130. Granne I, Southcombe JH, Snider JV*, et al.* ST2 and IL-33 in pregnancy and pre-eclampsia. *PloS one* 2011; **6**: e24463-e24463.
131. Sen S, Iyer C, Klebenov D, Histed A, Aviles JA, Meydani SN. Obesity impairs cell-mediated immunity during the second trimester of pregnancy. *American Journal of Obstetrics & Gynecology* 2013; **208**: 139.e131-139.e138.
132. Solders M, Gorchs L, Erkers T*, et al.* MAIT cells accumulate in placental intervillous space and display a highly cytotoxic phenotype upon bacterial stimulation. *Scientific reports* 2017; **7**: 6123-6123.
133. Kaipe H, Raffetseder J, Ernerudh J, Solders M, Tiblad E. MAIT Cells at the Fetal-Maternal Interface During Pregnancy. *Front Immunol* (10.3389/fimmu.2020.01788).2020; **11**: 1788.
134. Ravi K, Chan CYS, Akoto C*, et al.* Changes in the Vα7.2+ CD161++ MAIT cell compartment in early pregnancy are associated with preterm birth in HIV-positive women. *American Journal of Reproductive Immunology* (https://doi.org/10.1111/aji.13240).2020; **83**: e13240.
135. Raffetseder J, Lindau R, van der Veen S, Berg G, Larsson M, Ernerudh J. MAIT Cells Balance the Requirements for Immune Tolerance and Anti-Microbial Defense During Pregnancy. *Front Immunol* (10.3389/fimmu.2021.718168).2021; **12**: 3008.
136. Lima J, Martins C, Leandro MJ*, et al.* Characterization of B cells in healthy pregnant women from late pregnancy to post-partum: a prospective observational study. *BMC Pregnancy Childbirth* 2016; **16**: 139-139.
137. Rolle L, Memarzadeh Tehran M, Morell-García A*, et al.* Cutting Edge: IL-10-Producing Regulatory B Cells in Early Human Pregnancy. *American Journal of Reproductive Immunology* 2013; **70**: 448-453.

138. Guzman-Genuino RM, Hayball JD, Diener KR. Regulatory B Cells: Dark Horse in Pregnancy Immunotherapy? *Journal of Molecular Biology* 2021; **433**: 166596.
139. Palmeira P, Quinello C, Silveira-Lessa AL, Zago CA, Carneiro-Sampaio M. IgG placental transfer in healthy and pathological pregnancies. *Clin Dev Immunol* 2012; **2012**: 985646-985646.
140. Miller EC, Abel W. Changes in the immunoglobulins IgG, IgA and IgM in pregnancy and the puerperium. *Zentralblatt fur Gynakologie* 1984; **106(15)**: 1084-1091.
141. McDuffie JR, Riggs PA, Calis KA*, et al.* Effects of exogenous leptin on satiety and satiation in patients with lipodystrophy and leptin insufficiency. *J Clin Endocrinol Metab* 2004; **89**: 4258-4263.
142. Lam QL, Lu L. Role of leptin in immunity. *Cell Mol Immunol* 2007; **4**: 1-13.
143. Couce ME, Burguera B, Parisi JE, Jensen MD, Lloyd RV. Localization of Leptin Receptor in the Human Brain. *Neuroendocrinology* 1997; **66**: 145-150.
144. Frederich RC, Hamann A, Anderson S, Löllmann B, Lowell BB, Flier JS. Leptin levels reflect body lipid content in mice: Evidence for diet-induced resistance to leptin action. *Nat Med* 1995; **1**: 1311-1314.
145. Wabitsch M, Bo Jensen P, Blum WF*, et al.* Insulin and Cortisol Promote Leptin Production in Cultured Human Fat Cells. *Diabetes* 1996; **45**: 1435.
146. Ricci MR, Fried SK. Isoproterenol Decreases Leptin Expression in Adipose Tissue of Obese Humans. *Obesity Research* 1999; **7**: 233-240.
147. Trujillo ME, Lee M-J, Sullivan S*, et al.* Tumor Necrosis Factor α and Glucocorticoid Synergistically Increase Leptin Production in Human Adipose Tissue: Role for p38 Mitogen-Activated Protein Kinase. *The Journal of Clinical Endocrinology & Metabolism* 2006; **91**: 1484-1490.
148. Minokoshi Y, Toda C, Okamoto S. Regulatory role of leptin in glucose and lipid metabolism in skeletal muscle. *Indian J Endocrinol Metab* 2012; **16**: S562-S568.
149. Bruno A, Conus S, Schmid I, Simon H-U. Apoptotic Pathways Are Inhibited by Leptin Receptor Activation in Neutrophils. *The Journal of Immunology* 2005; **174**: 8090.
150. Francisco V, Pino J, Campos-Cabaleiro V*, et al.* Obesity, Fat Mass and Immune System: Role for Leptin. *Front Physiol* 2018; **9**: 640-640.
151. Cannon JG, Sharma G, Sloan G*, et al.* Leptin regulates CD16 expression on human monocytes in a sex-specific manner. *Physiol Rep* 2014; **2**: e12177.
152. Chehab FF, Lim ME, Lu R. Correction of the sterility defect in homozygous obese female mice by treatment with the human recombinant leptin. *Nature Genetics* 1996; **12**: 318-320.
153. Matkovic V, Ilich JZ, Skugor M*, et al.* Leptin Is Inversely Related to Age at Menarche in Human Females*. *The Journal of Clinical Endocrinology & Metabolism* 1997; **82**: 3239-3245.
154. Señarís R, Garcia-Caballero Ts, Casabiell Xs*, et al.* Synthesis of Leptin in Human Placenta. *Endocrinology* 1997; **138**: 4501-4504.
155. Trujillo-Güiza ML, Señarís R. Leptin resistance during pregnancy is also exerted at the periphery†. *Biology of Reproduction* 2018; **98**: 654-663.
156. Farley DM, Choi J, Dudley DJ*, et al.* Placental Amino Acid Transport and Placental Leptin Resistance in Pregnancies Complicated by Maternal Obesity. *Placenta* 2010; **31**: 718-724.
157. Tessier DR, Ferraro ZM, Gruslin A. Role of leptin in pregnancy: Consequences of maternal obesity. *Placenta* 2013; **34**: 205-211.

158. Jansson N, Greenwood SL, Johansson BR, Powell TL, Jansson T. Leptin Stimulates the Activity of the System A Amino Acid Transporter in Human Placental Villous Fragments. *The Journal of Clinical Endocrinology & Metabolism* 2003; **88**: 1205-1211.
159. Pomar L, Musso D, Malinger G, Vouga M, Panchaud A, Baud D. Zika virus during pregnancy: From maternal exposure to congenital Zika virus syndrome. *Prenatal Diagnosis* 2019; **39**: 420-430.
160. Wong SF, Chow KM, Leung TN*, et al.* Pregnancy and perinatal outcomes of women with severe acute respiratory syndrome. *American journal of obstetrics and gynecology* 2004; **191**: 292-297.
161. Somerville LK, Basile K, Dwyer DE, Kok J. The impact of influenza virus infection in pregnancy. *Future Microbiology* 2018; **13**: 263-274.
162. Mlakar J, Korva M, Tul N*, et al.* Zika Virus Associated with Microcephaly. *New England Journal of Medicine* 2016; **374**: 951-958.
163. Gynaecologists RCoOa. Coronavirus infection and pregnancy. Available from: https://www.rcog.org.uk/en/guidelines-research-services/guidelines/coronavirus-pregnancy/covid-19-virus-infection-and-pregnancy/#pregnancy.
164. Martinez-Perez O, Prats Rodriguez P, Muner Hernandez M*, et al.* The association between SARS-CoV-2 infection and preterm delivery: a prospective study with a multivariable analysis. *BMC Pregnancy Childbirth* 2021; **21**: 273.
165. Vousden N, Bunch K, Morris E*, et al.* The incidence, characteristics and outcomes of pregnant women hospitalized with symptomatic and asymptomatic SARS-CoV-2 infection in the UK from March to September 2020: A national cohort study using the UK Obstetric Surveillance System (UKOSS). *PLOS ONE* 2021; **16**: e0251123.
166. Zhang J-j, Dong X, Cao Y-y*, et al.* Clinical characteristics of 140 patients infected with SARS-CoV-2 in Wuhan, China. *Allergy* 2020; **75**: 1730-1741.
167. Knight M, Bunch K, Vousden N*, et al.* Characteristics and outcomes of pregnant women admitted to hospital with confirmed SARS-CoV-2 infection in UK: national population based cohort study. *BMJ (Clinical research ed)* 2020; **369**: m2107-m2107.
168. Hojyo S, Uchida M, Tanaka K*, et al.* How COVID-19 induces cytokine storm with high mortality. *Inflammation and Regeneration* 2020; **40**: 37.
169. Silberstein M. Correlation between premorbid IL-6 levels and COVID-19 mortality: Potential role for Vitamin D. *Int Immunopharmacol* 2020; **88**: 106995-106995.
170. O'Neill LAJ, Kishton RJ, Rathmell J. A guide to immunometabolism for immunologists. *Nature reviews Immunology* 2016; **16**: 553-565.
171. Newsholme P, Curi R, Gordon S, Newsholme EA. Metabolism of glucose, glutamine, long-chain fatty acids and ketone bodies by murine macrophages. *Biochemical Journal* 1986; **239**: 121-125.
172. Alonso D, Nungester W. Comparative study of host resistance of guinea pigs and rats. V. The effect of pneumococcal products on glycolysis and oxygen uptake by polymorphonuclear leucocytes. *J Infect Dis* 1956; **99**: 174-181.
173. Michl J, Ohlbaum D, Silverstein S. 2-Deoxyglucose selectively inhibits Fc and complement receptor-mediated phagocytosis in mouse peritoneal macrophages. I. Description of the inhibitory effect. *The Journal of Experimental Medicine* 1976; **144**: 1465-1483.
174. Hamilton JA, Vairo G, Lingelbach SR. CSF-1 stimulates glucose uptake in murine bone marrow-derived macrophages. *Biochemical and Biophysical Research Communications* 1986; **138**: 445-454.

175. van der Windt GJW, O'Sullivan D, Everts B*, et al.* CD8 memory T cells have a bioenergetic advantage that underlies their rapid recall ability. *Proceedings of the National Academy of Sciences of the United States of America* 2013; **110**: 14336-14341.
176. Joost H-G, Bell GI, Best JD*, et al.* Nomenclature of the GLUT/SLC2A family of sugar/polyol transport facilitators. *American Journal of Physiology-Endocrinology and Metabolism* 2002; **282**: E974-E976.
177. Baltazar F, Afonso J, Costa M, Granja S. Lactate Beyond a Waste Metabolite: Metabolic Affairs and Signaling in Malignancy. *Frontiers in Oncology* (10.3389/fonc.2020.00231).2020; **10**: 231.
178. Magistretti PJ, Allaman I. Lactate in the brain: from metabolic end-product to signalling molecule. *Nature Reviews Neuroscience* 2018; **19**: 235-249.
179. Vander Heiden MG, Cantley LC, Thompson CB. Understanding the Warburg effect: the metabolic requirements of cell proliferation. *Science (New York, NY)* 2009; **324**: 1029-1033.
180. WARBURG O. On the origin of cancer cells. *Science* 1956; **123**: 309-314.
181. Rodríguez-Prados J-C, Través PG, Cuenca J*, et al.* Substrate Fate in Activated Macrophages: A Comparison between Innate, Classic, and Alternative Activation. *The Journal of Immunology* 2010; **185**: 605.
182. Krawczyk CM, Holowka T, Sun J*, et al.* Toll-like receptor-induced changes in glycolytic metabolism regulate dendritic cell activation. *Blood* 2010; **115**: 4742-4749.
183. Donnelly RP, Loftus RM, Keating SE*, et al.* mTORC1-dependent metabolic reprogramming is a prerequisite for NK cell effector function. *Journal of immunology (Baltimore, Md : 1950)* 2014; **193**: 4477-4484.
184. Michalek RD, Gerriets VA, Jacobs SR*, et al.* Cutting edge: distinct glycolytic and lipid oxidative metabolic programs are essential for effector and regulatory CD4+ T cell subsets. *Journal of immunology (Baltimore, Md : 1950)* 2011; **186**: 3299-3303.
185. Doughty CA, Bleiman BF, Wagner DJ*, et al.* Antigen receptor-mediated changes in glucose metabolism in B lymphocytes: role of phosphatidylinositol 3-kinase signaling in the glycolytic control of growth. *Blood* 2006; **107**: 4458-4465.
186. Tannahill GM, Curtis AM, Adamik J*, et al.* Succinate is an inflammatory signal that induces IL-1β through HIF-1α. *Nature* 2013; **496**: 238-242.
187. Huynh A, DuPage M, Priyadharshini B*, et al.* Control of PI(3) kinase in Treg cells maintains homeostasis and lineage stability. *Nature immunology* 2015; **16**: 188-196.
188. Palsson-McDermott EM, Curtis AM, Goel G*, et al.* Pyruvate kinase M2 regulates Hif-1α activity and IL-1β induction and is a critical determinant of the warburg effect in LPS-activated macrophages. *Cell metabolism* 2015; **21**: 65-80.
189. Moon J-S, Hisata S, Park M-A*, et al.* mTORC1-Induced HK1-Dependent Glycolysis Regulates NLRP3 Inflammasome Activation. *Cell Rep* 2015; **12**: 102-115.
190. Infantino V, Convertini P, Cucci L*, et al.* The mitochondrial citrate carrier: a new player in inflammation. *Biochemical Journal* 2011; **438**: 433-436.
191. Michelucci A, Cordes T, Ghelfi J*, et al.* Immune-responsive gene 1 protein links metabolism to immunity by catalyzing itaconic acid production. *Proceedings of the National Academy of Sciences of the United States of America* 2013; **110**: 7820-7825.
192. Yankovskaya V, Horsefield R, Törnroth S*, et al.* Architecture of Succinate Dehydrogenase and Reactive Oxygen Species Generation. *Science* 2003; **299**: 700.

193. Grivennikova VG, Vinogradov AD. Generation of superoxide by the mitochondrial Complex I. *Biochimica et Biophysica Acta (BBA) - Bioenergetics* 2006; **1757**: 553-561.
194. Liguori I, Russo G, Curcio F*, et al.* Oxidative stress, aging, and diseases. *Clin Interv Aging* 2018; **13**: 757-772.
195. Heinz S, Freyberger A, Lawrenz B, Schladt L, Schmuck G, Ellinger-Ziegelbauer H. Mechanistic Investigations of the Mitochondrial Complex I Inhibitor Rotenone in the Context of Pharmacological and Safety Evaluation. *Scientific Reports* 2017; **7**: 45465.
196. Glatz JFC, Luiken JJFP, Bonen A. Membrane Fatty Acid Transporters as Regulators of Lipid Metabolism: Implications for Metabolic Disease. *Physiological Reviews* 2010; **90**: 367-417.
197. Yao C-H, Liu G-Y, Wang R, Moon SH, Gross RW, Patti GJ. Identifying off-target effects of etomoxir reveals that carnitine palmitoyltransferase I is essential for cancer cell proliferation independent of β-oxidation. *PLoS Biol* 2018; **16**: e2003782-e2003782.
198. Malandrino MI, Fucho R, Weber M*, et al.* Enhanced fatty acid oxidation in adipocytes and macrophages reduces lipid-induced triglyceride accumulation and inflammation. *American Journal of Physiology-Endocrinology and Metabolism* 2015; **308**: E756-E769.
199. Feingold KR, Shigenaga JK, Kazemi MR*, et al.* Mechanisms of triglyceride accumulation in activated macrophages. *Journal of leukocyte biology* 2012; **92**: 829-839.
200. Ecker J, Liebisch G, Englmaier M, Grandl M, Robenek H, Schmitz G. Induction of fatty acid synthesis is a key requirement for phagocytic differentiation of human monocytes. *Proceedings of the National Academy of Sciences of the United States of America* 2010; **107**: 7817-7822.
201. Hayat M, Khan A. WRF-TMH: predicting transmembrane helix by fusing composition index and physicochemical properties of amino acids. *Amino Acids* 2013; **44**: 1317-1328.
202. Devés R, Boyd CAR. Surface Antigen CD98(4F2): Not a Single Membrane Protein, But a Family of Proteins with Multiple Functions. *The Journal of Membrane Biology* 2000; **173**: 165-177.
203. Viola A, Munari F, Sánchez-Rodríguez R, Scolaro T, Castegna A. The Metabolic Signature of Macrophage Responses. *Front Immunol* (10.3389/fimmu.2019.01462).2019; **10**: 1462.
204. Murphy C, Newsholme P. Importance of glutamine metabolism in murine macrophages and human monocytes to L-arginine biosynthesis and rates of nitrite or urea production. *Clinical Science* 1998; **95**: 397-407.
205. MacMicking JD, Nathan C, Hom G*, et al.* Altered responses to bacterial infection and endotoxic shock in mice lacking inducible nitric oxide synthase. *Cell* 1995; **81**: 641-650.
206. Pesce JT, Ramalingam TR, Mentink-Kane MM*, et al.* Arginase-1-expressing macrophages suppress Th2 cytokine-driven inflammation and fibrosis. *PLoS Pathog* 2009; **5**: e1000371-e1000371.
207. Rutschman R, Lang R, Hesse M, Ihle JN, Wynn TA, Murray PJ. Cutting Edge: Stat6-Dependent Substrate Depletion Regulates Nitric Oxide Production. *The Journal of Immunology* 2001; **166**: 2173.
208. Ming X-F, Rajapakse AG, Yepuri G*, et al.* Arginase II Promotes Macrophage Inflammatory Responses Through Mitochondrial Reactive Oxygen Species, Contributing to Insulin Resistance and Atherogenesis. *Journal of the American Heart Association* 2012; **1**: e000992-e000992.

209. Weinlich G, Murr C, Richardsen L, Winkler C, Fuchs D. Decreased Serum Tryptophan Concentration Predicts Poor Prognosis in Malignant Melanoma Patients. *Dermatology* 2007; **214**: 8-14.
210. Yoshida R, Hayaishi O. Induction of pulmonary indoleamine 2,3-dioxygenase by intraperitoneal injection of bacterial lipopolysaccharide. *Proceedings of the National Academy of Sciences of the United States of America* 1978; **75**: 3998-4000.
211. Werner ER, Werner-Felmayer G, Fuchs D, Hausen A, Reibnegger G, Wachter H. Parallel induction of tetrahydrobiopterin biosynthesis and indoleamine 2,3-dioxygenase activity in human cells and cell lines by interferon-gamma. *The Biochemical journal* 1989; **262**: 861-866.
212. Pfefferkorn ER. Interferon gamma blocks the growth of Toxoplasma gondii in human fibroblasts by inducing the host cells to degrade tryptophan. *Proceedings of the National Academy of Sciences of the United States of America* 1984; **81**: 908-912.
213. Bessede A, Gargaro M, Pallotta MT*, et al.* Aryl hydrocarbon receptor control of a disease tolerance defence pathway. *Nature* 2014; **511**: 184-190.
214. Schröcksnadel H, Baier-Bitterlich G, Dapunt O, Wachter H, Fuchs D. Decreased plasma tryptophan in pregnancy. *Obstet Gynecol* 1996; **88**: 47-50.
215. Adu-Gyamfi C, Savulescu D, Mikhathani L*, et al.* Plasma Kynurenine-to-Tryptophan Ratio, a Highly Sensitive Blood-Based Diagnostic Tool for Tuberculosis in Pregnant Women Living With Human Immunodeficiency Virus (HIV). *Clinical infectious diseases : an official publication of the Infectious Diseases Society of America* 2021; **73**: 1027-1036.
216. Fallarino F, Grohmann U, You S*, et al.* The combined effects of tryptophan starvation and tryptophan catabolites down-regulate T cell receptor zeta-chain and induce a regulatory phenotype in naive T cells. *J Immunol* 2006; **176**: 6752-6761.
217. Chang R-Q, Li D-J, Li M-Q. The role of indoleamine-2,3-dioxygenase in normal and pathological pregnancies. *American Journal of Reproductive Immunology* (https://doi.org/10.1111/aji.12786).2018; **79**: e12786.
218. Munn DH, Zhou M, Attwood JT*, et al.* Prevention of allogeneic fetal rejection by tryptophan catabolism. *Science* 1998; **281**: 1191-1193.
219. Henrichs I, Benz R, Teller NM. Gluconeogenesis in human placenta: effects of insulin and hypoxia *in vitro Pediatric Research* 1986; **20**: 1180-1180.
220. Chen H, Chomyn A, Chan DC. Disruption of Fusion Results in Mitochondrial Heterogeneity and Dysfunction. *Journal of Biological Chemistry* 2005; **280**: 26185-26192.
221. Collins TJ, Berridge MJ, Lipp P, Bootman MD. Mitochondria are morphologically and functionally heterogeneous within cells. *EMBO J* 2002; **21**: 1616-1627.
222. Um J-H, Yun J. Emerging role of mitophagy in human diseases and physiology. *BMB Rep* 2017; **50**: 299-307.
223. Karaa A, Elsharkawi I, Clapp MA, Balcells C. Effects of mitochondrial disease/dysfunction on pregnancy: A retrospective study. *Mitochondrion* 2019; **46**: 214-220.
224. Feeney CL, Lim AZ, Fagan E*, et al.* A case-comparison study of pregnant women with mitochondrial disease – what to expect? *BJOG: An International Journal of Obstetrics & Gynaecology* (https://doi.org/10.1111/1471-0528.15667).2019; **126**: 1380-1389.
225. Boyle KE, Newsom SA, Janssen RC, Lappas M, Friedman JE. Skeletal muscle MnSOD, mitochondrial complex II, and SIRT3 enzyme activities are decreased in maternal

obesity during human pregnancy and gestational diabetes mellitus. *The Journal of clinical endocrinology and metabolism* 2013; **98**: E1601-E1609.

226. Spegiorin LCJF, Galão EA, Bagarelli LB, Oliani AH, de Godoy JMP. Prevalence of anticardiolipin antibodies in pregnancies with history of repeated miscarriages. *The open rheumatology journal* 2010; **4**: 28-30.
227. Aibibula M, Naseem KM, Sturmey RG. Glucose metabolism and metabolic flexibility in blood platelets. *Journal of Thrombosis and Haemostasis* (https://doi.org/10.1111/jth.14274).2018; **16**: 2300-2314.
228. Jones N, Blagih J, Zani F*, et al.* Fructose reprograms glutamine-dependent oxidative metabolism to support LPS-induced inflammation. Nature Communications; 2021.
229. Divakaruni AS, Hsieh WY, Minarrieta L*, et al.* Etomoxir Inhibits Macrophage Polarization by Disrupting CoA Homeostasis. *Cell metabolism* 2018; **28**: 490-503.e497.
230. Tracey TJ, Steyn FJ, Wolvetang EJ, Ngo ST. Neuronal Lipid Metabolism: Multiple Pathways Driving Functional Outcomes in Health and Disease. *Frontiers in Molecular Neuroscience* (10.3389/fnmol.2018.00010).2018; **11**: 10.
231. Fernández LP, Gómez de Cedrón M, Ramírez de Molina A. Alterations of Lipid Metabolism in Cancer: Implications in Prognosis and Treatment. *Frontiers in Oncology* (10.3389/fonc.2020.577420).2020; **10**: 2144.
232. Thirunavukkarasu S, Khader SA. Advances in Cardiovascular Disease Lipid Research Can Provide Novel Insights Into Mycobacterial Pathogenesis. *Frontiers in Cellular and Infection Microbiology* (10.3389/fcimb.2019.00116).2019; **9**: 116.
233. Lauber K, Bohn E, Kröber SM*, et al.* Apoptotic Cells Induce Migration of Phagocytes via Caspase-3-Mediated Release of a Lipid Attraction Signal. *Cell* 2003; **113**: 717-730.
234. Rong JX, Berman JW, Taubman MB, Fisher EA. Lysophosphatidylcholine Stimulates Monocyte Chemoattractant Protein-1 Gene Expression in Rat Aortic Smooth Muscle Cells. *Arteriosclerosis, Thrombosis, and Vascular Biology* 2002; **22**: 1617-1623.
235. Schmitz G, Ruebsaamen K. Metabolism and atherogenic disease association of lysophosphatidylcholine. *Atherosclerosis* 2010; **208**: 10-18.
236. Anderson SG, Dunn WB, Banerjee M*, et al.* Evidence that multiple defects in lipid regulation occur before hyperglycemia during the prodrome of type-2 diabetes. *PloS one* 2014; **9**: e103217-e103217.
237. Lu L, Koulman A, Petry CJ*, et al.* An Unbiased Lipidomics Approach Identifies Early Second Trimester Lipids Predictive of Maternal Glycemic Traits and Gestational Diabetes Mellitus. *Diabetes care* 2016; **39**: 2232-2239.
238. Alesi S, Ghelani D, Rassie K, Mousa A. Metabolomic Biomarkers in Gestational Diabetes Mellitus: A Review of the Evidence. *International journal of molecular sciences* 2021; **22**: 5512.
239. Hong X, Zhang B, Liang L*, et al.* Postpartum plasma metabolomic profile among women with preeclampsia and preterm delivery: implications for long-term health. *BMC Medicine* 2020; **18**: 277.
240. Liu Y, He B, Maurya MR*, et al.* Maternal blood lipidomics analyses link critical metabolic pathways associated with severe preeclampsia. *medRxiv* 2020: 2020.2007.2005.20145292.
241. Angelini R, Vortmeier G, Corcelli A, Fuchs B. A fast method for the determination of the PC/LPC ratio in intact serum by MALDI-TOF MS: An easy-to-follow lipid biomarker of inflammation. *Chemistry and Physics of Lipids* 2014; **183**: 169-175.

242. Williams TJ, Morley J. Prostaglandins as Potentiators of Increased Vascular Permeability in Inflammation. *Nature* 1973; **246**: 215-217.
243. Aronoff DM, Canetti C, Peters-Golden M. Prostaglandin E₂ Inhibits Alveolar Macrophage Phagocytosis through an E-Prostanoid 2 Receptor-Mediated Increase in Intracellular Cyclic AMP. *The Journal of Immunology* 2004; **173**: 559.
244. Kunkel SL, Wiggins RC, Chensue SW, Larrick J. Regulation of macrophage tumor necrosis factor production by prostaglandin E2. *Biochemical and Biophysical Research Communications* 1986; **137**: 404-410.
245. Hinson RM, Williams JA, Shacter E. Elevated interleukin 6 is induced by prostaglandin E2 in a murine model of inflammation: possible role of cyclooxygenase-2. *Proceedings of the National Academy of Sciences* 1996; **93**: 4885.
246. Harizi H, Juzan M, Pitard V, Moreau J-F, Gualde N. Cyclooxygenase-2-Issued Prostaglandin E₂ Enhances the Production of Endogenous IL-10, Which Down-Regulates Dendritic Cell Functions. *The Journal of Immunology* 2002; **168**: 2255.
247. Borgeat P, Naccache PH. Biosynthesis and biological activity of leukotriene B4. *Clinical Biochemistry* 1990; **23**: 459-468.
248. Powell WS, Chung D, Gravel S. 5-Oxo-6,8,11,14-eicosatetraenoic acid is a potent stimulator of human eosinophil migration. *The Journal of Immunology* 1995; **154**: 4123.
249. Powell WS, Rokach J. Biochemistry, biology and chemistry of the 5-lipoxygenase product 5-oxo-ETE. *Progress in Lipid Research* 2005; **44**: 154-183.
250. Stamatiou PB, Chan C-C, Monneret G, Ethier D, Rokach J, Powell WS. 5-Oxo-6,8,11,14-eicosatetraenoic Acid Stimulates the Release of the Eosinophil Survival Factor Granulocyte/Macrophage Colony-stimulating Factor from Monocytes. *Journal of Biological Chemistry* 2004; **279**: 28159-28164.
251. O'Flaherty JT, Kuroki M, Nixon AB*, et al.* 5-Oxo-eicosanoids and Hematopoietic Cytokines Cooperate in Stimulating Neutrophil Function and the Mitogen-activated Protein Kinase Pathway. *Journal of Biological Chemistry* 1996; **271**: 17821-17828.
252. Maddox JF, Serhan CN. Lipoxin A4 and B4 are potent stimuli for human monocyte migration and adhesion: selective inactivation by dehydrogenation and reduction. *Journal of Experimental Medicine* 1996; **183**: 137-146.
253. Patcha V, Wigren J, Winberg ME, Rasmusson B, Li J, Särndahl E. Differential inside-out activation of β2-integrins by leukotriene B4 and fMLP in human neutrophils. *Experimental Cell Research* 2004; **300**: 308-319.
254. Godson C, Mitchell S, Harvey K, Petasis NA, Hogg N, Brady HR. Cutting Edge: Lipoxins Rapidly Stimulate Nonphlogistic Phagocytosis of Apoptotic Neutrophils by Monocyte-Derived Macrophages. *The Journal of Immunology* 2000; **164**: 1663.
255. Mitchell S, Thomas G, Harvey K*, et al.* Lipoxins, Aspirin-Triggered Epi-Lipoxins, Lipoxin Stable Analogues, and the Resolution of Inflammation: Stimulation of Macrophage Phagocytosis of Apoptotic Neutrophils In Vivo. *Journal of the American Society of Nephrology* 2002; **13**: 2497.
256. Node K, Huo Y, Ruan X*, et al.* Anti-inflammatory Properties of Cytochrome P450 Epoxygenase-Derived Eicosanoids. *Science* 1999; **285**: 1276.
257. Heizer ML, McKinney JS, Ellis EF. 14,15-Epoxyeicosatrienoic acid inhibits platelet aggregation in mouse cerebral arterioles. *Stroke* 1991; **22**: 1389-1393.

258. Bednar MM, Gross CE, Balazy MK*, et al.* 16(R)-hydroxy-5,8,11,14-eicosatetraenoic acid, a new arachidonate metabolite in human polymorphonuclear leukocytes. *Biochemical Pharmacology* 2000; **60**: 447-455.
259. Hill E, Fitzpatrick F, Murphy RC. Biological activity and metabolism of 20-hydroxyeicosatetraenoic acid in the human platelet. *British Journal of Pharmacology* 1992; **106**: 267-274.
260. Arita M, Bianchini F, Aliberti J*, et al.* Stereochemical assignment, antiinflammatory properties, and receptor for the omega-3 lipid mediator resolvin E1. *Journal of Experimental Medicine* 2005; **201**: 713-722.
261. Schwab JM, Chiang N, Arita M, Serhan CN. Resolvin E1 and protectin D1 activate inflammation-resolution programmes. *Nature* 2007; **447**: 869-874.
262. Dona M, Fredman G, Schwab JM*, et al.* Resolvin E1, an EPA-derived mediator in whole blood, selectively counterregulates leukocytes and platelets. *Blood* 2008; **112**: 848-855.
263. Arita M, Ohira T, Sun Y-P, Elangovan S, Chiang N, Serhan CN. Resolvin E1 Selectively Interacts with Leukotriene B₄ Receptor BLT1 and ChemR23 to Regulate Inflammation. *The Journal of Immunology* 2007; **178**: 3912.
264. Duffield JS, Hong S, Vaidya VS*, et al.* Resolvin D Series and Protectin D1 Mitigate Acute Kidney Injury. *The Journal of Immunology* 2006; **177**: 5902.
265. Levy BD, Kohli P, Gotlinger K*, et al.* Protectin D1 Is Generated in Asthma and Dampens Airway Inflammation and Hyperresponsiveness. *The Journal of Immunology* 2007; **178**: 496.
266. Ariel A, Li P-L, Wang W*, et al.* The Docosatriene Protectin D1 Is Produced by TH2 Skewing and Promotes Human T Cell Apoptosis via Lipid Raft Clustering. *Journal of Biological Chemistry* 2005; **280**: 43079-43086.
267. Mukherjee PK, Marcheselli VL, de Rivero Vaccari JC, Gordon WC, Jackson FE, Bazan NG. Photoreceptor outer segment phagocytosis attenuates oxidative stress-induced apoptosis with concomitant neuroprotectin D1 synthesis. *Proceedings of the National Academy of Sciences* 2007; **104**: 13158.
268. Serhan CN, Yang R, Martinod K*, et al.* Maresins: novel macrophage mediators with potent antiinflammatory and proresolving actions. *Journal of Experimental Medicine* 2008; **206**: 15-23.
269. Eriksson L, Haglund B, Odlind V, Altman M, Ewald U, Kieler H. Perinatal conditions related to growth restriction and inflammation are associated with an increased risk of bronchopulmonary dysplasia. *Acta Paediatrica* 2015; **104**: 259-263.
270. Carlson SE, Colombo J, Gajewski BJ*, et al.* DHA supplementation and pregnancy outcomes. *The American journal of clinical nutrition* 2013; **97**: 808-815.
271. Olsen SF, Østerdal ML, Salvig JD*, et al.* Fish oil intake compared with olive oil intake in late pregnancy and asthma in the offspring: 16 y of registry-based follow-up from a randomized controlled trial. *The American Journal of Clinical Nutrition* 2008; **88**: 167-175.
272. Breckler LA, Hale J, Taylor A, Dunstan JA, Thornton CA, Prescott SL. Pregnancy IFN-γ responses to foetal alloantigens are altered by maternal allergy and gravidity status. *Allergy* (https://doi.org/10.1111/j.1398-9995.2008.01718.x).2008; **63**: 1473-1480.
273. Xu Z, Zhao F, Lin F*, et al.* Preeclampsia is associated with a deficiency of lipoxin A4, an endogenous anti-inflammatory mediator. *Fertility and Sterility* 2014; **102**: 282-290.e284.

274. Le Faouder P, Baillif V, Spreadbury I*, et al.* LC–MS/MS method for rapid and concomitant quantification of pro-inflammatory and pro-resolving polyunsaturated fatty acid metabolites. *Journal of Chromatography B* 2013; **932**: 123-133.
275. Ishikawa M, Maekawa K, Saito K*, et al.* Plasma and Serum Lipidomics of Healthy White Adults Shows Characteristic Profiles by Subjects' Gender and Age. *PLOS ONE* 2014; **9**: e91806.
276. Ditz T, Fuchs B. Determination of the Phosphatidylcholine/Lysophosphatidylcholine Ratio in Intact Serum by Matrix-Assisted Laser Desorption/Ionization Mass Spectrometry with Prior Enzymatic Albumin Digestion. *Lipids* 2018; **53**: 971-977.
277. Mukherjee S, Velez Edwards DR, Baird DD, Savitz DA, Hartmann KE. Risk of Miscarriage Among Black Women and White Women in a US Prospective Cohort Study. *American Journal of Epidemiology* 2013; **177**: 1271-1278.
278. Hamabata T, Nakamura T, Tachibana Y, Horikami D, Murata T. 5,6-DiHETE attenuates vascular hyperpermeability by inhibiting Ca(2+) elevation in endothelial cells. *Journal of lipid research* 2018; **59**: 1864-1870.
279. Clark SR, Guy CJ, Scurr MJ*, et al.* Esterified eicosanoids are acutely generated by 5-lipoxygenase in primary human neutrophils and in human and murine infection. *Blood* 2011; **117**: 2033-2043.
280. Lipp P, Ruhnau J, Lange A, Vogelgesang A, Dressel A, Heckmann M. Less Neutrophil Extracellular Trap Formation in Term Newborns than in Adults. *Neonatology* 2017; **111**: 182-188.
281. Endo J, Sano M, Isobe Y*, et al.* 18-HEPE, an n-3 fatty acid metabolite released by macrophages, prevents pressure overload–induced maladaptive cardiac remodeling. *Journal of Experimental Medicine* 2014; **211**: 1673-1687.
282. Liagre B, Vergne P, Rigaud M, Beneytout JL. Expression of arachidonate platelet-type 12-lipoxygenase in human rheumatoid arthritis typeB synoviocytes. *FEBS Letters* 1997; **414**: 159-164.
283. Katsube N, Maruyama M, Andoh T, Kuraishi Y. Involvement of Leukotriene B4 in Substance P-Induced Itch-Associated Response in Mice. *Journal of Investigative Dermatology* 2001; **117**: 1621-1626.
284. Mlodawski J, Mlodawska M, Armanska J, Swiercz G, Gluszek S. Misoprostol vs dinoprostone vaginal insert in labour induction: comparison of obstetrical outcome. *Scientific Reports* 2021; **11**: 9077.
285. Makhlouf AM, Al-Hussaini TK, Habib DM, Makarem MH. Second-trimester pregnancy termination: comparison of three different methods. *Journal of Obstetrics and Gynaecology* 2003; **23**: 407-411.
286. Singh Y, Mikrou P. Use of prostaglandins in duct-dependent congenital heart conditions. *Archives of disease in childhood - Education & practice edition* 2018; **103**: 137.
287. Kalinski P. Regulation of immune responses by prostaglandin E2. *Journal of immunology (Baltimore, Md : 1950)* 2012; **188**: 21-28.
288. Thomas J, Fairclough A, Kavanagh J, Kelly AJ. Vaginal prostaglandin (PGE2 and PGF2a) for induction of labour at term. *Cochrane Database of Systematic Reviews* 2014.
289. Behrman HR, Luborsky-Moore JL, Pang CY, Wright K, Dorflinger LJ. Mechanisms of PGF2α Action in Functional Luteolysis. In: Channing CP, Marsh JM, Sadler WA (eds). Ovarian Follicular and Corpus Luteum Function. Boston, MA: Springer US; 1979, pp 557-575.

290. Powell WS, Rokach J. The eosinophil chemoattractant 5-oxo-ETE and the OXE receptor. *Progress in lipid research* 2013; **52**: 651-665.
291. Sozzani S, Zhou D, Locati M*, et al.* Stimulating properties of 5-oxo-eicosanoids for human monocytes: synergism with monocyte chemotactic protein-1 and -3. *The Journal of Immunology* 1996; **157**: 4664.
292. Smárason AK, Gunnarsson A, Alfredsson JH, Valdimarsson H. Monocytosis and monocytic infiltration of decidua in early pregnancy. *Journal of clinical & laboratory immunology* 1986; **21(1)**: 1-5.
293. Serhan CN, Levy BD. Resolvins in inflammation: emergence of the pro-resolving superfamily of mediators. *J Clin Invest* 2018; **128**: 2657-2669.
294. Lee TH, Horton CE, Kyan-Aung U, Haskard D, Crea AEG, Spur BW. Lipoxin A4 and Lipoxin B4 Inhibit Chemotactic Responses of Human Neutrophils Stimulated by Leukotriene B4 and N-Formyl-l-Methionyl-l-Leucyl-l-Phenylalanine. *Clinical Science* 1989; **77**: 195-203.
295. Serhan CN, Levy BD. LIPID MEDIATORS | Lipoxins. In: Laurent GJ, Shapiro SD (eds). Encyclopedia of Respiratory Medicine. Oxford: Academic Press; 2006, pp 594-599.
296. Liu M, Boussetta T, Makni-Maalej K*, et al.* Protectin DX, a double lipoxygenase product of DHA, inhibits both ROS production in human neutrophils and cyclooxygenase activities. *Lipids* 2014; **49**: 49-57.
297. Xue L, Gyles SL, Wettey FR*, et al.* Prostaglandin D₂ Causes Preferential Induction of Proinflammatory Th2 Cytokine Production through an Action on Chemoattractant Receptor-Like Molecule Expressed on Th2 Cells. *The Journal of Immunology* 2005; **175**: 6531.
298. Jira W, Spiteller G, Richter A. Increased levels of lipid oxidation products in low density lipoproteins of patients suffering from rheumatoid arthritis. *Chemistry and Physics of Lipids* 1997; **87**: 81-89.
299. Yan J, Jiang X, West AA*, et al.* Pregnancy alters choline dynamics: results of a randomized trial using stable isotope methodology in pregnant and nonpregnant women. *The American journal of clinical nutrition* 2013; **98**: 1459-1467.
300. Heimerl S, Fischer M, Baessler A*, et al.* Alterations of plasma lysophosphatidylcholine species in obesity and weight loss. *PloS one* 2014; **9**: e111348-e111348.
301. Reder AT, Genc K, Byskosh PV, Porrini AM. Monocyte activation in multiple sclerosis. *Multiple Sclerosis Journal* 1998; **4**: 162-168.
302. Shornick L, Bhattacharya S, Tumala B. Increased PGD2 is associated with delayed dendritic cell maturation in neonates during respiratory viral infection (VIR2P.1031). *The Journal of Immunology* 2014; **192**: 75.20.
303. Li K, Underhill DM. C-Type Lectin Receptors in Phagocytosis. In: Yamasaki S (ed). C-Type Lectins in Immune Homeostasis. Cham: Springer International Publishing; 2020, pp 1-18.
304. Ezekowitz RA, Sastry K, Bailly P, Warner A. Molecular characterization of the human macrophage mannose receptor: demonstration of multiple carbohydrate recognition-like domains and phagocytosis of yeasts in Cos-1 cells. *Journal of Experimental Medicine* 1990; **172**: 1785-1794.
305. Schiff DE, Kline L, Soldau K*, et al.* Phagocytosis of Gram-negative bacteria by a unique CD14-dependent mechanism. *Journal of Leukocyte Biology* (https://doi.org/10.1002/jlb.62.6.786).1997; **62**: 786-794.

306. Patel SN, Serghides L, Smith TG*, et al.* CD36 Mediates the Phagocytosis of Plasmodium falciparum–Infected Erythrocytes by Rodent Macrophages. *The Journal of Infectious Diseases* 2004; **189**: 204-213.
307. Segawa K, Nagata S. An Apoptotic 'Eat Me' Signal: Phosphatidylserine Exposure. *Trends in Cell Biology* 2015; **25**: 639-650.
308. Penberthy KK, Ravichandran KS. Apoptotic cell recognition receptors and scavenger receptors. *Immunological Reviews* (https://doi.org/10.1111/imr.12376).2016; **269**: 44-59.
309. Devitt A, Moffatt OD, Raykundalia C, Capra JD, Simmons DL, Gregory CD. Human CD14 mediates recognition and phagocytosis of apoptotic cells. *Nature* 1998; **392**: 505-509.
310. Rosales C, Uribe-Querol E. Antibody - Fc Receptor Interactions in Antimicrobial Functions. *Curr Immunol Rev* 2013; **9**: 44-55.
311. Bezman N, Koretzky GA. Compartmentalization of ITAM and integrin signaling by adapter molecules. *Immunological Reviews* (https://doi.org/10.1111/j.1600-065X.2007.00541.x).2007; **218**: 9-28.
312. Sampath P, Moideen K, Ranganathan UD, Bethunaickan R. Monocyte Subsets: Phenotypes and Function in Tuberculosis Infection. *Front Immunol* (10.3389/fimmu.2018.01726).2018; **9**: 1726.
313. Gordon S, Taylor PR. Monocyte and macrophage heterogeneity. *Nature Reviews Immunology* 2005; **5**: 953-964.
314. Cros J, Cagnard N, Woollard K*, et al.* Human CD14dim monocytes patrol and sense nucleic acids and viruses via TLR7 and TLR8 receptors. *Immunity* 2010; **33**: 375-386.
315. Jurado KA, Iwasaki A. Zika virus targets blood monocytes. *Nature Microbiology* 2017; **2**: 1460-1461.
316. Michlmayr D, Andrade P, Gonzalez K, Balmaseda A, Harris E. CD14(+)CD16(+) monocytes are the main target of Zika virus infection in peripheral blood mononuclear cells in a paediatric study in Nicaragua. *Nature microbiology* 2017; **2**: 1462-1470.
317. Ayala-Nunez NV, Follain G, Delalande F*, et al.* Zika virus enhances monocyte adhesion and transmigration favoring viral dissemination to neural cells. *Nature Communications* 2019; **10**: 4430.
318. Quicke KM, Bowen JR, Johnson EL*, et al.* Zika Virus Infects Human Placental Macrophages. *Cell Host Microbe* 2016; **20**: 83-90.
319. Foo S-S, Chen W, Chan Y*, et al.* Asian Zika virus strains target CD14(+) blood monocytes and induce M2-skewed immunosuppression during pregnancy. *Nature microbiology* 2017; **2**: 1558-1570.
320. Rasanen J, Quinn MJ, Laurie A*, et al.* Maternal serum glycosylated fibronectin as a point-of-care biomarker for assessment of preeclampsia. *American Journal of Obstetrics and Gynecology* 2015; **212**: 82.e81-82.e89.
321. Chaemsaithong P, Madan I, Romero R*, et al.* Characterization of the myometrial transcriptome in women with an arrest of dilatation during labor. *J Perinat Med* 2013; **41**: 665-681.
322. Lachmandas E, Boutens L, Ratter JM*, et al.* Microbial stimulation of different Toll-like receptor signalling pathways induces diverse metabolic programmes in human monocytes. *Nature Microbiology* 2016; **2**: 16246.
323. Berg JM, Tymoczko JL, Stryer L, Gatto GJJ. Biochemistry. 7th edition. edn. W.H. Freeman: New York, 2012.

324. Raulien N, Friedrich K, Strobel S*, et al.* Fatty Acid Oxidation Compensates for Lipopolysaccharide-Induced Warburg Effect in Glucose-Deprived Monocytes. *Front Immunol* (Original Research).2017; **8**.
325. Herms A, Bosch M, Reddy BJN*, et al.* AMPK activation promotes lipid droplet dispersion on detyrosinated microtubules to increase mitochondrial fatty acid oxidation. *Nature communications* 2015; **6**: 7176-7176.
326. O'Connor JC, Lawson MA, André C*, et al.* Lipopolysaccharide-induced depressive-like behavior is mediated by indoleamine 2,3-dioxygenase activation in mice. *Molecular Psychiatry* (Original Article).2008; **14**: 511.
327. Sinclair LV, Neyens D, Ramsay G, Taylor PM, Cantrell DA. Single cell analysis of kynurenine and System L amino acid transport in T cells. *Nature Communications* 2018; **9**: 1981.
328. Melgert BN, Spaans F, Borghuis T*, et al.* Pregnancy and preeclampsia affect monocyte subsets in humans and rats. *PloS one* 2012; **7**: e45229-e45229.
329. Groen B, van der Wijk A-E, van den Berg PP*, et al.* Immunological Adaptations to Pregnancy in Women with Type 1 Diabetes. *Scientific Reports* 2015; **5**: 13618.
330. Blanpain C, Libert F, Vassart G, Parmentier M. CCR5 and HIV infection. *Recept Channels* 2002; **8**: 19-31.
331. Aldinucci D, Borghese C, Casagrande N. The CCL5/CCR5 Axis in Cancer Progression. *Cancers (Basel)* 2020; **12**: 1765.
332. Landsman L, Bar-On L, Zernecke A*, et al.* CX3CR1 is required for monocyte homeostasis and atherogenesis by promoting cell survival. *Blood* 2009; **113**: 963-972.
333. Bowers K, Tobias DK, Yeung E, Hu FB, Zhang C. A prospective study of prepregnancy dietary fat intake and risk of gestational diabetes. *The American journal of clinical nutrition* 2012; **95**: 446-453.
334. Anghebem-Oliveira MI, Martins BR, Alberton D, Ramos EAS, Picheth G, Rego FGM. Type 2 diabetes-associated genetic variants of FTO, LEPR, PPARg, and TCF7L2 in gestational diabetes in a Brazilian population. *Arch Endocrinol Metab* 2017; **61**: 238-248.
335. Thewissen MM, van de Gaar J, den Boer AT, Munsters MJ, Blaak EE, Duijvestijn A. Monocytes, but not T cells, respond to insulin with Akt(S473) phosphorylation independent of the donor glucometabolic state. *Diabetes/Metabolism Research and Reviews* 2014; **30**: 323-332.
336. Bunn RC, Cockrell GE, Ou Y, Thrailkill KM, Lumpkin CK, Fowlkes JL. Palmitate and insulin synergistically induce IL-6 expression in human monocytes. *Cardiovascular Diabetology* 2010; **9**: 73.
337. Cruz-Pineda WD, Parra-Rojas I, Rodríguez-Ruíz HA, Illades-Aguiar B, Matia-García I, Garibay-Cerdenares OL. The regulatory role of insulin in energy metabolism and leukocyte functions. *Journal of Leukocyte Biology* (https://doi.org/10.1002/JLB.2RU1220-847R).2021; **n/a**.
338. Liu Y, Dhall S, Castro A, Chan A, Alamat R, Martins-Green M. Insulin regulates multiple signaling pathways leading to monocyte/macrophage chemotaxis into the wound tissue. *Biol Open* 2018; **7**: bio026187.
339. Molvarec A, Szarka A, Walentin S*, et al.* Serum leptin levels in relation to circulating cytokines, chemokines, adhesion molecules and angiogenic factors in normal pregnancy and preeclampsia. *Reprod Biol Endocrinol* 2011; **9**: 124-124.

340. Naylor C, Petri WA, Jr. Leptin Regulation of Immune Responses. *Trends in Molecular Medicine* 2016; **22**: 88-98.
341. Chambers BJ, Salcedo M, Ljunggren H-G. Triggering of Natural Killer Cells by the Costimulatory Molecule CD80 (B7-1). *Immunity* 1996; **5**: 311-317.
342. Marlein CR, Piddock RE, Mistry JJ*, et al.* CD38-Driven Mitochondrial Trafficking Promotes Bioenergetic Plasticity in Multiple Myeloma. *Cancer Research* 2019; **79**: 2285.
343. Camacho-Pereira J, Tarragó MG, Chini CCS*, et al.* CD38 Dictates Age-Related NAD Decline and Mitochondrial Dysfunction through an SIRT3-Dependent Mechanism. *Cell metabolism* 2016; **23**: 1127-1139.
344. Schieke SM, Phillips D, McCoy JP*, et al.* The Mammalian Target of Rapamycin (mTOR) Pathway Regulates Mitochondrial Oxygen Consumption and Oxidative Capacity*. *Journal of Biological Chemistry* 2006; **281**: 27643-27652.
345. Xu S, Jay A, Brunaldi K, Huang N, Hamilton JA. CD36 Enhances Fatty Acid Uptake by Increasing the Rate of Intracellular Esterification but Not Transport across the Plasma Membrane. *Biochemistry* 2013; **52**: 7254-7261.
346. Mastroberardino L, Spindler B, Pfeiffer R*, et al.* Amino-acid transport by heterodimers of 4F2hc/CD98 and members of a permease family. *Nature* 1998; **395**: 288-291.
347. Erdman LK, Cosio G, Helmers AJ, Gowda DC, Grinstein S, Kain KC. CD36 and TLR interactions in inflammation and phagocytosis: implications for malaria. *Journal of immunology (Baltimore, Md : 1950)* 2009; **183**: 6452-6459.
348. Kuda O, Jenkins CM, Skinner JR*, et al.* CD36 protein is involved in store-operated calcium flux, phospholipase A2 activation, and production of prostaglandin E2. *J Biol Chem* 2011; **286**: 17785-17795.
349. Spangenburg EE, Pratt SJP, Wohlers LM, Lovering RM. Use of BODIPY (493/503) to visualize intramuscular lipid droplets in skeletal muscle. *J Biomed Biotechnol* 2011; **2011**: 598358.
350. Fukunaga Y, Katsuragi Y, Izumi T, Sakiyama F. Fluorescence Characteristics of Kynurenine and N' -Formylkynurenine, Their Use as Reporters of the Environment of Tryptophan 62 in Hen Egg-White Lysozyme 1. *The Journal of Biochemistry* 1982; **92**: 129-141.
351. Mándi Y, Vécsei L. The kynurenine system and immunoregulation. *Journal of Neural Transmission* 2012; **119**: 197-209.
352. Mellor AL, Munn DH. Ido expression by dendritic cells: tolerance and tryptophan catabolism. *Nature Reviews Immunology* 2004; **4**: 762-774.
353. Badawy AAB. Tryptophan metabolism, disposition and utilization in pregnancy. *Biosci Rep* 2015; **35**: e00261.
354. Assiri A, Abedi GR, Al Masri M, Bin Saeed A, Gerber SI, Watson JT. Middle East Respiratory Syndrome Coronavirus Infection During Pregnancy: A Report of 5 Cases From Saudi Arabia. *Clinical Infectious Diseases* 2016; **63**: 951-953.
355. Bekeredjian-Ding I, Roth SI, Gilles S*, et al.* T Cell-Independent, TLR-Induced IL-12p70 Production in Primary Human Monocytes. *The Journal of Immunology* 2006; **176**: 7438.
356. Webster NL, Kedzierska K, Azzam R*, et al.* Phagocytosis stimulates mobilization and shedding of intracellular CD16A in human monocytes and macrophages: inhibition by HIV-1 infection. *Journal of Leukocyte Biology* (https://doi.org/10.1189/jlb.0705382).2006; **79**: 294-302.

357. Lindner B, Burkard T, Schuler M. Phagocytosis assays with different pH-sensitive fluorescent particles and various readouts. *BioTechniques* 2020; **68**: 245-250.
358. Xu Y, Anjaneyulu M, Donelian A*, et al.* Assembly of the complexes of oxidative phosphorylation triggers the remodeling of cardiolipin. *Proceedings of the National Academy of Sciences* 2019; **116**: 11235.
359. Sinclair LV, Barthelemy C, Cantrell DA. Single Cell Glucose Uptake Assays: A Cautionary Tale. *Immunometabolism* 2020; **2**: e200029-e200029.
360. Zang X, Zheng X, Hou Y*, et al.* Regulation of proinflammatory monocyte activation by the kynurenine–AhR axis underlies immunometabolic control of depressive behavior in mice. *The FASEB Journal* (https://doi.org/10.1096/fj.201700853R).2018; **32**: 1944-1956.
361. El-Khoury TG, Bahr GM, Echtay KS. Muramyl-dipeptide-induced mitochondrial proton leak in macrophages is associated with upregulation of uncoupling protein 2 and the production of reactive oxygen and reactive nitrogen species. *The FEBS Journal* (https://doi.org/10.1111/j.1742-4658.2011.08226.x).2011; **278**: 3054-3064.
362. El-Jamal N, Bahr GM, Echtay KS. Effect of muramyl peptides on mitochondrial respiration. *Clinical and experimental immunology* 2009; **155**: 72-78.
363. Koumandakis E, Koumandaki I, Kaklamani E, Sparos L, Aravantinos D, Trichopoulos D. Enhanced phagocytosis of mononuclear phagocytes in pregnancy. *Br J Obstet Gynaecol* 1986; **93**: 1150-1154.
364. Lampé R, Kövér Á, Szűcs S*, et al.* Phagocytic index of neutrophil granulocytes and monocytes in healthy and preeclamptic pregnancy. *Journal of Reproductive Immunology* 2015; **107**: 26-30.
365. Dowling JK, Afzal R, Gearing LJ*, et al.* Mitochondrial arginase-2 is essential for IL-10 metabolic reprogramming of inflammatory macrophages. *Nature Communications* 2021; **12**: 1460.
366. Cervantes-Silva MP, Cox SL, Curtis AM. Alterations in mitochondrial morphology as a key driver of immunity and host defence. *EMBO reports* (https://doi.org/10.15252/embr.202153086).2021; **n/a**: e53086.
367. Oliva-Ramírez J, Moreno-Altamirano MMB, Pineda-Olvera B, Cauich-Sánchez P, Sánchez-García FJ. Crosstalk between circadian rhythmicity, mitochondrial dynamics and macrophage bactericidal activity. *Immunology* 2014; **143**: 490-497.
368. Tur J, Pereira-Lopes S, Vico T*, et al.* Mitofusin 2 in Macrophages Links Mitochondrial ROS Production, Cytokine Release, Phagocytosis, Autophagy, and Bactericidal Activity. *Cell Reports* 2020; **32**: 108079.
369. Lauterbach MA, Hanke JE, Serefidou M*, et al.* Toll-like Receptor Signaling Rewires Macrophage Metabolism and Promotes Histone Acetylation via ATP-Citrate Lyase. *Immunity* 2019; **51**: 997-1011.e1017.
370. Infantino V, Iacobazzi V, Palmieri F, Menga A. ATP-citrate lyase is essential for macrophage inflammatory response. *Biochemical and Biophysical Research Communications* 2013; **440**: 105-111.
371. Kumar P, Magon N. Hormones in pregnancy. *Niger Med J* 2012; **53**: 179-183.
372. Schock H, Zeleniuch-Jacquotte A, Lundin E*, et al.* Hormone concentrations throughout uncomplicated pregnancies: a longitudinal study. *BMC Pregnancy Childbirth* 2016; **16**: 146-146.

373. Teppa RJ, Ness RB, Crombleholme WR, Roberts JM. Free leptin is increased in normal pregnancy and further increased in preeclampsia. *Metabolism - Clinical and Experimental* 2000; **49**: 1043-1048.
374. Lain KY, Catalano PM. Metabolic Changes in Pregnancy. *Clinical Obstetrics and Gynecology* 2007; **50**: 938-948.
375. Confavreux C, Hutchinson M, Hours MM, Cortinovis-Tourniaire P, Moreau T. Rate of Pregnancy-Related Relapse in Multiple Sclerosis. *New England Journal of Medicine* 1998; **339**: 285-291.
376. Plemel JR, Michaels NJ, Weishaupt N*, et al.* Mechanisms of lysophosphatidylcholine-induced demyelination: A primary lipid disrupting myelinopathy. *Glia* (https://doi.org/10.1002/glia.23245).2018; **66**: 327-347.
377. Chu T, Zhang YP, Tian Z*, et al.* Dynamic response of microglia/macrophage polarization following demyelination in mice. *Journal of Neuroinflammation* 2019; **16**: 188.
378. Gjelstrup MC, Stilund M, Petersen T, Møller HJ, Petersen EL, Christensen T. Subsets of activated monocytes and markers of inflammation in incipient and progressed multiple sclerosis. *Immunology and cell biology* 2018; **96**: 160-174.
379. Mookerjee SA, Gerencser AA, Nicholls DG, Brand MD. Quantifying intracellular rates of glycolytic and oxidative ATP production and consumption using extracellular flux measurements. *J Biol Chem* 2018; **293**: 12649-12652.
380. Han K, Singh K, Rodman MJ*, et al.* Fasting-induced FOXO4 blunts human CD4+ T helper cell responsiveness. *Nature Metabolism* 2021; **3**: 318-326.
381. Fleming AF. 1 - Haematological Changes in Pregnancy. *Clinics in Obstetrics and Gynaecology* 1975; **2**: 269-283.
382. Mosimann B, Wagner M, Shehata H*, et al.* Natural killer cells and their activation status in normal pregnancy. *Int J Reprod Med* 2013; **2013**: 906813-906813.
383. Gregory CD, Lee H, Rees GB, Scott IV, Shah LP, Golding PR. Natural killer cells in normal pregnancy: analysis using monoclonal antibodies and single-cell cytotoxicity assays. *Clinical and experimental immunology* 1985; **62**: 121-127.
384. Kraus TA, Engel SM, Sperling RS*, et al.* Characterizing the Pregnancy Immune Phenotype: Results of the Viral Immunity and Pregnancy (VIP) Study. *Journal of Clinical Immunology* 2012; **32**: 300-311.
385. Beer AE, Kwak JY, Ruiz JE. Immunophenotypic profiles of peripheral blood lymphocytes in women with recurrent pregnancy losses and in infertile women with multiple failed in vitro fertilization cycles. *Am J Reprod Immunol* 1996; **35**: 376-382.
386. King K, Smith S, Chapman M, Sacks G. Detailed analysis of peripheral blood natural killer (NK) cells in women with recurrent miscarriage. *Human Reproduction* 2010; **25**: 52-58.
387. Bagkou Dimakou D, Lissauer D, Tamblyn J, Coomarasamy A, Richter A. Understanding human immunity in idiopathic recurrent pregnancy loss. *European Journal of Obstetrics & Gynecology and Reproductive Biology* 2022; **270**: 17-29.
388. Seshadri S, Sunkara SK. Natural killer cells in female infertility and recurrent miscarriage: a systematic review and meta-analysis. *Human Reproduction Update* 2014; **20**: 429-438.
389. Toth B, Vomstein K, Togawa R*, et al.* The impact of previous live births on peripheral and uterine natural killer cells in patients with recurrent miscarriage. *Reproductive Biology and Endocrinology* 2019; **17**: 72.

390. Al-ofi E, Coffelt SB, Anumba DO. Monocyte subpopulations from pre-eclamptic patients are abnormally skewed and exhibit exaggerated responses to Toll-like receptor ligands. *PloS one* 2012; **7**: e42217-e42217.
391. Huang C, Wang Y, Li X*, et al.* Clinical features of patients infected with 2019 novel coronavirus in Wuhan, China. *Lancet* 2020; **395**: 497-506.
392. Hadjadj J, Yatim N, Barnabei L*, et al.* Impaired type I interferon activity and inflammatory responses in severe COVID-19 patients. *Science* 2020; **369**: 718.
393. Kraus TA, Sperling RS, Engel SM*, et al.* Peripheral Blood Cytokine Profiling During Pregnancy and Post-partum Periods. *American Journal of Reproductive Immunology* (https://doi.org/10.1111/j.1600-0897.2010.00889.x).2010; **64**: 411-426.
394. Mor G, Aldo P, Alvero AB. The unique immunological and microbial aspects of pregnancy. *Nature Reviews Immunology* 2017; **17**: 469-482.
395. Dutta S, Sengupta P, Physiology LUC, Malaysia Pallav Sengupta. Defining pregnancy phases with cytokine shift. 2017; **1**.
396. Hamilton SA, Tower CL, Jones RL. Identification of chemokines associated with the recruitment of decidual leukocytes in human labour: potential novel targets for preterm labour. *PloS one* 2013; **8**: e56946-e56946.
397. Naccasha N, Gervasi M-T, Chaiworapongsa T*, et al.* Phenotypic and metabolic characteristics of monocytes and granulocytes in normal pregnancy and maternal infection. *American Journal of Obstetrics and Gynecology* 2001; **185**: 1118-1123.
398. Arya RP, Arankalle VA. Phenotypic analysis of monocytes and CD4+ T cells in hepatitis E patients with or without pregnancy. *Human Immunology* 2019; **80**: 855-862.
399. Lashen H, Fear K, Sturdee DW. Obesity is associated with increased risk of first trimester and recurrent miscarriage: matched case–control study. *Human Reproduction* 2004; **19**: 1644-1646.
400. Roberts JM, Bodnar LM, Patrick TE, Powers RW. The Role of Obesity in Preeclampsia. *Pregnancy Hypertens* 2011; **1**: 6-16.
401. Chu SY, Callaghan WM, Kim SY*, et al.* Maternal Obesity and Risk of Gestational Diabetes Mellitus. *Diabetes Care* 2007; **30**: 2070.
402. Boney CM, Verma A, Tucker R, Vohr BR. Metabolic Syndrome in Childhood: Association With Birth Weight, Maternal Obesity, and Gestational Diabetes Mellitus. *Pediatrics* 2005; **115**: e290.
403. NHS Digital LT. Statistics on Obesity, Physical Activity and Diet, England, 2019. England: NHS Digital. Available from: https://digital.nhs.uk/data-and-information/publications/statistical/statistics-on-obesity-physical-activity-and-diet/statistics-on-obesity-physical-activity-and-diet-england-2019.
404. Al-Goblan AS, Al-Alfi MA, Khan MZ. Mechanism linking diabetes mellitus and obesity. *Diabetes Metab Syndr Obes* 2014; **7**: 587-591.
405. Dağ ZÖ, Dilbaz B. Impact of obesity on infertility in women. *J Turk Ger Gynecol Assoc* 2015; **16**: 111-117.
406. Poirier P, Giles Thomas D, Bray George A*, et al.* Obesity and Cardiovascular Disease: Pathophysiology, Evaluation, and Effect of Weight Loss. *Circulation* 2006; **113**: 898-918.
407. Petrilli CM, Jones SA, Yang J*, et al.* Factors associated with hospitalization and critical illness among 4,103 patients with COVID-19 disease in New York City. *medRxiv* 2020: 2020.2004.2008.20057794.

408. Bytautiene E, Romero R, Vedernikov YP, El-Zeky F, Saade GR, Garfield RE. Induction of premature labor and delivery by allergic reaction and prevention by histamine H_1 receptor antagonist. *American Journal of Obstetrics & Gynecology* 2004; **191**: 1356-1361.
409. Gainaru G, Papadopoulos A, Tsangaris I, Lada M, Giamarellos-Bourboulis EJ, Pistiki A. Increases in inflammatory and CD14(dim)/CD16(pos)/CD45(pos) patrolling monocytes in sepsis: correlation with final outcome. *Critical care (London, England)* 2018; **22**: 56-56.
410. Lacerte P, Brunet A, Egarnes B, Duchêne B, Brown JP, Gosselin J. Overexpression of TLR2 and TLR9 on monocyte subsets of active rheumatoid arthritis patients contributes to enhance responsiveness to TLR agonists. *Arthritis Res Ther* 2016; **18**: 10-10.
411. Lumeng CN, Bodzin JL, Saltiel AR. Obesity induces a phenotypic switch in adipose tissue macrophage polarization. *The Journal of clinical investigation* 2007; **117**: 175-184.
412. Bulmer JN, Williams PJ, Lash GE. Immune cells in the placental bed. *Int J Dev Biol* 2010; **54**: 281-294.
413. Friis CM, Paasche Roland MC, Godang K*, et al.* Adiposity-related inflammation: Effects of pregnancy. *Obesity* (https://doi.org/10.1002/oby.20120).2013; **21**: E124-E130.
414. Sureshchandra S, Marshall NE, Mendoza N, Jankeel A, Zulu MZ, Messaoudi I. Functional and genomic adaptations of blood monocytes to pregravid obesity during pregnancy. *iScience* 2021; **24**: 102690-102690.
415. Talukdar S, Oh DY, Bandyopadhyay G*, et al.* Neutrophils mediate insulin resistance in mice fed a high-fat diet through secreted elastase. *Nat Med* 2012; **18**: 1407-1412.
416. Brotfain E, Hadad N, Shapira Y*, et al.* Neutrophil functions in morbidly obese subjects. *Clinical and experimental immunology* 2015; **181**: 156-163.
417. Scott HA, Gibson PG, Garg ML, Wood LG. Airway inflammation is augmented by obesity and fatty acids in asthma. *European Respiratory Journal* 2011; **38**: 594.
418. Grotta MB, Squebola-Cola DM, Toro AADC*, et al.* Obesity increases eosinophil activity in asthmatic children and adolescents. *BMC Pulm Med* 2013; **13**: 39-39.
419. Marijsse GS, Seys SF, Schelpe A-S*, et al.* Obese Individuals with Asthma Preferentially Have a High IL-5/IL-17A/IL-25 Sputum Inflammatory Pattern. *American Journal of Respiratory and Critical Care Medicine* 2014; **189**: 1284-1285.
420. Michelet X, Dyck L, Hogan A*, et al.* Metabolic reprogramming of natural killer cells in obesity limits antitumor responses. *Nature Immunology* 2018; **19**: 1330-1340.
421. Frasca D, Ferracci F, Diaz A, Romero M, Lechner S, Blomberg BB. Obesity decreases B cell responses in young and elderly individuals. *Obesity* 2016; **24**: 615-625.
422. Nishimura S, Manabe I, Nagasaki M*, et al.* CD8+ effector T cells contribute to macrophage recruitment and adipose tissue inflammation in obesity. *Nat Med* 2009; **15**: 914-920.
423. Reis BS, Lee K, Fanok MH*, et al.* Leptin receptor signaling in T cells is required for Th17 differentiation. *Journal of immunology (Baltimore, Md : 1950)* 2015; **194**: 5253-5260.
424. Seck A, Hichami A, Doucouré S*, et al.* Th1/Th2 Dichotomy in Obese Women with Gestational Diabetes and Their Macrosomic Babies. *Journal of Diabetes Research* 2018; **2018**: 8474617.
425. O'Shea D, Hogan AE. Dysregulation of Natural Killer Cells in Obesity. *Cancers (Basel)* 2019; **11**: 573.

426. Zhong J, Rao X, Braunstein Z*, et al.* T-Cell Costimulation Protects Obesity-Induced Adipose Inflammation and Insulin Resistance. *Diabetes* 2014; **63**: 1289.
427. Feuerer M, Herrero L, Cipolletta D*, et al.* Lean, but not obese, fat is enriched for a unique population of regulatory T cells that affect metabolic parameters. *Nat Med* 2009; **15**: 930-939.
428. Lynch L, Nowak M, Varghese B*, et al.* Adipose tissue invariant NKT cells protect against diet-induced obesity and metabolic disorder through regulatory cytokine production. *Immunity* 2012; **37**: 574-587.
429. Carolan E, Tobin LM, Mangan BA*, et al.* Altered Distribution and Increased IL-17 Production by Mucosal-Associated Invariant T Cells in Adult and Childhood Obesity. *The Journal of Immunology* 2015; **194**: 5775.
430. Toubal A, Kiaf B, Beaudoin L*, et al.* Mucosal-associated invariant T cells promote inflammation and intestinal dysbiosis leading to metabolic dysfunction during obesity. *Nature Communications* 2020; **11**: 3755.
431. Eliakim A, Schwindt C, Zaldivar F, Casali P, Cooper DM. Reduced tetanus antibody titers in overweight children. *Autoimmunity* 2006; **39**: 137-141.
432. Banga N, Guss P, Banga A, Rosenman KD. Incidence and variables associated with inadequate antibody titers after pre-exposure rabies vaccination among veterinary medical students. *Vaccine* 2014; **32**: 979-983.
433. Radulescu L, Munteanu O, Popa F, Cirstoiu M. The implications and consequences of maternal obesity on fetal intrauterine growth restriction. *Journal of medicine and life* 2013; **6**: 292-298.
434. de Barros Mucci D, Kusinski LC, Wilsmore P*, et al.* Impact of maternal obesity on placental transcriptome and morphology associated with fetal growth restriction in mice. *International Journal of Obesity* 2020; **44**: 1087-1096.
435. Biotec M. Flow cytometry analysis of T_H subsets. Available from: https://www.miltenyibiotec.com/_Resources/Persistent/6d2f11e6609ce4d3497f43ef9ee4e9331dcb1668/IM0021681.pdf.
436. Luckheeram RV, Zhou R, Verma AD, Xia B. CD4+T Cells: Differentiation and Functions. *Clinical and Developmental Immunology* 2012; **2012**: 12 (Abstract 925135).
437. Annunziato F, Romagnani S. Heterogeneity of human effector CD4+ T cells. *Arthritis research & therapy* 2009; **11**: 257-257.
438. O'Garra A, McEvoy LM, Zlotnik A. T-cell subsets: Chemokine receptors guide the way. *Current Biology* 1998; **8**: R646-R649.
439. Knieke K, Lingel H, Chamaon K, Brunner-Weinzierl MC. Migration of Th1 lymphocytes is regulated by CD152 (CTLA-4)-mediated signaling via PI3 kinase-dependent Akt activation. *PloS one* 2012; **7**: e31391-e31391.
440. Bonecchi R, Bianchi G, Bordignon PP*, et al.* Differential expression of chemokine receptors and chemotactic responsiveness of type 1 T helper cells (Th1s) and Th2s. *The Journal of experimental medicine* 1998; **187**: 129-134.
441. Mousset CM, Hobo W, Woestenenk R, Preijers F, Dolstra H, van der Waart AB. Comprehensive Phenotyping of T Cells Using Flow Cytometry. *Cytometry Part A* (https://doi.org/10.1002/cyto.a.23724).2019; **95**: 647-654.
442. Pandya JM, Lundell A-C, Hallström M, Andersson K, Nordström I, Rudin A. Circulating T helper and T regulatory subsets in untreated early rheumatoid arthritis and healthy control subjects. *Journal of Leukocyte Biology* (https://doi.org/10.1189/jlb.5A0116-025R).2016; **100**: 823-833.

443. Catalán V, Gómez-Ambrosi J, Ramirez B*, et al.* Proinflammatory Cytokines in Obesity: Impact of Type 2 Diabetes Mellitus and Gastric Bypass. *Obesity Surgery* 2007; **17**: 1464-1474.
444. Cox CL, Stanhope KL, Schwarz JM*, et al.* Circulating concentrations of monocyte chemoattractant protein-1, plasminogen activator inhibitor-1, and soluble leukocyte adhesion molecule-1 in overweight/obese men and women consuming fructose- or glucose-sweetened beverages for 10 weeks. *J Clin Endocrinol Metab* 2011; **96**: E2034-E2038.
445. Radzikowska U, Ding M, Tan G*, et al.* Distribution of ACE2, CD147, CD26, and other SARS-CoV-2 associated molecules in tissues and immune cells in health and in asthma, COPD, obesity, hypertension, and COVID-19 risk factors. *Allergy* 2020; **75**: 2829-2845.
446. Xu X, Su S, Wang X*, et al.* Obesity is associated with more activated neutrophils in African American male youth. *International Journal of Obesity* 2015; **39**: 26-32.
447. Kosaraju R, Guesdon W, Crouch MJ*, et al.* B Cell Activity Is Impaired in Human and Mouse Obesity and Is Responsive to an Essential Fatty Acid upon Murine Influenza Infection. *The Journal of Immunology* 2017; **198**: 4738.
448. Bolus WR, Kennedy AJ, Hasty AH. Obesity-induced reduction of adipose eosinophils is reversed with low-calorie dietary intervention. *Physiol Rep* 2018; **6**: e13919-e13919.
449. Lynch L, O'Shea D, Winter DC, Geoghegan J, Doherty DG, O'Farrelly C. Invariant NKT cells and CD1d+ cells amass in human omentum and are depleted in patients with cancer and obesity. *European Journal of Immunology* 2009; **39**: 1893-1901.
450. Fjeldborg K, Christiansen T, Bennetzen M, J. Møller H, Pedersen SB, Richelsen B. The Macrophage-Specific Serum Marker, Soluble CD163, Is Increased in Obesity and Reduced After Dietary-Induced Weight Loss. *Obesity* (https://doi.org/10.1002/oby.20376).2013; **21**: 2437-2443.
451. Bournat JC, Brown CW. Mitochondrial dysfunction in obesity. *Curr Opin Endocrinol Diabetes Obes* 2010; **17**: 446-452.
452. Yin X, Lanza IR, Swain JM, Sarr MG, Nair KS, Jensen MD. Adipocyte Mitochondrial Function Is Reduced in Human Obesity Independent of Fat Cell Size. *The Journal of Clinical Endocrinology & Metabolism* 2014; **99**: E209-E216.
453. Wang W, Sung N, Gilman-Sachs A, Kwak-Kim J. T Helper (Th) Cell Profiles in Pregnancy and Recurrent Pregnancy Losses: Th1/Th2/Th9/Th17/Th22/Tfh Cells. *Front Immunol* 2020; **11**: 2025-2025.
454. Sallusto F, Lanzavecchia A. Heterogeneity of CD4+ memory T cells: Functional modules for tailored immunity. *European Journal of Immunology* (https://doi.org/10.1002/eji.200939722).2009; **39**: 2076-2082.
455. Bardou M, Hadi T, Mace G*, et al.* Systemic increase in human maternal circulating CD14+CD16− MCP-1+ monocytes as a marker of labor. *American Journal of Obstetrics and Gynecology* 2014; **210**: 70.e71-70.e79.
456. Shynlova O, Tsui P, Dorogin A, Lye SJ. Monocyte Chemoattractant Protein-1 (CCL-2) Integrates Mechanical and Endocrine Signals That Mediate Term and Preterm Labor. *The Journal of Immunology* 2008; **181**: 1470.
457. Breslin N, Baptiste C, Gyamfi-Bannerman C*, et al.* Coronavirus disease 2019 infection among asymptomatic and symptomatic pregnant women: two weeks of confirmed presentations to an affiliated pair of New York City hospitals. *American journal of obstetrics & gynecology MFM* 2020; **2**: 100118-100118.

458. Pierce-Williams RAM, Burd J, Felder L*, et al.* Clinical course of severe and critical coronavirus disease 2019 in hospitalized pregnancies: a United States cohort study. *American Journal of Obstetrics & Gynecology MFM* 2020; **2**: 100134.
459. Savasi VM, Parisi F, Patanè L*, et al.* Clinical Findings and Disease Severity in Hospitalized Pregnant Women With Coronavirus Disease 2019 (COVID-19). *Obstetrics & Gynecology* 2020; **136**.
460. Knight M, Bunch K, Vousden N*, et al.* Characteristics and outcomes of pregnant women hospitalised with confirmed SARS-CoV-2 infection in the UK: a national cohort study using the UK Obstetric Surveillance System (UKOSS). *medRxiv* 2020: 2020.2005.2008.20089268.
461. Lokken EM, Walker CL, Delaney S*, et al.* Clinical characteristics of 46 pregnant women with a severe acute respiratory syndrome coronavirus 2 infection in Washington State. *American Journal of Obstetrics and Gynecology* 2020; **223**: 911.e911-911.e914.
462. McCartney SA, Kachikis A, Huebner EM, Walker CL, Chandrasekaran S, Adams Waldorf KM. Obesity as a contributor to immunopathology in pregnant and non-pregnant adults with COVID-19. *Am J Reprod Immunol* 2020; **84**: e13320.
463. Vankadari N, Wilce JA. Emerging COVID-19 coronavirus: glycan shield and structure prediction of spike glycoprotein and its interaction with human CD26. *Emerging Microbes & Infections* 2020; **9**: 601-604.
464. Wang K, Chen W, Zhou Y-S*, et al.* SARS-CoV-2 invades host cells via a novel route: CD147-spike protein. *bioRxiv* 2020: 2020.2003.2014.988345.
465. Cantuti-Castelvetri L, Ojha R, Pedro LD*, et al.* Neuropilin-1 facilitates SARS-CoV-2 cell entry and infectivity. *Science* 2020; **370**: 856.
466. Alhenc-Gelas F, Drueke TB. Blockade of SARS-CoV-2 infection by recombinant soluble ACE2. *Kidney International* 2020; **97**: 1091-1093.
467. Moin ASM, Sathyapalan T, Atkin SL, Butler AE. The relationship of soluble neuropilin-1 to severe COVID-19 risk factors in polycystic ovary syndrome. *Metabolism Open* 2021; **9**: 100079.
468. Baston-Buest DM, Porn AC, Schanz A, Kruessel J-S, Janni W, Hess AP. Expression of the vascular endothelial growth factor receptor neuropilin-1 at the human embryo–maternal interface. *European Journal of Obstetrics & Gynecology and Reproductive Biology* 2011; **154**: 151-156.
469. Maulik D, De A, Ragolia L*, et al.* Down-regulation of placental neuropilin-1 in fetal growth restriction. *American Journal of Obstetrics and Gynecology* 2016; **214**: 279.e271-279.e279.
470. Maynard SE, Min JY, Merchan J*, et al.* Excess placental soluble fms-like tyrosine kinase 1 (sFlt1) may contribute to endothelial dysfunction hypertension, and proteinuria in preeclampsia. *Journal of Clinical Investigation* (Article).2003; **111**: 649-658.
471. Erez O, Romero R, Espinoza J*, et al.* The change in concentrations of angiogenic and anti-angiogenic factors in maternal plasma between the first and second trimesters in risk assessment for the subsequent development of preeclampsia and small-for-gestational age. *Journal of Maternal-Fetal and Neonatal Medicine* (Article).2008; **21**: 279-287.
472. Chaiworapongsa T, Romero R, Tarca A*, et al.* A subset of patients destined to develop spontaneous preterm labor has an abnormal angiogenic/anti-angiogenic profile in maternal plasma: Evidence in support of pathophysiologic heterogeneity of preterm

labor derived from a longitudinal study. *Journal of Maternal-Fetal and Neonatal Medicine* (Article).2009; **22**: 1122-1139.

473. Zera CA, Seely EW, Wilkins-Haug LE, Lim K-H, Parry SI, McElrath TF. The association of body mass index with serum angiogenic markers in normal and abnormal pregnancies. *American Journal of Obstetrics and Gynecology* 2014; **211**: 247.e241-247.e247.
474. Mossanen JC, Jansen TU, Pracht J*, et al.* Elevated circulating CD14++CD16+ intermediate monocytes are independently associated with extracardiac complications after cardiac surgery. *Scientific Reports* 2020; **10**: 947.
475. Gómez-Olarte S, Bolaños NI, Echeverry M*, et al.* Intermediate Monocytes and Cytokine Production Associated With Severe Forms of Chagas Disease. *Frontiers in immunology* 2019; **10**: 1671-1671.
476. Christou KA, Christou GA, Karamoutsios A*, et al.* Metabolically Healthy Obesity Is Characterized by a Proinflammatory Phenotype of Circulating Monocyte Subsets. *Metabolic Syndrome and Related Disorders* 2019; **17**: 259-265.
477. Keustermans GC, Kofink D, Eikendal A*, et al.* Monocyte gene expression in childhood obesity is associated with obesity and complexity of atherosclerosis in adults. *Scientific Reports* 2017; **7**: 16826.
478. Etzerodt A, Moestrup SK. CD163 and inflammation: biological, diagnostic, and therapeutic aspects. *Antioxid Redox Signal* 2013; **18**: 2352-2363.
479. Parfieniuk-Kowerda A, Grubczak K, Eljaszewicz A*, et al.* High CD163 Expression on Classical Monocytes Is Associated with Immune Control of HBV Infection in Noncirrhotic Patients. *Mediators of Inflammation* 2020; **2020**: 6364258.
480. Møller HJ, Aerts H, Grønbaek H*, et al.* Soluble CD163: a marker molecule for monocyte/macrophage activity in disease. *Scand J Clin Lab Invest Suppl* 2002; **237**: 29-33.
481. Resende DP, da Costa AC, de Souza Rosa LP*, et al.* Non-classical circulating monocytes in severe obesity and obesity with uncontrolled diabetes: A comparison with tuberculosis and healthy individuals. *Tuberculosis* 2019; **114**: 30-41.
482. Amici SA, Young NA, Narvaez-Miranda J*, et al.* CD38 Is Robustly Induced in Human Macrophages and Monocytes in Inflammatory Conditions. *Front Immunol* (10.3389/fimmu.2018.01593).2018; **9**: 1593.
483. Wang L-F, Miao L-J, Wang X-N*, et al.* CD38 deficiency suppresses adipogenesis and lipogenesis in adipose tissues through activating Sirt1/PPARγ signaling pathway. *J Cell Mol Med* 2018; **22**: 101-110.
484. Escande C, Nin V, Price NL*, et al.* Flavonoid Apigenin Is an Inhibitor of the NAD⁺ase CD38. *Diabetes* 2013; **62**: 1084.
485. Bellissimo M, Fleischer C, Tran P*, et al.* Mitochondrial Bioenergetic Metabolism Is Associated with Total Body Composition and Influenced by Normal Weight Obesity (P21-039-19). *Current Developments in Nutrition* 2019; **3**.
486. Willig AL, Kramer PA, Chacko BK, Darley-Usmar VM, Heath SL, Overton ET. Monocyte bioenergetic function is associated with body composition in virologically suppressed HIV-infected women. *Redox Biology* 2017; **12**: 648-656.
487. Dicker D, Salook MA, Marcoviciu D, Djaldetti M, Bessler H. Role of peripheral blood mononuclear cells in the predisposition of obese individuals to inflammation and infection. *Obes Facts* 2013; **6**: 146-151.
488. Godfrey DI, Kronenberg M. Going both ways: immune regulation via CD1d-dependent NKT cells. *The Journal of clinical investigation* 2004; **114**: 1379-1388.

489. Southcombe J, Redman C, Sargent I. Peripheral blood invariant natural killer T cells throughout pregnancy and in preeclamptic women. *Journal of reproductive immunology* 2010; **87**: 52-59.
490. Li L, Tu J, Jiang Y, Zhou J, Schust DJ. Regulatory T cells decrease invariant natural killer T cell-mediated pregnancy loss in mice. *Mucosal Immunology* 2017; **10**: 613-623.
491. Rancourt RC, Ott R, Ziska T*, et al.* Visceral Adipose Tissue Inflammatory Factors (TNF-Alpha, SOCS3) in Gestational Diabetes (GDM): Epigenetics as a Clue in GDM Pathophysiology. *International journal of molecular sciences* 2020; **21**: 479.
492. Endo Y, Asou Hikari K, Matsugae N*, et al.* Obesity Drives Th17 Cell Differentiation by Inducing the Lipid Metabolic Kinase, ACC1. *Cell Rep* 2015; **12**: 1042-1055.
493. Chaouat G, Assal Meliani A, Martal J*, et al.* IL-10 prevents naturally occurring fetal loss in the CBA x DBA/2 mating combination, and local defect in IL-10 production in this abortion-prone combination is corrected by in vivo injection of IFN-tau. *The Journal of Immunology* 1995; **154**: 4261.
494. Fallon PG, Jolin HE, Smith P*, et al.* IL-4 Induces Characteristic Th2 Responses Even in the Combined Absence of IL-5, IL-9, and IL-13. *Immunity* 2002; **17**: 7-17.
495. Saito S, Nakashima A, Shima T, Ito M. Th1/Th2/Th17 and Regulatory T-Cell Paradigm in Pregnancy. *American Journal of Reproductive Immunology* (https://doi.org/10.1111/j.1600-0897.2010.00852.x).2010; **63**: 601-610.
496. Reinhard G, Noll A, Schlebusch H, Mallmann P, Ruecker AV. Shifts in the TH1/TH2 Balance during Human Pregnancy Correlate with Apoptotic Changes. *Biochemical and Biophysical Research Communications* 1998; **245**: 933-938.
497. Tranchot-Diallo J, Gras G, Benveniste O*, et al.* Modulations of Cytokine Expression in Pregnant Women. *American Journal of Reproductive Immunology* (https://doi.org/10.1111/j.1600-0897.1997.tb00218.x).1997; **37**: 215-226.
498. Matthiesen L, Khademi M, Ekerfelt C*, et al.* In-situ detection of both inflammatory and anti-inflammatory cytokines in resting peripheral blood mononuclear cells during pregnancy. *Journal of Reproductive Immunology* 2003; **58**: 49-59.
499. Matthiesen L, Berg G, Ekerfelt C, Ernerudh J. Increased Numbers of Circulating Interferon-γ-and Interleukin-4-Secreting Cells During Normal Pregnancy. *American Journal of Reproductive Immunology* (https://doi.org/10.1111/j.1600-0897.1998.tb00370.x).1998; **39**: 362-367.
500. Shimaoka Y, Hidaka YOH, Tada H*, et al.* Changes in Cytokine Production During and After Normal Pregnancy. *American Journal of Reproductive Immunology* (https://doi.org/10.1111/j.8755-8920.2000.440303.x).2000; **44**: 143-147.
501. Kaminski VdL, Ellwanger JH, Matte MCC, Savaris RF, Vianna P, Chies JAB. IL-17 blood levels increase in healthy pregnancy but not in spontaneous abortion. *Molecular Biology Reports* 2018; **45**: 1565-1568.
502. Darmochwal-Kolarz D, Michalak M, Kolarz B*, et al.* The Role of Interleukin-17, Interleukin-23, and Transforming Growth Factor-β in Pregnancy Complicated by Placental Insufficiency. *BioMed research international* 2017; **2017**: 6904325-6904325.
503. Gale C, Quigley MA, Placzek A*, et al.* Characteristics and outcomes of neonatal SARS-CoV-2 infection in the UK: a prospective national cohort study using active surveillance. *The Lancet Child & Adolescent Health* 2021; **5**: 113-121.
504. Radzikowska U, Ding M, Tan G*, et al.* Distribution of ACE2, CD147, CD26, and other SARS-CoV-2 associated molecules in tissues and immune cells in health and in asthma, COPD, obesity, hypertension, and COVID-19 risk factors. *Allergy* 2020; **n/a**.

505. Cypryk K, Szymczak W, Czupryniak L, Sobczak M, Lewiński A. Gestational diabetes mellitus - an analysis of risk factors. *Endokrynologia Polska* 2008; **59**: 393-397.
506. Sykes L, MacIntyre DA, Yap XJ, Teoh TG, Bennett PR. The Th1:th2 dichotomy of pregnancy and preterm labour. *Mediators of inflammation* 2012; **2012**: 967629-967629.
507. Khalil A, von Dadelszen P, Draycott T, Ugwumadu A, O'Brien P, Magee L. Change in the Incidence of Stillbirth and Preterm Delivery During the COVID-19 Pandemic. *JAMA* 2020; **324**: 705-706.
508. Noronha Ld, Zanluca C, Azevedo MLV, Luz KG, Santos CNDD. Zika virus damages the human placental barrier and presents marked fetal neurotropism. *Mem Inst Oswaldo Cruz* 2016; **111**: 287-293.
509. Bayer A, Lennemann NJ, Ouyang Y*, et al.* Type III Interferons Produced by Human Placental Trophoblasts Confer Protection against Zika Virus Infection. *Cell Host Microbe* 2016; **19**: 705-712.
510. Dong L, Pei S, Ren Q*, et al.* Evaluation of vertical transmission of SARS-CoV-2 in utero: nine pregnant women and their newborns. *medRxiv* 2021: 2020.2012.2028.20248874.
511. Kotlyar A, Grechukhina O, Chen A*, et al.* Vertical Transmission of COVID-19: A Systematic Review and Meta-analysis. *American journal of obstetrics and gynecology* 2020: S0002-9378(0020)30823-30821.
512. Shang J, Ye G, Shi K*, et al.* Structural basis of receptor recognition by SARS-CoV-2. *Nature* 2020; **581**: 221-224.
513. Levy A, Yagil Y, Bursztyn M, Barkalifa R, Scharf S, Yagil C. ACE2 expression and activity are enhanced during pregnancy. *American Journal of Physiology-Regulatory, Integrative and Comparative Physiology* 2008; **295**: R1953-R1961.
514. Dhaundiyal A, Kumari P, Jawalekar SS, Chauhan G, Kalra S, Navik U. Is highly expressed ACE 2 in pregnant women "a curse" in times of COVID-19 pandemic? *Life sciences* 2021; **264**: 118676-118676.
515. Taglauer E, Benarroch Y, Rop K*, et al.* Consistent localization of SARS-CoV-2 spike glycoprotein and ACE2 over TMPRSS2 predominance in placental villi of 15 COVID-19 positive maternal-fetal dyads. *Placenta* 2020; **100**: 69-74.
516. Conde-Agudelo A, Romero R. SARS-COV-2 infection during pregnancy and risk of preeclampsia: a systematic review and meta-analysis. *American journal of obstetrics and gynecology* 2021: S0002-9378(0021)00795-X.
517. Chu HY, Englund JA. Maternal immunization. *Clin Infect Dis* 2014; **59**: 560-568.
518. Zeng H, Xu C, Fan J*, et al.* Antibodies in Infants Born to Mothers With COVID-19 Pneumonia. *JAMA* 2020; **323**: 1848-1849.
519. Song D, Prahl M, Gaw SL*, et al.* Passive and active immunity in infants born to mothers with SARS-CoV-2 infection during pregnancy: prospective cohort study. *BMJ Open* 2021; **11**: e053036.
520. Jackson KM, Nazar AM. Breastfeeding, the Immune Response, and Long-term Health. *The Journal of the American Osteopathic Association* 2006; **106**: 203-207.
521. Erliana UD, Fly AD. The Function and Alteration of Immunological Properties in Human Milk of Obese Mothers. *Nutrients* 2019; **11**: 1284.
522. Perl SH, Uzan-Yulzari A, Klainer H*, et al.* SARS-CoV-2–Specific Antibodies in Breast Milk After COVID-19 Vaccination of Breastfeeding Women. *JAMA* 2021; **325**: 2013-2014.

523. Zhu F, Zozaya C, Zhou Q, De Castro C, Shah PS. SARS-CoV-2 genome and antibodies in breastmilk: a systematic review and meta-analysis. *Archives of Disease in Childhood - Fetal and Neonatal Edition* 2021: fetalneonatal-2020-321074.
524. Xiong X, Tortorici MA, Snijder J*, et al.* Glycan Shield and Fusion Activation of a Deltacoronavirus Spike Glycoprotein Fine-Tuned for Enteric Infections. *Journal of Virology* 2018; **92**: e01628-01617.
525. Inoue Y, Tanaka N, Tanaka Y*, et al.* Clathrin-Dependent Entry of Severe Acute Respiratory Syndrome Coronavirus into Target Cells Expressing ACE2 with the Cytoplasmic Tail Deleted. *Journal of Virology* 2007; **81**: 8722.
526. Epelman S, Tang WHW, Chen SY, Van Lente F, Francis GS, Sen S. Detection of soluble angiotensin-converting enzyme 2 in heart failure: insights into the endogenous counter-regulatory pathway of the renin-angiotensin-aldosterone system. *J Am Coll Cardiol* 2008; **52**: 750-754.
527. Igakura T, Kadomatsu K, Taguchi O*, et al.* Roles of Basigin, a Member of the Immunoglobulin Superfamily, in Behavior as to an Irritating Odor, Lymphocyte Response, and Blood–Brain Barrier. *Biochemical and Biophysical Research Communications* 1996; **224**: 33-36.
528. Philp NJ, Ochrietor JD, Rudoy C, Muramatsu T, Linser PJ. Loss of MCT1, MCT3, and MCT4 Expression in the Retinal Pigment Epithelium and Neural Retina of the 5A11/Basigin-Null Mouse. *Investigative Ophthalmology & Visual Science* 2003; **44**: 1305-1311.
529. Crosnier C, Bustamante LY, Bartholdson SJ*, et al.* Basigin is a receptor essential for erythrocyte invasion by Plasmodium falciparum. *Nature* 2011; **480**: 534-537.
530. Shilts J, Crozier TWM, Greenwood EJD, Lehner PJ, Wright GJ. No evidence for basigin/CD147 as a direct SARS-CoV-2 spike binding receptor. *Scientific Reports* 2021; **11**: 413.
531. Bian H, Zheng Z-H, Wei D*, et al.* Meplazumab treats COVID-19 pneumonia: an open-labelled, concurrent controlled add-on clinical trial. *medRxiv* 2020: 2020.2003.2021.20040691.
532. Mentlein R, Gallwitz B, Schmidt WE. Dipeptidyl-peptidase IV hydrolyses gastric inhibitory polypeptide, glucagon-like peptide-1(7–36)amide, peptide histidine methionine and is responsible for their degradation in human serum. *European Journal of Biochemistry* (https://doi.org/10.1111/j.1432-1033.1993.tb17986.x).1993; **214**: 829-835.
533. Meier JJ, Nauck MA, Kranz D*, et al.* Secretion, Degradation, and Elimination of Glucagon-Like Peptide 1 and Gastric Inhibitory Polypeptide in Patients with Chronic Renal Insufficiency and Healthy Control Subjects. *Diabetes* 2004; **53**: 654.
534. Röhrborn D, Wronkowitz N, Eckel J. DPP4 in Diabetes. *Front Immunol* 2015; **6**: 386-386.
535. Mamluk R, Gechtman Ze, Kutcher ME, Gasiunas N, Gallagher J, Klagsbrun M. Neuropilin-1 Binds Vascular Endothelial Growth Factor 165, Placenta Growth Factor-2, and Heparin via Its b1b2 Domain*. *Journal of Biological Chemistry* 2002; **277**: 24818-24825.
536. Chen H, Chédotal A, He Z, Goodman CS, Tessier-Lavigne M. Neuropilin-2, a Novel Member of the Neuropilin Family, Is a High Affinity Receptor for the Semaphorins Sema E and Sema IV but Not Sema III. *Neuron* 1997; **19**: 547-559.

537. Mercurio AM. VEGF/Neuropilin Signaling in Cancer Stem Cells. *International journal of molecular sciences* 2019; **20**: 490.
538. Nasarre C, Roth M, Jacob L*, et al.* Peptide-based interference of the transmembrane domain of neuropilin-1 inhibits glioma growth in vivo. *Oncogene* 2010; **29**: 2381-2392.
539. Mayi BS, Leibowitz JA, Woods AT, Ammon KA, Liu AE, Raja A. The role of Neuropilin-1 in COVID-19. *PLoS Pathog* 2021; **17**: e1009153.
540. Machhi J, Herskovitz J, Senan AM*, et al.* The Natural History, Pathobiology, and Clinical Manifestations of SARS-CoV-2 Infections. *Journal of Neuroimmune Pharmacology* 2020; **15**: 359-386.
541. Bechet D, Tirand L, Faivre B*, et al.* Neuropilin-1 Targeting Photosensitization-Induced Early Stages of Thrombosis via Tissue Factor Release. *Pharmaceutical Research* 2010; **27**: 468-479.
542. Brann DH, Tsukahara T, Weinreb C*, et al.* Non-neuronal expression of SARS-CoV-2 entry genes in the olfactory system suggests mechanisms underlying COVID-19-associated anosmia. *Science Advances* 2020; **6**: eabc5801.
543. Yang J, Nune M, Zong Y, Zhou L, Liu Q. Close and Allosteric Opening of the Polypeptide-Binding Site in a Human Hsp70 Chaperone BiP. *Structure* 2015; **23**: 2191-2203.
544. Corrigall VM, Bodman-Smith MD, Brunst M, Cornell H, Panayi GS. Inhibition of antigen-presenting cell function and stimulation of human peripheral blood mononuclear cells to express an antiinflammatory cytokine profile by the stress protein BiP: Relevance to the treatment of inflammatory arthritis. *Arthritis & Rheumatism* (https://doi.org/10.1002/art.20134).2004; **50**: 1164-1171.
545. Corrigall VM, Vittecoq O, Panayi GS. Binding immunoglobulin protein-treated peripheral blood monocyte-derived dendritic cells are refractory to maturation and induce regulatory T-cell development. *Immunology* 2009; **128**: 218-226.
546. Scheuner D, Mierde DV, Song B*, et al.* Control of mRNA translation preserves endoplasmic reticulum function in beta cells and maintains glucose homeostasis. *Nat Med* 2005; **11**: 757-764.
547. Kim Y, Lillo AM, Steiniger SCJ*, et al.* Targeting Heat Shock Proteins on Cancer Cells: Selection, Characterization, and Cell-Penetrating Properties of a Peptidic GRP78 Ligand. *Biochemistry* 2006; **45**: 9434-9444.
548. Ibrahim IM, Abdelmalek DH, Elshahat ME, Elfiky AA. COVID-19 spike-host cell receptor GRP78 binding site prediction. *Journal of Infection* 2020; **80**: 554-562.
549. Luo S, Mao C, Lee B, Lee AS. GRP78/BiP Is Required for Cell Proliferation and Protecting the Inner Cell Mass from Apoptosis during Early Mouse Embryonic Development. *Molecular and Cellular Biology* 2006; **26**: 5688.
550. Ni M, Lee AS. ER chaperones in mammalian development and human diseases. *FEBS Letters* (https://doi.org/10.1016/j.febslet.2007.04.045).2007; **581**: 3641-3651.
551. Lin P, Jin Y, Lan X*, et al.* GRP78 expression and regulation in the mouse uterus during embryo implantation. *Journal of Molecular Histology* 2014; **45**: 259-268.
552. Fradet S, Pierredon S, Ribaux P*, et al.* Involvement of Membrane GRP78 in Trophoblastic Cell Fusion. *PLOS ONE* 2012; **7**: e40596.
553. Nuzzo AM, Camm EJ, Sferruzzi-Perri AN*, et al.* Placental Adaptation to Early-Onset Hypoxic Pregnancy and Mitochondria-Targeted Antioxidant Therapy in a Rodent Model. *The American Journal of Pathology* 2018; **188**: 2704-2716.
554. Rezanezhad L, Zolghadri J, Gharesi-Fard B. Importance of Anti-GRP78 Antibody in Pre-Eclampsia. *Iranian Journal of Immunology* 2013; **10**: 238-246.

555. Black RA, Rauch CT, Kozlosky CJ*, et al.* A metalloproteinase disintegrin that releases tumour-necrosis factor-α from cells. *Nature* 1997; **385**: 729-733.
556. Heurich A, Hofmann-Winkler H, Gierer S, Liepold T, Jahn O, Pöhlmann S. TMPRSS2 and ADAM17 Cleave ACE2 Differentially and Only Proteolysis by TMPRSS2 Augments Entry Driven by the Severe Acute Respiratory Syndrome Coronavirus Spike Protein. *Journal of Virology* 2014; **88**: 1293.
557. Haga S, Yamamoto N, Nakai-Murakami C*, et al.* Modulation of TNF-alpha-converting enzyme by the spike protein of SARS-CoV and ACE2 induces TNF-alpha production and facilitates viral entry. *Proceedings of the National Academy of Sciences of the United States of America* 2008; **105**: 7809-7814.
558. Lambert DW, Yarski M, Warner FJ*, et al.* Tumor Necrosis Factor-α Convertase (ADAM17) Mediates Regulated Ectodomain Shedding of the Severe-acute Respiratory Syndrome-Coronavirus (SARS-CoV) Receptor, Angiotensin-converting Enzyme-2 (ACE2)*. *Journal of Biological Chemistry* 2005; **280**: 30113-30119.
559. Zipeto D, Palmeira JdF, Argañaraz GA, Argañaraz ER. ACE2/ADAM17/TMPRSS2 Interplay May Be the Main Risk Factor for COVID-19. *Front Immunol* (10.3389/fimmu.2020.576745).2020; **11**: 2642.
560. Schumacher N, Rose-John S. ADAM17 Activity and IL-6 Trans-Signaling in Inflammation and Cancer. *Cancers (Basel)* 2019; **11**.
561. Hoffmann M, Kleine-Weber H, Schroeder S*, et al.* SARS-CoV-2 Cell Entry Depends on ACE2 and TMPRSS2 and Is Blocked by a Clinically Proven Protease Inhibitor. *Cell* 2020; **181**: 271-280.e278.
562. Pan T, Jin Z, Yu Z*, et al.* Cathepsin L promotes angiogenesis by regulating the CDP/Cux/VEGF-D pathway in human gastric cancer. *Gastric Cancer* 2020; **23**: 974-987.
563. Canault M, Certel K, Schatzberg D, Wagner DD, Hynes RO. The Lack of ADAM17 Activity during Embryonic Development Causes Hemorrhage and Impairs Vessel Formation. *PLOS ONE* 2010; **5**: e13433.
564. Ma R, Gu Y, Groome LJ, Wang Y. ADAM17 regulates TNFα production by placental trophoblasts. *Placenta* 2011; **32**: 975-980.
565. Bloise E, Zhang J, Nakpu J*, et al.* Expression of severe acute respiratory syndrome coronavirus 2 cell entry genes, angiotensin-converting enzyme 2 and transmembrane protease serine 2, in the placenta across gestation and at the maternal-fetal interface in pregnancies complicated by preterm birth or preeclampsia. *American Journal of Obstetrics & Gynecology* 2021; **224**: 298.e291-298.e298.
566. Chen H, Guo J, Wang C*, et al.* Clinical characteristics and intrauterine vertical transmission potential of COVID-19 infection in nine pregnant women: a retrospective review of medical records. *The Lancet* 2020; **395**: 809-815.
567. Divya, Chhikara P, Mahajan VS, Datta Gupta S, Chauhan SS. Differential Activity of Cathepsin L in Human Placenta at Two Different Stages of Gestation. *Placenta* 2002; **23**: 59-64.
568. Chu H, Zhou J, Wong BH-Y*, et al.* Middle East Respiratory Syndrome Coronavirus Efficiently Infects Human Primary T Lymphocytes and Activates the Extrinsic and Intrinsic Apoptosis Pathways. *The Journal of infectious diseases* 2016; **213**: 904-914.
569. Gu J, Gong E, Zhang B*, et al.* Multiple organ infection and the pathogenesis of SARS. *Journal of Experimental Medicine* 2005; **202**: 415-424.
570. Pontelli MC, Castro IA, Martins RB*, et al.* Infection of human lymphomononuclear cells by SARS-CoV-2. *bioRxiv* 2020: 2020.2007.2028.225912.

571. Cheung CY, Poon LLM, Ng IHY*, et al.* Cytokine responses in severe acute respiratory syndrome coronavirus-infected macrophages in vitro: possible relevance to pathogenesis. *Journal of virology* 2005; **79**: 7819-7826.
572. Yilla M, Harcourt BH, Hickman CJ*, et al.* SARS-coronavirus replication in human peripheral monocytes/macrophages. *Virus Res* 2005; **107**: 93-101.
573. Law HKW, Cheung CY, Ng HY*, et al.* Chemokine up-regulation in SARS-coronavirus-infected, monocyte-derived human dendritic cells. *Blood* 2005; **106**: 2366-2374.
574. Tseng C-TK, Perrone LA, Zhu H, Makino S, Peters CJ. Severe Acute Respiratory Syndrome and the Innate Immune Responses: Modulation of Effector Cell Function without Productive Infection. *The Journal of Immunology* 2005; **174**: 7977.
575. Diao B, Wang C, Tan Y*, et al.* Reduction and Functional Exhaustion of T Cells in Patients With Coronavirus Disease 2019 (COVID-19). *Front Immunol* (10.3389/fimmu.2020.00827).2020; **11**: 827.
576. Zheng H-Y, Zhang M, Yang C-X*, et al.* Elevated exhaustion levels and reduced functional diversity of T cells in peripheral blood may predict severe progression in COVID-19 patients. *Cellular & Molecular Immunology* 2020; **17**: 541-543.
577. Veras FP, Pontelli MC, Silva CM*, et al.* SARS-CoV-2-triggered neutrophil extracellular traps mediate COVID-19 pathology. *The Journal of experimental medicine* 2020; **217**: e20201129.
578. Morimoto C, Schlossman SF. The structure and function of CD26 in the T-cell immune response. *Immunological Reviews* (https://doi.org/10.1111/j.1600-065X.1998.tb01571.x).1998; **161**: 55-70.
579. Jacks RD, Keller TJ, Nelson A, Nishimura MI, White P, Iwashima M. Cell intrinsic characteristics of human cord blood naïve CD4T cells. *Immunology letters* 2018; **193**: 51-57.
580. Iacono KT, Brown AL, Greene MI, Saouaf SJ. CD147 immunoglobulin superfamily receptor function and role in pathology. *Exp Mol Pathol* 2007; **83**: 283-295.
581. Koch C, Staffler G, Hüttinger R*, et al.* T cell activation-associated epitopes of CD147 in regulation of the T cell response, and their definition by antibody affinity and antigen density. *International Immunology* 1999; **11**: 777-786.
582. Zhang X, Chen Z, Huang H, Gordon JR, Xiang J. DNA microarray analysis of the gene expression profiles of naïve versus activated tumor-specific T cells. *Life Sciences* 2002; **71**: 3005-3017.
583. Helal MA, Shouman S, Abdelwaly A*, et al.* Molecular basis of the potential interaction of SARS-CoV-2 spike protein to CD147 in COVID-19 associated-lymphopenia. *J Biomol Struct Dyn* 2020: 1-11.
584. Fajnzylber J, Regan J, Coxen K*, et al.* SARS-CoV-2 viral load is associated with increased disease severity and mortality. *Nature Communications* 2020; **11**: 5493.
585. Trypsteen W, Van Cleemput J, Snippenberg Wv, Gerlo S, Vandekerckhove L. On the whereabouts of SARS-CoV-2 in the human body: A systematic review. *PLOS Pathogens* 2020; **16**: e1009037.
586. Raha Animesh A, Chakraborty S, Henderson J*, et al.* Investigation of CD26, a potential SARS-CoV-2 receptor, as a biomarker of age and pathology. *Biosci Rep* 2020; **40**.
587. Schlicht K, Rohmann N, Geisler C*, et al.* Circulating levels of soluble Dipeptidylpeptidase-4 are reduced in human subjects hospitalized for severe COVID-19 infections. *International Journal of Obesity* 2020; **44**: 2335-2338.

588. Abd El-Aziz TM, Al-Sabi A, Stockand JD. Human recombinant soluble ACE2 (hrsACE2) shows promise for treating severe COVID-19. *Signal Transduction and Targeted Therapy* 2020; **5**: 258.
589. Krishnamurthy S, Lockey RF, Kolliputi N. Soluble ACE2 as a potential therapy for COVID-19. *American Journal of Physiology-Cell Physiology* 2021; **320**: C279-C281.
590. Koenig JM, Simon J, Anderson DC, Smith EOb, Smith CW. Diminished Soluble and Total Cellular L-Selectin in Cord Blood Is Associated with Its Impaired Shedding from Activated Neutrophils. *Pediatric Research* 1996; **39**: 616-621.
591. Rebuck N, Gibson A, Finn A. Neutrophil adhesion molecules in term and premature infants: normal or enhanced leucocyte integrins but defective L-selectin expression and shedding. *Clinical & Experimental Immunology* (https://doi.org/10.1111/j.1365-2249.1995.tb02296.x).1995; **101**: 183-189.
592. Nargis T, Kumar K, Ghosh AR*, et al.* KLK5 induces shedding of DPP4 from circulatory Th17 cells in type 2 diabetes. *Molecular Metabolism* 2017; **6**: 1529-1539.
593. Duke-Cohan JS, Morimoto C, Rocker JA, Schlossman SF. A Novel Form of Dipeptidylpeptidase IV Found in Human Serum: Isolation, Characterization, and Comparison with T Lymphocyte Membrane Dipeptidylpeptidase IV (CD26). *Journal of Biological Chemistry* 1995; **270**: 14107-14114.
594. Atherton AJ, O'Hare MJ, Buluwela L*, et al.* Ectoenzyme regulation by phenotypically distinct fibroblast sub-populations isolated from the human mammary gland. *J Cell Sci* 1994; **107 (Pt 10)**: 2931-2939.
595. Blume C, Jackson CL, Spalluto CM*, et al.* A novel ACE2 isoform is expressed in human respiratory epithelia and is upregulated in response to interferons and RNA respiratory virus infection. *Nature Genetics* 2021; **53**: 205-214.
596. Ni M, Zhou H, Wey S, Baumeister P, Lee AS. Regulation of PERK Signaling and Leukemic Cell Survival by a Novel Cytosolic Isoform of the UPR Regulator GRP78/BiP. *PLOS ONE* 2009; **4**: e6868.
597. Zmora P, Moldenhauer A-S, Hofmann-Winkler H, Pöhlmann S. TMPRSS2 Isoform 1 Activates Respiratory Viruses and Is Expressed in Viral Target Cells. *PloS one* 2015; **10**: e0138380-e0138380.
598. Lücke K, Yan I, Krohn S*, et al.* Control of Listeria monocytogenes infection requires classical IL-6 signaling in myeloid cells. *PloS one* 2018; **13**: e0203395-e0203395.
599. American Diabetes A. Diagnosis and classification of diabetes mellitus. *Diabetes care* 2010; **33 Suppl 1**: S62-S69.
600. Kern PA, Ranganathan S, Li C, Wood L, Ranganathan G. Adipose tissue tumor necrosis factor and interleukin-6 expression in human obesity and insulin resistance. *American Journal of Physiology-Endocrinology and Metabolism* 2001; **280**: E745-E751.
601. Pradhan AD, Manson JE, Rifai N, Buring JE, Ridker PM. C-Reactive Protein, Interleukin 6, and Risk of Developing Type 2 Diabetes Mellitus. *JAMA* 2001; **286**: 327-334.
602. Pettitt DJ, Lawrence JM, Beyer J*, et al.* Association between maternal diabetes in utero and age at offspring's diagnosis of type 2 diabetes. *Diabetes care* 2008; **31**: 2126-2130.
603. Yu Y, Arah OA, Liew Z*, et al.* Maternal diabetes during pregnancy and early onset of cardiovascular disease in offspring: population based cohort study with 40 years of follow-up. *BMJ* 2019; **367**: l6398.
604. Taricco E, Radaelli T, Rossi G*, et al.* Effects of gestational diabetes on fetal oxygen and glucose levels in vivo. *BJOG: An International Journal of Obstetrics & Gynaecology* 2009; **116**: 1729-1735.

605. Gorar S, Alioglu B, Ademoglu E*, et al.* Is There a Tendency for Thrombosis in Gestational Diabetes Mellitus? *J Lab Physicians* 2016; **8**: 101-105.
606. Plows JF, Stanley JL, Baker PN, Reynolds CM, Vickers MH. The Pathophysiology of Gestational Diabetes Mellitus. *International journal of molecular sciences* 2018; **19**: 3342.
607. Hara CdCP, França EL, Fagundes DLG*, et al.* Characterization of Natural Killer Cells and Cytokines in Maternal Placenta and Fetus of Diabetic Mothers. *Journal of immunology research* 2016; **2016**: 7154524-7154524.
608. Sisino G, Bouckenooghe T, Aurientis S, Fontaine P, Storme L, Vambergue A. Diabetes during pregnancy influences Hofbauer cells, a subtype of placental macrophages, to acquire a pro-inflammatory phenotype. *Biochimica et Biophysica Acta (BBA) - Molecular Basis of Disease* 2013; **1832**: 1959-1968.
609. Mrizak I, Grissa O, Henault B*, et al.* Placental infiltration of inflammatory markers in gestational diabetic women. *General Physiology and Biophysics* 2014; **33**(2): 169-176.
610. Pantham P, Aye ILMH, Powell TL. Inflammation in maternal obesity and gestational diabetes mellitus. *Placenta* 2015; **36**: 709-715.
611. Schliefsteiner C, Peinhaupt M, Kopp S*, et al.* Human Placental Hofbauer Cells Maintain an Anti-inflammatory M2 Phenotype despite the Presence of Gestational Diabetes Mellitus. *Frontiers in immunology* 2017; **8**: 888-888.
612. De Luccia TPB, Pendeloski KPT, Ono E*, et al.* Unveiling the pathophysiology of gestational diabetes: Studies on local and peripheral immune cells. *Scandinavian Journal of Immunology* 2020; **91**: e12860.
613. Schober L, Radnai D, Spratte J*, et al.* The role of regulatory T cell (Treg) subsets in gestational diabetes mellitus. *Clinical & Experimental Immunology* 2014; **177**: 76-85.
614. Widlansky ME, Wang J, Shenouda SM*, et al.* Altered mitochondrial membrane potential, mass, and morphology in the mononuclear cells of humans with type 2 diabetes. *Translational Research* 2010; **156**: 15-25.
615. Du XL, Edelstein D, Rossetti L*, et al.* Hyperglycemia-induced mitochondrial superoxide overproduction activates the hexosamine pathway and induces plasminogen activator inhibitor-1 expression by increasing Sp1 glycosylation. *Proceedings of the National Academy of Sciences of the United States of America* 2000; **97**: 12222-12226.
616. Yu T, Robotham JL, Yoon Y. Increased production of reactive oxygen species in hyperglycemic conditions requires dynamic change of mitochondrial morphology. *Proceedings of the National Academy of Sciences of the United States of America* 2006; **103**: 2653-2658.
617. Mokgalaboni K, Dludla PV, Nyambuya TM, Yakobi SH, Mxinwa V, Nkambule BB. Monocyte-mediated inflammation and cardiovascular risk factors in type 2 diabetes mellitus: A systematic review and meta-analysis of pre-clinical and clinical studies. *JRSM cardiovascular disease* 2020; **9**: 2048004019900748-2048004019900748.
618. Hanenberg H, Kolb-Bachofen V, Kantwerk-Funke G, Kolb H. Macrophage infiltration precedes and is a prerequisite for lymphocytic insulitis in pancreatic islets of pre-diabetic BB rats. *Diabetologia* 1989; **32**: 126-134.
619. Takeda Y, Marumo M, Wakabayashi I. Attenuated phagocytic activity of monocytes in type 2 diabetic Goto–Kakizaki rats. *Immunobiology* 2011; **216**: 1094-1102.
620. Puchta A, Naidoo A, Verschoor CP*, et al.* TNF Drives Monocyte Dysfunction with Age and Results in Impaired Anti-pneumococcal Immunity. *PLOS Pathogens* 2016; **12**: e1005368.

621. Azizieh FY, Raghupathy RG. Tumor necrosis factor-α and pregnancy complications: a prospective study. *Medical principles and practice : international journal of the Kuwait University, Health Science Centre* 2015; **24**: 165-170.
622. Seidel A, Arolt V, Hunstiger M, Rink L, Behnisch A, Kirchner H. Major depressive disorder is associated with elevated monocyte counts. *Acta Psychiatrica Scandinavica* 1996; **94**: 198-204.
623. Hasselmann H, Gamradt S, Taenzer A*, et al.* Pro-inflammatory Monocyte Phenotype and Cell-Specific Steroid Signaling Alterations in Unmedicated Patients With Major Depressive Disorder. *Front Immunol* (10.3389/fimmu.2018.02693).2018; **9**: 2693.
624. Nowak W, Grendas LN, Sanmarco LM*, et al.* Pro-inflammatory monocyte profile in patients with major depressive disorder and suicide behaviour and how ketamine induces anti-inflammatory M2 macrophages by NMDAR and mTOR. *EBioMedicine* 2019; **50**: 290-305.
625. Corriger A, Pickering G. Ketamine and depression: a narrative review. *Drug design, development and therapy* 2019; **13**: 3051-3067.
626. Biaggi A, Conroy S, Pawlby S, Pariante CM. Identifying the women at risk of antenatal anxiety and depression: A systematic review. *Journal of affective disorders* 2016; **191**: 62-77.

Chapter 10 - Appendix

10.1 Differential expression of monocytes from pregnant women in comparison to non-pregnant women – full data

	Log2 fold change	std error (log2)	Confidence limit (log2)		Linear fold change	Confidence limit (linear)		P-value	BH.p.value
			Lower	Upper		Lower	Upper		
IDH1-mRNA	0.614	0.0582	0.5	0.728	1.53	1.41	1.66	9.69E-07	0.000502
TLR7-mRNA	1.15	0.138	0.885	1.42	2.23	1.85	2.68	7.77E-06	0.00201
STAT1-mRNA	1.2	0.159	0.889	1.51	2.3	1.85	2.85	1.95E-05	0.00337
IRF1-mRNA	0.831	0.117	0.601	1.06	1.78	1.52	2.09	3.37E-05	0.00437
PSME2-mRNA	0.846	0.127	0.598	1.09	1.8	1.51	2.14	5.55E-05	0.00507
ACSF3-mRNA	0.537	0.0813	0.378	0.696	1.45	1.3	1.62	6.04E-05	0.00507
PUDP-mRNA	0.449	0.069	0.314	0.584	1.36	1.24	1.5	6.85E-05	0.00507
ZNF136-mRNA	-0.308	0.0548	-0.415	-0.2	0.808	0.75	0.87	0.000224	0.0108
RIMKLB-mRNA	0.962	0.175	0.619	1.3	1.95	1.54	2.47	0.000261	0.0108
STAT3-mRNA	0.316	0.0575	0.203	0.429	1.25	1.15	1.35	0.000263	0.0108
SQSTM1-mRNA	-0.322	0.0588	-0.437	-0.207	0.8	0.738	0.866	0.000271	0.0108
RB1CC1-mRNA	-0.397	0.0724	-0.538	-0.255	0.76	0.689	0.838	0.000271	0.0108
JAK2-mRNA	0.596	0.11	0.381	0.811	1.51	1.3	1.75	0.000289	0.0108
ALOX5-mRNA	0.429	0.0791	0.274	0.584	1.35	1.21	1.5	0.000291	0.0108
FDX1-mRNA	-0.349	0.0659	-0.478	-0.22	0.785	0.718	0.858	0.000346	0.0117
PPM1A-mRNA	-0.298	0.0565	-0.408	-0.187	0.814	0.753	0.878	0.000361	0.0117
PDCD1LG2-mRNA	2.08	0.398	1.3	2.86	4.22	2.46	7.25	0.000386	0.0118
RBBP5-mRNA	0.503	0.0977	0.311	0.695	1.42	1.24	1.62	0.000434	0.0125
TLR2-mRNA	0.415	0.0831	0.252	0.577	1.33	1.19	1.49	0.000549	0.0144
PEMT-mRNA	-0.346	0.0694	-0.482	-0.21	0.787	0.716	0.865	0.000555	0.0144
MYC-mRNA	0.83	0.168	0.501	1.16	1.78	1.41	2.23	0.000586	0.0144
HAAO-mRNA	-0.396	0.0811	-0.555	-0.238	0.76	0.68	0.848	0.000632	0.0144
KMO-mRNA	0.611	0.125	0.366	0.856	1.53	1.29	1.81	0.000638	0.0144

GART-mRNA	0.467	0.0967	0.277	0.656	1.38	1.21	1.58	0.000693	0.015
CD14-mRNA	0.253	0.054	0.147	0.359	1.19	1.11	1.28	0.000866	0.0178
PSMB10-mRNA	0.381	0.0817	0.221	0.541	1.3	1.17	1.45	0.000896	0.0178
MSRB2-mRNA	0.567	0.123	0.325	0.809	1.48	1.25	1.75	0.00099	0.0184
HSF1-mRNA	-0.248	0.0541	-0.354	-0.142	0.842	0.782	0.906	0.00101	0.0184
SLC6A12-mRNA	0.842	0.185	0.479	1.2	1.79	1.39	2.31	0.00107	0.0184
FANCI-mRNA	-0.574	0.127	-0.822	-0.326	0.672	0.566	0.798	0.00109	0.0184
NCOR1-mRNA	-0.161	0.0356	-0.231	-0.0913	0.894	0.852	0.939	0.0011	0.0184
H6PD-mRNA	0.303	0.068	0.17	0.436	1.23	1.12	1.35	0.00122	0.0188
TKT-mRNA	-0.388	0.0871	-0.558	-0.217	0.764	0.679	0.86	0.00123	0.0188
SERINC1-mRNA	-0.153	0.0344	-0.221	-0.0857	0.899	0.858	0.942	0.00124	0.0188
PNOC-mRNA	1.49	0.336	0.83	2.15	2.81	1.78	4.43	0.00127	0.0188
TLR4-mRNA	0.292	0.0667	0.161	0.423	1.22	1.12	1.34	0.00138	0.0195
GLRX-mRNA	0.292	0.0668	0.161	0.423	1.22	1.12	1.34	0.00141	0.0195
RUNX1-mRNA	0.422	0.0968	0.232	0.611	1.34	1.17	1.53	0.00143	0.0195
VEGFA-mRNA	-1.08	0.248	-1.56	-0.59	0.474	0.338	0.664	0.00147	0.0196
ATOX1-mRNA	0.211	0.0493	0.115	0.308	1.16	1.08	1.24	0.00159	0.0206
SCD-mRNA	1.37	0.327	0.727	2.01	2.58	1.65	4.03	0.00188	0.0233
SLC16A3-mRNA	0.32	0.0766	0.17	0.47	1.25	1.13	1.39	0.00189	0.0233
KDM3B-mRNA	0.0756	0.0186	0.0391	0.112	1.05	1.03	1.08	0.00227	0.0268
ATP6V1F-mRNA	-0.215	0.0528	-0.318	-0.111	0.862	0.802	0.926	0.00228	0.0268
MYD88-mRNA	0.354	0.0876	0.182	0.526	1.28	1.13	1.44	0.00235	0.027
STK3-mRNA	0.436	0.108	0.224	0.648	1.35	1.17	1.57	0.0024	0.027
PIK3CD-mRNA	0.2	0.0499	0.103	0.298	1.15	1.07	1.23	0.00245	0.027
SOS1-mRNA	0.509	0.131	0.253	0.765	1.42	1.19	1.7	0.00297	0.0321
MAP2K3-mRNA	-0.249	0.0643	-0.375	-0.123	0.841	0.771	0.918	0.00307	0.0325
PIK3R4-mRNA	0.434	0.114	0.211	0.657	1.35	1.16	1.58	0.00339	0.0351
PSMA3-mRNA	0.241	0.0639	0.116	0.366	1.18	1.08	1.29	0.00362	0.0368

RPL23-mRNA	-0.168	0.0449	-0.256	-0.0804	0.89	0.837	0.946	0.00377	0.0375
AMPD2-mRNA	-0.453	0.121	-0.69	-0.216	0.731	0.62	0.861	0.00384	0.0375
MLYCD-mRNA	0.445	0.123	0.203	0.686	1.36	1.15	1.61	0.00476	0.0457
TYMP-mRNA	0.682	0.19	0.31	1.05	1.6	1.24	2.08	0.00489	0.0458
RICTOR-mRNA	-0.189	0.0527	-0.292	-0.0857	0.877	0.817	0.942	0.00495	0.0458
GMPS-mRNA	-0.239	0.067	-0.37	-0.107	0.847	0.774	0.928	0.00517	0.0466
PCK2-mRNA	0.364	0.102	0.163	0.564	1.29	1.12	1.48	0.00521	0.0466
APOM-mRNA	-0.524	0.148	-0.815	-0.234	0.695	0.568	0.85	0.00535	0.047
NPM1-mRNA	-0.208	0.0599	-0.326	-0.0912	0.865	0.798	0.939	0.00589	0.0492
PRR5-mRNA	-0.937	0.269	-1.47	-0.409	0.522	0.362	0.753	0.00593	0.0492
FBP1-mRNA	0.418	0.12	0.182	0.654	1.34	1.13	1.57	0.00595	0.0492
MS4A4A-mRNA	0.857	0.247	0.372	1.34	1.81	1.29	2.53	0.00607	0.0492
NFKB1-mRNA	0.182	0.0526	0.0791	0.285	1.13	1.06	1.22	0.00608	0.0492
ADORA2A-mRNA	-0.87	0.254	-1.37	-0.372	0.547	0.388	0.772	0.00646	0.0515
CD84-mRNA	0.381	0.112	0.161	0.601	1.3	1.12	1.52	0.00675	0.053
SREBF2-mRNA	0.356	0.105	0.149	0.562	1.28	1.11	1.48	0.00705	0.054
CTSL-mRNA	0.885	0.262	0.371	1.4	1.85	1.29	2.64	0.00709	0.054
HIF1A-mRNA	-0.423	0.126	-0.67	-0.175	0.746	0.629	0.886	0.00738	0.0544
GLUD1-mRNA	-0.151	0.045	-0.239	-0.0624	0.901	0.847	0.958	0.00742	0.0544
AKT1-mRNA	-0.196	0.0588	-0.312	-0.0811	0.873	0.806	0.945	0.0075	0.0544
HSF2-mRNA	-0.848	0.254	-1.35	-0.35	0.556	0.393	0.785	0.00756	0.0544
GMPR-mRNA	0.71	0.215	0.288	1.13	1.64	1.22	2.19	0.00804	0.0558
TECR-mRNA	-0.172	0.0522	-0.274	-0.0696	0.888	0.827	0.953	0.00811	0.0558
NDUFB1-mRNA	0.123	0.0373	0.0495	0.196	1.09	1.03	1.15	0.0082	0.0558
SDHC-mRNA	0.132	0.0401	0.053	0.21	1.1	1.04	1.16	0.00826	0.0558
HK3-mRNA	0.286	0.0871	0.115	0.457	1.22	1.08	1.37	0.00829	0.0558
ATF4-mRNA	-0.302	0.0925	-0.483	-0.121	0.811	0.716	0.92	0.00852	0.0566
PDK2-mRNA	-0.354	0.109	-0.567	-0.14	0.782	0.675	0.907	0.00874	0.057

PDK3-mRNA	0.376	0.116	0.148	0.603	1.3	1.11	1.52	0.00889	0.057
BCL2L1-mRNA	0.269	0.0831	0.106	0.432	1.21	1.08	1.35	0.00892	0.057
HERC1-mRNA	-0.258	0.0823	-0.42	-0.0972	0.836	0.748	0.935	0.0105	0.0663
IMPDH2-mRNA	-0.323	0.104	-0.527	-0.12	0.799	0.694	0.921	0.0111	0.0683
OGDH-mRNA	-0.185	0.0594	-0.301	-0.0683	0.88	0.812	0.954	0.0111	0.0683
CS-mRNA	-0.186	0.0602	-0.304	-0.0681	0.879	0.81	0.954	0.0114	0.0697
LY96-mRNA	0.323	0.105	0.117	0.529	1.25	1.08	1.44	0.0118	0.0702
ACAT1-mRNA	0.305	0.0993	0.11	0.5	1.24	1.08	1.41	0.0118	0.0702
PTK2-mRNA	-0.72	0.235	-1.18	-0.259	0.607	0.441	0.836	0.012	0.0708
CMKLR1-mRNA	0.904	0.296	0.323	1.48	1.87	1.25	2.8	0.0123	0.0714
CAT-mRNA	-0.174	0.0578	-0.287	-0.0608	0.886	0.819	0.959	0.0131	0.0753
MAPK1-mRNA	-0.144	0.0484	-0.238	-0.0488	0.905	0.848	0.967	0.0141	0.08
MPC2-mRNA	-0.194	0.0653	-0.322	-0.0655	0.874	0.8	0.956	0.0142	0.08
SLC7A5-mRNA	-1.05	0.357	-1.75	-0.35	0.483	0.297	0.785	0.0148	0.0824
VHL-mRNA	-0.161	0.0549	-0.268	-0.0533	0.895	0.83	0.964	0.015	0.0827
ZNF254-mRNA	0.504	0.172	0.166	0.842	1.42	1.12	1.79	0.0152	0.0828
NFKB2-mRNA	-0.442	0.152	-0.74	-0.144	0.736	0.599	0.905	0.0156	0.0844
NDUFA3-mRNA	0.153	0.0529	0.0493	0.257	1.11	1.03	1.19	0.016	0.0855
IL7-mRNA	0.856	0.296	0.275	1.44	1.81	1.21	2.71	0.0162	0.0855
PRDX1-mRNA	0.176	0.0615	0.0556	0.297	1.13	1.04	1.23	0.0169	0.0874
APRT-mRNA	-0.152	0.053	-0.256	-0.0479	0.9	0.838	0.967	0.0169	0.0874
GUSB-mRNA	-0.159	0.0559	-0.269	-0.0499	0.895	0.83	0.966	0.0172	0.0881
TRAF6-mRNA	-0.209	0.0746	-0.355	-0.0628	0.865	0.782	0.957	0.0187	0.0946
KMT2E-mRNA	-0.219	0.0781	-0.372	-0.0656	0.859	0.773	0.956	0.0188	0.0946
NDUFB2-mRNA	0.121	0.0436	0.036	0.207	1.09	1.03	1.15	0.0193	0.0959
ITGAM-mRNA	0.211	0.0758	0.0622	0.359	1.16	1.04	1.28	0.0194	0.0959
SEC13-mRNA	-0.0913	0.0332	-0.156	-0.0263	0.939	0.897	0.982	0.0204	0.0988
D2HGDH-mRNA	0.252	0.0914	0.0724	0.431	1.19	1.05	1.35	0.0204	0.0988

BRIP1-mRNA	-0.36	0.132	-0.619	-0.102	0.779	0.651	0.932	0.0212	0.1
CD180-mRNA	0.727	0.267	0.203	1.25	1.65	1.15	2.38	0.0215	0.1
SLC7A11-mRNA	-2.04	0.752	-3.51	-0.566	0.243	0.0875	0.676	0.0219	0.1
PRIM1-mRNA	0.407	0.15	0.113	0.701	1.33	1.08	1.63	0.0219	0.1
RAD51AP1-mRNA	0.927	0.342	0.256	1.6	1.9	1.19	3.03	0.022	0.1
GMPR2-mRNA	0.17	0.0628	0.0466	0.293	1.12	1.03	1.23	0.0223	0.1
SLC16A7-mRNA	0.227	0.0842	0.0624	0.393	1.17	1.04	1.31	0.0223	0.1
MRAS-mRNA	-0.586	0.217	-1.01	-0.16	0.666	0.496	0.895	0.0225	0.1
STAM2-mRNA	0.355	0.132	0.0965	0.613	1.28	1.07	1.53	0.0226	0.1
TP53-mRNA	0.214	0.0793	0.058	0.369	1.16	1.04	1.29	0.0226	0.1
SERINC3-mRNA	-0.147	0.055	-0.255	-0.0397	0.903	0.838	0.973	0.023	0.101
CCL4-mRNA	-1.65	0.622	-2.87	-0.435	0.318	0.136	0.74	0.024	0.103
EHHADH-mRNA	1.02	0.383	0.267	1.77	2.03	1.2	3.41	0.024	0.103
PYCR2-mRNA	0.188	0.0708	0.0493	0.327	1.14	1.03	1.25	0.024	0.103
SLC27A1-mRNA	-0.282	0.107	-0.492	-0.0716	0.823	0.711	0.952	0.0253	0.107
STAT5A-mRNA	0.182	0.0693	0.0459	0.317	1.13	1.03	1.25	0.0255	0.107
HACD2-mRNA	-0.175	0.0672	-0.307	-0.0438	0.885	0.808	0.97	0.026	0.109
IDH3B-mRNA	-0.107	0.0414	-0.189	-0.0263	0.928	0.877	0.982	0.0267	0.111
CD4-mRNA	-0.289	0.112	-0.509	-0.0692	0.819	0.703	0.953	0.0276	0.113
PSMC1-mRNA	-0.162	0.0629	-0.285	-0.0388	0.894	0.82	0.973	0.0276	0.113
NKG7-mRNA	0.567	0.221	0.133	1	1.48	1.1	2	0.0284	0.115
AKT1S1-mRNA	-0.101	0.0396	-0.179	-0.0235	0.932	0.884	0.984	0.0287	0.115
PRDX5-mRNA	0.212	0.0834	0.0486	0.375	1.16	1.03	1.3	0.0292	0.116
IDO1-mRNA	1.01	0.398	0.23	1.79	2.01	1.17	3.46	0.0294	0.116
NUP62-mRNA	0.186	0.0737	0.0414	0.33	1.14	1.03	1.26	0.0303	0.119
BIRC3-mRNA	-0.279	0.112	-0.498	-0.0605	0.824	0.708	0.959	0.0313	0.122
IDH3G-mRNA	-0.141	0.0569	-0.253	-0.0294	0.907	0.839	0.98	0.0327	0.126

NFE2L2-mRNA	-0.174	0.0709	-0.313	-0.0352	0.886	0.805	0.976	0.0339	0.13
PIK3R1-mRNA	-0.262	0.107	-0.472	-0.0523	0.834	0.721	0.964	0.0343	0.13
COX5A-mRNA	-0.133	0.0543	-0.239	-0.0261	0.912	0.847	0.982	0.0348	0.13
ZNF93-mRNA	0.621	0.254	0.122	1.12	1.54	1.09	2.17	0.0349	0.13
PTGES-mRNA	-1.85	0.761	-3.34	-0.362	0.277	0.0985	0.778	0.0351	0.13
CBL-mRNA	0.222	0.0914	0.0433	0.402	1.17	1.03	1.32	0.0353	0.13
UQCR10-mRNA	0.124	0.0509	0.0241	0.224	1.09	1.02	1.17	0.0353	0.13
CTSZ-mRNA	0.123	0.0512	0.0228	0.223	1.09	1.02	1.17	0.037	0.134
CD63-mRNA	0.219	0.091	0.0403	0.397	1.16	1.03	1.32	0.0371	0.134
ZNF675-mRNA	0.377	0.157	0.0689	0.684	1.3	1.05	1.61	0.0374	0.134
SLC16A13-mRNA	0.592	0.247	0.107	1.08	1.51	1.08	2.11	0.0378	0.135
ECHS1-mRNA	0.272	0.114	0.0475	0.496	1.21	1.03	1.41	0.0389	0.138
MAP2K1-mRNA	-0.104	0.044	-0.19	-0.0173	0.931	0.877	0.988	0.0404	0.142
PRKAG2-mRNA	-0.16	0.0688	-0.295	-0.0254	0.895	0.815	0.983	0.0421	0.146
MAP3K12-mRNA	0.306	0.131	0.0485	0.563	1.24	1.03	1.48	0.0421	0.146
GATM-mRNA	-1.08	0.471	-2	-0.156	0.473	0.25	0.897	0.0448	0.155
COX14-mRNA	0.156	0.0682	0.0224	0.29	1.11	1.02	1.22	0.0451	0.155
GBA-mRNA	0.135	0.059	0.019	0.25	1.1	1.01	1.19	0.0456	0.155
RPS6KB2-mRNA	-0.145	0.0635	-0.269	-0.0202	0.905	0.83	0.986	0.046	0.156
SLC25A1-mRNA	0.213	0.0939	0.0294	0.397	1.16	1.02	1.32	0.0463	0.156
TNF-mRNA	-0.845	0.374	-1.58	-0.112	0.557	0.335	0.925	0.0473	0.158
PGM2-mRNA	0.217	0.096	0.0285	0.405	1.16	1.02	1.32	0.0477	0.158
SLC2A6-mRNA	-0.317	0.142	-0.595	-0.039	0.803	0.662	0.973	0.0494	0.162
SLC3A2-mRNA	-0.248	0.111	-0.467	-0.0304	0.842	0.724	0.979	0.0496	0.162
CCNA2-mRNA	1.1	0.491	0.134	2.06	2.14	1.1	4.17	0.0496	0.162
SOD1-mRNA	-0.161	0.0725	-0.303	-0.0195	0.894	0.81	0.987	0.05	0.162
GNS-mRNA	0.168	0.0755	0.0197	0.316	1.12	1.01	1.24	0.0506	0.163
HRAS-mRNA	-0.318	0.145	-0.602	-0.0348	0.802	0.659	0.976	0.0524	0.167

CD209-mRNA	0.765	0.349	0.0809	1.45	1.7	1.06	2.73	0.0532	0.169
GPI-mRNA	-0.102	0.0466	-0.193	-0.0106	0.932	0.875	0.993	0.0536	0.169
KYAT1-mRNA	-0.327	0.151	-0.623	-0.0309	0.797	0.649	0.979	0.0557	0.175
L2HGDH-mRNA	0.461	0.214	0.0411	0.88	1.38	1.03	1.84	0.0569	0.176
CTSD-mRNA	0.19	0.0884	0.017	0.364	1.14	1.01	1.29	0.0569	0.176
NDUFA12-mRNA	0.297	0.138	0.026	0.568	1.23	1.02	1.48	0.0572	0.177
COX6A1-mRNA	0.104	0.0489	0.00859	0.2	1.08	1.01	1.15	0.0585	0.179
NDUFB8-mRNA	-0.113	0.0532	-0.217	-0.00896	0.925	0.86	0.994	0.0592	0.18
TRAF1-mRNA	-0.344	0.162	-0.662	-0.0257	0.788	0.632	0.982	0.0602	0.182
UQCR11-mRNA	0.291	0.138	0.0195	0.562	1.22	1.01	1.48	0.062	0.186
CD36-mRNA	0.382	0.182	0.0251	0.738	1.3	1.02	1.67	0.0623	0.186
ZNF253-mRNA	0.828	0.395	0.0538	1.6	1.78	1.04	3.04	0.0625	0.186
CTPS1-mRNA	-0.326	0.156	-0.632	-0.0195	0.798	0.645	0.987	0.0637	0.189
ATF7-mRNA	0.148	0.0712	0.00863	0.288	1.11	1.01	1.22	0.0641	0.189
MTOR-mRNA	0.167	0.081	0.00778	0.325	1.12	1.01	1.25	0.0668	0.196
NADK-mRNA	0.17	0.0829	0.00754	0.333	1.13	1.01	1.26	0.0674	0.196
NRAS-mRNA	-0.168	0.0818	-0.328	-0.00715	0.89	0.797	0.995	0.0678	0.196
TET2-mRNA	-0.0885	0.0436	-0.174	-0.00294	0.941	0.886	0.998	0.0701	0.201
PEBP1-mRNA	-0.291	0.144	-0.573	-0.00935	0.817	0.672	0.994	0.0704	0.201
CEACAM3-mRNA	0.753	0.373	0.0218	1.48	1.69	1.02	2.8	0.0712	0.203
TELO2-mRNA	0.22	0.11	0.0037	0.435	1.16	1	1.35	0.0742	0.209
KYAT3-mRNA	-0.161	0.081	-0.32	-0.0026	0.894	0.801	0.998	0.0744	0.209
MLST8-mRNA	-0.187	0.095	-0.374	-0.00121	0.878	0.772	0.999	0.0768	0.215
SOD2-mRNA	-0.372	0.19	-0.743	-0.000411	0.773	0.597	1	0.0782	0.217
BCL2-mRNA	-0.429	0.219	-0.859	0.000584	0.743	0.551	1	0.0788	0.217
HLA-A-mRNA	0.3	0.154	-0.000953	0.601	1.23	0.999	1.52	0.0792	0.217

RANBP2-mRNA	-0.279	0.143	-0.559	0.000903	0.824	0.679	1	0.0793	0.217
MTF1-mRNA	0.215	0.111	-0.00172	0.432	1.16	0.999	1.35	0.0805	0.219
NEDD8-mRNA	0.0897	0.0464	-0.00127	0.181	1.06	0.999	1.13	0.0821	0.223
SNF8-mRNA	0.0753	0.039	-0.0012	0.152	1.05	0.999	1.11	0.0825	0.223
YWHAZ-mRNA	-0.165	0.0862	-0.334	0.00435	0.892	0.794	1	0.0853	0.229
PDK1-mRNA	-0.291	0.153	-0.591	0.00986	0.818	0.664	1.01	0.0872	0.233
NDUFB7-mRNA	0.0965	0.0511	-0.00363	0.197	1.07	0.997	1.15	0.0882	0.234
KMT2D-mRNA	0.0756	0.0405	-0.00382	0.155	1.05	0.997	1.11	0.0916	0.242
BRAF-mRNA	-0.0716	0.039	-0.148	0.00483	0.952	0.903	1	0.0962	0.251
IDH2-mRNA	0.234	0.128	-0.0161	0.485	1.18	0.989	1.4	0.0965	0.251
DERA-mRNA	-0.111	0.0605	-0.23	0.00763	0.926	0.853	1.01	0.0966	0.251
ACACA-mRNA	0.38	0.208	-0.0264	0.787	1.3	0.982	1.73	0.0968	0.251
GNLY-mRNA	0.534	0.293	-0.0399	1.11	1.45	0.973	2.15	0.0982	0.253
ACAA2-mRNA	0.175	0.0965	-0.0145	0.364	1.13	0.99	1.29	0.1	0.258
KRAS-mRNA	0.186	0.104	-0.0171	0.389	1.14	0.988	1.31	0.103	0.262
GLYCTK-mRNA	-0.227	0.127	-0.476	0.0223	0.855	0.719	1.02	0.105	0.266
NOD2-mRNA	0.24	0.136	-0.0264	0.505	1.18	0.982	1.42	0.108	0.271
PPARG-mRNA	0.114	0.0645	-0.0126	0.24	1.08	0.991	1.18	0.108	0.271
LAMTOR2-mRNA	0.102	0.0581	-0.0116	0.216	1.07	0.992	1.16	0.109	0.272
KEAP1-mRNA	0.223	0.129	-0.0299	0.477	1.17	0.98	1.39	0.115	0.285
HK2-mRNA	-0.26	0.151	-0.556	0.036	0.835	0.68	1.03	0.116	0.286
PGAM2-mRNA	0.678	0.394	-0.094	1.45	1.6	0.937	2.73	0.116	0.286
CAD-mRNA	0.222	0.13	-0.0319	0.477	1.17	0.978	1.39	0.117	0.288
COX5B-mRNA	0.0718	0.042	-0.0106	0.154	1.05	0.993	1.11	0.119	0.29
NDUFA13-mRNA	0.0952	0.0561	-0.0146	0.205	1.07	0.99	1.15	0.12	0.292
FCAR-mRNA	-0.497	0.293	-1.07	0.0776	0.709	0.476	1.06	0.121	0.293
IRF4-mRNA	-0.498	0.296	-1.08	0.0824	0.708	0.474	1.06	0.124	0.296
COX4I1-mRNA	-0.0771	0.0459	-0.167	0.0129	0.948	0.891	1.01	0.124	0.296

ADAL-mRNA	0.304	0.181	-0.0512	0.66	1.23	0.965	1.58	0.124	0.296
MAP1LC3B-mRNA	-0.324	0.193	-0.702	0.0545	0.799	0.615	1.04	0.124	0.296
RELA-mRNA	-0.0769	0.0461	-0.167	0.0133	0.948	0.891	1.01	0.126	0.297
SLC16A6-mRNA	-0.186	0.111	-0.404	0.0325	0.879	0.756	1.02	0.126	0.297
ASH1L-mRNA	0.0959	0.0578	-0.0174	0.209	1.07	0.988	1.16	0.128	0.3
PTPN5-mRNA	-0.485	0.293	-1.06	0.0889	0.714	0.48	1.06	0.129	0.3
MPC1-mRNA	-0.13	0.0789	-0.285	0.0247	0.914	0.821	1.02	0.131	0.3
CDK9-mRNA	-0.153	0.0929	-0.335	0.0291	0.899	0.793	1.02	0.131	0.3
CPT1A-mRNA	0.276	0.168	-0.0527	0.605	1.21	0.964	1.52	0.131	0.3
RPLP0-mRNA	-0.141	0.0856	-0.308	0.0271	0.907	0.807	1.02	0.131	0.3
CACNB4-mRNA	-0.699	0.426	-1.53	0.136	0.616	0.346	1.1	0.132	0.3
HSPA4-mRNA	0.108	0.0658	-0.0211	0.237	1.08	0.985	1.18	0.132	0.3
MS4A1-mRNA	-0.891	0.544	-1.96	0.175	0.539	0.258	1.13	0.132	0.3
EEA1-mRNA	0.137	0.0842	-0.0278	0.302	1.1	0.981	1.23	0.134	0.302
RBKS-mRNA	0.478	0.294	-0.0974	1.05	1.39	0.935	2.08	0.135	0.302
HLA-DQA1-mRNA	-3.65	2.25	-8.05	0.75	0.0796	0.00376	1.68	0.135	0.302
ATP5F1D-mRNA	-0.0784	0.0484	-0.173	0.0165	0.947	0.887	1.01	0.136	0.303
ACOX1-mRNA	0.144	0.0898	-0.0314	0.32	1.11	0.978	1.25	0.139	0.307
RPTOR-mRNA	0.228	0.143	-0.0519	0.508	1.17	0.965	1.42	0.141	0.31
RRAGC-mRNA	-0.121	0.0757	-0.269	0.0276	0.92	0.83	1.02	0.142	0.31
CYP1B1-mRNA	0.261	0.164	-0.0604	0.583	1.2	0.959	1.5	0.143	0.31
HEXB-mRNA	-0.0929	0.0584	-0.207	0.0216	0.938	0.866	1.02	0.143	0.31
PRKAB1-mRNA	0.106	0.0669	-0.0248	0.237	1.08	0.983	1.18	0.143	0.31
SELENOK-mRNA	-0.352	0.222	-0.788	0.084	0.783	0.579	1.06	0.145	0.311
ATF7IP-mRNA	0.146	0.0928	-0.0353	0.328	1.11	0.976	1.26	0.145	0.311
RPS6KA1-mRNA	0.158	0.1	-0.0383	0.355	1.12	0.974	1.28	0.146	0.311

TK1-mRNA	-0.549	0.348	-1.23	0.133	0.683	0.426	1.1	0.146	0.311
GPX4-mRNA	-0.11	0.0696	-0.246	0.0269	0.927	0.843	1.02	0.147	0.311
SDSL-mRNA	0.466	0.299	-0.12	1.05	1.38	0.92	2.07	0.15	0.318
ERN1-mRNA	0.125	0.0801	-0.0325	0.282	1.09	0.978	1.22	0.151	0.318
KPNA2-mRNA	-0.163	0.105	-0.369	0.0428	0.893	0.774	1.03	0.152	0.318
USP8-mRNA	0.109	0.0702	-0.0288	0.246	1.08	0.98	1.19	0.152	0.318
COX7B-mRNA	0.0872	0.0564	-0.0233	0.198	1.06	0.984	1.15	0.153	0.318
FAH-mRNA	-0.209	0.135	-0.475	0.0562	0.865	0.72	1.04	0.153	0.318
CTSA-mRNA	0.157	0.102	-0.0426	0.357	1.11	0.971	1.28	0.154	0.318
ASL-mRNA	0.0823	0.0535	-0.0226	0.187	1.06	0.984	1.14	0.155	0.318
INSR-mRNA	-0.152	0.0988	-0.345	0.042	0.9	0.787	1.03	0.156	0.318
FASN-mRNA	0.264	0.172	-0.0732	0.6	1.2	0.951	1.52	0.156	0.318
PRKAA1-mRNA	0.0695	0.0456	-0.0199	0.159	1.05	0.986	1.12	0.159	0.321
PTPRC-mRNA	0.21	0.138	-0.0604	0.481	1.16	0.959	1.4	0.159	0.321
SERINC2-mRNA	-0.401	0.264	-0.917	0.115	0.757	0.529	1.08	0.159	0.321
ME2-mRNA	0.118	0.078	-0.0354	0.27	1.08	0.976	1.21	0.163	0.327
TIGAR-mRNA	0.253	0.169	-0.0789	0.584	1.19	0.947	1.5	0.166	0.332
CXCL9-mRNA	-0.63	0.427	-1.47	0.206	0.646	0.362	1.15	0.17	0.339
TFRC-mRNA	-0.228	0.154	-0.53	0.0752	0.854	0.692	1.05	0.171	0.339
GLS-mRNA	0.104	0.0704	-0.0343	0.242	1.07	0.976	1.18	0.172	0.339
DCK-mRNA	0.102	0.0696	-0.0345	0.238	1.07	0.976	1.18	0.174	0.342
GCLC-mRNA	0.138	0.0946	-0.0474	0.323	1.1	0.968	1.25	0.175	0.344
ITGB1-mRNA	-0.0835	0.0575	-0.196	0.0293	0.944	0.873	1.02	0.177	0.347
NDUFB11-mRNA	-0.0897	0.0622	-0.212	0.0322	0.94	0.864	1.02	0.18	0.35
NAGLU-mRNA	-0.134	0.0932	-0.317	0.0484	0.911	0.803	1.03	0.18	0.35
ARID1A-mRNA	0.0898	0.0625	-0.0327	0.212	1.06	0.978	1.16	0.181	0.35
PIK3R2-mRNA	0.108	0.0755	-0.0399	0.256	1.08	0.973	1.19	0.183	0.352
CHMP2A-mRNA	0.0861	0.0604	-0.0324	0.204	1.06	0.978	1.15	0.185	0.354

IL21R-mRNA	0.606	0.426	-0.229	1.44	1.52	0.853	2.72	0.185	0.354
GABARAP-mRNA	0.0598	0.0422	-0.0229	0.143	1.04	0.984	1.1	0.187	0.355
TXNRD1-mRNA	-0.0775	0.0549	-0.185	0.03	0.948	0.88	1.02	0.188	0.355
VPS28-mRNA	-0.11	0.078	-0.263	0.0427	0.926	0.833	1.03	0.188	0.355
CD244-mRNA	-0.197	0.14	-0.471	0.0777	0.873	0.722	1.06	0.19	0.359
LTA4H-mRNA	0.273	0.195	-0.11	0.655	1.21	0.927	1.57	0.192	0.361
CYBB-mRNA	0.114	0.0822	-0.0474	0.275	1.08	0.968	1.21	0.197	0.367
ADK-mRNA	-0.554	0.401	-1.34	0.232	0.681	0.395	1.17	0.197	0.367
SPIB-mRNA	-0.654	0.474	-1.58	0.275	0.635	0.334	1.21	0.198	0.367
GAPDH-mRNA	-0.084	0.061	-0.204	0.0356	0.943	0.868	1.02	0.198	0.367
PIK3CB-mRNA	-0.0541	0.0395	-0.132	0.0233	0.963	0.913	1.02	0.201	0.37
PSMD13-mRNA	-0.0716	0.0525	-0.174	0.0313	0.952	0.886	1.02	0.203	0.372
NUP205-mRNA	-0.104	0.0761	-0.253	0.0455	0.931	0.839	1.03	0.203	0.372
ZNF682-mRNA	-0.415	0.306	-1.02	0.185	0.75	0.495	1.14	0.205	0.375
MGST3-mRNA	0.223	0.165	-0.101	0.547	1.17	0.932	1.46	0.207	0.377
NCAPH-mRNA	-0.23	0.172	-0.567	0.107	0.853	0.675	1.08	0.21	0.381
TLR10-mRNA	0.331	0.25	-0.159	0.821	1.26	0.896	1.77	0.214	0.387
SLC16A1-mRNA	-0.129	0.0985	-0.322	0.0637	0.914	0.8	1.05	0.219	0.393
SLC7A9-mRNA	0.507	0.391	-0.259	1.27	1.42	0.836	2.42	0.223	0.4
NDUFA1-mRNA	0.0622	0.0483	-0.0325	0.157	1.04	0.978	1.11	0.227	0.405
PRPS1-mRNA	-0.145	0.113	-0.366	0.076	0.904	0.776	1.05	0.228	0.405
PDK4-mRNA	0.821	0.641	-0.435	2.08	1.77	0.74	4.22	0.229	0.406
AFMID-mRNA	-0.183	0.143	-0.463	0.0971	0.881	0.726	1.07	0.229	0.406
PIK3C2A-mRNA	0.125	0.0986	-0.0682	0.318	1.09	0.954	1.25	0.233	0.411
DGUOK-mRNA	0.0673	0.0533	-0.0371	0.172	1.05	0.975	1.13	0.235	0.412
AMPD3-mRNA	0.249	0.197	-0.138	0.636	1.19	0.909	1.55	0.236	0.412
LAMC1-mRNA	-0.644	0.512	-1.65	0.359	0.64	0.319	1.28	0.237	0.412
HLA-DRB1-mRNA	-0.702	0.558	-1.8	0.392	0.615	0.288	1.31	0.237	0.412

COPS6-mRNA	-0.0592	0.0471	-0.152	0.0332	0.96	0.9	1.02	0.238	0.412
PDPK1-mRNA	0.102	0.0824	-0.06	0.263	1.07	0.959	1.2	0.246	0.425
GAPVD1-mRNA	0.0481	0.0394	-0.0291	0.125	1.03	0.98	1.09	0.25	0.43
PTGS2-mRNA	-0.338	0.279	-0.884	0.208	0.791	0.542	1.15	0.253	0.433
LAT-mRNA	0.131	0.109	-0.0814	0.344	1.1	0.945	1.27	0.254	0.434
PFKL-mRNA	-0.0784	0.0652	-0.206	0.0494	0.947	0.867	1.03	0.257	0.438
GLUL-mRNA	0.109	0.0913	-0.0697	0.288	1.08	0.953	1.22	0.259	0.438
NSD1-mRNA	0.0845	0.0706	-0.054	0.223	1.06	0.963	1.17	0.259	0.438
CAB39-mRNA	0.102	0.0852	-0.0652	0.269	1.07	0.956	1.2	0.26	0.438
NDUFA6-mRNA	-0.0832	0.0701	-0.221	0.0542	0.944	0.858	1.04	0.263	0.44
SHMT2-mRNA	-0.13	0.11	-0.345	0.085	0.914	0.787	1.06	0.263	0.44
ITCH-mRNA	-0.101	0.0851	-0.268	0.0659	0.932	0.831	1.05	0.263	0.44
UCKL1-mRNA	-0.103	0.0871	-0.273	0.0682	0.931	0.827	1.05	0.267	0.444
IMPDH1-mRNA	0.106	0.091	-0.0722	0.285	1.08	0.951	1.22	0.27	0.448
BRCA2-mRNA	0.34	0.292	-0.233	0.913	1.27	0.851	1.88	0.272	0.45
CHMP6-mRNA	0.0731	0.0634	-0.0512	0.197	1.05	0.965	1.15	0.276	0.455
FNIP1-mRNA	-0.0915	0.0805	-0.249	0.0664	0.939	0.841	1.05	0.282	0.464
ZNF708-mRNA	0.224	0.198	-0.164	0.612	1.17	0.893	1.53	0.284	0.466
KANSL1-mRNA	0.0474	0.042	-0.0349	0.13	1.03	0.976	1.09	0.286	0.467
IL4I1-mRNA	0.295	0.264	-0.221	0.812	1.23	0.858	1.76	0.289	0.471
MCAT-mRNA	-0.273	0.246	-0.754	0.209	0.828	0.593	1.16	0.293	0.475
NAALAD2-mRNA	0.194	0.176	-0.151	0.539	1.14	0.901	1.45	0.296	0.478
ZNF85-mRNA	0.322	0.292	-0.251	0.894	1.25	0.841	1.86	0.296	0.478
CDA-mRNA	-0.197	0.18	-0.55	0.155	0.872	0.683	1.11	0.298	0.48
MAPK8IP1-mRNA	-0.455	0.419	-1.28	0.365	0.729	0.413	1.29	0.302	0.485
MAP2K2-mRNA	-0.065	0.061	-0.185	0.0547	0.956	0.88	1.04	0.312	0.497
KMT2A-mRNA	0.07	0.0658	-0.059	0.199	1.05	0.96	1.15	0.312	0.497

ALDOA-mRNA	-0.0395	0.0371	-0.112	0.0333	0.973	0.925	1.02	0.313	0.497
ATP5ME-mRNA	-0.0448	0.0424	-0.128	0.0382	0.969	0.915	1.03	0.315	0.499
EFNA4-mRNA	0.202	0.194	-0.179	0.582	1.15	0.884	1.5	0.323	0.51
CSF3R-mRNA	-0.0881	0.0864	-0.257	0.0812	0.941	0.837	1.06	0.332	0.523
EPC1-mRNA	-0.0662	0.0656	-0.195	0.0624	0.955	0.874	1.04	0.337	0.528
PLA2G15-mRNA	0.105	0.106	-0.103	0.314	1.08	0.931	1.24	0.344	0.538
AP2S1-mRNA	0.0617	0.0626	-0.061	0.184	1.04	0.959	1.14	0.347	0.542
CD68-mRNA	0.078	0.0795	-0.0778	0.234	1.06	0.947	1.18	0.35	0.544
IL6-mRNA	0.832	0.86	-0.854	2.52	1.78	0.553	5.72	0.356	0.552
PTGER4-mRNA	-0.216	0.227	-0.661	0.228	0.861	0.632	1.17	0.362	0.558
HLA-E-mRNA	0.0582	0.0611	-0.0616	0.178	1.04	0.958	1.13	0.363	0.558
BCL2A1-mRNA	0.172	0.181	-0.183	0.527	1.13	0.881	1.44	0.364	0.558
PSPH-mRNA	-0.237	0.249	-0.726	0.252	0.848	0.605	1.19	0.364	0.558
PDP1-mRNA	-0.122	0.129	-0.374	0.13	0.919	0.771	1.09	0.365	0.558
FAHD1-mRNA	0.156	0.165	-0.167	0.479	1.11	0.891	1.39	0.366	0.558
NRF1-mRNA	0.131	0.141	-0.146	0.408	1.1	0.904	1.33	0.375	0.568
SLC2A8-mRNA	-0.171	0.184	-0.531	0.189	0.888	0.692	1.14	0.375	0.568
PSMB1-mRNA	0.15	0.162	-0.169	0.468	1.11	0.89	1.38	0.379	0.572
CBR4-mRNA	0.128	0.139	-0.145	0.4	1.09	0.905	1.32	0.38	0.572
IDH3A-mRNA	0.0822	0.0897	-0.0936	0.258	1.06	0.937	1.2	0.381	0.572
PLCG1-mRNA	-0.35	0.383	-1.1	0.401	0.785	0.466	1.32	0.383	0.573
MAT2A-mRNA	0.158	0.174	-0.182	0.499	1.12	0.881	1.41	0.384	0.573
NCR1-mRNA	0.269	0.3	-0.318	0.857	1.21	0.802	1.81	0.39	0.58
UQCRQ-mRNA	0.0715	0.0808	-0.0869	0.23	1.05	0.942	1.17	0.397	0.588
PNP-mRNA	-0.341	0.385	-1.1	0.414	0.79	0.468	1.33	0.397	0.588
UBE2T-mRNA	-0.415	0.473	-1.34	0.513	0.75	0.394	1.43	0.401	0.592
NFS1-mRNA	0.0987	0.114	-0.124	0.321	1.07	0.918	1.25	0.405	0.595
CCL5-mRNA	0.304	0.35	-0.383	0.991	1.23	0.767	1.99	0.406	0.595

BRCA1-mRNA	-0.146	0.169	-0.476	0.185	0.904	0.719	1.14	0.407	0.596
RRM1-mRNA	0.134	0.156	-0.172	0.441	1.1	0.888	1.36	0.411	0.599
AK3-mRNA	-0.0998	0.117	-0.329	0.13	0.933	0.796	1.09	0.414	0.602
WRN-mRNA	-0.138	0.163	-0.456	0.181	0.909	0.729	1.13	0.417	0.606
DEPTOR-mRNA	-0.168	0.2	-0.56	0.224	0.89	0.678	1.17	0.42	0.608
SREBF1-mRNA	-0.0714	0.0866	-0.241	0.0984	0.952	0.846	1.07	0.429	0.619
MAT1A-mRNA	0.427	0.521	-0.594	1.45	1.34	0.663	2.73	0.431	0.62
GSK3B-mRNA	-0.0497	0.0611	-0.17	0.0701	0.966	0.889	1.05	0.435	0.622
ITGA1-mRNA	0.222	0.274	-0.314	0.759	1.17	0.805	1.69	0.435	0.622
PRKAB2-mRNA	-0.11	0.136	-0.376	0.156	0.926	0.77	1.11	0.436	0.622
TBXAS1-mRNA	0.0383	0.0474	-0.0547	0.131	1.03	0.963	1.1	0.438	0.623
PDHA1-mRNA	-0.0529	0.0656	-0.181	0.0758	0.964	0.882	1.05	0.439	0.623
GOT1-mRNA	0.172	0.217	-0.254	0.597	1.13	0.839	1.51	0.447	0.632
PIK3CA-mRNA	0.051	0.0646	-0.0756	0.178	1.04	0.949	1.13	0.448	0.632
CD276-mRNA	-0.207	0.263	-0.722	0.308	0.866	0.606	1.24	0.45	0.632
PGD-mRNA	0.0574	0.0732	-0.086	0.201	1.04	0.942	1.15	0.451	0.632
ALDH2-mRNA	0.0823	0.106	-0.125	0.29	1.06	0.917	1.22	0.454	0.632
FANCD2-mRNA	-0.144	0.186	-0.508	0.22	0.905	0.703	1.16	0.455	0.632
TIMELESS-mRNA	0.124	0.16	-0.189	0.437	1.09	0.877	1.35	0.455	0.632
PGK1-mRNA	0.0604	0.0777	-0.092	0.213	1.04	0.938	1.16	0.455	0.632
ARF5-mRNA	-0.0476	0.0625	-0.17	0.0748	0.968	0.889	1.05	0.463	0.642
NDUFS8-mRNA	-0.0568	0.0752	-0.204	0.0906	0.961	0.868	1.06	0.468	0.644
HSPE1-mRNA	0.0662	0.0876	-0.106	0.238	1.05	0.929	1.18	0.468	0.644
DGLUCY-mRNA	0.071	0.0944	-0.114	0.256	1.05	0.924	1.19	0.469	0.645
RPS6KB1-mRNA	-0.0425	0.0577	-0.156	0.0706	0.971	0.898	1.05	0.478	0.654
SLC1A5-mRNA	0.114	0.155	-0.19	0.418	1.08	0.877	1.34	0.479	0.654
FNIP2-mRNA	-0.0419	0.0576	-0.155	0.0709	0.971	0.898	1.05	0.483	0.658
UCK1-mRNA	0.0402	0.0553	-0.0682	0.149	1.03	0.954	1.11	0.484	0.658

BRCC3-mRNA	0.0576	0.0806	-0.1	0.216	1.04	0.933	1.16	0.491	0.666
PSMA7-mRNA	0.0275	0.0387	-0.0483	0.103	1.02	0.967	1.07	0.493	0.667
CTCF-mRNA	0.0437	0.0618	-0.0774	0.165	1.03	0.948	1.12	0.496	0.668
SRM-mRNA	-0.0657	0.0934	-0.249	0.117	0.955	0.842	1.08	0.498	0.668
SERINC5-mRNA	-0.0591	0.0841	-0.224	0.106	0.96	0.856	1.08	0.498	0.668
ZNF91-mRNA	-0.0965	0.138	-0.367	0.174	0.935	0.775	1.13	0.501	0.67
NQO1-mRNA	-0.469	0.674	-1.79	0.851	0.722	0.289	1.8	0.502	0.67
ENO3-mRNA	-0.203	0.296	-0.783	0.377	0.869	0.581	1.3	0.509	0.676
ARID1B-mRNA	0.0515	0.0752	-0.0959	0.199	1.04	0.936	1.15	0.509	0.676
STK11-mRNA	-0.0634	0.0943	-0.248	0.122	0.957	0.842	1.09	0.517	0.681
LTB-mRNA	-0.118	0.176	-0.463	0.227	0.921	0.725	1.17	0.518	0.681
OAT-mRNA	-0.0809	0.121	-0.318	0.156	0.945	0.802	1.11	0.519	0.681
UPP1-mRNA	0.0847	0.127	-0.164	0.333	1.06	0.893	1.26	0.519	0.681
NEU1-mRNA	0.0878	0.132	-0.17	0.346	1.06	0.889	1.27	0.52	0.681
PRF1-mRNA	0.445	0.669	-0.866	1.76	1.36	0.549	3.38	0.521	0.681
ACACB-mRNA	-0.112	0.171	-0.448	0.223	0.925	0.733	1.17	0.527	0.687
PRIM2-mRNA	0.0688	0.106	-0.14	0.277	1.05	0.908	1.21	0.532	0.693
STAT6-mRNA	0.0291	0.0452	-0.0595	0.118	1.02	0.96	1.09	0.534	0.693
TXN2-mRNA	0.0595	0.0935	-0.124	0.243	1.04	0.918	1.18	0.538	0.697
SMAD2-mRNA	0.0571	0.0898	-0.119	0.233	1.04	0.921	1.18	0.539	0.697
AKT3-mRNA	-0.121	0.191	-0.496	0.254	0.919	0.709	1.19	0.541	0.697
MAPK8-mRNA	-0.0532	0.0844	-0.219	0.112	0.964	0.859	1.08	0.543	0.698
WASHC4-mRNA	0.0595	0.0949	-0.126	0.245	1.04	0.916	1.19	0.544	0.698
COX8A-mRNA	-0.0264	0.0422	-0.109	0.0564	0.982	0.927	1.04	0.546	0.698
MYCL-mRNA	-0.066	0.107	-0.276	0.144	0.955	0.826	1.1	0.551	0.7
KYNU-mRNA	-0.0897	0.146	-0.375	0.196	0.94	0.771	1.15	0.551	0.7
MSH2-mRNA	-0.124	0.202	-0.519	0.271	0.918	0.698	1.21	0.553	0.7
CTSW-mRNA	0.186	0.303	-0.408	0.781	1.14	0.754	1.72	0.553	0.7

ARPC4-mRNA	-0.0211	0.0345	-0.0887	0.0466	0.985	0.94	1.03	0.555	0.701
NDUFS7-mRNA	-0.0377	0.0621	-0.159	0.0839	0.974	0.895	1.06	0.557	0.702
SIGLEC5-mRNA	-0.185	0.31	-0.794	0.423	0.879	0.577	1.34	0.564	0.709
ODC1-mRNA	-0.0813	0.139	-0.353	0.191	0.945	0.783	1.14	0.571	0.716
ZNF43-mRNA	0.258	0.442	-0.608	1.12	1.2	0.656	2.18	0.573	0.717
SHMT1-mRNA	0.123	0.213	-0.294	0.541	1.09	0.816	1.45	0.575	0.718
ADA-mRNA	-0.136	0.247	-0.621	0.349	0.91	0.65	1.27	0.594	0.74
ACOT12-mRNA	-0.252	0.461	-1.15	0.651	0.84	0.449	1.57	0.597	0.742
ERCC6-mRNA	-0.058	0.108	-0.269	0.153	0.961	0.83	1.11	0.603	0.747
WDR45-mRNA	-0.0453	0.085	-0.212	0.121	0.969	0.863	1.09	0.606	0.749
CD163-mRNA	0.0785	0.148	-0.212	0.369	1.06	0.863	1.29	0.608	0.75
ASNS-mRNA	-0.281	0.538	-1.33	0.773	0.823	0.396	1.71	0.613	0.754
LEPR-mRNA	-0.169	0.33	-0.815	0.477	0.889	0.568	1.39	0.619	0.758
NME2-mRNA	0.0437	0.0854	-0.124	0.211	1.03	0.918	1.16	0.62	0.758
RUNX2-mRNA	0.322	0.632	-0.916	1.56	1.25	0.53	2.95	0.621	0.758
NDC1-mRNA	-0.0871	0.171	-0.423	0.249	0.941	0.746	1.19	0.622	0.758
TPR-mRNA	0.034	0.0674	-0.0981	0.166	1.02	0.934	1.12	0.625	0.76
TFAM-mRNA	0.0719	0.146	-0.214	0.358	1.05	0.862	1.28	0.633	0.768
NFAT5-mRNA	-0.0827	0.17	-0.415	0.25	0.944	0.75	1.19	0.636	0.77
HMOX1-mRNA	0.0567	0.119	-0.176	0.29	1.04	0.885	1.22	0.644	0.777
GPX1-mRNA	-0.0365	0.0781	-0.19	0.117	0.975	0.877	1.08	0.65	0.782
EZH2-mRNA	-0.0515	0.11	-0.268	0.165	0.965	0.831	1.12	0.651	0.782
HLA-C-mRNA	0.0637	0.138	-0.207	0.334	1.05	0.867	1.26	0.654	0.784
TXN-mRNA	-0.0387	0.0842	-0.204	0.126	0.974	0.868	1.09	0.656	0.784
POLE-mRNA	-0.0453	0.101	-0.243	0.152	0.969	0.845	1.11	0.663	0.787
LDHB-mRNA	-0.0339	0.0755	-0.182	0.114	0.977	0.882	1.08	0.663	0.787
MYBL1-mRNA	0.14	0.313	-0.473	0.754	1.1	0.72	1.69	0.664	0.787
PKM-mRNA	0.0337	0.0754	-0.114	0.181	1.02	0.924	1.13	0.664	0.787

GOT2-mRNA	-0.0216	0.0501	-0.12	0.0766	0.985	0.92	1.05	0.675	0.798
FDXR-mRNA	-0.148	0.346	-0.825	0.529	0.902	0.564	1.44	0.677	0.799
UMPS-mRNA	0.0787	0.187	-0.288	0.446	1.06	0.819	1.36	0.683	0.804
ABL1-mRNA	-0.0212	0.0529	-0.125	0.0825	0.985	0.917	1.06	0.697	0.818
SRR-mRNA	0.103	0.261	-0.408	0.614	1.07	0.754	1.53	0.7	0.82
CTSS-mRNA	0.0324	0.0837	-0.132	0.197	1.02	0.913	1.15	0.707	0.827
SLC2A14-mRNA	-0.0656	0.177	-0.412	0.28	0.956	0.752	1.21	0.718	0.838
BAD-mRNA	-0.0415	0.114	-0.265	0.182	0.972	0.832	1.13	0.723	0.842
AMDHD1-mRNA	-0.147	0.409	-0.948	0.655	0.903	0.518	1.57	0.727	0.844
IDNK-mRNA	-0.0383	0.111	-0.256	0.179	0.974	0.837	1.13	0.737	0.85
LTC4S-mRNA	0.0696	0.203	-0.328	0.467	1.05	0.797	1.38	0.738	0.85
ENO1-mRNA	0.022	0.0642	-0.104	0.148	1.02	0.931	1.11	0.739	0.85
BTK-mRNA	0.0328	0.0958	-0.155	0.221	1.02	0.898	1.17	0.739	0.85
ITGB2-mRNA	0.0325	0.0951	-0.154	0.219	1.02	0.899	1.16	0.74	0.85
HSD17B8-mRNA	0.0965	0.292	-0.475	0.668	1.07	0.72	1.59	0.748	0.857
SOS2-mRNA	0.0301	0.0922	-0.151	0.211	1.02	0.901	1.16	0.751	0.857
UCK2-mRNA	0.0387	0.119	-0.194	0.272	1.03	0.874	1.21	0.751	0.857
ACAT2-mRNA	-0.0413	0.133	-0.302	0.22	0.972	0.811	1.16	0.763	0.866
ATG2B-mRNA	-0.0219	0.0706	-0.16	0.116	0.985	0.895	1.08	0.763	0.866
AGXT-mRNA	0.11	0.355	-0.587	0.806	1.08	0.666	1.75	0.764	0.866
COX7C-mRNA	-0.0168	0.0553	-0.125	0.0915	0.988	0.917	1.07	0.767	0.867
NME1-mRNA	-0.0676	0.23	-0.518	0.383	0.954	0.698	1.3	0.775	0.874
LDHA-mRNA	0.0259	0.0913	-0.153	0.205	1.02	0.899	1.15	0.782	0.876
TBK1-mRNA	0.0203	0.0717	-0.12	0.161	1.01	0.92	1.12	0.783	0.876
GPS1-mRNA	-0.0188	0.067	-0.15	0.113	0.987	0.901	1.08	0.784	0.876
SDHB-mRNA	0.0249	0.0887	-0.149	0.199	1.02	0.902	1.15	0.784	0.876
HPRT1-mRNA	-0.0238	0.0849	-0.19	0.143	0.984	0.877	1.1	0.785	0.876
KLRB1-mRNA	-0.166	0.595	-1.33	1	0.891	0.397	2	0.786	0.876

TALDO1-mRNA	-0.0221	0.081	-0.181	0.137	0.985	0.882	1.1	0.791	0.879
FABP5-mRNA	-0.0583	0.216	-0.481	0.364	0.96	0.716	1.29	0.792	0.879
TK2-mRNA	-0.0456	0.173	-0.385	0.294	0.969	0.766	1.23	0.798	0.883
SLC2A3-mRNA	-0.0728	0.281	-0.623	0.477	0.951	0.649	1.39	0.801	0.884
THBS1-mRNA	-0.219	0.858	-1.9	1.46	0.859	0.268	2.76	0.804	0.886
GCDH-mRNA	-0.0336	0.14	-0.308	0.24	0.977	0.808	1.18	0.815	0.894
ITGB5-mRNA	-0.0943	0.396	-0.87	0.681	0.937	0.547	1.6	0.816	0.894
NDUFA4-mRNA	0.0102	0.0433	-0.0747	0.0951	1.01	0.95	1.07	0.819	0.894
PYCR3-mRNA	0.0825	0.353	-0.609	0.774	1.06	0.656	1.71	0.82	0.894
ARID2-mRNA	-0.0173	0.0743	-0.163	0.128	0.988	0.893	1.09	0.821	0.894
NDUFB10-mRNA	0.00855	0.0374	-0.0648	0.0819	1.01	0.956	1.06	0.824	0.894
RRM2-mRNA	0.122	0.541	-0.938	1.18	1.09	0.522	2.27	0.826	0.894
NCOA2-mRNA	-0.0199	0.0881	-0.193	0.153	0.986	0.875	1.11	0.826	0.894
IL10-mRNA	-0.161	0.716	-1.56	1.24	0.894	0.338	2.37	0.826	0.894
PRKAG1-mRNA	0.0184	0.0834	-0.145	0.182	1.01	0.904	1.13	0.829	0.895
REST-mRNA	-0.0169	0.0778	-0.169	0.136	0.988	0.889	1.1	0.832	0.895
ATG101-mRNA	-0.0133	0.0615	-0.134	0.107	0.991	0.911	1.08	0.833	0.895
FH-mRNA	0.0129	0.0618	-0.108	0.134	1.01	0.928	1.1	0.839	0.9
BUB1B-mRNA	-0.0464	0.227	-0.492	0.399	0.968	0.711	1.32	0.842	0.9
SMAD3-mRNA	0.0166	0.0829	-0.146	0.179	1.01	0.904	1.13	0.845	0.9
ACAP2-mRNA	0.00928	0.0464	-0.0816	0.1	1.01	0.945	1.07	0.845	0.9
UBE2C-mRNA	0.0336	0.169	-0.298	0.365	1.02	0.813	1.29	0.846	0.9
HK1-mRNA	0.012	0.062	-0.109	0.133	1.01	0.927	1.1	0.85	0.901
NDUFA2-mRNA	0.0215	0.111	-0.197	0.239	1.02	0.873	1.18	0.851	0.901
NDUFB4-mRNA	-0.00649	0.0344	-0.074	0.061	0.996	0.95	1.04	0.854	0.902
LAMTOR5-mRNA	0.0111	0.0592	-0.105	0.127	1.01	0.93	1.09	0.855	0.902
CLOCK-mRNA	0.0232	0.129	-0.23	0.276	1.02	0.853	1.21	0.861	0.905
A2M-mRNA	-0.0641	0.357	-0.763	0.635	0.957	0.589	1.55	0.861	0.905

LY86-mRNA	-0.0207	0.12	-0.256	0.215	0.986	0.837	1.16	0.867	0.909
KAT6A-mRNA	0.00883	0.0545	-0.0979	0.116	1.01	0.934	1.08	0.874	0.915
SMAD4-mRNA	0.0188	0.12	-0.217	0.255	1.01	0.86	1.19	0.879	0.918
HADH-mRNA	-0.0162	0.114	-0.24	0.208	0.989	0.847	1.16	0.89	0.928
NDUFA7-mRNA	-0.0118	0.0903	-0.189	0.165	0.992	0.877	1.12	0.899	0.93
COX6B1-mRNA	-0.00474	0.0364	-0.0761	0.0667	0.997	0.949	1.05	0.899	0.93
FOLR3-mRNA	-0.081	0.628	-1.31	1.15	0.945	0.403	2.22	0.9	0.93
PPAT-mRNA	0.0235	0.182	-0.333	0.38	1.02	0.794	1.3	0.9	0.93
LAMTOR4-mRNA	0.00765	0.0658	-0.121	0.137	1.01	0.919	1.1	0.91	0.939
PTEN-mRNA	0.00718	0.0656	-0.121	0.136	1	0.919	1.1	0.915	0.941
AKT2-mRNA	0.00614	0.0567	-0.105	0.117	1	0.93	1.08	0.916	0.941
RPIA-mRNA	0.00537	0.0522	-0.097	0.108	1	0.935	1.08	0.92	0.944
PSMB3-mRNA	0.00861	0.0881	-0.164	0.181	1.01	0.892	1.13	0.924	0.946
S100A12-mRNA	-0.0215	0.252	-0.516	0.473	0.985	0.699	1.39	0.934	0.953
PTK6-mRNA	0.0235	0.28	-0.525	0.572	1.02	0.695	1.49	0.935	0.953
MAPKAP1-mRNA	-0.0038	0.0503	-0.102	0.0947	0.997	0.932	1.07	0.941	0.958
ZNF100-mRNA	-0.0123	0.17	-0.345	0.321	0.991	0.787	1.25	0.944	0.958
PFKM-mRNA	-0.00961	0.159	-0.321	0.302	0.993	0.8	1.23	0.953	0.966
NADK2-mRNA	0.00595	0.14	-0.268	0.28	1	0.83	1.21	0.967	0.977
FPR1-mRNA	0.0102	0.243	-0.466	0.486	1.01	0.724	1.4	0.967	0.977
HEXA-mRNA	-0.00225	0.0778	-0.155	0.15	0.998	0.898	1.11	0.978	0.985
PTGS1-mRNA	-0.00407	0.191	-0.379	0.371	0.997	0.769	1.29	0.983	0.987
ATXN7-mRNA	-0.000917	0.0461	-0.0912	0.0894	0.999	0.939	1.06	0.985	0.987
CENPA-mRNA	0.00682	0.354	-0.686	0.7	1	0.621	1.62	0.985	0.987
FLT1-mRNA	4.61E-16	0.297	-0.582	0.582	1	0.668	1.5	1	1